IMPERIAL COLLEGE OF SCIENCE, TECHNOLOGY & MEDICINE

DEPARTMENT OF AERONAUTICS

A Windows® based conceptual design and analysis package for next generation passenger aircraft.

By

Joseph Leon Amodeo

January 1998

Thesis submitted for the degree of
Doctor of Philosophy of the University of London
and for the Diploma of Imperial College

BIBL
LONDON

‘ The funny thing about regret is, it’s better to regret something you have done than to regret something you haven’t done ’

- B. Surfers

Abstract

A software package has been developed for the purpose of the conceptual design and analysis of passenger aircraft. The package is compatible with both the Window 95 and Windows 3.1 operating systems, and fully utilises the graphical user interface features of these environments. Both the aircraft design methods and the program features are described in detail.

The ethos behind the program is to bring the usability of Windows based software into the arena of engineering design. While the program concentrates on the design of aircraft, the graphical interface and the document based structure of the program, and the inclusion of optimisation, sensitivity, trade-off, and correlation tools, mean that it is a valid concept for any engineering design problem.

The design methods used within the program are a mixture of established techniques, techniques based on published research, and new techniques developed specifically for the program. Many of the new methods are based on correlations of existing and projected data, as these tend to give more reliable and accurate answers than ones based on theoretical methods.

The program allows the incorporation of advanced technologies into the aircraft designs. The choice of technologies includes winglets, advanced materials, laminar flow control, riblets, and ultra high bypass ratio engines. Equations have been developed to describe the impacts of these technologies and their possible future benefits.

Particular attention has been paid to the design of next generation ultra high capacity aircraft. A selection of unconventional fuselage types are included, and the emphasis of the aircraft design methods is towards large aircraft. The special considerations and problems involved with the design of large aircraft have been investigated and practical solutions have been proposed.

The accuracy of the program has been verified using existing Airbus and Boeing aircraft data and some Airbus UHCA concept data. The average error of each major output design parameter is approximately 5 percent. The range of the aircraft, possibly the best indicator of the design accuracy, is calculated using a step iteration approach and gives excellent agreement with actual data.

Acknowledgements

The greatest thanks and appreciation goes to my parents whose support in every respect has been appreciated throughout, and without whom this research, or indeed my existence would not have been possible.

I would also like to acknowledge the contributions, help, and advice provided by the supervision of Dr. Varnavas Serghides, and to thank him for his continued support throughout this research.

A debt of gratitude also goes to Dave, Richard, Tony, Krups, Phillips, Sony, Ideal, Electrolux, Sue Clarke, and ID Software for contributing to a pleasant and hard working environment. I would also like to mention ICU bar, Jules, Sebastian Nutvento and Mr. Gasson.

Contents

Abstract 3

Acknowledgements 4

Contents 5

Nomenclature 14

List of Tables 30

List of Figures 32

Chapter 1 - Introduction 36

1 .1 Background 36

1 .2 Objectives 37

1 .3 Ultra High Capacity Aircraft 37

1 .4 Advanced Technologies 38

1 .5 The Aircraft Design Program 39

1 .6 Design Methods 39

1 .7 Design Results 40

Chapter 2 - Future Aircraft 41

2 .1 The Future of Air Transportation 41

2 .2 The UHCA: Long Overdue ? 43

2 .3 UHCA Constraints 46

2 .3 .1 Airport Compatibility 47

2 .3 .2 Environmental Compatibility 49

2 .4 UHCA Configurations 54

Chapter 3 - Advanced Technologies 57

3 .1 Background 57

3 .2 Propulsion 58

3 .2 .1 Turbofan Engines 58
3 .2 .2 Propfan 62
3 .2 .3 Advanced Ducted Propfan (ADP) 64
3 .2 .4 ContraFan 65
3 .3 Materials & Structures 65
3 .3 .1 Materials 65
3 .3 .2 Structures 69
3 .4 Aerodynamics 69
3 .4 .1 Airfoils 69
3 .4 .2 Winglets 71
3 .4 .3 Wing Tip Devices 73
3 .4 .4 Wing Tip Blowing 73
3 .4 .5 Natural Laminar Flow (N.L.F.) 74
3 .4 .6 Laminar Flow Control (L.F.C.) 78
3 .4 .7 Hybrid Laminar Flow Control (H.L.F.C.) 81
3 .4 .8 Riblets 82
3 .4 .9 Large Eddy Breakup Devices 83
3 .4 .10 Variable Camber Wings 84
3 .5 Miscellaneous 88
3 .5 .1 Undercarriage 88
3 .5 .2 Advanced Fuels 88
3 .5 .3 Systems and Avionics 89

Chapter 4 - Program Overview 90
4 .1 The Aircraft Design Process 90
4 .2 The Aircraft Design Program 91
4 .2 .1 Objectives 91
4 .2 .2 Program Methods 92
4 .2 .3 Program Features & Functionality 97
4 .2 .4 Existing Design Syntheses 104

Chapter 5 - Airfoil & Engine Data Methods 108
5 .1 Airfoil Data 108
5 .2 Engine Data 109
5 .2 .1 Engine Size & Weight 109
5 .2 .2 Engine Thrust Performance 113

5 .2 .3 S.F.C. Performance....115
5 .2 .4 Engine Interpolation \ Scaling....119
5 .3 Data Evaluation....120

Chapter 6 - Initial Sizing Methods....122
6 .1 Payload Weight....122
6 .2 Flight profile Parameters....122
6 .3 Aircraft Performance Parameters....124
6 .3 .1 Wing Loading....124
6 .3 .2 Lift to Drag Ratio....125
6 .3 .3 Lift Coefficients....128
6 .3 .4 Thrust Settings....129
6 .4 Effect of advanced technologies on L\D....132
6 .4 .1 Wing Tip Devices....132
6 .4 .2 Laminar Flow Technologies....133
6 .5 Weight Effect of Advanced Technologies....142
6 .5 .1 Weight Reductions Due To Advanced Materials....142
6 .5 .2 Weight Adjustments due to Active Drag Devices....147
6 .6 Weight Fractions....149
6 .6 .1 Takeoff....149
6 .6 .2 Climb To The Cruise Altitude....150
6 .6 .3 Main Cruise....150
6 .6 .4 Descent From The Cruise Altitude....152
6 .6 .5 Aborted Landing....152
6 .6 .6 Climb To The Diversion Altitude....153
6 .6 .7 Diversion....154
6 .6 .8 Descent From The Diversion Altitude....155
6 .6 .9 Loiter....155
6 .6 .10 Descent From The Loiter Altitude....156
6 .6 .11 Landing....156
6 .6 .12 Final Weight Fraction....157
6 .7 Takeoff Weight Estimation....157
6 .8 Weight Adjustment and iteration....160
6 .9 Thrust & Thrust To Weight Ratios....161

Chapter 7 - Wing Design Methods 162
7 .1 Wing Planform 162
7 .2 Mean Aerodynamic Chord Location 165
7 .3 Aerodynamic Centre Location 165
7 .4 Lift Coefficients & Wing Incidence 166
7 .4 .1 Cruise lift coefficient 166
7 .4 .2 Landing Lift Coefficient 166
7 .4 .3 Takeoff Lift Coefficient 167
7 .4 .4 Wing Incidence 167
7 .4 .5 Ground Roll Lift Coefficient 168
7 .5 Equivalent Wing 168
7 .5 .1 Wing Lift Distribution (Cruise) 169
7 .5 .2 Maximum Clean Lift Coefficient 171
7 .5 .3 Flap Lift Increments 171

Chapter 8 - Geometry Methods 175
8 .1 Fuselage Geometry 175
8 .1 .1 Plan View 175
8 .1 .2 Side View 178
8 .2 Fuselage Cross-Sections 182
8 .2 .1 Elliptical (Ovoid) Cross Sections 182
8 .2 .2 747-Type Cross-Sections 182
8 .2 .3 Double Bubble Cross-Sections 185
8 .3 Fuselage Wetted Area 187
8 .3 .1 Elliptical (Ovoid) Fuselage Shapes 188
8 .3 .2 747-Type Fuselage Shapes 188
8 .3 .3 Double Bubble Fuselage Shapes 189
8 .4 Fuselage Frontal Area 190
8 .5 Fuselage Freight Volume 192
8 .6 Nacelle Geometry 193

Chapter 9 - Weight Estimation Methods 200
9 .1 Detailed Weight Estimation 200
9 .1 .1 Maximum Zero Fuel & Landing Weights 200
9 .1 .2 Ultimate Load Factor 201

9 .1 .3 Wing Structural Weight Estimation 201
9 .1 .4 Fuselage Structural Weight 204
9 .1 .5 Undercarriage Weight 208
9 .1 .6 Surface Control Weight 208
9 .1 .7 Nacelle Weight 208
9 .1 .8 Propulsion Group Weight 209
9 .1 .9 Airframe Services & Equipment Weight 209
9 .2 Operational Items Weight 213
9 .2 Centres Of Gravity 214
9 .3 Tail Sizing 216
9 .3 .1 Tail Volume Coefficients 216
9 .3 .2 Initial Configuration 218
9 .3 .3 Initial Tail Estimate 219
9 .3 .4 Tail Weight Estimation 219
9 .3 .5 Tail Centres Of Gravity 220
9 .3 .6 Tail Iteration 221
9 .4 Undercarriage Sizing 221
9 .5 Undercarriage Drag 222
Chapter 10 - Drag Prediction Methods 224
10 .1 Wetted Area Calculation 224
10 .1 .1 Wing Wetted Area 224
10 .1 .2 Tail Wetted Areas 224
10 .1 .3 Pylon Wetted Area 224
10 .1 .4 Nacelle Wetted Area 225
10 .2 Parasite Drag Components 225
10 .2 .1 Wing Component Drag 226
10 .2 .2 Tail Component drag 229
10 .2 .3 Pylon Component Drag 230
10 .2 .4 Fuselage Component Drag 230
10 .2 .5 Nacelle Drag 231
10 .3 Compressibility Drag 232
10 .3 .1 Drag Divergence Mach Number 232
10 .3 .2 Transonic Drag Rise Estimation 233
10 .3 .3 Zero Lift Drag Increment Due To High Lift Devices 235
10 .4 Windmilling Engine Drag 235

10 .5 Lift Induced Drag....236
10 .5 .1 The Span Efficiency Factor (e)....236
10 .5 .2 Wing Twist Parameters....237
10 .5 .3 Variable Camber Wings....237
10 .6 Ground Effect....238
10 .7 Effect of Winglets....239
10 .7 .1 Upper And Lower Winglets....239
10 .7 .2 Upper Winglet....240
10 .7 .3 Wing Tip Fences....241
10 .7 .4 Winglet Efficiency....242
10 .8 Drag Summary....242

Chapter 11 - Stability Analysis Methods....243
11 .1 Aircraft Trim Condition....243
11 .1 .1 Aircraft Incidence Solution....243
11 .1 .2 Wing Pitching Moment....244
11 .1 .3 Flap Pitching Moment....245
11 .1 .4 Fuselage Pitching Moment....246
11 .1 .5 Horizontal Tail Pitching Moment....246
11 .1 .6 Thrust Pitching Moment....246
11 .2 Neutral Point....247
11 .3 Static Margin....247
11 .4 Trim Drag....248

Chapter 12 - Performance Prediction Methods....249
12 .1 Calculation Process....249
12 .2 Common Procedures....250
12 .3 Takeoff analysis....251
12 .3 .1 Ground Roll....251
12 .3 .2 Rotation....252
12 .3 .3 Transition....252
12 .3 .4 initial Climb....254
12 .4 Climb At Maximum Gamma (γ)....254
12 .5 Climb at Constant Calibrated Airspeed....256
12 .6 Acceleration....257

12 .7 Cruise 257
12 .8 Deceleration 258
12 .9 Descent 258
12 .10 Loiter 259
12 .11 Aborted Landing 259
12 .12 Landing 260
12 .12 .1 Final Approach 260
12 .12 .2 Flare 260
12 .12 .3 Free Roll 261
12 .12 .4 Ground Roll (with thrust Reversal) 261
12 .12 .5 Ground Roll (without thrust Reversal) 262
12 .13 FAR Landing Distance 262
12 .14 Balanced Field Length 262

Chapter 13 - Design Tool Methods 264
13 .1 Fuselage Sizing 264
13 .1 .1 Cross-section Layout 264
13 .1 .2 Seating plan 271
13 .1 .3 747-Type Fuselage Methods 277
13 .1 .4 Double Deck Fuselage Methods 278
13 .1 .5 Horizontal Double Bubble Methods 279
13 .1 .6 Vertical Double Bubble Methods 279
13 .2 Optimisation Methods 279
13 .2 .1 Hooke & Jeeves Method 279
13 .2 .2 Rosenbrock Method 280
13 .3 Correlation Method 281

Chapter 14 - Design Method Validation 282
14 .1 Airfoil & Engine Results 282
14 .1 .1 Airfoil Data 283
14 .1 .2 Engine Data 283
14 .2 Initial Sizing Results 284
14 .3 Wing Design Results 287
14 .3 .1 Wing Planform 287
14 .3 .2 Wing Lift Distribution 288

14 .3 .3 Flap Performance 289
14 .4 Geometry Results 290
14 .4 .1 Fuselage Geometry 290
14 .4 .2 Nacelle Dimensions 291
14 .5 Weight Estimation Results 292
14 .5 .1 Operating Empty Weight 292
14 .5 .2 Tail Surface Sizing 294
14 .5 .3 Undercarriage Sizing 296
14 .6 Drag Prediction Results 297
14 .7 Stability Results 299
14 .7 .1 Static Margin 299
14 .7 .2 Trim Calculations 301
14 .8 Performance Module results 302
14 .8 .1 Flight Range 302
14 .8 .2 Takeoff and Landing Distances 305
14 .9 Fuselage Sizing Results 308
14 .9 .1 Fuselage Cross Section 308
14 .9 .2 Fuselage length 309

Chapter 15 - Design Study Results 311
15 .1 800 Seat Concept Designs 311
15 .1 .1 Design Goals and Constraints 311
15 .1 .2 Design Assumptions 312
15 .1 .3 Design Procedure 313
15 .1 .4 Design Results 313
15 .2 1000 Seat Concept 319
15 .3 Effect of Advanced Technologies 321
15 .3 .1 Advanced Engines 322
15 .3 .2 Wing Tip Devices 324
15 .3 .3 Advanced Materials 326
15 .3 .4 Variable Camber Wings 328
15 .3 .5 Laminar Flow Control 330
15 .3 .6 Hybrid Laminar Flow Control 336
15 .3 .7 Natural Laminar Flow (NLF) 341
15 .3 .8 Riblets 342
15 .3 .9 Summary of Advanced Technologies 343

15 .4 Future Designs.....346

Discussion 349

Conclusions.....368

References 370

Appendix A - User Guide.....378

Nomenclature

Symbols

a	Speed of sound
A	Wing Aspect Ratio
a'_{nose}	Coefficient of the ellipse describing part of the fuselage nose (side view)
a_0	Speed of sound at sea level
a_{bubble}	Coefficient of ellipse of bubble portion of '747'-type fuselage cross-section
A_{bypass}	Cross-sectional area of engine bypass flow
A_{cargo}	Cross-sectional area of cargo hold
A_{core}	Cross-sectional area of engine core flow
$a_{ellipse}$	Coefficient of elliptical equation
A_{fan}	Frontal area of engine fan
a_{lower}	Coefficient of lower elliptical portion of fuselage cross-section
$a_{lower\,i}$	Coefficient of internal lower elliptical portion of fuselage cross-section
A_{max}	Maximum lateral cross-sectional area of aircraft
a_{nose}	Coefficient of the ellipse describing part of the fuselage nose (plan view)
a_{tail}	Coefficient of the ellipse describing part of the fuselage tail (plan view)
a_{upper}	Coefficient of upper elliptical portion of fuselage cross-section
A_{ws}	Area of cockpit windshield
b/a_{fuse}	Eccentricity of ellipse describing fuselage cross-section
b'_{nose}	Coefficient of ellipse describing part of the fuselage nose (side view)
$b_{aileron\,i}$	Innermost aileron span
$b_{aileron\,o}$	Outermost aileron span
$b_{armrest}$	Width of single armrest of passenger seat
b_{bubble}	Coefficient of ellipse of bubble portion of '747'-type fuselage cross-section
b_{cabin}	Maximum width of cabin
$b_{ellipse}$	Coefficient of elliptical equation
BFL	Balanced field length
$b_{flap\,i}$	Innermost flap span
$b_{flap\,o}$	Outermost flap span
b_{fuse}	Maximum width of the fuselage
$b_{fuse\,bubble}$	Width of ellipse describing upper bubble of '747'-type fuselage
$b_{lower\,i}$	Coefficient of internal lower elliptical portion of fuselage cross-section

b_{nose}	Coefficient of the ellipse describing part of the fuselage nose (plan view)
BPR	Bypass ratio of engine
b_{ref}	Span of reference wing
b_{tail}	Coefficient of the ellipse describing part of the fuselage tail (plan view)
$b_{tyre\ main}$	Width of main undercarriage tyres
$b_{tyre\ nose}$	Width of nose undercarriage tyres
C	Specific fuel consumption
c	Chord length
C^*	Non-dimensionalised values of sfc, $C^*=C/(\theta^{0.5}\delta)$
C'	Ratio of s.f.c. of engine to that of a pure jet engine ($C/C_{BPR=0}$)
c'	Flap extended airfoil cord
$C'_{ellipse\ bubble}$	Perimeter of the fuselage upper bubble section that is exposed
$C'_{ellipse\ lower}$	Perimeter of the fuselage lower ellipse section that is exposed
$C'_{ellipse\ upper}$	Perimeter of the fuselage upper ellipse section that is exposed
$C'_{fairing}$	Perimeter of the fuselage cross-section fairing
c'_{root}	Length of chord at wing root, neglecting cranked portion of wing
c_{cg}	Length of wing chord along which the centre of gravity lies
$C_{circular}$	Perimeter of exposed circular parts of double bubble fuselages
c_{crank}	Length of wing chord at wing/crank intersection
$C_{cross\text{-}section}$	Perimeter of fuselage cross-section
$C_{cross\text{-}section.d.d}$	Perimeter of double deck part of '747' type fuselage
$C_{cross\text{-}section.s.d.}$	Perimeter of single deck part of '747' type fuselage
C_d	Drag coefficient (2-dimensional)
C_D	Drag coefficient (3 dimensional)
C_{D0}	Parasite drag coefficient
$C_{D0fuse\text{-}base}$	Fuselage parasite drag coefficient, neglecting base drag
C_{D0nac}'	Nacelle parasite drag coefficient calculated using flat plate analogy
C_{Dbfuse}	Fuselage base drag coefficient
$C_{Dengine}$	Additional drag coefficient due to stopped engine
$C_{Dfuse/nac}$	Additional nacelle drag coefficient due to fuselage interference
C_{Di}	Lift induced drag coefficient
C_{Dint}	Interference drag coefficient
$C_{Dprofile}$	Profile drag coefficient
C_{Dtrim}	Additional drag coefficient due to the tail lift required to trim the aircraft
C_{Dwave}	Wave drag coefficient due to transonic effects
$C_{Dwing/nac}$	Additional nacelle drag coefficient due to wing interference

$C_{ellipse\ lower}$	Perimeter of lower elliptical portion of fuselage cross-section
$C_{ellipse\ upper}$	Perimeter of upper elliptical portion of fuselage cross-section
C_f	Skin friction coefficient
$C_{flaminar}$	Skin friction coefficient assuming laminar flow
$C_{f\ turbulent}$	Skin friction coefficient assuming turbulent flow
c_{flap}	Flap chord length
$c_{flap\ i}$	Length of wing chord at innermost flap location
$c_{flap\ o}$	Length of wing chord at outermost flap location
c_g	Mean geometric chord
C_{ht}	Horizontal tail volume coefficient
C_L	Lift coefficient (3-dimensional)
C_l	Lift coefficient (2-dimensional)
C_{la}	Additional lift coefficient of wing lift distribution
C_{lb}	Basic lift coefficient of wing lift distribution
$C_{L\ crl}$	Mid-cruise lift coefficient
$C_{L\ la(max)}$	Maximum landing lift coefficient
$C_{L\ max}$	Maximum wing lift coefficient (3-dimensional)
$C_{l\ max}$	Maximum wing lift coefficient (2-dimensional)
$C_{l\ max(clean)}$	Maximum wing lift coefficient (2-dimensional) without high lift devices
$C_{l\ max}$'	Maximum lift coefficient of flap extended airfoil section
$C_{L\ to(max)}$	Maximum takeoff lift coefficient
C_{l0}	Zero incidence lift coefficient
$C_{l\alpha}$	Lift curve slope (2-dimensional)
$C_{L\alpha}$	Lift curve slope (3-dimensional)
$C_{L\alpha\ wing}$	Wing lift curve slope (3-dimensional)
C_m	Pitching moment coefficient
$C_{m\alpha}$	Pitching moment curve slope
c_{mac}	Mean aerodynamic chord length
c_{pylon}	Length of wing chord at pylon location
c_{root}	Length of chord at wing root
$c_{root\ e}$	Length of chord at root of equivalent wing
c_{slat}	Length of chord of wing with leading edge slats extended
c_{tip}	Length of chord at wing tip
$c_{tip\ e}$	Length of chord at tip of equivalent wing
C_{vt}	Vertical tail volume coefficient
$c_{wing/fuse}$	Length of the wing chord at the fuselage/wing interface

D	Drag force
D/q	Drag force divided by dynamic head
$D/q_{\ sears\text{-}hack}$	Drag force to dynamic head ratio of Sears-Hack body
$D/q_{\ strut\ main}$	Total drag force to dynamic head ratio of main undercarriage struts
$D/q_{\ strut\ nose}$	Total drag force to dynamic head ratio of nose undercarriage struts
$D/q_{\ tyre\ main}$	Total drag force to dynamic head ratio of main undercarriage tyres
$D/q_{\ tyre\ nose}$	Total drag force to dynamic head ratio of nose undercarriage tyres
$D/q_{\ wave}$	Drag force to dynamic head ratio of transonic wave drag
D_{fan}	Diameter of engine fan
D_{fc}	Maximum diameter of nacelle fan cowling
$D_{fc\,i}$	Diameter of nacelle fan cowling inlet
$D_{fc\,o}$	Diameter of nacelle fan cowling outlet
D_{fuse}	Diameter of component fuselage of double bubble fuselage
$D_{ge\,i}$	Diameter of nacelle gas generator inlet
$D_{ge\,o}$	Diameter of nacelle gas generator outlet
D_{main}	Diameter of tyres on main undercarriage
D_{oleo}	Diameter of main undercarriage oleo
$d_{outer\ main}$	Outer diameter of main undercarriage tyres
$d_{outer\ nose}$	Outer diameter of nose undercarriage tyres
D_{pl}	Diameter of nacelle plug inlet
e	Span efficiency factor (Oswald's efficiency factor)
e_{th}	Theoretical span efficiency factor
FAR_{la}	FAR landing field length
FAR_{to}	FAR takeoff field length
FF	Drag form factor of component
F_p	Vertical force at engine inlet front face due to turning air
$F_{p\alpha}$	Gradient of vertical force at inlet front face due to turning air vs. incidence
ft	feet to metre conversion factor (3.80665)
g	Gravitational constant (9.80665 ms^{-2})
h	altitude
h'_{fuse}	Maximum height of fuselage (including '747' upper bubble)
h_{bubble}	Height of ellipse describing upper bubble of '747' type fuselage
h_{cabin}	Maximum height of cabin
h_{crl}	Main design cruise altitude
h_{deck}	Height of cabin floor (measured from centre of main cross-section)
$h_{deck\,L}$	Height of lower cabin floor (measured from centre of main cross-section)

$h_{deck\,U}$	Height of upper cabin floor (measured from centre of main cross-section)
h_{fuse}	Maximum fuselage height
$h_{fuse\,tail}$	Height of fuselage at tail extremity
h_{max}	Maximum operational altitude of aircraft
h_{seat}	Total height of passenger seat
i_{wing}	Wing fixed incidence relative to fuselage
K_{buf}	Factor in determining weight of food preparation equipment
$K_{efficiency\,v.camber}$	User defined efficiency of variable camber wing
$K_{ellipse}$	Factor that accounts for eccentricity in the weight of elliptical fuselages
$K_{engtype}$	Fuel consumption scaling factor, dependant on engine configuration
K_{join}	Factor that accounts for the weight of joining two circular fuselages
K_{lav}	Factor in determining weight of toilets
$K_{roughness}$	Skin friction roughness constant (0.0000208)
$K_{tune\,aero.effic}$	Tuning factor for overall aerodynamic efficiency
$K_{tune\,apu}$	Tuning factor for the weight of the auxiliary power unit
$K_{tune\,cht}$	Tuning factor for horizontal tail volume coefficient
$K_{tune\,cvt}$	Tuning factor for vertical tail volume coefficient
$K_{tune\,furn}$	Tuning factor for the weight of the cabin furnishings
$K_{tune\,hlfc.weight}$	Tuning factor for weight of HLFC system
$K_{tune\,hlfc.wt.ht}$	Tuning factor for weight of HLFC system applied to horizontal tail
$K_{tune\,hlfc.wt.vt}$	Tuning factor for weight of HLFC system applied to vertical tail
$K_{tune\,iae}$	Tuning factor for the weight of instrumentation, avionics, and electronics
$K_{tune\,L/D}$	Tuning factor for lift to drag ratio
$K_{tune\,lfc.weight}$	Tuning factor for weight of LFC system
$K_{tune\,lfc.wt.ht}$	Tuning factor for weight of LFC system applied to horizontal tail
$K_{tune\,lfc.wt.vt}$	Tuning factor for weight of LFC system applied to vertical tail
$K_{tune\,Macrit}$	Tuning factor for critical Mach number
$K_{tune\,sc}$	Tuning factor for the weight of the surface controls
$K_{tune\,t/c}$	Tuning factor for airfoil thickness to chord ratio
$K_{tune\,W/S}$	Tuning factor for design wing loading
$K_{tune\,w0}$	Tuning factor for maximum takeoff weight
$K_{tune\,winglet}$	Tuning factor for winglet efficiency
$K_{tune\,wtail}$	Tuning factor for weight of tails
K_{uc}	Factor in determining weight of the undercarriage
L	Lift force
L/D	Lift to drag ratio

L/D'	Lift to drag ratio estimated from correlation
L/D_{crl}	Lift to drag ratio at the main cruise mid-point
l'_{nose}	Length of the nose portion of the fuselage (side view)
l'_{nosell}	Length of the elliptical part of the lower fuselage nose (side view)
l'_{noselu}	Length of the elliptical part of the upper fuselage nose (side view)
l'_{nose2l}	Length of the cubic spline part of the lower fuselage nose (side view)
l'_{nose2u}	Length of the cubic spline part of the flight deck (side view)
l'_{nose3u}	Length of the linear part of the flight deck (side view)
l'_{nose4u}	Length of the cubic spline part of the upper fuselage nose (side view)
l'_{taill}	Length of the lower tail portion of the fuselage (side view)
l'_{taill1}	Length of the circular part of the fuselage tail (side view)
l'_{tail2l}	Length of the linear part of the fuselage tail (side view)
l'_{tailu}	Length of the upper tail portion of the fuselage (side view)
L_a	Additional lift of wing lift distribution
l_{ac}	Length along the cabin for which air conditioning is used
lb	Pound to kilogram conversion factor (2.205)
L_b	Basic lift of wing lift distribution
l_{cargo}	Total length of cargo hold
$l_{correct}$	Correction applied to fuselage width to allow for cabin/seat intersection
$l_{ddcylinder}$	Length of double deck region in 'quasi-cylindrical' portion of '747' fuselage
$L_{elliptical}$	Lift of ideal elliptical wing lift distribution
L_{eng}	Total Length of engine
l_{fc}	Length of nacelle fan cowling
LF_{DD}	Lift factor for calculation of drag divergence Mach number
l_{fuse}	Length of the fuselage
l_{galley}	Length of galley
l_{ge}	Length of nacelle gas generator
l_{ht}	Length of horizontal tail arm
l_{na}	Total Length of nacelle
l_{nose}	Length of the nose portion of the fuselage (plan view)
l_{nose1}	Length of the elliptical part of the fuselage nose (plan view)
l_{nose2}	Length of the cubic spline part of the fuselage nose (plan view)
l_{pl}	Length of nacelle plug
l_{pylon}	Maximum length of pylon
$l_{seating}$	Length along which the fuselage contains passenger seating
l_{tail}	Length of the tail portion of the fuselage (plan view)

l_{tail1}	Length of the cubic spline part of the fuselage tail (plan view)
l_{tail1u}	Length of the cubic spline part of the upper fuselage tail (plan view)
l_{tail2}	Length of the linear part of the fuselage tail (plan view)
l_{tail3}	Length of the elliptical part of the fuselage tail (plan view)
$l_{transonic}$	Length of the aircraft along which its cross-sectional area varies
l_{vt}	Length of vertical tail arm
$l_{windows}$	Total length of fuselage which includes cabin windows
Ma	Mach number
Ma_{crit}	Critical Mach number
M_{DD}	Drag divergence Mach number
$M_{DDL=0}$	Drag divergence Mach number at zero lift
N'_{pass}	Number of passengers per deck
$N_{1st.class}$	Number of 1st class passengers for design range
N_{bogey}	Number of bogeys of main undercarriage
N_{cc}	Estimate of the number of cabin crew
N_{crew}	Total number of crew specified by the user
N_e	Number of engines
N_{exit}	Number of emergency exits
N_{fdc}	Estimate of the number of flight deck crew
$N_{manoeuvre}$	Manoeuvre load factor
N_{meal}	Number of meals per passenger per flight
N_{pass}	Total number of passengers for design range
$N_{pass\ 1stClass}$	Total number of 1st class passengers (for fuselage size determination)
$N_{pass\ business}$	Total number of business class passengers (for fuselage size determination)
$N_{pass\ tourist}$	Total number of tourist class passengers (for fuselage size determination)
$N_{surfaces}$	Number of components surfaces to which LFC or HLFC is applied (1 or 2)
$N_{toilets}$	Total number of toilets for fuselage internal layout
N_{ult}	Ultimate load factor
N_{wheel}	Number of wheels on each bogey of main undercarriage
$N_{windows}$	Number of cabin windows along one side of fuselage
P_0	Atmospheric pressure at sea level
P_c	Cabin pressure
P_s	Excess power
q	Dynamic head ($1/2\rho V^2$)
Q	Drag interference factor of component
Q_{fuel}	Mass of fuel consumed

r	radius of circle
R	Distance travelled (Range)
R_{cl1}	Range travelled during climb to main cruise altitude
R_{cl2}	Range travelled during climb to diversion altitude
R_{cr1}	Main design cruise range (no reserves)
R_{db}	Radius of constituent circular cross-sections of double-bubble fuselages
R_{de1}	Range travelled during descent from main cruise altitude
R_{de2}	Range travelled during descent from diversion altitude
Re	Reynolds number
Re_{cutoff}	Reynolds number cut-off value for skin friction calculations
R_{les}	Leading edge suction parameter
R_{total}	Total range of the aircraft including reserves
$S_{aileron}$	Reference area of ailerons
$S_{airbrake}$	Total area of air-brakes
S_{bh}	Area of fuselage bulkheads
$S_{cylinder}$	Wetted area of 'quasi-cylindrical' portion of fuselage
$S_{exposed}$	Exposed area of wing
S_{flap}	Reference area of flaps
$S_{frontal}$	Frontal area of fuselage
S_{hlfc}	Area to which hybrid laminar flow control suction is applied
S_{lef}	Reference area of all leading edge devices
S_{lfc}	Area to which laminar flow control suction is applied
SM	Static margin
S_{nose}	Wetted area of fuselage nose
$S_{planform}$	Fuselage planform area
S_{ref}	Reference area of wing
S_{refe}	Reference area of equivalent wing
S_{refht}	Reference area of horizontal tail
S_{refvt}	Reference area of vertical tail
S_{riblet}/S	Portion of component surface area to which riblets are applied
$S_{spoiler}$	Total area of spoilers
S_{tail}	Wetted area of fuselage tail
S_{tef}	Reference area of all trailing edge devices
S_{uc}	Stroke length of undercarriage
S_{wetfc}	Wetted area of the nacelle fan cowling
$S_{wetfuse}$	Total wetted area of the fuselage

$S_{wet\,ge}$	Wetted area of the nacelle gas generator
$S_{wet\,pl}$	Wetted area of the nacelle plug
$S_{wet\,pylon}$	Wetted area of the pylons
$S_{wet\,wing}$	Wetted area of the wing
S_{wf}	Wetted area of flaps
t	Time
t	Thickness of a component
T	Thrust
T^*	Non-dimensionalised values of thrust, $T^* = T/(T_{nominal} \times \delta)$
t/c '	Thickness to chord ratio corrected for supercritical wings
t/c	Thickness to chord ratio
T/W	Thrust to weight ratio
T'	Ratio of thrust of engine to the thrust of a pure jet engine ($T/T_{BPR=0}$)
T_0	Uninstalled maximum sea-level static thrust
$t_{laminar}/t_{turbulent}$	Portion of flight time for which laminar flow can be maintained
t_{lo}	Loiter time
$T_{nominal}$	Nominal installed engine thrust
t_{root}	Maximum thickness of wing root airfoil
V	Velocity
V_c	Calibrated airspeed
V_{cargo}	Volume of cargo hold
V_{eng}	Engine volume parameter
V_{galley}	Total aircraft galley volume
$V_{\gamma max}$	Velocity that maximises climb path angle
V_{la}	Landing velocity
V_{to}	Takeoff velocity
$V_{to\,stall}$	Takeoff stall velocity
v_{twist}	Factor of induced drag due to linear twist of wing
V_v	Vertical velocity
W	Weight
W/S	Wing loading ($W'/S \times K_{tune\,W/S}$)
W/S'	Wing loading estimated from correlation
W_0	Maximum takeoff weight
W_{ac}	Weight of air conditioning
W_{al}	Weight at the end of aborted landing

W_{apu}	Weight of auxiliary power systems
W_{ase}	Weight of airframe services and equipment
$W_{ase\ misc}$	Weight of miscellaneous airframe services and equipment items
W_{cl1}	Weight at end of the climb to main cruise altitude
W_{cl2}	Weight at end of the climb to diversion altitude
$W_{composite}$	Weight of composite materials present in the aircraft
W_{cr1}	Weight at end of the main cruise
W_{crew}	Weight of all crew and their baggage
W_{de1}	Weight at the end of the descent from the main cruise altitude
W_{de2}	Weight at the end of the descent from the diversion altitude
W_{de3}	Weight at the end of the descent from the loiter altitude
W_{des}	Design weight (assumed to equal 0.85 times the maximum takeoff weight)
W_{el}	Weight of electrical equipment
W_{end}	Weight at the end of the flight
W_{eng}	Dry weight of engine
W_{fixed}	Weight of fixed components in tail sizing analysis
W_{floor}	Weight of cabin floor
W_{fuel}	Weight of fuel for the design cruise range
W_{fuel}/NR	Weight of fuel consumed during entire flight per passenger per kilometre
W_{furn}	Weight of furnishings
W_{fuse}	Total fuselage weight
$W_{fuse\ circular}$	Weight of component circular fuselages for double bubble fuselages
W_{hld}	Weight of wing high lift devices
W_{ht}	Weight of horizontal tail
W_{hyd}	Weight of hydraulics and pneumatics
W_{iae}	Weight of flight instruments, avionics, and electronics
$W_{land\text{-}max}$	Maximum landing weight
W_{lo}	Weight at the end of the loiter
$W_{meal\ 1st.class}$	Weight of first class meals per flight per passenger
$W_{meal\ standard}$	Weight of economy meals per flight per passenger
$W_{mid\text{-}cr1}$	Weight at the mid-point of the main cruise
W_{nac}	Nacelle weight
$W_{non\text{-}struct}$	Non-structural weight
W_{oew}	Operating empty weight
W_{oil}	Weight of oil
W_{ope}	Weight of operational items

W_{ox}	Weight of passenger oxygen system
$W_{payload}$	Weight of maximum payload for design range
W_{pg}	Weight of propulsion group items (engine and relevant systems)
$W_{residual}$	Weight of residual fuel
W_{safety}	Weight of safety equipment
W_{sc}	Weight of surface controls
W_{sp}	Weight of wing spoilers
W_{struct}	Structural weight
W_{to}	Weight at end of the takeoff section of flight
$W_{toilet.supply}$	Weight of toilet supplies per passenger
W_{total}	Total aircraft weight at any point during performance calculations
w_{twist}	Factor of zero lift drag due to linear twist of wing
W_{uc}	Undercarriage weight
$W_{variable}$	Weight of variable components in tail sizing analysis
W_{vt}	Weight of vertical tail
W_{wheel}	Weight loading on each wheel of main undercarriage
W_{window}	Weight of windows
W_{wing}	Total weight of wing
$W_{wing\ basic}$	Weight of the wing neglecting high lift devices and spoilers
$W_{zero\text{-}fuel}$	Maximum zero fuel weight
x	General longitudinal co-ordinate
$\overline{X}$	Longitudinal distance normalised by the mean wing chord length
X''_{ht}	Longitudinal location of horizontal tail c. of g. from leading edge of chord
X''_{vt}	Longitudinal location of vertical tail c. of g. from leading edge of chord
$X'_{ac\,wing}$	Longitudinal location of wing AC measured from wing apex
$X'_{ac.location}$	Longitudinal distance between aircraft c. of g. and wing AC
$X'_{cg\,nac}$	Longitudinal location of nacelles c. of. g. measured from wing apex
$X'_{cg\,pg}$	Longitudinal location of propulsion group c. of. g. from wing apex
$X'_{cg\,sc}$	Longitudinal location of surface controls c. of. g. measured from wing apex
$X'_{cg\,wing}$	Longitudinal location of wing c. of. g. measured from wing apex
X'_{e}	Longitudinal location of the engine front face measured from wing apex
$X_{ac\,wing}$	Longitudinal location of wing aerodynamic centre from fuselage nose
X_{cg}	Longitudinal location of aircraft c. of. g. from fuselage nose
$X_{cg\,ase}$	Longitudinal location of ASE c. of. g. measured from fuselage nose
$X_{cg\,fixed}$	Longitudinal location of fixed components c. of. g. from fuselage nose
$X_{cg\,fuse}$	Longitudinal location of fuselage c. of. g. measured from fuselage nose

$X_{cg\,nac}$	Longitudinal location of nacelles c. of. g. measured from fuselage nose
$X_{cg\,pg}$	Longitudinal location of propulsion group c. of. g. from fuse. nose
$X_{cg\,sc}$	Longitudinal location of surface controls c. of. g. measured from fuse. nose
$X_{cg\,variable}$	Longitudinal location of variable components c. of. g. from fuselage nose
$X_{cg\,wing}$	Longitudinal location of wing c. of. g. measured from fuse. nose
X_m	Longitudinal location of maximum thickness normalised by length
x_{tr}	Longitudinal transition location
$X_{tr\,crl}$	User specified main cruise transition location for LFC and HLFC systems
$X_{tr\,limit.lower}$	Lower surface transition limit normalised by component length
$X_{tr\,limit.upper}$	Upper surface transition limit normalised by component length
$X_{tr\,lower}$	Lower surface transition location normalised by component length
$X_{tr\,upper}$	Upper surface transition location normalised by component length
$X_{transition}$	Average transition location normalised by component length
y	General lateral co-ordinate
$Y_{cg\,wing}$	Lateral location of wing c. of. g.
Y_e	Lateral location of the engines (twin-engined)
$Y_{e\,i}$	Lateral location of the inboard engines (four-engined)
$Y_{e\,o}$	Lateral location of the outboard engines (four-engined)
Year	Year of entry into service of engine
y_{mac}	Spanwise location of mean aerodynamic chord
y_{max}	Maximum width of fuselage at a given longitudinal location
y_{pylon}	lateral location of pylon
$Y_{wing/fusel}$	Lateral location of the lower wing surface and fuselage intersection
z	General co-ordinate perpendicular to both longitudinal and lateral axes
$\overline{Z}$	Distance along z-axis normalised by the mean wing chord length
z_{bubble}	Vertical distance of centre of '747' upper bubble from centre of main ellipse
z_t	Vertical distance between engine centre line and aircraft c. of g.

α	Thrust lapse ratio (T/T_0)
α	incidence
$\alpha'_{nose.l}$	Join angle of elliptical and cubic parts of the lower fuselage nose (side view)
$\alpha'_{nose.u}$	Join angle of elliptical and cubic parts of the upper fuselage nose (side view)
α_0	Zero lift incidence
α_δ'	Flap element incidence
α_{inlet}	Engine inlet incidence

α_{nose}	Join angle of the elliptical and cubic parts of the fuselage nose (plan view)
α_{tail}	Join angle of the elliptical and cubic parts of the fuselage tail (plan view)
β	Compressibility correction factor
β_{fc}	Location of maximum fan cowling diameter (as ratio of l_{fc})
δ	Atmospheric pressure ratio
$\delta_{aileron}/\delta_{flap}$	User defined ratio of the aileron deflection to the flap deflection
$\Delta c/c_f$	Flap chord extension ratio
ΔC_D	Change in drag coefficient
$\Delta C_{D winglet}$	Change in drag coefficient due to winglets or wing tip devices
ΔC_{Dge}	Change in drag coefficient due to ground effect
δ_f	flap element deflection
$\Delta_f C_{l0}'$	Change in airfoil zero incidence lift coefficient due to flap deflection
$\Delta_f C_{l0}''$	Change in airfoil zero incidence lift coefficient due to flap element
$\Delta_f C_{lmax}$	Change in maximum lift coefficient (2-d) due to flap deflection
$\Delta_f C_{Lmax}$	Change in maximum lift coefficient (3-d) due to flap deflection
δ_{flap}	flap system deflection
Δp	Maximum operational differential cabin pressure
Δt	Time step
$\Delta W/W$	Weight reduction of a component due to advanced materials
$\Delta W_{oew\ composite}$	Reduction in operating empty weight due to use of composite materials
$\Delta y/c$	Leading edge sharpness parameter
ε	Downwash angle
ε_p	Upwash at engine inlet
ε_t	Total wing twist angle between wing root and tip
$\phi_{ac.location}$	Percentage MAC length between aircraft c. of g. and wing AC (set by user)
ϕ_{crank}	Ratio of cranked wing span to un-cranked wing span
ϕ_{db}	Join distance between sections of double-bubble fuselage (as fraction of R_{db})
ϕ_{fuse}	Ratio of double deck length to overall fuselage length of '747' type fuselage
γ	Flight path angle
γ_{max}	Maximum flight path angle
η_d	Flap effectiveness factor
η_h	Tail dynamic head ratio (assumed = 0.8)
λ	Wing taper ratio
$\Lambda_{0.5c\,ht}$	Sweep of mid-chord line of horizontal tail
$\Lambda_{0.5c\,vt}$	Sweep of mid-chord line of vertical tail

$\Lambda_{1/4c}$	Sweep of wing at quarter chord line
$\Lambda_{1/4c\,e}$	Sweep of equivalent wing at quarter chord line
Λ_{β}	Sweep of wing quarter chord corrected for Mach number
Λ_{crank}	Sweep of wing at trailing edge of cranked portion
λ_{e}	Taper of equivalent wing
Λ_{le}	Sweep of wing at leading edge
$\Lambda_{le\,e}$	Sweep of leading edge of equivalent wing
Λ_{m}	Sweep of wing along line of maximum thickness
Λ_{te}	Sweep of wing at trailing edge
μ	Coefficient of friction
θ	Atmospheric temperature ratio
$\theta_{fairing}$	Arc angle of joint of fairing of double-bubble fuselage cross-sections
θ_{lower}	Arc angle of joint of fairing to lower ellipse of '747' type cross-section
θ_{nose}	Arc angle of the elliptical part of the fuselage nose (plan view)
θ_{sfc}	Exponent of θ for non-dimensionalised engine s.f.c. values
θ_{upper}	Arc angle of joint of fairing to upper ellipse of '747' type cross-section
ρ	atmospheric air density
$\rho_{h\,stall}$	Air density at specified stall altitude

Subscripts

ac	Aerodynamic centre
aileron	Trailing edge ailerons
airfoil	Refers to root, tip, and tail airfoils
component	Generalisation for any main aircraft component
cp	Centre of Pressure
cr1	Main cruise section of flight
cr2	Diversion cruise section of flight
e	Denotes properties of equivalent wing
final	Value at end of step
flap	Trailing edge flaps
flaps	Combined ailerons and trailing edge flaps
flare	Flare portion of landing section

fuse	Fuselage
gr	Ground roll
hld	High lift devices
ht	Horizontal tail
initial	Value at beginning of step
L	Lower cabin (fuselage geometry calculations)
la	Landing section of flight
lef	Leading edge flaps
lo	Loiter section of flight
mac	Mean aerodynamic chord
max	Maximum
mid	Value at mid point of step
min	Minimum
nac	Nacelle
np	Neutral point
pg	Propulsion group
pylon	Pylon
riblets	Refers to application of riblets to a component
root	Wing root
sc	Surface Controls
surface	Refers to wing, tail, nacelle, or fuselage surface
tef	Trailing edge flaps
tip	Wing tip
to	Takeoff section of flight
U	Upper cabin (fuselage geometry calculations)
v.camber	Variable camber wing
vt	Vertical tail

Acronyms

AC	Aerodynamic Centre
ADP	Advanced Ducted Propeller engine
ASE	Airframe Services and Equipment
AMWS	Advanced Material Weight Saving

CSE	Component Specification Editor
HLFC	Hybrid Laminar Flow Control
LFC	Laminar Flow Control
MAC	Mean Aerodynamic Chord
NLF	Natural Laminar Flow
SFC	Specific Fuel Consumption
TF	Tuning factor
UHCA	Ultra High Capacity Aircraft

List of Tables

Table 2.1 - Minimum regulatory flight separations 49
Table 2.2 - Callaghan and Liebeck[17] results part 1 55
Table 2.3 - Callaghan and Liebeck[17] results part 2 55
Table 5.1 - Manufacturers engine data 111
Table 6.1 - Aircraft wing loading and range data 124
Table 6.2- Assumed aircraft lift to drag ratios 126
Table 6.3 - Assumed aircraft thrust settings 130
Table 6.4 - Initial sizing parameters of example aircraft 158
Table 6.5 - Calculation of sizing parameter Xw0 for example aircraft 159
Table 14.1- Main sizing parameters of sample aircraft 285
Table 14.2 - Initial sizing results of sample aircraft 286
Table 14.3- Wing design results of sample aircraft 288
Table 14.4- Flap deflection results for sample aircraft 290
Table 14.5- Results of freight volume estimation for sample aircraft 291
Table 14.6 - Results of nacelle sizing for sample aircraft 292
Table 14.7- Results of detailed weight estimation for sample aircraft 293
Table 14.8 - Horizontal tail sizing results for sample aircraft 295
Table 14.9 - Vertical tail sizing results for sample aircraft 296
Table 14.10 - Results of undercarriage sizing for sample aircraft 297
Table 14.11- Results of wing location for sample aircraft 300
Table 14.12 - Results of trim calculations for sample aircraft 302
Table 14.13- Results of range calculations for sample aircraft 304
Table 14.14 - Results of takeoff field length calculations for sample aircraft 306
Table 14.15 - Results of landing field length calculations for sample aircraft 308
Table 14.16 - Results of fuselage cross-section sizing for sample aircraft 309
Table 14.17 - Results of fuselage length estimation for sample aircraft 310
Table 15.1- UHCA design example assumptions 312
Table 15.2- Main results of 800 seat fuselage configuration study 318
Table 15.3- Main results of 1000 seat UHCA design (X1000) 321
Table 15.4 - Effect of advanced technology engines on X800 aircraft 322
Table 15.5- Effect of advanced technology engines on X1000 aircraft 323
Table 15.6 - Effect of wing tip devices on X800 aircraft 324
Table 15.7- Effect of wing tip devices on X1000 aircraft 325
Table 15.8- Effect of extra span on X800 and X1000 aircraft 325
Table 15.9 - Advanced material strategy (Years 2010 and 2020) 326
Table 15.10 - Effect of year 2010 materials on X800 and X1000 aircraft 327

Table 15.11- Effect of year 2020 materials on X800 and X1000 aircraft 327
Table 15.12- Effect of variable camber wing efficiency parameter for X800 aircraft 328
Table 15.13- Effect of variable camber wing efficiency parameter for X1000 aircraft 329
Table 15.14 - Effect of LFC transition location on X800 aircraft..... 331
Table 15.15 - Effect of LFC transition location on X1000 aircraft..... 331
Table 15.16 - Effect of LFC flight time on X800 and X1000 aircraft 332
Table 15.17 - Effect of additional LFC lower surface suction on X800 and X1000 aircraft..... 333
Table 15.18 - Effect of LFC vertical tail on X800 and X1000 aircraft 335
Table 15.19 - Effect of LFC horizontal tail on X800 and X1000 aircraft..... 336
Table 15.20 - Effect of HLFC transition location on X800 aircraft..... 337
Table 15.21- Effect of HLFC transition location on X1000 aircraft 337
Table 15.22- Effect of HLFC flight time on X800 and X1000 aircraft..... 338
Table 15.23 - Effect of HLFC vertical tail on X800 and X1000 aircraft 340
Table 15.24- Effect of HLFC horizontal tail on X800 and X1000 aircraft..... 341
Table 15.25 - Effect of NLF nacelles on X800 and X1000 aircraft..... 341
Table 15.26 - Effect of riblets on X800 aircraft 342
Table 15.27- Effect of riblets on X1000 aircraft 343
Table 15.28 - Summary of advanced technologies applied to X800..... 344
Table 15.29 - Summary of advanced technologies applied to X1000..... 345
Table 15.30 - Summary of advanced technologies (average values) 345
Table 15.31 - Effect of year 2010 technology applied to X800 and X1000 aircraft 347
Table 15.32 - Effect of year 2020 technology applied to X800 and X1000 aircraft 348

List of Figures

Figure 2.1- Predicted air traffic development 41
Figure 2.2- Maximum takeoff weight vs. time 44
Figure 2.3- Predicted aircraft seating capacity (1967) 44
Figure 2.4- Predicted aeroplane weight trend (1967) 45
Figure 2.5- Projected UHCA demand 46
Figure 2.6 -Predicted UHCA size limits 47
Figure 2.7 - Aircraft noise history 49
Figure 2.8 - Fly-over point noise limits 51
Figure 2.9 - Sideline point noise limits 51
Figure 2.10 - Approach point noise limits 52
Figure 2.11- Landing and takeoff engine emissions 53
Figure 2.12 - Cruise engine emissions 53
Figure 2.13- Aerodynamic efficiency vs. time 54
Figure 3.1- Summary of Callaghan and Liebeck[17] study 57
Figure 3.2 - Engine performance history 59
Figure 3.3 - Prototype propfan engine 63
Figure 3.4 - Theoretical advanced engine efficiencies 63
Figure 3.5- Advanced ducted propeller designs 64
Figure 3.6 - Typical aircraft material composition breakdown 65
Figure 3.7 - Comparison of conventional and supercritical airfoils 70
Figure 3.8 - Summary of winglet test results 72
Figure 3.9 - Optimum pressure gradients for wing flow stability 75
Figure 3.10 - Natural laminar flow limits of wing 76
Figure 3.11- Comparison of conventional and NLF nacelles 77
Figure 3.12- Lockheed laminar flow control test article 79
Figure 3.13 - Douglas laminar flow control test article 80
Figure 3.14 - Typical hybrid laminar flow control design 82
Figure 3.15- Schematic of variable camber system operation 85
Figure 3.16 - Comparison of variable camber and conventional airfoil profile drag 86
Figure 3.17 - Cruise lift coefficient distribution for variable camber wing 87
Figure 3.18 - Manoeuvre lift coefficient distribution for variable camber wing 87
Figure 4.1- Aircraft design environment flow chart 94
Figure 4.2- Layout of Main Design Parameter Window 95
Figure 4.3 - Aircraft Design module flow chart 96
Figure 4.4 - Screen-shot of Fuselage Sizing Window 98
Figure 4.5 - Screen-shot of Drag Data Window 100

Figure 4.6 - Rendered image of design based on Deutsche Airbus 702 concept 102
Figure 4.7 - Rendered image of design based on Boeing 747-600 102
Figure 5.1- Engine uninstalled weight vs. volume parameter 112
Figure 5.2- Thrust vs. bypass ratio 113
Figure 5.3 - Fuel consumption vs. bypass ratio 115
Figure 5.4 - S.F.C. scaling factors for advanced engines 116
Figure 5.5 - Specific fuel consumption vs. year 117
Figure 5.6 - Cutting edge bypass ratio vs. time 118
Figure 6.1- Estimation of wing loading 125
Figure 6.2 - Estimation of cruise lift to drag ratio 127
Figure 6.3 - Estimation of diversion lift to drag ratio 127
Figure 6.4 - Estimation of loiter lift to drag ratio 128
Figure 6.5- Estimation of cruise lift coefficient (first estimate) 129
Figure 6.6- Estimation of cruise thrust 131
Figure 6.7 - Estimation of diversion thrust 131
Figure 6.8 - Estimation of loiter thrust 132
Figure 6.9 - Estimation of wing MAC length 133
Figure 6.10- Estimation of horizontal tail MAC length 134
Figure 6.11- Estimation of vertical tail MAC length 134
Figure 6.12- Estimation of wing drag fraction 137
Figure 6.13 - Estimation of vertical tail drag fraction 137
Figure 6.14- Estimation of horizontal tail drag fraction 138
Figure 6.15 - Estimation of nacelle drag fraction 138
Figure 6.16- Estimation of fuselage drag fraction 140
Figure 6.17 - Effect of variable camber efficiency on cruise L\D improvement 141
Figure 6.18 - Estimation of the main component weight ratios 143
Figure 6.19 - Estimation of the weight ratios of aerodynamic surfaces 144
Figure 6.20- Estimation of the ASE component weight ratios 145
Figure 6.21- Estimation of the takeoff weight fraction 149
Figure 6.22- Estimation of the climb to cruise altitude weight fraction 150
Figure 6.23- Estimation of the range to climb to the main cruise altitude 150
Figure 6.24- Estimation of the range of the descent from the main cruise altitude 151
Figure 6.25- Estimation of the descent from cruise altitude weight fraction 152
Figure 6.26 - Estimation of the aborted landing weight fraction 153
Figure 6.27 - Estimation of the climb to diversion weight fraction 153
Figure 6.28 - Estimation of the range of the descent from diversion altitude 154
Figure 6.29 - Estimation of the descent from the diversion altitude weight fraction 155
Figure 6.30 - Estimation of the descent from the loiter altitude weight fraction 156

Figure 6.31- Estimation of the landing weight fraction 156
Figure 6.32 - Estimation of takeoff weight 160
Figure 7.1 - Wing planform geometry 163
Figure 7.2- Determination of wing areas 163
Figure 7.3 - Available flaps geometries 171
Figure 8.1 - Geometry of the fuselage in plan view 175
Figure 8.2 - Geometry of the fuselage nose in plan view 176
Figure 8.3 - Construction of fuselage nose geometry 176
Figure 8.4 - Geometry of fuselage tail in plan view 178
Figure 8.5 - Geometry of fuselage in side view 179
Figure 8.6 - Geometry of fuselage nose in side view 179
Figure 8.7 - Geometry of fuselage tail in side view 181
Figure 8.8 - Geometry of '747'- type fuselage cross-section 183
Figure 8.9 - Geometry of horizontal double bubble cross-section 185
Figure 8.10 - Determination of '747' frontal area ($\theta_{lower}>0$) 191
Figure 8.11 - Geometry of cargo hold cross-section 192
Figure 8.12 - Assumed nacelle geometry 194
Figure 8.13 - Estimation of the total nacelle length 194
Figure 8.14 - Estimation of maximum nacelle fan cowling diameter 195
Figure 8.15 - Estimation of nacelle fan cowling length 195
Figure 8.16 - Estimation of nacelle gas generator length 196
Figure 8.17 - Estimation of nacelle fan cowling inlet diameter 196
Figure 8.18 - Estimation of nacelle fan cowling outlet diameter 197
Figure 8.19 - Estimation of nacelle gas generator inlet diameter 197
Figure 8.20 - Estimation of nacelle gas generator outlet diameter 198
Figure 8.21 - Estimation of nacelle plug diameter 199
Figure 9.1 - Estimation of maximum zero fuel and landing weights 200
Figure 9.2 - Estimation of horizontal tail volume coefficient 216
Figure 9.3 - Estimation of vertical tail volume coefficient 217
Figure 10.1 - Transonic drag rise profile 233
Figure 10.2 - Estimation of drag reduction due to upper and lower winglets 239
Figure 10.3 - Estimation of drag reduction due to upper winglet 241
Figure 12.1 - Construction of transition flight path 254
Figure 12.2 - Determination of maximum climb angle 255
Figure 13.1 - Layout of elliptical single deck fuselage cross-section 264
Figure 13.2 - Determination of correction length for cabin/seat intersection 266
Figure 13.3 - Construction of '747' type fuselage cross-section 267
Figure 13.4 - Construction of elliptical double deck fuselage cross-section 268

Figure 13.5 - Construction of horizontal double bubble fuselage cross-section 270
Figure 13.6 - Construction of vertical double bubble fuselage cross-section 271
Figure 13.7 - Example of automated internal cabin layout generation 272
Figure 13.8 - Estimation of nose and tail lengths of the fuselage 272
Figure 13.9 - Determination of fore and aft cabin limits 273
Figure 13.10 - Possible galley arrangements 275
Figure 14.1- The effect of bypass ratio on engine specific fuel consumption 283
Figure 14.2 - Effect of bypass ratio on engine weight 284
Figure 14.3 - Example wing lift distribution 289
Figure 14.4 - Example parasite drag plot 298
Figure 14.5 - Example drag polar 298
Figure 14.6 - Example trim plot 301
Figure 15.1- UHCA design example constraints 311
Figure 15.2 - 800 Seat - Double Deck (X800-DD) 314
Figure 15.3 - 800 Seat - '747' Type Fuselage (X800-747) 315
Figure 15.4 - 800 Seat - Horizontal Double Bubble (X800-HDB) 316
Figure 15.5 - 800 Seat - Vertical Double Bubble (X800-HDB) 317
Figure 15.6 - 1000 Seat - Double Deck (X1000-DD) 320
Figure 15.7- Weight reduction due to variable camber wing (X800) 329
Figure 15.8 - Weight reduction due to variable camber wing (X1000) 330
Figure 15.9 - Weight reductions due to LFC wing on X800 aircraft 334
Figure 15.10 - Weight reductions due to LFC wing on X1000 aircraft 334
Figure 15.11 - Weight reductions due to HLFC wing on X800 aircraft 339
Figure 15.12 - Weight reductions due to HLFC wing on X1000 aircraft 339
Figure 15.13 - Fuel savings for X-800 and X-1000 due to advanced technologies 346
Figure 15.14 - Assumed year 2010 technology 347
Figure 15.15 - Assumed year 2020 technology 347

1 .Introduction

1 .1 BACKGROUND

The world of civil aviation has developed tremendously over the last century, and will continue to do so as we approach the next millennium. The demand for more economical and convenient air travel is the main driving force behind the technological and operational improvements that we have witnessed.

As the cost of travelling by air has fallen, the demand has risen accordingly, leading to a situation where the current capacity of the world aviation infra-structure is only just enough to keep up with the demands placed on it. With predictions that airline revenue will continue to grow well into the next century, a number of important issues need to be addressed in order to meet the needs of the aviation markets of the future.

Possible remedies to this potential problem include the construction of more airports and the expansion of existing airports. Although these approaches will almost certainly play some part in future aviation strategies, there are a number of drawbacks and potential obstacles associated with them, especially since environmental issues have become so close to the forefront of public consciousness in recent times.

One of the perennial solutions to the required increases in capacity has been to build larger and larger aircraft, and in many ways this is the most logical approach. For a number of years the idea of Ultra High Capacity Aircraft (UHCA) has been suggested as the way forward, however for technical, economic, and safety reasons these ideas have remained on the drawing board.

The technical issues involved in the production of a suitable large aircraft have been and continue to be addressed by the leading aircraft manufacturers, and in fact the prospect of an ultra high capacity aircraft becoming reality has increased dramatically over the last five years. An important aspect of any future UHCA design will be the effect of advanced technologies that can improve flight efficiency, and can lead to a more technically and economically viable UHCA.

The kinds of technologies that are likely to evolve, their relative merits, and the effect of their application on all aspects of the aircraft performance need to be assessed. The operational and economic validity of these proposed technologies also needs to be investigated, so that a balanced picture of the potential benefits to be gained from each technology can be formed, and future directions for research can be established.

In order to perform the quantitative evaluation of such future civil aircraft concepts, there is a need for a specifically written comprehensive computer software package. This package will need to provide a flexible platform for performing the conceptual design and analysis of both present and future civil aircraft, with the inclusion of candidate advanced technologies, and including methods specifically adapted for the design of UHCA.

This computer software package will be then used to demonstrate that not only the aviation market, but that aeronautical technology, has also progressed to a stage which means that the UHCA has become a viable proposition for the beginning of the next century.

1 .2 OBJECTIVES

The key objectives of this research programme are:-

- To produce a user-friendly interactive program which performs the conceptual design and analysis of subsonic civil passenger aircraft.
- To provide facility for the incorporation of candidate advanced technologies into the aircraft designs, and to adequately reflect their impact on the aircraft designs.
- To use this program to develop new methodologies suitable for UHCA and to then incorporate these methods into the program.
- To use this final program to come up with results and conclusions concerning the configurations and technology requirements for viable and efficient UHCA's

With these objectives in mind the research is based around the five main areas of assessing UHCA ideas, the evaluation of advanced technologies, developing the Aircraft Design Program, creating new methods and techniques applicable for advanced technologies and UHCA and incorporating them into the Aircraft Design Program, and using the final program to analyse advanced UHCA designs.

1 .3 ULTRA HIGH CAPACITY AIRCRAFT

The important question of whether there actually is or will be a demand for Ultra High Capacity Aircraft is one that needs to be carefully considered. The facts and figures on air transport growth need to be examined and a number of possible solutions to the expected future congestion of the global air transport system, including UHCA, need to be considered.

The fact that the worlds current largest civil aircraft, the Boeing 747, was designed over 30 years ago would suggest that a stagnation has occurred in the accepted maximum size for a civil transport, and predictions made some years ago of the size of civil transports for the late 20th century have now been shown to be wildly inaccurate. The reasons for this apparent delay in the uptake of UHCA designs should be examined, and any possible reasons why this may change in the near future must be explored.

One of the main stumbling blocks for the production of UHCA could be the need to provide compatibility with existing airport infra-structure and operational requirements. The physical size limits that define airport compatibility regulations, and any possible future changes in these, along with the main operational concerns that are synonymous with UHCA,need investigation.

The environmental impact of UHCA on both noise and air pollution is also a very important issue, and one that could have great bearing on any future UHCA designs. Any difficulties of gaining certification for the regulations governing air and noise pollution need to be highlighted and possible solutions suggested.

The overall configuration of a next generation large aircraft has been the subject of debate for some time, with many new and unconventional ideas having been suggested. An overview of current thinking has to be made, and various configurations evaluated.

1 .4 Advanced Technologies

The effect of ever advancing technological achievements has been to greatly increase the efficiency of modern aircraft. The most significant of contributions to these improvements over the last twenty years has probably come from the use of high bypass ratio engines and supercritical wings. Predictions for the future directions of technology give us no reason to suggest that similar developments will not continue well into the next century.

Candidate future technologies can be split into three distinct types. The first type can be described as 'derivative technologies', and includes such advancements as very high bypass ratio engines, new alloy and composite materials, and improved wing and winglet designs, all of which are merely refinements or progressions of current technologies. The second type of technologies are still experimental, yet have been thoroughly investigated and evaluated over recent years. This type of 'established technology' would include such concepts as laminar flow control, natural laminar flow, hybrid laminar flow control, variable camber wings, riblets, and propfan engines. The third group contains 'unestablished technologies', which have undergone some experimental testing, yet are still much an

unknown quantity. This would include such things as advanced ducted propellers, contra fan engines, wing tip turbines/sails, and large eddy break-up devices.

The merits and possible drawbacks of each technology, including operational and environmental characteristics, needs to be explored in-depth for each technology. An assessment can then made of the likelihood of this technology actually coming into use on future civil aircraft.

1 .5 The Aircraft Design Program

The role of conceptual design in the complete aircraft design process needs to be appraised and the main targets for this design stage assessed. This will allow the objectives of the Aircraft Design Program to be more clearly set.

The layout of the program itself will be Windows based and operated via easy to use pull down menus and buttons, the fully installed program will be complete with comprehensive context-sensitive help information and design examples. The program should not only perform the design process but provide many functions for the analysis of the design. These functions include the graphing of pertinent output data, as well as optimisation, correlation, trade-off, and sensitivity tools.

Although there are a number of conceptual design programs within the industrial and educational community with which the Aircraft Design program will have some common features, no package has been identified as combining an integrated design synthesis with interactive user friendly analysis features, while simultaneously allowing the design of UHCA incorporating future advanced technologies. This means that the completed Aircraft Design Program will provide a unique design tool for the computerised conceptual design syntheses of advanced civil aircraft.

1 .6 Design Methods

The ultimate aim when selecting the appropriate design methods is to ensure that the maximum accuracy can be achieved given the data resources available. This means that new methods need to be developed, many based on correlations of existing aircraft data, which will give a higher degree of accuracy than existing semi-empirical or theoretical methods.

Another important goal of the program is to gain maximum accuracy while minimising the need for input and judgement from the user. This should be done without compromising the accuracy of the output data, and while maintaining a degree of flexibility that could be appreciated by more experienced users.

The facility to incorporate advanced technologies into the designs means that many new methods need to be created to account for the effect of these components. These methods will invariably be based upon the results of published research in the particular field of interest, and will correctly reflect the expected physical and mechanical effects of the technologies.

The first stage of gathering results from the program is to use the input data from existing designs to verify the accuracy of the output data. Data for existing and concept aircraft from Airbus and Boeing could be used for this purpose. An average accuracy of about 10% could reasonably be expected for this kind of synthesis.

Once these methods contained within the program have been verified, then a number of studies could be undertaken to investigate any modifications and new methods that need to be introduced to account for any changes in the design process peculiar to the design of UHCA.

1 .7 Design Results

The final stage of gathering results from the program can then concentrate on investigating the viability and optimum configuration of UHCA, and the effects of advanced technologies on their performance. The studies shall concentrate on concept aircraft capable of carrying 800 and 1000 passengers for a range of 7000 nautical miles. These specifications have been chosen to provide aircraft with a greater payload-range than any existing aircraft, and greater than that of any of the concept aircraft produced by Boeing or Airbus. This will therefore provide some interesting insights into aircraft of this size, especially with regards to their technical and operational feasibility.

These results should give clear indications of the properties of UHCA, and the types of technology that would be of most benefit to them. It is expected that these results should quantitatively confirm many assumptions and arguments that have been made so far for advanced technology UHCA studies, and perhaps reveal some unexpected trends.

2 .Future Aircraft

2 .1 The Future of Air Transportation

There can be no doubt that air transportation is a growth industry. Based on data from Sutton[1], figure 2.1 shows the increase in traffic, in terms of revenue passenger kilometres over the last fifteen years, and the predicted increase for next fifteen. This data is in agreement with the Acton[2] prediction of a long-term growth trend between 5-6%, with a disproportionate amount of this growth coming from south-east Asia and the Pacific Rim area. Orlowski and Callaghan[3] forecast similar figures of an average 7% growth in Revenue Passenger Kilometres world-wide over the next 20 years, with the North Atlantic region contributing 4.5% growth, compared to the 11% of the Far East and Pacific region.

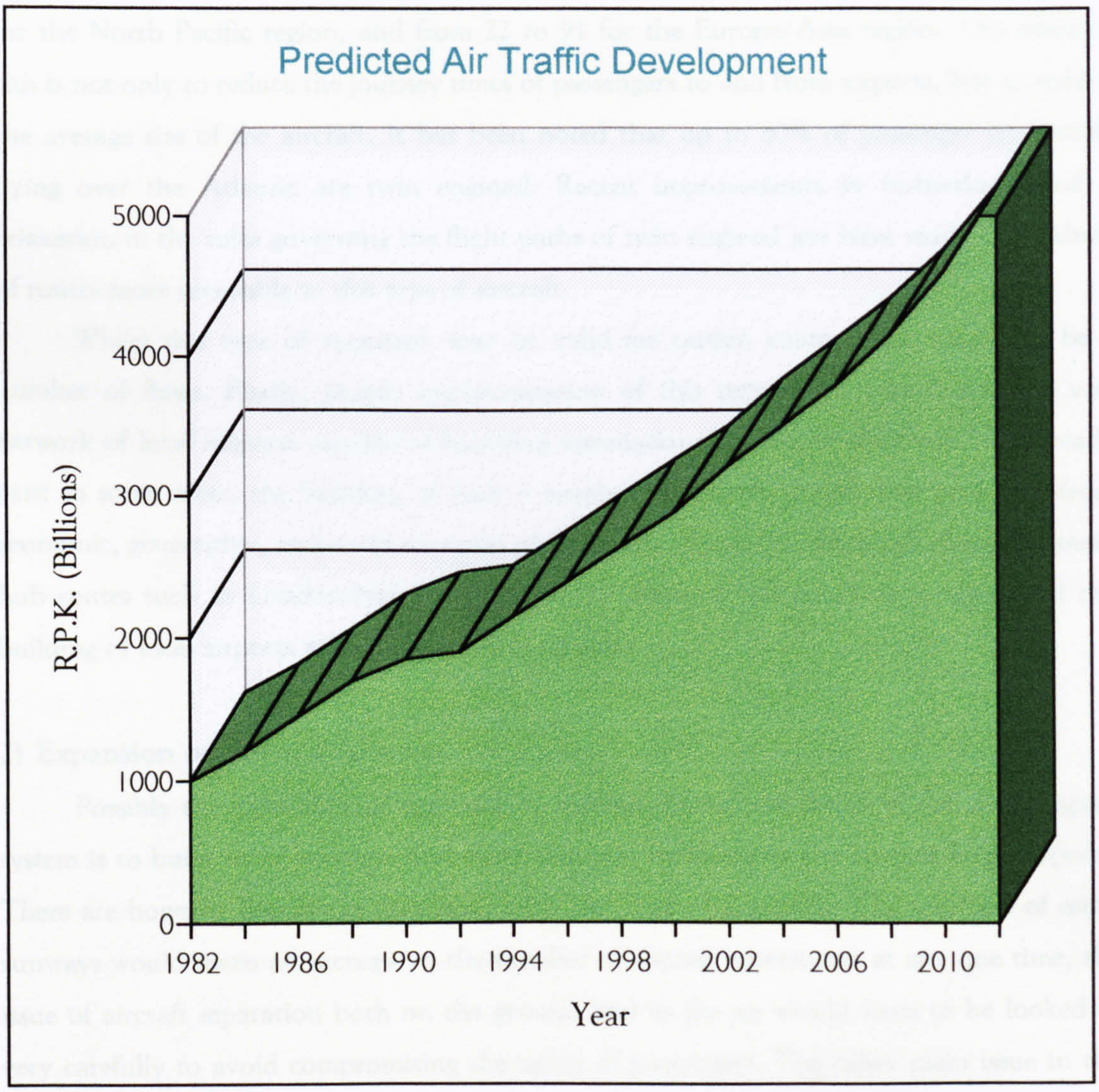


Figure 2.1- Predicted air traffic development

There is less agreement however on how to deal with these increases in demand. There appear to be three distinct views on the strategy that should be adopted to avert future over crowding and congestion of the air transport system.

1) Route Dispersion

Air traffic has traditionally been concentrated in a few large cities, this creation of airline hubs has created an artificial demand for flights from these hubs. A large proportion of passengers travelling from these airports may not actually live or work anywhere near these cities.

The demand for flights world-wide has been increasingly toward a 'point to point' service to and from the smaller local airports rather than the larger more congested arterial airports. This dispersion of routes is illustrated by the increase in served city pairs across the world, Orlowski and Callaghan[3] have estimated this increase over the fifteen year period between 1975 and 1990 to be from 47 to 122 for the North Atlantic region, from 17 to 56 for the North Pacific region, and from 22 to 91 for the Europe/Asia region. The effect of this is not only to reduce the journey times of passengers to and from airports, but to reduce the average size of the aircraft. It has been noted that up to 80% of passenger jet aircraft flying over the Atlantic are twin engined. Recent improvements in technology, and a relaxation in the rules governing the flight paths of twin engined jets have made these kinds of routes more accessible to this type of aircraft.

Whilst this type of approach may be valid for certain routes there appear to be a number of flaws. Firstly, proper implementation of this type of strategy requires a vast network of local airports capable of handling international traffic, whilst these may already exist in some areas, the building of such a number of airports could pose problems from economic, geographic, and environmental stand points. Secondly, there will always be main hub routes such as London-New York where the demand will continue to grow and the building of local airports will not be a viable option.

2) Expansion of Existing Airports

Possibly the most obvious approach to solving the capacity needs of the air transport system is to build more runways and more terminal buildings at the current large airports. There are however drawbacks associated with this type of approach. The addition of more runways would mean an increase in the number of aircraft movements at any one time, the issue of aircraft separation both on the ground and in the air would have to be looked at very carefully to avoid compromising the safety of passengers. The other main issue in the expansion of airports debate has been the environmental pollution caused by the airports, in particular the aircraft noise. This is an issue which has become of much greater significance

over the last decade, and it is unlikely that the expansion of existing airports will continue at the same pace due to the increased influence of environmental lobbyists, and the likelihood of tougher noise regulations to be introduced by the aviation authorities.

It must also be considered that many airports, especially those located in or around major cities, or those situated near residential or business areas simply do not have any room to expand into.

3) Larger Aircraft

It is almost inevitable that the time will come, if it already has not, that the airlines will demand aircraft capable of carrying more passengers than the current largest passenger aircraft the Boeing 747-400. This seems to be the best approach for solving the congestion problems certain to occur on the more popular routes, especially in Europe and Japan, where a shortage of runway slots means that it is simply not possible to increase the frequency of flights to fit more aircraft into an already congested flight path.

While carrying more passengers per flight seems an attractive prospect, there are a number of issues that need to be addressed. Any increase in the separation of aircraft on the ground, or in the air, as well as any increase in turnaround and boarding time due to the additional size of these new large aircraft could negate any potential benefit.

It is clear that none of the solutions to air traffic congestion presented above are by any means perfect, and that the way forward is to realise that each situation is unique. Each occurrence of congestion difficulties may require a different solution, perhaps combining the ideas above to produce a more efficient and flexible system.

2 .2 The UHCA: Long Overdue ?

As outlined above, it seems certain that one day air transports will be built that are larger than today's giants. The graph shown below in figure 2.2 compiled recently by Airbus4 shows the increase in size of aircraft over the last 75 years, and their projected growth for the turn of the next century. It is interesting to note the rapid increases in size that took place up until 1970, culminating with the introduction of the Boeing 747. This is followed by very little growth over the following 27 years up until the present day, with that small amount of growth coming from stretched versions of the 747.

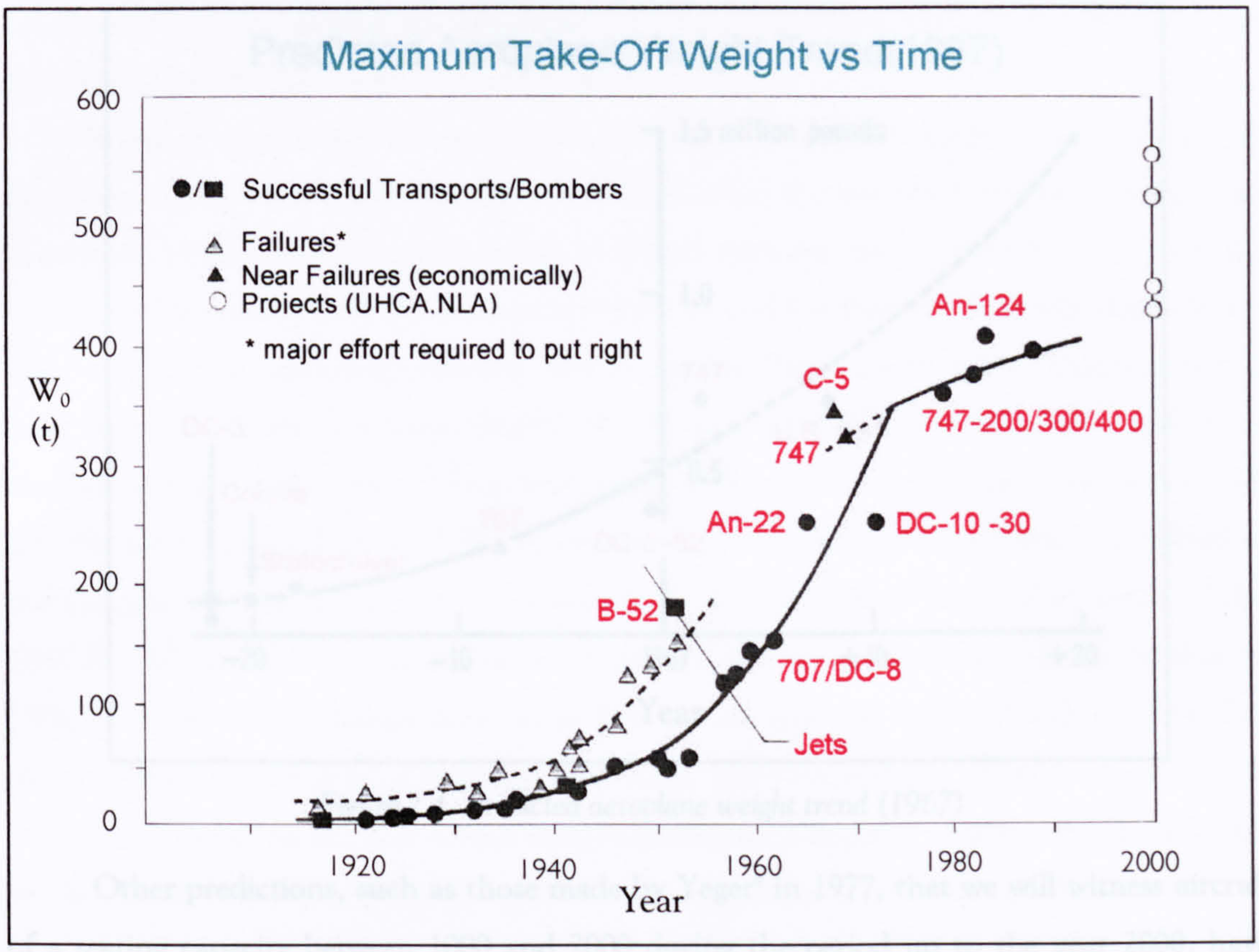


Figure 2.2-Maximum takeoff weight vs. time

Since the introduction of the Boeing 747 in the late 60's, there has been constant speculation on the size of future aircraft. In 1967 Schriever and Seifert[5] published a book entitled 'Air transportation 1975 and beyond', which attempted to predict the nature of aircraft flying in the 70's and beyond. Figure 2.3 and Figure 2.4 show the predictions made in this book for both the seating capacity and the weight of aircraft up to 1987.

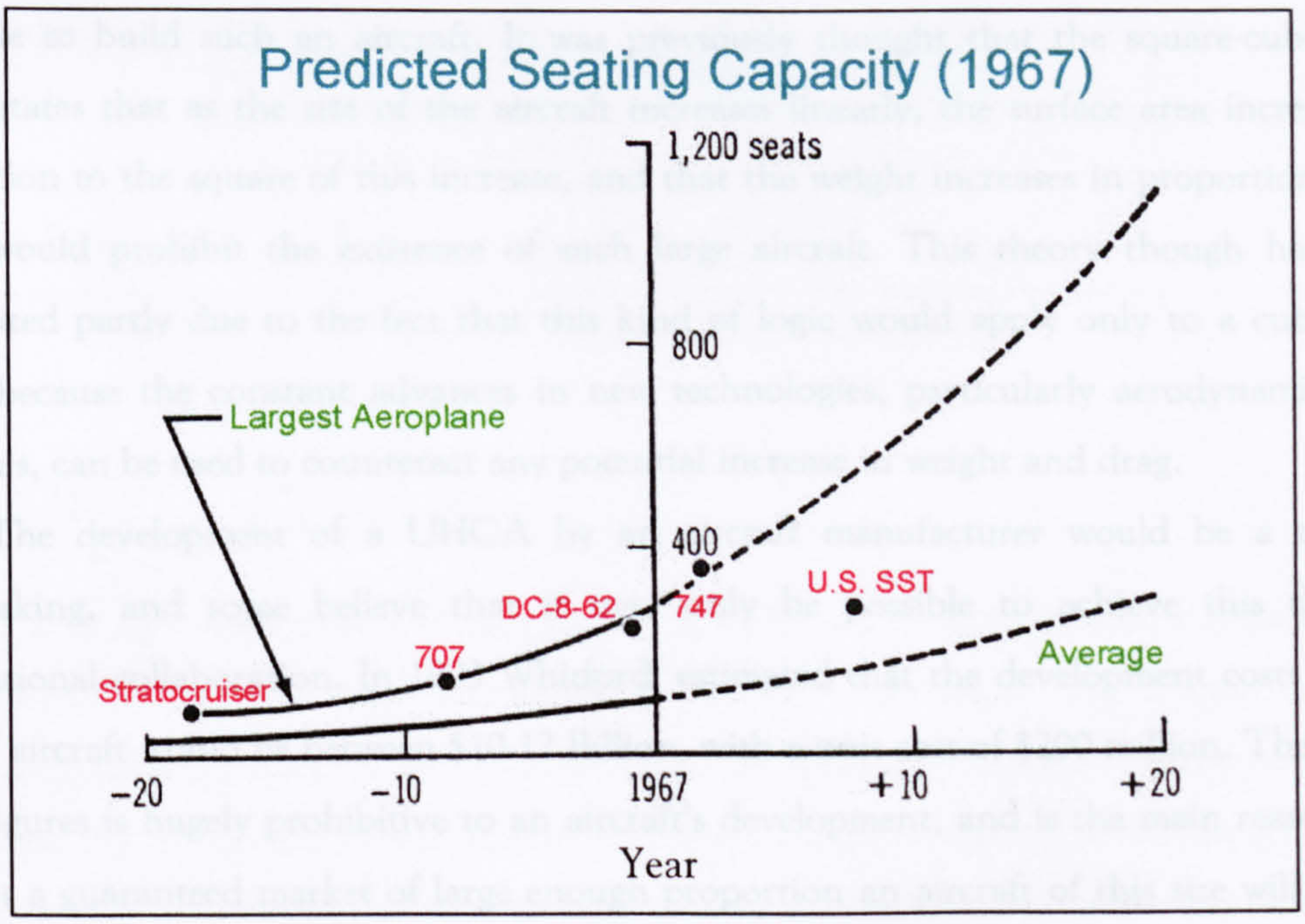


Figure 2.3- Predicted aircraft seating capacity (1967)

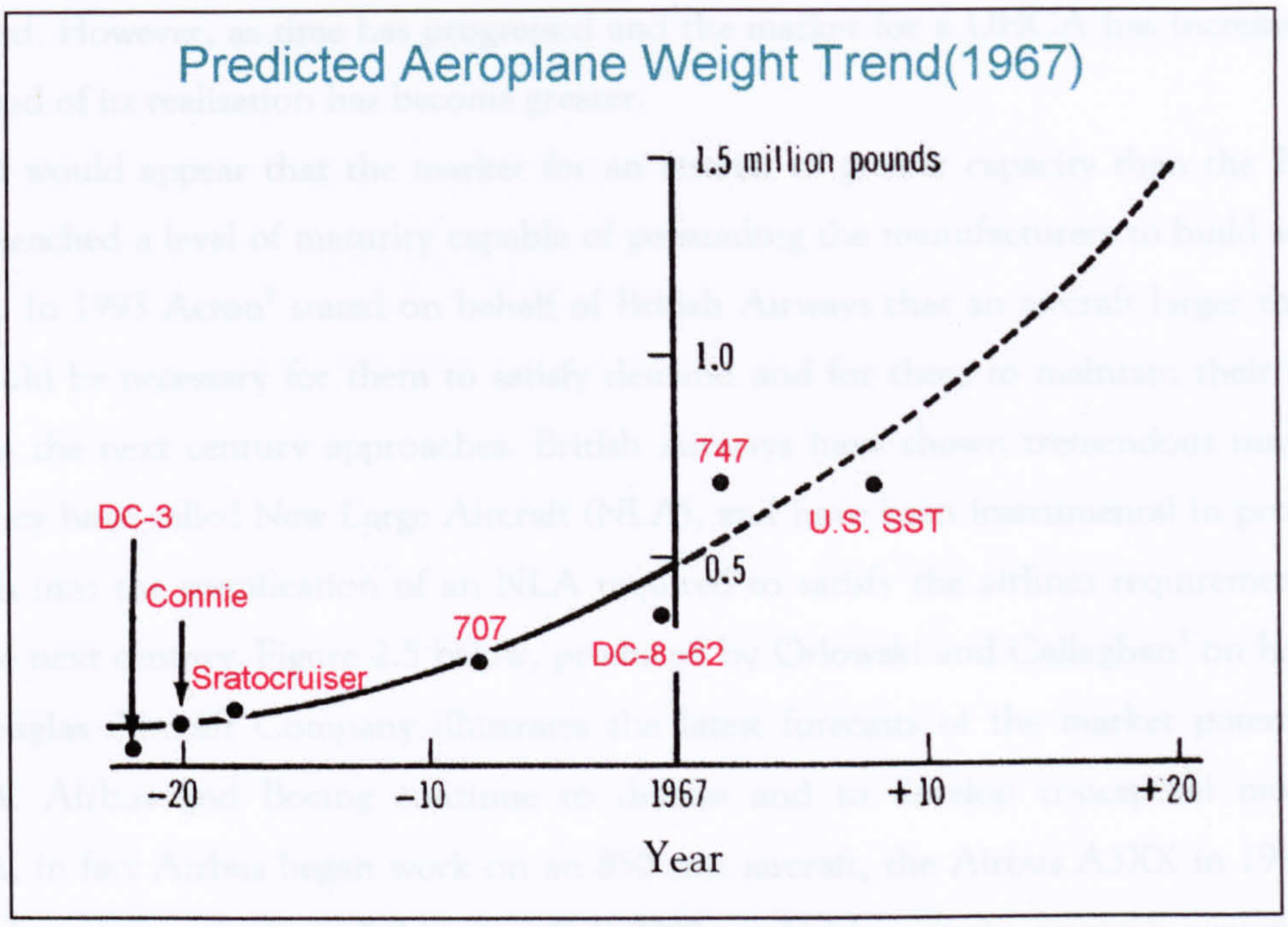


Figure 2.4- Predicted aeroplane weight trend (1967)

Other predictions, such as those made by Yeger[6] in 1977, that we will witness aircraft of a seating capacity between 1000 and 2000 during the period up to the year 2000, have been shown with time to be wildly inaccurate. It would seem that in theory the production of an ultra high capacity aircraft is long over due. The reasons for the lack of very large aircraft would seem to be based on economic rather than technical constraints, after all the Antonov 225 which first flew in 1988, and is currently the worlds largest aircraft with a wingspan of 88m, length of 84m, and takeoff weight of 600 tons, demonstrates that an aircraft of such large proportions is capable of flying, and that the technology has long been available to build such an aircraft. It was previously thought that the square-cubic law, which states that as the size of the aircraft increases linearly, the surface area increases in proportion to the square of this increase, and that the weight increases in proportion to its cube, would prohibit the existence of such large aircraft. This theory though has been discredited partly due to the fact that this kind of logic would apply only to a cube, and partly because the constant advances in new technologies, particularly aerodynamics and materials, can be used to counteract any potential increase in weight and drag.

The development of a UHCA by an aircraft manufacturer would be a massive undertaking, and some believe that it may only be possible to achieve this through international collaboration. In 1993 Whitford[7] estimated that the development costs of this type of aircraft would be between $10-12 Billion, with a unit cost of $200 million. The size of these figures is hugely prohibitive to an aircraft's development, and is the main reason that without a guaranteed market of large enough proportion an aircraft of this size will not be

produced. However, as time has progressed and the market for a UHCA has increased, the likelihood of its realisation has become greater.

It would appear that the market for an aircraft of greater capacity than the 747 has finally reached a level of maturity capable of persuading the manufacturers to build such an aircraft. In 1993 Acton[2] stated on behalf of British Airways that an aircraft larger than the 747 would be necessary for them to satisfy demand and for them to maintain their market share as the next century approaches. British Airways have shown tremendous interest in what they have called New Large Aircraft (NLA), and have been instrumental in producing research into the specification of an NLA required to satisfy the airlines requirements well into the next century. Figure 2.5 below, produced by Orlowski and Callaghan[3] on behalf of the Douglas Aircraft Company illustrates the latest forecasts of the market potential for UHCA. Airbus and Boeing continue to discuss and to develop conceptual models of UHCA, in fact Airbus began work on an 850 seat aircraft, the Airbus A3XX in 1994. The planned service entry date of this aircraft is 2003, and although the research programme is continuing, there has yet been a firm announcement on a decision to proceed fully with this project. It can only be a matter of time before such a project is given the go ahead.

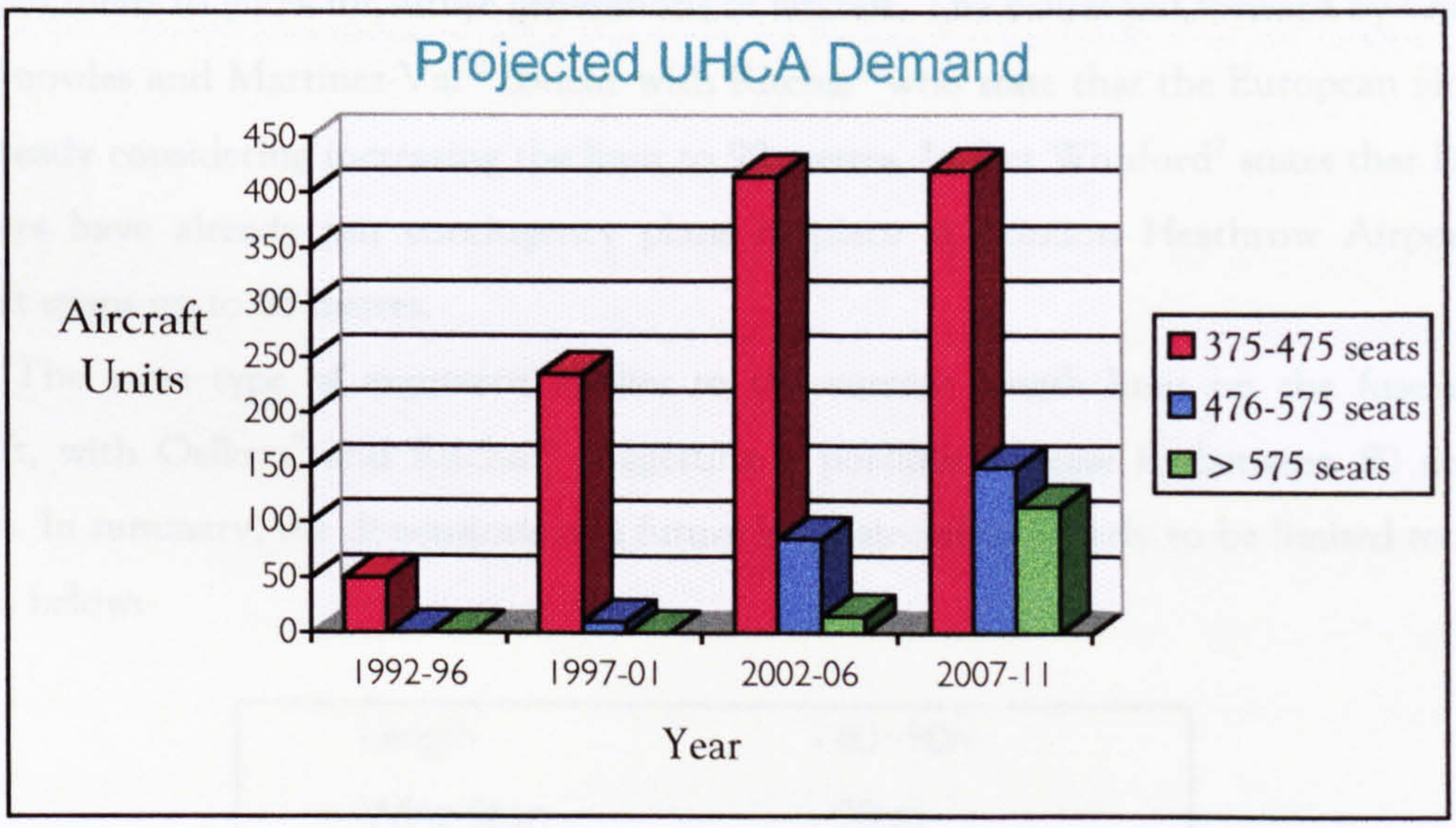


Figure 2.5- Projected UHCA demand

2 .3 UHCA Constraints

The design requirements of new aircraft are dictated by a combination of constraints imposed by the customer (the airlines) and the aviation authorities. The lengths to which the aircraft manufacturers will go to satisfy these demands are illustrated by the example of the Boeing 777, which includes an option for folding wings, to allow it to occupy the airport gates currently used by DC-10 aircraft. This was an option specified by a small number of airlines, but was included in the design at great expense to Boeing. For the case of the design

of a UHCA, the airlines requirements will be dominated by issues of airport compatibility and economic efficiency.

2 .3 .1 AIRPORT COMPATIBILITY

The current limit on the wing span of an aircraft set by the regulatory authorities is 65 metres, this corresponds to the span of the wings of a Boeing 747. Studies have shown that it may be possible by the use of unconventionally configured aircraft to design aircraft capable of carrying 800 passengers to fit within this current size limit (Serghides[8]). This design concept from Serghides[8] featured a front coupled canard that allows a reduced wing span of 65 metres and a wide body fuselage that was also confined to 65m. As discussed later, it seems that these unconventionally configured aircraft are for a number of reasons out of favour with the aircraft manufacturers.

With more conventional designs seemingly more probable, it seems very likely that this size limit will be increased in the near future. Oelkers[9] reports that discussions have already taken place between aircraft manufacturers and the authorities, aimed at increasing the span limits to allow for future generations of aircraft. The values put forward by Oelkers[9] and Knowles and Martinez-Val[10] concur with Ritchie[11] who state that the European airports are already considering increasing the limit to 90 metres. In fact Whitford[7] states that British Airways have already put contingency plans in place at London Heathrow Airport for aircraft spans up to 85 metres.

The same type of argument applies to the current length limit on the fuselage of aircraft, with Oelkers[9] and Ritchie[11] suggesting a possible increase to between 80 and 90 metres. In summary, the dimensions of a future large aircraft are likely to be limited to those shown below:-

Length	- 80~90m
Wing Span	- 90 m
Wheel Track	- 17 m
Wheel Base	- 35 m
Outer Engine Span	- 56m
Max. Weight	- 635,000 kg

Figure 2.6 -Predicted UHCA size limits

Of possibly greater concern to the airlines than the length and span of the aircraft, are the overall height and deck heights of some of the proposed new aircraft. Overall aircraft heights greater than 22 metres are likely to cause problems in maintenance hangars, and the

increased heights of the decks will require a new approach to passenger boarding and evacuation.

The inference of bigger aircraft impinges on every aspect of airport operation, apart from the physical size of the aircraft, the services required by the aircraft such as refuelling, baggage loading/unloading, and aircraft turn-around will all require a degree of modification. There also remains the task of ensuring that the greatly increased number of passengers can embark and disembark to and from their journeys as smoothly as possible, as well as the critical issue of passenger emergency evacuation. This has repercussions across the airport, from check-in facilities to restaurants and shops.

It is without doubt that the introduction of UHCA will require some modification to airport terminal facilities, although expensive, this situation is not unprecedented. The introduction of the Boeing 747 required the alteration of passenger handling facilities at many airports.

Apart from modifications to terminal buildings and equipment, larger aircraft would put other strains on the airport infra-structure. As yet there is no ICAO ruling on the physical separations of aircraft greater in size than the Boeing 747, however assuming that the size of the new aircraft is within the new limits suggested above, Ritchie[11] argues that this would infer an increase in runway width to 60 metres, a possible increase in taxiway width from 23m to 26m, an increase in taxiway separation distance from 182.5m to 192.5m, and the possible redesign of apron stands containing more fixed provisions optimised especially for these particular aircraft. These values are purely speculative, and with the aid of modern guidance equipment some of these changes may not be deemed necessary.

As well as the separation of aircraft on the ground, the separation of aircraft in flight is of paramount importance. Due to the disturbance of the air following an aircraft, caused mainly by the wake vortices, constraints are applied on the minimum separations allowed between aircraft leaving and departing an airport. In an airport such as Heathrow this is the main constraint on operations. According to Critchley and Greenwood[12] the strength of the wake vortices appear to increase with the weight of the aircraft, and to decrease with the speed of the aircraft. It is also suggested that the rate of vortex decay may increase with wing span. These factors would appear to infer that the wake vortices produced by a UHCA would be of greater strength than those of existing aircraft. The current UK minimum separations to avoid an aircraft flying into the wake vortices of an aircraft preceeding are shown below in table 2.1. A heavy aircraft is defined as weighing 136,000 kg or greater, a medium weight aircraft as weighing more than 40,000kg (and less than 136,000kg), and the weight of a small aircraft is defined as being greater than 17,000kg (and less than 40,000kg).

Lead Aircraft	Following Aircraft	Minimum Separation (nm)
Heavy	Heavy	4
Heavy	Medium	5
Heavy	Small	6
Heavy	Light	8
Medium	Medium	3
Medium	Small	4
Medium	Light	6
Small	Light	4

Table 2.1- Minimum regulatory flight separations

If it is deemed necessary to increase the separations for a new class of large aircraft, this could have serious impacts on the effectiveness of these aircraft in reducing airport congestion. It would become necessary to evaluate the effect of the trade off between increased capacity per aircraft, and the reduced overall capacity of the airport.

2 .3 .2 Environmental Compatibility

The two main areas of concern for environmental compatibility are those of aircraft noise and aircraft emissions. The importance of these two characteristics has escalated dramatically over the last 10 years and is fast becoming one of the leading issues in modern civil aircraft design.

Aircraft Noise

The noise produced by aircraft has been greatly reduced over the last 40 years, as illustrated in figure 2.7, which depicts the past and predicted 1500ft sideline noise of aircraft with a total of 100,000lb sea level static thrust (from Russell and Streckenback[13]).

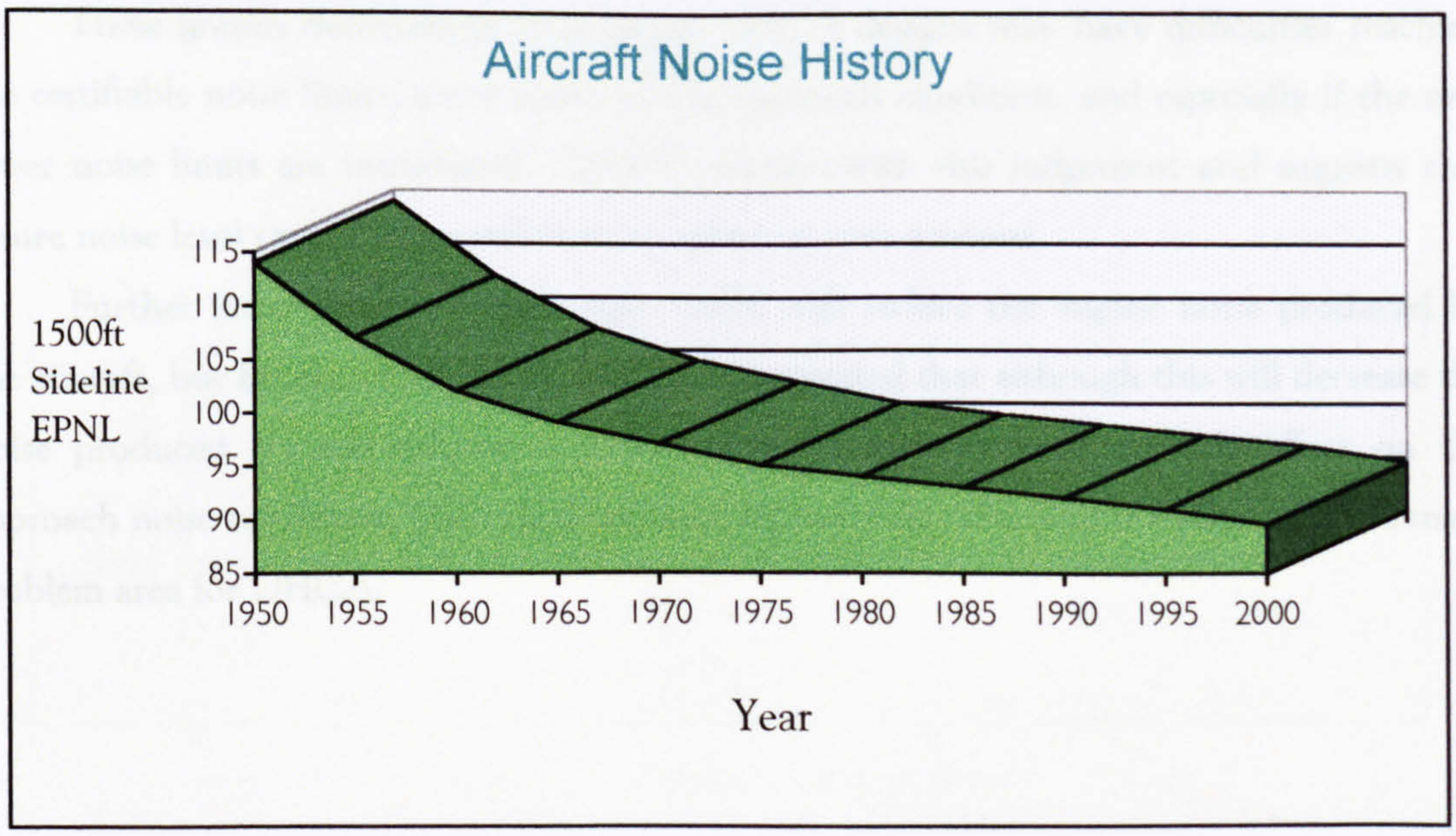


Figure 2.7 - Aircraft noise history

BIBL LONDON

The initial reductions were mainly due to the improvements and greater attention to acoustic detail in first and second generation pure jet and low bypass ratio engines. Further improvements were then made by the introduction of high bypass ratio engines. As we can see from this graph the rate of reduction of aircraft noise is slowing, probably due to the fact that the potential improvements to modern engines are becoming smaller and smaller as the engines have become more highly developed.

The mechanisms responsible for producing aircraft noise are largely dependant on the size of the aircraft. A larger aircraft will produce higher amounts of both engine noise and airframe noise. The current ICAO regulations governing the noise levels of aircraft require an aircraft to meet the set requirements at three particular conditions. These conditions are takeoff flyover, approach, and sideline, with the actual noise limit in each case depending on the weight of the aircraft. As the rules stand at the moment a deficit in one particular category may be balanced by superior performance in another.

However, Airbus Industrie[5], Jagger[14], Eccelseton and Metcalfe[15], and Oelkers[9], are all in agreement with respect to a likely tightening of the current noise regulations in the very near future, by introducing noise limits -3dB below the current ones, and scrapping the 'trade off' policy described above.

It is important to note that currently, for each noise category, there is a weight limit above which the noise limit is constant. This means that as the size of the aircraft increases it becomes more difficult for them to stay within the prescribed noise limits. A study by Eccelseton and Metcalfe[15] has illustrated the possible difficulties that will be encountered in obtaining noise level certification for future large aircraft. The figures 2.8, 2.9, and 2.10 below show the current and predicted noise limits, with their relationship to current aircraft (from Jagger[14]), and to future aircraft (as predicted by Eccelseton and Metcalfe[15]).

These graphs demonstrate that future UHCA designs may have difficulties reaching the certifiable noise limits, particularly in the approach condition, and especially if the new lower noise limits are introduced. Oelkers[9] concurs with this judgement and suggests that future noise level certifications will have to take this into account.

Further increasing the bypass ratio could well reduce the engine noise produced by the aircraft, but Eccelseton and Metcalfe[15] have suggested that although this will decrease the noise produced for the sideline and flyover requirements, this has little effect on the approach noise condition, which is dominated by airframe noise and is likely to be the main problem area for UHCA.

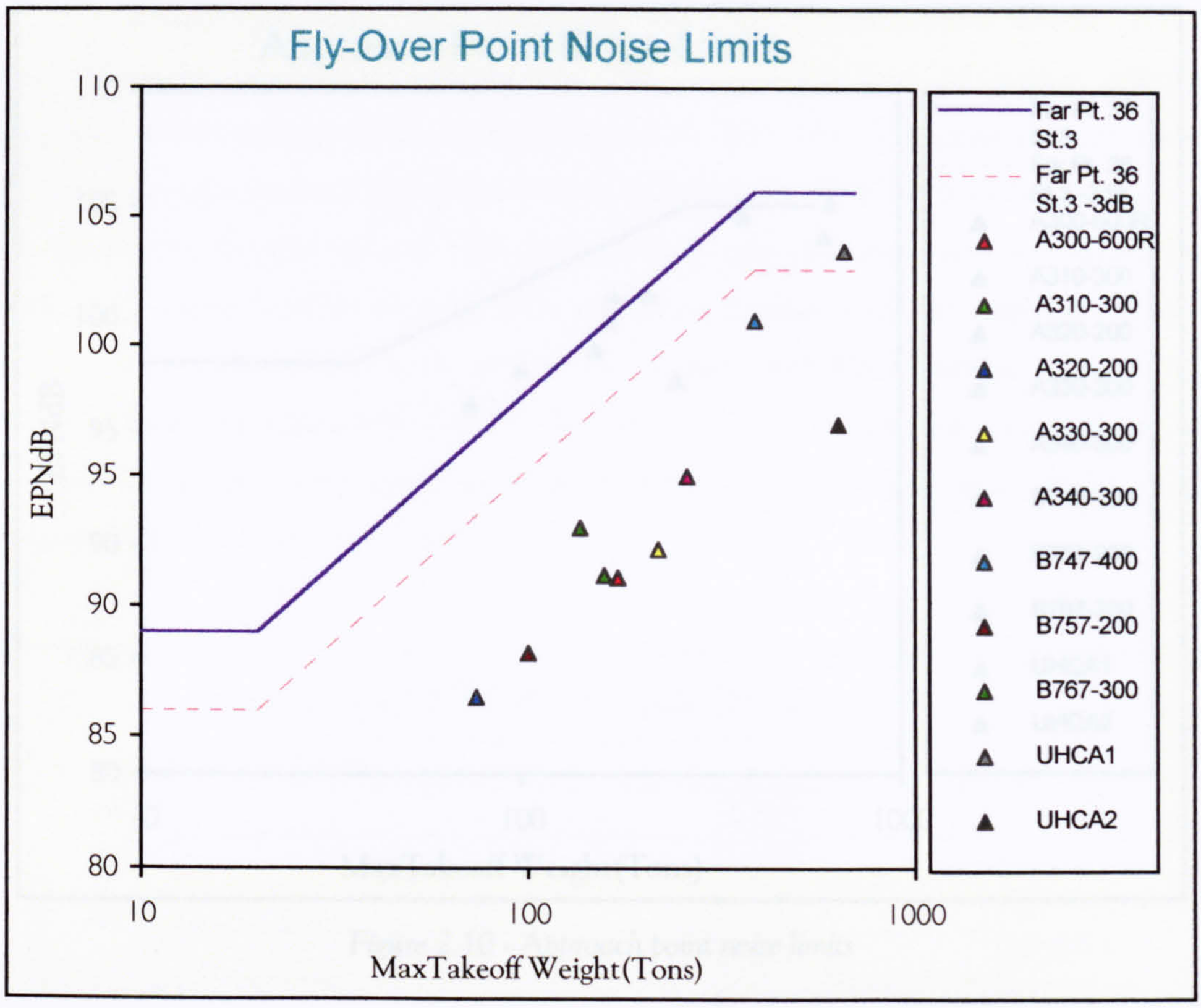


Figure 2.8 - Fly-over point noise limits

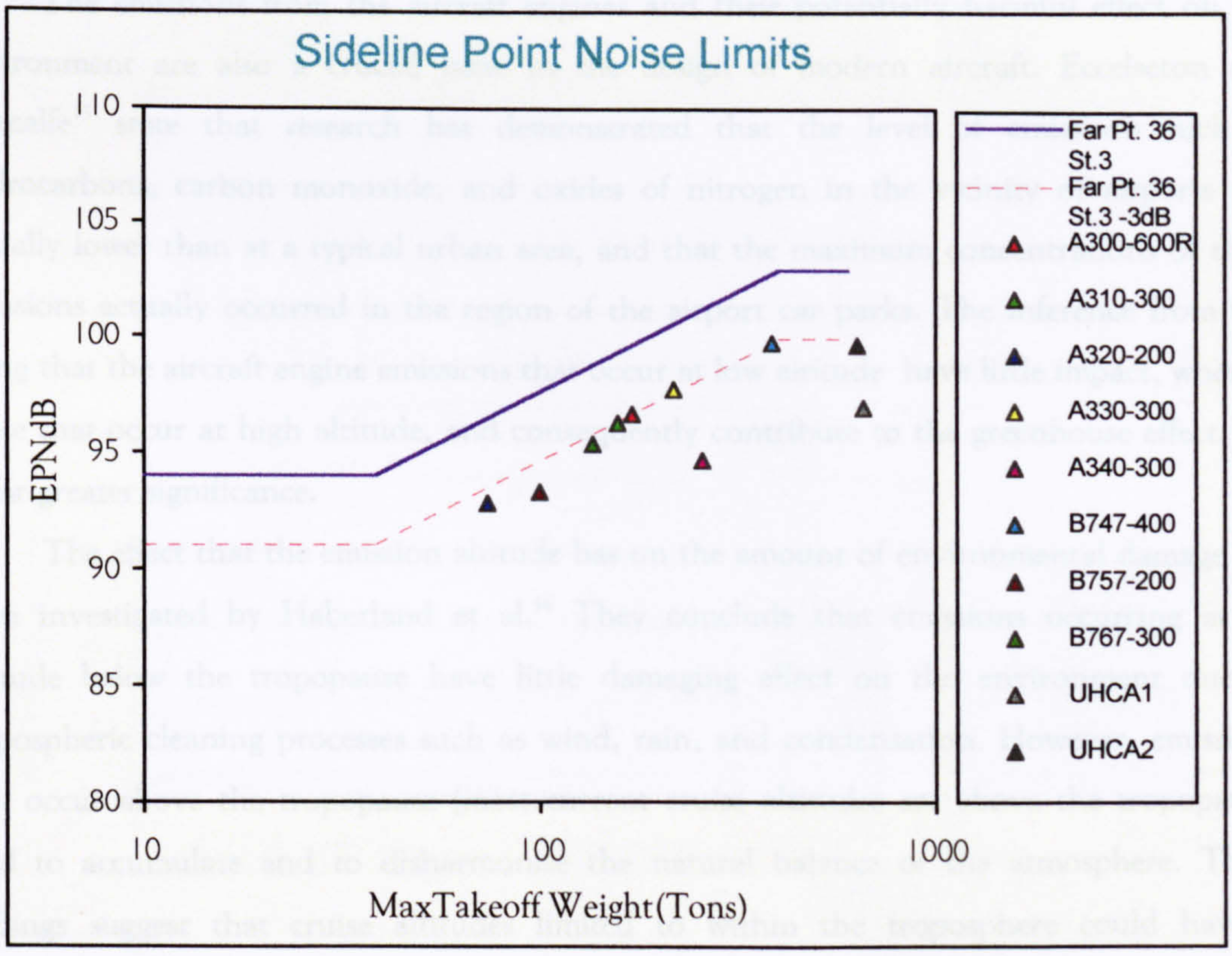


Figure 2.9 - Sideline point noise limits

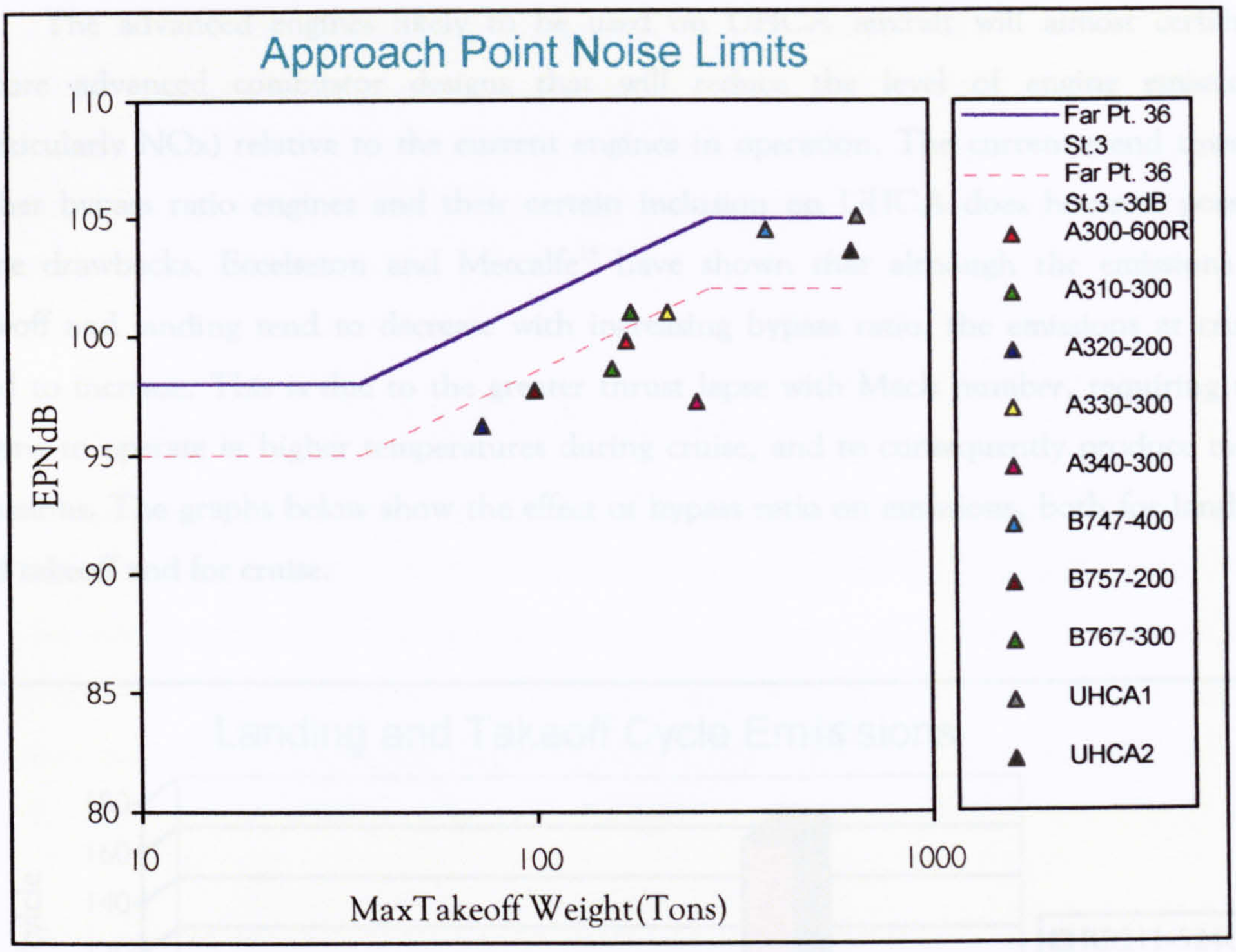


Figure 2.10 - Approach point noise limits

Engine Emissions

The emissions from the aircraft engines and their potentially harmful effect on the environment are also a crucial issue in the design of modern aircraft. Eccelseton and Metcalfe[15] state that research has demonstrated that the level of emissions such as hydrocarbons, carbon monoxide, and oxides of nitrogen in the vicinity of airports was actually lower than at a typical urban area, and that the maximum concentrations of these emissions actually occurred in the region of the airport car parks. The inference from this being that the aircraft engine emissions that occur at low altitude have little impact, whereas those that occur at high altitude, and consequently contribute to the greenhouse effect, are of far greater significance.

The effect that the emission altitude has on the amount of environmental damage has been investigated by Haberland et al.[16] They conclude that emissions occurring at an altitude below the tropopause have little damaging effect on the environment due to tropospheric cleaning processes such as wind, rain, and condensation. However, emissions that occur above the tropopause (most current cruise altitudes are above the tropopause) tend to accumulate and to disharmonise the natural balance of the atmosphere. These findings suggest that cruise altitudes limited to within the troposphere could have a beneficial impact on the environment.

The advanced engines likely to be used on UHCA aircraft will almost certainly feature advanced combustor designs that will reduce the level of engine emissions (particularly NOx) relative to the current engines in operation. The current trend toward higher bypass ratio engines and their certain inclusion on UHCA does however possess some drawbacks. Eccelseton and Metcalfe[15] have shown that although the emissions at takeoff and landing tend to decrease with increasing bypass ratio, the emissions at cruise tend to increase. This is due to the greater thrust lapse with Mach number, requiring the engine to operate at higher temperatures during cruise, and to consequently produce more emissions. The graphs below show the effect of bypass ratio on emissions, both for landing and takeoff and for cruise.

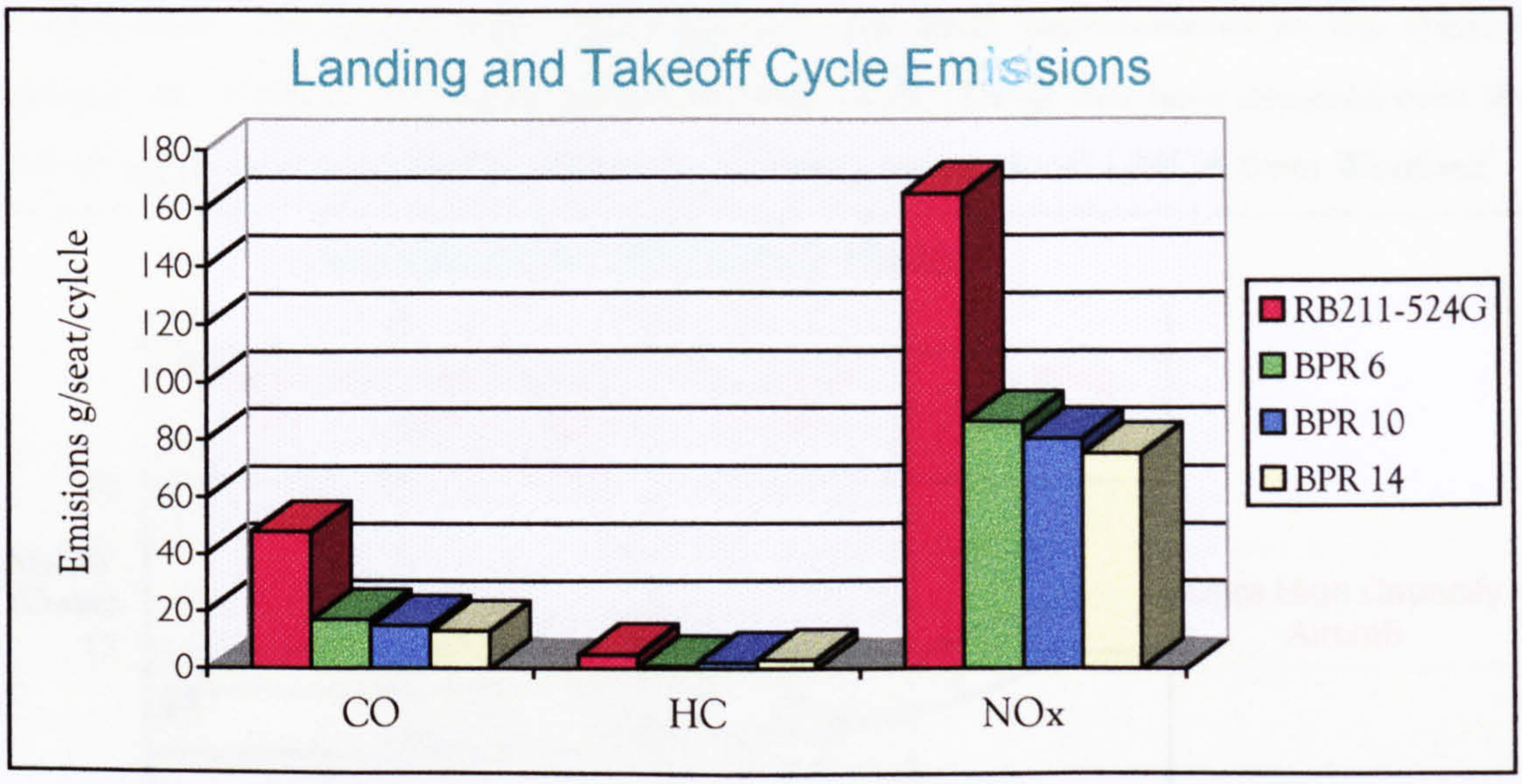


Figure 2.11- Landing and takeoff engine emissions

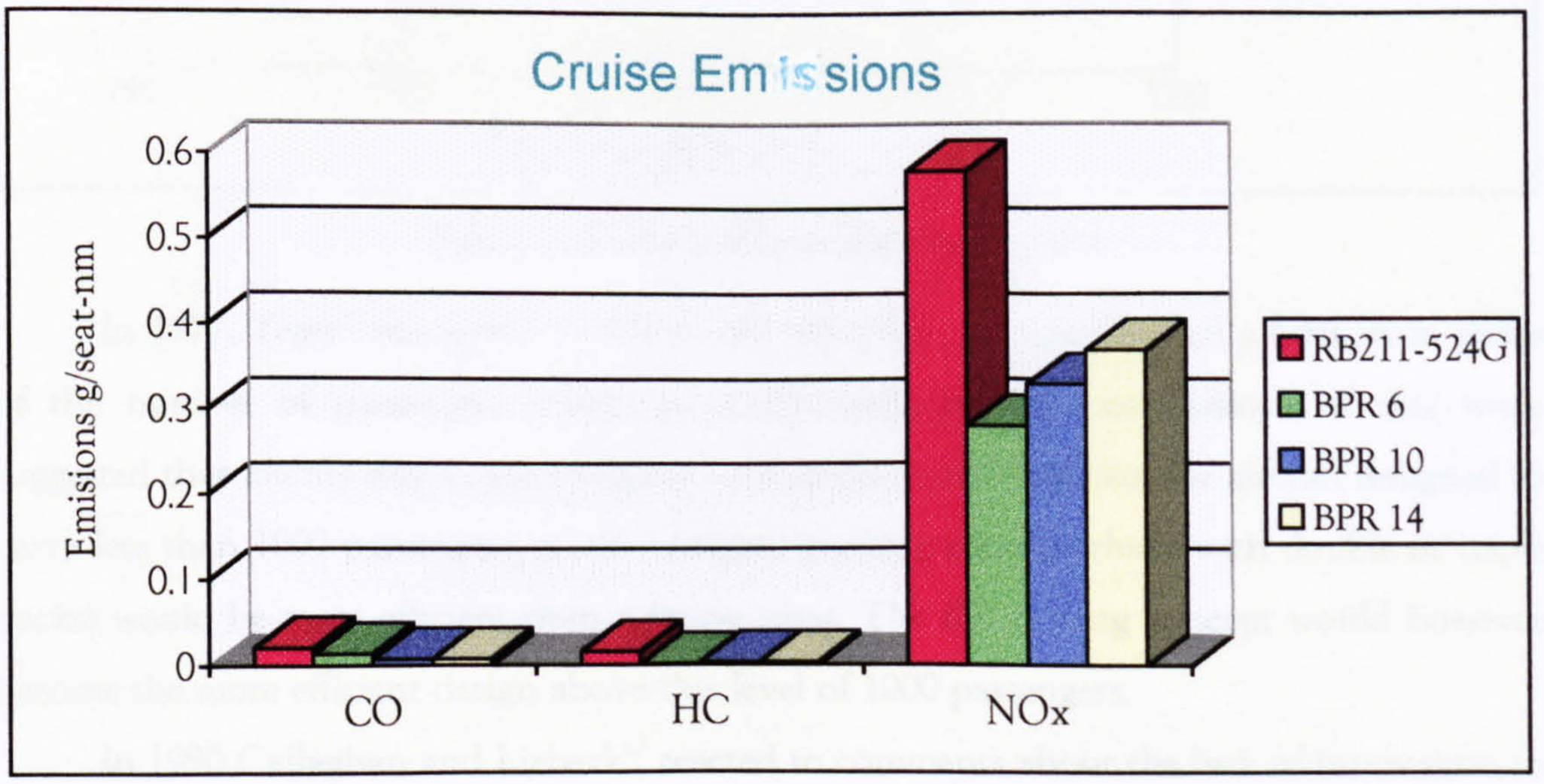


Figure 2.12 - Cruise engine emissions

Figures 2.11 and 2.12 illustrate the point that although the engines of the future will have better efficiencies and hence lower emissions compared to older engines of similar bypass ratio, there will need to be a compromise to balance the beneficial reductions in fuel consumption and noise, and the potentially harmful effect of increased emissions from engines of higher bypass ratio.

2 .4 UHCA CONFIGURATIONS

It has been suggested that the development of transport aircraft as a whole has been somewhat stagnant since the development of aircraft such as the DC-8 and the B-707. The changes seen in aircraft produced since these has been more evolutionary as opposed to revolutionary. The graph below illustrates the very small improvements in the classical aerodynamic efficiency parameter (Mach Number x Lift \ Drag) that have occurred over the past 30 years, and the predicted efficiency of a future conventional UHCA from Whitford[8].

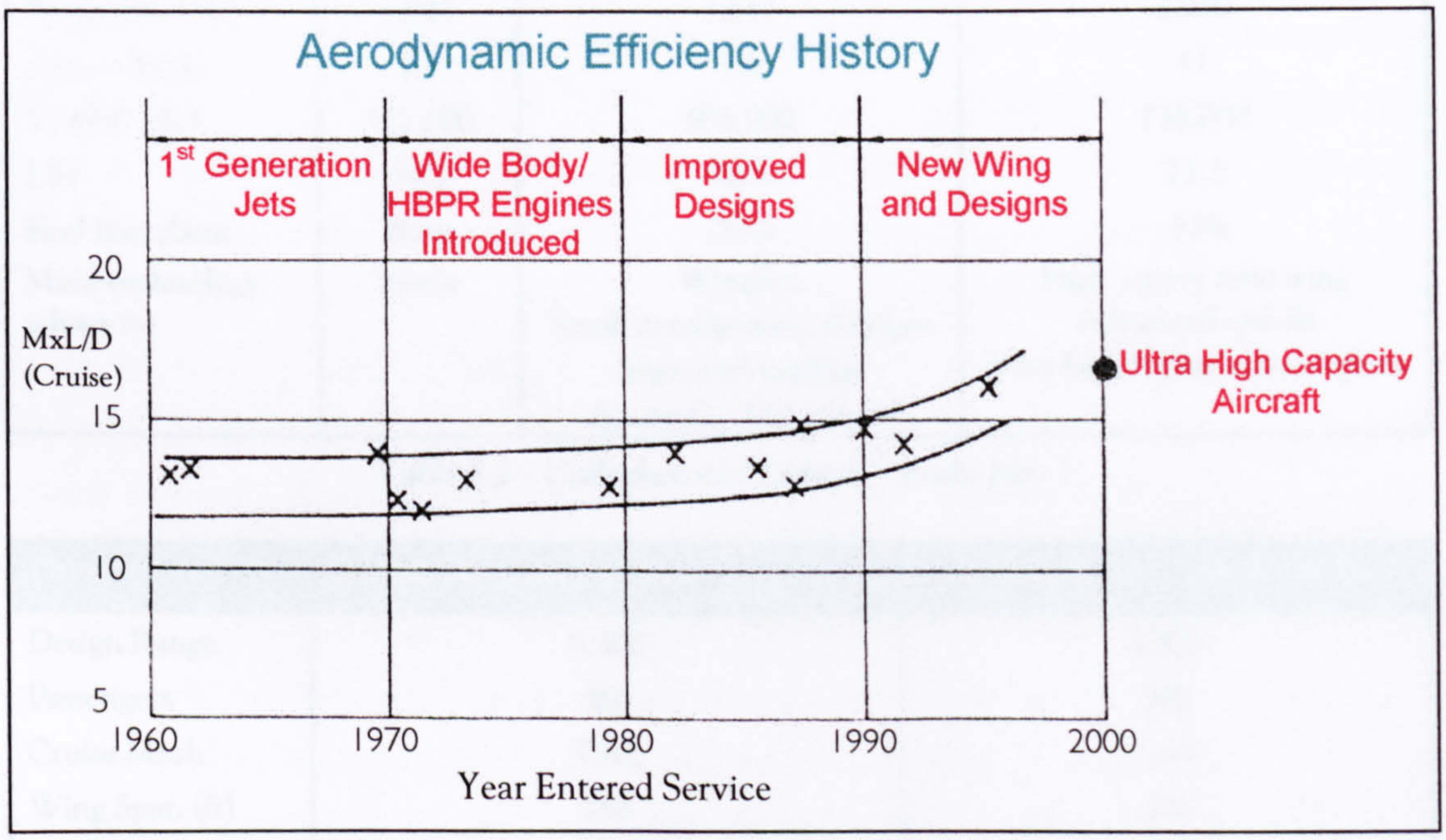


Figure 2.13- Aerodynamic efficiency vs. time

In 1977, Yeger[6] attempted to qualify the optimum configuration of a UHCA in terms of the number of passengers using theoretical methods. The conclusions of this work suggested that mainly due to aerodynamic and weight considerations, for aircraft designed to carry less than 1000 passengers, a conventional configuration (perhaps with double or triple decks) would be more efficient than a flying wing. The flying wing concept would however become the more efficient design above this level of 1000 passengers.

In 1990 Callaghan and Liebeck[17] reacted to comments about the lack of innovation in air transport design by producing and evaluating a number of concepts for future civil aircraft. Their aim was to highlight the differences between future evolutionary concepts and

a revolutionary concept such as a blended wing body (flying wing) aircraft. Using the DC-10 as a starting point for their work, three conventional designs were evaluated. These are the MD-11, the Super-Stretch Advanced Derivative, and the Synergistic Technology Transport, each design being loosely based on the previous one, yet becoming successively more advanced in terms of technology. Finally, an advanced blended wing body concept was evaluated to fulfil the same design objectives, and for the same level of technology as included in the Synergistic Technology Transport. The results of these studies are shown in tables 2.2 and 2.3 below:-

Parameter	DC-10	MD-11	Super-Stretch Advanced Derivative
Range (nm)	5,800	7,000	8,500
Passengers	231	293	368
Cruise Mach	0.82	0.82	0.85
Wing Span (ft)	165	170	211
Length (ft)	183	201	236
Wing Area (ft^2)	3,647	3,647	3,900
Aspect Ratio	7.5	7.5	11
TOGW (lb.)	572,000	605,000	738,000
L\D	14.2	18.1	21.2
Fuel Burn/Seat	Base	-33%	-52%
Main technology advances	None	Winglets Small aerodynamic changes Improved engines Active C. of G. control	High aspect ratio wing Advanced airfoils Very high bypass ratio engines

Table 2.2 - Callaghan and Liebeck[17] results part 1

Parameters	Synergistic Technology Transport	Blended Wing Body
Design Range	8,500	8,500
Passengers	368	368
Cruise Mach	0.85	0.85
Wing Span (ft)	188	260
Length (ft)	236	167
Wing Area (ft^2)	2,020	4,500
Aspect Ratio	17.5	15.0
TOGW (lb.)	367,200	338,800
L\D	23.1	33.3
Fuel Burn/Seat	-83.5%	-87.7%
Main technology advances	Very high aspect ratio wings Laminar flow control Riblets Highly advanced engines Improved materials Advanced systems	Laminar flow control Riblets Highly advanced engines Improved materials Advanced systems

Table 2.3 - Callaghan and Liebeck[17] results part 2

These results illustrate that there is still an enormous potential for improvement of the conventionally configured aircraft. The blended wing body concept shows a marginal improvement over the Synergistic Technology Transport, with the size of this improvement being partially overstated by the inclusion of laminar flow control on the upper and lower surfaces of the B.W.B. as opposed to only the upper surface of the S.T.T.

The other unconventional configurations that have been of much interest are the canard and tri-surface aircraft. A study performed by Martinez-Val et al.[18] compared the economic efficiencies of a conventional aircraft to those of a tri-surface aircraft, for the cases of both present technology and future technologies. The results of the estimated direct operating costs of these aircraft show that using present technologies the tri-surface aircraft would have a small benefit of about 1%. However, with future technologies the conventional aircraft would have a relative benefit of approximately 1%.

A similar study by Knowles and Martinez-Val[10] comparing a conventional, a canard, and a tri-surface aircraft, each capable of carrying 1000 passengers, concluded that the conventional and the canard design were the two best designs, with very little between them in terms of direct operating cost. Similarly the work by Serghides[8] demonstrated that although the unconventional canard concept could have some compatibility advantages, there was little performance benefit over a conventionally configured aircraft.

The facts above indicate that the conventional configuration is still a competitive design for a civil aircraft. When one considers the huge costs that would be incurred from the development of such an aircraft as the blended wing body (flying wing) concept, or the canard concept, there would need to be a massive operational benefit due to the introduction of these aircraft. It would seem that there may be some potential benefit associated with these designs, but the fact is that the conventional double-decker still represents the lowest possible technological and financial risk for a new UHCA concept. It is for these reasons that most serious UHCA programmes have been based on a double-deck configuration, including the Airbus A3XX, which is almost certain to be the worlds first UHCA. Therefore the remainder of my work shall concentrate on this conventional type of aircraft, although with some consideration of alternative fuselage cross-sections.

3 .Advanced Technologies

3 .1 BACKGROUND

Since the inception of commercial passenger aircraft, designers have striven to increase the efficiency of operation. Improvements have been made in virtually every aspect of the aircraft, with the aerodynamic, propulsive, and material advances being of particular significance.

As discussed in chapter 2, Callaghan and Liebeck[17], on behalf of the Douglas Aircraft Corporation, presented data in 1990 which aimed to estimate the potential improvements in efficiencies of civil aircraft up to the year 2000 and beyond. A summary of their conclusions is shown below in figure 3.1. These values were described as 'optimistic' and have been proven to be so, however the results of this analysis are still valid, as the conclusions of this work are based on the 'potential' of cutting edge technology. It would appear that much of this potential still exists and has yet to be exploited.

Aerodynamics	- 35% Lift/Drag ratio improvement
Materials	- 40% structural weight reduction
Systems	- 28% average weight reduction
Propulsion	- 40% S.F.C. reduction
Propulsion	- 20% Weight Reduction

Figure 3.1- Summary of Callaghan and Liebeck[17] study

It is interesting to note that an improvement in one area will generally have a 'snowball' effect as it impacts on other areas of the aircraft design. For example, a small structural weight reduction will allow a smaller wing, which will reduce the drag, and allow for a smaller engine. This produces a further decrease in structural weight and the process begins again.

There are a number of technologies that will be discussed, their potential merits will be evaluated, and their likelihood of coming into being assessed. The technologies can be split into three groups in terms of their current status of development. The first group contains those technologies that are natural developments of existing technologies (derivative technologies), and are almost certain to be included in future aircraft. The next group contains technologies that have not yet featured on production aircraft, but have been extensively researched and evaluated over a number of years (established technologies).

The final group contains those technologies that are much more innovative, undeveloped, and speculative, and have only a small chance of appearing on near future aircraft designs.

Derivative Technologies
Very High Bypass Ratio Turbofans
Advanced Composite and Alloy Materials
Improved Supercritical Airfoils
Improved Winglet Design
Lightweight Landing Gears

Established Technologies
Propfan Engines
Smart Structures
Natural Laminar Flow
Laminar Flow Control
Hybrid Laminar Flow Control
Variable Camber Wings
Riblets

Unestablished Technologies
Advanced Ducted Prop Engines
Contrafan Engine
Large Eddy Break-up Devices
Wing Tip Turbines / Sails

Each technology will be discussed below within the context of the major design area to which it belongs:-

3 .2 PROPULSION

3 .2 .1 TURBOFAN ENGINES

The advances made in engine technology have certainly contributed more to the increased aircraft efficiencies of today than any other technology area. Turbofan engines have become not only much more powerful but have become much more fuel efficient.

Fuel Efficiency

The graph displayed in figure 3.2 below, taken from Webb[19], shows the huge improvements made in engine fuel consumption since the introduction of the jet engine in 1950.

On average, fuel consumption has been reduced by 40% since the early turbojets, and by 16% since 1970. These improvements have been made possible by a combination of increased bypass ratio, advanced materials, and improved aerodynamic design, with the effect of the increasing bypass ratio probably being the most significant of these changes. The role of each of these factors in previous and any future performance improvements is discussed below.

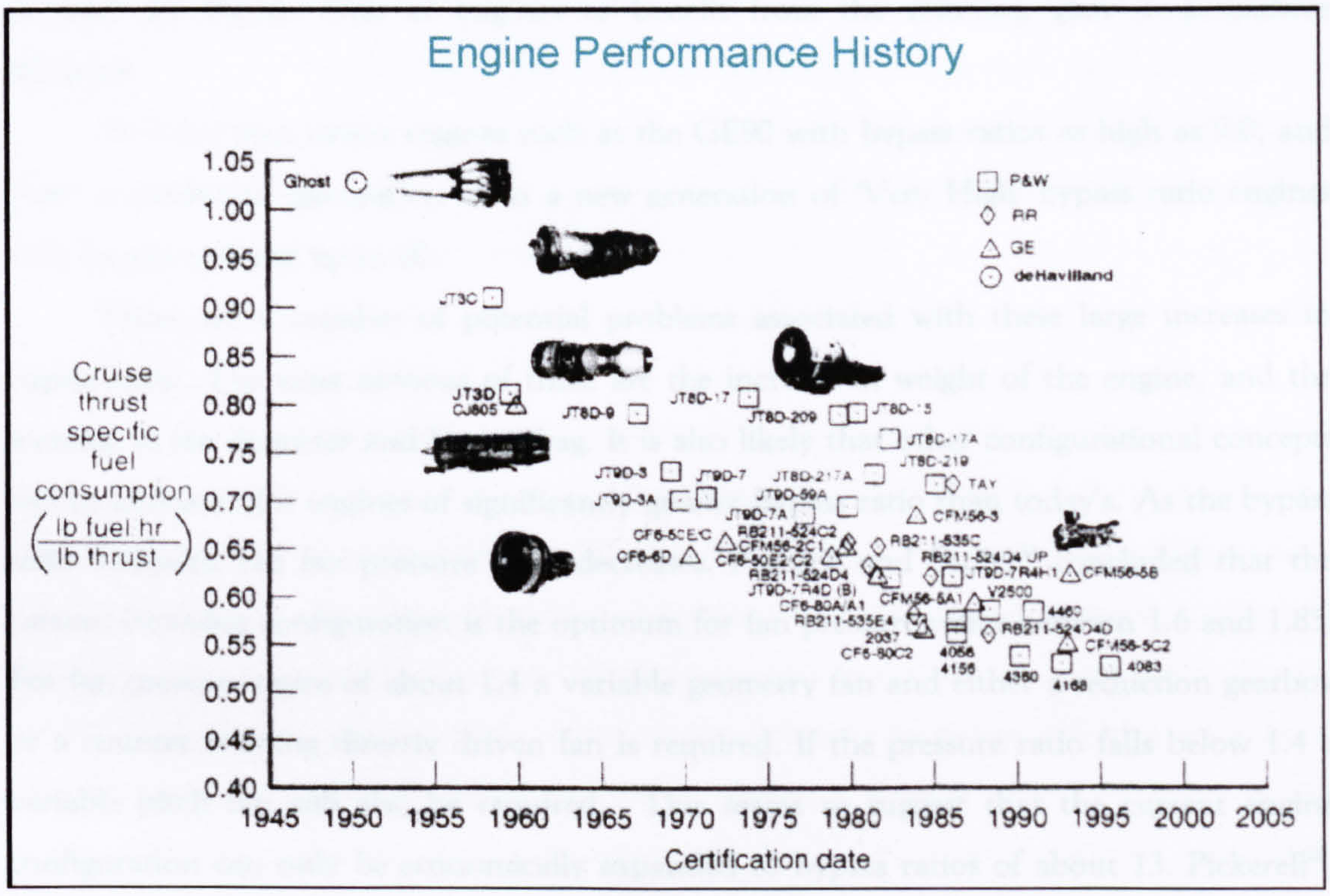


Figure 3.2 - Engine performance history

Propulsive Efficiency

It had been known since the early days of the jet engine that the propulsive efficiency is a function of the ratio of the jet velocity to the aircraft velocity. This means that a high propulsive efficiency is achieved by accelerating a large mass of air by a relatively small amount. Pickerell[20] notes that this is the reason that propeller aircraft have such high propulsive efficiencies (about 95%) compared to those of jet engines (50%). In fact Whittle and others had experimented with these ideas and the concept of bypass engines in the 1930's, but the lack of suitably advanced materials and fabrication techniques was prohibitive to their development at that time.

The first commercial gas turbine engine was the DeHavilland Ghost 50 introduced in 1950. This was a pure jet engine i.e. a bypass ratio of zero, as were most of the early commercial engines, which were largely based on military engines. In the chase for improved efficiency it was not long before engine manufacturers realised the potential of the bypass engine and began adding a compression stage to the engines, and discharging some of the air from this stage directly into the atmosphere. These engines became the first turbofans. It was not until the late 1960's that the first 'High Bypass Ratio' engines were developed. These were General Electric's TF39 and Pratt & Whitneys JT9D engine used to power the Boeing 747. These engines had bypass ratios of approximately five and had massive performance advantages over other engines of the time. The current trend is and will continue to be to increase the bypass ratio of engines to benefit from the resulting gain in propulsive efficiency.

We have seen recent engines such as the GE90 with bypass ratios as high as 9.0, and there is continued speculation as to a new generation of 'Very High' bypass ratio engines with bypass ratios of up to 20.

There are a number of potential problems associated with these large increases in bypass ratio. The most obvious of these are the increase in weight of the engine, and the increase in fan diameter and hence drag. It is also likely that other configurational concepts will be necessary for engines of significantly greater bypass ratio than today's. As the bypass ratio increases, the fan pressure ratio decreases. Peacock and Sadler[21] concluded that the current front-fan configuration is the optimum for fan pressure ratios between 1.6 and 1.85. For fan pressure ratios of about 1.4 a variable geometry fan and either a reduction gearbox or a counter rotating directly driven fan is required. If the pressure ratio falls below 1.4 a variable pitch fan will also be required. This seems to suggest that the current engine configuration can only be economically expanded to bypass ratios of about 13. Pickerell[20], NAS-NRC[22] , and Stryker[23] all agree that a bypass ratio of 15 is not possible for evolutions of current turbofan engines. A bypass ratio of 13 would bring about a fuel consumption decrease of between 5-6% based purely on the bypass ratio increase over an engine with a bypass ratio of 6.

Core Efficiency

Over the past 30 years the overall thermal efficiency of the engine core has been increased from around 35% to 45% and above. This has been achieved through the use of advanced higher temperature materials, improved cooling effectiveness, and increased component aerodynamic efficiencies.

Data from Knip[24] and NAS-NRC[22] illustrates the point that maximum turbine temperatures have been increased from 1000F to 2600F over the last 50 years due to these new high temperature materials and advanced cooling methods, and overall pressure ratios

have increased from 5 to 50. The detailed study conducted by NAS-NRC[22] concluded that these trends will continue in the future, with turbine inlet temperatures of between 2900-3000F by the year 2005, and temperatures of between 3200-3400F by the year 2015. This will be accompanied by overall pressure ratios of 60-75 by the year 2005, and over 75 by the year 2015. Component and fan efficiencies are also predicted to increase by about 2% up to the year 2005, and 3% by the year 2015. These advances are expected to bring about a 15-20% fuel burn reduction over mid 90's engines by the year 2005, and a 30% reduction by the year 2015. These fuel reductions also take into account the effect of increasing bypass ratio.

Thrust

There is little to be said on the direction of thrust ratings for future engines. Engines currently in use such as the GE90 and the Trent 800 series already have the thrust and the potential for thrust growth to serve the needs of most conceivable near future aircraft designs. One can only see the thrust ratings of modern turbofans following the trend of the last 50 years and increasing further into the next century.

Engine Weight

The use of advanced materials has not only increased turbine temperatures and pressures but has had a large impact on the weight of modern engines. Both Knip[24] and NAS-NRC[22] expect that the current trend for engine weight reduction will continue with the introduction of new materials such as polymer and metal matrix composites, titanium aluminides, nickel aluminides, carbon-carbon composites, and new high-temperature ceramic materials. Neglecting any secondary effects due to increases in bypass ratio, an analysis of the data provided by Knip[24] shows that we can expect a massive weight reduction in the region of 44% from the year 1987 to the year 2010, due to advances in materials alone. This compares well with predicted 20% weight reduction from 1990 to 2000 as estimated by Callaghan and Liebeck[17].

Engine Noise

As discussed in Chapter 2, engine noise is a major issue in the certification of any new large aircraft. Figure 2.7 shows the reduction of aircraft noise over the past 40 years. Most of this reduction has come from improvements in the acoustic properties of the engines, and from increases in Bypass ratio. These improvements are predicted to continue, with developments coming in a number of areas.

The design of the nacelle is an important factor in the noise production of an engine. A long cowl mixed exhaust as used on the Airbus A330 reduces engine noise by lowering the velocity of the gasses at exit. The longer cowl also allows a greater area where acoustic

treatment can be applied, however the longer cowl can also cause problems of aerodynamic interference with the wing.

Increasing the engine bypass ratio also reduces the velocity of gases, and therefore reduces noise as described in Chapter 2. Other methods of reducing noise are to optimise the numbers and spacing of the fan and turbine blades themselves, and the addition of sound suppressers to the engines.

Engine Emissions

The main focus for the improvement in the emissions of future aircraft engines is to reduce the amount of oxides of nitrogen (NOx) which contribute to the greenhouse effect, smog, and acid rain. NOx is formed from a combination of oxygen and nitrogen that occurs at the high temperatures present in the combustor of an engine. Webb[19] reports that NOx only tends to form when the fuel/air mixture is near stoichiometric and that research has indicated reductions in NOx could be made by introducing staged combustion where the local fuel/air mixture is controlled carefully. It is estimated that this approach could reduce these emissions by up to 30%.

Miscellaneous

Small improvements in the design of pylons and nacelles from both aerodynamic and propulsive stand points can be expected in the future, but it is unlikely that the size of these benefits will be of the same magnitude as those from other aspects of engine and wing design.

One could also expect that the reliability and maintainability standards of new turbofan engines will be at least as good as those of current engines.

3 .2 .2 PROPFAN

With the above limitations on the bypass ratio and hence propulsive efficiency of turbofan engines in mind, much research on future engine concepts has centred on the propfan engine. Conventional propellers are only efficient up to mach number of about 0.5. However, research has shown (Pickerell[20]) that by careful redesign of the blades and by use of two contra-rotating rows of blades, the propulsive efficiency may be maintained up to Mach numbers of 0.8, this gives a theoretical fuel consumption improvement over today's turbofan engines of the order of 30%. The figures below show a picture of a propfan with bypass ratio of 40, and a graph illustrating that the propfan has the potential for the highest propulsive efficiency of any engine. In fact Pratt & Whitney successfully tested a propfan

engine in the late 80's, with the flight test results showing an installed fuel consumption improvement of between 15 ~ 20% (Stryker[23]).

There are however many problems related to the installation and use of a propfan on a civil aircraft. The main problem being the noise generated by this type of engine, which because of the speeds involved is significantly greater than that generated by a conventional propeller engine. Other potential problems include blade loss certification and the impracticality of high thrust engines. It is likely that any application of these engines would be in a rear fuselage mounted, twin engined configuration, where only relatively small amounts of thrust are required. On realisation of these limitations Pratt & Whitney ceased work on this type of engine.

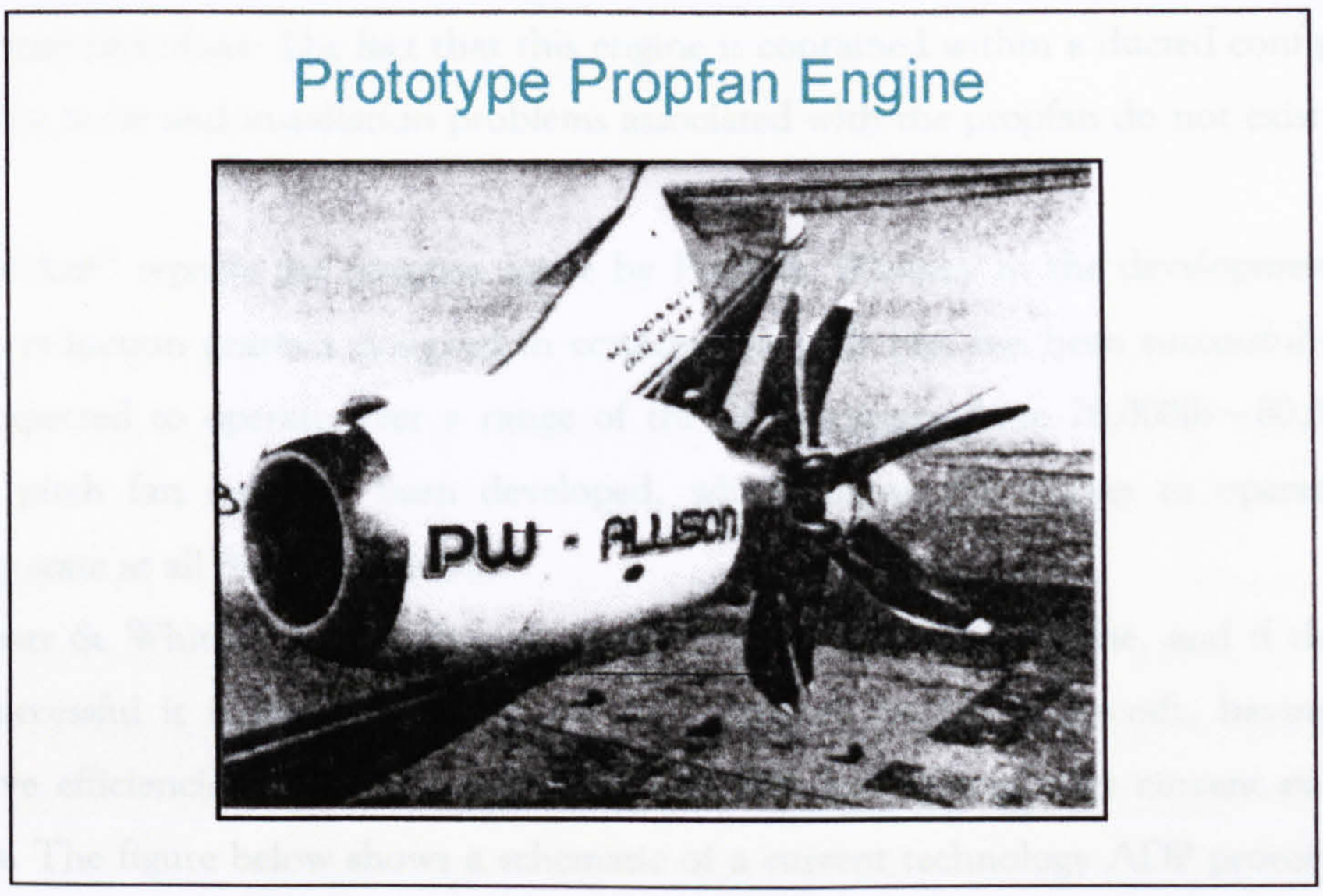


Figure 3.3 - Prototype propfan engine

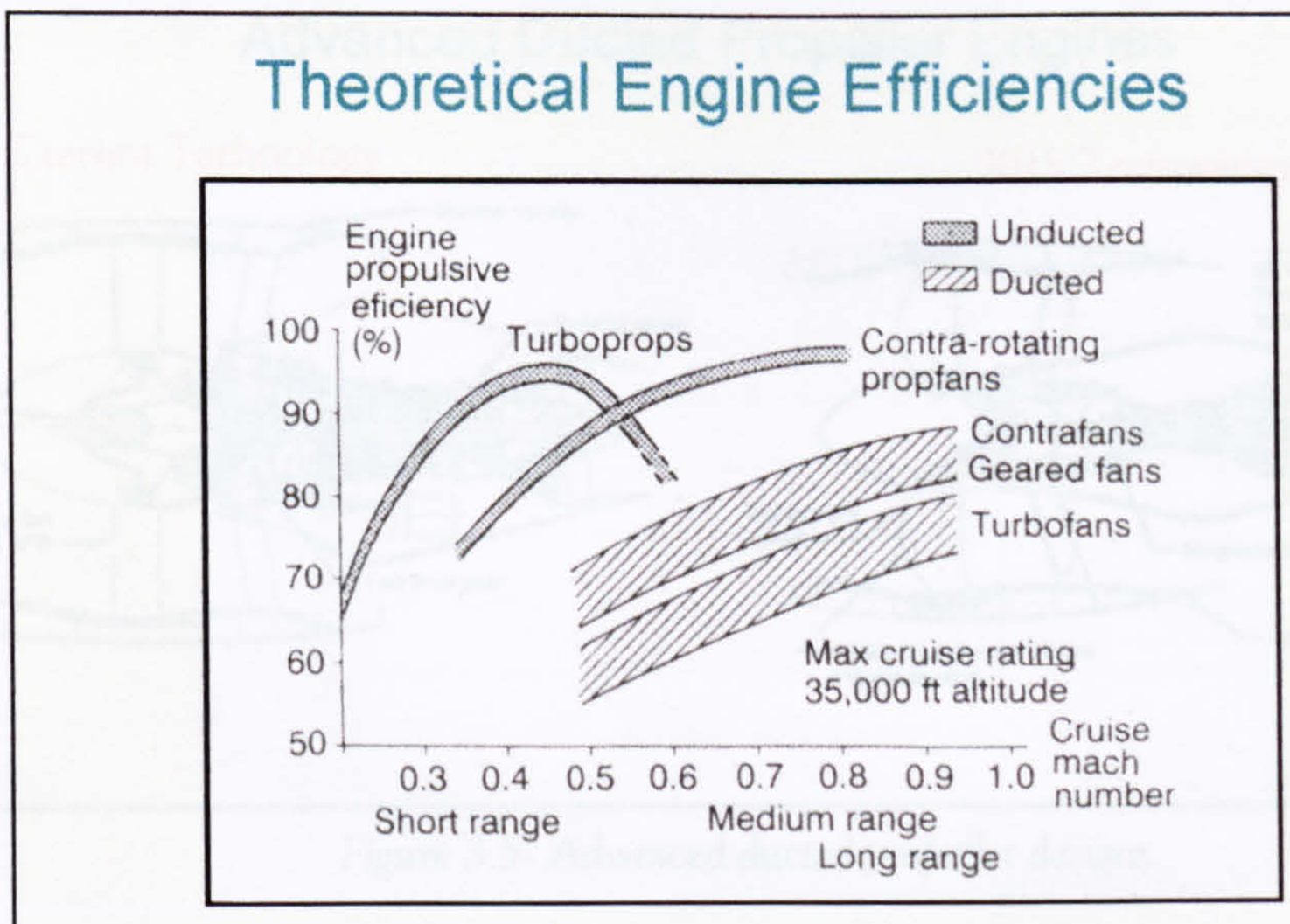


Figure 3.4 - Theoretical advanced engine efficiencies

3 .2 .3 ADVANCED DUCTED PROPFAN (ADP)

The concept of the advanced ducted prop is one of compromise between a conventional turbofan and a propfan. This configuration has been suggested as a solution to the technical difficulties associated with conventional turbofans of bypass ratios 15 and above (Stryker[23], Peacock and Sadler[21], and Pickerell[20]). These bypass ratios are achieved by the introduction of a reduction gear box to allow for the disparity between the low rotational speeds of the fan, and the high speeds of the low pressure turbine. This would allow all parts of the engine to operate at their optimum speeds, and therefore increase component efficiency. It is estimated that this configuration could operate at a propulsive efficiency of approximately 70%, giving fuel consumption reductions of between 10~12% over current turbofans. The fact that this engine is contained within a ducted configuration means that noise and installation problems associated with the propfan do not exist for this engine.

Stryker[23] reports the progress made by Pratt & Whitney in the development of the ADP. A reduction gearbox designed in conjunction with Fiat has been successfully tested, and is expected to operate over a range of thrust conditions from 20,000lb~80,000lb. A variable pitch fan has also been developed, which allows the engine to operate in its optimum state at all flight conditions.

Pratt & Whitney are continuing to test prototypes of this engine, and if these tests prove successful it is likely we could see ADP engines on future aircraft, having higher propulsive efficiencies and hence giving at least 10% fuel savings over current propulsion methods. The figure below shows a schematic of a current technology ADP prototype, and an ADP aimed at the year 2015 with a bypass ratio of 25.

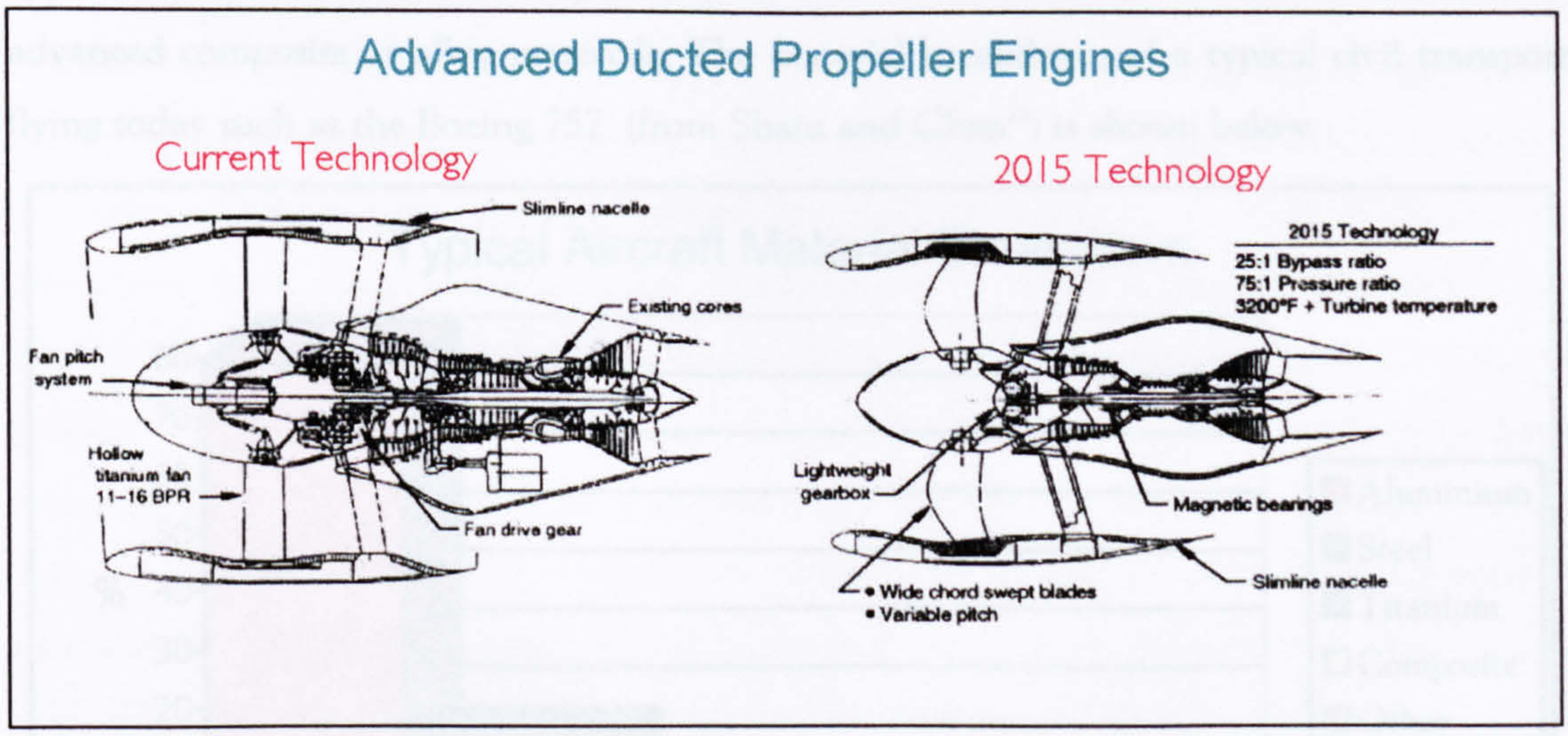


Figure 3.5- Advanced ducted propeller designs

3 .2 .4 ContraFan

An alternative to the introduction of gear box is the use of a directly driven counter rotating aft fan. Due to the contra rotation of the aft fan, the effective speed of the turbine is increased, and thus the need for a gearbox is eliminated. The aft mounting of the fan also has potential beneficial effects, allowing the gas generator to be designed for smaller diameters, which could in turn allow for higher component efficiencies. It has been estimated (Pickerell[20]) that this kind of design could lead to a 15% fuel consumption reduction over current turbofans.

3 .3 Materials & Structures

3 .3 .1 Materials

Since the beginning of flight the need to reduce the weight of the aircraft has been seen as of paramount importance. The strength of the aircraft structure though is of equal if not greater importance, especially for civil transport applications, as any failure can have catastrophic consequences. Up until the 1960's, civil aircraft were built almost entirely from aluminium alloys. In 1969 Concorde became the first aircraft to contain composite material, but the introduction of advanced composite, metallic, and plastic materials into the structure of civil aircraft has been a very slow process. There are in existence military aircraft such as the V-22 whose airframe consists of 60% composite material by weight. By contrast, even the latest civil aircraft such as the Boeing 777 and the Airbus A340 have only approximately 9% and 13% respectively of their airframe structure manufactured from advanced composite or alloy materials. The material breakdown of a typical civil transport flying today such as the Boeing 757 (from Shaiu and Chen[25]) is shown below.

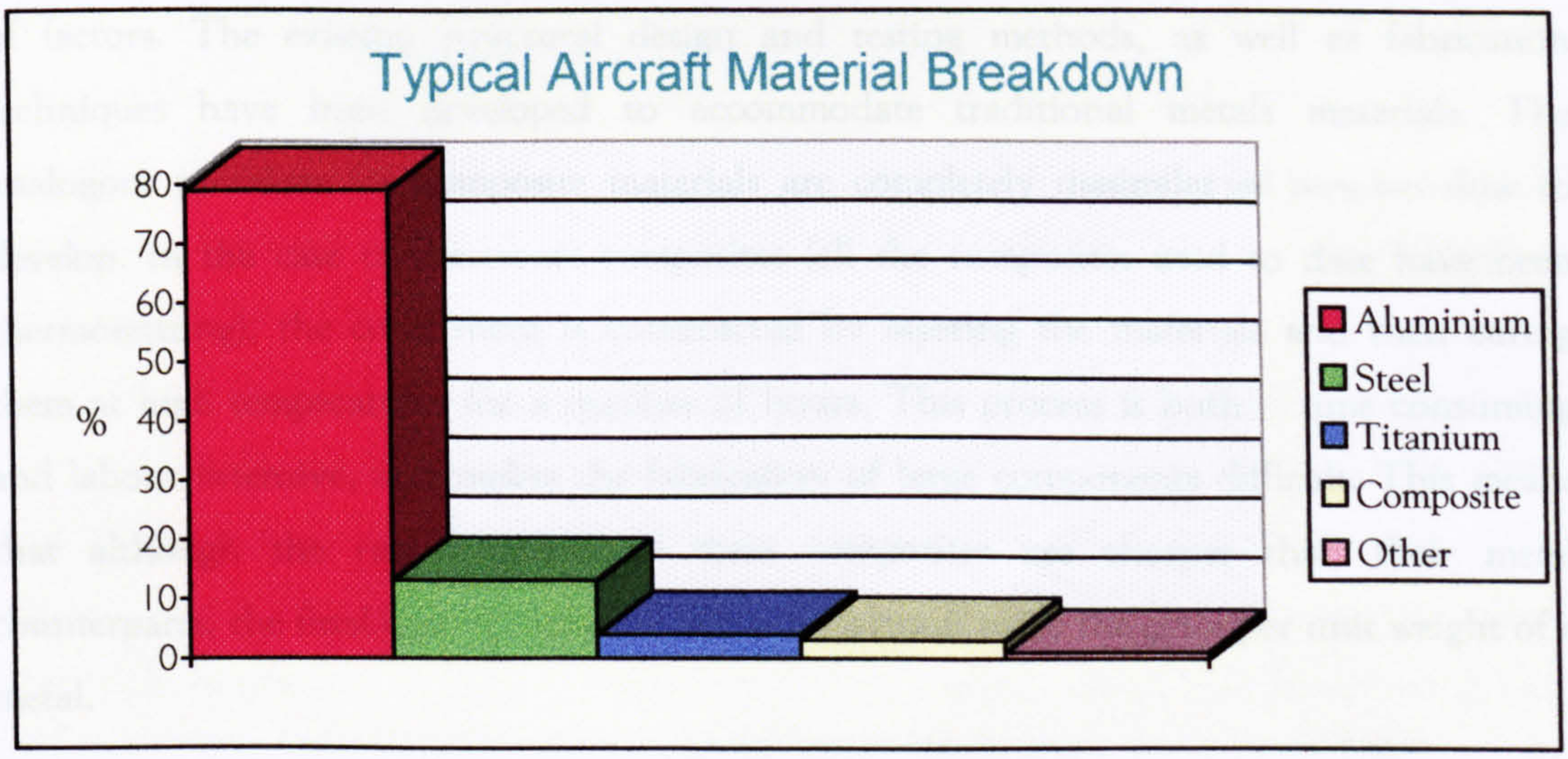


Figure 3.6 - Typical aircraft material composition breakdown

Aircraft of the future will certainly be comprised of higher proportions of advanced material. The materials that are likely to replace the aluminium alloys, and steel in certain parts of the aircraft are discussed below:-

3 .3 .1 .1 Composites

The term composite is used to describe materials consisting of two constituent parts. These parts are the fibre and the matrix. The matrix holds the fibres together and distributes the load between the fibres, while the fibres give the material its strength and stiffness, and is thus the load bearing element of the material.

The advantages of composite materials over traditional airframe materials are that they tend to exhibit a greater strength and stiffness per unit weight, increased corrosion and fatigue properties, and the potential for lower manufacturing costs.

Composite materials have been in existence since the glass reinforced plastics used in the 1940's. The 1960's saw the introduction of carbon fibre composite materials which showed great strength and stiffness. To date, the composite materials used in aircraft have been carbon, kevlar, aramid, or boron fibres in an epoxy matrix. These generally have been used sparingly in secondary structures such as flaps, elevators, rudders, fairings, landing gear doors, and certain wing surface panels. The flaps, elevators and rudders on almost all modern transport aircraft are made from CFRP (carbon fibre reinforced plastic) or KFRP (kevlar fibre reinforced plastic). The Airbus A310 was the first civil transport aircraft to use composite materials for primary structure. The fin of this aircraft is made almost entirely from carbon fibre material, and all subsequent Airbus designs have incorporated similar fin designs.

Although composite materials tend to give a weight saving between 25% and 30% (Bartlett et al.[26], Vogelesang and Gunnink[27], and Resetar et al.[28]) the slow rate of adoption of composite materials into current aircraft, especially in primary structure, is due to a number of factors. The existing structural design and testing methods, as well as fabrication techniques have been developed to accommodate traditional metals materials. The analogous processes for composite materials are completely dissimilar and have been slow to develop. In the case of thermoset composites (all the composites used to date have been thermosettting), the component is constructed by layering the materials and then curing them at high temperatures for a number of hours. This process is both time consuming and labour intensive, and makes the fabrication of large components difficult. This means that although the raw materials of these composites are cheaper than their metal counterparts, the final cost can in some cases be around twice the price per unit weight of a metal.

One of the other main hindrances to the inclusion of composite materials into critical structural areas has been the lack of adequate analytical techniques. As a composite material is not a homogeneous one, the analysis of its behaviour is very complex, with fibre orientation and interaction between the two materials being of major concern. Also the methods required for the manufacture and production of large structures are still being developed, as current composite materials cannot be as easily bolted or riveted as their metallic counterparts. The issue of maintenance and repair is also an area of major concern.

There are however a number of new composite materials on the horizon which can potentially solve some of the problems associated with thermoset composites, and bring composite materials more to the forefront in primary and secondary aircraft structures.

Thermoplastic Composites

Thermoplastic composites have been the subject of intense research since the early 1980's. The main advantage of thermoplastics is their ability to be reheated and then reshaped. They also have much shorter fabrication times than thermosets (a number of minutes), they are less temperature sensitive and more resistant to impact damage and cracking than thermosets, and they can be welded, unlike thermosets. As well as many as yet unknown mechanical properties of thermoplastics there are a number of potential drawbacks. The high temperatures needed to process them (650-800F) could prove prohibitive, as could be their relatively poor high temperature strength and solvent resistance.

Metal Matrix Composites

The development of materials using metals as the matrix is still in an early stage of development, but is showing a large potential. These materials offer superior operating temperatures than conventional composites while maintaining better compression strength than conventional superalloys. The matrix materials tested so far have included aluminium, titanium, magnesium, copper, or superalloys, while the fibres include graphite, boron, silicon oxide, and aluminium oxide. The potential of the superior performance and weight savings is obviously appealing, and tests have already been conducted on vertical tail structures. Potential drawbacks are the high cost of manufacture and a wide variation in properties between batches.

One of the most exciting prospects in this area is an aramid aluminium laminate called ARALL (Vogelesang and Gunnin[27]). It is built up as a laminated sheet from thin aluminium alloy sheets and unidirectional aramid fibres. The result of this is a material with a high tensile strength, good fatigue crack properties, high impact strength, combined with simple fabrication methods. The material can be easily cut, drilled, milled, and joined using bolts and rivets. The main use of ARALL would likely be in the fatigue critical areas of the

aircraft, such as the lower skin of the wing, and the fuselage. This material could directly replace aluminium giving approximately 30% weight savings.

Although not a mature technology, the potential benefits will ensure that knowledge of the properties of metal matrix composites will be increased rapidly in the time to come.

Ceramic Matrix Composites (CMC)

Still at a very early stage of development, ceramic matrix composites have greater wear resistance and high temperature strength than metals. The matrix can include such materials as glass, carbon, silicon carbide, and alumina. The main problem with CMC's is their poor fracture toughness, often resulting in catastrophic failure, which excludes them from use in most primary structure applications. The main application of CMC's will be in high temperature environments such as the aircraft engine.

There are two approaches that can be adopted for the use of composite materials. They can either be used to directly substitute a metal, bringing obvious weight benefits, or by fully utilising the properties of composites, careful redesign can reduce the number of parts for construction and further reduce the weight. An example of this being the construction of the composite A330/A340 rudder, where a 20% weight saving and 10% cost saving was produced by using a 'sandwich' construction. Rather than using the conventional skin-stringer type of construction, the sandwich skin construction method creates a skin with integral internal stiffeners that is only possible if using composite materials.

A study by Jackson et al.[29] shows that by using this and other kinds of techniques in conjunction with the advanced types of composites described above, it is possible to use composite materials in the primary structures of both wing and fuselage to obtain an average of about 30% reduction in weight, and a 20% reduction in cost.

3 .3 .1 .2 Metals and Alloys

Aluminium alloys continue to be the most widespread material used in aircraft manufacture. Steel, titanium, and titanium alloys tend to make up most of the remaining metallic parts. The most promising new metal and alloy materials are described below:-

Aluminium-Lithium Alloys (Al-Li)

The development of aluminium lithium alloys goes back 60 years to the 1930's, however it seems that their development has only just reached a point where their inclusion in aircraft structures is a serious proposition. Al-Li alloys are approximately 10% lighter and 5% stronger than current aluminium alloys. Research has shown (Resetar et al.[28]) that they may be used to replace conventional aluminium alloys, or as an alternative to composites in certain areas.

Powder Metallurgy

This is a process from which materials are produced by mixing metals in powder form, allowing a more homogeneous mixture and therefore more desirable properties. This technique may be applied to many materials, and has already been shown to enhance the properties of aluminium-lithium alloys.

3 .3 .1 .3 Summary

In summary, the ability to fabricate advanced materials and to design structures based specifically on these materials will improve in the foreseeable future, with the most notable benefit being an average 30% weight reduction where composite materials are used in place of conventional metal or alloy, or a 10% weight reduction when an Al-Li alloy is used in place of a conventional one. It would seem that the amount of composites used in primary structure will continue to increase, with perhaps an all composite wings and fuselage appearing some time in the next century.

3 .3 .2 STRUCTURES

As well as the incorporation of advanced materials into structures, as discussed above, there are a number of concepts being researched that have become known as smart structures.

The first type of smart structure under consideration is one that can actively alter its shape under a control input. This kind of structure could be used for a wing section and would play an important part in a variable camber system. Research by Austin et al.[30] has shown that actuators could be successfully used to deflect the surface of a 2d-model, and that transonic drag reductions were possible as a result of this. This kind of work is discussed more thoroughly in 3.4.10.

The other type of smart structure under investigation is a self-diagnostic system using embedded sensors to allow real time damage and crack detection. This technology seems a long way off and will not affect the performance or the weight of the aircraft significantly.

3 .4 AERODYNAMICS

3 .4 .1 AIRFOILS

The supercritical airfoil first came into being in the early 1970's. A supercritical airfoil is designed for use in the transonic regime, and is characterised by a large leading-edge radius, a flattened upper surface, and a substantially cambered trailing edge. This geometry

gives a flattened pressure distribution for both the upper and lower surfaces (shown in figure 3.7 from Harris[31]) which in turn results in a much delayed and weaker shock system. The main effect of this is to increase the drag divergence Mach number at a particular lift coefficient markedly above that for a conventional airfoil, without any significant loss in low speed or stall performance. This means that for a given drag divergence Mach number and drag level, a thicker airfoil may be used, and hence the structural weight of the wings reduced, while the useful useable volume inside the wing is increased. This also infers that for cruise Mach numbers comparable to those of aircraft using conventional airfoils, it was possible to increase the aspect ratio and to decrease the sweep of the wings, hence reducing the drag.

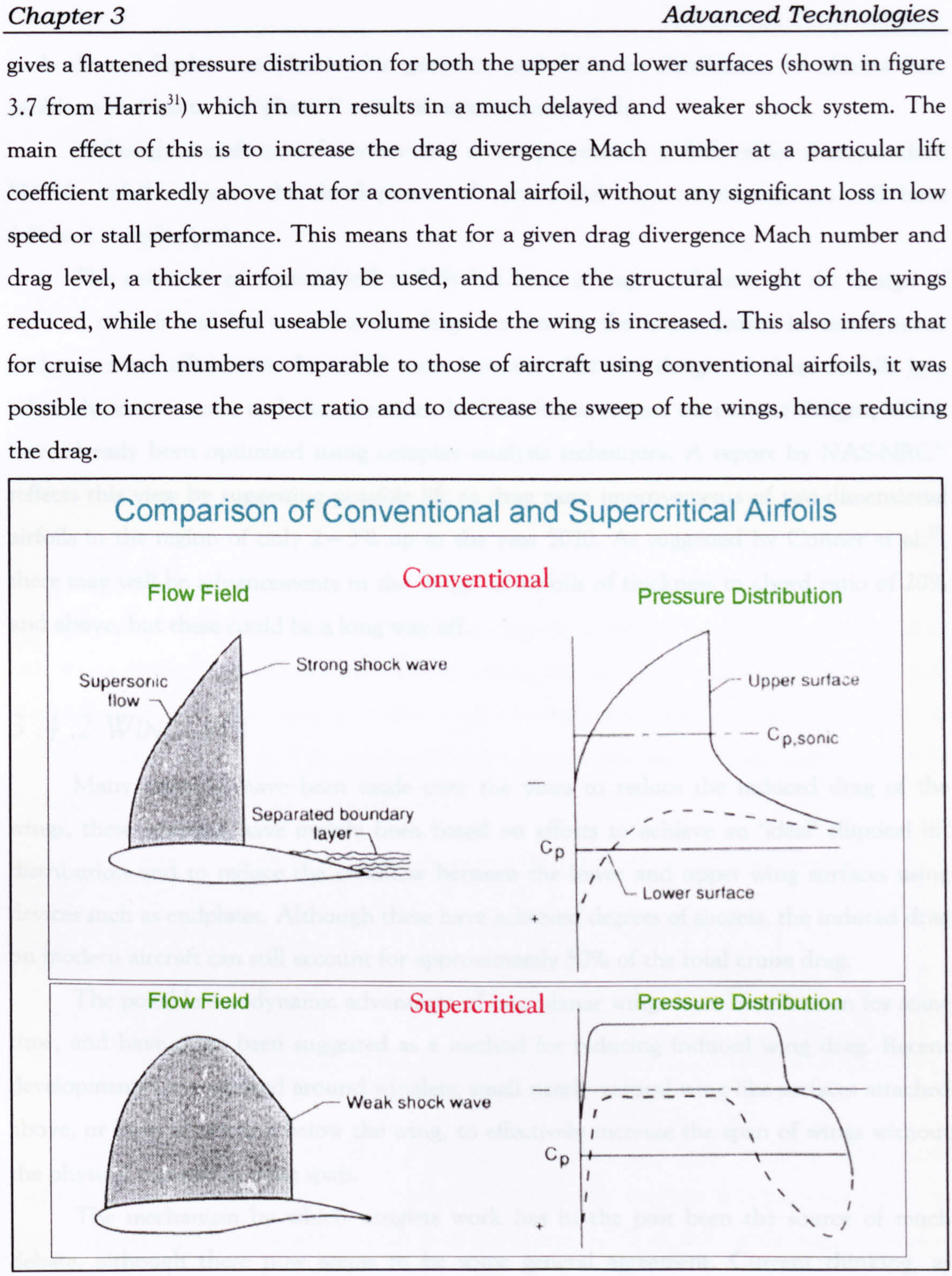


Figure 3.7 - Comparison of conventional and supercritical airfoils

Initial efforts by NASA produced the 'phase 1' supercritical airfoils, which suffered from a gradual increase in drag just before the final drag rise, known as drag creep. Refinements in geometry were made to correct this problem and resulted in improved 'phase 1' airfoils. New analysis techniques and insights learnt from previous experiments then led to the 'phase 2' supercritical airfoils. However, these airfoils still possessed relatively unfavourable low speed characteristics, large nose-down pitching moments, and little rear structural depth for the application of flaps. Increased availability of computerised design

tools allowed further modifications in geometry and thickness distribution to address these problems and led to the 'phase 3' series of supercritical airfoils.

Although aircraft manufacturers tend to use proprietary airfoils rather than standard NASA airfoil sections, the development of commercial supercritical sections will have followed a similar path.

The existence of supercritical airfoils has been a major influence on the design of modern aircraft and has contributed a large amount to the improvement in aerodynamic and structural efficiencies. It would seem however that the design of these airfoils is a relatively mature area, and that there can be little improvement on current designs, which have already been optimised using complex analysis techniques. A report by NAS-NRC[22] reflects this view by suggesting possible lift to drag ratio improvements of two-dimensional airfoils in the region of only 2~3% up to the year 2020. As suggested by Conner et al.[32], there may well be advancements in the design of airfoils of thickness to chord ratio of 20% and above, but these could be a long way off.

3 .4 .2 WINGLETS

Many attempts have been made over the years to reduce the induced drag of the wings, these attempts have mainly been based on efforts to achieve an 'ideal' elliptical lift distribution and to reduce the crossflow between the lower and upper wing surfaces using devices such as endplates. Although these have achieved degrees of success, the induced drag on modern aircraft can still account for approximately 50% of the total cruise drag.

The possible aerodynamic advantages of non-planar wings have been known for some time, and have often been suggested as a method for reducing induced wing drag. Recent developments have centred around winglets, small nearly vertical wing like surfaces attached above, or both above and below the wing, to effectively increase the span of wings without the physical increase in wing span.

The mechanism by which winglets work has in the past been the source of much debate, although there now seems to be some general agreement. Current thinking, as reported by Merkl and Marsden[33], and Thomas[34], indicates that the winglet not only produces a thrust component in the streamwise direction due to the alignment of the lift produced by the winglet, but that the winglets reduce the induced drag along the entire span of the wing.

The other main effects of these winglets are to increase the bending moment of the wings and to reduce the vortex tip strength (Barber and Selegan[35]). In terms of stability, Flechner[36] demonstrated that winglets can increase longitudinal stability and significantly increase the dihedral effect, while other research has indicated that winglets can potentially

incur a significant flutter penalty. However, the addition of winglets appears to have little or no effect on the wing lift curve slope, or on the lift characteristics of the aircraft generally.

The configuration of the winglets is of major significance and can have a huge impact on their performance. The main parameters of significance are the inclusion or exclusion of a lower winglet, the span of the winglets, the sweep and taper of the winglets, the cant angle of the winglets, and the inclusion of leading edge devices.

It is clear that the greater the span of the winglet the greater the drag reduction potential, but with greater corresponding increase in wing root bending moment. The results of 'The DC-10 Winglet Flight Evaluation' (Douglas Aircraft Co.[37]) indicated that removal of the lower winglet detracted from cruise performance, and that leading edge devices could be used to improve low speed performance. Data on the amount of cant angle required to reduce wing-winglet interference, and the optimum values of sweep and taper are however less conclusive.

Results from wind tunnel and flight testing of optimised winglets give cruise drag reductions of the order of the values shown below, the large differences in values probably arising from the disparate nature of the wings on which the winglets were being tested, as well as experimental error. The drag reduction tends to increase with lift coefficient, while being relatively independent of Mach number.

DC-10 Upper and Lower Winglet	-2.5%	(Taylor[38])
DC-10 Upper Winglet	-1.5%	(Taylor[38])
KC-135 Upper Winglet	-6%	(Barber and Selegan[35])
Boeing 747 Upper Winglet	-3.3%	(Boeing Airplane Company[39])

Figure 3.8 - Summary of winglet test results

The main disagreement about the use of winglets has been whether it is more beneficial to increase the span of the wings rather than use winglets. It is interesting to note that Airbus decided to use winglets on their A340 and A330 models, while Boeing decided against their use on the Boeing 777. Most research seems to agree that for a given bending moment increase, winglets will give approximately twice the drag reduction of increased span. Boeing however argue that when designing a new aircraft, extra span will give better performance than a winglet of the same size, particularly at low speeds (Sweetman and Gregory[40]). However, Körner[41] argues that winglets would be the optimal solution on a new aircraft when the cruise lift coefficient is above 0.45, which would include most large transport aircraft.

It would seem that there is still disagreement over the role that winglets have to play in the design of a new aircraft, but we can say with certainty that the use of winglets is of

definite benefit both when the span of the aircraft is of critical importance and when being fitted to an existing aircraft. However, the retrofit of winglets to an existing aircraft may not be straightforward and may cause technical difficulties, mainly due to the increased bending moment. The winglet span may need to be significantly reduced, which may result in a compromise design being reached, such as in the case of the A310, where wing tip-fences have been fitted giving a 1.5% drag reduction (Poisson-Quiton[42]).

In the future we are unlikely to see new aircraft incorporating winglets, even the provisional designs for the Airbus A3XX, where wing span is of crucial significance, do not include winglets in the original design. It is more likely that they will be used as a retrofit device to increase the capacity of the aircraft at a later date.

3 .4 .3 Wing Tip Devices

Other devices that have been suggested for reducing the induced drag are wing tip sails and wing tip turbines.

Wing tip sails described by Thomas[34], Spillman[43], and Schmitt[44] are a logical extension of winglets, they are multiple vanes or winglets applied to the wing in a spiral array around the tip. Induced drag reductions of 30% have been reported, however this technology remains very much an experimental one, with little hard evidence with regards to their application on transport aircraft at the present time.

The principle behind the wing tip turbine is to simultaneously extract energy from the wing tip vortex, and to convert this energy into thrust. The effect of this is to both reduce aircraft drag, increase the aircraft thrust, while reducing the strength of trailing edge vortices. Tests by Patterson[45] indicate total drag reductions in the region of 10%, although the development of this technology is still at a very early stage.

3 .4 .4 Wing Tip Blowing

The blowing of air from the tip of the wing spanwise across the wing has often been suggested as a method for reducing drag. A comprehensive study by Mineck[46] concluded that spanwise blowing is only effective for reducing drag on high aspect ratio wings, at speeds below a Mach number of 0.5, and that blowing appears to have more of an effect on the lift than on the drag. This excludes this technology from use in modern transport aircraft.

3 .4 .5 NATURAL LAMINAR FLOW (N.L.F.)

Possibly the largest potential for improvements in aircraft efficiency is the realisation of significant portions of laminar flow over the aircraft surface. If we look at the equations governing the skin friction coefficient:-

$$C_f = \frac{1.328}{\sqrt{Re}} \qquad \text{(laminar)}$$

$$C_f = \frac{0.455}{\left(\log_{10} Re\right)^{2.58}\left(1+0.144\,Ma^2\right)^{0.65}} \qquad \text{(turbulent)}$$

We can see that for a representative Reynolds number of 50 million and Mach number of 0.8 we get a laminar skin friction coefficient of $1.878\text{x}10^{-4}$, and a turbulent skin friction coefficient of $2.218\text{x}10^{-3}$. There is an order of difference between these two numbers, and if we make the usual assumption that skin friction drag is proportional to the skin friction coefficient, then this infers a parasite drag reductions in the region of 90%. This kind of potential benefit has lead to a considerable amount of research activity in this area over the years. As early as the 1930's it was recognised that laminar boundary layers can be stabilised by a favourable pressure gradient or by wall suction. The reduction of instabilities by shaping and by pressure gradient tailoring became known as 'natural' laminar flow.

The introduction of advanced production techniques and advanced materials have been responsible for the high precision aircraft skins we see today. The accuracy and waviness of these components are of such a level that the maintenance of laminar flow over these surfaces is a realistic prospect. The development of more complex computational methods also gives designers a great advantage in the design of natural laminar flow components.

Natural Laminar Flow Wings

The main objective in the design of N.L.F. airfoils is to shape the airfoil appropriately in order to maximise the extent of the region which supports a favourable pressure gradient. This favourable pressure region must however be followed by an appropriate recovery in the adverse pressure region, to maintain attached flow.

This approach has led to many successful designs, especially for airfoils designed for use at low speed and low Reynolds numbers. Many sailplanes and smaller aircraft currently flying today make use of N.L.F. airfoils. The NLF(1)-0414F airfoil has been reported by Viken et al. [47] to produce only 38% of the drag of its turbulent counterparts. It has only been recently that airfoils have been developed that are capable of sustaining portions of

laminar flow at Mach numbers representative of large subsonic transports. Khalid & Jones[48] have reported the development of a series of airfoils ranging from 10%-21% thickness to chord ratio capable of sustaining up to 70% laminar flow. The 10% thick airfoil was estimated to give a 60% region of laminar flow at a Mach number of 0.8, while maintaining lift and moment characteristics comparable with turbulent airfoils. Similarly, Boeing[49] have designed an airfoil which is claimed to exhibit 35% and 50% regions of laminar flow on its upper and lower surfaces respectively, at a Mach number of 0.78 and a Reynolds number of 20 million.

The main problem is the integration of these two dimensional airfoils into a three dimensional wing design. In the two dimensional case one is only concerned with Tollmien-Schlichting (T-S) type disturbances, which are responsible for streamwise instabilities. However in the case of a three dimensional swept wing one must also consider the effect of crossflow stability. The optimum pressure gradients for the two cases of T-S stability and crossflow stability are very different (as shown below in figure 3.9), and therefore the introduction of sweep has a profound effect on the amounts of laminar flow attainable. In fact the negative pressure gradients associated with preventing streamwise disturbances have a detrimental effect on the crossflow stability.

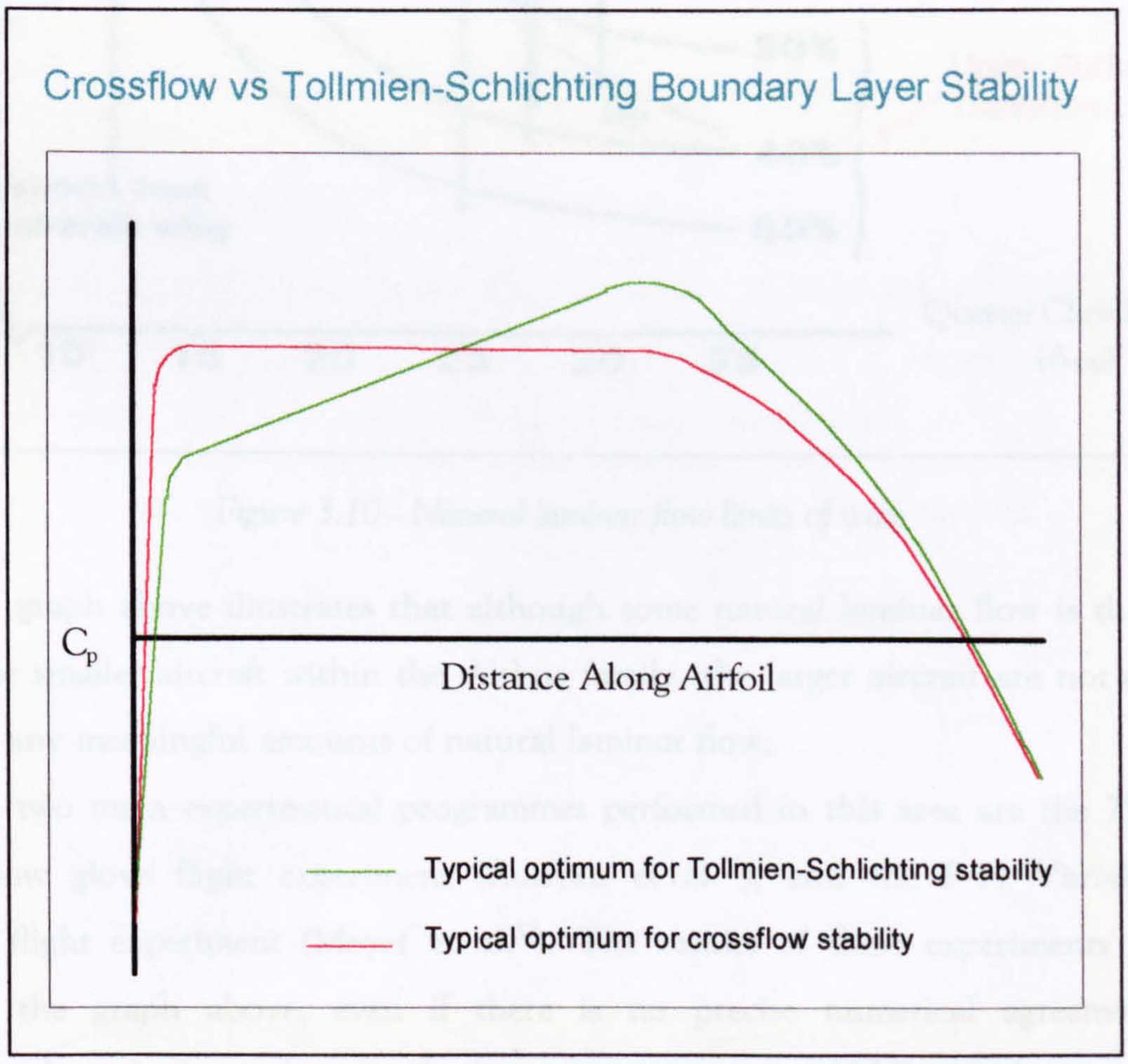


Figure 3.9 - Optimum pressure gradients for wing flow stability

At high sweep one must also consider the effect of disturbances from the fuselage being propagated along the attachment line and causing transition (attachment line transition). A study by Reneaux and Blanchard[50] produced the diagram shown below in

figure 3.10. This depicts the predicted transition points of an infinite swept wing at various sweep angles, and Reynolds numbers, taking all the forms of instability into account. The graph also depicts the sweep and Reynolds number of aircraft contained within the Airbus family.

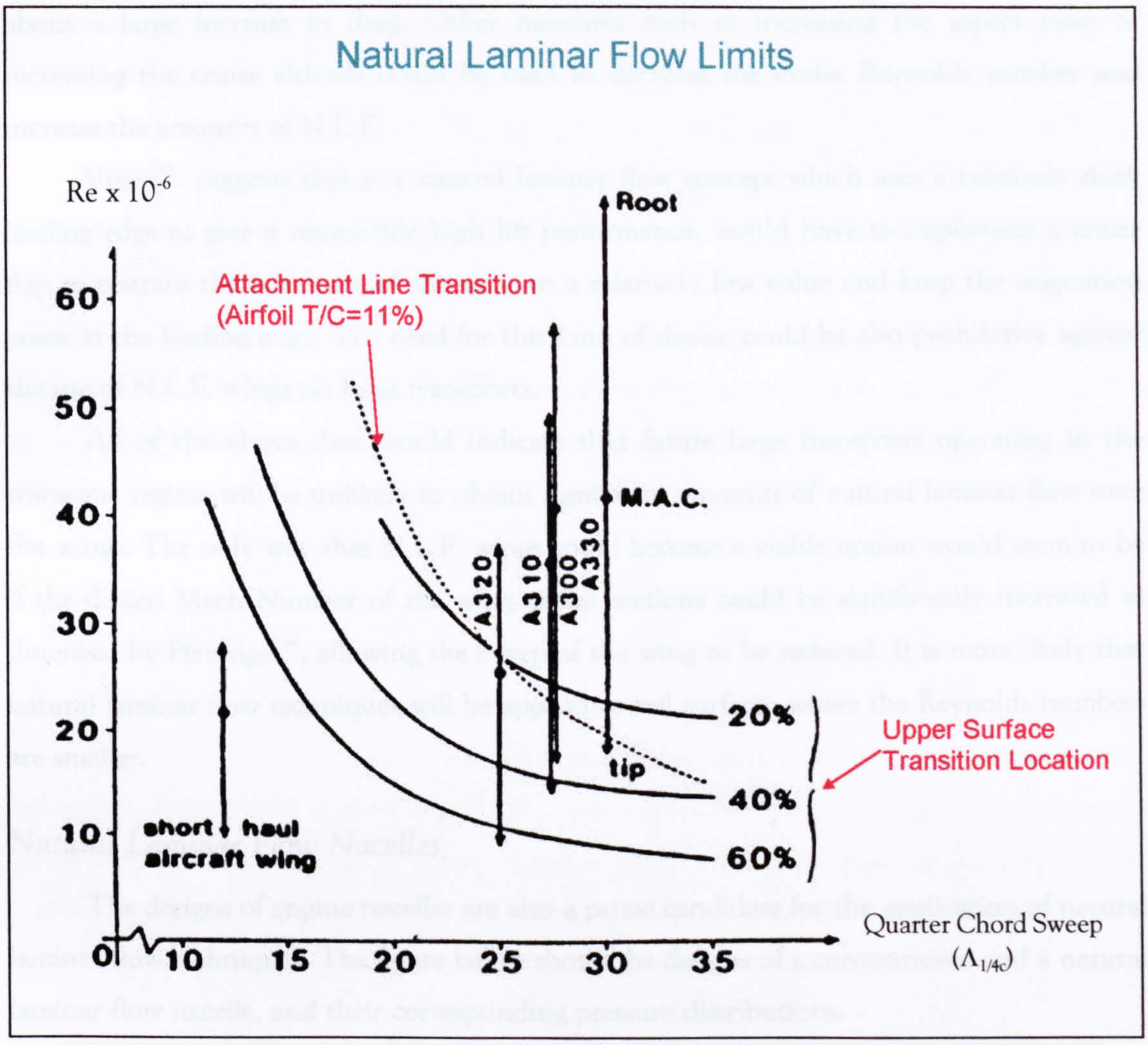


Figure 3.10 - Natural laminar flow limits of wing

The graph above illustrates that although some natural laminar flow is theoretically possible for smaller aircraft within the Airbus family, the larger aircraft are not capable of sustaining any meaningful amounts of natural laminar flow.

The two main experimental programmes performed in this area are the 757 natural laminar flow glove flight experiment (Runyan et al.[51]), and the F-14 Variable Sweep transition flight experiment (Meyer et al.[52]). The results of these experiments verify the trends of the graph above, even if there is no precise numerical agreement. These experiments have been used to verify that some portions of N.LF. can be maintained at Mach numbers up to 0.8, for moderate Reynolds numbers, and that the effect of engine noise on boundary layer instability is insignificant.

The applicability of N.L.F. does however appear at this stage be limited to small and medium sized aircraft. The only way to achieve significant natural laminar flow on the wings of larger aircraft may be to reduce the wing sweep. However the wing sweep is essential for reducing the local maximum Mach numbers, and any decrease in wing sweep would bring about a large increase in drag. Other measures such as increasing the aspect ratio or increasing the cruise altitude could be used to decrease the cruise Reynolds number and increase the amounts of N.L.F.

Viken[53] suggests that any natural laminar flow concept which uses a relatively thick leading edge to give a reasonable high lift performance, would have to implement a cruise flap to restrain the incidence of the wing to a relatively low value and keep the stagnation point at the leading edge. The need for this kind of device could be also prohibitive against the use of N.L.F. wings on large transports.

All of the above data would indicate that future large transports operating in the transonic regime will be unlikely to obtain significant amounts of natural laminar flow over the wings. The only way that N.L.F. wings could become a viable option would seem to be if the design Mach Number of the wing airfoil sections could be significantly increased as discussed by Pfenniger[54], allowing the sweep of the wing to be reduced. It is more likely that natural laminar flow techniques will be applied to tail surfaces where the Reynolds numbers are smaller.

Natural Laminar Flow Nacelles

The designs of engine nacelles are also a prime candidate for the application of natural laminar flow techniques. The figure below shows the designs of a conventional and a natural laminar flow nacelle, and their corresponding pressure distributions.

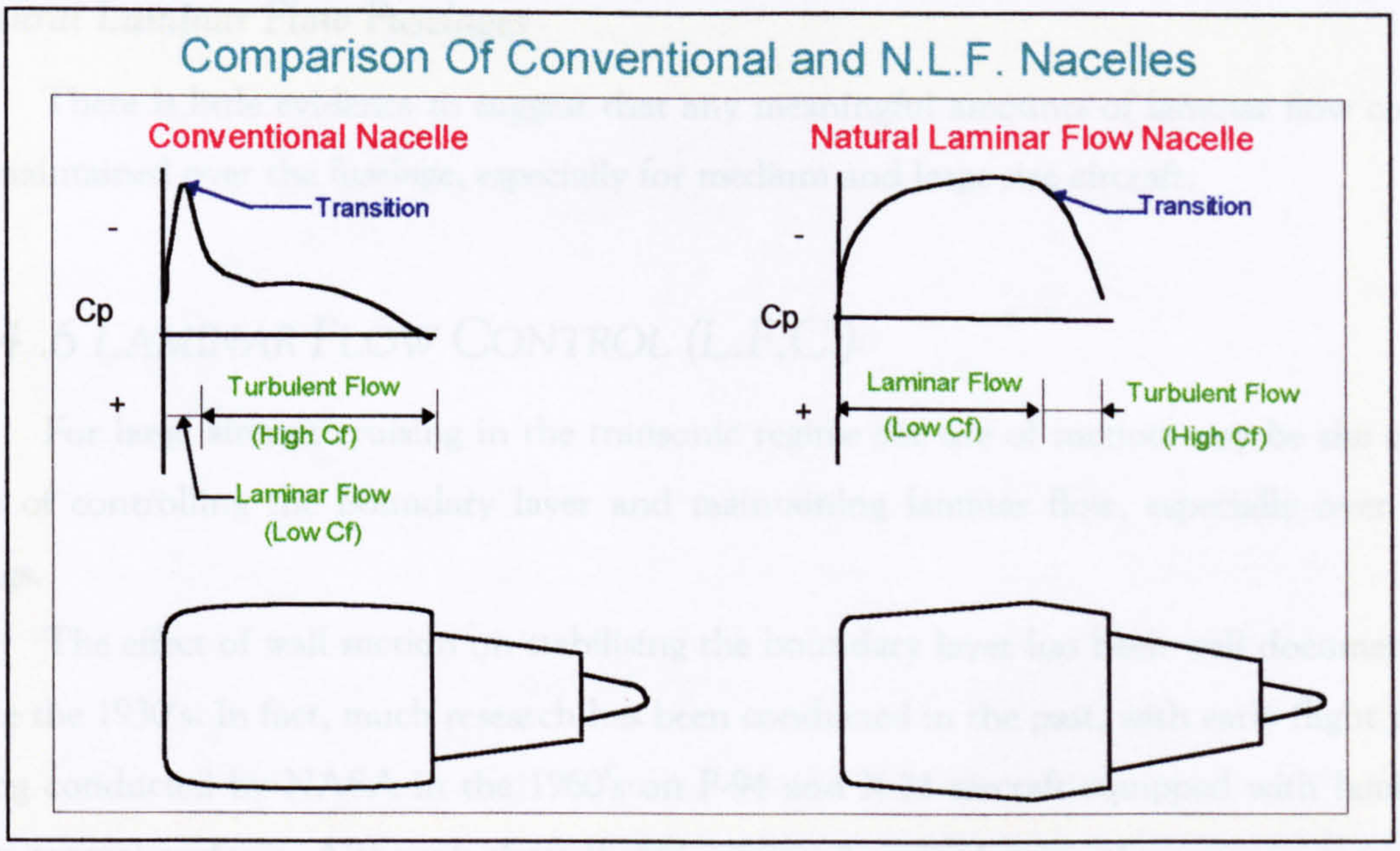


Figure 3.11- Comparison of conventional and NLF nacelles

Aircraft engine nacelles generally have lower Reynolds numbers than the wing surfaces, and as they are not used to provide lift they can be more freely shaped to provide favourable pressure gradients without the need to design for lift and moment characteristics.

In the past, nacelles have been designed to have a 'peaky' distribution, which creates suction at the nacelle lip and improves flow through the nacelle. The natural laminar flow nacelle must have both sharper internal and external lips. Achieving good off-design flow and avoiding separation with these designs is the major challenge yet to be fully resolved.

Faust[55] states that this kind of design could result in a 40% to 50% reduction in nacelle friction drag if the transition is delayed to approximately 70% of the nacelle length, while Radespiel et al.[56] expect transition to occur at 60% of the nacelle length at cruise conditions. This is in agreement with wind tunnel tests described by Lamb et al.[57], which demonstrated that laminar flow could be maintained up to lengths in excess of 60% of the nacelle, at Mach numbers up to 0.8. They also showed that installation had no effect on this laminar flow and its related drag reduction. Furthermore, flight test results published by Obara and Dodbele[58] demonstrate a transition location greater than 50%, with the possibility of this reaching 60% using a revised design. Rolls Royce have been working on laminar flow nacelles for some time, and Mullender et al.[59] report significant drag reductions have been predicted by the use of N.L.F. techniques.

It would seem wholly reasonable to expect future nacelles to be capable of sustaining laminar flow up to 60% of their length. This kind of achievement would preclude the use of active laminar flow control of hybrid laminar flow control on nacelles, as any further improvements due to the implementation of these technologies would be outweighed by the weight and maintenance penalties associated with them.

Natural Laminar Flow Fuselages

There is little evidence to suggest that any meaningful amounts of laminar flow could be maintained over the fuselage, especially for medium and large size aircraft.

3 .4 .6 Laminar Flow Control (L.F.C.)

For large aircraft cruising in the transonic regime the use of suction may be the only way of controlling the boundary layer and maintaining laminar flow, especially over the wings.

The effect of wall suction on stabilising the boundary layer has been well documented since the 1930's. In fact, much research has been conducted in the past, with early flight tests being conducted by NASA in the 1960's on F-94 and X-21 aircraft equipped with laminar flow control surfaces. Although these flights exhibited some degrees of success in terms of

drag reduction, even at Reynolds numbers up to 40 million, these programs were abandoned due to question marks over reliability and maintenance of such a system for aircraft at that time. Research in L.F.C. systems was rejuvenated in the 1980's due to the increased drive toward more efficient aircraft.

A better understanding of laminar flow problems, more advanced materials and production techniques such as electron beam drilling, combined with highly sophisticated computational techniques mean that laminar flow control is now a much more realistic prospect.

Wind Tunnel research produced by NASA has shown encouraging results, while the main flight research in this area has been produced by the Lockheed-Georgia company, and the Douglas Aircraft Company, with both companies flight testing L.F.C. devices on a NASA Jetstar aircraft.

Brooks et al.[60] reports the success achieved in the wind tunnel tests conducted by NASA. A model of a supercritical wing with 23 degree sweep was constructed with slots along both the full chord of the upper and lower surfaces to enable boundary layer suction. The results showed that full chord laminar flow was maintained up to a Mach number of 0.82 and Reynolds number of 22 million. This led to an upper surface drag reduction of 80%, and a lower surface drag reduction of 60%, even accounting for suction drag.

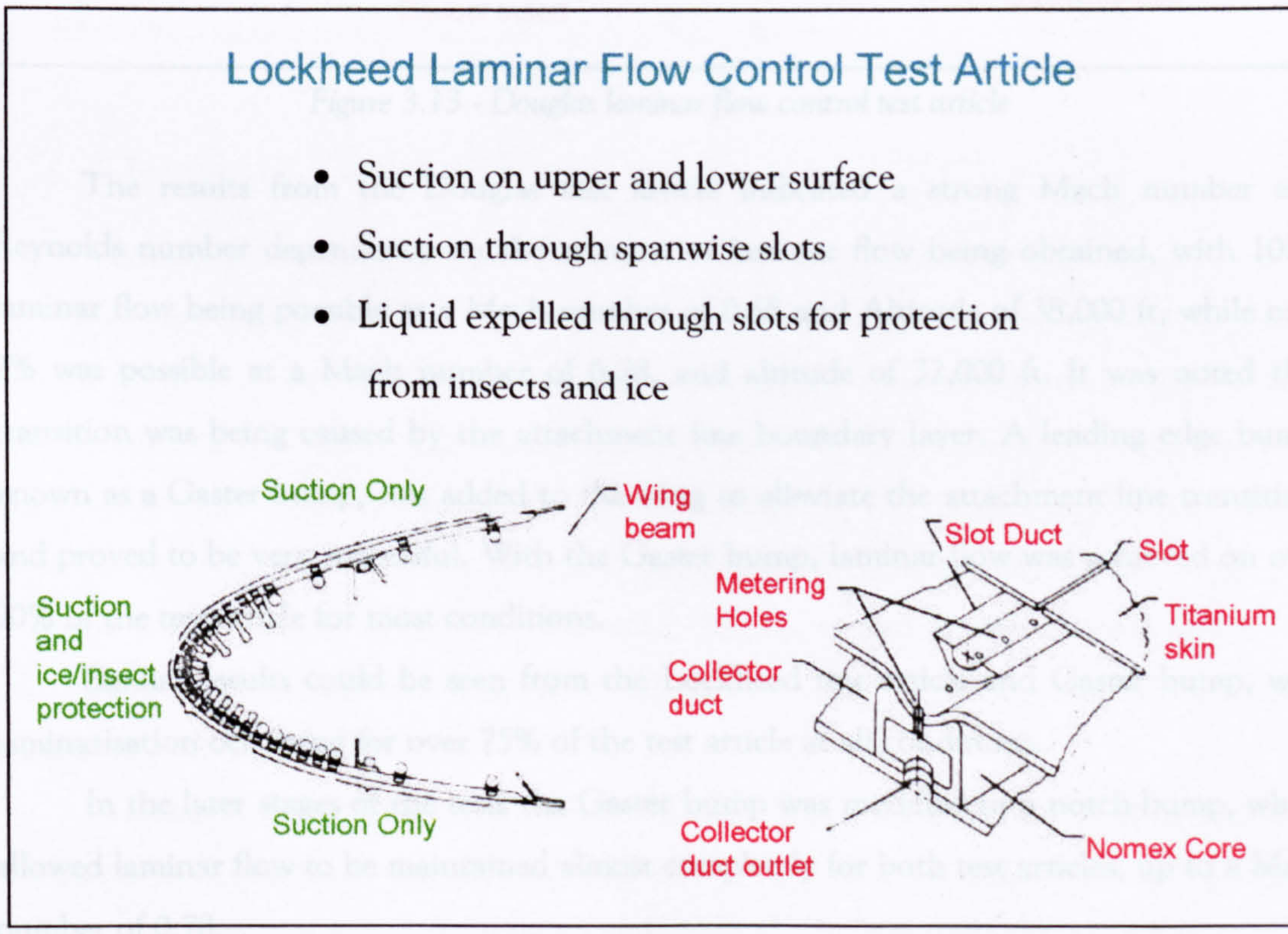


Figure 3.12- Lockheed laminar flow control test article

The Lockheed leading edge L.F.C. flight test results, described by Fisher and Fischer[61], were based on a slotted test article providing suction on both the lower and upper

leading edge surfaces and incorporating an integrated insect/ice protection system, as shown above.

The Douglas test article differed in that suction was provided through porous holes on the upper surface only, and incorporated a Krueger type flap for insect and ice protection, as shown below in figure 3.13 (Fisher and Fischer[61]).

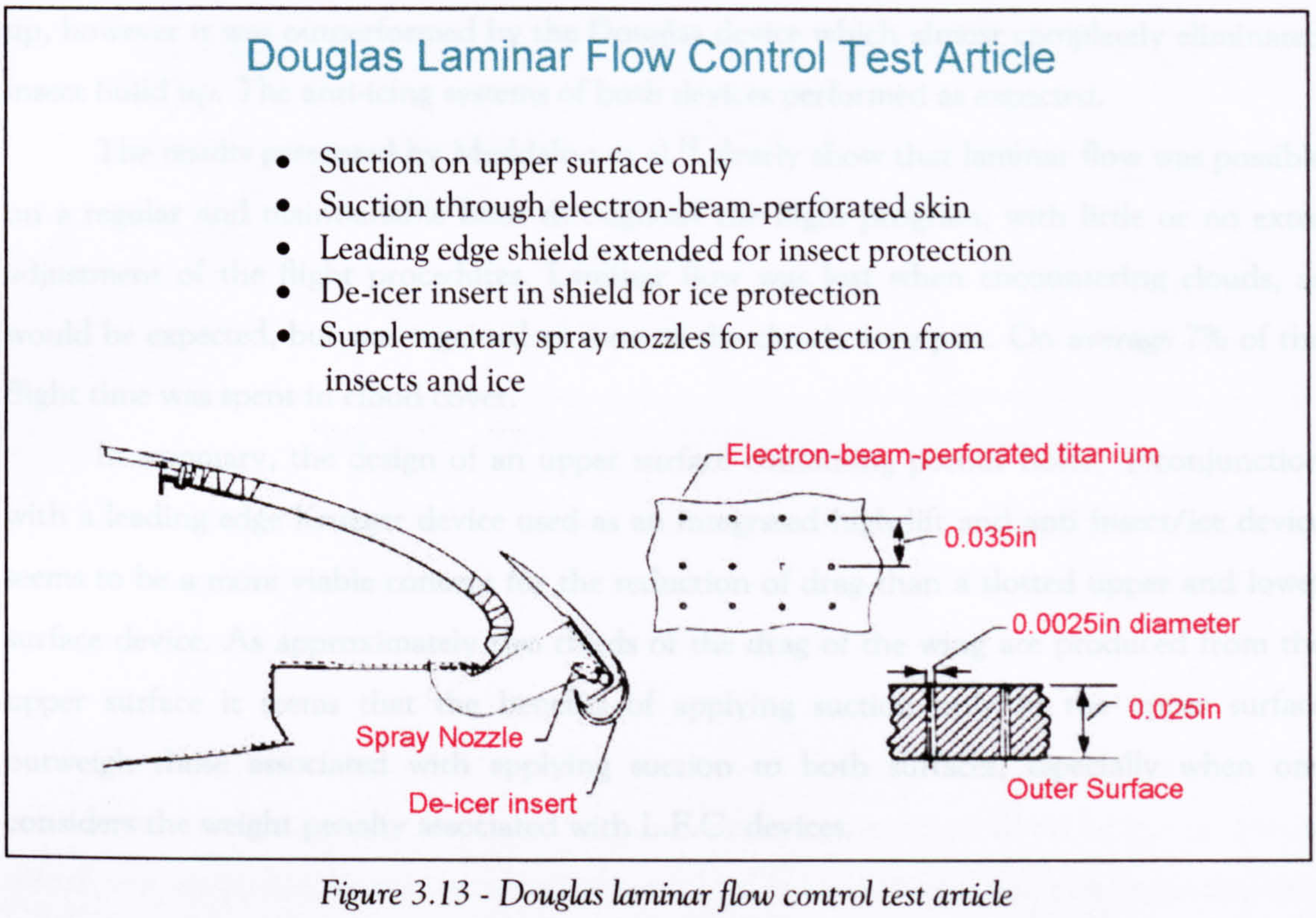


Figure 3.13 - Douglas laminar flow control test article

The results from the Douglas test article indicated a strong Mach number and Reynolds number dependency on the amount of laminar flow being obtained, with 100% laminar flow being possible at a Mach number of 0.68 and Altitude of 38,000 ft, while only 7% was possible at a Mach number of 0.78, and altitude of 32,000 ft. It was noted that transition was being caused by the attachment line boundary layer. A leading edge bump, known as a Gaster bump, was added to the wing to alleviate the attachment line transition, and proved to be very successful. With the Gaster bump, laminar flow was achieved on over 90% of the test article for most conditions.

Similar results could be seen from the Lockheed test article and Gaster bump, with laminarisation occurring for over 75% of the test article at all conditions.

In the later stages of the tests the Gaster bump was modified to a notch-bump, which allowed laminar flow to be maintained almost completely for both test articles, up to a Mach number of 0.78.

The operational impacts of these laminar flow control devices were investigated (Maddalon et al.[62]) through a series of 62 flights between domestic airports. The Lockheed article used surface slots to eject freezing point depressant fluid to stop the build up of ice

and insects, while the Douglas article, because of its lack of suction on the lower surface was able to incorporate a Krueger flap. The Krueger flap, stored in the lower part of the wing could be deployed at low altitude and used as a direct line of sight insect shield, and also contains nozzles for the ejection of freezing point depressant liquid, as well as being used as a high lift device. The Lockheed test article performed reasonably well in terms of insect build up, however it was outperformed by the Douglas device which almost completely eliminated insect build up. The anti-icing systems of both devices performed as expected.

The results presented by Maddalon et al.[62] clearly show that laminar flow was possible on a regular and maintainable basis throughout the flight program, with little or no extra adjustment of the flight procedures. Laminar flow was lost when encountering clouds, as would be expected, but was regained as soon as the clouds were past. On average 7% of the flight time was spent in cloud cover.

In summary, the design of an upper surface containing porous holes, inconjunction with a leading edge Krueger device used as an integrated high lift and anti insect/ice device seems to be a more viable concept for the reduction of drag than a slotted upper and lower surface device. As approximately two thirds of the drag of the wing are produced from the upper surface it seems that the benefits of applying suction only to the upper surface outweigh those associated with applying suction to both surfaces, especially when one considers the weight penalty associated with L.F.C. devices.

3 .4 .7 Hybrid Laminar Flow Control (H.L.F.C.)

Research has recently focused on a more promising method of maintaining laminar flow over wing and tail surfaces. In the past, laminar flow control studies applied suction to a major portion of the wing chord, this approach required major reconstruction of the load bearing part of the wing, and studies have shown that full chordwise suction actually inhibits the effectiveness of laminar flow control (Attar[63]). The concept of Hybrid Laminar Flow Control is to combine the effects of suction at the leading edge of the wing, thus retaining a conventional wing box, with airfoil shaping toward natural laminar flow in the mid and rear portions of the wing. A typical design of a Hybrid Laminar Flow Wing is shown below in figure 3.14.

A number of computational, flight, and wind tunnel experiments have been carried out successfully. Thibert[64] reports that 50% of the flow over an A320 fin could be made laminar at cruise conditions by applying suction to the first 20% of the chord. Flight experiments conducted on a Boeing 757 and a Falcon 50 described by Collier[65] illustrate that large portions of laminar flow are possible using H.L.F.C. at cruise conditions. The Boeing

757 flight test in particular showed almost complete laminarisation of the wing up to the flap region at a Mach number of 0.82, producing a 29% drag reduction.

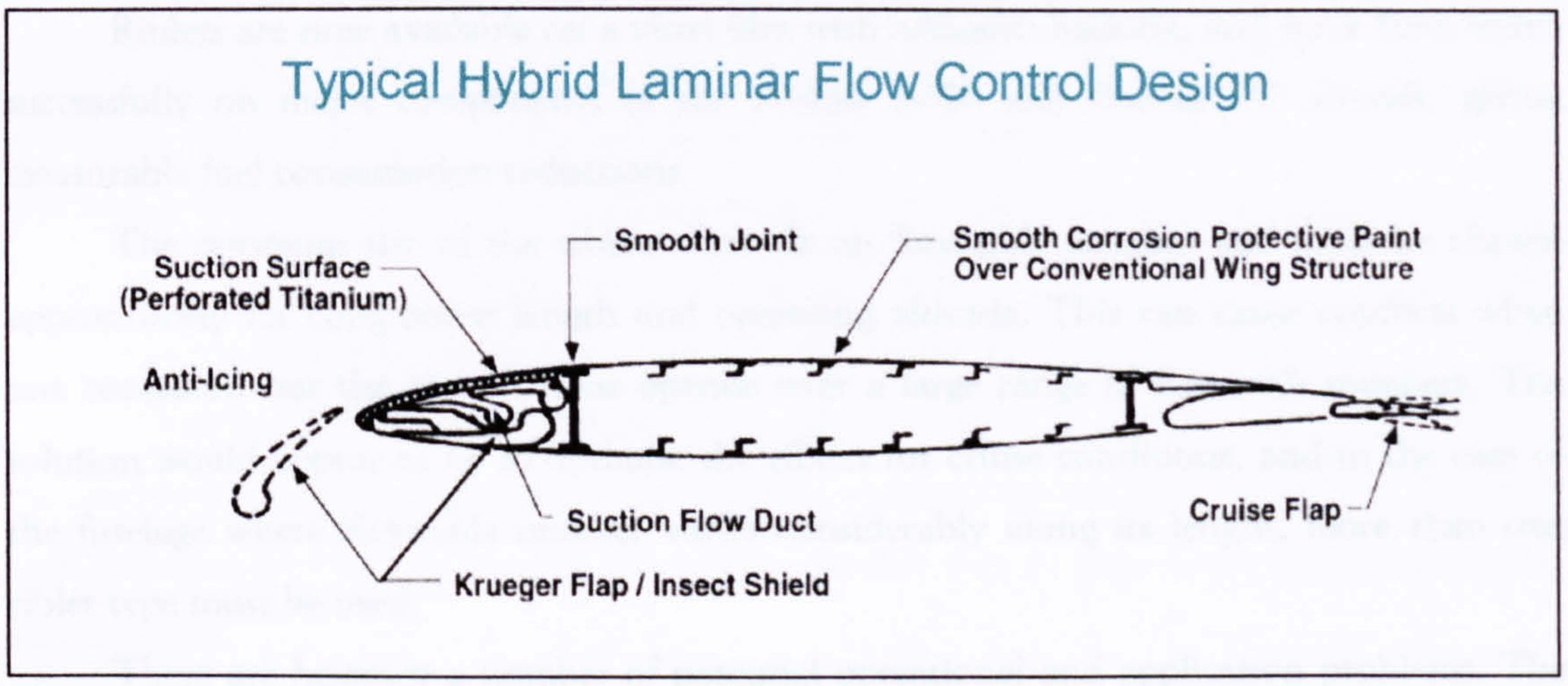


Figure 3.14 - Typical hybrid laminar flow control design

It would appear that hybrid laminar flow offers the greatest overall potential for use on future large civil transports. Drag reductions of the order of 30% may be possible, with corresponding weight increments being of the order of a few percent.

Supposing that laminar flow could be achieved by any of the above methods, there still remains the issue of certification. It is possible that laminar flow could be lost on a wing due to contamination from insects, ice, or rain. In this kind of situation it is important that the aircraft maintains adequate handling and performance properties. The flying qualities of the aircraft which could be affected by a loss of laminar flow include stall speed (Green[66] indicates that the effect of laminar flow on stall speed is still inconclusive), longitudinal stability, and lateral stability in the case of an asymmetric loss of laminar flow. The use of a Krueger flap on an active drag reduction system in place of a conventional slat also raises issues of high lift and stall behaviour. The fuel reserve policy of any aircraft relying on large amounts of laminar flow would also have to be reviewed to take into account the extra fuel required in the event of the loss of laminar flow.

3 .4 .8 RIBLETS

Riblets are small flow aligned grooves created on a flow surface that alter the structure of the turbulence and reduce skin friction drag. Research has demonstrated (Lynch and Klinge[67], and Walsh[68]) that the optimum shape for riblets is a symmetric v-groove, the riblet appears to reduce the turbulent drag by thickening the viscous region near the wall and providing a 'slip layer' at the surface, giving an average drag reduction of approximately 7%. The application of riblets has been shown to reduce the drag on a supercritical airfoil at

transonic speeds by between 6～12% (Viswanath and Mikund[69]), and to reduce the drag of a nacelle at transonic speeds by up to 6.2% (Stockman et al.[70]).

Riblets are now available on a vinyl film with adhesive backing, and have been tested successfully on major components of the Airbus A320 and Boeing 757 aircraft, giving measurable fuel consumption reductions.

The optimum size of the riblets depends on Reynolds number and must be chosen appropriately for component length and operating altitude. This can cause conflicts when one considers that the aircraft must operate over a large range of Reynolds numbers. The solution would appear to be to optimise the riblets for cruise conditions, and in the case of the fuselage where Reynolds number varies considerably along its length, more than one riblet type must be used.

There are however a number of potential operational and application problems. The riblets themselves need to be aligned to within 10 degrees of the flow direction for them to be effective, and they also need to be kept sharp else their performance will degrade rapidly. The use of riblets on the wing and tail surfaces could present problems in terms of buffet, stall, and control effectiveness, all of which will need to be researched thoroughly before riblets may be used in these areas. It is also apparent that riblets can be irreparably damaged by many of the fluids used in aircraft maintenance.

The time of application of the riblet film is also a major drawback. It has been estimated that to cover three quarters of an MD-11 aircraft with riblets would take 1000 man hours (Lynch and Kynge[67]). With little information on riblet lifetime, riblet application, riblet replacement, and the large expense of the riblet material, there is at the present time no economic benefit associated with the use of riblets. However, future advancements in these area could lead to the 6% drag reductions becoming a reality.

3 .4 .9 Large Eddy Breakup Devices

Large eddy breakup devices are thin plates or small airfoils immersed within the turbulent boundary layer. They work by altering the structure of the turbulence in such a way as to produce a net drag reduction. Hefner[71] and Anders[72] have both observed skin friction drag reductions of the order of 10%.

These devices are still however at a very early experimental stage, and one can see no immediate likelihood of their inclusion on production aircraft.

3 .4 .10 VARIABLE CAMBER WINGS

The wings of modern civil aircraft must be designed to operate in a wide range of conditions. Lift coefficients can range from the order of 0.5 to the order of 2.5, while flight loads can vary from 1g at cruise to 2.5g or above for manoeuvres. The problems of gust alleviation must also be addressed. This means that the final design of the wings must be a compromise design that satisfies all of the flight criteria, this compromise usually means optimising the wing lift distribution for one particular cruise lift coefficient.

A solution to this problem would be to allow the wing to change its geometry in both the chordwise and spanwise direction, as deemed necessary by the flight conditions. The first approach to achieving this kind of wing uses a flexible skin to deform the wing and to alter its properties.

3 .4 .10 .1 Flexible Skin Adaptive Wing

Research has been conducted by Austin and Nostrand[73] on models of an active rib for an aircraft wing. The model consists of series of actuators and a flexible skin. Results showed that control laws could be created that could accurately deform the surface to the desired shape. However, this kind of approach is far from being a reality, with major question marks over the internal complexity of such a system, and the kind of materials required to form such a flexible yet tough surface. The weight increment associated with such a system is also a point of major concern.

3 .4 .10 .2 Multi-Element Airfoils

A far more attractive prospect than a flexible skin approach, is that of using trailing edge and leading edge devices to vary the camber of the airfoil. Research published from Cranfield Institute by Rao[74], Spillman[75], Fielding et al.[76], as well as NASA research by Hilbig and Koerner[77], and Airbus research by MBB[78], indicate that this kind of approach to variable camber wings has a large potential for increasing the efficiency of future aircraft, without needing to change the design of existing wing box sections. This variable camber approach has advantages in both two-dimensional performance as well as three-dimensional.

Two Dimensional Variable Camber

There are a number of possible configurations of a variable camber system consisting of various trailing edge and leading edge pieces with stiff and flexible surfaces. The general operation of the system though is illustrated below by the variable camber system designed by Rao[74].

The forward camber is achieved using a leading edge element attached to the spar at the 20% chord position. This element travels in a circular arc, maintaining a smooth

junction between itself and the centre section. The effect of the leading edge droop is to avoid large leading edge suction peaks at high lift coefficients. The leading edge element is designed such that the inclusion of a leading edge slat would be possible.

The trailing edge element is attached to the main centre section at the 60% chord location. The element is deployed along a circular arc pathway, thus keeping the surface curvature constant. The system described by Fielding at Al[76] also contains an upper flexible closing plate, and a lower solid closing plate, to keep the surface continuous during the translational motion of the trailing edge element.

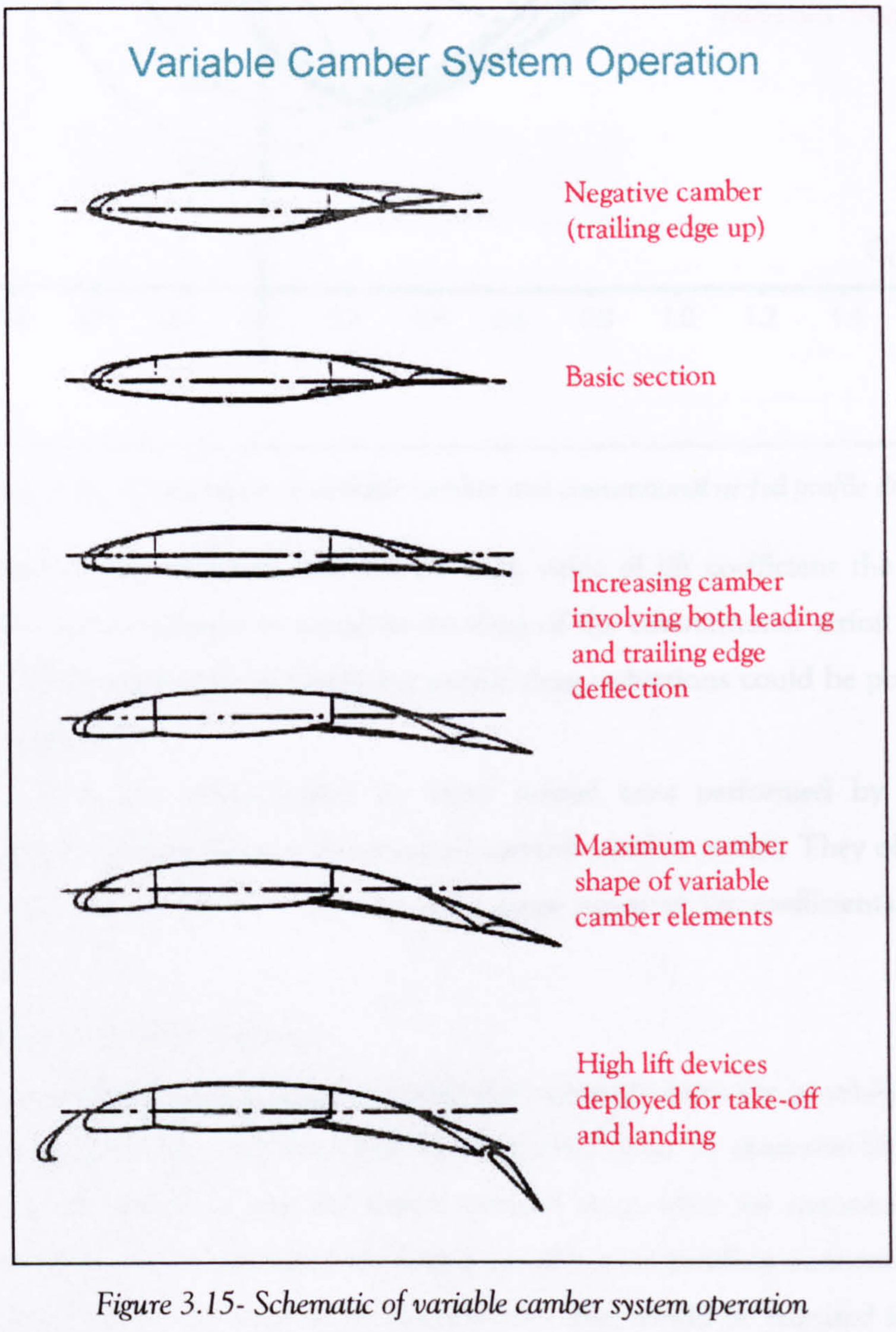


Figure 3.15- Schematic of variable camber system operation

For an airfoil of given thickness there is a particular lift coefficient which corresponds to its minimum drag. This lift coefficient varies with the camber of the airfoil. This means that by varying the camber of the airfoil it is possible to minimise drag over a range of lift coefficients. The diagram below (from Rao[74]), illustrates the results of wind tunnel tests of various camber configurations.

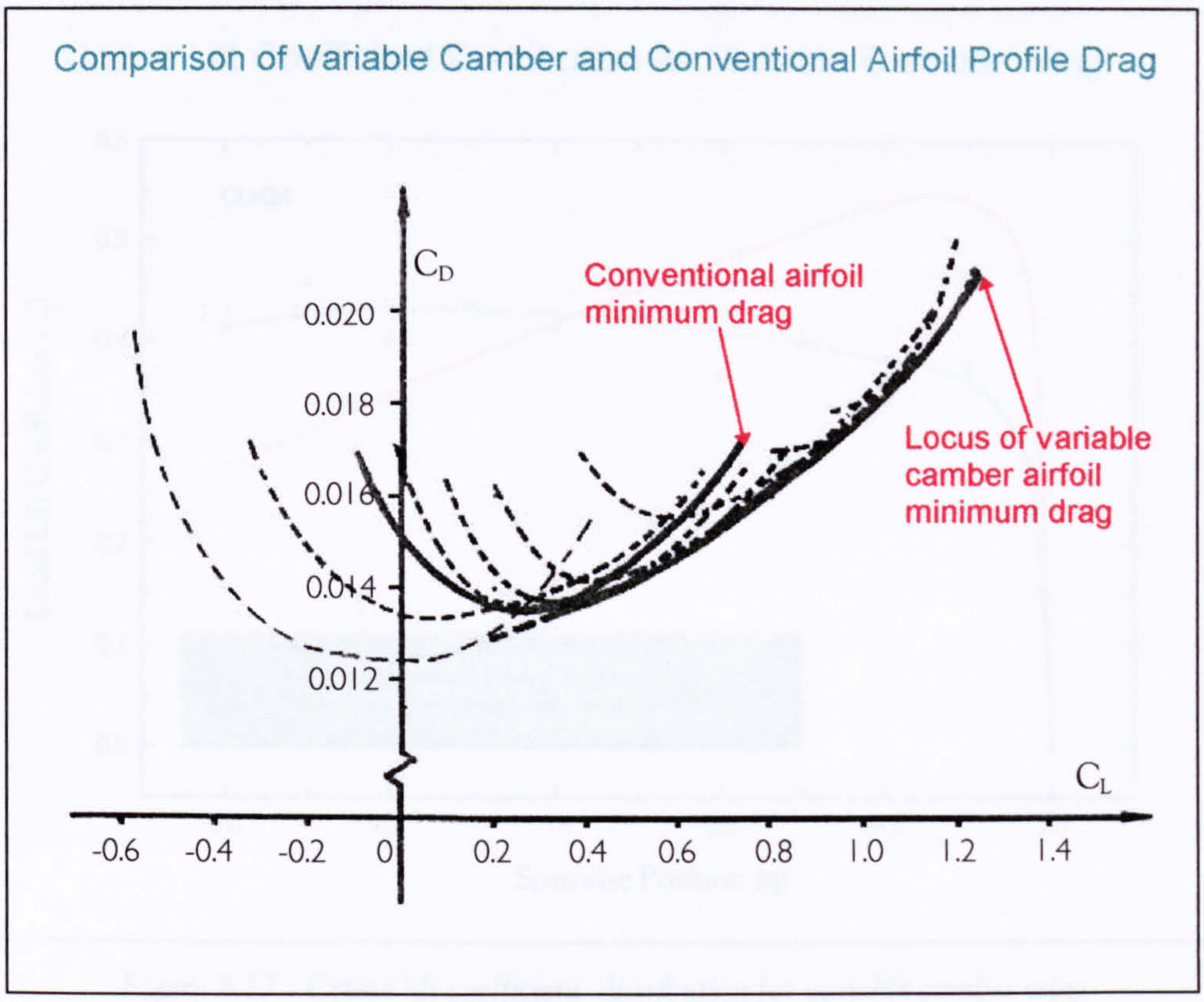


Figure 3.16 - Comparison of variable camber and conventional airfoil profile drag

The graph clearly indicates that the for each value of lift coefficient the drag of the variable camber airfoil is lower or equal to the drag of the conventional airfoil at the same lift coefficient. This suggests that significant profile drag reductions could be possible under most flight conditions.

These results are substantiated by wind tunnel tests performed by Hilbig and Koerrner[77], using a very similar two dimensional variable camber model. They observed very significant increments in lift to drag ratio for a large range of lift coefficients, at a Mach number of 0.82.

Three Dimensional Variable Camber

Splitting the wing into independent spanwise segments gives the possibility of further optimising the wing for all conditions. For 1g flight conditions the spanwise lift distribution of the wing can be altered to give the lowest induced drag, while for manoeuvre and gust conditions the wing can be optimised for lowest possible root bending moment. The figures below (from Rao[74]) show the kind of lift distributions that would be required for these two different conditions, and compares them with those of existing aircraft, and a computational analysis of the distributions attainable with the spanwise camber model devised by Rao[74].

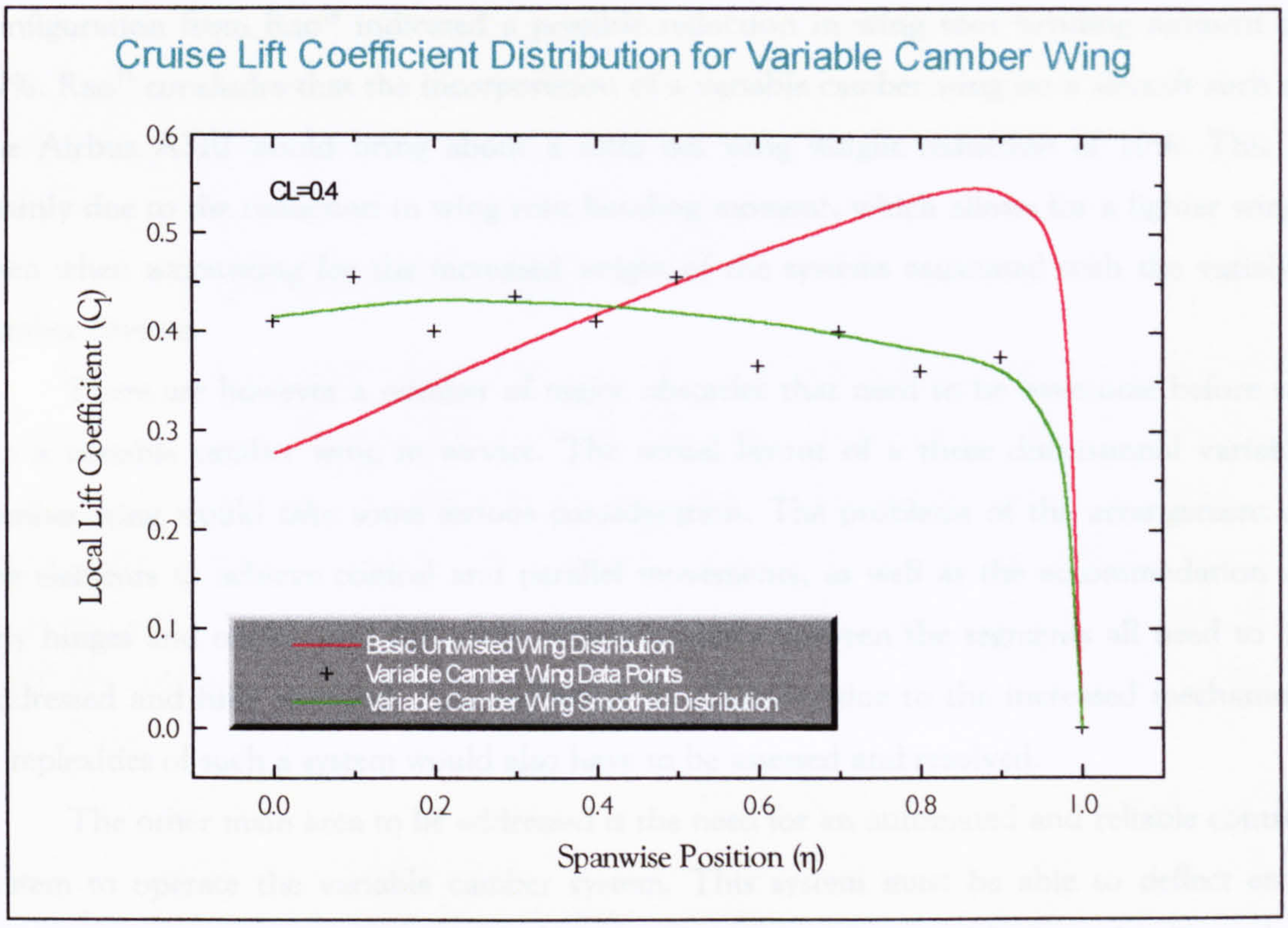


Figure 3.17 - Cruise lift coefficient distribution for variable camber wing

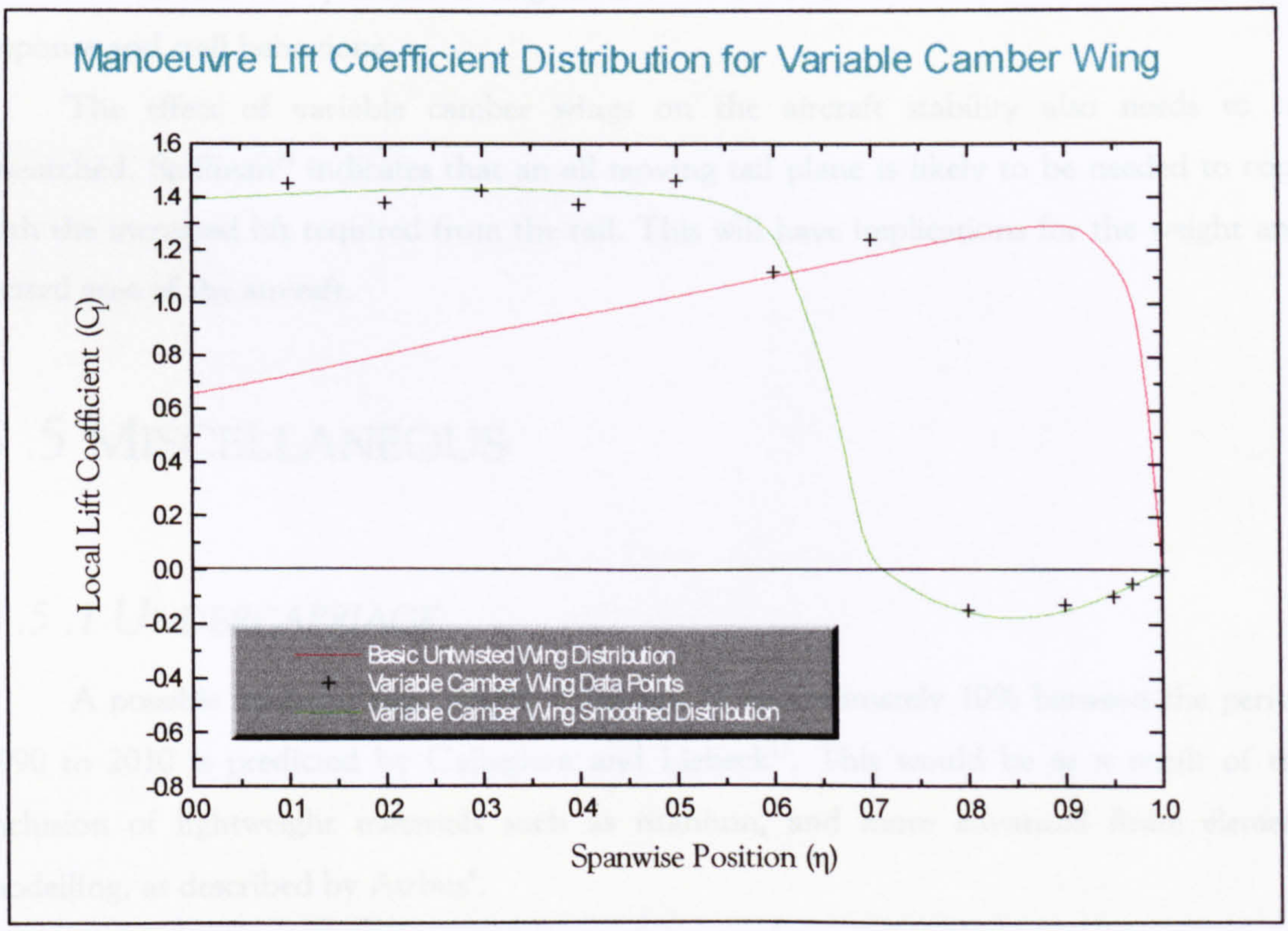


Figure 3.18 - Manoeuvre lift coefficient distribution for variable camber wing

Wind tunnel tests on independent spanwise variable camber models by Rao[74] and Fielding et al.[76] have provided encouraging results. Although the cruise configuration drag results produced by Rao[74] were inconclusive, the results produced by Fielding et al.[76] showed potential drag reductions for lift coefficients above 0.42. The results of the manoeuvre wing

configuration from Rao[74] indicated a possible reduction in wing root bending moment of 29%. Rao[74] concludes that the incorporation of a variable camber wing on a aircraft such as the Airbus A310 would bring about a total net wing weight reduction of 10%. This is mainly due to the reduction in wing root bending moment, which allows for a lighter wing, even when accounting for the increased weight of the systems associated with the variable camber devices.

There are however a number of major obstacles that need to be overcome before we see a variable camber wing in service. The actual layout of a three dimensional variable camber wing would take some serious consideration. The problems of the arrangement of the elements to achieve conical and parallel movements, as well as the accommodation of any hinges and tracks, and the effect of discontinuity between the segments all need to be addressed and fully resolved. Any reduction in reliability due to the increased mechanical complexities of such a system would also have to be assessed and resolved.

The other main area to be addressed is the need for an automated and reliable control system to operate the variable camber system. This system must be able to deflect each portion of the wing dependent on the flight conditions at that time. Much work will need to be done to assess the optimum setting at each condition, and to allow for adequate gust response and stall behaviour.

The effect of variable camber wings on the aircraft stability also needs to be researched. Spillman[75] indicates that an all moving tail plane is likely to be needed to cope with the increased lift required from the tail. This will have implications for the weight and wetted area of the aircraft.

3 .5 MISCELLANEOUS

3 .5 .1 UNDERCARRIAGE

A possible undercarriage weight reduction of approximately 10% between the period 1990 to 2010 is predicted by Callaghan and Liebeck[17]. This would be as a result of the inclusion of lightweight materials such as titanium, and more advanced finite element modelling, as described by Airbus[4].

3 .5 .2 ADVANCED FUELS

There will in the future need to be a move away from petroleum based fuels as the supply of this type of fuel begins to expire. The main contenders to replace traditional

aviation fuels are synthetic kerosene, cryogenic methane, and cryogenic hydrogen. Conner et al.[32] suggest that the know how is already in place for the use of these fuels, and their performance could at least equal that of traditional fuels, especially for long range aircraft.

3 .5 .3 Systems and Avionics

Great advances have already been made in areas such as fly-by-wire and active centre of gravity control on the new Airbus aircraft. The use of these technologies allows the static margin to be actively controlled and the trim drag to be correspondingly reduced. The further reliance on computers in future aircraft may see the longitudinal stability relaxed to such an extent that the aircraft is in fact unstable, as with modern fighter aircraft. This could give potential reductions in drag of the order of up to 4% (Rising et al.[79]), due to reduced control surface area, and reduced trim drag.

Other possible improvements could come in the form of advanced electrical power systems, designed to replace hydraulic and pneumatic secondary power systems. Murray et al.[80] concluded that this replacement could save 5.5% of total takeoff weight of an MD-11 aircraft.

The increased use of fibre optics in the distribution of avionics could also be a source of weight savings, with potential savings of up to 50% of the total systems and avionics weight (Callaghan and Liebeck[17]).

4 .Program Overview

4 .1 The Aircraft Design Process

The process of the design and production of a new aircraft is a long and complex one. The period from its first conception to its final realisation can span the best part of a decade, and will involve interaction between many teams of engineers and designers of various disciplines. The impetus for a new civil aircraft will usually stem from the capacity needs of the major airlines, who will specify a set of design requirements. The main requirements will invariably be related to the range and payload of the aircraft, with secondary requirements including takeoff and landing distances, passenger comfort levels, airport compatibility, and operating efficiencies. As well as meeting the demands of the customer, an aircraft design must comply with the safety and environmental regulations laid down by the aviation authorities. The most critical of these regulations are those pertaining to passenger evacuation, reserve fuel policies, engine emissions, and aircraft noise. The complete design process can be split into three main phases:-

Conceptual Design

The purpose of the conceptual design phase is to establish a baseline configuration for the aircraft which can then be refined in later design phases. It is in this initial phase of the design process that innovative ideas can be proposed and the feasibility of these ideas evaluated. Many configurations can be examined in an attempt to meet the design requirements in the most efficient and effective manner, these configurations are then evaluated and refined or discarded accordingly.

The evaluation of a concept will be carried out using some theoretical methods, but mainly using empirical or semi-empirical techniques based on, and proven to work with past aircraft designs. Using this approach it is possible to evaluate the main properties of the design, including aerodynamics, weights, geometry, performance, and stability, to a relatively high degree of accuracy. A margin of error in the region of 10% would be a reasonable outcome for this type of design work.

Ever since the late 1930's aircraft designers have realised the importance of producing baseline designs during the conceptual design process that are as close to optimal as possible. Now with the advent of modern computers it is possible to evaluate a virtually unlimited number of possibilities, and to isolate the best configuration as a baseline for the next stages of the design process.

Preliminary Design

Once the general features of the aircraft have been selected, the design teams can begin to fine tune the design and to turn their attention to the more detailed aspects of the aircraft. This will include more thorough analysis of structures, landing gear, control systems, aerodynamics, stability, economics, and production methods.

More theoretically based methods will be utilised in this phase of design evaluation, with computational fluid dynamics and finite element analysis techniques being used extensively to estimate the aerodynamic and structural performance of the aircraft.

It is at this stage of the design process that models and mock-ups will be built of the aircraft, to test its aerodynamic properties in the wind-tunnel, and to assist with its structural and material design. The aircraft may also be 'lofted', this ensures that the aircraft geometry is producible, fits together correctly, and allows for acceptable installation of the aircraft's internal features.

Detailed Design

At the end of the preliminary design phase, the aircraft's specification will be 'frozen', this means that no further changes are made to the geometry or parameters of the design. This final phase of the design process deals with all the fine detail necessary to manufacture the aircraft. This will include detailed drawings of each component to be built, the individual ribs, spars, and skins in the case of the wings, or the stringers, longerons, and frames in the case of the fuselage. A program of testing of the major items of the aircraft will be initiated, and compatibility with safety regulations confirmed.

The manufacturing processes and tools necessary to produce the components will be addressed, and any implications of necessary modifications will be evaluated. The computer systems of the aircraft will be designed, with the control laws for the flight navigation systems being assessed on a flight simulator. The process will be completed with the construction of the aircraft.

4 .2 THE AIRCRAFT DESIGN PROGRAM

4 .2 .1 OBJECTIVES

The three main phases of the design process described above are now almost exclusively carried out with the aid of computers. This does not mean however that there is no longer a place for the skilled design engineer. A skilled engineer can use his judgement

and knowledge to make important design decisions and to steer a design to a more effective and realistic optimum.

The work described herein concentrates on the creation of an automated design synthesis for use in the conceptual phase. Whilst the accuracy of any conceptual design must be as high as possible, it is of equal if not greater importance that the design reflects correctly the effects of any variations in input parameter, technology level, and configuration. The reason for this being that the baseline design produced by the conceptual process should be as close to the optimum as possible, as the details of this design can be refined and calculated to a higher degree of accuracy during the preliminary design process.

The finished software package should not be limited in its applicability to a small number of designs within the passenger aircraft field, but be flexible enough to deal with a wide range of aircraft. This flexibility, along with the inclusion of a user friendly interface and comprehensive analysis tools means that the scope of the program should be broad enough to encourage users from both educational and professional establishments.

With these points in mind, the Aircraft Design program was written with a number of definite goals in mind:-

- To provide accurate results of the conceptual design phase.
- To allow the design of candidate configurations for next generation UHCA.
- To allow the incorporation of advanced technologies into the aircraft.
- To provide a platform for quantitative comparison of the effects of these technologies
- To utilise a minimised set of input data.
- To minimise any conceptual design guesswork.
- To provide an integrated design & analysis environment.
- To operate from a user friendly interface, compatible with Microsoft Windows®.
- To allow complete freedom and flexibility within the design environment.

4 .2 .2 PROGRAM METHODS

The program was written using Microsoft Visual Basic version 3.0. Visual Basic proved to be an intuitive and easy to use language, and was an excellent choice for designing a Windows® program of such complexity. The completed program consists of approximately 80,000 lines of code, with most of this code (63,000 lines) being related to the operation of the design environment and tools, with the remaining 17,000 lines being responsible for the actual design calculations. The compiled program exists in the form of a standard Windows® executable, with versions available that are compatible with both Window 95 and Windows 3.1x. The complete environment is installed from a custom written setup interface, and occupies 4 installation disks (including design examples).

The program has been compiled using Visual Basic versions 4 and 5, but although these newer development kits provided extra features, the speed of execution of the Aircraft Design program was reduced. It was therefore decided to continue to use Visual Basic version 3.0

The program itself can be split in two main areas of functionality, the design environment and analysis tools, and the design calculations. These are described separately below.

4 .2 .2 .1 The Design Environment & Analysis Tools

The format of the Aircraft Design environment will be familiar to most Windows users. Each window within the environment is made up of standard windows controls such as scroll bars, spin boxes, list boxes, and dialogue boxes. All of the sub-windows are contained within one main Aircraft Design window, and each design is treated as a self-contained document. This document contains all the relevant input, output, and unit data for a particular aircraft design. It is possible to open up to twenty documents simultaneously, and for these documents to be directly compared, either graphically or numerically.

The program gives the user the complete freedom within the environment to open as many windows at one time as necessary, and for the contents of these windows to be customised as required. Each window may be tailored in terms of the size of the window, the document displayed, any method of comparison of the data displayed, the units of the data, and the size and axes of any graphs.

A parameter may be input in a number ways, by typing the number directly, by using the spin box to increase or decrease its value, or by using the cut, copy, and paste facilities to transfer the values from another document.

Although each window can be manipulated independently of the others, the windows are all in fact integrated internally into the Aircraft Design environment. Any change in parameter value or document property in one window is automatically updated in every other relevant window. Similarly, when a set of calculations is performed on a particular document, all relevant windows are updated with the new data values.

Analysis of the data is simplified with the inclusion of a mathematical language written specifically for the Aircraft Design program. Each parameter within the design calculations is given a variable name, and these names can be combined with mathematical functions and operators to create complex user defined expressions. It is even possible to refer to expressions or variables created by the user in other parts of the Aircraft Design environment. These expressions can then be used as part of the complex analysis techniques associated with the Correlation, Optimisation, Trade Off, and Sensitivity windows. Writing the interpreter routines responsible for evaluating these mathematical expressions proved to

be a major challenge. However, the completed expression interpreter can evaluate expressions with up to 20 levels of parenthesis, and containing any combination of mathematical and trigonometric functions.

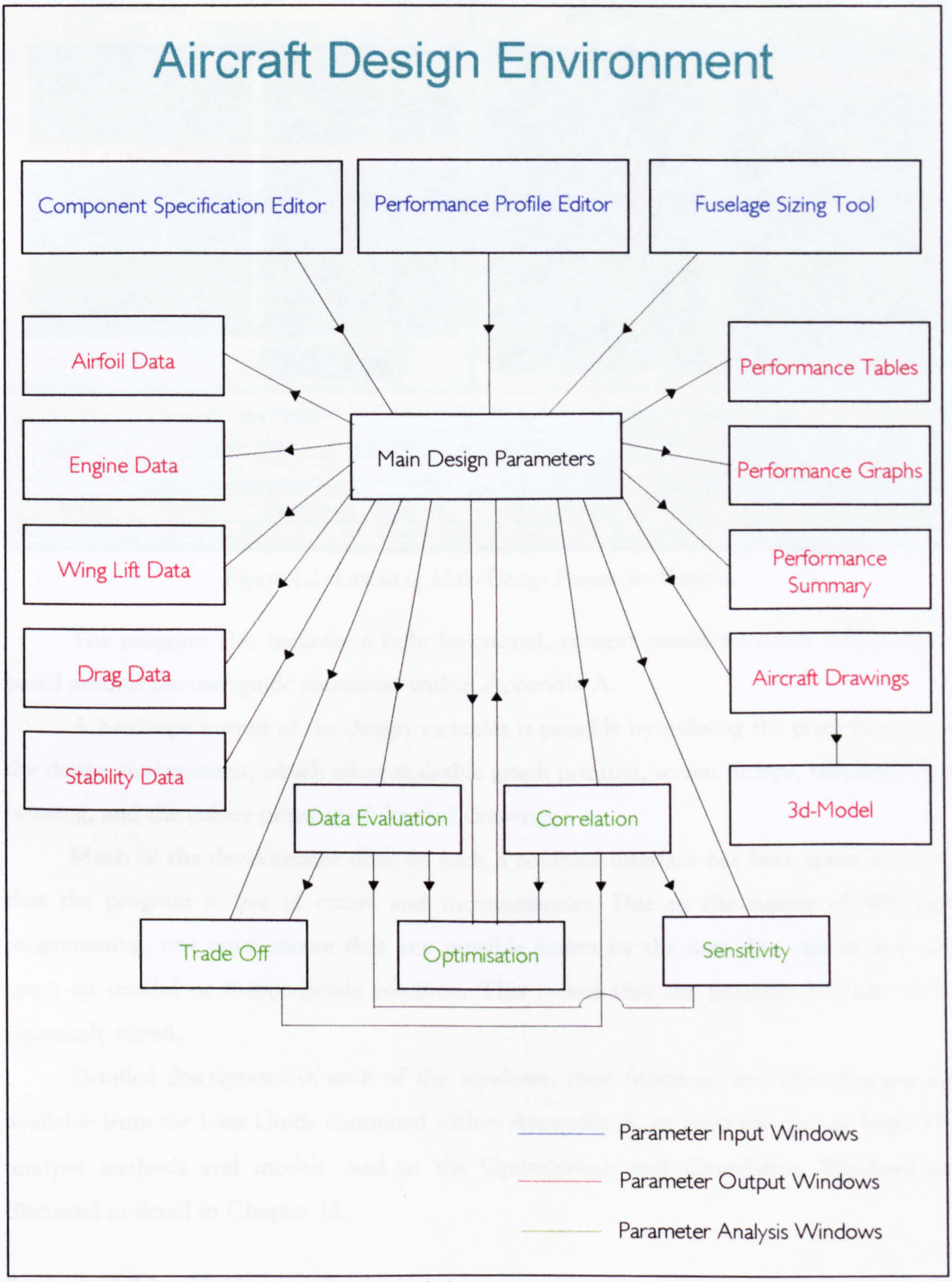


Figure 4.1- Aircraft design environment flow chart

A schematic of the design environment, and the relation of each main window to each other is shown above. The Main Design Parameter Window is the window that automatically appears when a document is opened, and is the window from which all others are launched. The format of this window is shown below in figure 4.2.

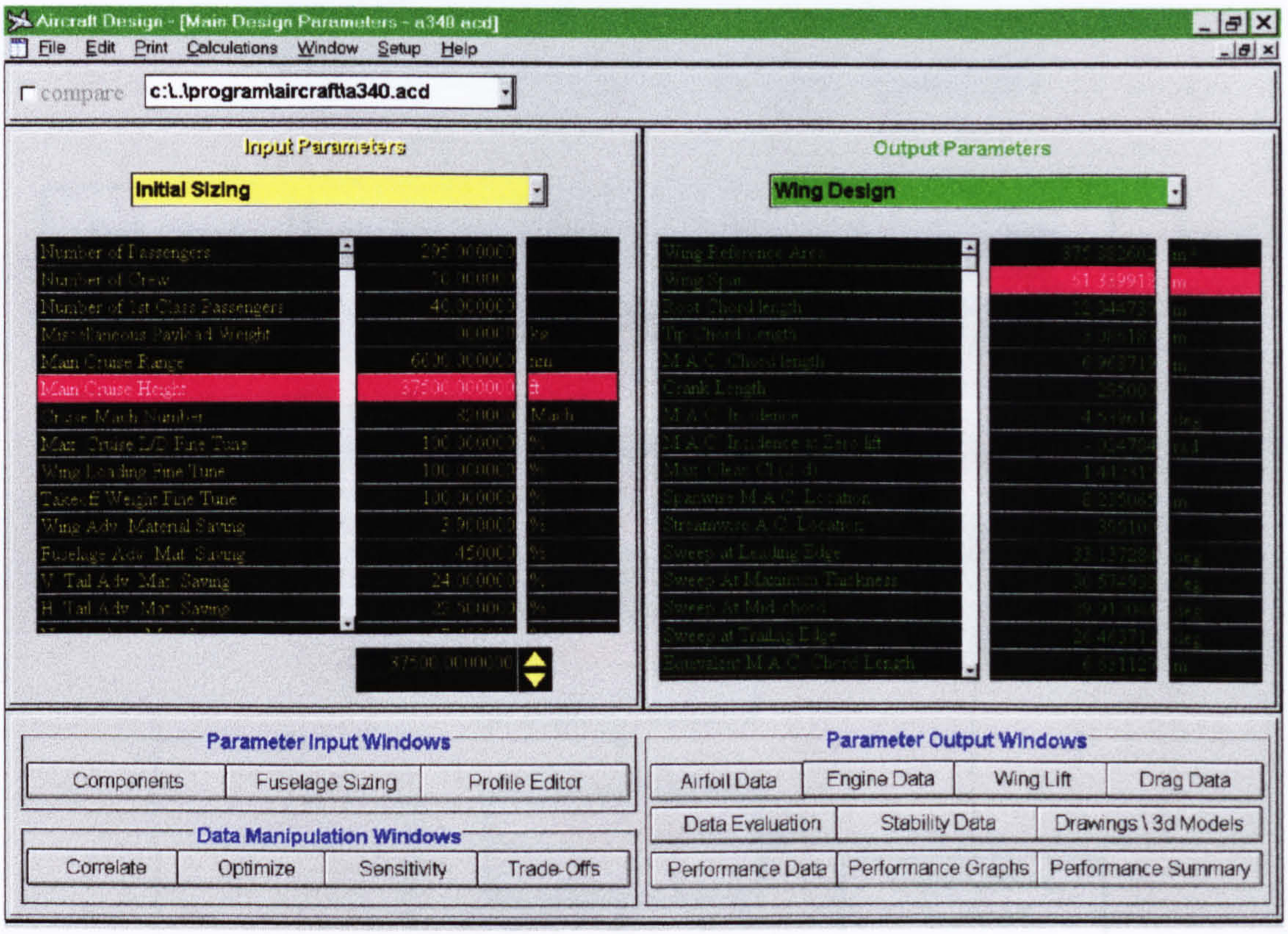


Figure 4.2- Layout of Main Design Parameter Window

The program also includes a fully functional, context sensitive on-line help feature, based around the user guide contained within Appendix A.

A hardcopy output of the design variables is possible by utilising the print features of the design environment, which allow scaleable graph printing, screen dumps, tabulated data printing, and the colour printing of detailed drawings.

Much of the development time on such a complex interface has been spent ensuring that the program is free of errors and inconsistencies. Due to the nature of Windows programming, one must ensure that any possible action by the user does not in any way cause an invalid or inappropriate response. This means that the program has had to be rigorously tested.

Detailed descriptions of each of the windows, their function, and their features are available from the User Guide contained within Appendix A, or from the on-line help. The analysis methods and models used in the Optimisation and Correlation Windows are discussed in detail in Chapter 13.

4 .2 .2 .2 The Design Calculations

The design calculations can be performed at any time on the currently selected document, from almost any window within the design environment. The complete calculations have been split into a set of 8 modules, with each module having its own set of input and output parameters. The modular nature of the program is represented below:-

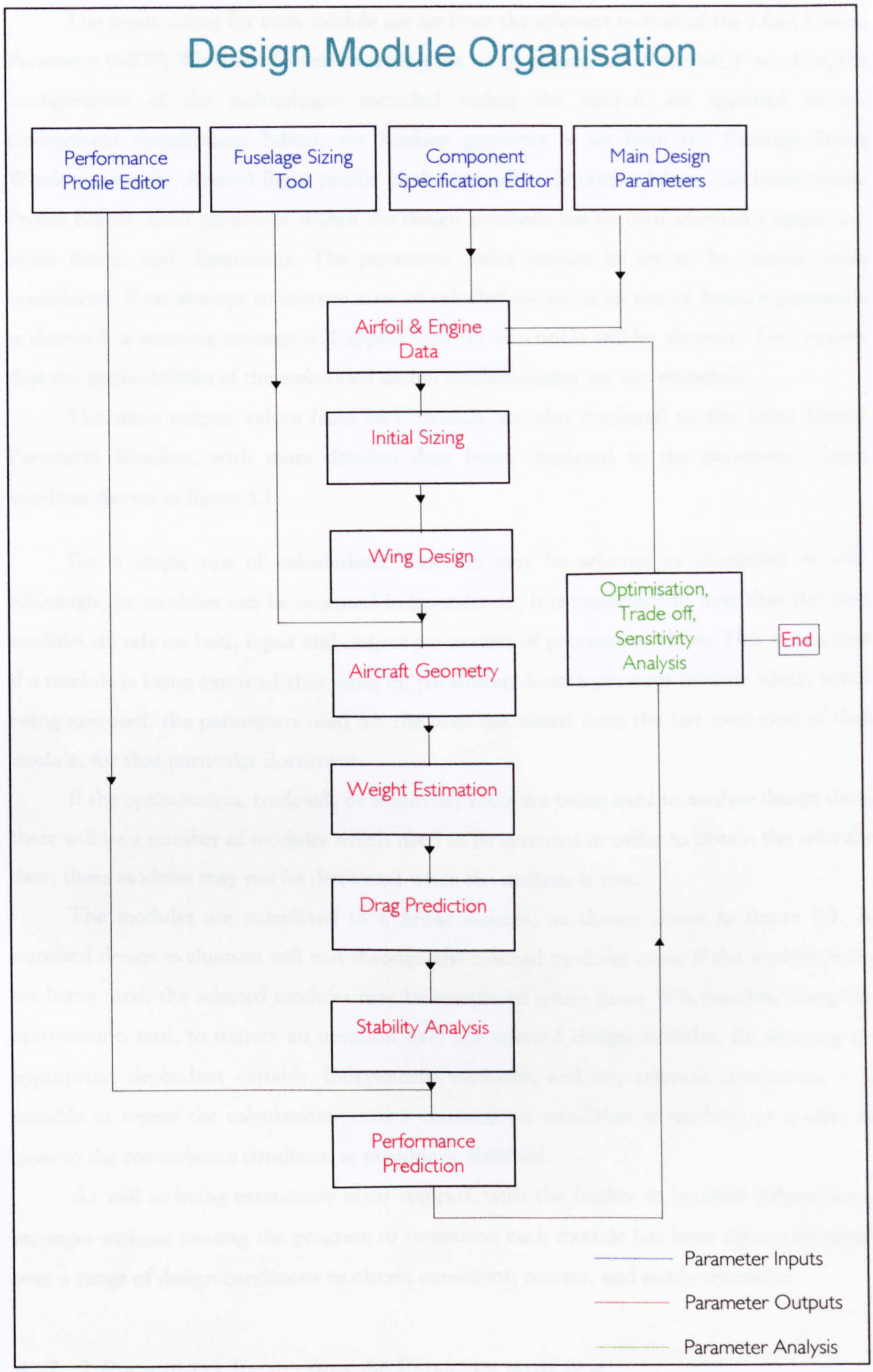


Figure 4.3 - Aircraft design module flow chart

The input values for each module are set from the relevant section of the Main Design Parameter (MDP) Window. As well as setting the input parameters in the MDP window, the configuration of the technologies included within the aircraft are specified in the Component Specification Editor, the fuselage geometry is set from the Fuselage Sizing Window, and the detailed flight profile of the aircraft is determined from the Performance Profile Editor. Each parameter within the design synthesis has its own associated upper and lower limits, and dimensions. The parameter value cannot be set to be outside these boundaries. If an attempt to execute a set of calculations using an out of bounds parameter is detected, a warning message will appear and the execution will be aborted. This ensures that the applicabilities of the embedded design methodologies are not exceeded.

The main output values from each module are also displayed in the Main Design Parameter Window, with more detailed data being displayed in the parameter output windows shown in figure 4.1.

For a single run of calculations, modules may be selected or deselected at will. Although the modules can be executed independently, it is important to note that the later modules do rely on both input and output parameters of previous modules. This means that if a module is being executed that relies on parameters from a previous module which is not being executed, the parameters used are the ones calculated from the last execution of that module, for that particular document.

If the optimisation, trade-off, or sensitivity tools are being used to analyse design data, there will be a number of modules which need to be executed in order to obtain the relevant data, these modules may not be deselected when the analysis is run.

The modules are completed in a linear fashion, as shown above in figure 4.3. A standard design evaluation will run through the selected modules once, if the analysis tools are being used, the selected modules may be completed many times. It is possible, using the optimisation tool, to imitate an iteration over the selected design modules. By selecting an appropriate dependent variable, independent variables, and any relevant constraints, it is possible to repeat the calculations until a convergence condition is reached, or a state as close to the convergence condition as possible is obtained.

As well as being extensively error trapped, with the facility to produce helpful error messages without causing the program to terminate, each module has been rigorously tested over a range of design conditions to obtain consistent, correct, and stable operation.

4 .2 .3 PROGRAM FEATURES & FUNCTIONALITY

The completed program fulfils and surpasses all of the main objectives laid out in section 4.2.1. The main features and functions of the program are discussed below.

4 .2 .3 .1 Design Features

As discussed later in Chapter 14, the design modules produce consistently accurate results for designs ranging from 100 passenger aircraft up to and above 1000 passenger aircraft.

The program allows the incorporation of advanced technologies such as laminar flow control, variable camber wings, riblets, extensive use of composite materials, and ultra high bypass ratio engines. Each technology is easily setup with only a few parameters needing to be specified, and the impact of the technology on each aspect of the aircraft design is estimated and appropriately assessed.

The Fuselage Sizing Window (figure 4.4) provides a fully automated and powerful tool for determining the internal and external layout of a transport fuselage. The seat sizes, seat pitch, and horizontal arrangement must be specified for each class, and from this the program automatically calculates and draws the required fuselage and its internal layout, including galleys, toilets, and emergency exits. A number of fuselage styles are available, including an ovoid double deck, a '747' type fuselage with an upper deck part of the way along the fuselage, a horizontal double bubble, and a vertical double bubble.

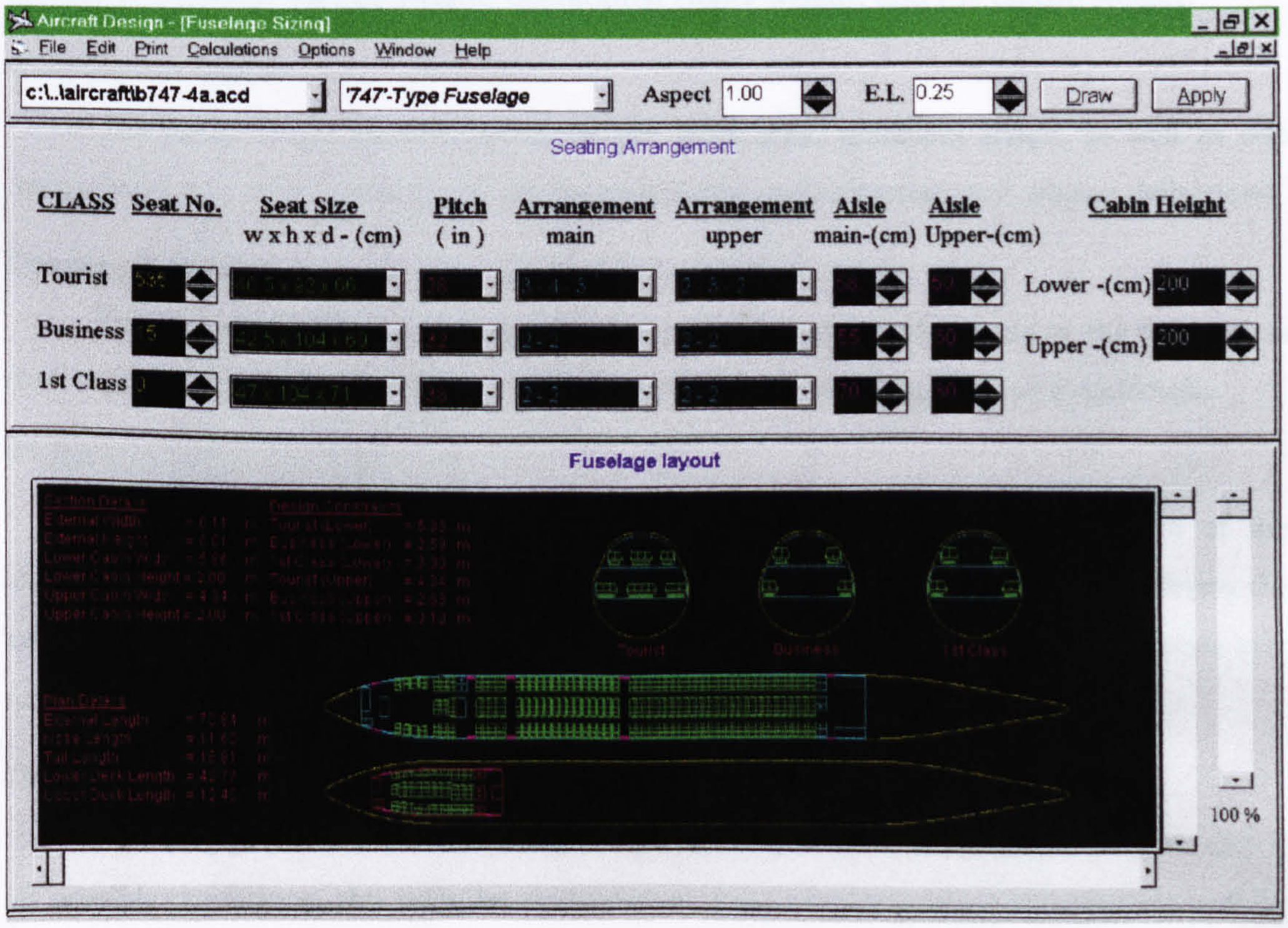


Figure 4.4 - Screen-shot of Fuselage Sizing Window

Much of the guesswork involved in the aircraft design has been partly removed by the introduction of empirical estimates of crucial design parameters such as wing loading, and tail volume coefficients. The program will make an estimate of these parameters using

correlations based on a database of previous aircraft designs and including any adjustments due to the incorporation of advanced technologies. If the user is not satisfied with the estimate, the value may be altered by making use of the 'tuning factors' associated with these variables. Although normally these tuning factors can be set to their default value of 100%. This kind of approach, and the use of intelligent programming to concentrate effort on the key design areas, leads to a much reduced set of input parameters, compared to the numbers normally associated with this kind of synthesis. In total there are only 88 input parameters which need to be set to give a full aircraft design.

The function of each design module corresponds to one of the main conceptual design disciplines for a civil aircraft. The function of each module is briefly described below:-

Airfoil & Engine Module

The Airfoil & Engine module simply creates a suitable data set for the airfoils and engine selected for the particular calculations.

Initial Sizing Module

The main function of the initial sizing module is to provide target estimates of the maximum values of the fuel weight, operational empty weight, and the takeoff weight.

Wing Design Module

The wing design module calculates the wing area, planform shape, as well as two dimensional and three dimensional lift characteristics, including flap and aileron deflections.

Geometry Module

The geometry module is concerned with calculating the surface area of the fuselage, as well as the size and shape of the nacelles, and other geometric properties of the aircraft.

Weight Estimation Module

The weight estimation module produces detailed weight estimates of most of the aircraft components, calculates the centres of gravity of these components, and performs the tail sizing iteration. This module also calculates the geometry and the drag of the main and nose undercarriage components.

Drag Prediction Module

The drag prediction module is responsible for producing a 'map' of the aircraft drag at all possible conditions, this includes skin friction drag, transonic drag, lift dependent drag, and drag due to flaps.

Stability Module

The stability module is concerned with static longitudinal stability only, and creates the data necessary for a trim plot, static margin and trim drag analysis.

Performance Module

The final module is the Performance module which brings all the previous elements together to accurately predict the range, fuel consumption, and takeoff and landing distances of the aircraft. The flight profile is entered in the Performance Profile Editor. The flight may be made up of any combination of segments such as 'Cruise', 'Climb', 'Loiter', and all other types of segment that would be encountered in a transport aircraft flight. A number of parameters must be set to numerically describe each segment adequately. This profile is then followed using a step-by-step iteration approach in the Performance Module. Each segment is split into a number of steps and each variable encountered during the flight such as s.f.c., lift, drag, and thrust are accurately modelled at each point.

The output from the modules described above may be interactively viewed using the relevant output window. The main design variables with a single numeric value are displayed in the Main Design Parameter Window. More complex data, such as the drag polars for example, may be viewed in graphical form from within the Drag Data Window (figure 4.5). For the example of the drag polars, it is possible to use the window controls to view the data at any particular Mach number, lift coefficient, or altitude. The graph may also be customised, in terms of line style, axes, origin, and units, to suit the user.

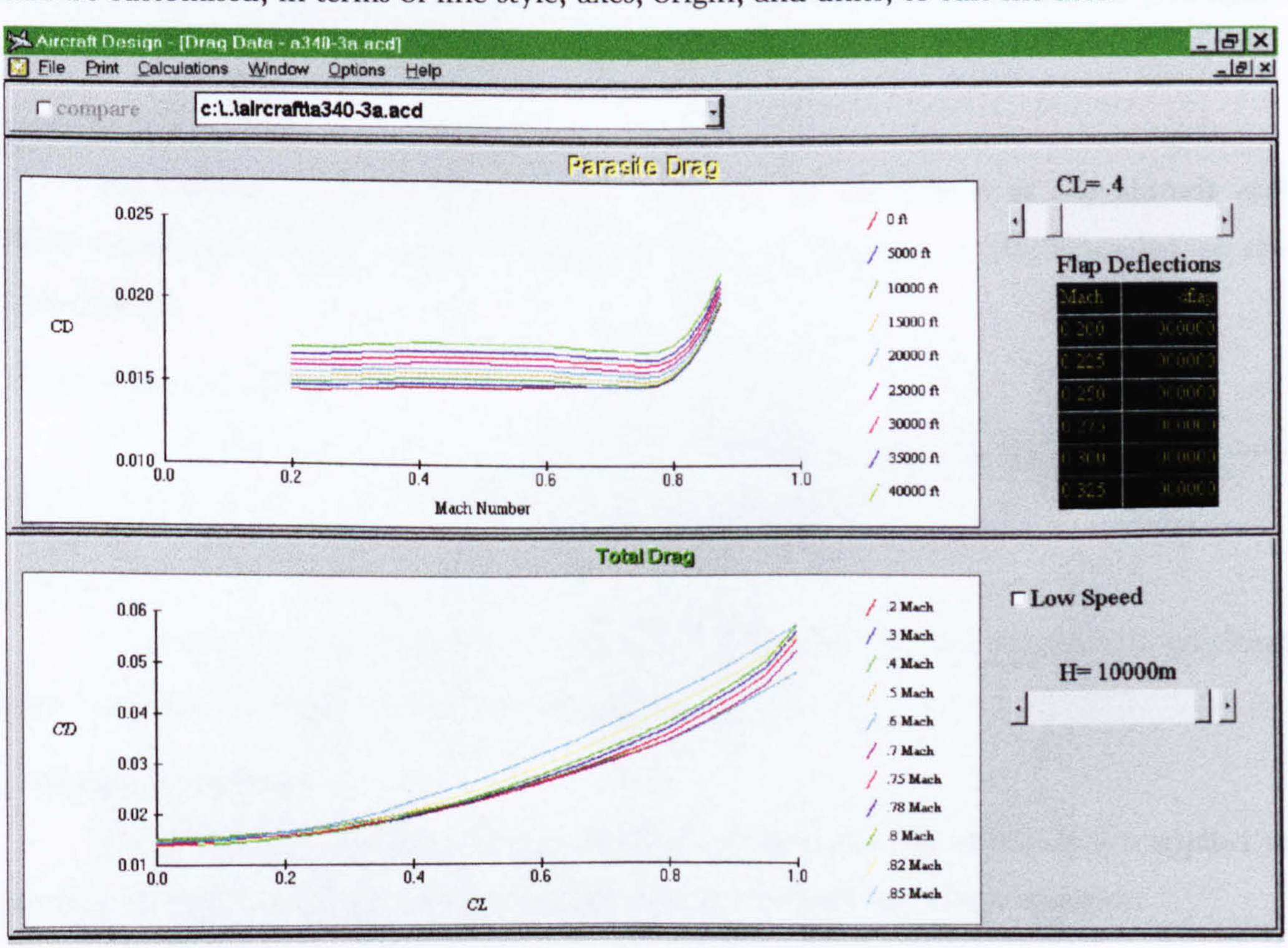


Figure 4.5 - Screen-shot of Drag Data Window

A full list of data display windows and their use is given below:-

Airfoil Data Window

This window displays the lift, drag, and pitching moment data for the selected root, tip, and tail airfoils that have been selected from the airfoil data library. The data can be presented at any chosen Reynolds number.

Engine Data

The engine thrust and fuel consumption data is displayed in this window. The thrust data can be displayed as either a thrust lapse or as an actual thrust value, at any altitude and Mach number, and for takeoff, climb, continuous power, cruise, and idle settings. Similarly the values of fuel consumption can be viewed for any altitude and Mach number, and can be expressed in terms of specific fuel consumption or fuel flow.

Wing Lift Distribution Window

The wing lift distribution at cruise conditions is plotted alongside the ideal elliptical lift distribution.

Drag Data Window

Both the parasite (skin friction) drag and the total drag including lift induced drag are plotted in this window. These drag curves can be viewed at any particular lift coefficient and altitude, and any flap deflections at the set values are calculated and tabulated. (See figure 4.5)

Stability Data Window

The stability data window provides a trim plot of the aircraft at any altitude and Mach number, as well as a graph showing the effect of altitude and Mach number on the static margin.

Performance Data Window

The detailed output from the performance calculations is tabulated, with the main flight variables at each step of the flight profile being displayed.

Performance Graphs Window

The detailed output from the performance calculations can be displayed in graphical form. The *x*-axis and *y*-axis functions can be set by the user.

Performance Summary

The performance output is summarised, and further analysis of the data is applied to provide information on the change of flight variables between each flight segment.

Drawings\ Models Window

A 3-view orthogonal drawing of the aircraft can be generated from within the Drawings\Model Window. Each drawing can be zoomed and panned independently, and

the option of including centres of gravity and the equivalent wing profile are also available. The drawings show the main features of the aircraft and are updated automatically when any feature is altered.



Figure 4.6 - Rendered image of design based on Deutsche Airbus 702 concept

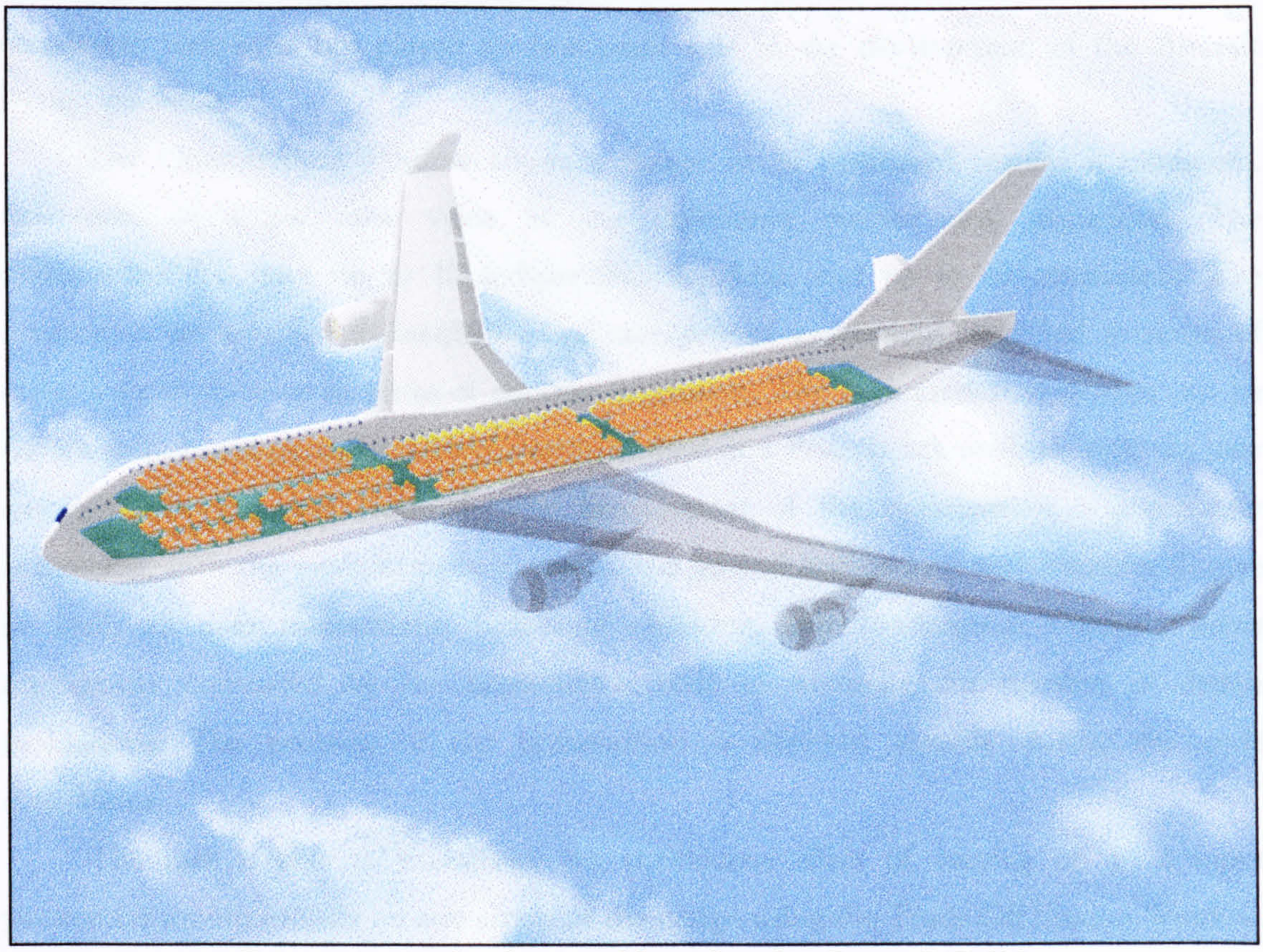


Figure 4.7 - Rendered image of design based on Boeing 747-600

It is also possible to create a highly detailed three dimensional mesh of the aircraft. A file can be generated which can be automatically interpreted by AutoCAD to produce a three dimensional model of the aircraft, including such details as seats, windows, flaps, and cabin floors. The model may then be rendered to produce results such as the drawings shown above in figures 4.6 and 4.7. It is important to note that a licensed copy of AutoCAD version 12 or later must be available.

4 .2 .3 .2 Analysis Features

Much emphasis has been placed on the ability to analyse designs within the Aircraft Design environment. Each data window has the ability to compare two or more designs. The graphical based windows can compare all the open documents on the same graph, which can be plotted in terms of absolute values or values relative to a chosen baseline design. Text based windows can compare the data of two designs, using either a subtraction or division algorithm.

Further analyses can be performed from the four data manipulation windows, which all utilise with the expression interpreter described previously. The Correlation Window allows the user to investigate the relationships between up to fifteen user defined expressions for all open documents. The values of the expressions can be plotted in any combination, and a suitable line fit can be automatically calculated from a comprehensive set of line fit functions. The line fit method is based upon the Gauss-Jordan elimination technique. This correlation technique has played an important role in the development of the Aircraft Design synthesis.

The Optimisation Window allows a design to be optimised toward a minimum, maximum, or a particular value of any dependent mathematical expression. The optimisation can have up to 10 independent variables, and up to 10 constraints. The constraints are specified as inequalities of user defined expressions, specified in terms of either a fixed value or in terms of another expression. The optimisation algorithm can be chosen to be based on either a Hook-Jeeves method or a Rosenbrock method, with the user specifying the accuracy required. The management of the optimisation is completely automated, with the modules to be executed, the goal of any performance iteration (Range or fuel), all data transactions, constraint checking, and convergence checking being intelligently controlled by the optimisation code to minimise the number of design evaluations. The progress of the optimisation is depicted visually during the code evaluations.

The user is able to investigate the continuous effect of varying up to 2 input parameters simultaneously on any aspect of the design using the Trade Off Studies Window.

The trade off parameters are varied a discrete number of steps, between a lower and upper limit, as set by the user, and the design is evaluated at each point. The design variables at each point are then stored by the program, and expressions can be evaluated and plotted for each combination of parameters in the trade off study.

The Sensitivity Window can be used to estimate the dependency of up to 10 user defined expressions on up to 10 independent input parameters. Once the dependent expression, and the independent variables are set, a coefficient will automatically be calculated, which reflects the strength of the inter-dependency between the value of the expression, and the value of the parameter. This can be particularly useful when considering candidate variables for optimisation.

4 .2 .3 .3 Summary

The windows based program brings a whole new dimension to this kind of synthesis. The program provides a complete user-friendly environment in almost which every tool and visualisation aid is provided for the conceptual design of civil aircraft. The program can be used to evaluate the effectiveness of advanced technologies, and suggest which technologies are worthwhile and suitable for follow up research. The program reduces much of the guesswork associated with conceptual design, and relies on a very much reduced set of input data to produce its results, which have been shown on average to be accurate within approximately 5% for all trial cases. The program is suited to both the professional and educational environments, and will soon be available for the teaching of undergraduates, particularly as an aid for undergraduate projects, for which no other public domain software is currently available.

4 .2 .4 Existing Design Syntheses

Most main aeronautical establishments rely upon their own computer based design syntheses. Commercial aeronautical organisations tend to be very secretive about their design systems, and thus there is little literature in the public domain about the systems employed by the major aircraft companies. It would seem safe to assume that with the financial and human resources available to them, that their computer based design systems are state of the art, and well beyond the scope of this work. From the little information I have gleaned, it would seem that most of their work concentrates on the later stages of the design process, with computational fluid dynamics and finite element modelling being of most importance.

However, educational institutes, government agencies such as NASA, and commercial software developers such DAR Corporation[81] tend to be more forthcoming with information about their systems.

The design program with the most in common with the Aircraft Design program described herein, in terms of user interface, is the Advanced Aircraft Analysis (AAA) program developed by DAR Corporation[81]. The program is essentially a Windows based aircraft design tool, based upon the Roskam[82] series of books. Although the design methods used within the synthesis are based upon proven methods, and give relatively good results, there a number of major differences in approach between the AAA program and the Aircraft Design program. The AAA program does not incorporate any provision for advanced technologies, and is not geared toward the design of large civil aircraft. The main difference though comes in the layout of the design environment, which does not provide a fully integrated and automated design synthesis. The calculations are split into a large number of areas, and each calculation must be performed at the request of the user. The synthesis also relies on a large number of detailed input parameters. While this provides the good basis of a teaching, or of a manual design aid, it does not appear to be aimed toward the same objective as the Aircraft Design program described here.

The ACSYNT program developed over the last 20 or so years by NASA, and described by Mason and Arledge[83], provides a low level graphical user interface to an advanced conceptual design program, aimed at providing accurate initial sizing and optimisation analysis for all types of current technology aircraft. The program consists of modules to deal with geometry, weights, propulsion, performance, aerodynamics, stability and control, takeoff, balance, and economics. The calculations are performed using mainly empirical methods, with the aerodynamics module using similar methods to those used in the Aircraft Design program. Despite the resources available for the creation of this program, the graphical interface and the geometric models produced form the program are still fairly simplistic. While the results of the program give good agreement with flight data, they do rely heavily on 'matching factors' to tune the initial estimates to more realistic values. It would seem that the program undoubtedly gives good results, but that a lot of effort is required to achieve them.

CAPDA (Haberland et al.[84]) is another conceptual design synthesis aiming to provide accurate results and optimisation of design concepts. The program allows the detailed interactive design of almost every part of the aircraft, and provides a set of optimisation tools allowing the design to be optimised for a number of merit functions. Although there appears to be little information about the results and operation of this program, it would seem that it provides an excellent design tool, but does not have provision to include

advanced technologies, is not a completely integrated design program, and requires much time and judgement on the part of the user to fully explore the programs' depth.

The Optimum Preliminary Design Of Transports (OPDOT) is a program developed by NASA to evaluate the impact of new technologies upon transport aircraft (Arbuckle and Silwa[85]). The structure and goals of the program are very similar to the Aircraft Design program. The design variables are specified, a mission profile is estimated using a step-by-step analysis, and this can then be optimised for a specific merit function and constraints. The main focus of the program however is on the optimisation process, and there appears to be no inclusion of methods to estimate the initial design parameters. The program is simply a performance and optimisation tool for advanced technologies and unconventional configurations.

Despite its name, CASP (Combat Aircraft Synthesis Program), described by Sieron et Al[86], performs analysis of all types of aircraft, including transport aircraft. The user must supply a geometric description of the aircraft, and the program uses standard Datcom methods to provide weight, aerodynamic, and stability information. The mission analysis performs a similar task to the Performance Module of the Aircraft Design program. While containing certain elements of the Aircraft Design program, CASP is more suited to combat aircraft, as its name would suggest. The mission analysis does not appear to provide the features one would associate with the flight of a civil transport aircraft, it does not appear to have the flexibility of other programs, and has no provision for the inclusion of advanced technologies.

Vaziry-Z and Fielding[87] report on a program developed at Cranfield Institute called 'Computer Aided Conceptual Aircraft Design' (CACAD). The program is aimed at the conceptual design of turbofan powered transport aircraft. The methods of calculation are similar to those of the Aircraft Design program. The general input data, and the mission input data is set, and the aircraft is sized using the maximum number of passengers, the weights, aerodynamics, and performance of the aircraft are then calculated. The design is then optimised for a number of fixed 'quasi-dependent' variables. One of the main strengths of the program is its detailed economic and reliability analysis. The main differences between CACAD and the Aircraft Design program are CACAD's tendency toward the economic aspects of the aircraft design, the lack of flexibility of CACAD's design and optimisation processes, the lack of any kind of user interface for the CACAD program, and the inclusion of only one advanced technology (variable camber wings) in the CACAD program.

Summary

Each program described above has been created with a different set of goals in mind. No one program is likely to be able achieve every goal and to be the ultimate conceptual design tool. The Aircraft Design program has achieved its goals of providing an integrated

design and analysis environment from within a Windows based user friendly interface, while providing accurate and detailed design methods for transport aircraft to include the design of UHCA, and the effects advanced technologies, without relying too heavily on subjective decisions and judgement of the user.

Although the Aircraft Design program does have limitations in its applicability, such as a lack of facilities for the analysis of high wing configurations, aft-mounted engines, and unconventional layouts (other than unconventional fuselages), these omissions are relatively minor, especially when one considers the likely configurations for future UHCA.

5 .Airfoil & Engine Data Methods

Each method and equation contained within the eight design modules are described in detail in the subsequent eight chapters. The reasons behind the choice of these methods, and any information regarding their application is also included. New or revised techniques are described in complete detail, while standard existing methods are described in less detail, or are simply referred to their source.

Many new equations have been developed using correlations to existing and projected data. The error of each correlation is calculated as a variance based on the percentage error at each point of the correlation. Y_{data} is the value of the original data point at value X, Y_{line} is the estimated value at that particular value of X, and N_{points} is the number of data points.

$$Error = \frac{1}{N_{\text{points}}} \sum_{i=1,N_{\text{points}}} \left(\frac{(Y_{data} - Y_{line}) \times 100}{Y_{data}} \right)^2 \tag{0.1}$$

5 .1 Airfoil Data

The user selects the root, tip, and tail airfoils from the Component Specification Editor. The selection is made from a user defined set of airfoil library files. The purpose of the airfoil data routines within this module are to simply take the data for the relevant airfoil data files and to convert the data into a format that is compatible with the internal data requirements of the program structure, and that can be saved in a document format.

The only change that can occur in the numeric properties of the data is the tuning of the thickness to chord ratio of the airfoil by the thickness to chord tuning parameter (see eqn. 1.1). This has no other effect on the airfoil data, and is used mainly to specify a thickness to chord ratio other than those available from the airfoils in the data library. This is useful, as the thickness to chord ratio is the main parameter used for determining the wing weight and the aerodynamic properties of the wing. The contents of the airfoil data files are described in detail in section A.6.1., and are mainly used to estimate the 2-d airfoil lift curve slope and the 2-d airfoil pitching moment.

$$t\backslash c_{airfoil} = t\backslash c_{library\,airfoil} \times K_{Tune_{\text{t\backslash c.airfoil}}} \tag{1.1}$$

Since the properties of the airfoil sections at the wing extremities are known, then the properties at any spanwise section of the wing can be estimated using interpolation.

5 .2 ENGINE DATA

The engine data routines provide a method for predicting both the thrust and fuel consumption at all conditions, of an engine of any bypass ratio, thrust rating, and technology level. The type of engine is selected by the user from the Component Specification Editor. If the engine is simply one of the engines from the engine data library, then no calculations need to be made, and the data can simply be copied from the relevant data file.

However, if the engine is a 'custom' engine, the new properties of this engine have to be determined. The method used is to first determine which engines from the engine data library are closest to this new engine, in terms of thrust rating. If the engine has greater thrust than all the library engines, then the most powerful is chosen, and if the new engine has a smaller thrust rating than the smallest library engine, then the least powerful is chosen, else the two closest engines above and below the desired thrust rating are chosen. The engine data library supplied with the Aircraft Design program should however provide a wide enough range in thrust ratings to enable both an engine of greater thrust and smaller thrust to be found for most cases.

Assuming that two engines have been found, the data from these two engine data files act as base points from which the properties of the new engine are calculated by interpolation. The thrust, fuel consumption, size, and weight data of each baseline engine is first modified to reflect the impacts of any changes to the desired 'custom' engine values of bypass ratio and year of service. A complete list of the contents of the engine data files is given in A.6.2.

It is believed that this approach to predicting engine performance characteristics gives more accurate and reliable results than methods based on theoretical calculations of engine thermodynamic properties. The reason being, that the basis for all the calculations are sets of data which give the engine performance characteristics for a wide range of real engines of various sizes and at all operational conditions. This data was kindly supplied by Rolls Royce. It seems that the alteration of this data to take into account bypass ratio, thrust, and technology level changes is more appropriate than trying to accurately model the performance of an engine at all conditions using theoretically based methods.

5 .2 .1 ENGINE SIZE & WEIGHT

The physical dimensions of the baseline engines are resized to reflect changes in bypass ratio and year of service using the following methods. The fan diameter (D_{fan}), and bypass ratio (BPR) of the baseline engines are known from the engine data files.

In the analysis below the subscript '*1*' refers to the original engine, while the '*a*' subscript refers to the resized engine of same thrust rating.

For all engines:-

$$A_{fan} = \frac{\pi \cdot D_{fan}{}^2}{2} \tag{1.2}$$

$$BPR = \frac{\dot{m}_{bypass}}{\dot{m}_{core}} \tag{1.3}$$

Assuming that the flow area is proportional to the mass flow at inlet conditions:-

$$A_{core} = \frac{A_{bypass}}{BPR} \tag{1.4}$$

and since

$$A_{fan} = A_{core} + A_{bypass} \tag{1.5}$$

$$A_{bypass} = \frac{A_{fan}}{\left(1/BPR + 1\right)} \tag{1.6}$$

Therefore, re-sizing the existing engine, assuming that $A_{core\,a} \approx A_{core1}$, which should be valid for engines of moderate to high bypass ratios, as the fuel burn and power requirements of the core should not vary that dramatically.

$$A_{bypass_a} = A_{core1} \times BPR_a \tag{1.7}$$

$$A_{fan_a} = A_{core_a} + A_{bypass_a} \tag{1.8}$$

$$D_{fan_a} = 2\sqrt{\frac{A_{fan_a}}{\pi}} \tag{1.9}$$

The length of the new engine is assumed to be unchanged. The uninstalled dry weight of the engine can be calculated using a relationship found between the uninstalled engine weight (W_{eng}), and an engine volume parameter (V_{eng}). Using data from approximately 30 turbofan engines (table 5.1), a volume parameter could be created which gives a reasonably accurate relationship to the weight of the engines.

This volume parameter is based on characteristic engine lengths and areas, and assumes an area equal to the fan area for the first 40% of the engine length, and an area equal to the average of the core and the fan area over the remaining 60% of the engine length.

$$V_{eng} = \left(0.4 L_{eng} A_{fan}\right) + \left(0.6 L_{eng} \frac{\left(A_{fan} + A_{core}\right)}{2}\right) \tag{1.10}$$

Analysis of the engine weight data provides the relationship:-

$$W_{eng} = 1233.6 + 295.7V_{eng} - 3.31V_{eng}^{\ 2} \tag{1.11}$$

The data and the graph from which this equation is derived are shown in table 5.1 and figure 5.1 below.

Engine Name	D_{fan} (mm)	L_{eng} (mm)	A_{inlet} (m^2)	A_{bypass} (m^2)	A_{core} (m^2)	Volume (m^3)	Weight (kg)
CFM56-3c	1524	2360	1.824	1.52	0.304	3.229	1951
JT8D-219	1250	3911	1.227	0.614	0.614	4.08	2092
CFM56-2B	1735	2430	2.364	2.026	0.338	4.268	2119
CFM56-5A	1735	2422	2.364	2.026	0.338	4.254	2275
CFM56-7B	1549	2507	1.884	1.576	0.309	3.539	2361
CFM56-5c	1836	2616	2.647	2.299	0.348	5.121	2492
V2522-A5	1600	3200	2.011	1.67	0.341	4.831	2500
V2527-A5	1600	3200	2.011	1.661	0.35	4.839	2500
V2528-D5	1600	3200	2.011	1.664	0.347	4.837	2500
V2533-A5	1600	3200	2.011	1.638	0.372	4.861	2500
RB535E4B	1892	2995	2.811	2.281	0.53	6.371	3261
RB535C	1877	3010	2.767	2.255	0.512	6.293	3309
PW2040	2154	3729	3.644	3.123	0.521	10.094	3311
Cf6-80A2/A3	2195	3998	3.784	3.108	0.676	11.401	3819
JT9D-7R4h	2463	3371	4.765	3.943	0.821	12.074	4029
Cf6 80C2	2362	4087	4.382	3.658	0.724	13.424	4144
RB211-22b	2154	3033	3.644	3.037	0.607	8.289	4171
PW4000	2463	3371	4.765	3.95	0.814	12.066	4264
RB211-524B	2180	3106	3.733	3.041	0.691	8.759	4452
RB211-524H	2192	3175	3.774	3.062	0.712	9.065	4479
Trent 700	2474	3912	4.807	4.019	0.788	14.089	4785
Cf6-80E1	2438	4405	4.668	3.897	0.772	15.414	5075
Trent 800	2794	4369	6.131	5.257	0.875	19.897	5957
PW 4084	2845	4868	7.297	6.049	1.247	26.685	6335
GE90-76B	3404	5182	9.101	8.191	0.91	34.426	7559
GE90-85B	3404	5182	9.101	8.162	0.938	34.47	7559
GE90-90B	3404	5182	9.101	8.132	0.968	34.517	7559
GE90-92B	3404	5182	9.101	8.122	0.979	34.533	7559

Table 5.1 - Manufacturers engine data

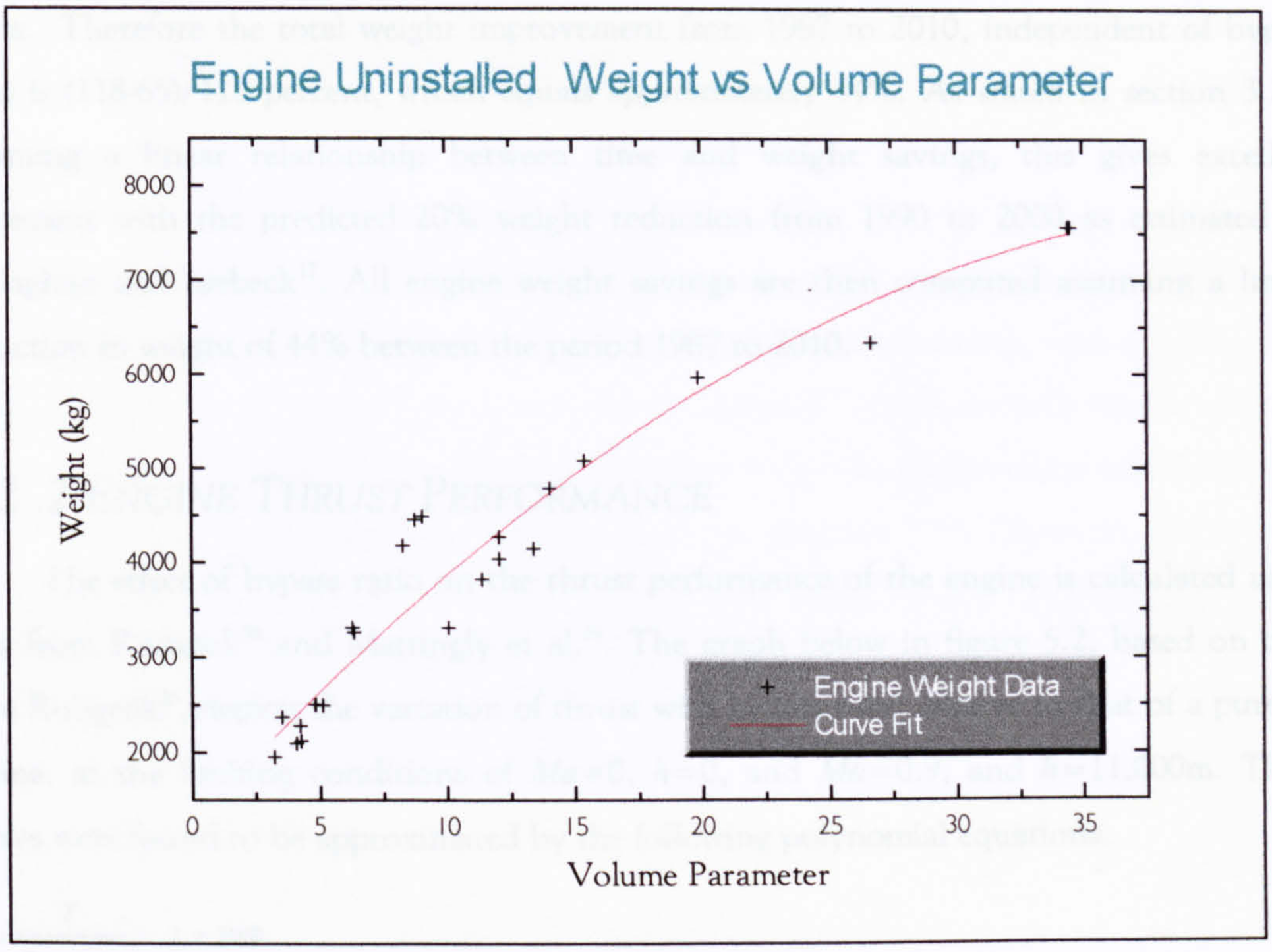


Figure 5.1- Engine uninstalled weight vs. volume parameter

These results allow estimates W'_{eng1} and W'_{enga} to be made of the original engine weight and the new engine weight. As the actual original engine weight is obtainable from the engine library data file, a more accurate estimate of the new engine weight can be made by scaling the original value.

W'_{eng1} - Initial estimate of original engine weight

W'_{eng_a} - Initial estimate of new engine weight

$$W_{eng_a} = W_{eng_1} \frac{W'_{enga}}{W'_{eng1}} \tag{1.12}$$

This weight estimate does not yet include any of the effects of the inclusion of advanced technologies. This is done by using the analysis of advanced turbofan engines provided by Knip[24]. Knip[24] presents detailed designs for a high bypass ratio engine built for 1987, and a very high bypass ratio engine built for 2010, with the latter providing a weight saving of 35% over the former. Performing the weight analysis from equations 1.11 and 1.12 on the engines designed by Knip[24] gives an estimate of the weight of those engines if they were to be built using today's technologies. This allows for the weight improvement from the period 1987 to the year 2010 to be estimated independently of the effect of bypass ratio. From the calculations purely based on the engine dimensions, the weight of the very high bypass ratio would be 18% higher if both engines were built using the same technology

levels. Therefore the total weight improvement from 1987 to 2010, independent of bypass ratio is (118-65)/118 percent, which equals approximately 44%. As stated in section 3.2.1, assuming a linear relationship between time and weight savings, this gives excellent agreement with the predicted 20% weight reduction from 1990 to 2000 as estimated by Callaghan and Liebeck[17]. All engine weight savings are then computed assuming a linear reduction in weight of 44% between the period 1987 to 2010.

5 .2 .2 Engine Thrust Performance

The effect of bypass ratio on the thrust performance of the engine is calculated using data from Ruijgrok[88] and Mattingly et al.[89]. The graph below in figure 5.2, based on data from Ruijgrok[88], depicts the variation of thrust with bypass ratio relative to that of a pure jet engine, at the limiting conditions of $Ma=0$, $h=0$, and $Ma=0.9$, and $h=11{,}000$m. These curves were found to be approximated by the following polynomial equations.

$$T' = \frac{T}{T_{BPR=0}}, \quad \lambda = \text{BPR}$$

$$T'_{Ma=0,h=0m} = -3.75\times10^{-6}\lambda^4 - 3.40\times10^{-4}\lambda^3 - 0.128\lambda^2 + 0.275\lambda + 1.01 \tag{1.13}$$

$$T'_{Ma=0.9,h=11km} = 1.21\times10^{-8}\lambda^6 + 1.35\times10^{-5}\lambda^5 - 5.91\times10^{-6}\lambda^4 + 0.0126\lambda^3 - 0.0144\lambda^2 - 0.116\lambda + 0.999 \tag{1.14}$$

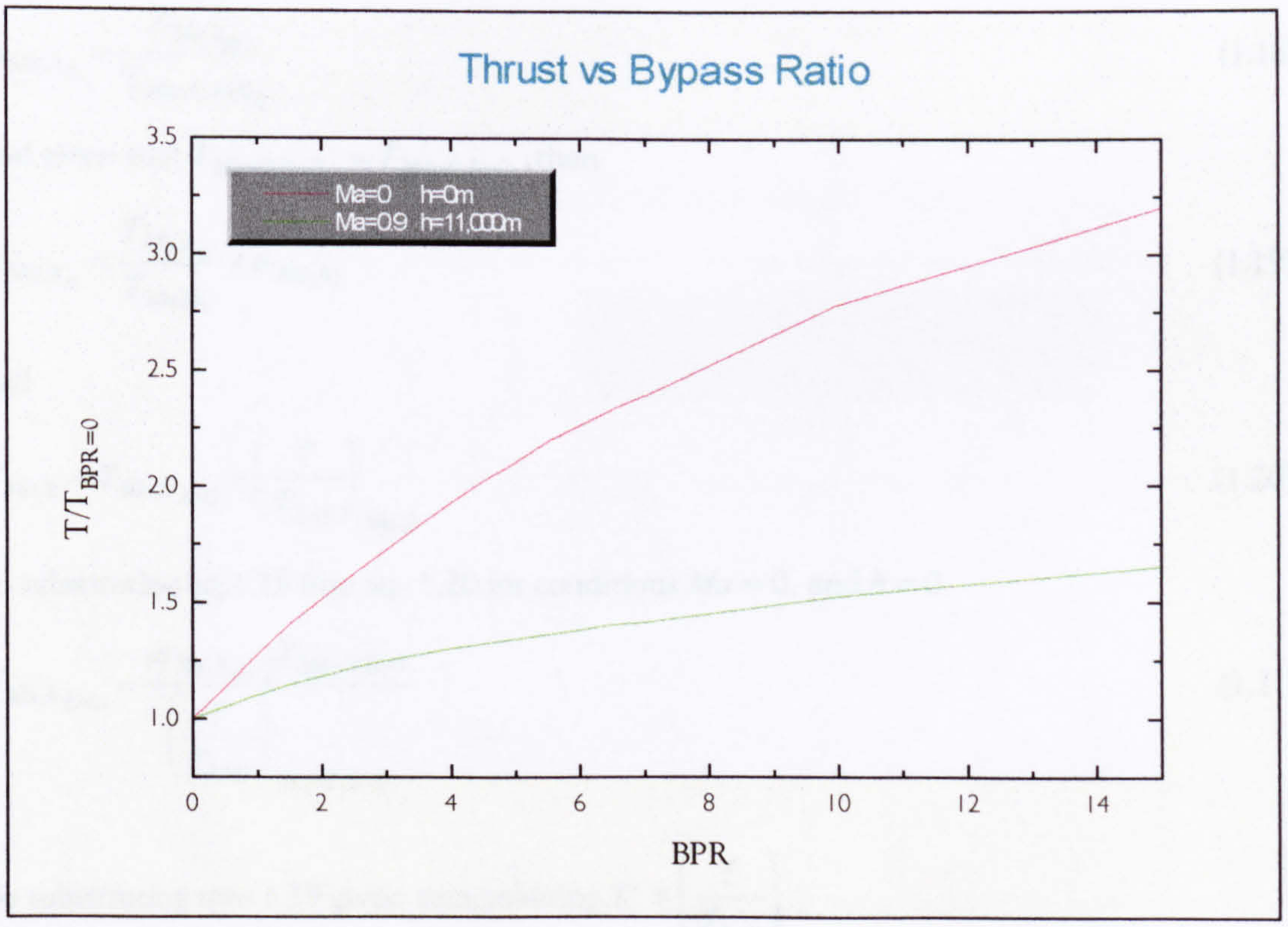


Figure 5.2- Thrust vs. bypass ratio

and from Mattingly et al.[89]page 36:-

$\alpha = \dfrac{T}{T_0}$, θ = Atmospheric Temperature Ratio

$$\alpha = \left(0.568 + 0.25(1.2 - \mathrm{Ma})^3\right)\theta^{0.6} \tag{1.15}$$

The information from these two sets of equations can be combined to give an estimate of the thrust lapse of an engine for any bypass ratio, Mach number, and altitude. It is assumed that the thrust lapse values given by the Ruijgrok[88] graph for each bypass ratio are correct at the two limiting atmospheric conditions given. The intermediate values are then found by scaling these values using information from equation 1.15. Given the thrust lapse data (α) for the original engine, the thrust lapse at these Mach numbers and altitudes can be found for the new engine using the following relationships.

ϕ = Interpolation factor between data at $T'_{Ma=0,h=0}$ and $T'_{Ma=0.9,h=11km}$

$$\phi = \frac{\alpha_{Ma,h} - \alpha_{Ma=0,h=0}}{\alpha_{Ma=0.9,h=11km} - \alpha_{Ma=0,h=0}} \tag{1.16}$$

so interpolating:-

$$T'_{Ma,h} = T'_{Ma=0,h=0} + \left(T'_{Ma=0.9,h=11km} - T'_{Ma=0,h=0}\right)\phi \tag{1.17}$$

and since

$$\alpha_{Ma,h_a} = \frac{T_{Ma,h_a}}{T_{Ma=0,h=0_a}} \tag{1.18}$$

and given that $T_{Ma=0,h=0_a} = T_{Ma=0,h=0_1}$, then

$$\alpha_{Ma,h_a} = \frac{T_{Ma,h_a}}{T_{Ma,h_1}} \times \alpha_{Ma,h_1} \tag{1.19}$$

and

$$T_{Ma,h} = T_{Ma,h\,\lambda=0} \times \left(\frac{T}{T_{\lambda=0}}\right)_{Ma,h} \tag{1.20}$$

so substituting eq.1.18 into eq. 1.20 for conditions $Ma = 0$, and $h = 0$

$$T_{Ma,h\,\lambda=0} = \frac{\alpha_{Ma,h\,\lambda=0} T_{Ma=0,h=0}}{\left(\dfrac{T}{T_{\lambda=0}}\right)_{Ma=0,h=0}} \tag{1.21}$$

So substituting into 1.19 gives, remembering $T' = \left(\dfrac{T}{T_{\lambda=0}}\right)$

$$\alpha_{Ma,h_a} = \frac{\frac{\alpha_{Ma,h\,\lambda=0} T_{Ma=0,h=0_a}}{T'_{Ma=0,h=0_a}} \times T'_{Ma,h_a}}{\frac{\alpha_{Ma,h\,\lambda=0} T_{Ma=0,h=0_1}}{T'_{Ma=0,h=0_1}} \times T'_{Ma,h_1}} \times \alpha_{Ma,h_1}$$

which reduces to

$$\alpha_{Ma,h_a} = \frac{T'_{Ma=0,h=0_1} \times T'_{Ma,h_a}}{T'_{Ma=0,h=0_a} \times T'_{Ma,h_1}} \times \alpha_{Ma,h_1} \qquad (1.22)$$

This relationship can be used to estimate the thrust lapse for the new engine at the data points provided by the data file of the original engine.

5 .2 .3 S.F.C. PERFORMANCE

5 .2 .3 .1 Effect of Bypass Ratio

The effect of bypass ratio on specific fuel consumption is estimated using similar methods to those above. The graph below (figure 5.3) reproduced from data in Ruijgrok[88] shows the variation of s.f.c. with bypass ratio. This allow the fuel consumption to be scaled for bypass ratio, given the non-dimensionalised s.f.c. and respective thrust values supplied from the original engine data file (see A.6.2.).

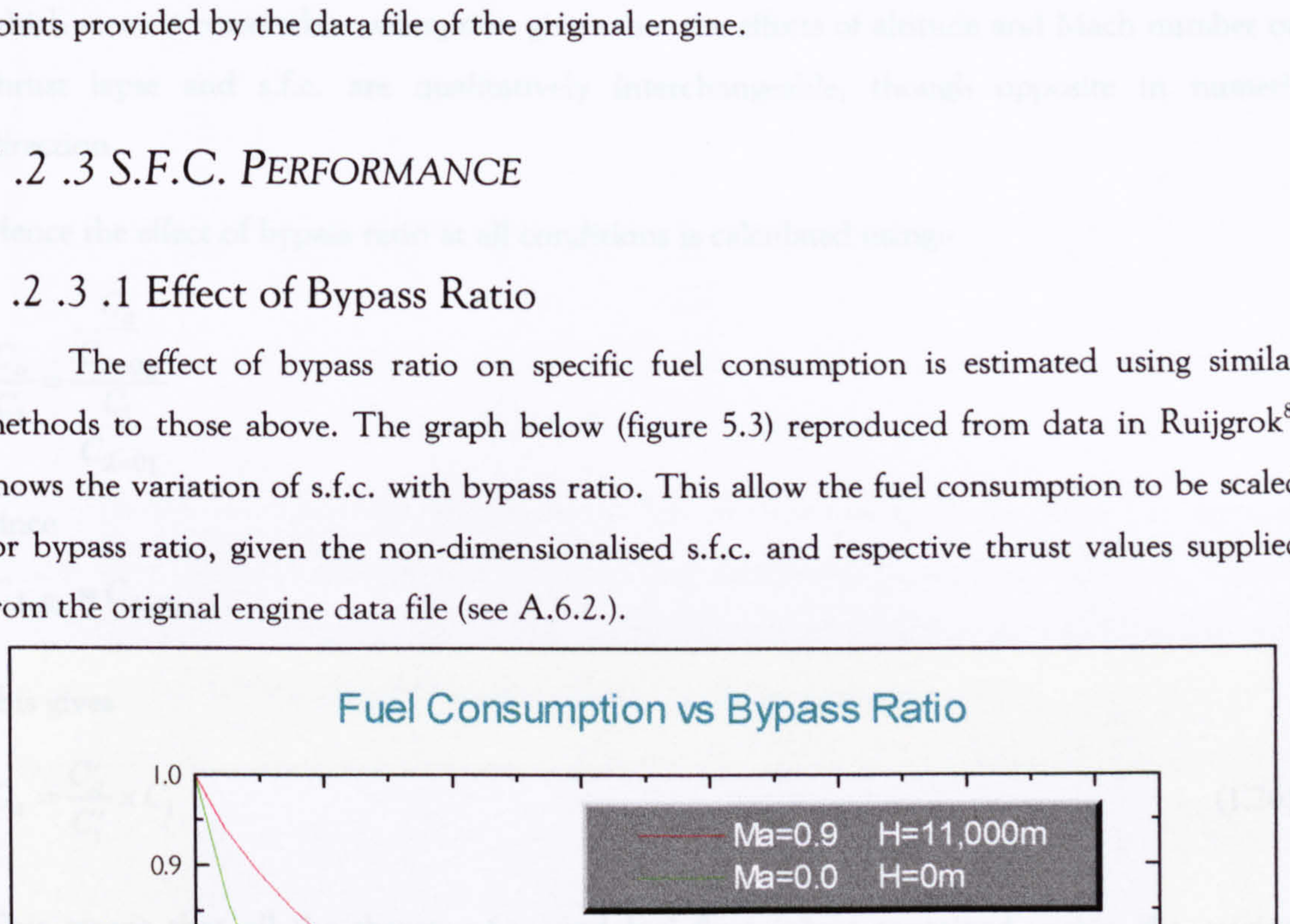


Figure 5.3 - Fuel consumption vs. bypass ratio

These curves can then be approximated:-

$$C' = \frac{C}{C_{\lambda=0}}, \text{ where } \lambda = \text{BPR}$$

$$C'_{Ma=0,h=0} = 0.32744 + 0.5269e^{-\frac{(\lambda-0.04971)}{2.077}} + 1.457e^{-\frac{(\lambda-0.04971)}{10.95}} \quad (1.23)$$

$$C'_{Ma=0.9,h=11km} = 0.66501 + 0.2403e^{-\frac{(\lambda-0.03582)}{1.661}} + 0.09153e^{-\frac{(\lambda-0.03582)}{17.54}} \quad (1.24)$$

assuming that -

$$C'_{Ma,h} = C'_{Ma=0,h=0} + \left(C'_{Ma=0.9,h=11km} - C'_{Ma=0,h=0}\right)\phi \quad (1.25)$$

which seems a reasonable assumption given that the effects of altitude and Mach number on thrust lapse and s.f.c. are qualitatively interchangeable, though opposite in numeric direction.

Hence the effect of bypass ratio at all conditions is calculated using:-

$$\frac{C_a}{C_1} = \frac{\frac{C_a}{C_{\lambda=0_a}}}{\frac{C_1}{C_{\lambda=0_1}}}$$

since

$$C_{\lambda=0_1} \approx C_{\lambda=0_a}$$

this gives

$$C_a = \frac{C'_a}{C'_1} \times C_1 \quad (1.26)$$

This means that all the thrust, s.f.c., and fuel flow values contained within the original engine data file can be scaled using equation 1.26 to produce the fuel consumption data for the engine of required BPR.

The configuration of the engine is also considered, with a factor $K_{engtype}$ providing a fuel consumption scaling factor depending on the type of engine. The values of this factor are shown below, and have been based on the findings described in chapter 3.

Turbofan	-	1.0
Advanced Ducted Propeller	-	0.9
Contrafan	-	0.85

Figure 5.4 - S.F.C. scaling factors for advanced engines

5 .2 .3 .2 Effect of Year of Service

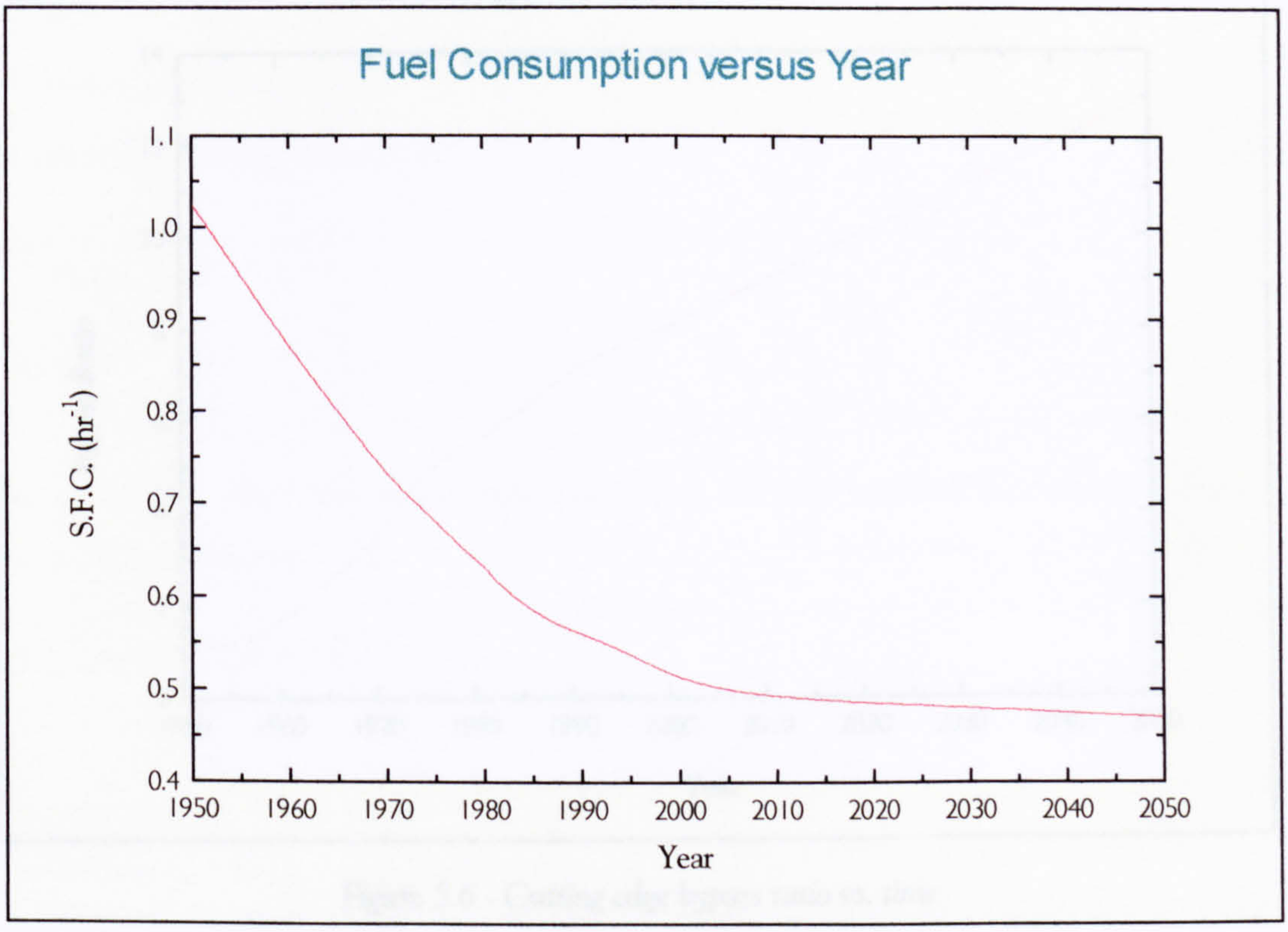


Figure 5.5 - Specific fuel consumption vs. year

The effect of the year of service on the fuel efficiency must also be taken into account. This is done using the historic and predicted fuel consumption data from Stryker[23], Webb[19], and NAS-NRC[22]. The graph shown above was constructed from this data to show the effect of time on the cutting edge technology value of turbofan fuel consumption.

Using a non dimensionalised Year parameter Y'

$$Y' = \frac{Year - 1950}{100}$$

the cutting edeg techgnology s.f.c. C″ could be expressed as a polynomial in terms of Y'

$$C'' = -10.5Y'^6 + 33.95Y'^5 - 40.63Y'^4 + 21.41Y'^3 - 3.51Y'^2 - 1.343Y' + 1.0239 \qquad (1.27)$$

However, much of this s.f.c. improvement is due to increases in bypass ratios. The amount of s.f.c. improvement that is due to this effect needs to be quantified. For this reason the graph shown below in figure 5.6 was constructed which shows an estimate of the past and predicted bypass ratios of cutting edge technology engines versus time.

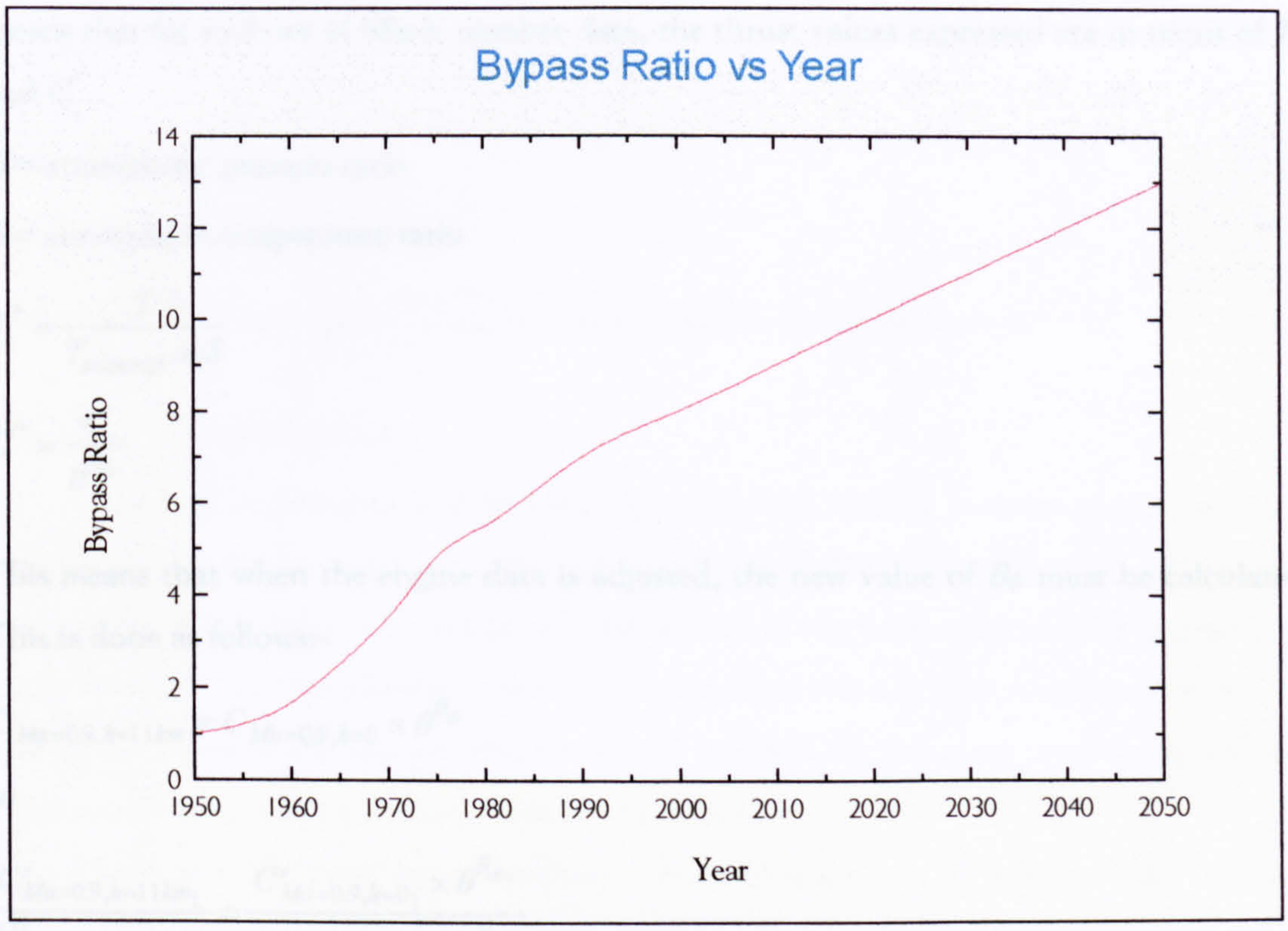


Figure 5.6 - Cutting edge bypass ratio vs. time

The cutting edge technology bypass ratio λ' can be expressed as a polynomial in terms of Y'

$$\lambda' = -.218.5Y'^{6} - 781.5Y'^{5} + 1083.8Y'^{4} - 719.0Y'^{3} + 219.7Y'^{2} - 9.51Y' + 1.0 \qquad (1.28)$$

This means that C' can be calculated for the bypass ratio λ'.

As the bypass ratio is being changed from λ_1 to λ_a, and the year is being changed from Y'_1 to Y'_a, the expected bypass ratios for the two years can be calculated (λ_1' and λ_a'). This means that from the period Y'_1 to Y'_a the fuel consumption will be expected to change by the factor C''_{BPR} purely based on bypass ratio, where:-

$$C''_{BPR} = \frac{C'_{\lambda_a'}}{C'_{\lambda_1'}} \qquad (1.29)$$

so the full transformation of the original s.f.c. to the new s.f.c. at all conditions is given by

$$C_a = \frac{C'_a}{C'_1} \times \frac{1}{C''_{BPR}} \times K_{engtype} \times C_1 \qquad (1.30)$$

The s.f.c. exponent (θ_{sfc})

The s.f.c. data in the data file has been specified in terms of non-atmospheric dependent values, and an atmospheric coefficient θ_{sfc} (as described in section A.6.1). This

means that for each set of Mach number data, the thrust values expressed are in terms of T^*, and C^*.

δ = atmospheric pressure ratio

θ = atmospheric temperature ratio

$$T^* = \frac{T}{T_{nominal} \times \delta}$$

$$C^* = \frac{C}{\theta^{\theta_{sfc}}}$$

This means that when the engine data is adjusted, the new value of θ_{sfc} must be calculated. This is done as follows:-

$$C_{Ma=0.9,h=11km} = C_{Ma=0.9,h=0} \times \theta^{\theta_{sfc}}$$

so

$$\frac{C'_{Ma=0.9,h=11km_1}}{C'_{Ma=0.9,h=11km_a}} = \frac{C'_{Ma=0.9,h=0_1} \times \theta^{\theta_{sfc_1}}}{C'_{Ma=0.9,h=0_a} \times \theta^{\theta_{sfc_a}}}$$

taking logs of both sides gives:-

$$\theta_{sfc_a} = \frac{\log\left(\frac{C'_{Ma=0.9,h=11km_1} \times C'_{Ma=0.9,h=0_a}}{C'_{Ma=0.9,h=11km_a} \times C'_{Ma=0.9,h=0_1}}\right)}{\log(\theta)} - \theta_{sfc_1} \qquad (1.31)$$

5 .2 .4 *Engine Interpolation \ Scaling*

Once the data from the baseline engine(s) has been modified to reflect any changes in bypass ratio and technology level, the final engine data set can be computed

5 .2 .4 .1 Scaling

If the desired thrust rating is outside the bounds of the current engine data library, then the final engine data can only be based on the modified data of the one engine closest to it in terms of thrust rating. The engine thrust lapse ratios and fuel consumption data are based on the values of the baseline engine, scaled using the methods of sections 5.2.2 and 5.2.3. The weight of the engine is calculated using the method of section 5.2.1., with the size of the engine being found using the relationships from Raymer[90], as shown below.

$$\tau = \frac{T_{0_a}}{T_{0_1}}$$

$$L_{eng_a} = L_{eng_1} \times \tau^{0.4} \tag{1.32}$$

$$D_{fan_a} = D_{fan_1} \times \tau^{0.5} \tag{1.33}$$

The nominal installed thrust $T_{nominal}$ is simply scaled by the thrust ratio τ.

5 .2 .4 .2 Interpolation

If the final engine data is to be based upon an interpolation between two sets of data, one of a smaller thrust engine, one of a greater thrust engine, then each value within these sets must be interpolated. The weight and dimensions of the final engine can be interpolated easily, however the interpolation of the performance data sets can be a complex process. The data points between the sets are not necessarily specified for the same conditions, and the sets may not even contain the same number of points.

Great care has been taken to write a comprehensive set of routines that carefully interpolate between the two sets of data, to maximise the number of final data points, and to minimise error. These routines use linear methods to convert the data within the two sets to compatible values, these values can then be linearly interpolated between the two sets. In the case of the fuel consumption data, routines are provided that can intelligently extrapolate the data of one set to the conditions of the other set. This greatly enhances the quality of the final data.

5 .3 Data Evaluation

Subroutines have been written which allow the airfoil properties, and engine properties to be evaluated at any particular condition. This subroutine is globally available to any part of the Aircraft Design program.

The airfoil data subroutine, once supplied with the Reynolds number of interest, interpolates the data sets to provide a new data set for that particular Reynolds number, and calculates the 2-d lift curve slope of the airfoils at that Reynolds number. If the desired Reynolds number is outside the bounds of either the lowest or highest Reynolds number data set, then the values from the closest Reynolds number data set are assumed. As the data is mainly used to estimate the 2-d lift curve slope, which is relatively insensitive to Reynolds number, then this approach provides acceptable accuracy.

The thrust routine requires the altitude, Mach number, and engine mode of operation to be specified. This allows the engine thrust to be calculated at this point, if the altitude or Mach number are out of the range of the data available, then the closest data point is used.

The calculation of fuel consumption requires the thrust setting, Mach number, and altitude to be specified. The routine will automatically detect whether the engine is running in 'idle' mode, and will use the correct data accordingly. Again, if the altitude or Mach number are out of the range of the data available the closest data point is used

6 .Initial Sizing Methods

This module uses a weight fraction method, along with data correlations, and some advanced technology predictions, to compute an estimate of the takeoff weight, the operational empty weight, the payload weight, and the fuel weight, as well as many other sizing parameters.

Some of the correlations are based on actual data of current civil aircraft designs, while the remainder are based on estimates of the values of data for current civil aircraft designs. These data estimates were achieved from the outputs of the Weight, Aerodynamics, and Performance modules of the design program, by setting all the input parameters and the output parameters from the Initial Sizing and Wing Design modules to the actual values of the aircraft, or as close to the actual values as possible. These provide the Initial Sizing module with methods and design parameter values that are more appropriate and reliable than those achievable with current empirical methods. It is worth noting that many of the correlation equations rely on the fact that:-

$$W_0 = f\left(N_{pass} . R_{cr1}\right)$$

6 .1 Payload Weight

The weight of the payload is calculated using standard weights for passengers and baggage. A passenger is assumed to weigh 175 pounds, while standard baggage is assumed to weigh 40 pounds, with first class baggage weighing 60 pounds.

$$W_{payload} = \frac{\left(N_{pass} - N_{1st.Class}\right) \times 40 + N_{1st.Class} \times 60 + N_{pass} \times 175}{lb} \qquad (2.1)$$

6 .2 Flight profile Parameters

The flight profile parameters are used to describe the estimated flight profile of the aircraft, including any loiter or diversion. This profile is then used in the weight fraction analysis to determine the empty weight fraction. Although the cruise portion of the flight profile is specified by the user, the remaining flight profile parameters are determined automatically. The flight profile is chosen to be consistent with the FAA regulations governing reserve fuel provisions. The chosen profiles are summarised below:-

For a total cruise range of less than 3000nm:-

- Warm up
- Takeoff
- Climb to Cruise Altitude
- Cruise for R_{crl} nm (at altitude h_{crl}, at a Mach Number Ma_{crl})
- Cruise for further 1 hour at same conditions
- Descent
- Aborted Landing
- Climb to Diversion Altitude
- Cruise for further 200 nm (at altitude $h_{crl}/2$, at a Mach Number 0.6)
- Descent
- Landing

For a total cruise range of greater than 3000nm:-

- Warm up
- Takeoff
- Climb to Cruise Altitude
- Cruise for R_{crl} nm (at altitude h_{crl}, at a Mach Number Ma_{crl})
- Cruise for further 10% of cruise range
- Descent
- Aborted Landing
- Climb to Diversion Altitude
- Cruise for further 200 nm (at altitude $h_{crl}/2$, at a Mach Number 0.6)
- Descent to Loiter Altitude
- Loiter for 30 minutes (At Altitude of 1500ft, and Ma=0.35)
- Landing

The atmospheric properties at each relevant altitude are calculated using a subroutine which returns the value of density, pressure, speed of sound, viscosity, and temperature, for any input value of altitude, and for any temperature deviation from the international standard atmosphere. The flight profiles above are assumed to occur within the international standard atmosphere.

6 .3 AIRCRAFT PERFORMANCE PARAMETERS

Aircraft performance parameters such as wing loading, lift to drag ratios, cruise lift coefficients, and cruise thrust ratings, need to be estimated as accurately as possible to provide the highest quality information necessary for the determination of the weight fractions. At this early stage in the design process, very little information is known, therefore the estimations of these parameters must be based on empirical results.

6 .3 .1 WING LOADING

The maximum wing loading of the aircraft is estimated using a correlation based upon actual data from the designs of the 13 civil aircraft. This data is shown below:-

Aircraft	*Wing Loading* ($kgm^{-1}sec^{-2}$)	*Range* (*km*)
Airbus A300	6430	7315
Airbus A310	7343	9574
Airbus A320	5888	5000
Airbus A330	5725	8333
Airbus A340	6941	12222
Boeing 737	5254	2963
Boeing 747	7372	13148
Boeing 757	5282	5518
Boeing 767	6076	10667
Boeing 777	5355	7852
DA502 concept	6791	12963
DA602 concept	6653	12963
DA702 concept	6675	12963

Table 6.1 - Aircraft wing loading and range data

Finding an accurate method of estimating the wing loading proved to be a difficult task, no existing methods gave accurate results, and the choice of wing loading for a particular aircraft design can be fairly arbitrary. It was found that the wing loading ($Kgm^{-1}sec^{-2}$) could be loosely related to the range (km) using the following equation.

$$\frac{W'}{S} = 1.67 \times 10^{-4} R_{cr1} + 4729.0 \qquad \text{(error } \sim 2.0\text{)} \qquad (2.2)$$

This value of wing loading may be adjusted by the user, via the wing loading tuning factor ($K_{tune\ W\backslash S}$) found in the initial sizing input parameter section.

$$\frac{W}{S} = \left(1.67 \times 10^{-4} R_{cr1} + 4729.0\right) \times \mathrm{K}_{\mathrm{tune\ W\backslash S}} \tag{2.3}$$

The graph below illustrates the agreement with the aircraft data. Although the agreement is relatively poor, this method still proves to be more reliable and accurate than other techniques. In choosing this approach, rather than a classical design point calculation based upon thrust to weight ratio, stall velocity, and many other parameters, the calculation has been greatly simplified and made less reliant on parameters that at this stage of the calculation are unknown. This estimated value of wing loading provides an excellent first guess estimate and should ideally be refined by the user from the wing loading tuning value.

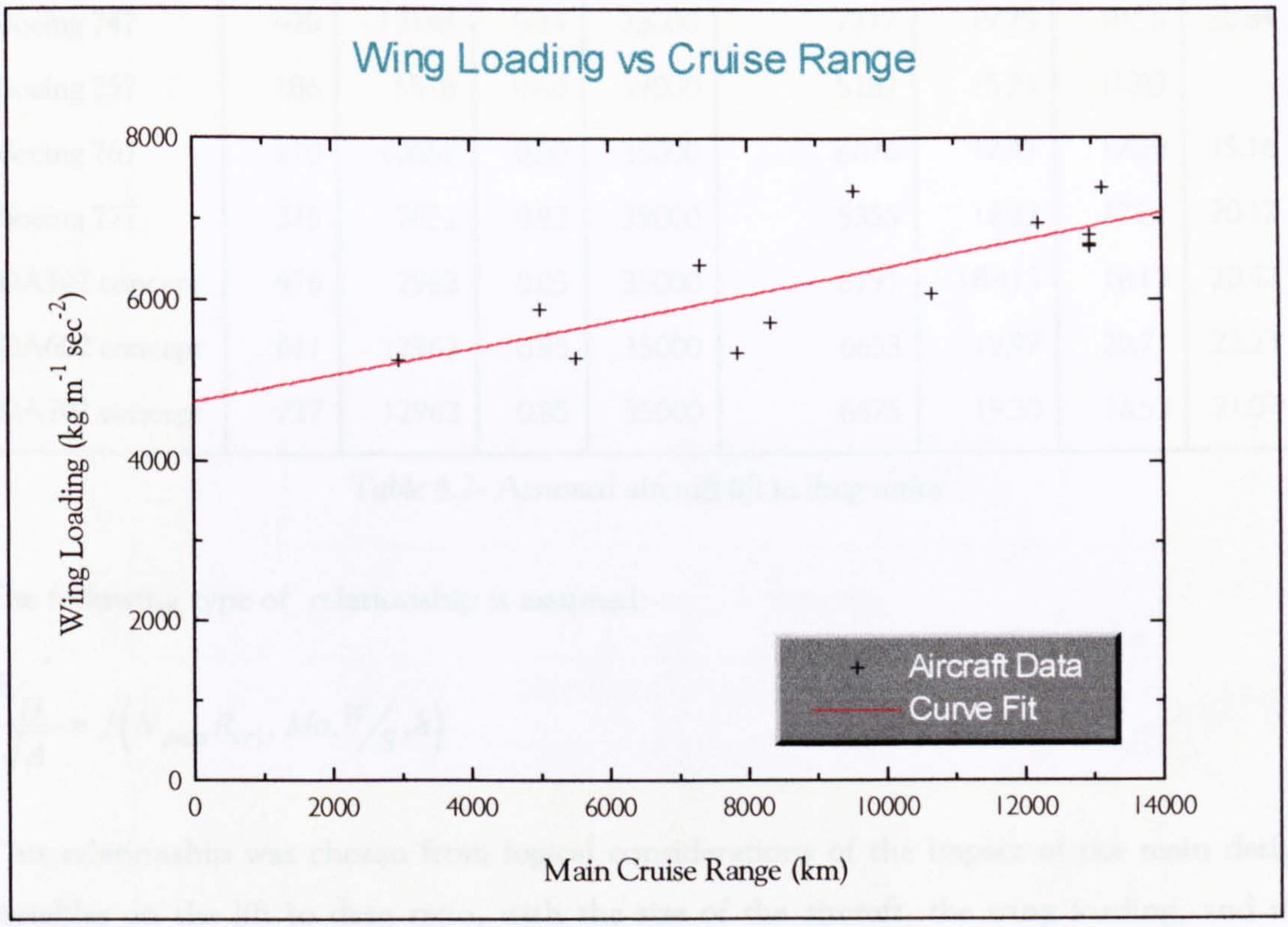


Figure 6.1- Estimation of wing loading

6 .3 .2 LIFT TO DRAG RATIO

An initial estimate of the lift to drag ratio of the aircraft, neglecting any advanced technologies (L/D') is made at the cruise, diversion, and loiter conditions. The following data collated from the Aerodynamics and Performance Modules was used to find an estimate of these lift to drag ratios. These values were created using the Aerodynamics and Performance Modules to calculate the properties of designs with the exact geometric, weight,

and powerplant properties as the aircraft shown below. Confidence in these results comes from the small margins of error produced in the final range calculations of the Performance Module, which would indicate that the lift to drag ratios are accurate and consistent.

Aircraft	N_{pass}	R_{cr1} *(km)*	Ma_{cr1}	h_{cr1} *(ft)*	$W\backslash S$ *(kg m^{-1} sec^{-2})*	$L\backslash D_{cr1}$	$L\backslash D_{cr2}$	$L\backslash D_{lo}$
Airbus A300	266	7315	0.80	31000	6430	16.41	16.09	18.27
Airbus A310	220	9574	0.80	36000	7343	17.03	16.74	19.63
Airbus A320	150	5000	0.78	31000	5888	16.59	15.85	-
Airbus A330	335	8333	0.82	37500	5725	20.42	19.49	24.30
Airbus A340	295	12222	0.82	37500	6941	20.21	16.25	20.24
Boeing 737	140	2963	0.75	35000	5254	15.00	14.35	-
Boeing 747	420	13148	0.83	35000	7372	19.75	19.55	20.84
Boeing 757	186	5518	0.80	39000	5282	15.24	15.03	-
Boeing 767	210	10667	0.80	35000	6076	17.41	17.30	19.16
Boeing 777	375	7852	0.83	39000	5355	18.32	17.21	20.12
DA502 concept	476	12963	0.85	35000	6791	18.413	18.13	20.42
DA602 concept	611	12963	0.85	35000	6653	19.97	20.71	22.23
DA702 concept	727	12963	0.85	35000	6675	19.30	16.53	21.07

Table 6.2- Assumed aircraft lift to drag ratios

The following type of relationship is assumed:-

$$\frac{L/D'}{\sqrt{A}} = f\left(N_{pass} R_{cr1}, Ma, W/S, h\right)$$

This relationship was chosen from logical considerations of the impact of the main design variables on the lift to drag ratio, with the size of the aircraft, the wing loading, and the cruise Mach number having been assumed to have the most profound effect on the lift to drag ratio of the aircraft. A process of trial and error was used to find the expressions to give the best agreement with the data, both in terms of numeric value and trend. The functions that relate the expressions, and their error are given below.

Cruise (error ~ 1.01)

$$\frac{L/D_{cr1}'}{\sqrt{A}} = 5.48 + 0.5443 \log\left(\frac{N_{pass}}{100} \times R_{cr1} \times \frac{Ma_{cr1}}{W \backslash S}\right) \qquad (2.4)$$

Diversion (error ~ 2.31)

$$\frac{L/D_{cr2}}{\sqrt{A}}' = 0.923 + 0.5322 \log\left(\frac{N_{pass}}{100} \times R_{cr1} \times \frac{Ma_{cr1}}{W \setminus S} \times h_{cr2}\right) \tag{2.5}$$

Loiter (error ~ 1.53)

$$\frac{L/D_{lo}}{\sqrt{A}}' = 6.32 + 0.4368 \times \log\left(\frac{N_{pass}}{100} \times R_{cr1} \times \frac{Ma_{cr1}}{W \setminus S}\right) \tag{2.6}$$

The agreement of these expressions with the data is shown below.

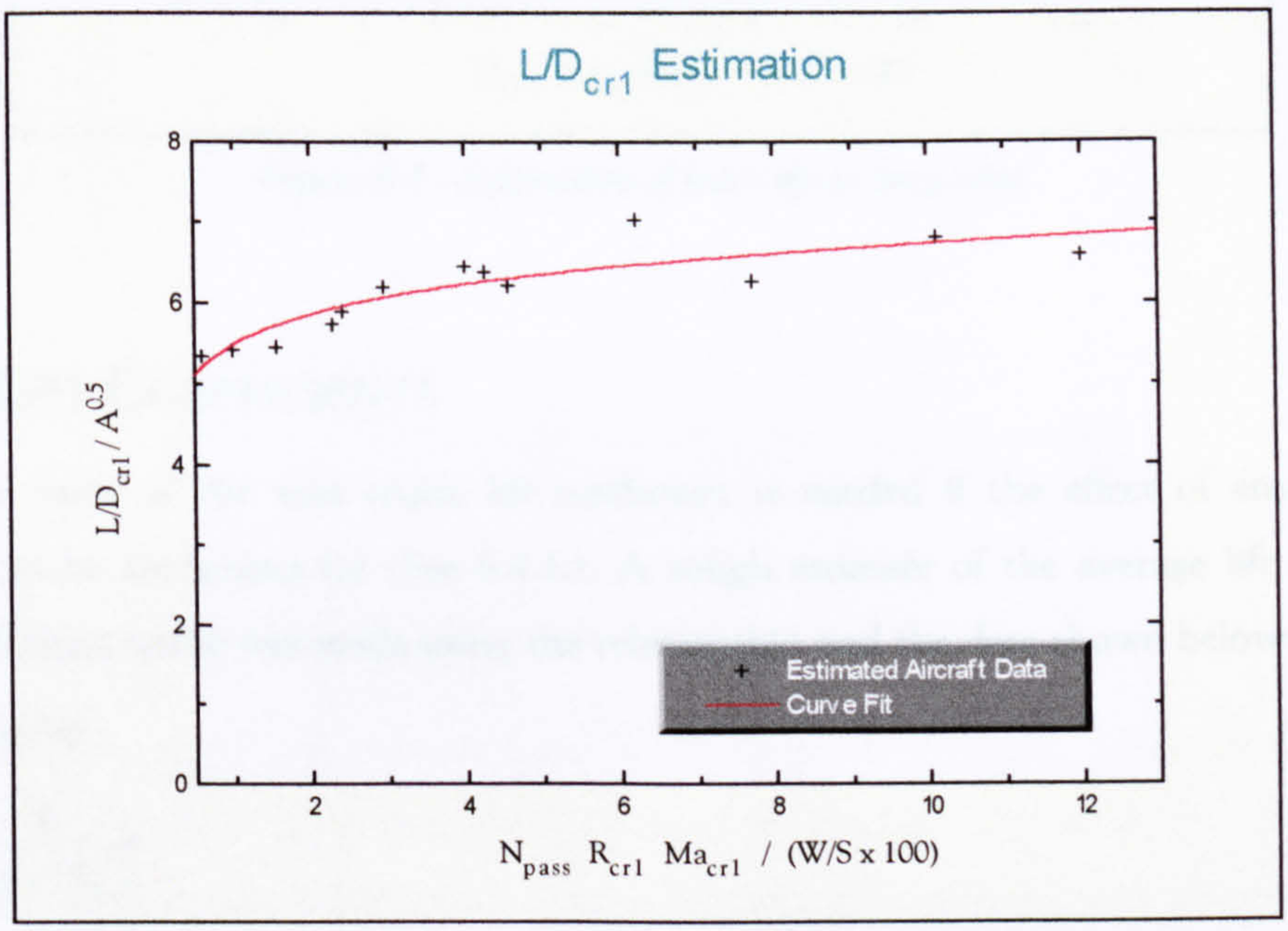


Figure 6.2 - Estimation of cruise lift to drag ratio

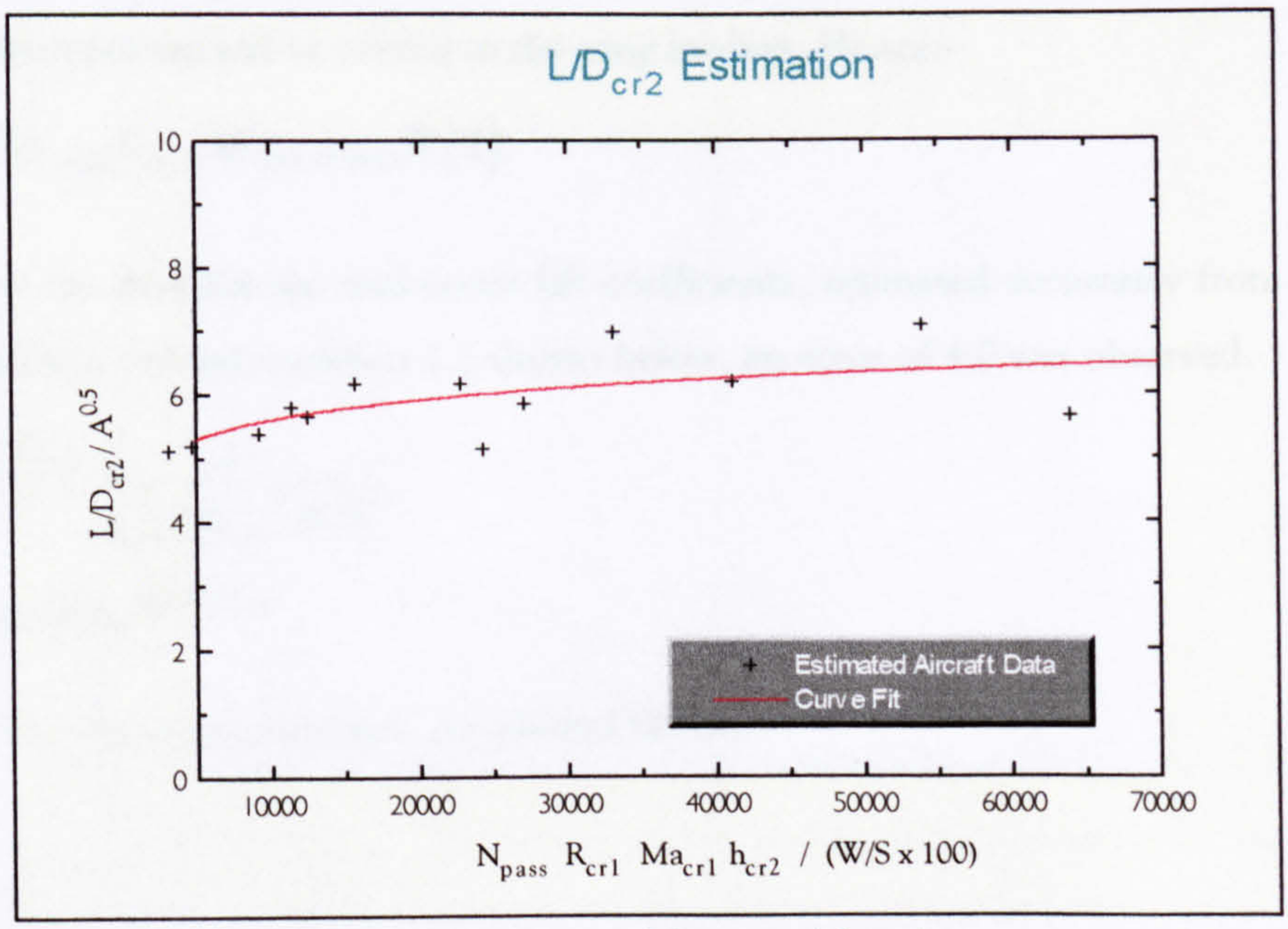


Figure 6.3 - Estimation of diversion lift to drag ratio

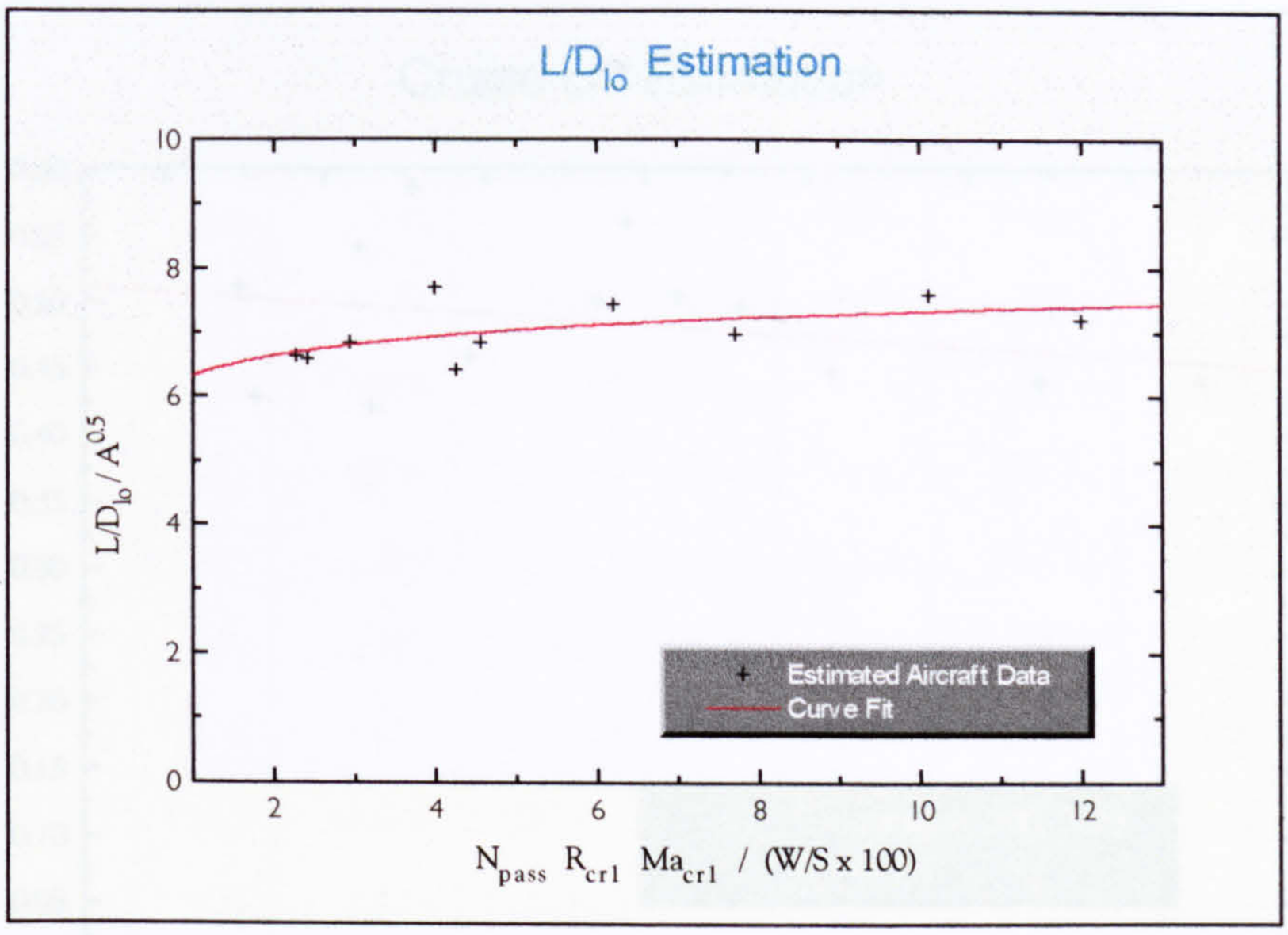


Figure 6.4 - Estimation of loiter lift to drag ratio

6 .3 .3 LIFT COEFFICIENTS

The value of the mid cruise lift coefficient is needed if the effect of any wing tip devices is to be accounted for (See 6.4.1.). A rough estimate of the average lift coefficient during the main cruise was made using the relationship and the data shown below:-

Since at cruise

$$C_L = \frac{W}{0.5\rho V^2 S_{ref}}$$

Assuming that the weight is a function of $N_{pass} \times R_{crl}$, the velocity is a function of Ma_{crl}, and the wing reference are will be related to the wing loading. Hence:-

$$C_{L_{crl}} = f\left(N_{pass} R_{crl}, Ma_{crl}, \rho_{crl}, W/S\right)$$

Analysis of the data for the mid-cruise lift coefficients, estimated accurately from the Wing Design Module, yielded equation 2.7 shown below, an error of 4.0 was observed.

$$X = \frac{N_{pass} R_{crl}}{100} \frac{1}{\rho_{crl} Ma_{crl}{}^2 W/S}$$

$$C_{L_{crl}} = 0.50068 e^{-0.00192 X} \qquad (2.7)$$

The data and this approximation are plotted below.

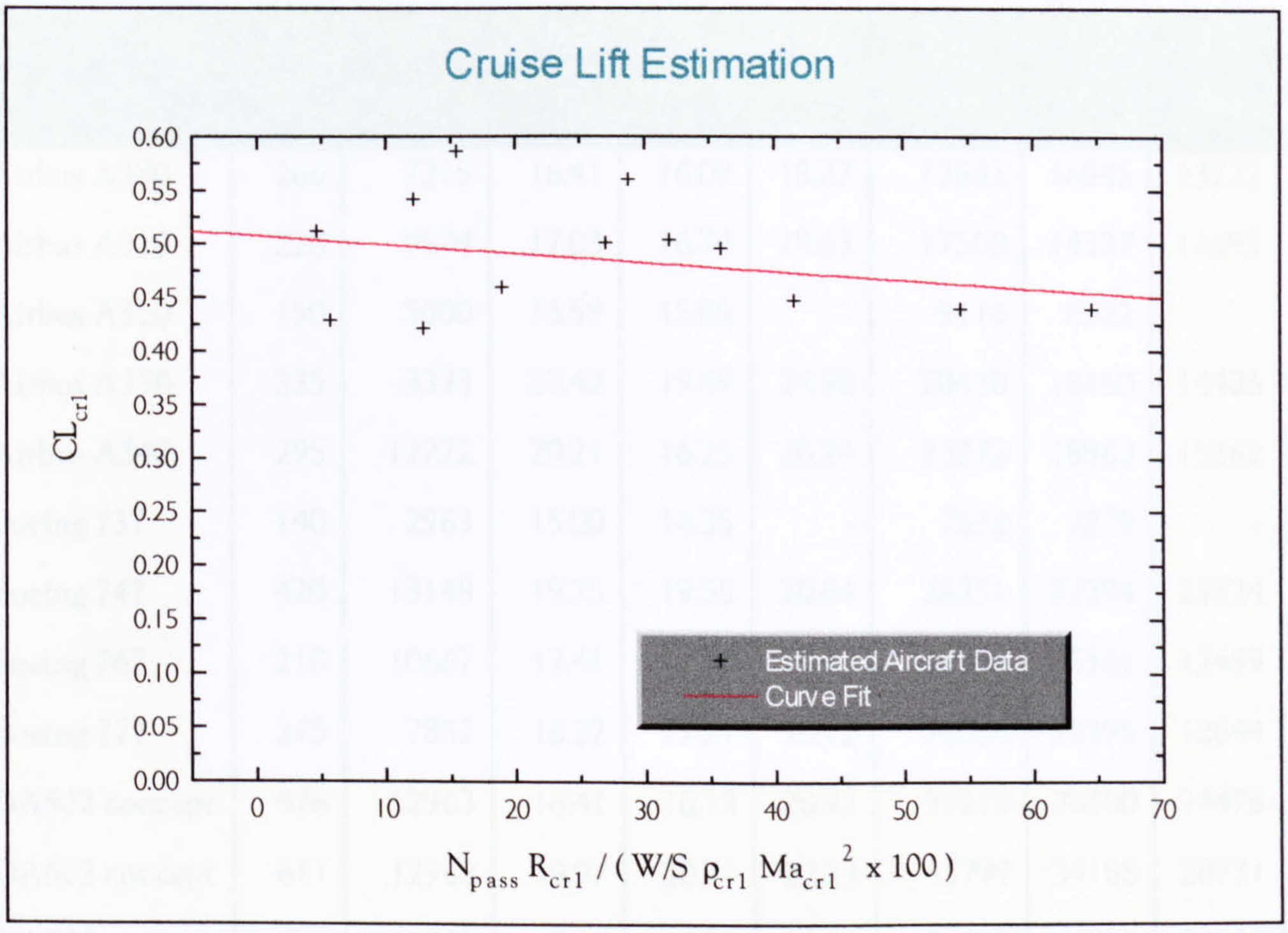


Figure 6.5- Estimation of cruise lift coefficient (first estimate)

6 .3 .4 THRUST SETTINGS

To enable a more accurate estimate of the weight fractions at cruise, diversion, and loiter, the average thrust required during these stages must be calculated. This thrust value can then be used in-conjunction with the engine data to provide a more accurate value of the s.f.c. at these conditions.

For these conditions

$T = D$

therefore

$$\frac{T}{W} = \frac{D}{L}$$

so a function of the form below is assumed.

$$T = f\left(N_{pass} R_{cr1}, \frac{1}{L/D}\right)$$

Using the values of thrust shown below, which were calculated using the detailed drag data estimated for the designs, assuming that for cruise, loiter, and diversion, the thrust force is equal to the drag force.

Aircraft Name	N_{pass}	R_{cr1} (km)	$L\backslash D_{cr1}$	$L\backslash D_{cr2}$	$L\backslash D_{lo}$	T_{cr1} (lb)	T_{cr2} (lb)	T_{lo} (lb)
Airbus A300	266	7315	16.41	16.09	18.27	19863	16845	13722
Airbus A310	220	9574	17.03	16.74	19.63	17508	14337	11695
Airbus A320	150	5000	16.59	15.85	-	9114	8522	-
Airbus A330	335	8333	20.42	19.49	24.30	20438	18160	14486
Airbus A340	295	12222	20.21	16.25	20.24	23272	18963	15362
Boeing 737	140	2963	15.00	14.35	-	7572	7279	-
Boeing 747	420	13148	19.75	19.55	20.84	36251	27394	23324
Boeing 767	210	10667	17.41	17.30	19.16	17994	15161	12499
Boeing 777	375	7852	18.32	17.21	20.12	26030	22395	18844
DA502 concept	476	12963	18.41	18.13	20.42	39218	30300	24478
DA602 concept	611	12963	19.97	20.71	22.23	45799	34188	28731
DA702 concept	727	12963	19.30	16.53	21.07	54822	41850	34550

Table 6.3 - Assumed aircraft thrust settings

The following equations were found.

Cruise (error ~1.5)

$$\frac{T_{cr1}}{T_0 N_e} = 46.9\left(\frac{N_{pass}}{100} \times R_{cr1} \times \frac{1}{L/D_{cr1}}\right) + 2.32 \times 10^4 \tag{2.8}$$

Diversion (error ~ 1.7)

$$\frac{T_{cr2}}{T_0 N_e} = 34.5\left(\frac{N_{pass}}{100} \times R_{cr1} \times \frac{1}{L/D_{cr1}}\right) + 2.40 \times 10^4 \tag{2.9}$$

Loiter (error ~ 1.7)

$$\frac{T_{lo}}{T_0 N_e} = 33.7\left(\frac{N_{pass}}{100} \times R_{cr1} \times \frac{1}{L/D_{cr1}}\right) + 2.12 \times 10^4 \tag{2.10}$$

The data and the expressions are plotted on the graphs below.

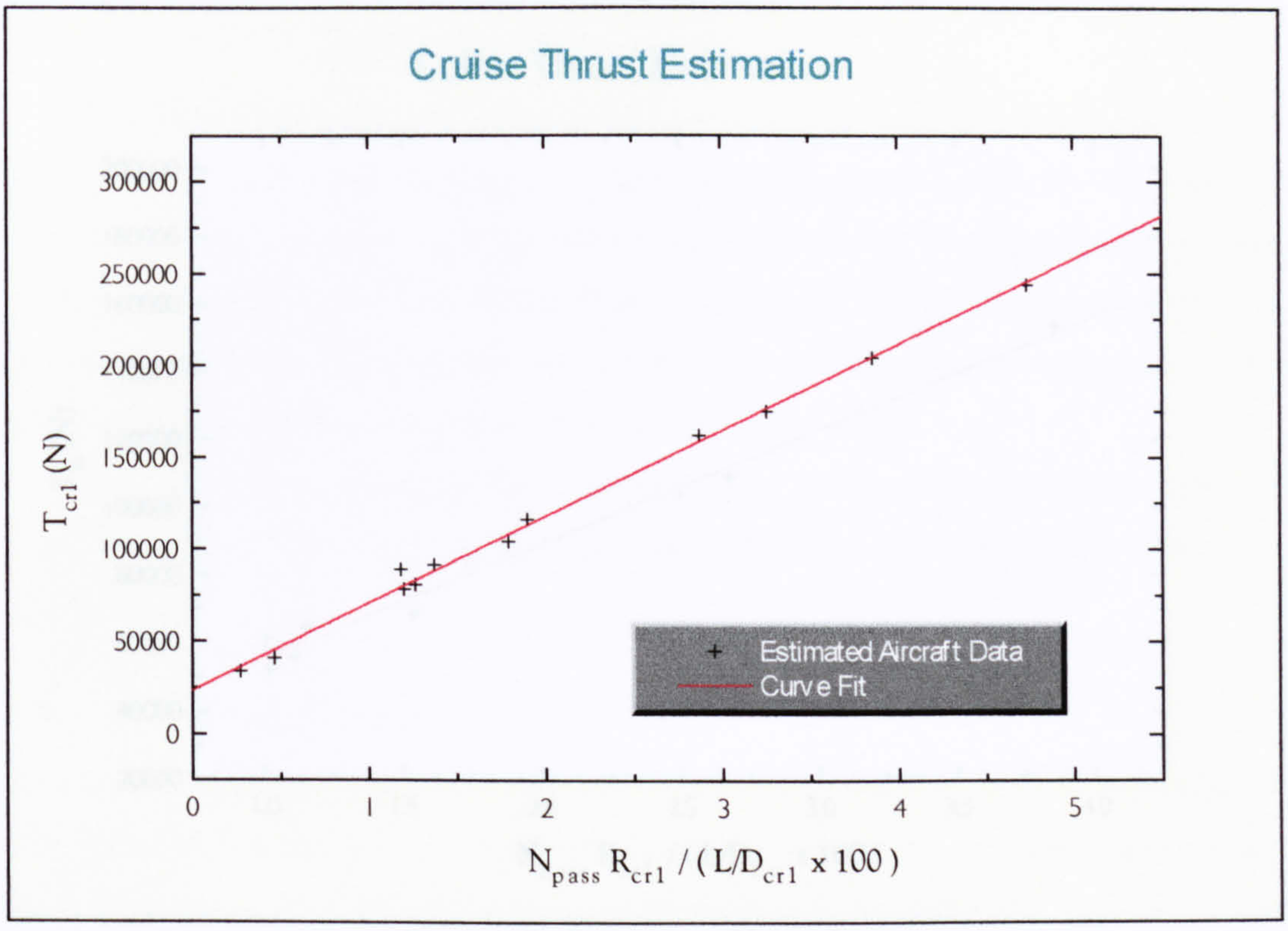


Figure 6.6- Estimation of cruise thrust

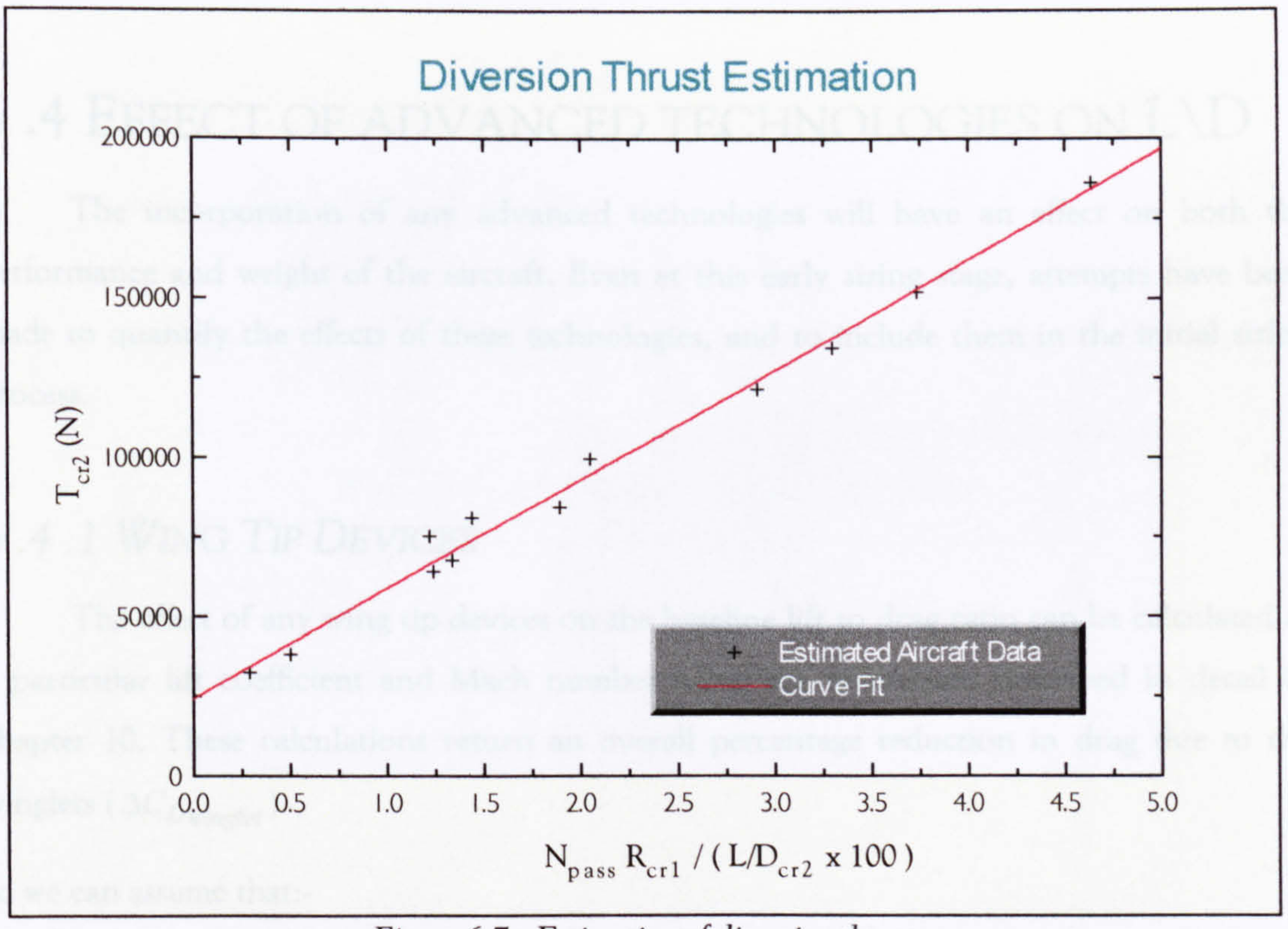


Figure 6.7 - Estimation of diversion thrust

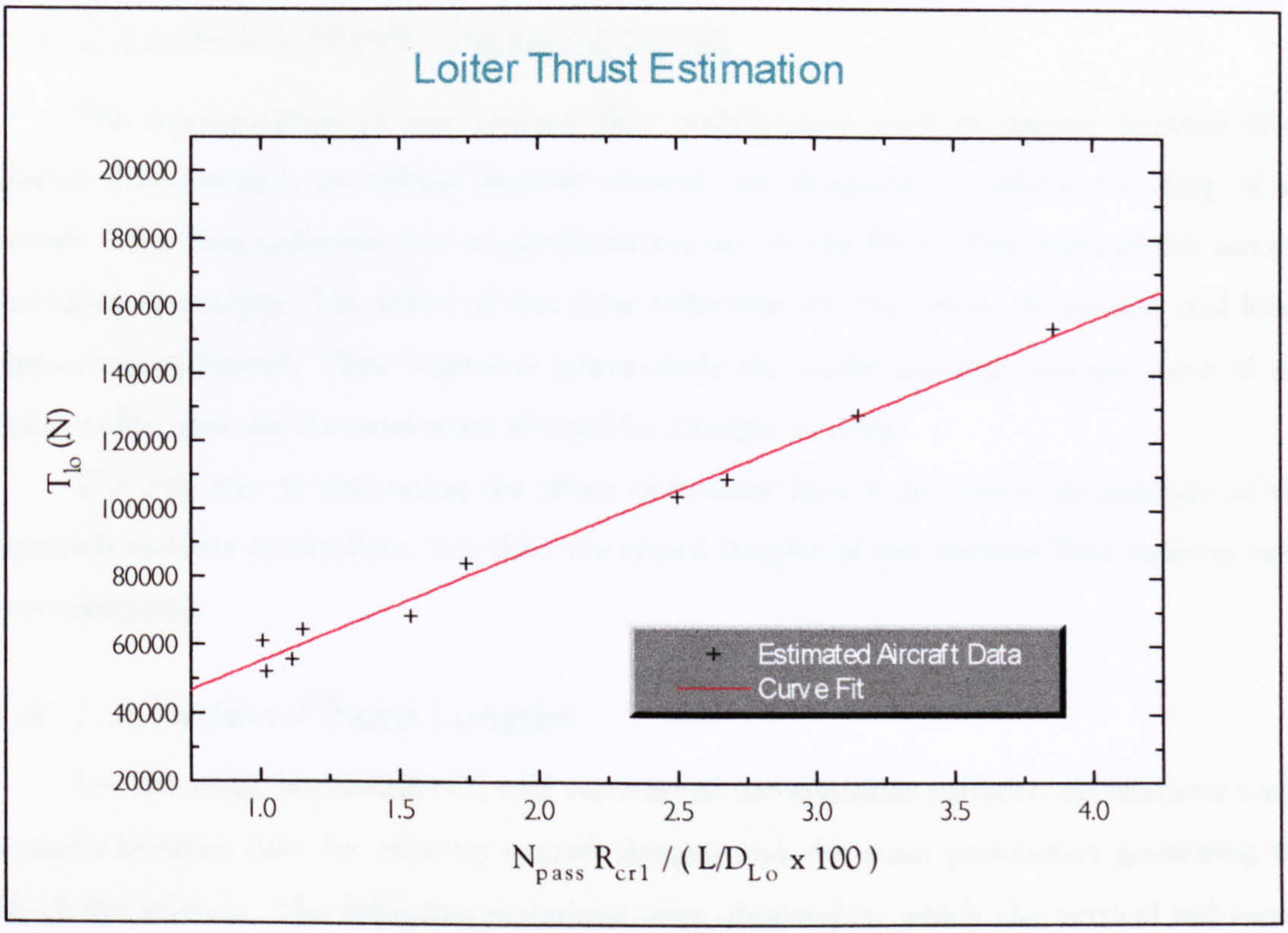


Figure 6.8 - Estimation of loiter thrust

6 .4 Effect of advanced technologies on L\D

The incorporation of any advanced technologies will have an effect on both the performance and weight of the aircraft. Even at this early sizing stage, attempts have been made to quantify the effects of these technologies, and to include them in the initial sizing process.

6 .4 .1 Wing Tip Devices

The effect of any wing tip devices on the baseline lift to drag ratio can be calculated at a particular lift coefficient and Mach number using the techniques described in detail in chapter 10. These calculations return an overall percentage reduction in drag due to the winglets ($\Delta C_{D\,winglet}$).

so we can assume that:-

$$L/D = L/D' \times \left(1 - \frac{\Delta C_{D\,winglet}}{100}\right) \qquad (2.11)$$

6 .4 .2 LAMINAR FLOW TECHNOLOGIES

The incorporation of any laminar flow technologies such as natural laminar flow, laminar flow control, or hybrid laminar control, are designed to reduce the drag of an aircraft. This drag reduction has a significant impact on the lift to drag ratio of the aircraft and hence its weight. The effect of this drag reduction on the cruise, diversion, and loiter segments is estimated. These segments (particularly the cruise segment) occupy most of the flight profile, and are the ones most affected by changes in drag.

The first step to estimating the effect of laminar flow is to obtain an estimate of the Reynolds number of the flow. For this, the chord lengths of the laminar flow surfaces need to be estimated.

6 .4 .2 .1 Surface Chord Lengths

For the wing, horizontal tail, and vertical tail aerodynamic surfaces, correlations could be made between data for existing aircraft designs and the main parameters governing the size of the surfaces. The following equations were obtained in which the vertical tail aspect ratio (A_{vt}) is defined with reference area extending to the fuselage centreline.

$$c_{mac} = 9.425\left(\frac{N_{pass} \times R_{cr1}}{100 \times W/S \times A}\right)^{0.378} \tag{2.12}$$

$$c_{mac\,ht} = 2.609 \times 10^{-4}\left(\frac{N_{pass} \times R_{cr1}}{100 \times A_{ht}}\right) + 2.78 \tag{2.13}$$

$$c_{mac\,vt} = 1.161 \times 10^{-4}\left(\frac{N_{pass} \times R_{cr1}}{100 \times A_{vt}}\right) + 3.94 \tag{2.14}$$

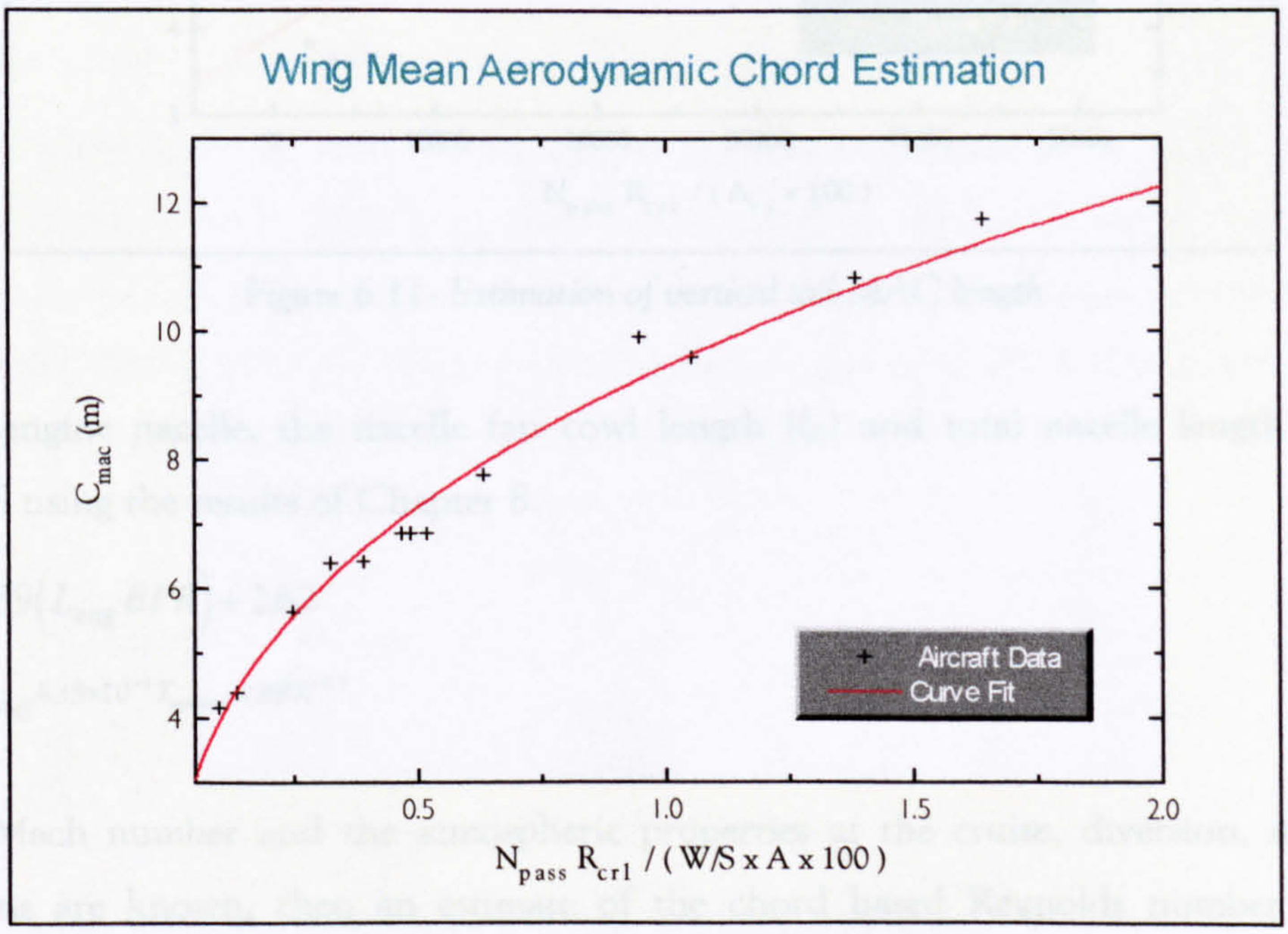


Figure 6.9 - Estimation of wing MAC length

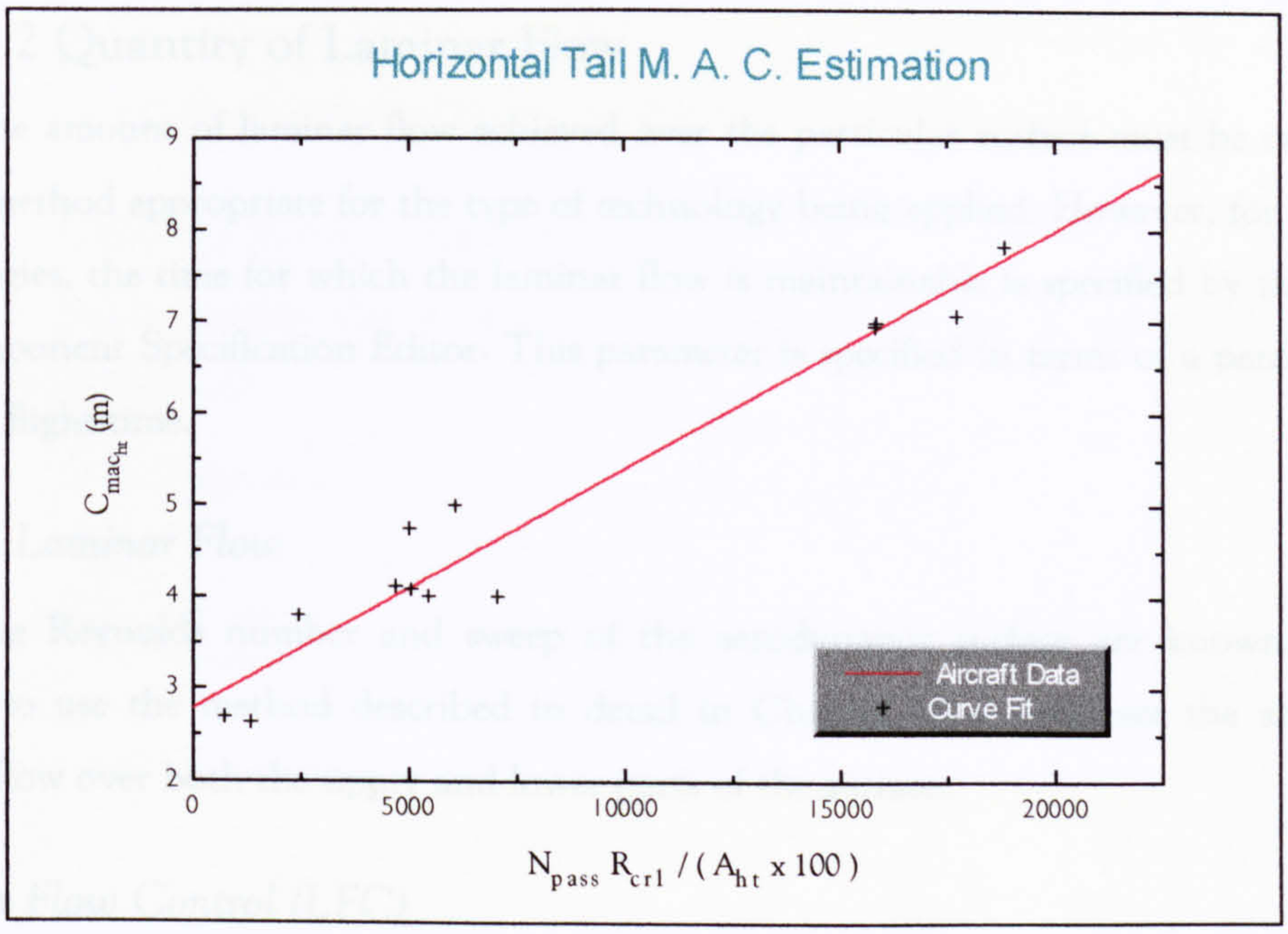


Figure 6.10- Estimation of horizontal tail MAC length

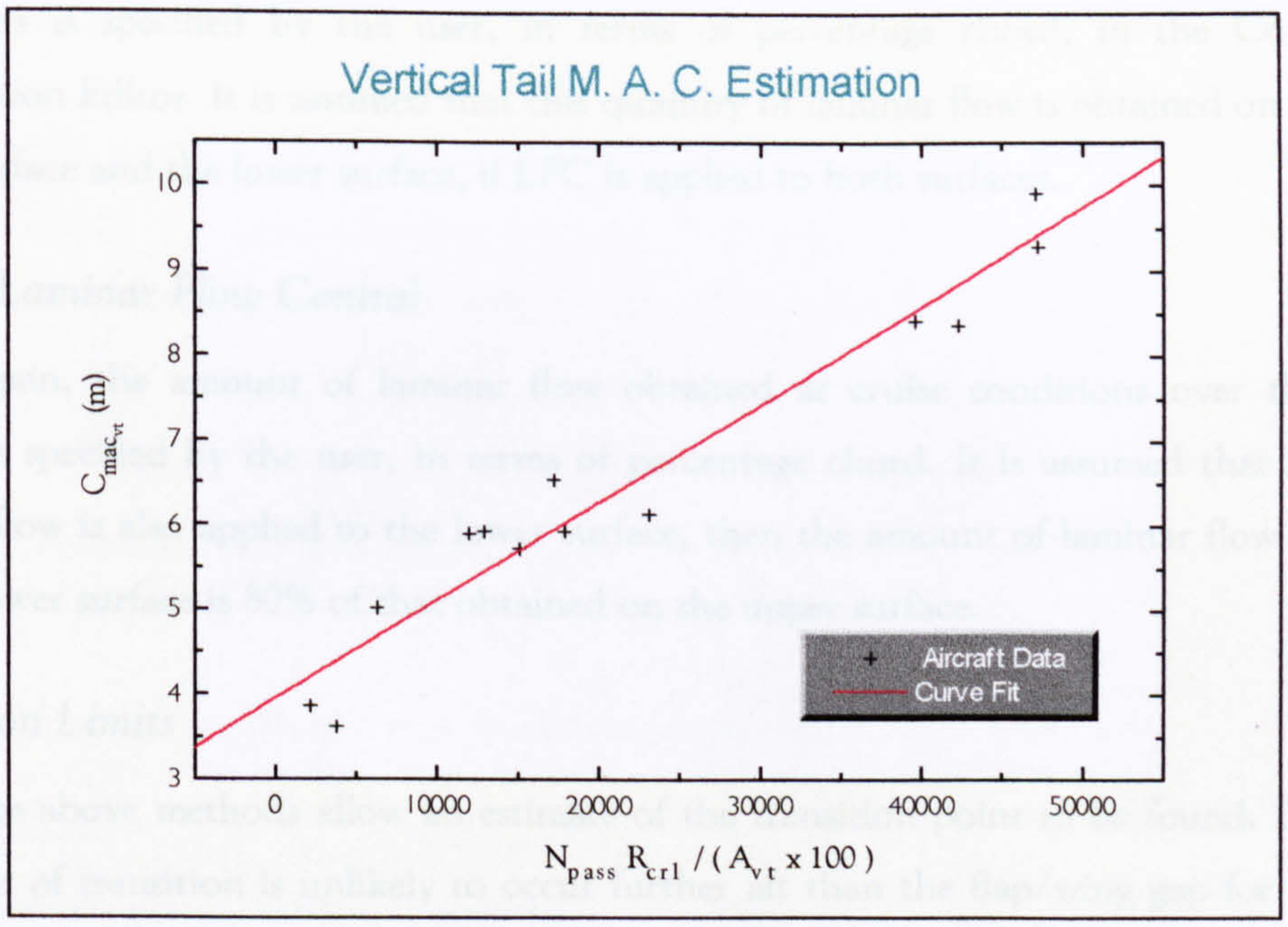


Figure 6.11- Estimation of vertical tail MAC length

For the engine nacelle, the nacelle fan cowl length (l_{fc}) and total nacelle length (l_{na}) are estimated using the results of Chapter 8.

$$l_{fc} = 0.739\left(L_{eng}\,BPR\right) + 2.60$$

$$l_{na} = 3.74e^{4.35\times10^{-6}\,T_{nominal}\times BPR^{-0.5}}$$

As the Mach number and the atmospheric properties at the cruise, diversion, and loiter conditions are known, then an estimate of the chord based Reynolds number at these conditions is possible.

6 .4 .2 .2 Quantity of Laminar Flow

The amount of laminar flow achieved over the particular surface must be calculated, using a method appropriate for the type of technology being applied. However, for all of the technologies, the time for which the laminar flow is maintainable is specified by the user in the Component Specification Editor. This parameter is specified in terms of a percentage of the total flight time.

Natural Laminar Flow

The Reynolds number and sweep of the aerodynamic surface are known, so it is possible to use the method described in detail in Chapter 10 to evaluate the amount of laminar flow over both the upper and lower parts of the surface.

Laminar Flow Control (LFC)

The amount of laminar flow achieved over a laminar flow control surface at cruise conditions is specified by the user, in terms of percentage chord, in the Component Specification Editor. It is assumed that this quantity of laminar flow is obtained on both the upper surface and the lower surface, if LFC is applied to both surfaces.

Hybrid Laminar Flow Control

Again, the amount of laminar flow obtained at cruise conditions over the upper surface is specified by the user, in terms of percentage chord. It is assumed that if hybrid laminar flow is also applied to the lower surface, then the amount of laminar flow achieved on the lower surface is 80% of that obtained on the upper surface.

Transition Limits

The above methods allow an estimate of the transition point to be found. However, this point of transition is unlikely to occur further aft than the flap/wing gap for the wing surface, or further aft than the elevator/tail, rudder/tail gaps for the horizontal and vertical tails. Laminar flow is limited to the cowl section for the case of NLF nacelles. For this reason the transition point is limited to the values show below.

Wing

$$\left(\frac{x_{tr}}{c}\right)_{\text{limit}} = 1 - {}^{c_{flap}}\!/_{c} \tag{2.15}$$

Tail Surfaces

$$\left(\frac{x_{tr}}{c}\right)_{\text{limit}} = 0.7 \tag{2.16}$$

where the assumed value of 0.7 has been found to be the average value for the normalised chordwise location of the elevator/rudder for existing civil aircraft.

6 .4 .2 .3 Laminar Flow Drag Reduction

The drag reduction due to significant portions of laminar is quantified using the methods from Raymer[90].

For Ma < 0.875 (Subsonic)

$$Re_{cutoff} = 38.21\left(\frac{C_{mac} \times ft}{K_{roughness}}\right)^{1.053}$$

For Ma >= 0.875 (Transonic)

$$Re_{cutoff} = 44.62\left(\frac{C_{mac} \times ft}{K_{roughness}}\right)^{1.053} \times Ma^{1.16}$$

Where $K_{roughness} = 0.0000208$

The Reynolds number (Re) is chosen to be the smaller of the chord based Reynolds number and the cut-off Reynolds number (Re_{cutoff}). The laminar and turbulent skin friction coefficients can then be calculated using the equations below.

$$C_{f\,\text{laminar}} = \frac{1.328}{\sqrt{Re}}$$

$$C_{f\,\text{turbulent}} = \frac{0.455}{\left(\log_{10} Re\right)^{2.58}\left(1 + 0.144\,Ma^2\right)^{0.65}}$$

Since the wing drag coefficient is proportional to the skin friction coefficient.

$$\frac{C_{D\,surface}}{C_{D100\%.turbulent\,surface}} = \left(\frac{x_{tr}}{c_{mac}} \times \frac{C_{f\,\text{laminar}}}{C_{f\,turbulent}}\right) + \left(1 - \frac{x_{tr}}{c_{mac}}\right) \tag{2.17}$$

To evaluate the overall drag reduction effect due to the improvements in the particular surface, an estimate has to be made of the proportion of the total aircraft drag that is due to the skin friction drag of this surface. An analysis was made of the output data from the Aerodynamics Module for the 13 existing aircraft designs at cruise conditions, and the following relationships were made.

$$\frac{C_{D\,wing}}{C_{D\,Total}} = 6.71 \times 10^{-7}\,\frac{N_{pass} R_{crl}}{100} + 0.2230 \quad \text{(error ~ 2.6)} \tag{2.18}$$

$$\frac{C_{D\,vt}}{C_{D\,Total}} = 3.40 \times 10^{-8}\,\frac{N_{pass} R_{crl}}{100 \times A_{vt}} + 0.0407 \quad \text{(error ~ 4.5)} \tag{2.19}$$

$$\frac{C_{D\,ht}}{C_{D\,Total}} = 5.76 \times 10^{-7} \frac{N_{pass} R_{cr1}}{100 \times A_{ht}} + 0.0583 \quad \text{(error } \sim \text{ 2.6)} \tag{2.20}$$

$$\frac{C_{D\,nac}}{C_{D\,Total}} = 1.32 \times 10^{-7} \frac{N_{pass} R_{cr1}}{100} + 0.0743 \quad \text{(error } \sim \text{ 3.4)} \tag{2.21}$$

The data and the curve fits are shown in the figures 6.12 ~ 6.15 below.

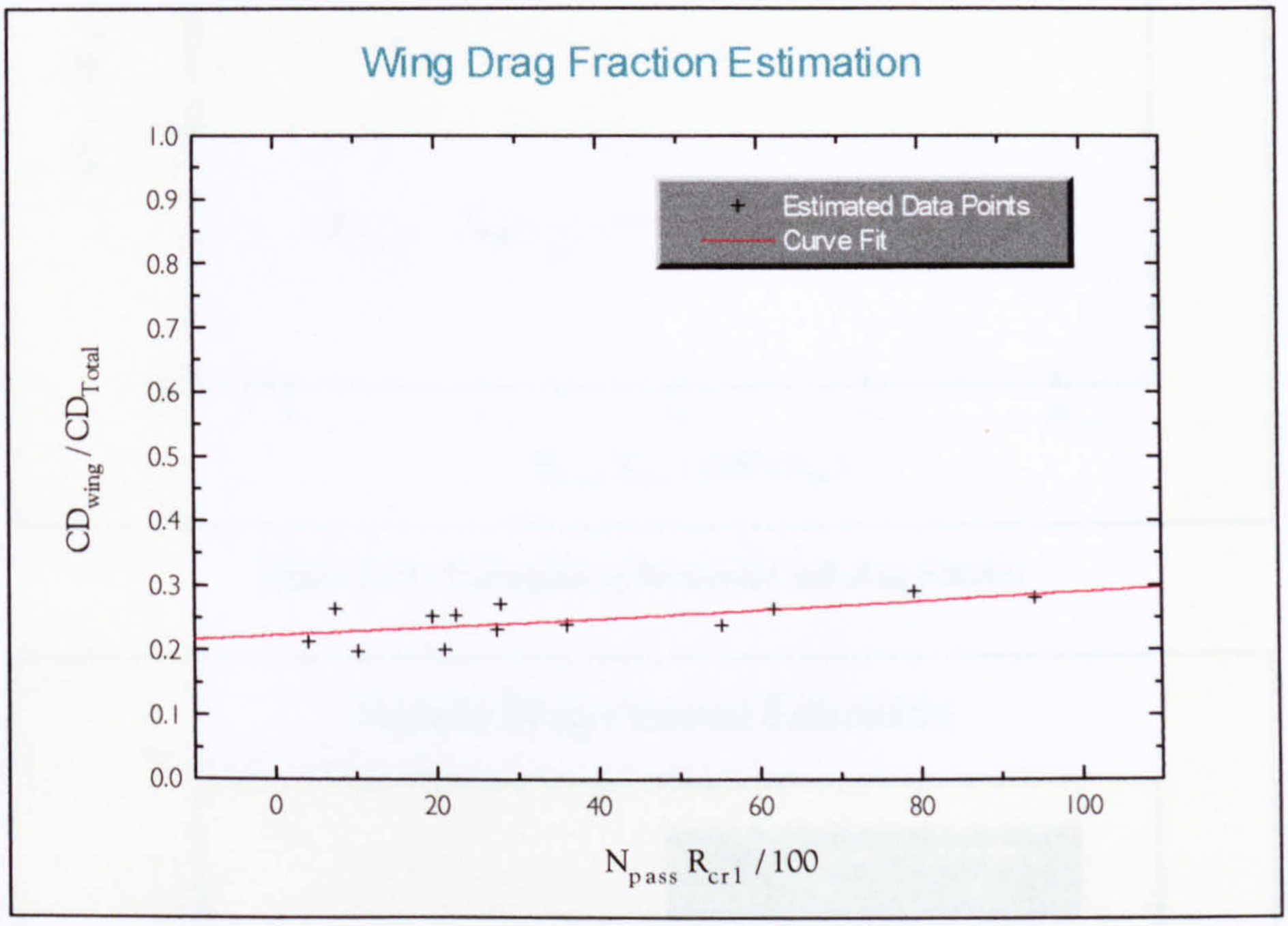


Figure 6.12- Estimation of wing drag fraction

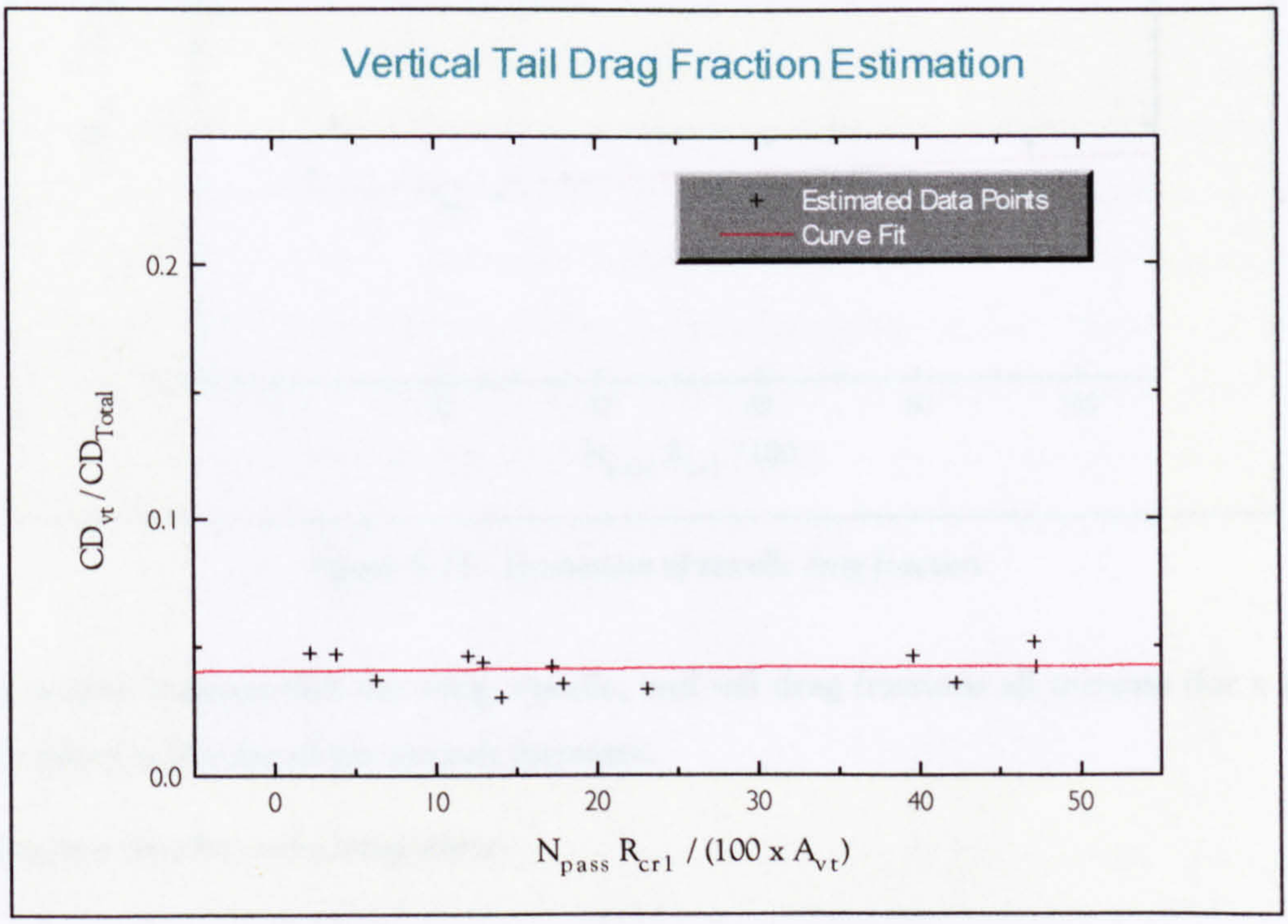


Figure 6.13 - Estimation of vertical tail drag fraction

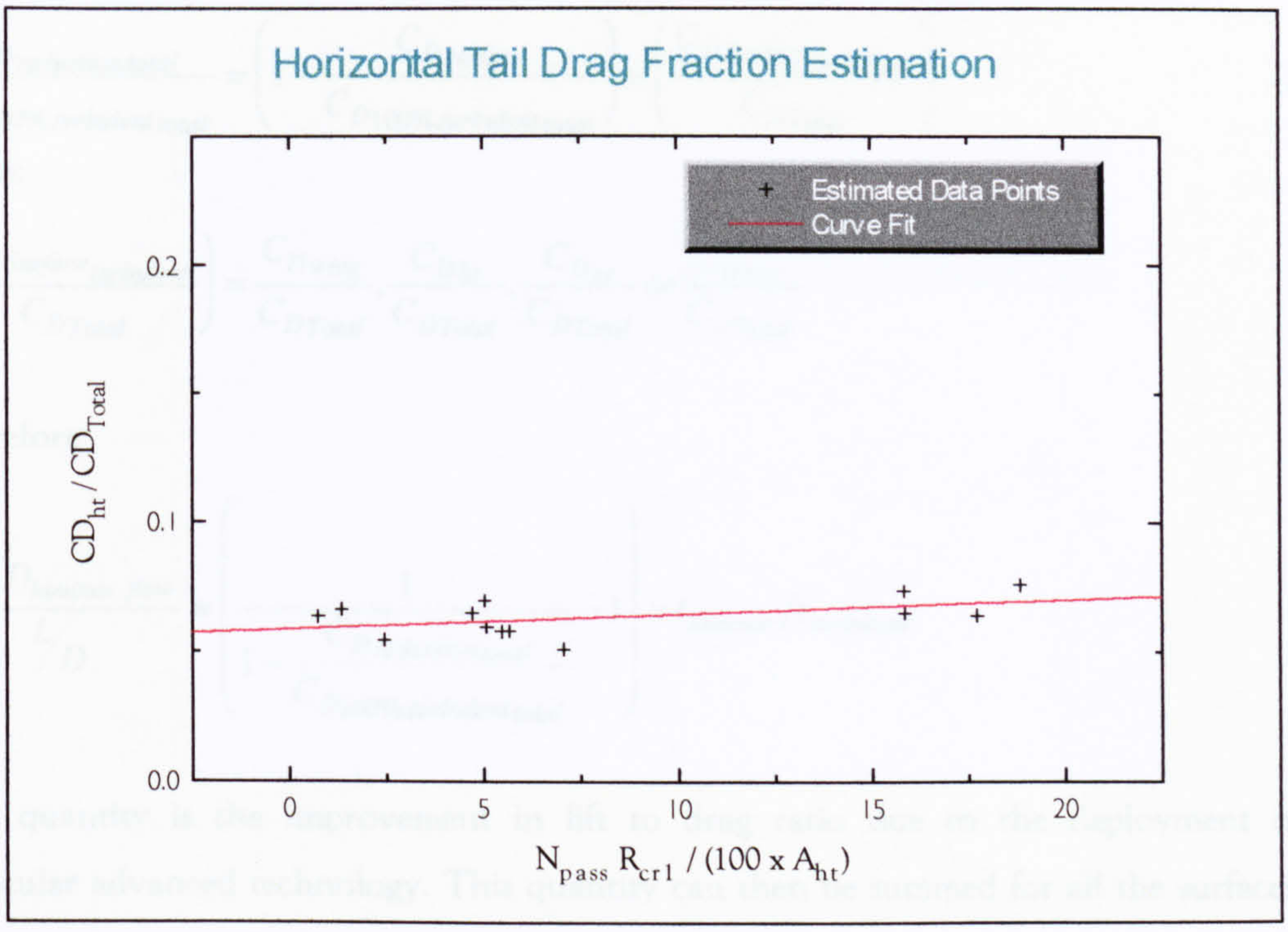


Figure 6.14- Estimation of horizontal tail drag fraction

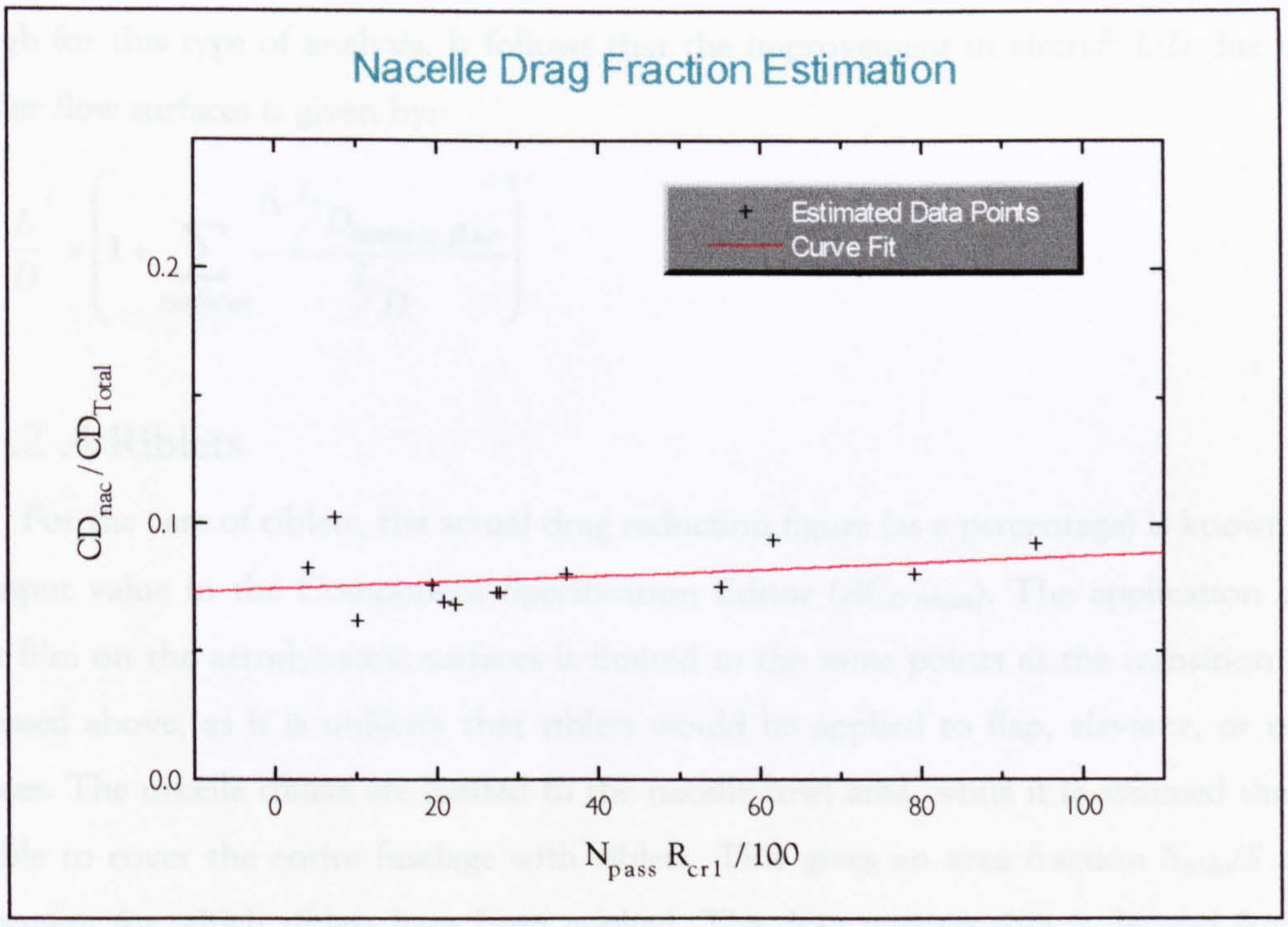


Figure 6.15 - Estimation of nacelle drag fraction

These graphs indicate that the wing, nacelle, and tail drag fractions all increase (for a given aspect ratio) as the size of the aircraft increases.

This means that for each component:-

$$\frac{C_{D\,reduction.total}}{C_{D100\%.turbulent\,total}} = \left(1 - \frac{C_{D\,surface}}{C_{D100\%.turbulent\,total}}\right) \times \left(\frac{C_{D\,Surface\,turbulent}}{C_{D\,Total}}\right) \tag{2.22}$$

where

$$\left(\frac{C_{D\,Surface\,turbulent}}{C_{D\,Total}}\right) = \frac{C_{D\,wing}}{C_{D\,Total}}, \frac{C_{D\,ht}}{C_{D\,Total}}, \frac{C_{D\,vt}}{C_{D\,Total}} \; or \; \frac{C_{D\,nac}}{C_{D\,Total}}$$

Therefore

$$\frac{\Delta L/D_{laminar.flow}}{L/D} \approx \left(\frac{1}{1 - \frac{C_{D\,reduction\,total}}{C_{D100\%.turbulent\,total}}} - 1\right) \times t_{laminar}/t_{turbulent} \tag{2.23}$$

This quantity is the improvement in lift to drag ratio due to the deployment of the particular advanced technology. This quantity can then be summed for all the surfaces that implement some kind of laminar flow technology. Although this summing procedure ignores any secondary effects and the inter dependency of each component, this should be accurate enough for this type of analysis. It follows that the improvement in aircraft *L\D* due to the laminar flow surfaces is given by:-

$$\frac{L}{D} = \frac{L}{D}' \times \left(1 + \sum_{surfaces} \frac{\Delta L/D_{laminar.flow}}{L/D}\right) \tag{2.24}$$

6 .4 .2 .4 Riblets

For the case of riblets, the actual drag reduction figure (as a percentage) is known from the input value in the Component Specification Editor ($\Delta C_{D\,riblets}$). The application of the riblet film on the aerodynamic surfaces is limited to the same points as the transition limits expressed above, as it is unlikely that riblets would be applied to flap, elevator, or rudder surfaces. The nacelle riblets are limited to the nacelle cowl area, while it is assumed that it is possible to cover the entire fuselage with riblets. This gives an area fraction S_{riblet}/S of the component for which riblets have been applied. The drag portion that is derived from the fuselage is estimated from the equation below.

$$\frac{C_{D\,fuselage}}{C_{D\,Total}} = 0.20806 \times e^{-3.53\times10^{-6}\frac{N_{pass}R_{cr1}}{100}} \tag{2.25}$$

The graph of figure 6.16 clearly indicates that as the aircraft size increase, the fuselage becomes relatively more efficient and its contribution to the overall drag decreases.

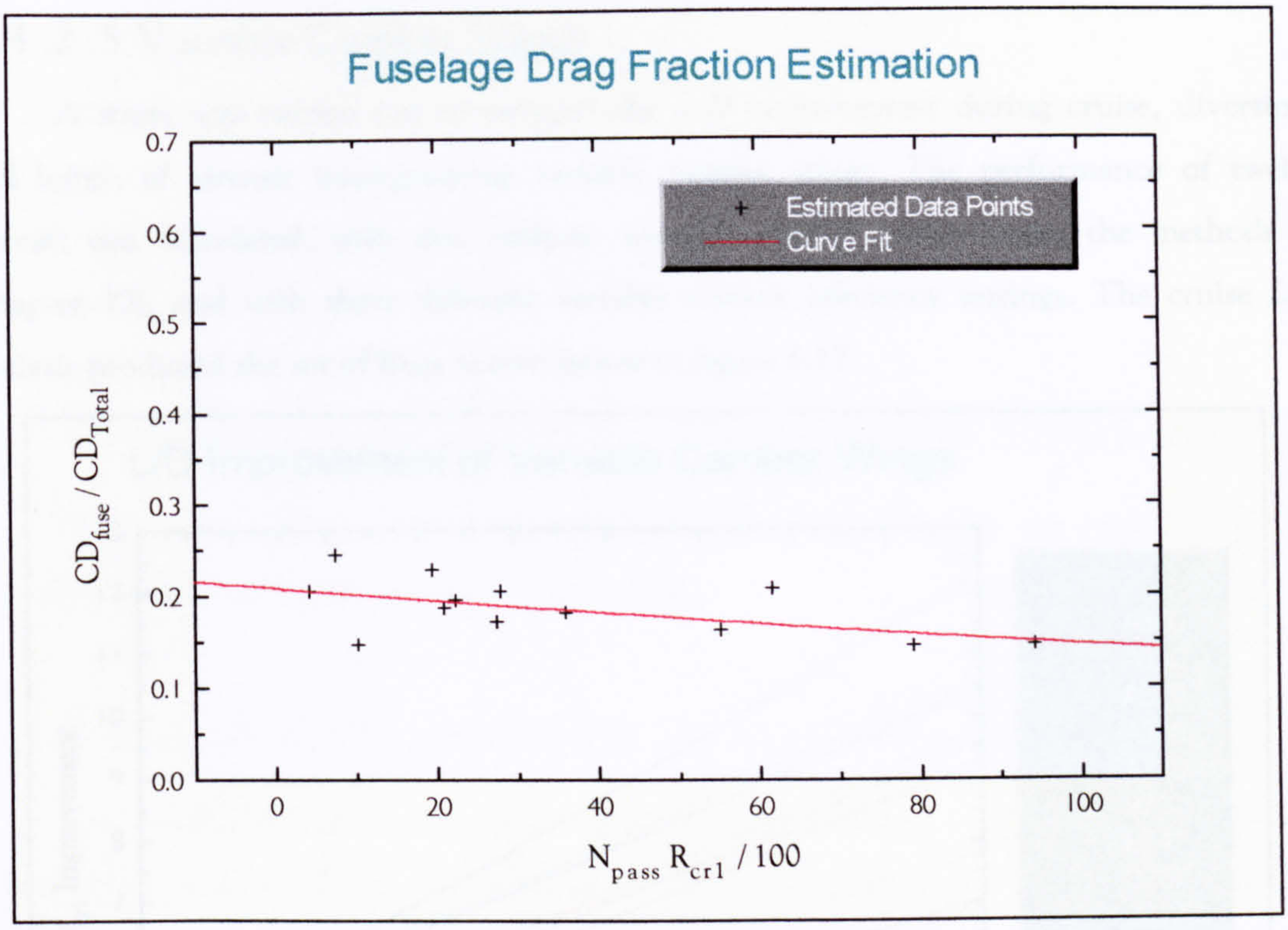


Figure 6.16- Estimate of fuselage drag fraction

The lift to drag ratio improvement is then calculated as follows.

$$\frac{C_{D\,riblets\,surface}}{C_{D\,surface}} = \left(1 - \Delta C_{D\,riblets}\right) \times \frac{S_{riblets}}{S} \tag{2.26}$$

so for each component

$$\frac{C_{D\,reduction.total}}{C_{D\,total}} = \left(1 - \frac{C_{D\,riblets\,surface}}{C_{D\,surface}}\right) \times \left(\frac{C_{D\,Surface}}{C_{D\,Total}}\right) \tag{2.27}$$

where

$$\left(\frac{C_{D\,Surface}}{C_{D\,Total}}\right) = \frac{C_{D\,wing}}{C_{D\,Total}}, \frac{C_{D\,ht}}{C_{D\,Total}}, \frac{C_{D\,vt}}{C_{D\,Total}}, \frac{C_{D\,nac}}{C_{D\,Total}}, or \frac{C_{D\,fuse}}{C_{D\,Total}}$$

as before,

$$\frac{\Delta L/D_{riblets}}{L/D} \approx \left(\frac{1}{1 - \frac{C_{D\,reduction\,total}}{C_{D\ total}}} - 1\right) \tag{2.28}$$

$$\frac{L}{D} = \frac{L}{D}' \times \left(1 + \sum_{surfaces} \frac{\Delta L/D_{riblets}}{L/D}\right) \tag{2.29}$$

6 .4 .2 .5 Variable Camber Wings

A study was carried out to estimate the *L/D* improvement during cruise, diversion, and loiter, of aircraft incorporating variable camber wings. The performance of twelve aircraft was calculated, with and without variable camber wings (using the methods of Chapter 10), and with three different variable camber efficiency settings. The cruise *L/D* analysis produced the set of lines shown below in figure 6.17.

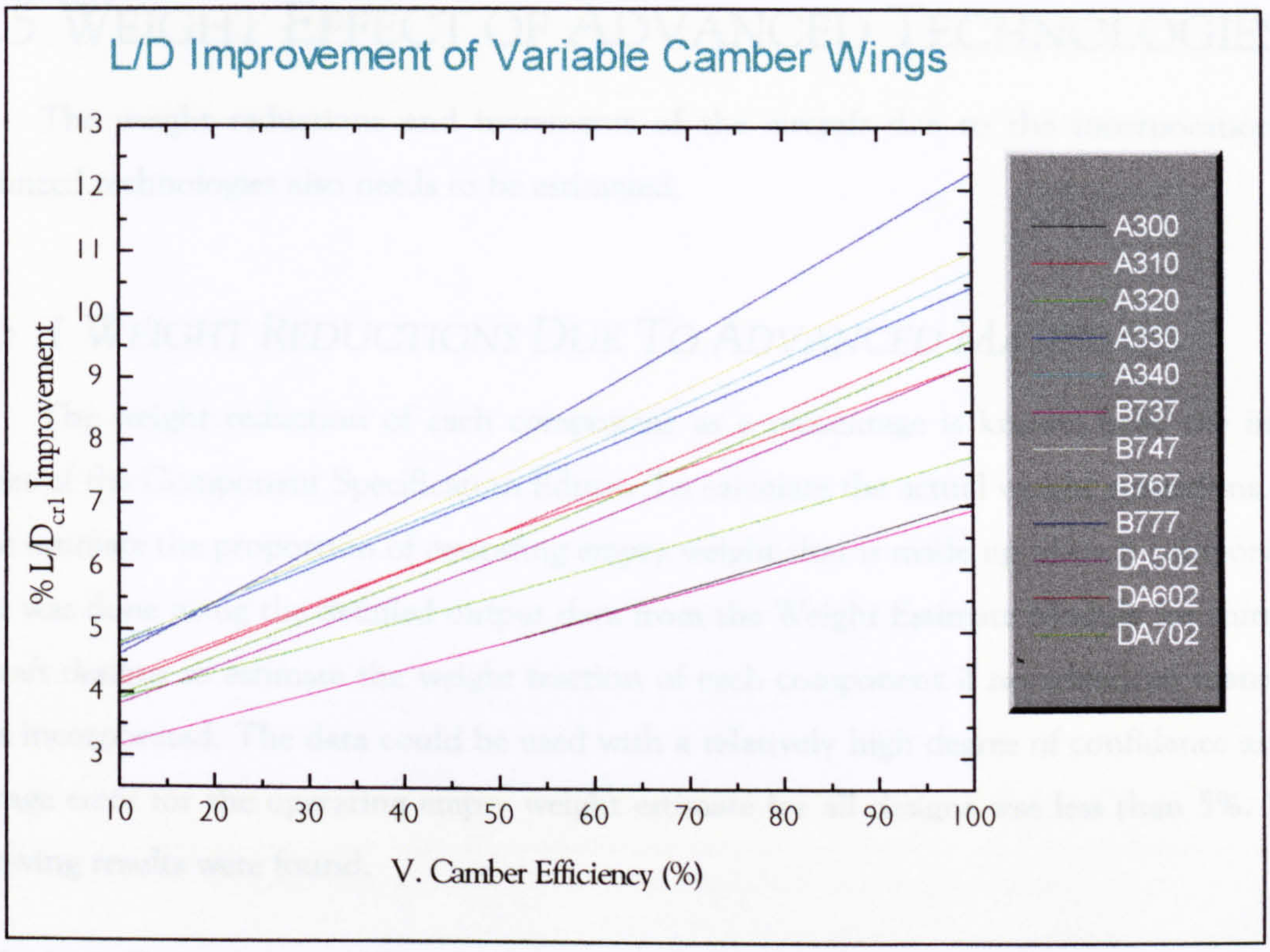


Figure 6.17 - Effect of variable camber efficiency on cruise L\D improvement

It was found that it was possible to relate the lines with the following equations.

Assuming that the line is given by $y = mx + c$

$$m = 1.934 \times 10^{-7}\left(\frac{N_{pass} R_{cr1}}{100}\right) + 0.0541 \qquad (2.30)$$

$$c = 5.701 \times 10^{-7}\left(\frac{N_{pass} R_{cr1}}{100}\right) + 3.49 \qquad (2.31)$$

This means that the percentage *L/D* improvement during the main cruise can be found by calculating the linear coefficients m and c, and then calculating the point occupied on this line occupied at the particular variable camber efficiency.

It was subsequently discovered that approximations for the diversion and loiter *L/D* improvements could be expressed as:-

$$\left(\frac{\Delta L/D_{v.camber}}{L/D_{conventional}}\right)_{diversion} \approx \left(\frac{\Delta L/D_{v.camber}}{L/D_{conventional}}\right)_{cruise} \times \frac{1}{1.8} \tag{2.32}$$

$$\left(\frac{\Delta L/D_{v.camber}}{L/D_{conventional}}\right)_{loiter} \approx \left(\frac{\Delta L/D_{v.camber}}{L/D_{conventional}}\right)_{cruise} \tag{2.33}$$

6 .5 Weight Effect of Advanced Technologies

The weight reductions and increments of the aircraft due to the incorporation of advanced technologies also needs to be estimated.

6 .5 .1 Weight Reductions Due To Advanced Materials

The weight reduction of each component as a percentage is known from the input values of the Component Specification Editor. To calculate the actual weight reductions one must estimate the proportion of operating empty weight that is made up of each component. This was done using the detailed output data from the Weight Estimate Module for thirteen aircraft designs to estimate the weight fraction of each component if no advanced materials were incorporated. The data could be used with a relatively high degree of confidence as the average error for the operating empty weight estimate for all designs was less than 5%. The following results were found.

6 .5 .1 .1 Component Weight Ratios

For the main component areas it was discovered that the ratio of the component weight to the operating empty weight appeared to be a function takeoff weight. Thus, a correlation with the parameter N_{pass} x R_{cr1} was used, and the equations shown below were derived from the data plotted in figure 6.18.

$$\frac{W_{nac}}{W'_{oew}} \approx 3.94\times10^{-2} e^{-2.52\times10^{-6}\left(\frac{N_{pass}R_{cr1}}{100}\right)} \qquad \text{(error } \sim \text{ 2.3)} \tag{2.34}$$

$$\frac{W_{uc}}{W'_{oew}} \approx 2.45\times10^{-7}\left(\frac{N_{pass}R_{cr1}}{100}\right)+0.0681 \qquad \text{(error } \sim \text{ 1.7)} \tag{2.35}$$

$$\frac{W_{fuse}}{W'_{oew}} \approx -1.90\times10^{-7}\left(\frac{N_{pass}R_{cr1}}{100}\right)+0.1825 \qquad \text{(error } \sim \text{ 1.9)} \tag{2.36}$$

$$\frac{W_{pg}}{W'_{oew}} \approx 0.895e^{-0.200\left(\frac{N_{pass}R_{cr1}}{100}\right)} \qquad \text{(error } \sim \text{ 2.7)} \tag{2.37}$$

$$\frac{W_{ase}}{W'_{oew}} \approx 0.48\left(\frac{N_{pass}R_{cr1}}{100}\right)^{-0.112} \qquad \text{(error } \sim 1.4\text{)} \qquad (2.38)$$

$$\frac{W_{sc}}{W'_{oew}} \approx 0.0387e^{-1.39\times10^{-5}\left(\frac{N_{pass}R_{cr1}}{100}\right)} \qquad \text{(error } \sim 1.6\text{)} \qquad (2.39)$$

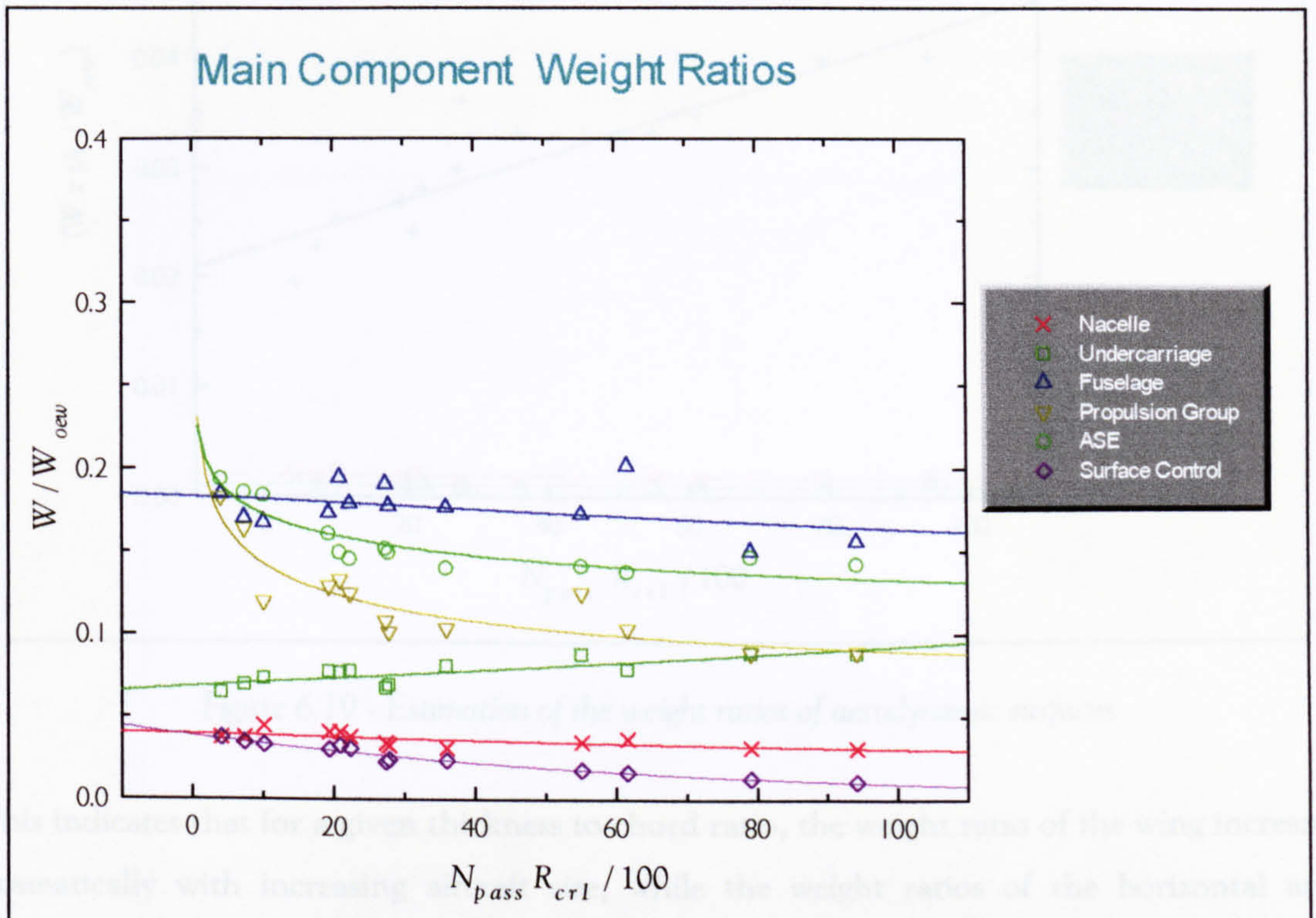


Figure 6.18 - Estimation of the main component weight ratios

The graph clearly shows that the weight ratios of all the main non-aerodynamic components, with the exception of the airframe services and equipment, have a tendency to decrease with increasing aircraft size. For the aerodynamic surfaces, it was more difficult to find a reasonable data trend, however, the final results are accurate enough for initial sizing purposes. The thickness to chord ratio of the surface has been introduced to give more qualitative accuracy. The equations are shown below.

$$\frac{W_{wing}\times t/c_{root}}{W'_{oew}}t \approx 2.06\times10^{-7}\left(\frac{N_{pass}R_{cr1}}{100}\right)+0.0228 \qquad \text{(error } \sim 2.8\text{)} \qquad (2.40)$$

$$\frac{W_{ht}\times t/c_{tail}}{W'_{oew}} \approx 0.00194e^{-1.51\times10^{-6}\left(\frac{N_{pass}R_{cr1}}{100}\right)} \qquad \text{(error } \sim 4.9\text{)} \qquad (2.41)$$

$$\frac{W_{vt}\times t/c_{tail}}{W'_{oew}} \approx 0.00109e^{-1.95\times10^{-6}\left(\frac{N_{pass}R_{cr1}}{100}\right)} \qquad \text{(error } \sim 7.3\text{)} \qquad (2.42)$$

The data from which these equations were derived is plotted below.

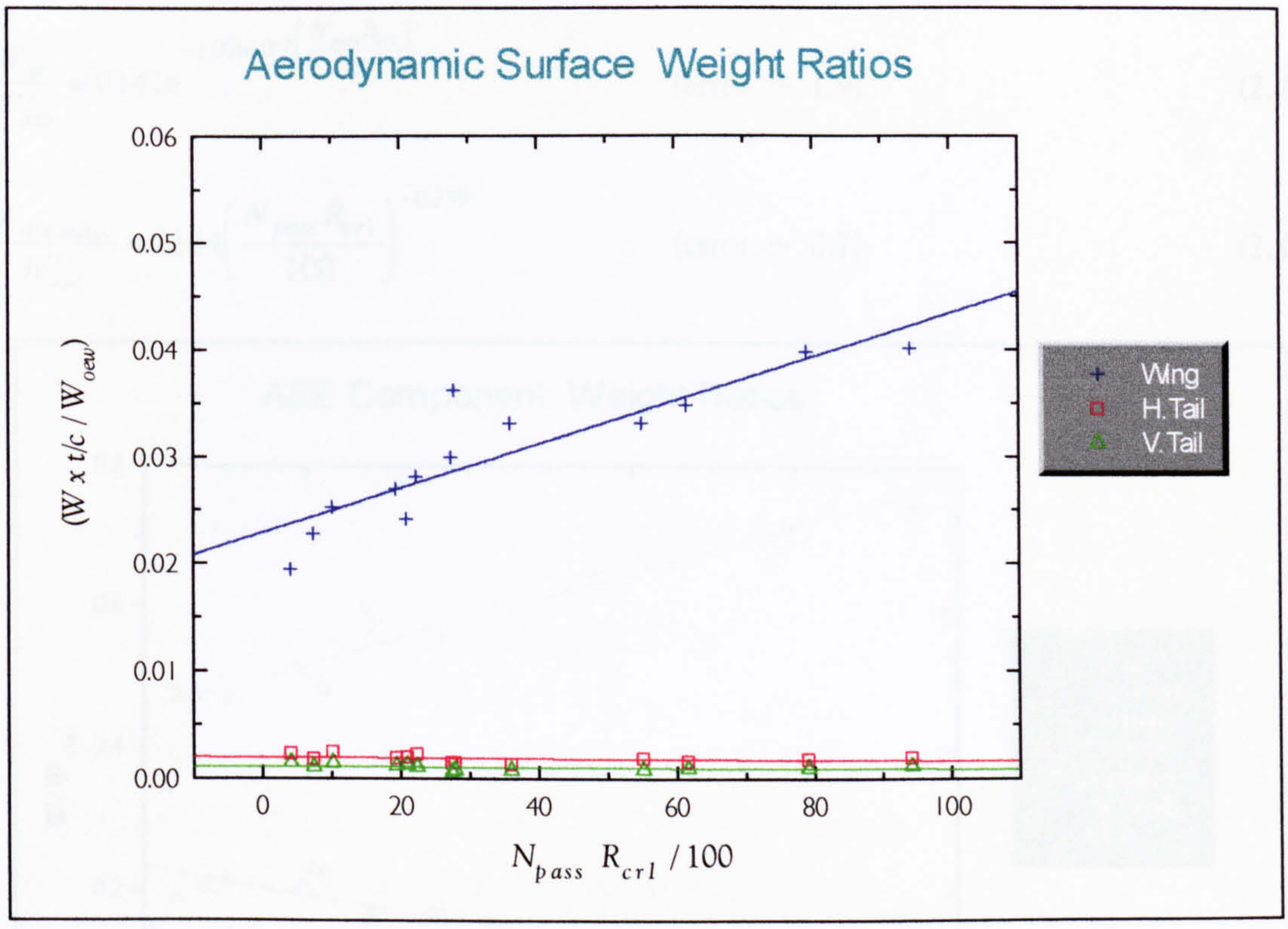


Figure 6.19 - Estimation of the weight ratios of aerodynamic surfaces

This indicates that for a given thickness to chord ratio, the weight ratio of the wing increases dramatically with increasing aircraft size, while the weight ratios of the horizontal and vertical tails remain virtually constant.

Equations and data for the detailed breakdown of the airframe services and equipment (ASE) parts are given below.

$$\frac{W_{apu}}{W'_{ase}} \approx 6.85\left(\frac{N_{pass}R_{cr1}}{100}\right)^{-0.548} \qquad \text{(error } \sim \text{ 1.4)} \qquad (2.43)$$

$$\frac{W_{iae}}{W'_{ase}} \approx 0.0516e^{-5.87\times10^{-6}\left(\frac{N_{pass}R_{cr1}}{100}\right)} \qquad \text{(error } \sim \text{ 2.0)} \qquad (2.44)$$

$$\frac{W_{hyd}}{W'_{ase}} \approx 0.0798e^{-1.28\times10^{-6}\left(\frac{N_{pass}R_{cr1}}{100}\right)} \qquad \text{(error } \sim \text{ 0.9)} \qquad (2.45)$$

$$\frac{W_{el}}{W'_{ase}} \approx 0.235e^{-9.85\times10^{-6}\left(\frac{N_{pass}R_{cr1}}{100}\right)} \qquad \text{(error } \sim \text{ 2.9)} \qquad (2.46)$$

$$\frac{W_{furn}}{W'_{ase}} \approx 3.26\times10^{-6}\left(\frac{N_{pass}R_{cr1}}{100}\right)+0.453 \qquad \text{(error } \sim \text{ 1.3)} \qquad (2.47)$$

$$\frac{W_{ac}}{W'_{ase}} \approx 0.141e^{-1.07\times10^{-5}\left(\frac{N_{pass}R_{cr1}}{100}\right)} \quad \text{(error ~ 1.9)} \tag{2.48}$$

$$\frac{W_{ase.misc.}}{W'_{ase}} \approx 0.144\left(\frac{N_{pass}R_{cr1}}{100}\right)^{-0.259} \quad \text{(error ~ 0.7)} \tag{2.49}$$

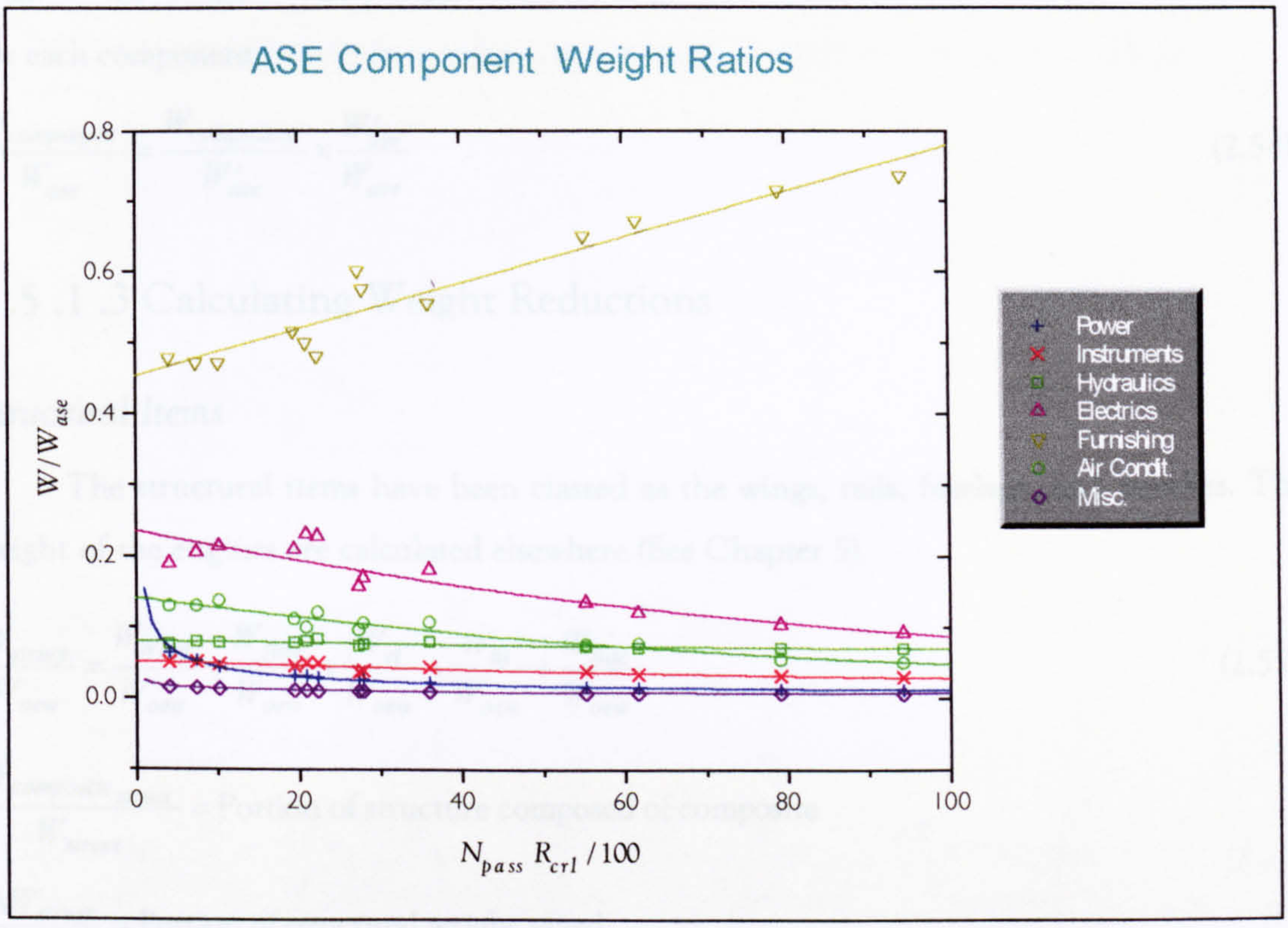


Figure 6.20- Estimation of the ASE component weight ratios

It is clear from the above graph that the weight ratios of all the ASE components, with the exception of the furnishings, tend to decrease with increasing aircraft size.

6 .5 .1 .2 Normalising Component Weights

As these component weights are only estimates they will not sum exactly to 100%, therefore they need to be normalised.

$$\frac{W_{oew}}{W'_{oew}} = \frac{W_{Wing}}{W'_{oew}} + \frac{W_{fuse}}{W'_{oew}} + \frac{W_{vt}}{W'_{oew}} + \frac{W_{ht}}{W'_{oew}} + \frac{W_{nac}}{W'_{oew}} + \frac{W_{pg}}{W'_{oew}} + \frac{W_{ase}}{W'_{oew}} + \frac{W_{ope}}{W'_{oew}} + \frac{W_{uc}}{W'_{oew}} + \frac{W_{sc}}{W'_{oew}} \tag{2.50}$$

where the operational item weight fraction is estimated from a data correlation:-

$$\frac{W_{ope}}{W'_{oew}} \approx 7.65\times10^{-7}\left(\frac{N_{pass}R_{cr1}}{100}\right) + 0.124 \tag{2.51}$$

Therefore for each component:-

$$\frac{W_{component}}{W_{oew}} = \frac{W_{component}}{W'_{oew}} \times \frac{W'_{oew}}{W_{oew}} \tag{2.52}$$

Similarly, for the ASE components

$$\frac{W_{ase}}{W'_{ase}} = \frac{W_{apu}}{W'_{ase}} + \frac{W_{iae}}{W'_{ase}} + \frac{W_{hyd}}{W'_{ase}} + \frac{W_{el}}{W'_{ase}} + \frac{W_{ac}}{W'_{ase}} + \frac{W_{ase.misc}}{W'_{ase}} + \frac{W_{furn}}{W'_{ase}} \tag{2.53}$$

for each component

$$\frac{W_{component}}{W_{ase}} = \frac{W_{component}}{W'_{ase}} \times \frac{W'_{ase}}{W_{ase}} \tag{2.54}$$

6 .5 .1 .3 Calculating Weight Reductions

Structural Items

The structural items have been classed as the wings, tails, fuselage, and nacelles. The weight of the engines are calculated elsewhere (See Chapter 5).

$$\frac{W_{struct}}{W_{oew}} = \frac{W_{Wing}}{W_{oew}} + \frac{W_{fuse}}{W_{oew}} + \frac{W_{vt}}{W_{oew}} + \frac{W_{ht}}{W_{oew}} + \frac{W_{Nac}}{W_{oew}} \tag{2.55}$$

$\frac{W_{composite_{struct}}}{W_{struct}}$ = Portion of structure composed of composite

$\frac{\Delta W_{struct}}{W_{struct}}$ = Portion of structural weight saved

$\frac{\Delta W_{oew\,struct}}{W_{oew}}$ = Portion of O.E.W. weight saved due to reductions in structural weight

$\frac{W_{composite_{comp.}}}{W_{comp}}$ = Portion of each component composed of composite (set in C.S.E.)

$\frac{\Delta W_{comp}}{W_{comp}}$ = Portion of component weight saved (Calculated in Component Specification Editor)

$$\frac{W_{composite_{struct}}}{W_{struct}} = \sum_{struct} \frac{W_{comp}}{W_{oew}} \times \frac{W_{composite_{comp}}}{W_{comp}} \times \frac{W_{oew}}{W_{struct}} \tag{2.56}$$

$$\frac{\Delta W_{struct}}{W_{struct}} = \sum_{struct} \frac{W_{comp}}{W_{oew}} \times \frac{\Delta W_{comp}}{W_{comp}} \times \frac{W_{oew}}{W_{struct}} \tag{2.57}$$

$$\frac{\Delta W_{oew\,struct}}{W_{oew}} = \sum_{struct} \frac{W_{comp}}{W_{oew}} \times \frac{\Delta W_{comp}}{W_{comp}} \tag{2.58}$$

Non-structural Items

$\frac{\Delta W_{non-struct}}{W_{non-struct}}$ = Portion of non structural weight saved

$\frac{\Delta W_{oew\,non-struct}}{W_{oew}}$ = Portion of O.E.W. weight saved due to reductions in non structural weight

$\frac{\Delta W_{comp}}{W_{comp}}$ = Portion of component weight saved (Set in Component Specification Editor)

$$\frac{W_{non-struct}}{W_{oew}} = 1 - \frac{W_{struct}}{W_{oew}} \tag{2.59}$$

and

$$\frac{W_{ase}}{W_{non-struct}} = \frac{W_{ase}}{W_{oew}} \times \frac{W_{oew}}{W_{non-struct}} \tag{2.60}$$

So

$$\frac{\Delta W_{oew\,non-struct}}{W_{oew}} = \frac{W_{uc}}{W_{oew}}\frac{\Delta W_{uc}}{W_{uc}} + \frac{W_{sc}}{W_{oew}}\frac{\Delta W_{sc}}{W_{sc}} + \frac{\Delta W_{oew\,ase}}{W_{oew}} \tag{2.61}$$

and

$$\frac{\Delta W_{non-struct}}{W_{non-struct}} = \frac{W_{uc}}{W_{oew}}\frac{\Delta W_{uc}}{W_{uc}}\frac{W_{oew}}{W_{non-struct}} + \frac{W_{sc}}{W_{oew}}\frac{\Delta W_{sc}}{W_{sc}}\frac{W_{oew}}{W_{non-struct}} + \frac{\Delta W_{non-struct\,ase}}{W_{non-struct}} \tag{2.62}$$

The weight savings of the airframe services and equipment are calculated as follows:-

$$\frac{\Delta W_{oew\,ase}}{W_{oew}} = \sum_{ase.items} \frac{W_{comp}}{W_{ase}} \times \frac{\Delta W_{comp}}{W_{comp}} \times \frac{W_{ase}}{W_{oew}} \tag{2.63}$$

$$\frac{\Delta W_{non-struct\,ase}}{W_{non-struct}} = \sum_{ase.items} \frac{W_{comp}}{W_{ase}} \times \frac{\Delta W_{comp}}{W_{comp}} \times \frac{W_{ase}}{W_{non-struct}} \tag{2.64}$$

Therefore the total amount of weight saving of operational empty weight is given by:-

$$\frac{\Delta W_{oew\,ad.material}}{W_{oew}} = \frac{\Delta W_{oew\,struct}}{W_{oew}} + \frac{\Delta W_{oew\,non-struct}}{W_{oew}} \tag{2.65}$$

6 .5 .2 *Weight Adjustments due to Active Drag Devices*

The only adjustments considered of significant importance at this initial sizing stage are the increases/decreases of the wing weight due to the implementation of variable camber wings, laminar flow control, and hybrid laminar flow control.

6 .5 .2 .1 Variable Camber Wings

The amount of wing weight increase or decrease due to the implementation of variable camber wings ($\Delta W_{Wing\,v.camber}/W_{wing}$)is set by the user in the Component Specification Editor (the default setting is a reduction of 10%).

6 .5 .2 .2 Laminar Flow Control

An analysis of the output from the Weight Estimation Module for a range of designs incorporating L.F.C. showed that for an aircraft incorporating laminar control surfaces into its wings, the average weight increase of the wings for each surface (upper and lower) is approximately 4.2%. This is with the laminar flow control weight tuning parameter from the C.S.E. set to 100%. Therefore:-

For one surface LFC

$$\frac{\Delta W_{wing\,lfc}}{W_{wing}} = \frac{4.2}{100} \times K_{tune\,lfc.weight} \tag{2.66}$$

For two surface LFC

$$\frac{\Delta W_{wingl\,lfc}}{W_{wing}} = \frac{8.4}{100} \times K_{tune\,lfc.weight} \tag{2.67}$$

6 .5 .2 .3 Hybrid Laminar Flow Control

A similar analysis performed for hybrid laminar flow systems has shown an average wing weight increment of 1% per surface. This is also with the hybrid laminar flow control weight tuning parameter set to 100%.

For one surface HLFC

$$\frac{\Delta W_{wing\,hlfc}}{W_{wing}} = \frac{1.0}{100} \times K_{tune\,hlfc.weight} \tag{2.68}$$

For two surface H.L.F.C.

$$\frac{\Delta W_{wing\,hlfc}}{W_{wing}} = \frac{2.0}{100} \times K_{tune\,hlfc.weight} \tag{2.69}$$

6 .5 .2 .4 Weight Adjustment

The adjustment to operational empty weight is given by:-

$$\frac{\Delta W_{oew\,active.drag}}{W_{oew}} = \frac{\Delta W_{wing\,activedrag}}{W_{wing}} \times \frac{W_{Wing}}{W_{oew}} \tag{2.70}$$

6 .6 WEIGHT FRACTIONS

The method used to calculate the fraction W_{fuel}/W_0 is based upon the standard methods described in Raymer[90] and Roskam[82]. However, the actual values given to the component fractions have been modified to more realistically reflect the flight profile of a medium to large subsonic civil transport. The detailed output from the Performance Module has been analysed for thirteen different aircraft designs. It was possible to assign values or expressions to each of the weight fractions based upon this analysis. The Performance Module produced in the region of 30 flight profiles, based upon differing cruise requirements for the different designs. The average error of these profiles was approximately 3%. This would suggest that the data for each segment is reliable, and is therefore applicable for this type of analysis. The equations used to approximate the weight fractions have been designed to incorporate some of the factors that will most directly influence the value of those fractions.

6 .6 .1 TAKEOFF

$$\frac{W_{takeoff}}{W_0} = 2.67\times10^{-9}\left(\frac{N_{pass}R_{cr1}}{100}\right)+0.9987 \qquad \text{(error} \sim 0.003\text{)} \qquad (2.71)$$

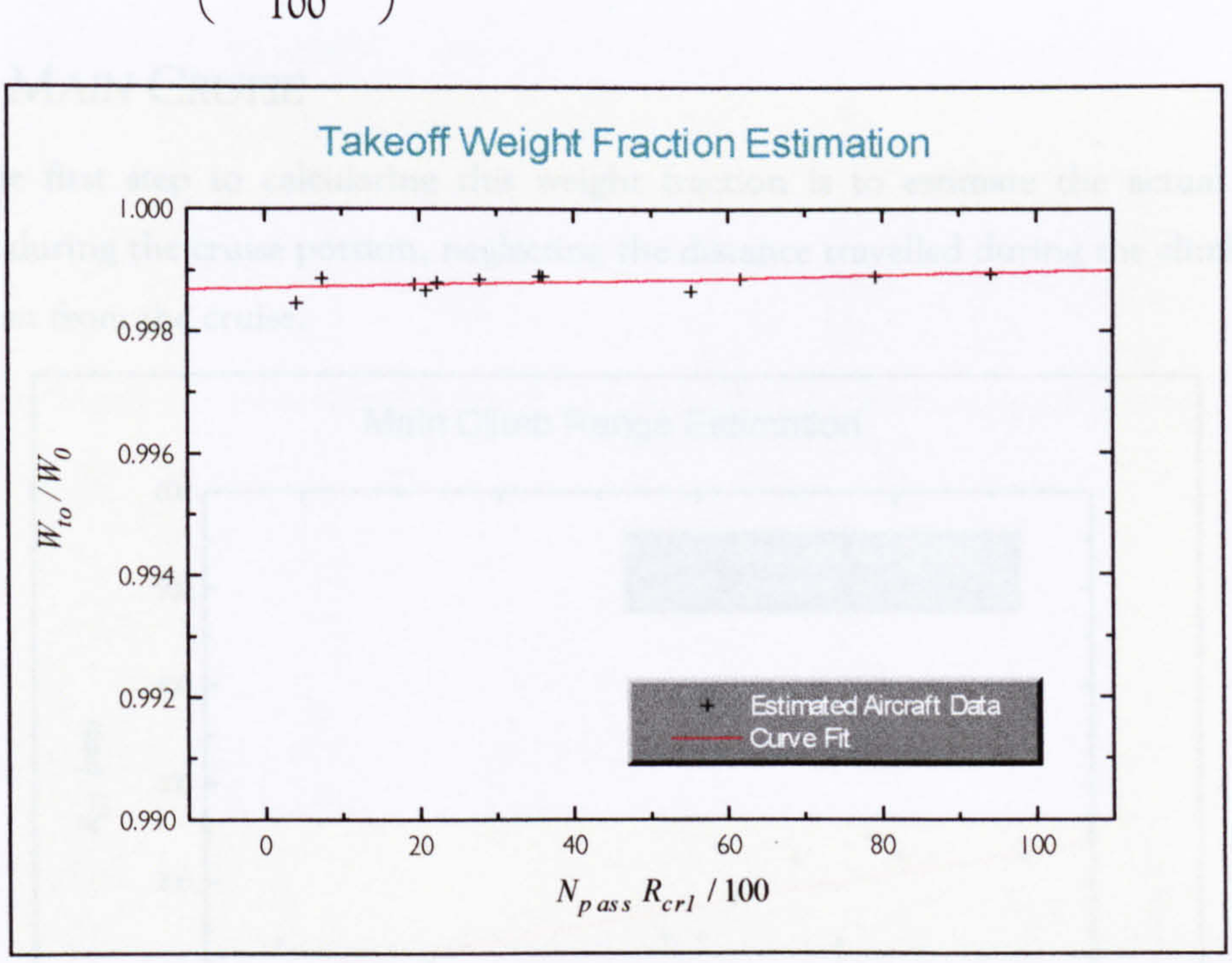


Figure 6.21- Estimation of the takeoff weight fraction

6 .6 .2 CLIMB TO THE CRUISE ALTITUDE

$$\frac{W_{cl1}}{Wto} = -4.86\times10^{-9}\left(\frac{N_{pass}R_{cr1}Ma_{cr1}h_{cr1}\times10}{T_{\text{nominal}}N_e}\right)+0.9795 \quad (\text{error}\sim 0.0085) \tag{2.72}$$

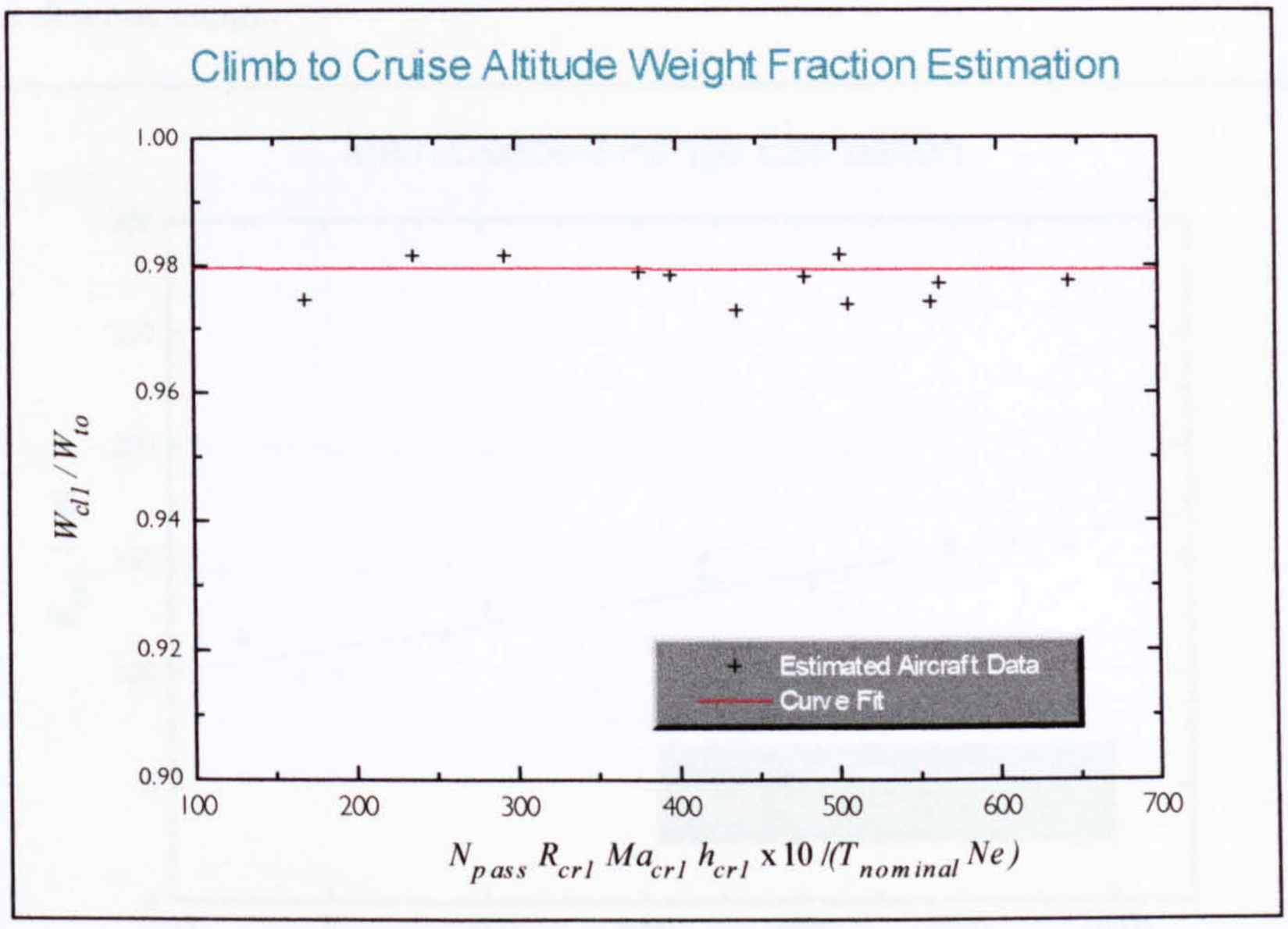


Figure 6.22- Estimation of the climb to cruise altitude weight fraction

6 .6 .3 MAIN CRUISE

The first step to calculating this weight fraction is to estimate the actual distance travelled during the cruise portion, neglecting the distance travelled during the climb to, and the descent from the cruise.

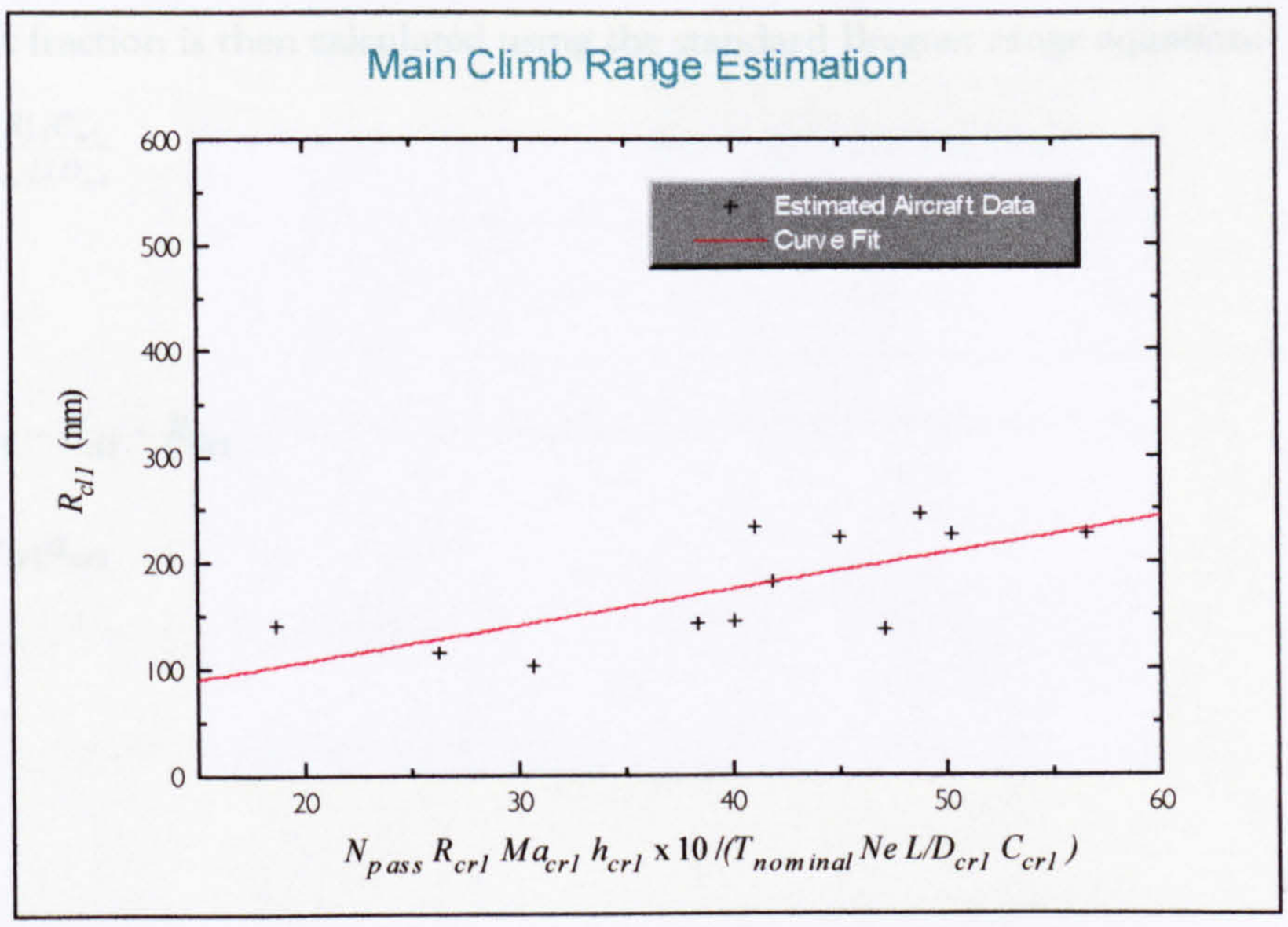


Figure 6.23- Estimation of the range to climb to the main cruise altitude

R_{cl1} in nm.

$$R_{cl1} = 3.41\left(\frac{N_{pass} R_{cr1} Ma_{cr1} h_{cr1} \times 10}{T_{nominal} N_e L/D_{cr1} C_{cr1}}\right) + 38.2 \qquad \text{(error} \sim 6.73\text{)} \qquad (2.73)$$

and for the descent range:-

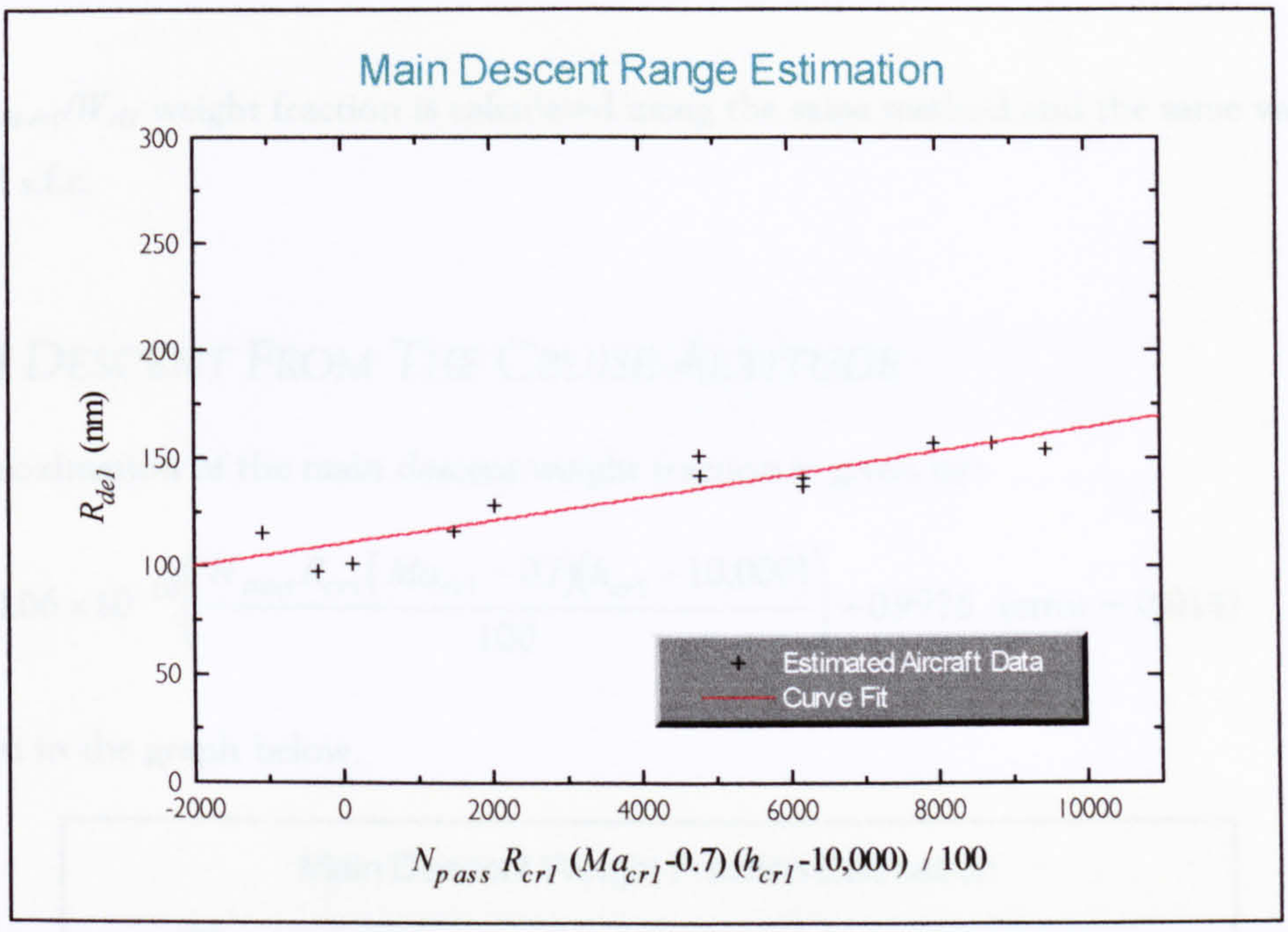


Figure 6.24- Estimation of the range of the descent from the main cruise altitude

R_{del} in nm.

$$R_{del} = 5.37 \times 10^{-6}\left(\frac{N_{pass} R_{cr1}\left(Ma_{cr1} - 0.7\right)\left(h_{cr1} - 10{,}000\right)}{100}\right) + 110.4 \qquad \text{(error} \sim 1.9\text{)} \qquad (2.74)$$

The weight fraction is then calculated using the standard Breguet range equation:-

$$\frac{W_{cr1}}{W_{cl1}} = e^{\frac{-R'_{cr1} C_{cr1}}{V_{cr1} L/D_{cr1}}} \qquad (2.75)$$

where

$$R'_{cr1} = R_{cr1} - R_{cl1} - R_{del} \qquad (2.76)$$

$$V_{cr1} = Ma_{cr1} a_{cr1} \qquad (2.77)$$

and

$$L/D_{criuse} = L/D'_{criuse}\left(1+\sum_{surfaces}\frac{\Delta L/D_{riblets}}{L/D}+\sum_{surfaces}\frac{\Delta L/D_{laminar.flow}}{L/D}+\left(\frac{\Delta L/D_{v.camber}}{L/D}\right)_{cruise}\right)$$

$$\times\left(1-\frac{\Delta C_{D\,winglet}}{100}\right)K_{tune\,L/D}K_{tune\,aero.effic} \qquad (2.78)$$

The $W_{mid\text{-}cr1}/W_{cl1}$ weight fraction is calculated using the same method and the same values of $L\backslash D$ and s.f.c.

6 .6 .4 *Descent From The Cruise Altitude*

An approximation of the main descent weight fraction is given by:-

$$\frac{W_{de1}}{W_{cr1}} = 1.06\times10^{-10}\left(\frac{N_{pass}R_{cr1}\left(Ma_{cr1}-0.7\right)\left(h_{cr1}-10{,}000\right)}{100}\right)+0.9976 \quad (\text{error}\sim 0.014) \qquad (2.79)$$

as shown in the graph below.

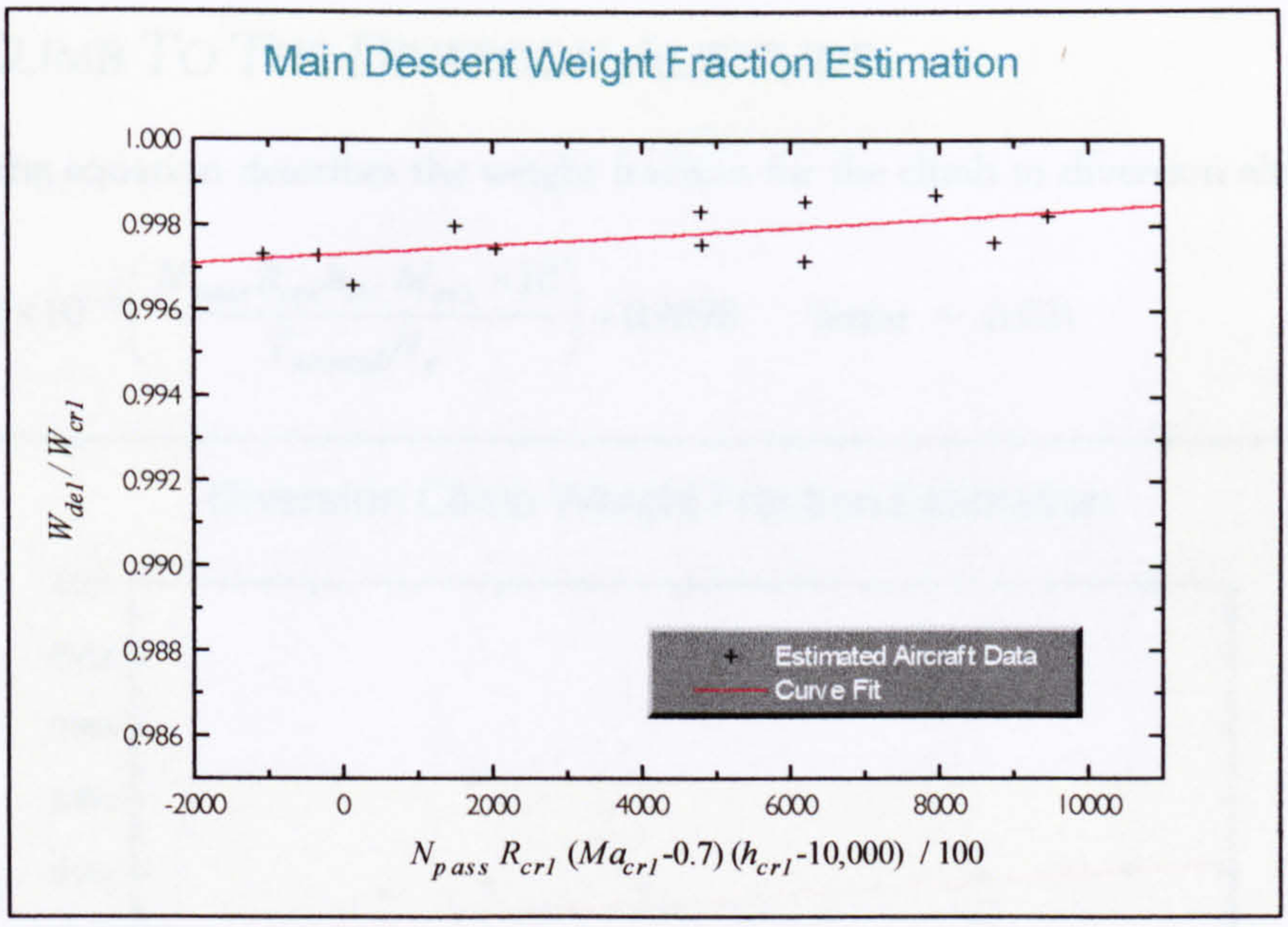


Figure 6.25- Estimation of the descent from cruise altitude weight fraction

6 .6 .5 *Aborted Landing*

This weight fraction is estimated as follows.

$$\frac{W_{al}}{W_{de1}} = 0.999e^{-1.2\times10^{-8}\left(\frac{N_{pass}R_{cr1}}{100}\right)} \qquad (\text{error}\sim 0.008) \qquad (2.80)$$

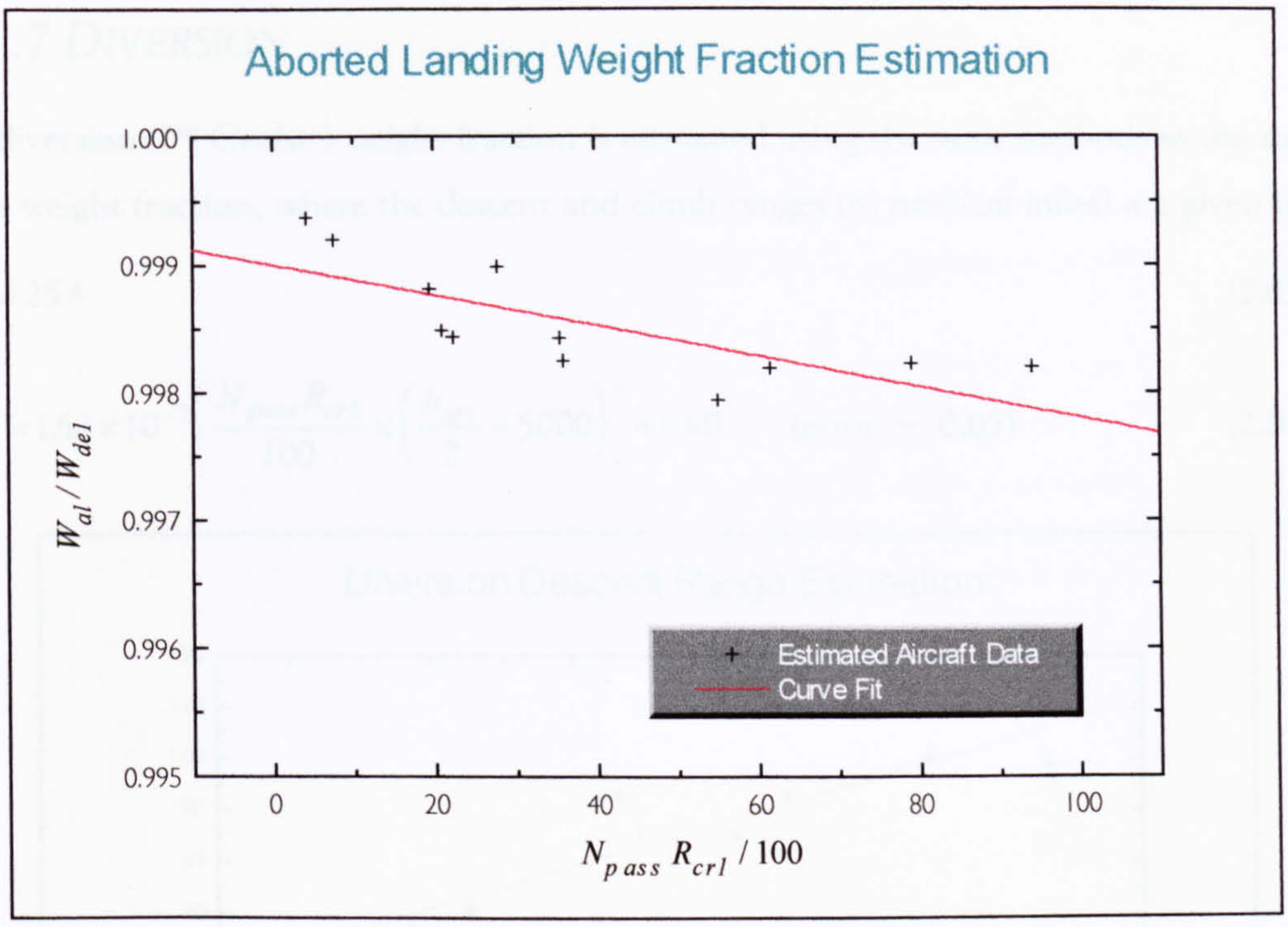


Figure 6.26 - Estimation of the aborted landing weight fraction

6 .6 .6 Climb To The Diversion Altitude

The following equation describes the weight fraction for the climb to diversion altitude.

$$\frac{W_{cl2}}{W_{al}} = 3.52 \times 10^{-6}\left(\frac{N_{pass} R_{cr1} h_{cr1} M_{cr1} \times 10}{T_{nominal} N_e}\right) + 0.9898 \qquad \text{(error } \sim \text{ 0.02)} \tag{2.81}$$

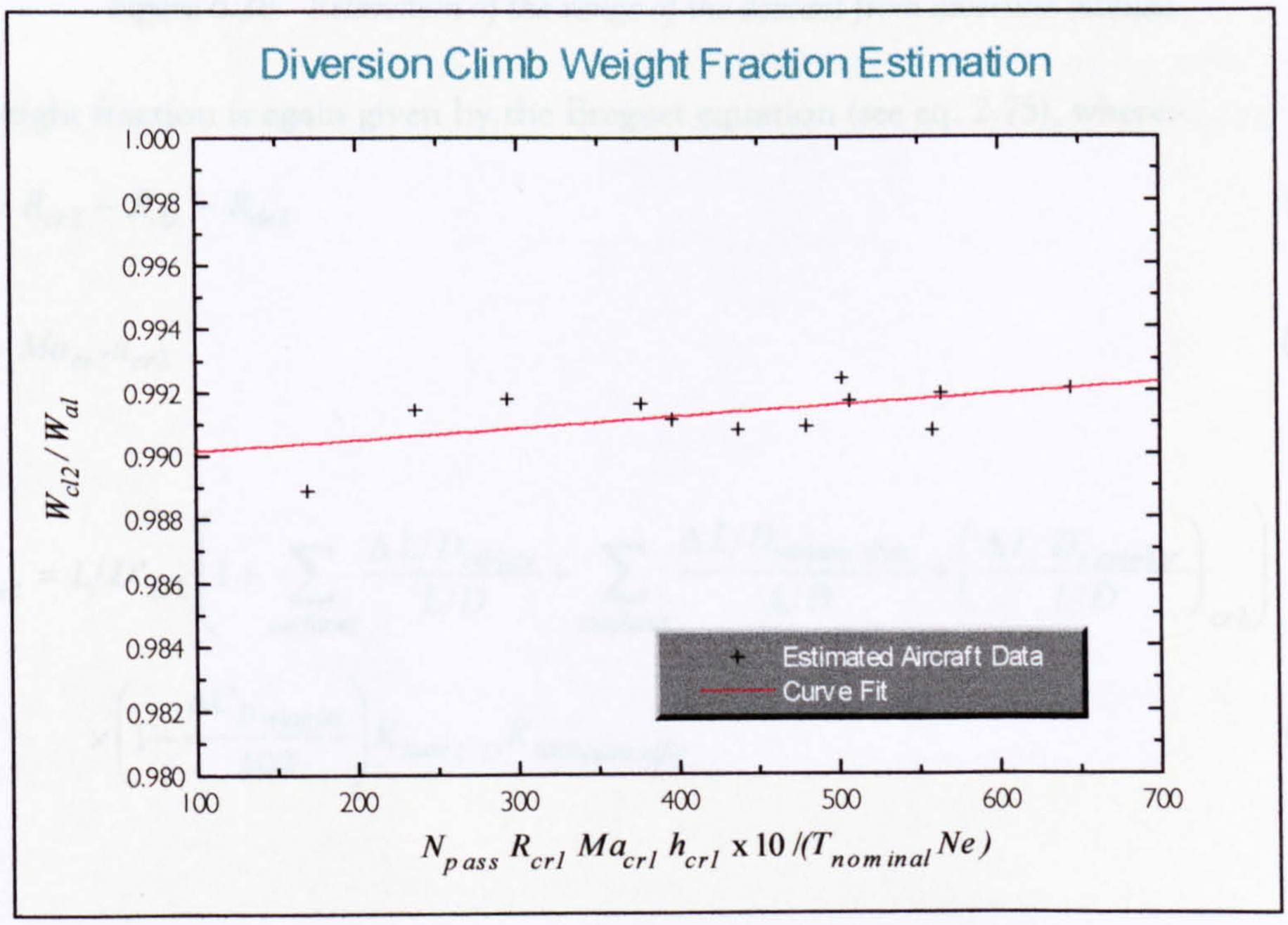


Figure 6.27 - Estimation of the climb to diversion weight fraction

6 .6 .7 DIVERSION

The diversion (2nd Cruise) weight fraction is estimated using the same methods as the main cruise weight fraction, where the descent and climb ranges (in nautical miles) are given by:-

$$R_{cl2} = 25.4 \tag{2.82}$$

$$R_{de2} = 1.62 \times 10^{-7}\left(\frac{N_{pass} R_{cr1}}{100} \times \left(\frac{h_{cr1}}{2} - 5000\right)\right) + 63.0 \qquad \text{(error } \sim \text{ 0.05)} \tag{2.83}$$

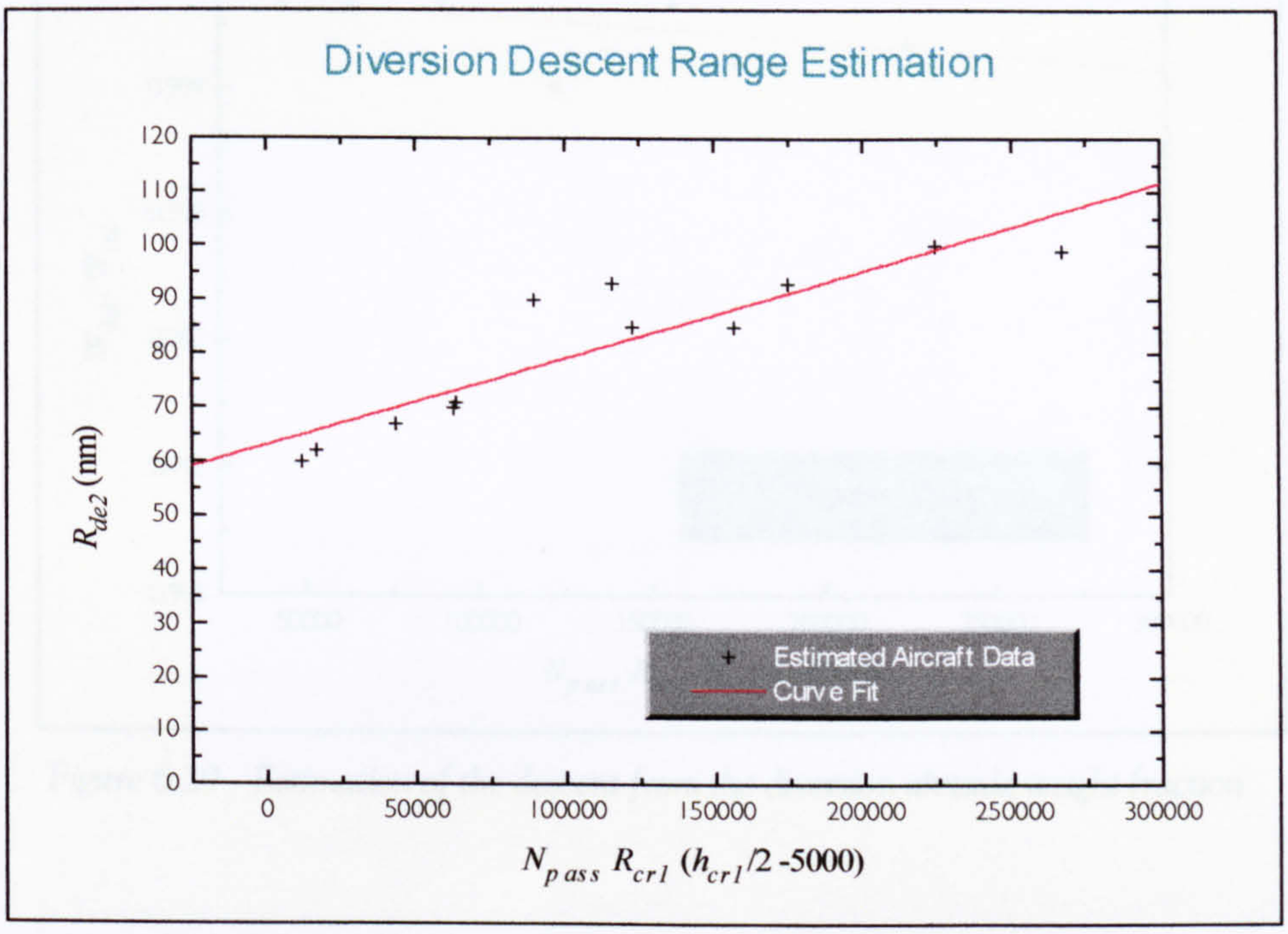


Figure 6.28 - Estimation of the range of the descent from diversion altitude

The weight fraction is again given by the Breguet equation (see eq. 2.75), where:-

$$R'_{cr2} = R_{cr2} - R_{cl2} - R_{de2} \tag{2.84}$$

$$V_{cr2} = Ma_{cr2} a_{cr2} \tag{2.85}$$

and

$$L/D_{cr2} = L/D'_{cr2}\left(1 + \sum_{surfaces} \frac{\Delta L/D_{riblets}}{L/D} + \sum_{surfaces} \frac{\Delta L/D_{laminar.flow}}{L/D} + \left(\frac{\Delta L/D_{v.camber}}{L/D}\right)_{cr2}\right)$$
$$\times\left(1 - \frac{\Delta C_{D\,winglet}}{100}\right) K_{tune\,L/D} K_{tune\,aero.effic} \tag{2.86}$$

6 .6 .8 DESCENT FROM THE DIVERSION ALTITUDE

This weight fraction is approximated by:-

$$\frac{W_{de2}}{W_{cr2}} = -2.20\times10^{-12}\left(\frac{N_{pass}R_{cr1}}{100}\times\left(\frac{h_{cr1}}{2}-5000\right)\right)+0.9998 \qquad \text{(error } \sim 0.007\text{)} \qquad (2.87)$$

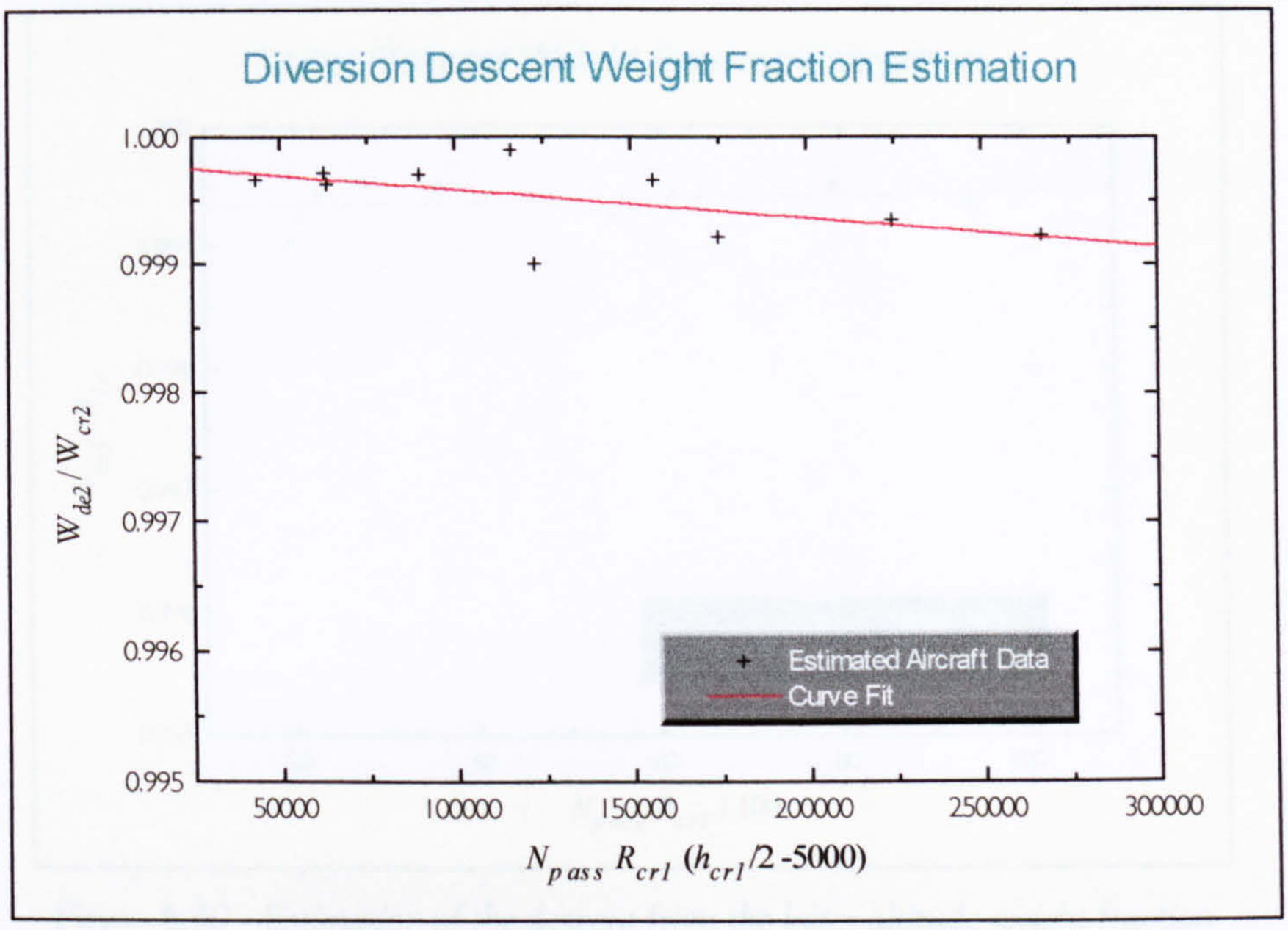


Figure 6.29 - Estimation of the descent from the diversion altitude weight fraction

6 .6 .9 LOITER

The loiter weight fraction is estimated using the endurance equation below (Raymer[90]).

$$\frac{W_{lo}}{W_{de2}} = e^{-\frac{t_{lo}C_{lo}}{L/D_{lo}}} \qquad (2.88)$$

where

t_{lo} = loiter time

and

$$L/D_{lo} = L/D'_{lo}\left(1+\sum_{surfaces}\frac{\Delta L/D_{riblets}}{L/D}+\sum_{surfaces}\frac{\Delta L/D_{laminar.flow}}{L/D}+\left(\frac{\Delta L/D_{v.camber}}{L/D}\right)_{lo}\right)$$

$$\times\left(1-\frac{\Delta C_{D\,winglet}}{100}\right)K_{tune\,L/D}K_{tune\,aero.effic} \qquad (2.89)$$

6 .6 .10 DESCENT FROM THE LOITER ALTITUDE

The following approximation is made for this weight fraction:-

$$\frac{W_{de3}}{W_{lo}} = 1.59 \times 10^{-9}\left(\frac{N_{pass} R_{cr1}}{100}\right) + 0.9993 \qquad \text{(error } \sim 0.005\text{)} \qquad (2.90)$$

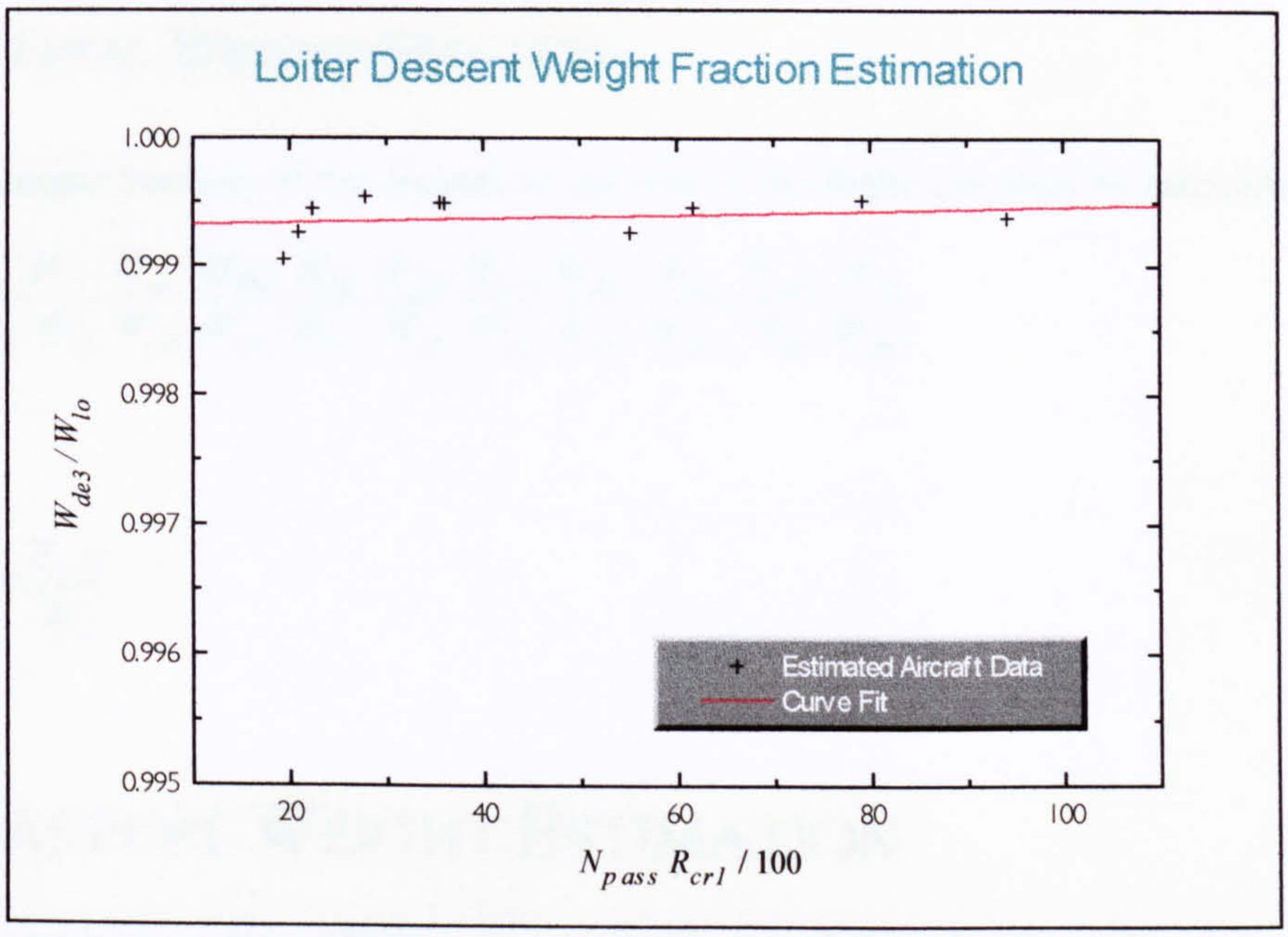


Figure 6.30 - Estimation of the descent from the loiter altitude weight fraction

6 .6 .11 LANDING

The final weight fraction is estimated from:-

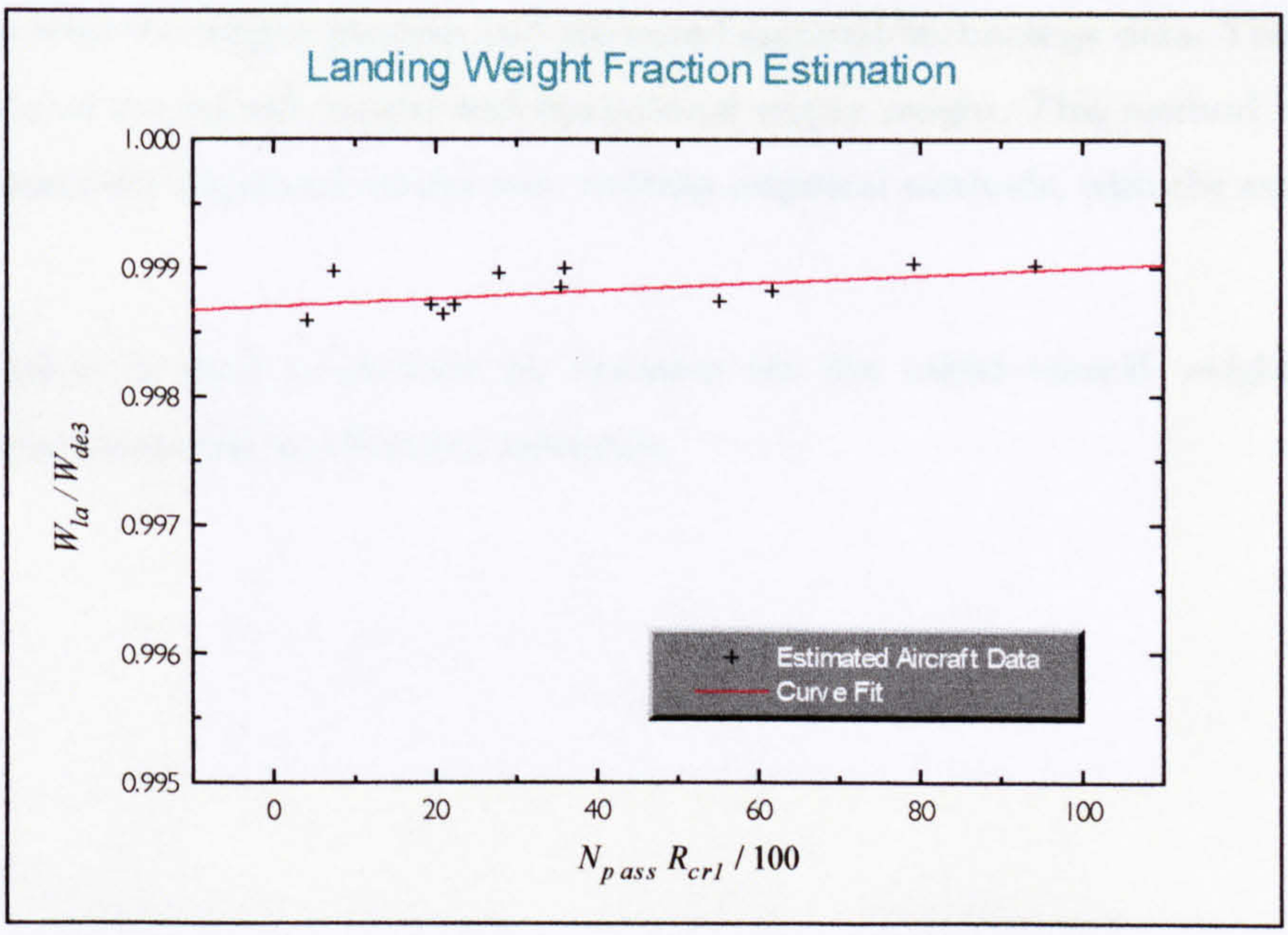


Figure 6.31- Estimation of the landing weight fraction

The resulting expression is:-

$$\frac{W_{la}}{W_{de3}} = 2.99 \times 10^{-9}\left(\frac{N_{pass} R_{cr1}}{100}\right) + 0.9987 \qquad \text{(error } \sim 0.003\text{)} \qquad (2.91)$$

6 .6 .12 Final Weight Fraction

The final weight fraction of the aircraft at the end of the flight can thus be calculated:-

$$\frac{W_{end}}{W_0} = \frac{W_{to}}{W_0}\frac{W_{cl1}}{W_{to}}\frac{W_{cr1}}{W_{cl1}}\frac{W_{de1}}{W_{cr1}}\frac{W_{al}}{W_{de1}}\frac{W_{cl2}}{W_{al}}\frac{W_{cr2}}{W_{cl2}}\frac{W_{de2}}{W_{cr2}}\frac{W_{lo}}{W_{de2}}\frac{W_{de3}}{W_{lo}}\frac{W_{la}}{W_{de3}} \qquad (2.92)$$

and

$$\frac{W_{fuel}}{W_0} = 1 - \frac{W_{end}}{W_0} \qquad (2.93)$$

6 .7 Takeoff Weight Estimation

The method used to calculate an initial estimate of the takeoff weight of the aircraft is similar to the method suggested by Sieron et Al[86]. This method relies on the basic premise that the aircraft weight is a function of the product of its payload and its range to provide a weight estimate. This idea has been extended to take into account cruise Mach number, engine efficiency, and aerodynamic efficiency. An initial guess of the basic aircraft weight neglecting any advanced materials or technologies is made, this guess is then refined, in-conjunction with the weight fraction and advanced material/technology data. The result is a final estimate of the takeoff weight and operational empty weight. This method has proved to give substantially improved results over existing empirical methods, with the average error below 5%.

The data below is used to provide an equation for the initial takeoff weight estimate, neglecting any composite or advanced materials.

Aircraft	N_{pass}	R_{cr1} (nm)	Ma_{cr1}	h_{cr1} (ft)	W_0 (kg)	W_{oew} (kg)	$(\%_{composite})_{structure}$
Boeing 737	140	1600	0.75	31000	56450	31895	3
Airbus A320	150	2700	0.78	31000	73500	41782	15
Boeing 757	186	2820	0.80	39000	99800	57180	3
Airbus A300	266	3950	0.80	31000	170500	90339	12
Airbus A310	220	5170	0.80	35000	164000	82488	10
Boeing 767	210	5760	0.80	35000	175575	89130	3
Airbus A330	335	4500	0.82	37500	212000	120012	13
Boeing 777	375	3950	0.83	39000	229575	135580	9
Airbus 340	295	6600	0.82	37500	257004	126873	13
Boeing 747	420	7100	0.83	35000	396873	182754	3
DAP 502	476	7000	0.85	35000	411120	188996	25
DAP 602	611	7000	0.85	35000	519140	236394	25
DAP 702	727	7000	0.85	35000	614827	277791	25

Table 6.4 - Initial sizing parameters of example aircraft

The above information is used to calculate the following parameters:-

R_{total} - Total range, including diversion and loiter

$W_{compsite}$ - Weight of composite material in complete aircraft

It is also necessary to obtain an estimate of the proportion of the operating empty weight that is composed of structural items (W_{struct}/W_{oew}). This is taken from the results of the Weight Estimation Module.

It has arbitrarily been assumed that the proportion of advanced materials in the non-structural areas of the aircraft is some function of the proportion of materials in the structural areas. As very little information was available in this area it has been assumed that:-

$$\frac{W_{composite_{non-struct}}}{W_{non-struct}} = \frac{1}{6} \times \frac{W_{composite_{struct}}}{W_{struct}}$$

This means that

$$W_{composite} = \frac{\%composite_{struct}}{100} \frac{W_{struct}}{W_{oew}} W_{oew} + \frac{\%composite_{struct}}{100 \times 6} \left(1 - \frac{W_{struct}}{W_{oew}}\right) W_{oew} \qquad (2.94)$$

Assuming a 30% weight saving due to the use of advanced materials, an estimate of the aircraft weight without any advanced materials can be made (W_0').

$$W_0' = W_0 + \left(\frac{1}{0.7} - 1\right) W_{composite} \tag{2.95}$$

The parameters $L\backslash D_{cr1}$ and C_{cr1} are estimated from the detailed output of the performance and aerodynamics modules for example designs of the exact weight and geometry as the sample designs. A parameter X_{W0} is then estimated and plotted.

$$X_{W0} = \frac{R_{total} W_{payload} C_{cr1}{}^{0.3}}{L/D_{cr1}{}^{0.25}} \left(\frac{0.815}{M_{cr1}}\right) \tag{2.96}$$

Aircraft	$W_{struct}\backslash W_{oew}$	$W_{composite}$ (kg)	R_{total} (nm)	$L\backslash D_{cr1}$	C_{cr1} (hr^{-1})	X_{W0}	W'_0 (kg)
Boeing 737	0.5132	568.7	2250	15.19	0.597	144.82	56693.7
Airbus A320	0.4661	3478.6	3357	16.10	0.572	218.24	74990.8
Boeing 757	0.4928	990.4	3417	15.15	0.555	270.38	100224.5
Airbus A300	0.5100	6413.9	4660	16.41	0.590	527.11	173248.8
Airbus A310	0.5426	5104.3	6002	17.44	0.566	540.82	166187.6
Boeing 767	0.5582	1689.6	6475	17.70	0.568	565.62	176299.1
Airbus A330	0.6013	10418.1	5265	20.33	0.561	682.79	216464.9
Boeing 777	0.6211	8505.9	4660	18.69	0.566	857.84	271265.4
Airbus 340	0.5807	10730.0	7575	20.08	0.570	875.43	261602.6
Boeing 747	0.5772	3550.9	8125	19.19	0.590	1347.58	398394.8
DAP 502	0.6216	32348.6	8015	18.95	0.560	1446.59	424983.7
DAP 602	0.5555	37208.5	8015	20.51	0.553	1812.49	535086.5
DAP 702	0.5915	45808.5	8015	19.90	0.563	2193.25	634459.2

Table 6.5 - Calculation of sizing parameter X_{w0} for example aircraft

This gives the following graph:-

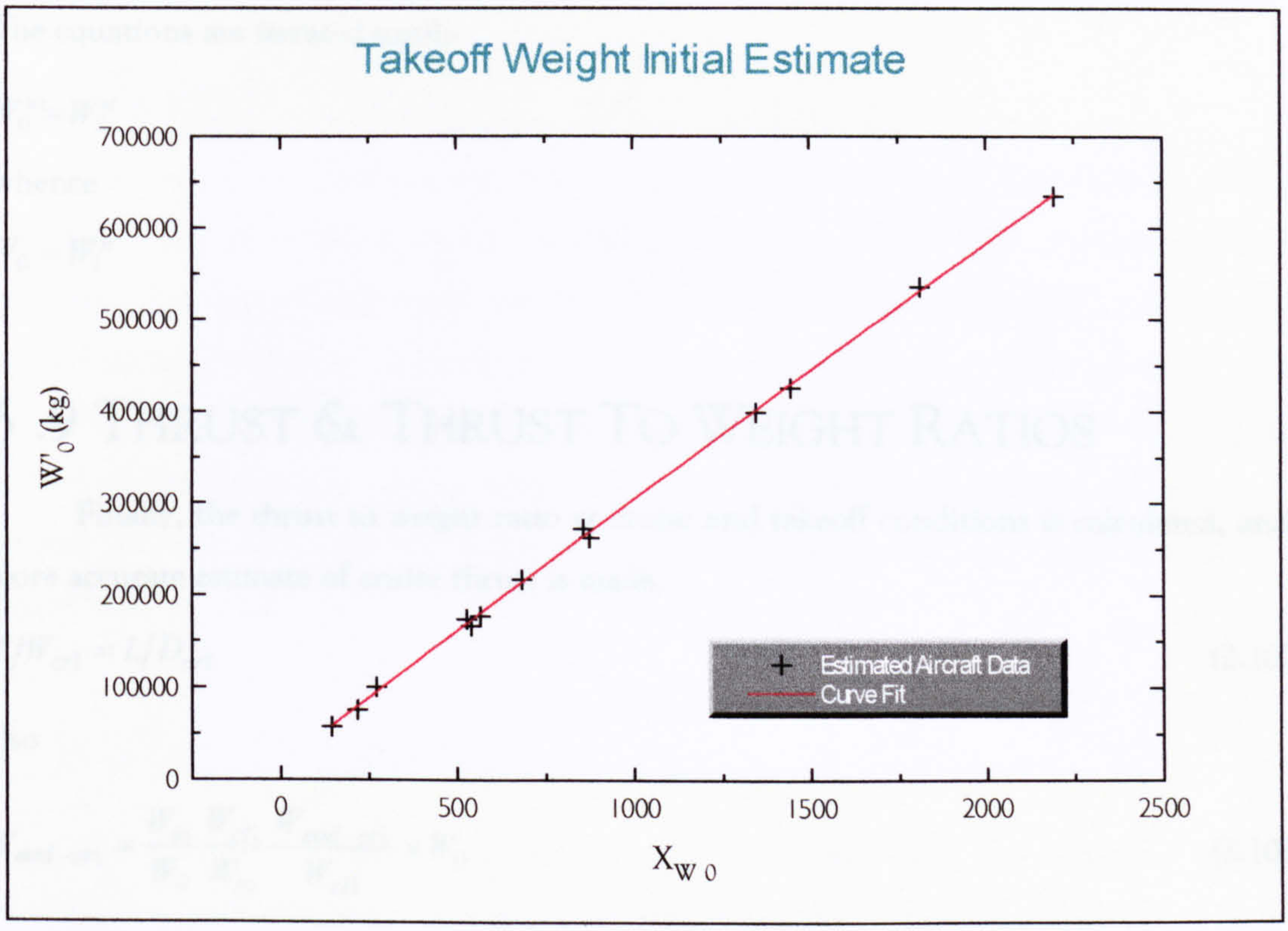


Figure 6.32 - Estimation of takeoff weight

This graph is approximated by:-

$$W_0' = 1.83 \times 10^{-6} X_{W0}{}^3 - 0.0101 X_{W0}{}^2 + 296.7 X_{W0} + 14672.3 \quad (2.97)$$

6 .8 Weight Adjustment and Iteration

The initial takeoff weight estimate now needs to be adjusted to take into account the effect of advanced technologies. As the weight savings due to advanced materials depends on the operational empty weight, and the operational empty weight depends on the takeoff weight, then the process is an iterative one. The following equations are solved until a convergent solution is found:-

$$W_0'' = W_0' \times K_{tuneW0} \quad (2.98)$$

$$W_{fuel} = \frac{W_{fuel}}{W_0} W'' \quad (2.99)$$

$$W_{oew} = \left(W_0'' - W_{payload} - W_{fuel}\right)\left(1 + \frac{\Delta W_{oew\,active.drag}}{W_{oew}}\right) \quad (2.100)$$

$$W_0''' = W_0'' - \frac{\Delta W_{oew\,ad.material}}{W_{oew}} W_{oew} + \frac{\Delta W_{oew\,active.drag}}{W_{oew}} W_{oew} \quad (2.101)$$

The equations are iterated until:-

$W_0'' = W_0''$

whence

$W_0 = W_1''$

6 .9 Thrust & Thrust To Weight Ratios

Finally, the thrust to weight ratio at cruise and takeoff conditions is calculated, and a more accurate estimate of cruise thrust is made.

$$T/W_{cr1} = L/D_{cr1} \tag{2.102}$$

also

$$W_{mid-cr1} = \frac{W_{to}}{W_0}\frac{W_{cl1}}{W_{to}}\frac{W_{mid-cr1}}{W_{cl1}} \times W_0 \tag{2.103}$$

so

$$T_{cr1} = \frac{W_{mid-cr1}\,g}{L/D_{cr1}} \tag{2.104}$$

and at takeoff

$$T/W_{to} = \frac{T_{nominal}N_e}{W_0 g} \tag{2.105}$$

7 .Wing Design Methods

The wing design module performs the necessary calculations to determine the physical size of the wing planform, as well as its main geometric properties. The lift properties of the wing are calculated for high speed and low speed conditions, and the flap lift coefficients and deflections are estimated. The wing lift distribution at cruise is also calculated. Some of the methods rely on the digitisation and interpolation of graphical data presented in recognised aircraft design texts. It is worth noting that all of the interpolations contained within this module are controlled such that if any value is out of the bounds of the available data, the closest value is used.

7 .1 Wing Planform

The geometric properties of the wing are calculated using the following standard relationships and equations.

$$S_{ref} = \frac{W_0}{W/S} \tag{3.1}$$

$$b_{ref} = \sqrt{S_{ref} A} \tag{3.2}$$

The flap and aileron locations can simply be calculated from the non-dimensionalised flap and aileron parameters set in the Wing Design section of the input parameters. The '*i*' and '*o*' subscripts refer to the innermost spanwise location of the flaps/ailerons, and the outermost location of the flaps/ailerons respectively.

$$b_{flap_o} = \left(\frac{b_{flap_o}}{b_{ref}} \right) \times b_{ref} \tag{3.3}$$

$$b_{flap_i} = \left(\frac{b_{flap_i}}{b_{ref}} \right) \times b_{ref} \tag{3.4}$$

$$b_{aileron_o} = \left(\frac{b_{aileron_o}}{b_{ref}} \right) \times b_{ref} \tag{3.5}$$

$$b_{aileron_i} = \left(\frac{b_{aileron_i}}{b_{ref}} \right) \times b_{ref} \tag{3.6}$$

The planform shape is assumed to be of the type shown below in figure 3.1. The unknown planform parameters are calculated using an iterative approach. The value of the tip chord is

found such that the area of the planform, including the cranked section, is exactly equal to the reference area calculated from equation 3.1. In some cases it may not be possible to find an exact solution that satisfies all of the conditions of the iteration process, these cases will provide negative values of tip chord or taper ratio. It is possible to rectify this problem by adjusting the crank length (ϕ_{crank}) appropriately, from its initial value as set by the user, such that a sensible solution is found.

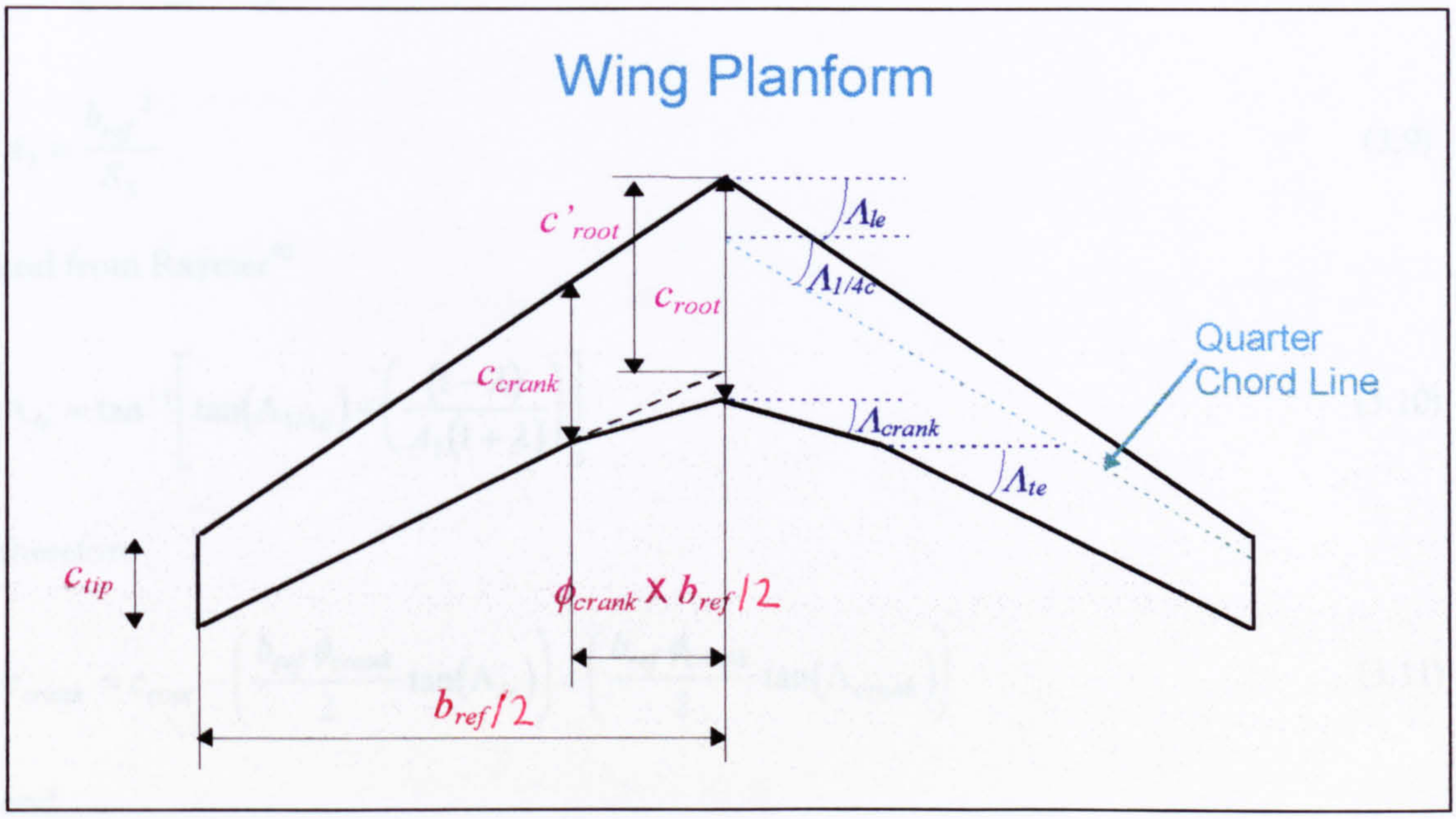


Figure 7.1- Wing planform geometry

The wing is split into the following areas for calculation purposes.

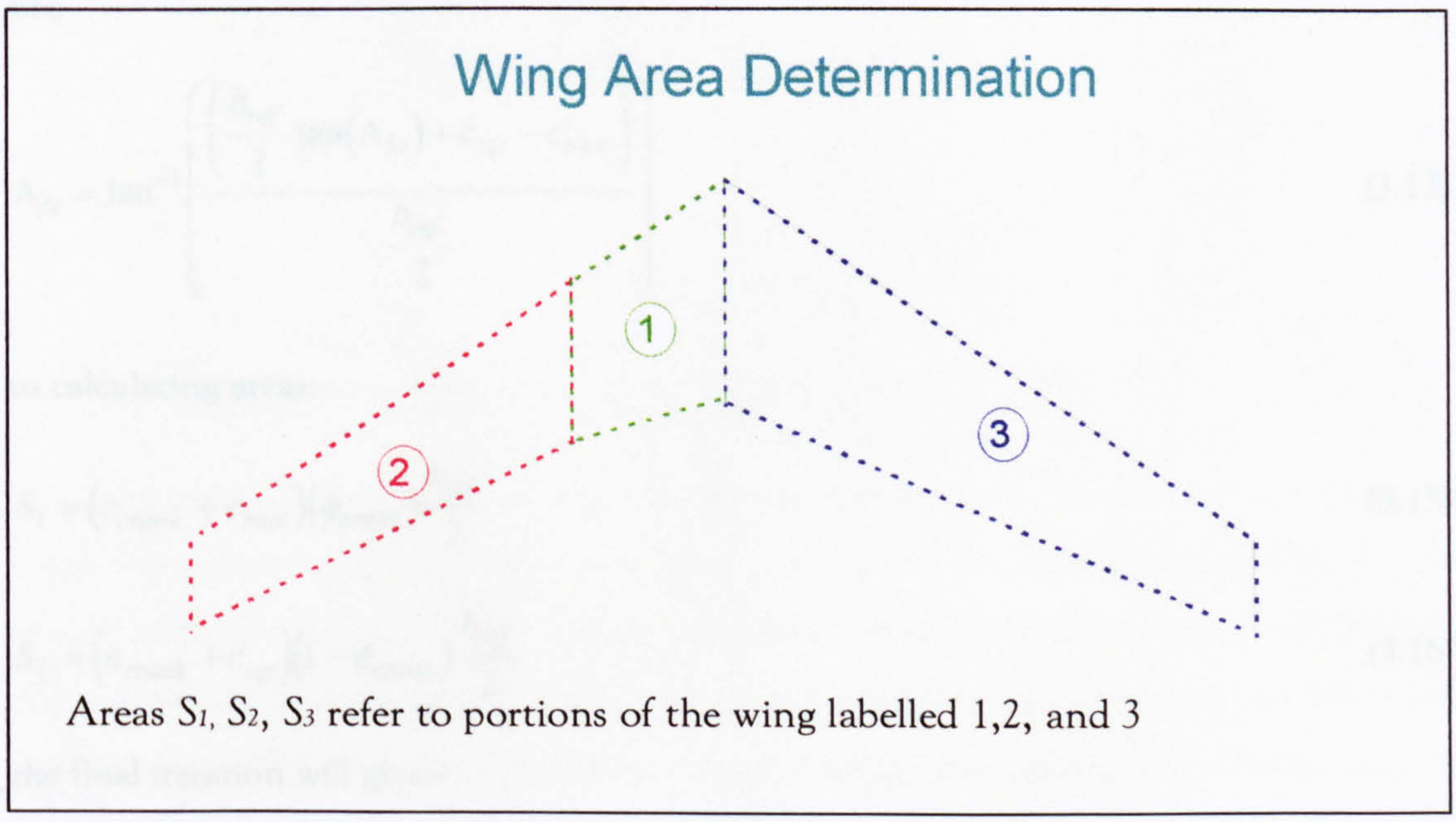


Figure 7.2- Determination of wing areas

Suitable initial values are chosen, and then the iteration process is automatically performed to find the solution of c_{tip} and ϕ_{crank}, such that:-

$$c_{root} = \frac{c_{tip}}{\lambda} \tag{3.7}$$

$$S_3 = \left(\frac{c_{root} + c_{tip}}{2}\right) b_{ref} \tag{3.8}$$

$$A_3 = \frac{{b_{ref}}^2}{S_3} \tag{3.9}$$

and from Raymer[90]

$$\Lambda_{le} = \tan^{-1}\left[\tan\left(\Lambda_{1/4c}\right) + \left(\frac{(1-\lambda)}{A_3(1+\lambda)}\right)\right] \tag{3.10}$$

therefore

$$c_{crank} = c_{root} - \left(\frac{b_{ref}\,\phi_{crank}}{2}\tan\left(\Lambda_{le}\right)\right) + \left(\frac{b_{ref}\,\phi_{crank}}{2}\tan\left(\Lambda_{crank}\right)\right) \tag{3.11}$$

and

$$c'_{root} = c_{crank} + \left(\left(c_{crank} - c_{tip}\right)\frac{\phi_{crank}}{1-\phi_{crank}}\right) \tag{3.12}$$

also

$$\Lambda_{te} = \tan^{-1}\left(\frac{\left(\frac{b_{ref}}{2}\tan\left(\Lambda_{le}\right) + c_{tip} - c'_{root}\right)}{\frac{b_{ref}}{2}}\right) \tag{3.13}$$

so calculating areas:-

$$S_1 = \left(c_{crank} + c_{root}\right)\left(\phi_{crank}\right)\frac{b_{ref}}{2} \tag{3.15}$$

$$S_2 = \left(c_{crank} + c_{tip}\right)\left(1-\phi_{crank}\right)\frac{b_{ref}}{2} \tag{3.16}$$

the final iteration will give:-

$$S_{ref} = \left(S_1 + S_2\right) \times 2$$

7 .2 Mean Aerodynamic Chord Location

The mean aerodynamic chord length (c_{mac}), and its spanwise location (y_{mac}) are calculated using the following methods.

For $\phi_{crank} > 0$

Using the method from ESDU[92], where:-

$$\lambda_1 = \frac{c_{crank}}{c_{root}}, \text{ and } \lambda_2 = \frac{c_{tip}}{c_{crank}}$$

$$\frac{c_{mac}}{c_{root}} = \frac{2}{3}\frac{\phi_{crank}\left(1+\lambda_1+\lambda_1^2\right)+\lambda_1^2\left(1-\phi_{crank}\right)\left(1+\lambda_2+\lambda_2^2\right)}{\phi_{crank}+\lambda_1+\lambda_1\lambda_2\left(1-\phi_{crank}\right)} \tag{3.17}$$

so if $c_{mac} > c_{crank}$ then:-

$$y_{mac} = \frac{b_{ref}}{2}\phi_{crank}\left(\frac{c_{root}-c_{mac}}{c_{root}-c_{tip}}\right) \tag{3.18}$$

else

$$y_{mac} = \frac{b_{ref}}{2}\phi_{crank} + \left(\frac{\left(1-\phi_{crank}\right)b_{ref}}{2}\right)\left(\frac{c_{crank}-c_{mac}}{c_{crank}-c_{tip}}\right) \tag{3.19}$$

However, if $\phi_{crank}=0$, using the methods from Raymer[90]

$$\frac{c_{mac}}{c_{root}} = \frac{2}{3}\frac{\left(1+\lambda+\lambda^2\right)}{1+\lambda} \tag{3.20}$$

$$y_{mac} = \frac{b_{ref}}{6}\left(\frac{1+2\lambda}{1+\lambda}\right) \tag{3.21}$$

7 .3 Aerodynamic Centre Location

The streamwise location of the aerodynamic centre, relative to the leading edge of the mean aerodynamic chord, is calculated using the data in Torenbeek[93] (page 478), for the aerodynamic centre of a lifting surface at subsonic speeds. In this analysis the location parameter $X'_{ac\,wing}$ is dependant on wing aspect ratio, taper ratio, sweep, and the flow Mach number. As these dependant parameters are known, the aerodynamic centre can be calculated. The calculation if performed for cruising conditions where:-

$$\beta = \sqrt{1 - Ma_{cr1}{}^2} \tag{3.22}$$

The graphs shown in Torenbeek[93] have been converted into a series of 5 data sets for each given value of βA. These sets are then further divided into data points for 5 values of taper ratio. To calculate the aerodynamic centre, the data is first linearly interpolated for the relevant value of βA, then this new data set is interpolated for taper, followed by sweep. This procedure is used to calculate the aerodynamic centres of both the wing and the tail surfaces.

7 .4 Lift Coefficients & Wing Incidence

Throughout the Wing Design Module, and the other calculation modules, the following assumption has been made to relate 2-dimensional lift coefficients to 3-dimensional ones. This assumption is valid for moderate to high aspect ratio wings only, which is appropriate for the wing designs being considered.

$$C_L = C_l \times \cos \Lambda_{1/4c} \tag{3.23}$$

Where C_L represents the 3-dimensional lift coefficient, and C_l represents the 2-dimensional counterpart. This is a fairly standard assumption made by both Raymer[90] and Torenbeek[93].

7 .4 .1 Cruise lift coefficient

The results of the weight fraction estimation of the Initial Sizing Module are used to provide a more accurate estimate of the mid cruise three dimensional lift coefficient than the estimate made from data correlation (see 6.3.3).

$$C_{L_{cr1}} = \frac{W_{mid-cr1} \times g}{1/2 \rho_{cr1} V_{cr1}{}^2 S_{ref}} \tag{3.24}$$

7 .4 .2 Landing Lift Coefficient

The maximum lift coefficient during landing is calculated from the minimum landing touchdown velocity entered by the user. As stated in the FAR regulations, the stall velocity at landing is assumed to be 1.15 times smaller than the actual touchdown velocity. As the stall velocity is then known, the maximum possible lift coefficient can be calculated. The standard assumptions are also made that the maximum weight at landing is no more than 85% of the takeoff weight, and that the landing occurs at sea level conditions. Hence

$$C_{L_{la(max)}} = \frac{0.85 W_0 \times g}{1/2 \rho_{la} \left(\frac{V_{la}}{1.15} \right)^2 S_{ref}} \tag{3.25}$$

7 .4 .3 TAKEOFF LIFT COEFFICIENT

The maximum takeoff coefficient is calculated using the assumption that the lift increment between cruise and takeoff conditions is 0.7 times the lift increment between landing and cruise conditions. This assumption has been made to provide an estimate of the magnitude of the takeoff lift coefficient that should be expected for the kind of aircraft to which these methods are applied.

$$C_{L_{to(\max)}} = C_{L_{cr}} + 0.7\left(C_{L_{la(\max)}} - C_{L_{cr}}\right) \tag{3.26}$$

Using the fact that the aircraft takeoff velocity must be at least 1.1 times the stall speed, and assuming a warm-up, taxi, and takeoff weight fraction of 0.998.

$$V_{to.stall} = \sqrt{\frac{0.998W_0 \times g}{1/2\rho_{to}S_{ref}C_{L_{to(\max)}}}} \tag{3.27}$$

therefore

$$V_{to} = 1.1V_{to.stall} \tag{3.28}$$

7 .4 .4 WING INCIDENCE

The value of mid-cruise lift coefficient calculated from equation 3.24 is converted into a 2-dimensional lift coefficient and is used to provide an estimate of the necessary wing fixed incidence that will give the correct lift at cruise conditions with zero aircraft incidence. As the Reynolds number at cruise is known, the airfoil data interpolation routine is used to provide sets of lift data for the wing root and wing tip airfoils at the relevant Reynolds number. This information is then used to provide the values for the incidences of the root and tip airfoils ($i'_{wing_{root}}$ and $i'_{wing_{tip}}$) that would provide the 2-dimensional cruise lift coefficient. Any twist of the tip airfoil relative to the root airfoil is assumed to follow a linear distribution in the spanwise direction. The fixed incidence (the incidence relative to the fuselage) of the mean aerodynamic chord at cruise conditions can then be calculated:-

$$i_{wing_{mac}} = i'_{wingroot} + \left(i'_{wing_{tip}} - i'_{wing_{root}}\right)\left(\frac{y_{mac}}{b_{ref}/2}\right) \tag{3.29}$$

taking into account the desired wing twist ε_t

$$i_{wing_{root}} = i_{wing_{mac}} + \varepsilon_t\left(\frac{y_{mac}}{b_{ref}/2}\right)$$

$$i_{wing_{tip}} = i_{wing_{mac}} + \varepsilon_t \left(\frac{b_{ref}/2 - y_{mac}}{b_{ref}/2} \right) \tag{3.31}$$

also the aerodynamic twist is given by:-

$$\alpha_{0_{mac}} = \alpha_{0_{root}} + \left(\alpha_{0_{tip}} - \alpha_{0_{root}} \right) \frac{y_{mac}}{b_{ref}/2} \tag{3.32}$$

For a variable camber wing the geometric twist is assumed to be zero.

7 .4 .5 Ground Roll Lift Coefficient

During the ground roll portion of the takeoff segment it has been assumed that the aircraft has zero incidence. This means that without any flaps deployed, the total lift will be approximately equal to lift achieved with the fixed incidences calculated above. By calculating the Reynolds number at takeoff, it is possible to obtain the 2-d root and tip airfoil data sets at this Reynolds number by using the airfoil interpolation routine. The 2-d lift values for both the root and tip airfoils ($C_{lgr.root}$ and $C_{lgr.tip}$) can then be calculated for their respective fixed incidences. As the lift vs. incidence data values will be relatively insensitive to small changes in Reynolds number, the lift values at takeoff ($V = V_{to}$) are assumed for all velocities leading up to takeoff. Therefore:-

$$C_{lgr} = C_{lgr.root} + \left(C_{lgr.tip} - C_{lgr.root} \right) \left(\frac{y_{mac}}{b_{ref}/2} \right) \tag{3.33}$$

The 2-d lift curve slope during the ground roll is also calculated using the values of root and tip 2-d lift curve slope returned by the airfoil interpolation routine.

$$C_{l\alpha.gr} = C_{l\alpha.gr.root} + \left(C_{l\alpha.gr.tip} - C_{l\alpha.gr.root} \right) \left(\frac{y_{mac}}{b_{ref}/2} \right) \tag{3.34}$$

7 .5 Equivalent Wing

The equivalent wing is the straight tapered wing that best approximates to the actual cranked wing planform, which can be used to simplify aerodynamic analysis. The equivalent wing planform is calculated from geometric considerations:-

subscript e denotes equivalent wing

$c_{tip_e} = c_{tip}$

$$S_{ref_e} = S_{ref}$$

$$\Lambda_{le_e} = \Lambda_{le}$$

therefore

$$C_{root_e} = \frac{S_{ref}}{1/2\, b_{ref}} - c_{tip_e} \tag{3.35}$$

this means that the shape of the planform is defined, and all other geometric properties, such as quarter chord sweep angle, and mean aerodynamic chord location can be easily calculated.

7 .5 .1 Wing Lift Distribution (Cruise)

The spanwise lift distribution at cruise conditions is calculated for the equivalent wing using the methods of Diederich and Anderson described in appendix E of Torenbeek[93]. This method assumes that at each spanwise ordinate η, the lift can be split into a basic lift C_{lb} and an additional lift C_{la}, such that:-

$$C_l = C_{la} + C_{lb} \tag{3.36}$$

where

$$C_{la} = \frac{L_a C_L c_g}{c} \tag{3.37}$$

c - chord at spanwise coordinate η

c_g - mean geometric chord $\left(S_{ref}/b_{ref}\right)$

and

$$C_{lb} = \frac{L_b c_g C_{l\alpha} \varepsilon_t}{cE} \tag{3.38}$$

E - Jones edge velocity correction $\left(1 + \frac{2\lambda_e}{A_e(1+\lambda_e)}\right)$

The lift values L_a and L_b are calculated using the expressions below, where ε is the local geometric twist at the spanwise ordinate η.

$$L_a = C_1 \frac{c}{c_g} + C_2 \frac{4}{\pi}\sqrt{1-\eta^2} + C_3 f \tag{3.39}$$

$$\frac{L_b}{\beta E} = L_a C_4 \cos\left(\Lambda_\beta\right)\left(\frac{\varepsilon}{\varepsilon_t} + \alpha_{0l}\right) \tag{3.40}$$

β is found from equation 3.22 and,

$$\tan\Lambda_\beta = \frac{\tan\Lambda_{1/4c_e}}{\beta} \tag{3.41}$$

C_1, C_2, C_3, C_4 are constants that are dependant on aspect ratio, quarter chord sweep, and lift curve slope, and are found from the graph E.5 in Torenbeek[93]. This graph has been converted into a data file, and the data points are interpolated to find the values of these parameters. The value of f is dependant on η and Λ_β, and is found from the graph E.6 of Torenbeek[93], which has also been converted into a data file. The value of α_{0l} is found from the relationship:-

$$\alpha_{0l} = -\int_0^1 \frac{\varepsilon}{\varepsilon_t} L_a d\eta \tag{3.42}$$

this can be evaluated using a simple trapezoidal strip integration method, and the 2-dimensional local lift distribution can then be evaluated. The 2-dimensional local lift coefficient is then converted into a lift force value using:-

$$L = C_l \frac{1}{2}\rho_{cr1} {V_{cr1}}^2 b_{ref} c \tag{3.43}$$

The ideal elliptical lift distribution is then calculated using the fact that the area of the lift distribution graph should be equal to the cruise lift. Therefore:-

assuming $\dfrac{\eta^2}{{a_{ellipse}}^2} + \dfrac{{L_{elliptical}}^2}{{b_{ellipse}}^2} = 1$

$$a_{ellipse} = 1 \tag{3.44}$$

$$b_{ellipse} = \left(\frac{4C_{Lcr1}}{\pi}\right)\frac{1}{2}\rho_{cr1}{V_{cr1}}^2 S_{ref} \tag{3.45}$$

If variable camber wings are used, then the lift distribution can be calculated by making the following assumption, noting that the efficiency parameter ($K_{efficiency\ v.camber}$) is set by the user in the Component Specification Editor (the default value is 60%).

$$L_{v.camber} = L + \left(L_{elliptical} - L\right)\frac{K_{efficiency_{v.camber}}}{100} \tag{3.46}$$

7 .5 .2 MAXIMUM CLEAN LIFT COEFFICIENT

The maximum three dimensional lift of the wing in the clean configuration is calculated using the methods of Raymer[90], assuming the wing is of high aspect ratio. The maximum lift coefficient is given by:-

$$C_{Lmax} = C_{lmax(clean)}\left(\frac{C_{Lmax}}{C_{lmax}}\right) + \Delta C_{Lmax} \qquad (3.47)$$

The value of $Cl_{max(clean)}$ is known from 2-d airfoil data. The value of (CL_{max}/Cl_{max}) can be estimated from figure 12.8 of Raymer[90], which plots this parameter against leading edge sweep and leading edge sharpness parameter. As the values of both of these inputs are known, the data points created from this figure can be linearly interpolated and the value of (CL_{max}/Cl_{max}) evaluated.

Similarly the value of ΔCL_{max} can be estimated from figure 12.9 of Raymer[90]. This parameter is again dependant on leading edge sweep, leading edge sharpness parameter, as well as Mach number. The data from these graphs has been converted into a suitable format, and using linear interpolation, along with a small amount of second order extrapolation, it is possible to evaluate ΔCL_{max}. This calculation has been performed in such a manner that the maximum clean lift coefficient at any Mach number is globally available to all modules.

7 .5 .3 FLAP LIFT INCREMENTS

The span and the chord width of both the trailing edge flaps and ailerons are set by the user from parameters within the Wing Design section of the input parameters. The ailerons are assumed to be plain flaps, whereas the type of main trailing edge flaps used can be selected from one of six available types. These types are:-

1 - Single Slotted Fixed Hinge Flaps
2 - Single Slotted Fowler Flaps
3 - Double Slotted Fixed Vane Flaps
4 - Double Slotted Variable Geometry Flaps
5 - Double Slotted Fowler Flaps
6 - Triple Slotted Fowler Flaps

Figure 7.3 - Available Flaps geometries

The method used to estimate the lift increment due to deflections of these flaps is taken from Torenbeek[93]. The values of the flap lift effectiveness factor (η_δ) is calculated from data sets based on figures G.4, G.5, and G.6 from Torenbeek[93]. For plain flaps the value is

dependent on deflection angle and flap chord length, for the other types of flap the value is only dependent on deflection angle. For the plain, single slotted fixed hinge, single slotted Fowler, and double slotted fixed vane configurations, the total lift effectiveness of the flap system can be directly calculated from the graph. For double slotted variable geometry, double slotted Fowler, and triple slotted Fowler configurations, the contribution of each portion of the flap must be considered. The initial portion of the flap system is modelled as a single slotted flap, and the remaining portions are assumed to be an auxiliary flap.

The flap chord extension $\Delta c/c_f$ is calculated from figure G.7 of Torenbeek[93], and is dependent on deflection only.

The calculations described below are performed for a number of flap deflections (δ_{flap}) from 0 degrees to a maximum of 50 degrees. This provides a complete set of data that can be used to calculate the necessary flap deflection for any desired lift coefficient. The calculations use the following techniques.

$$\frac{c'}{c} = 1 + \frac{\Delta c}{c_f}\frac{c_f}{c} \tag{3.48}$$

where c' is the extended airfoil chord, $\Delta c/c_f$ is described above, and c_f/c is set by the user.

So

$$\frac{c_f}{c'} = \frac{c_f}{c}\frac{c}{c'} \tag{3.49}$$

The maximum 2-d lift with flap deflected is given by:-

$$C_{l\,max} = C_{l\,max}{}' \frac{c'}{c} \tag{3.50}$$

where C_{lmax}' is the lower of the following two expressions:-

$$C_{l\,max}{}' = 0.533\frac{\Delta y}{c}\left(\frac{Re}{3\times 10^6}\right)^{0.8} + 0.5\left(C_{l0} + \Delta_f C_{l0}{}'\right) \tag{3.51}$$

or

$$C_{l\,max}{}' = C_{l\,max(clean)} + \Delta_f C_{l0}{}' \tag{3.52}$$

Re is the Reynolds number of the equivalent wing mean aerodynamic chord at landing conditions. The effect of velocity will be relatively insignificant and can be ignored for small perturbations around the landing velocity.

$C_{l\max(clean)}$ is known from the 2-d airfoil data and $\Delta_f C_{l0}{}'$ is calculated as follows:-

$$\Delta_f C_{l0}{}' = \sum_{\textit{flap elements}} \Delta_f C_{l0}{}'' \tag{3.53}$$

and for each element

$$\Delta_f C_{l0}{}'' = 2\pi\eta_d \alpha_\delta{}' \delta_f \tag{3.54}$$

where

$$\alpha_\delta{}' = 1 - \frac{\theta_f{}' - \sin\theta_f{}'}{\pi} \tag{3.55}$$

and

$$\theta_f{}' = \cos^{-1}\left(\frac{2c_f}{c'} - 1\right) \tag{3.56}$$

For a single element flap system $\delta_f = \delta_{flap}$. In the case of a system with two elements, the first element is assumed to have a deflection of δ_{flap} while the second element is arbitrarily assumed to have a deflection of $\delta_{flap}/2$ relative to the first element. For a triple slotted flap the third element is assumed to have a deflection $\delta_{flap}/4$ relative to the second element. These deflections have been chosen after a brief analysis of the operation of the relevant flap systems, and keep the total deflection of the flap system within sensible limits (the total trailing edge deflection will never be greater than 90 degrees).

As detailed airfoil data is available, this means that the 2-dimensional lift increment due to flaps can be given by equation 3.57. This approach was used rather then estimating the maximum 2-d lift increment from equation G-13 of Torenbeek[93], as it proved to give more reasonable and appropriate results.

$$\Delta_f C_{l\,max} = C_{l\,max} - C_{l\,max\,clean} \tag{3.57}$$

This can be converted into a 3-dimensional lift increment using the equation below from Torenbeek[93].

$$\Delta_f C_{L\,max} = .92 \Delta_f C_{l\,max} \frac{S_{wf}}{S_{ref}} \cos\Lambda_{1/4c_e} \tag{3.58}$$

and the area ratio $S_{wf}\backslash S_{ref}$ is given by:-

$$\frac{S_{wf}}{S_{ref}} = \frac{b_{flap_o} - b_{flap_i}}{b_{ref}} \left\{ 1 + \frac{1-\lambda_e}{1+\lambda_e} \left(1 - \frac{b_{flap_o} + b_{flap_i}}{b_{ref}} \right) \right\} \tag{3.59}$$

Now the 3-d lift increment has been calculated for a full range of deflections of the trailing edge flaps. It is also possible to use the ailerons to augment the lift capabilities of the trailing edge flaps. This is done by setting the input parameter $\delta_{aileron}/\delta_{flap}$ to any value greater than 0 (and less than 1). This will provide an additional deflection of the ailerons that is of the value $\delta_{aileron}/\delta_{flap}$x δ_{flap}. The above analysis is then repeated for the ailerons and their lift contribution is added.

The flap lift analysis is now complete, and the flap and aileron deflection can be computed for any desired lift coefficient.

8 .Geometry Methods

The main function of the geometry module is to mathematically model the detailed shape of the fuselage, and to calculate its properties such as wetted area and frontal area. The shape of the nacelles is also estimated, and some preliminary calculations are made to ensure that the major components fit together correctly.

8 .1 Fuselage Geometry

The cross-sectional properties of the fuselage and its nose and tail lengths are set elsewhere (see Chapter 13). These properties are used in this module to calculate an estimate of the detailed 3-dimensional shape of the fuselage. The composition of the fuselage parts, in terms of selection of the types and properties of the curves, was decided from an analysis of the fuselage structures of all recent medium to large transport aircraft. The methods chosen provide simple but effective approximations to the actual fuselage shapes used for this type of aircraft. The fuselage shown in the examples below is a based on a double deck 500 seat concept, and shows the main features of the fuselage geometry. Although this approach places certain constraints on fuselage shape, there is still a reasonably large scope of fuselage geometries that can be produced by the program, which can differ in a number of respects from the example shown below.

8 .1 .1 Plan View

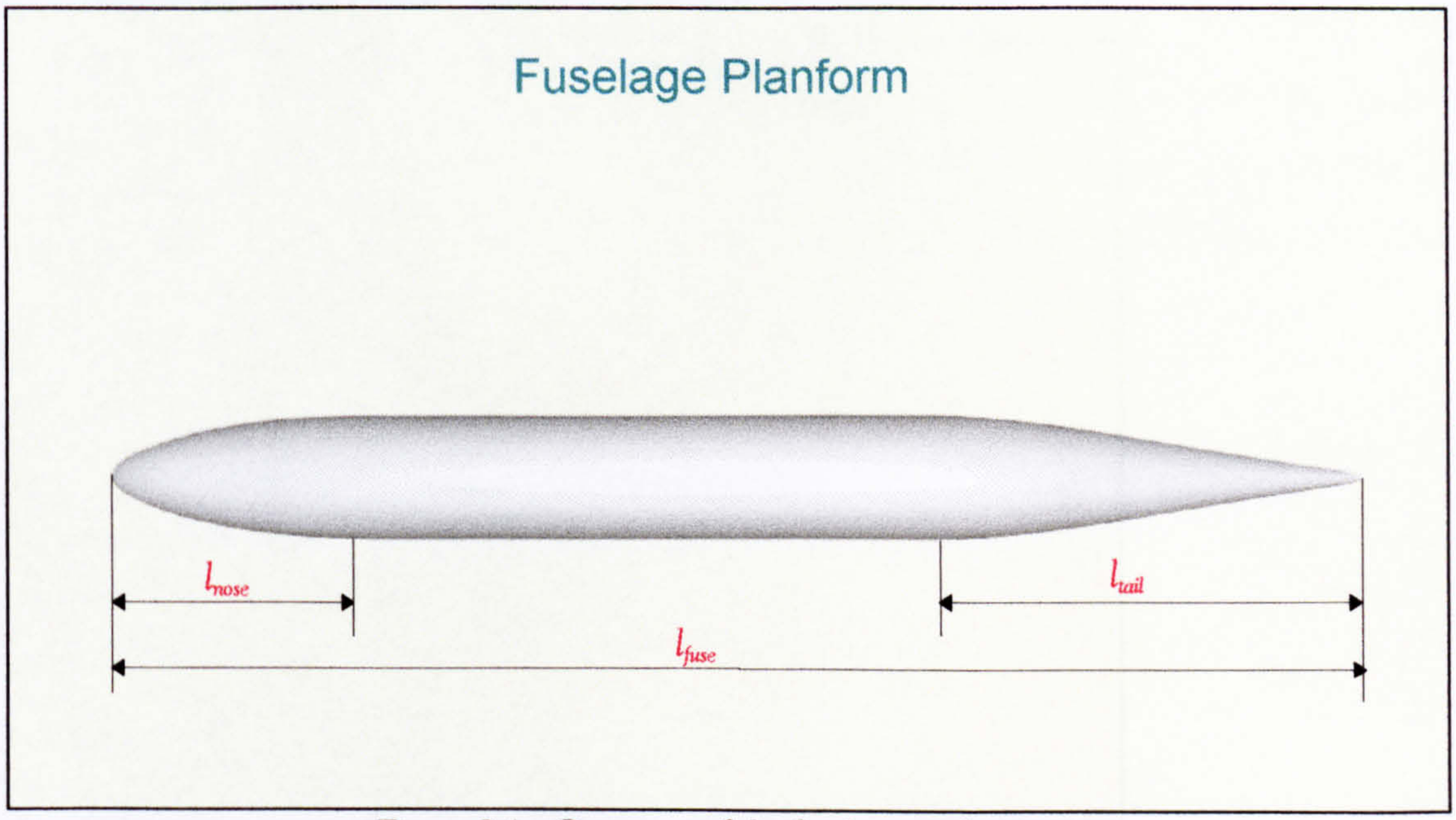


Figure 8.1 - Geometry of the fuselage in plan view

The main features of the fuselage planform are assumed to be of the form shown above in figure 8.1. The detailed geometries of the nose and tail sections, in planform view, are discussed below.

Nose Planform

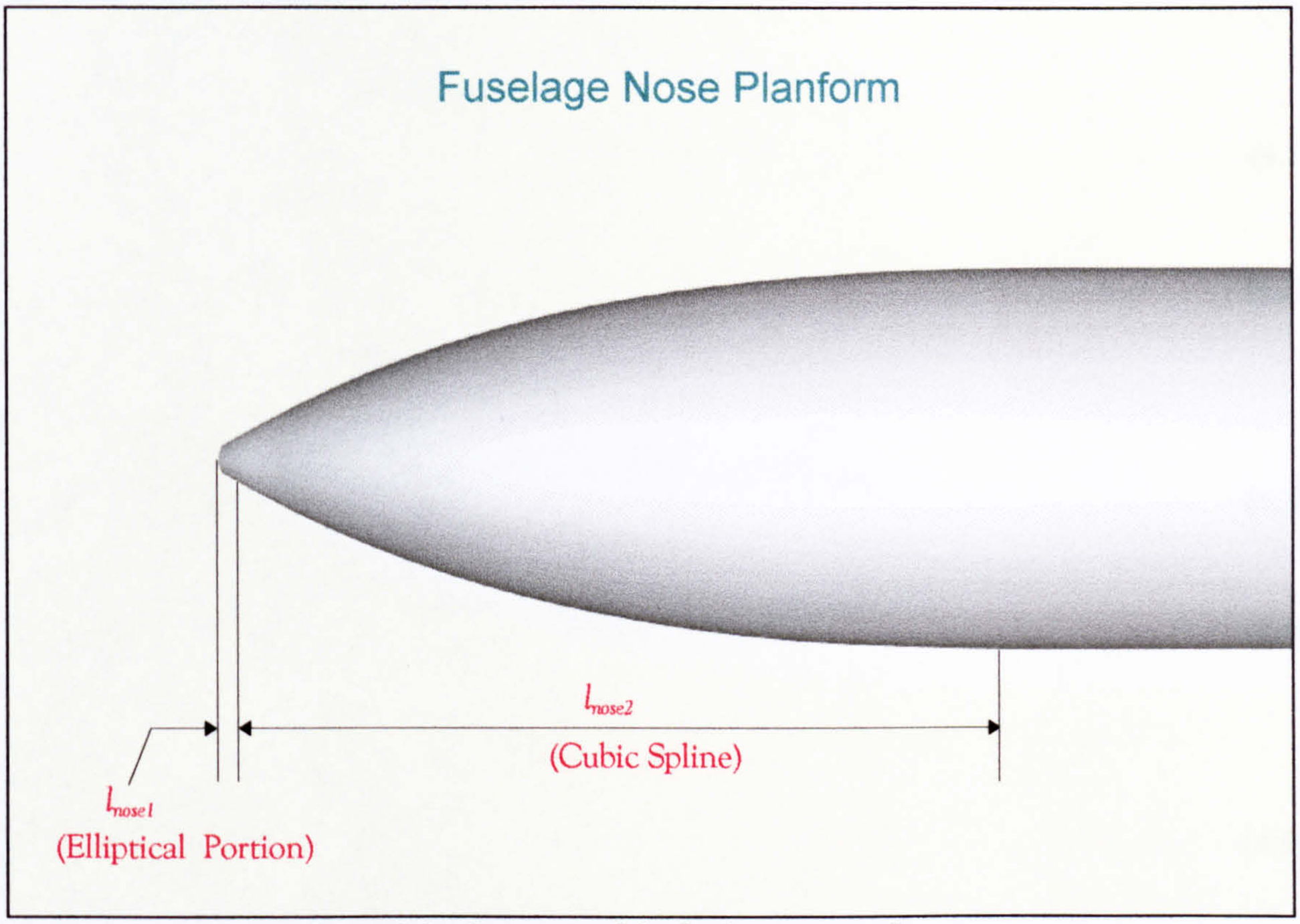


Figure 8.2 - Geometry of the fuselage nose in plan view

The parameters describing the curves are found using the following methods, assuming that the origin is at the very foremost point of the nose:-

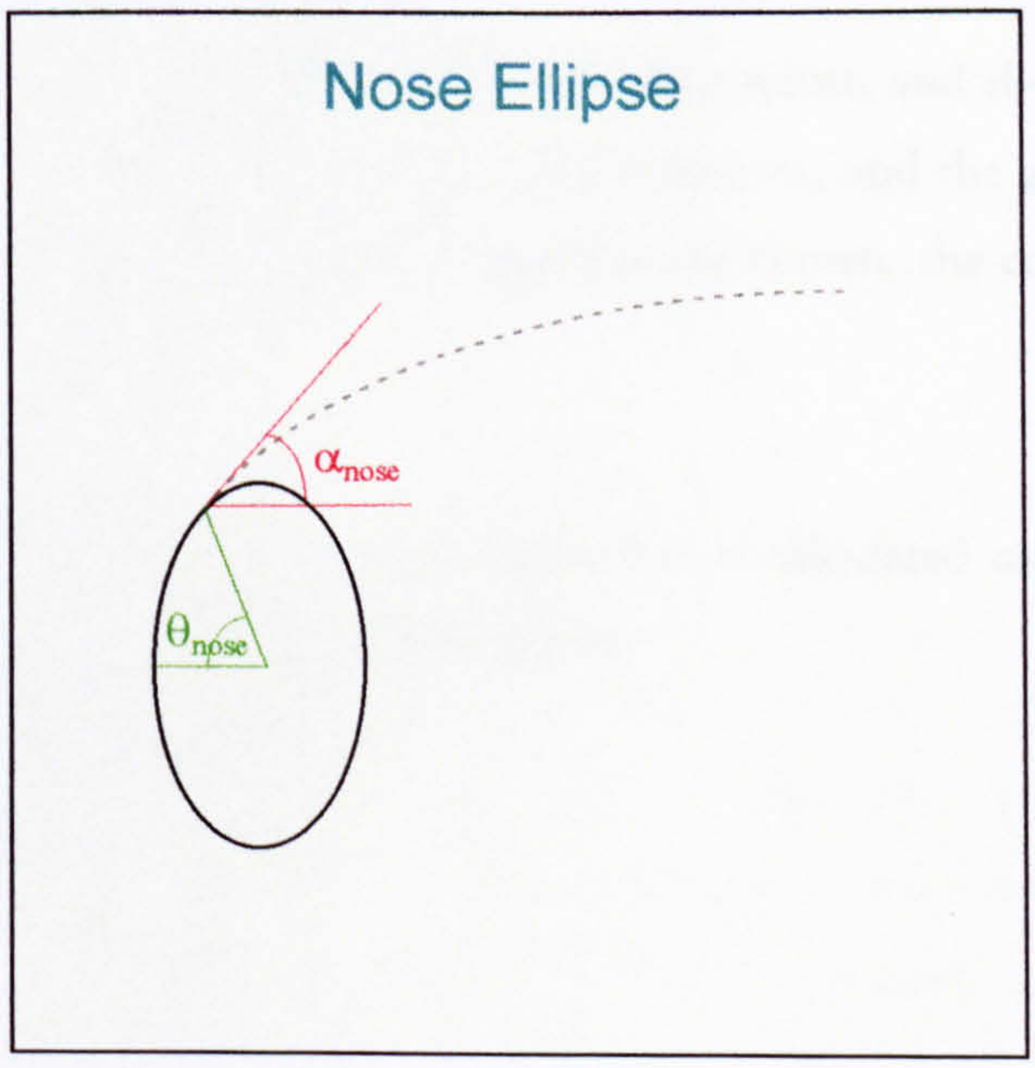


Figure 8.3 - Construction of fuselage nose geometry

Assuming that the ellipse is given by $\frac{x^2}{a_{nose}^2}+\frac{y^2}{b_{nose}^2}=1$, it joins the fuselage at an angle θ_{nose}, as shown above in figure 8.3. The parameters are then estimated using the following approximations:-

If $b_{fuse}<10$m then

$$\alpha_{nose}=\frac{\pi}{6} \tag{4.1}$$

$$\frac{b_{nose}}{a_{nose}}=\frac{b_{fuse}}{l_{nose}} \tag{4.2}$$

else

$$\alpha_{nose}=\frac{\pi}{8} \tag{4.3}$$

$$\frac{b_{nose}}{a_{nose}}=\frac{2b_{fuse}}{l_{nose}} \tag{4.4}$$

and

$$a_{nose}=\frac{l_{nose}}{6} \tag{4.5}$$

so

$$\theta_{nose}=\tan^{-1}\left(\frac{b_{nose}}{a_{nose}}\tan(\alpha_{nose})\right) \tag{4.6}$$

This means the point where the ellipse joins the cubic spline, and the gradient at this point are both known. The other extreme of the cubic is known, and the gradient at this extreme is zero. As four conditions for the cubic equation are known, the coefficients can be easily calculated.

Tail Planform

The tail planform (shown below in figure 8.4) is calculated using similar methods to those used for the nose planform described above.

The tail ellipse is described by.

$$\alpha_{tail}=\frac{\pi}{18} \tag{4.7}$$

$$\frac{b_{tail}}{a_{tail}} = \frac{b_{fuse}}{l_{nose}} \tag{4.8}$$

and

$$a_{tail} = \frac{l_{tail}}{20} \tag{4.9}$$

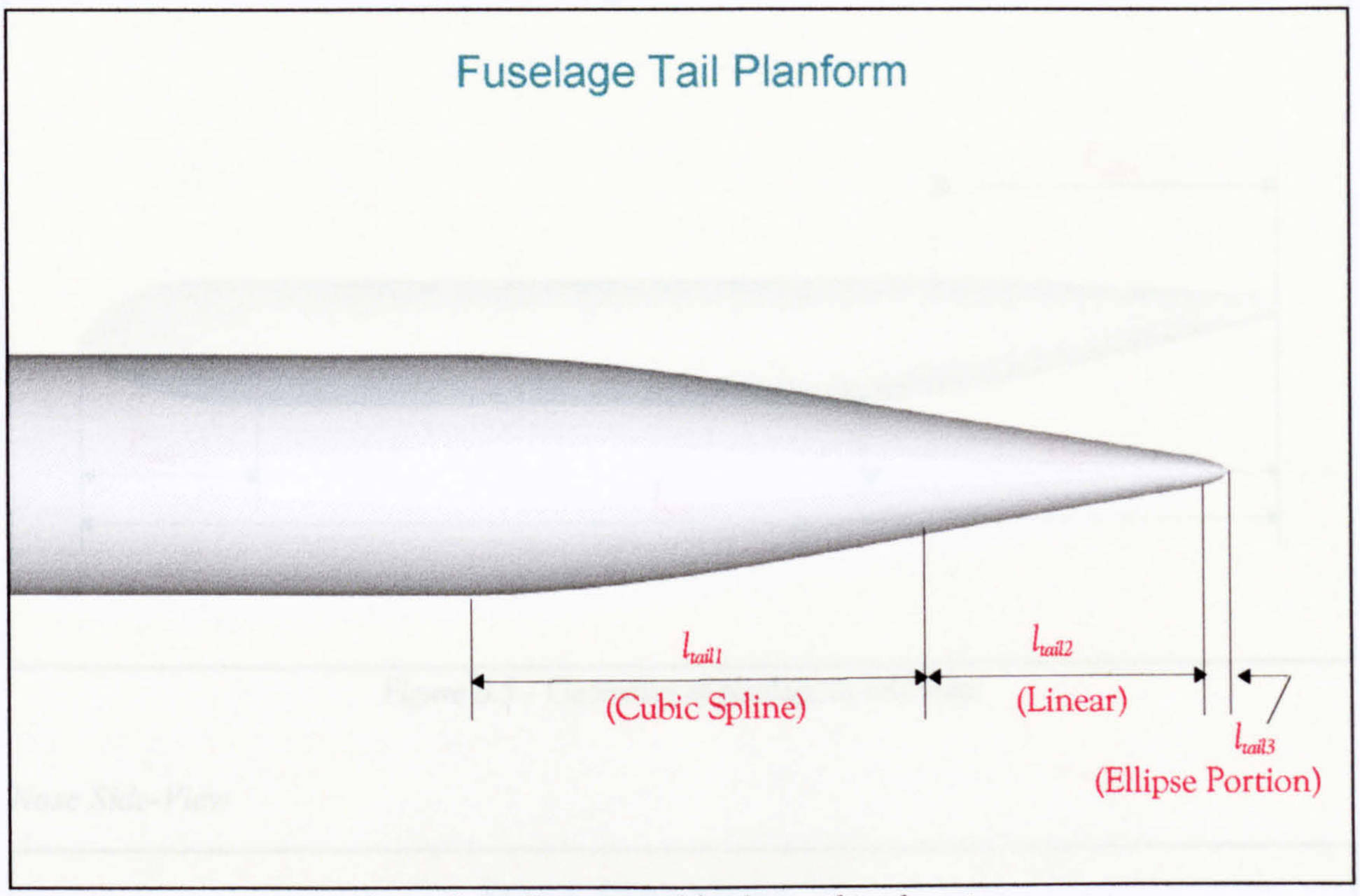


Figure 8.4 - Geometry of fuselage tail in plan view

A straight line is then constructed that joins the ellipse and continues with the same gradient for a length of $l_{tail2}=0.3l_{tail}$. As the beginning and end points of the cubic, and the gradients at these points are known, the equation of the cubic can be solved.

The overall planform area is estimated by calculating the value of y_{max} at a number of points along the fuselage, and then multiplying by the distance between the points.

8 .1 .2 Side View

Figure 8.5 shows the assumed geometry of the fuselage from a side view. The upper and lower parts of the fuselage are non-symmetrical and take into account such details as the integration of the cabin with the fuselage body, and a sufficient rear upsweep angle. The figures 8.6 and 8.7 show the detailed breakdown of the nose and tail sections. The variables denoting parameters for the side view are distinguished by an apostrophe.

The side-view nose length and the upper and lower tail length are given by:-

$$l'_{nose} = 0.6 l_{nose} \tag{4.10}$$

$$l'_{tail\,u} = 0.95 l_{tail} \tag{4.11}$$

$$l'_{tail\,l} = 1.2 l_{tail} \tag{4.12}$$

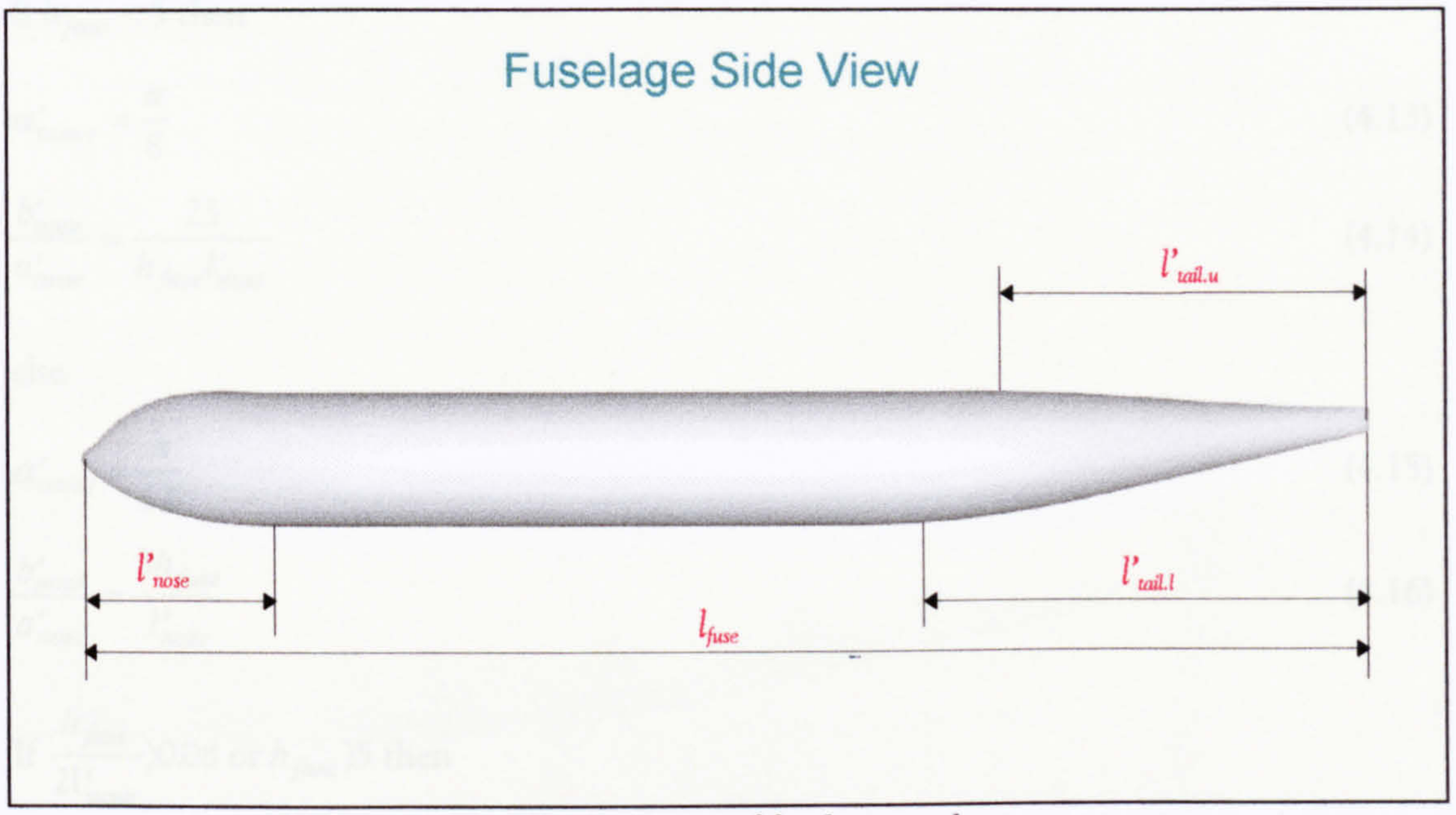


Figure 8.5 - Geometry of fuselage in side view

Nose Side-View

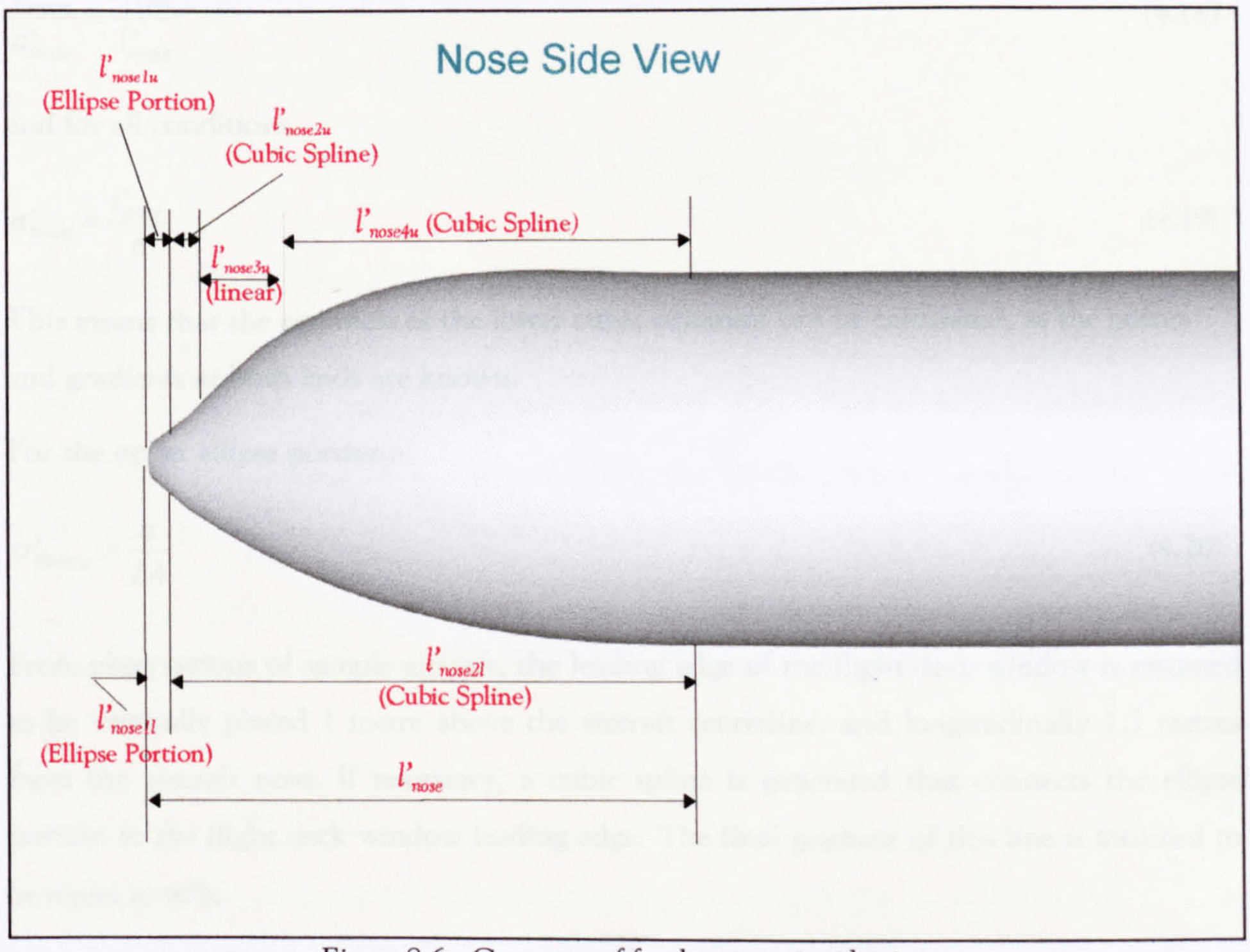


Figure 8.6 - Geometry of fuselage nose in side view

The shape of the front elliptical portion is defined using an approach similar to the one used to define the front ellipse of the planform view. For the lower portion:-

If $\frac{h_{fuse}}{2l'_{\text{nose}}} < 0.08$ or $h_{fuse} < 5$ then

If $h_{fuse} < 5$ then

$$\alpha'_{\text{nose}l} = \frac{\pi}{8} \tag{4.13}$$

$$\frac{b'_{nose}}{a'_{nose}} = \frac{25}{h_{fuse} l'_{nose}} \tag{4.14}$$

else

$$\alpha'_{\text{nose}l} = \frac{\pi}{12} \tag{4.15}$$

$$\frac{b'_{nose}}{a'_{nose}} = \frac{3h_{fuse}}{l'_{nose}} \tag{4.16}$$

If $\frac{h_{fuse}}{2l'_{\text{nose}}} > 0.08$ or $h_{fuse} > 5$ then

$$\alpha'_{\text{nose}l} = \frac{\pi}{4.9} \tag{4.17}$$

$$\frac{b'_{nose}}{a'_{nose}} = \frac{h_{fuse}}{l'_{nose}} \tag{4.18}$$

and for all conditions

$$a'_{nose} = \frac{l'_{nose}}{6} \tag{4.19}$$

This means that the equation of the lower cubic equation can be calculated, as the points and gradients at both ends are known.

For the upper ellipse portion:-

$$\alpha'_{\text{nose}u} = \frac{\pi}{2.4} \tag{4.20}$$

From observations of sample aircraft, the leading edge of the flight deck window is assumed to be vertically placed 1 metre above the aircraft centreline, and longitudinally 1.3 metres from the aircraft nose. If necessary, a cubic spline is generated that connects the ellipse portion to the flight deck window leading edge. The final gradient of this line is assumed to be equal to $\pi/6$.

The flight deck window is then assumed to be a linear shape of length 1 metre, placed at an angle of $\pi/3.6$ to the horizontal. The final cubic spline can then calculated which connects the trailing edge of the flight deck window to the main fuselage. The initial gradient is assumed to be equal to $\pi/3$.

Tail Side-View

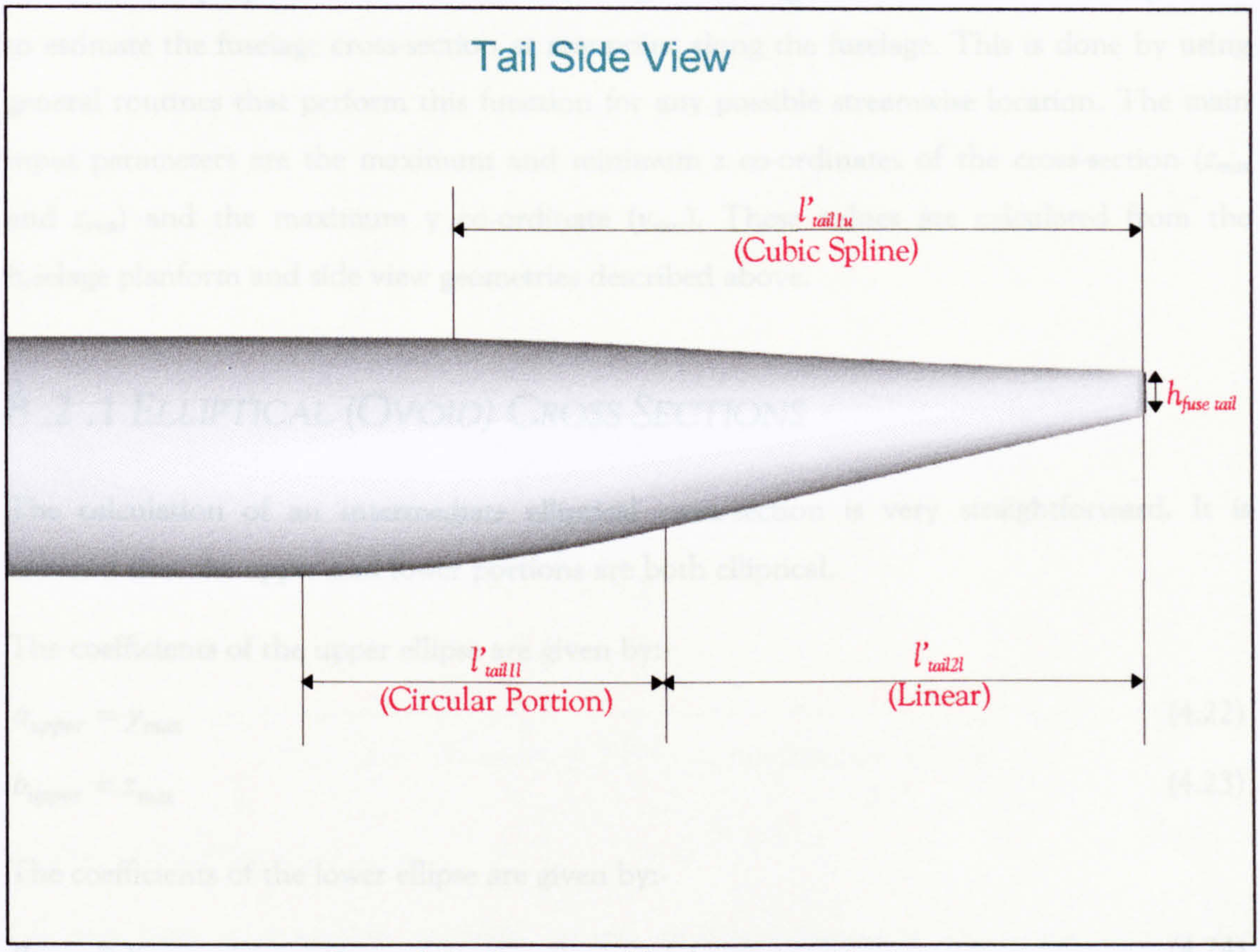


Figure 8.7 - Geometry of fuselage tail in side view

The first part of the lower surface consists of a circular arc which occupies the length l'_{tail1l} and smoothly sweeps the rear of the fuselage up until the target fuselage upsweep angle is reached. The radius of this circle is assumed to be $2l'_{tail1}$. The fuselage upsweep angle is assumed to be 13 degrees for all fuselage shapes, except for a vertical double bubble which has an increased upsweep of 20 degrees. The remainder of the lower surface is a straight line.

As the lower surface has already been determined, the upper surface can be resolved by assuming that the height of the fuselage at its very end ($h_{fuse\ tail}$) is equal to the following expression.

$$h_{fuse_{tail}} = 1.5(t \setminus c)_{tail} c_{root\ tail} \tag{4.21}$$

If a value of the horizontal tail root chord has not yet been made, then an estimate is made using equation 2.13.

A cubic equation can then be used to describe the upper surface as the co-ordinates and gradients at both extremes are known.

8 .2 Fuselage Cross-Sections

For the purposes of accurately calculating the fuselage wetted areas it must be possible to estimate the fuselage cross-section at any point along the fuselage. This is done by using general routines that perform this function for any possible streamwise location. The main input parameters are the maximum and minimum z co-ordinates of the cross-section (z_{max} and z_{min}) and the maximum y co-ordinate (y_{max}). These values are calculated from the fuselage planform and side view geometries described above.

8 .2 .1 Elliptical (Ovoid) Cross Sections

The calculation of an intermediate elliptical cross-section is very straightforward. It is assumed that the upper and lower portions are both elliptical.

The coefficients of the upper ellipse are given by:-

$$a_{upper} = y_{max} \tag{4.22}$$

$$b_{upper} = z_{max} \tag{4.23}$$

The coefficients of the lower ellipse are given by:-

$$a_{lower} = y_{max} \tag{4.24}$$

$$b_{lower} = z_{min} \tag{4.25}$$

8 .2 .2 747-Type Cross-Sections

The double deck portion of the 747-type fuselage cross-section is shown below in figure 8.8. It is composed of the upper deck and the main deck, both ellipses, connected tangentially by a fairing. It is possible for the upper deck to be wider or narrower than the main deck.

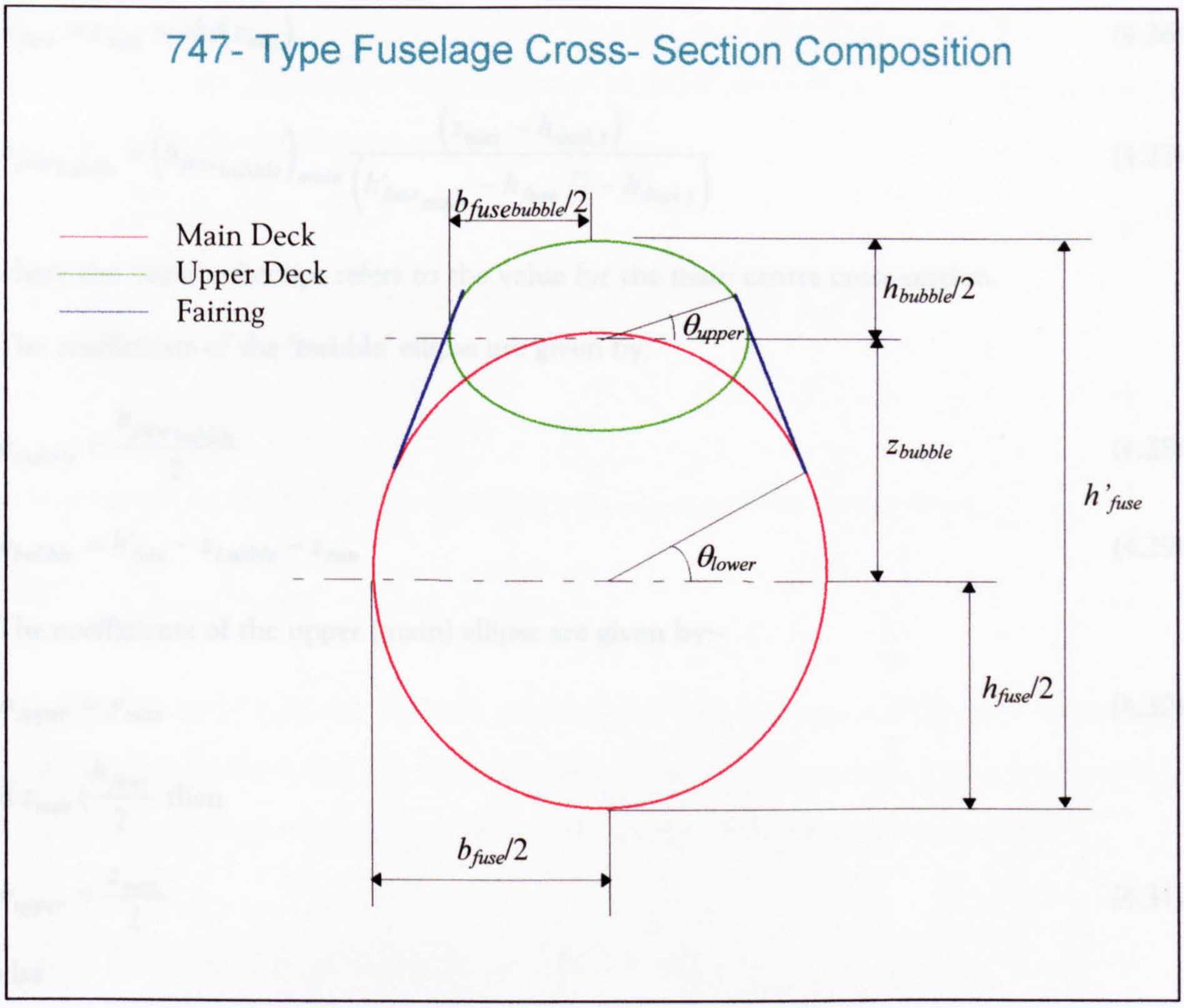


Figure 8.8 - Geometry of '747'- type fuselage cross-section

Main Cross-Section

For the main cross-section specified by the Fuselage Geometry input parameters, the following are known:-

h_{fuse}, b_{fuse}, h'_{fuse}, $b_{fuse\,bubble}$

The bubble height z_{bubble} is calculated from the height of the upper deck, specified in the Fuselage Geometry input parameters. It has been assumed that $z_{bubble}=h_{deckU}+0.5$ (see chapter 13).

Intermediate Cross-Section

For an intermediate cross-section only the values of z_{max}, z_{min}, y_{max} are known. So the fuselage section is created using the following method.

If $z_{max} \leq z_{bubble}$ then a single deck elliptical cross-section (see 8.2.1.) is assumed, where the coefficients of the upper and lower ellipses are given by equations 4.22 to 4.25

If $z_{max} \rangle z_{bubble}$ then a double deck 747 - type cross - section is assumed where:-

$$h'_{fuse} = z_{max} + abs(z_{min}) \tag{4.26}$$

$$b_{fuse_{bubble}} = \left(b_{fuse_{bubble}}\right)_{main} \frac{\left(z_{max} - h_{deck_2}\right)}{\left(h'_{fuse_{main}} - h_{fuse}/2 - h_{deck_2}\right)} \tag{4.27}$$

where the '*main*' subscript refers to the value for the main centre cross-section.

The coefficients of the 'bubble' ellipse are given by:

$$a_{bubble} = \frac{b_{fuse_{bubble}}}{2} \tag{4.28}$$

$$b_{bubble} = h'_{fuse} - z_{bubble} - z_{min} \tag{4.29}$$

The coefficients of the upper (main) ellipse are given by:-

$$a_{upper} = y_{max} \tag{4.30}$$

if $z_{max} \langle \frac{h_{fuse}}{2}$ then

$$b_{upper} = \frac{z_{max}}{2} \tag{4.31}$$

else

$$b_{upper} = \frac{h_{fuse}}{2} \tag{4.32}$$

if $a_{bubble} \rangle a_{upper}$ then

$$b_{upper} = b_{lower} \tag{4.33}$$

The coefficients of the lower ellipse are given by equations 4.24 and 4.25

Fairing Calculation

Once the coefficients of the relevant ellipses, and their respective positions are known, the geometry of the fairing connecting the 'bubble' ellipse and the main upper ellipse can be calculated. The join angle of the fairing from the main ellipse to the bubble will be positive (using the convention of figure 8.8) if $b_{bubble} < b_{fuse}$, otherwise it will be negative. If the axis is assumed to be at then centre of main ellipse, and assuming that θ_{lower} is positive (therefore the join will take place on the upper portion of the main ellipse), then at an angle $\theta_{lower} = \theta$, the y and z co-ordinates of the upper part of the main ellipse are given by:-

$$y_{main} = a_{upper} \cos\theta \tag{4.34}$$

$$z_{main} = b_{upper} \sin\theta \tag{4.35}$$

The correct position of the fairing is such that it is also tangential to the 'bubble' ellipse. From Scott[94] the equation of a line tangential to an ellipse with gradient m, where m is the gradient of the ellipse at a point (x_1,y_1) is given by:-

$$y = mx + \sqrt{a^2m^2 + b^2} \tag{4.36}$$

and since the equation of the tangent from an ellipse at point (x_1,y_1) is:-

$$y = \left(\frac{b^2}{a^2}\frac{x_1}{y_1}\right)x + \frac{b^2}{y_1} \tag{4.37}$$

the fairing will be situated at the value of $\theta = \theta_{lower}$ that satisfies the equality:-

$$\frac{{b_{upper}}^2}{y_{main}} = \sqrt{{a_{bubble}}^2 {m_{upper}}^2 + \left({b_{bubble}}^2 + z_{bubble}\right)} \tag{4.38}$$

This equality can be solved for both positive and negative values of θ using an iteration approach (the coefficients of the lower ellipse are used if θ is negative). The upper join angle θ_{upper} can be calculated and the geometry of the section is then completely defined.

8 .2 .3 Double Bubble Cross-Sections

A diagram of a horizontal double bubble cross-section is shown below in figure 8.9. A vertical double cross section is an identical cross-section rotated through 90 degrees.

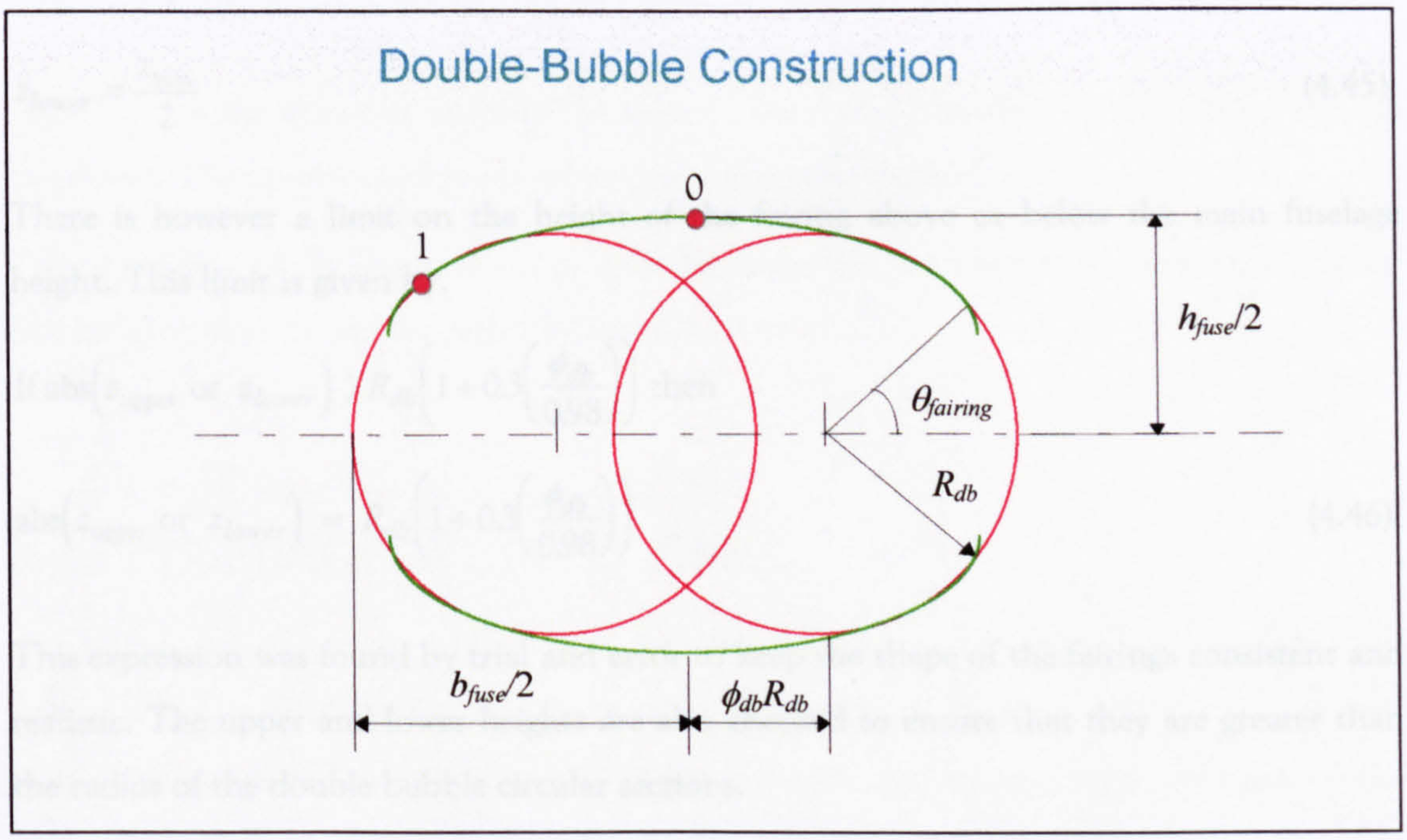


Figure 8.9- Geometry of horizontal double bubble cross-section

For the main cross-section, the values of h_{fuse} and b_{fuse} correspond to the values set in the Fuselage Geometry parameters. For an intermediate nose or tail section :-

$$b_{fuse} = 2y_{max} \tag{4.39}$$

$$h_{fuse} = z_{max} + abs(z_{min}) \tag{4.40}$$

The value of ϕ_{db} is assumed to be constant throughout the section, and is equal to the value set by the user in the Fuselage Geometry Section. This parameter allows the user to set the join distance between the two component fuselages.

The radius of the circular portions can be calculated using:-

$$R_{db} = \frac{b_{fuse}}{2(1+\phi_{db})} \tag{4.41}$$

The fairing then may be computed. For a symmetrical section, such as the main section:

$$z_{upper} = \frac{h_{fuse}}{2} \tag{4.42}$$

$$z_{lower} = \frac{h_{fuse}}{2} \tag{4.43}$$

However, some intermediate sections may not be symmetrical and:-

$$z_{upper} = \frac{z_{max}}{2} \tag{4.44}$$

$$z_{lower} = \frac{z_{min}}{2} \tag{4.45}$$

There is however a limit on the height of the fairing above or below the main fuselage height. This limit is given by.

$$\text{If } \text{abs}\left(z_{upper} \text{ or } z_{lower}\right) \rangle R_{db}\left(1+0.3\left(\frac{\phi_{db}}{0.98}\right)\right) \text{ then}$$

$$\text{abs}\left(z_{upper} \text{ or } z_{lower}\right) = R_{db}\left(1+0.3\left(\frac{\phi_{db}}{0.98}\right)\right) \tag{4.46}$$

This expression was found by trial and error to keep the shape of the fairings consistent and realistic. The upper and lower heights are also checked to ensure that they are greater than the radius of the double bubble circular sections.

The two extremes of the fairing position are denoted by the subscripts '*0*' and '*1*', as shown above in figure 8.9. The cubic equation of the upper fairing is then calculated as follows.

$$\phi_{fairing} = \frac{z_{upper} - R_{db}}{R_{db}} \tag{4.47}$$

$$y_0 = 0 \tag{4.48}$$

$$z_0 = R_{db}\left(1 + \phi_{fairing}\right) \tag{4.49}$$

Upper and lower limits have also been placed on the of the horizontal positioning of the fairing, so as to keep the geometry sensible.

$$y_{lower\ limit} = -R_{db}\left(0.75 + \phi_{db}\right) \tag{4.50}$$

$$y_{upper\ limit} = -R_{db}\left(\phi_{db}\right) \tag{4.51}$$

then

$$y_1 = y_{upper\ limit} + \left(y_{lower\ limit} - y_{upper\ limit}\right)\frac{\phi_{fairing}}{0.5} \tag{4.52}$$

and

$$z_1 = \sqrt{{R_{db}}^2 + \left(y_1 - y_{upper\ limit}\right)^2} \tag{4.53}$$

The gradient at point '1' is given by:-

$$m_1 = \cos^{-1}\left(\frac{z_1}{R_{db}}\right) \tag{4.54}$$

Therefore as the gradient at point '0' is zero, the cubic equation of the fairing can be calculated. The lower fairing is calculated using the same method.

The calculation of the properties of a vertical double bubble section used the same methods, but with the axes turned through 90 degrees.

8 .3 Fuselage Wetted Area

The wetted area of the fuselage is calculated using a strip integration approach. The nose and tail parts of the fuselage are split into a number of segments and the area of each segment is calculated. The evaluation of the circumference of an ellipse, or parts of the circumference of an ellipse, is carried out using a numerical integration technique. The method used may to calculate the segment area varies depending on the type of fuselage cross-section:-

8 .3 .1 ELLIPTICAL (OVOID) FUSELAGE SHAPES

The dimensions of the main cross section are known, therefore the wetted area of the quasi-cylindrical section can be calculated as:-

$$S_{cylinder} = C_{cross-section}\left(l_{fuse} - l_{nose} - l_{tail}\right) \tag{4.55}$$

where

$C_{cross\text{-}section}$ is the circumference of the cross - section of the 'cylindrical' portion of the fuselage

For the nose and the tail sections, the maximum and minimum z co-ordinate (z_{max} and z_{min}), and the maximum y co-ordinate (y_{max}) are known at any point. It is therefore possible to calculate an approximation of the intermediate sections (See 8.2.1).

So

$$C_{cross-section} = \frac{C_{ellipse_{lower}}}{2} + \frac{C_{ellipse_{upper}}}{2} \tag{4.56}$$

The wetted area of each strip (of length δx) is then found by multiplying the circumference of the cross-section by the width of the strip. The width of each strip depends on the nose\tail lengths and the number of strips (related to the Wetted Area Accuracy Parameter).

So

$$S_{nose} = \sum_{nose} C_{cross-section}\delta x \tag{4.57}$$

$$S_{tail} = \sum_{tail} C_{cross-section}\delta x \tag{4.58}$$

therefore

$$S_{wet\ fuse} = S_{cylinder} + S_{nose} + S_{tail} \tag{4.59}$$

8 .3 .2 747-TYPE FUSELAGE SHAPES

The circumference of the double deck cross-section is given by:-

$$C_{cross-section\,d.d.} = C'_{ellipse_{lower}} + C'_{ellipse_{upper}} + C'_{ellipse_{bubble}} + C_{fairing} \tag{4.60}$$

where

$C'_{ellipse_{lower}}$ = the perimeter of the lower ellipse that is exposed

$C'_{ellipse_{upper}}$ = the perimeter of the upper ellipse that is exposed

$C'_{ellipse_{bubble}}$ = the perimeter of the bubble ellipse that is exposed

$C_{fairing}$ = the perimeter of the fairing

These quantities can easily be calculated using simple geometry and a sub-routine that calculates the circumference of elliptical arcs. The single deck cross-section ($C_{cross-section_{s.d.}}$) can also be calculated in a straightforward manner.

The quasi-cylindrical wetted area can then be calculated. The length of the double-deck region in this 'cylindrical' main portion ($l_{d.d.cylinder}$) is calculated from the fuselage dimension inputs, and the wetted area is then computed:-

$$S_{cylinder} = C_{cross-section_{d.d}} l_{d.d\,cylinder} + C_{cross-section_{s.d}} \left(l_{fuse} - l_{nose} - l'_{tail\,l} - l_{d.d\,cylinder} \right) \qquad (4.61)$$

The tail portion of the fuselage is treated as elliptical, and the tail wetted area is calculated using the method described in 8. 2.1

For the nose portion of this type of fuselage, intermediate fuselage cross-sections are calculated at the point of each strip in the wetted area calculation. This technique allows a smooth transition from an elliptical cross-section to the desired double-deck cross-section. The wetted area of each strip is calculated using the appropriate method, depending whether it is a straightforward elliptical, or double deck cross-section.

For the purpose of weight calculations, a fuselage of this type is split into two component ovoid fuselages. The first fuselage is the main fuselage without any double deck region, and the second fuselage is the double deck region itself. It is assumed that the second fuselage has no tail area, and has a nose length equal to $0.9l_{nose}$. The heights, widths, and lengths of these are fuselages easily calculated from the fuselage input data. The wetted areas of these component fuselages are then computed using the techniques of section 8.2.1.

8 .3 .3 Double Bubble Fuselage Shapes

The double bubble fuselages (both horizontal and vertical) are assumed to be comprised of a double bubble cross section along the entire length of the fuselage. Using the techniques of section 8.2.3 it is possible to derive intermediate double bubble cross-sections, with fairings, for any suitable combination of fuselage width, fuselage height, and join distance between sections. The circumference of any section is given by:-

$$C_{cross-section} = C_{circular} + C_{fairing} \qquad (4.62)$$

Once the geometry of the section has been calculated, the circumference of the exposed circular portion is easily calculated, and the perimeter of the fairing is calculated by means of a discrete summation along its length. The total of the areas of the cross-sections is then summed, and the wetted area is found.

For the purposes of weight estimation, the properties of the two circular component fuselages must also be estimated. The radius of each fuselage is equal to R_{db} (see 8.2.3), and the methods of 8.3.1 are used to calculate their wetted area.

8 .4 Fuselage Frontal Area

The frontal area of the fuselage types are calculated using simple geometric methods. The methods used are described very briefly below.

Elliptical Fuselages

The frontal area of an elliptical section is simply the area of the ellipse:-

$$S_{frontal} = \pi a_{ellipse} b_{ellipse} \tag{4.63}$$

747-Type Fuselage

The frontal area is found by splitting the cross-section into a number of triangles and circular portions. This results in the expression below, where the area (A) of portions of the 'main' and 'bubble' ellipses are calculated between an initial and a final angular position, using a strip integration sub-routine.

If $\theta_{lower} > 0$

$$\frac{S_{frontal}}{2} = \left[A_{ellipse_{lower}}\right]_0^{\pi/2} + \left[A_{ellipse_{upper}}\right]_0^{\theta_{lower}} + \left[A_{ellipse_{bubble}}\right]_{\theta_{upper}}^{pi/2} + A_{triangle_1} + A_{triangle_2} \tag{4.64}$$

where

$$A_{triangle_1} = \frac{1}{2} z_{bubble} \sin\left(\frac{\pi}{2} - \theta_{lower}\right) \sqrt{\left(a_{upper} \cos\theta_{lower}\right)^2 + \left(b_{upper} \sin\theta_{lower}\right)^2} \tag{4.65}$$

$$A_{triangle_2} = \frac{1}{2} \sqrt{\left(a_{bubble} \cos\theta_{upper}\right)^2 + \left(b_{bubble} \sin\theta_{upper}\right)^2} \times b_{triangle_2} \tag{4.66}$$

where

$$b_{triangle_2} = \sqrt{\left(b_{bubble} \sin\theta_{upper} + z_{bubble} - b_{upper} \sin\theta_{lower}\right)^2 + \left(a_{bubble} \cos\theta_{upper} - a_{upper} \cos\theta_{lower}\right)^2} \tag{4.67}$$

If $\theta_{lower} < 0$

$$\frac{S_{frontal}}{2} = \left[A_{ellipse_{lower}}\right]_{-\theta_{lower}}^{\pi/2} + \left[A_{ellipse_{bubble}}\right]_{0}^{pi/2} + \left[A_{ellipse_{bubble}}\right]_{0}^{-\theta_{upper}} + A_{triangle_1} + A_{triangle_2} \tag{4.68}$$

Where these equations have been determined from the geometry shown below:-



Figure 8.10 - Determination of '747' Frontal area ($\theta_{lower} > 0$)

Double Bubble Fuselages

The frontal area of a double bubble fuselage is calculated by first computing the radial angle at which the fairing joins the circular part of the fuselage ($\theta_{fairing}$). This is easily done from the information available on the cross-sectional geometry. This means that area of the circular portion can be calculated that occupies the radial angle between $\theta_{fairing}$ and $-\theta_{fairing}$. As the equation and co-ordinates of the fairing are known. The area can be expressed as:-

$$S_{frontal} = 2\pi R_{db}{}^2 \frac{2\theta_{fairing}}{2\pi} - 4\frac{1}{2} y_1 z_1 + \sum_{i=1,N} \delta A \tag{4.69}$$

where δA is the area of a strip at between y_i and y_{i+1} where these are given by:-

$$y_i = y_1\left(\frac{i-1}{N}\right)$$

and the area of the strip is:-

$$\delta A = 2(y_{i+1} - y)(z_i + z_{i+1}) \tag{4.70}$$

8 .5 FUSELAGE FREIGHT VOLUME

A rough estimate of the volume available for the transportation of cargo is made using some simple approximations. The layout of the freight hold is assumed to be as shown in figure 8.11 below.

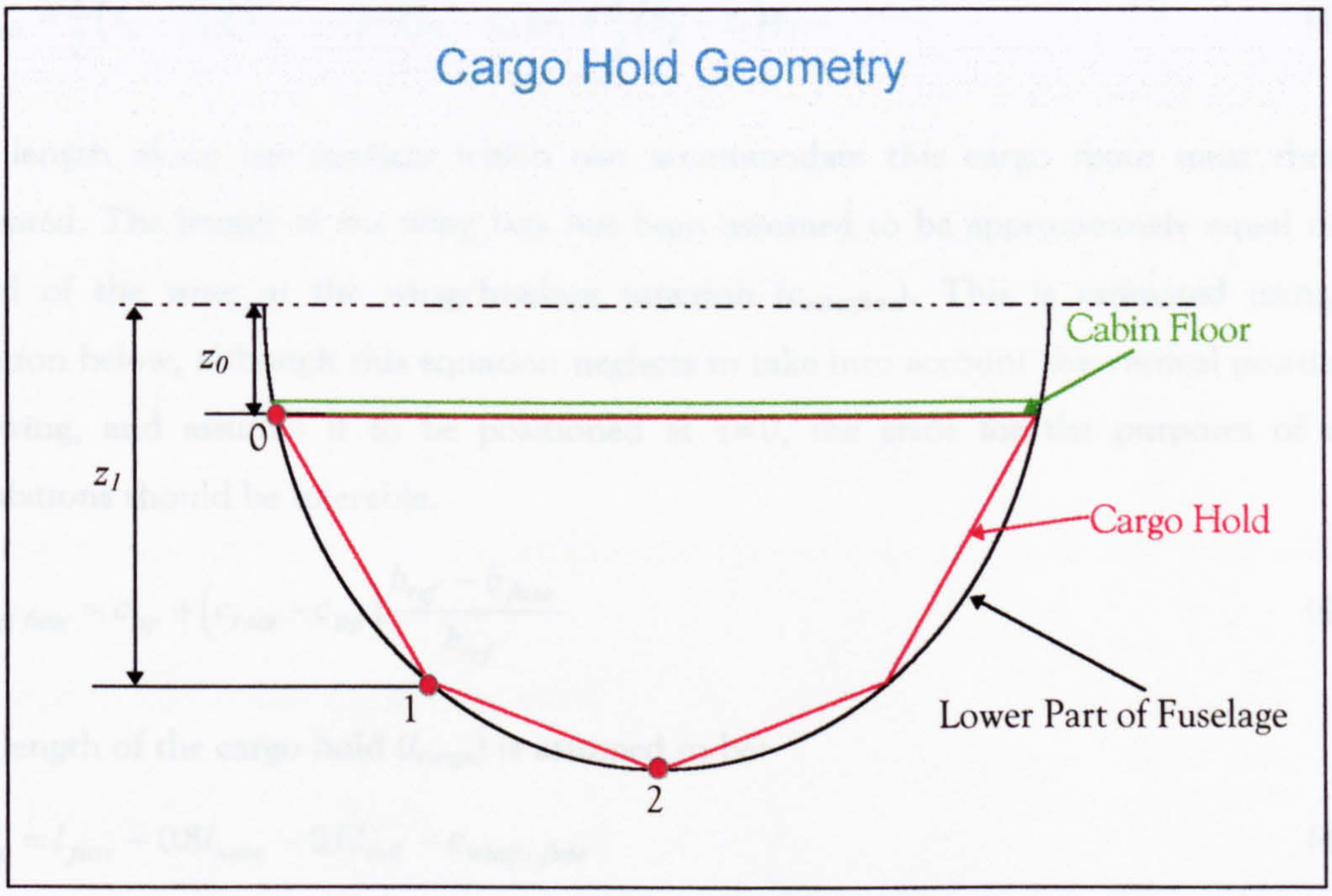


Figure 8.11 - Geometry of cargo hold cross-section

$$z_0 = h_{deck\,L} - 0.125 \tag{4.71}$$

If the lower part of the internal fuselage has the elliptical coefficients $a_{lower\,i}$ and $b_{lower\,I}$, then using the subscripts '*0*', '*1*', '*2*' to represent the coefficients at the points marked appropriately:-

$$y_0 = \sqrt{a_{lower\,i}{}^2\left(1 - \frac{z_0{}^2}{b_{lower\,i}{}^2}\right)} \tag{4.72}$$

and assuming that

$$z_1 = \frac{z_0 + b_{lower\,i}}{2} \tag{4.73}$$

then

$$y_1 = \sqrt{a_{lower\,i}{}^2\left(1-\frac{z_1{}^2}{b_{lower\,i}{}^2}\right)} \tag{4.74}$$

and

$$z_2 = b_{lower\,i} \tag{4.75}$$

$$y_2 = 0 \tag{4.76}$$

so the cargo hold area is given by:-

$$A_{cargo} = \frac{1}{2}(z_0 - z_1)(y_1 - y_0) + (z_1 - z_0)y_1 + \frac{1}{2}(z_2 - z_1)y_1 \tag{4.77}$$

The length along the fuselage which can accommodate this cargo space must then be estimated. The length of the wing box has been assumed to be approximately equal to the chord of the wing at the wing/fuselage junction ($c_{wing/fuse}$). This is estimated using the equation below, although this equation neglects to take into account the vertical position of the wing, and assumes it to be positioned at $z=0$, the error for the purposes of these calculations should be tolerable.

$$c_{wing/fuse} = c_{tip} + \left(c_{root} - c_{tip}\right)\frac{b_{ref} - b_{fuse}}{b_{ref}} \tag{4.78}$$

The length of the cargo hold (l_{cargo}) is assumed to be:-

$$l_{cargo} = l_{fuse} - 0.8l_{nose} - 0.8l_{tail} - c_{wing/fuse} \tag{4.79}$$

so

$$V_{cargo} = A_{cargo}l_{cargo} \tag{4.80}$$

8 .6 Nacelle Geometry

The geometry of the nacelles has been estimated using data values for the physical engine size, along with empirical correlations of the nacelle sizes of existing aircraft. The geometry of the nacelle is assumed to be as shown below in figure 8.12, where the 'gas generator' descriptor refers to the portion of the engine gas generator that is not covered by the fan cowling part of the engine nacelle.

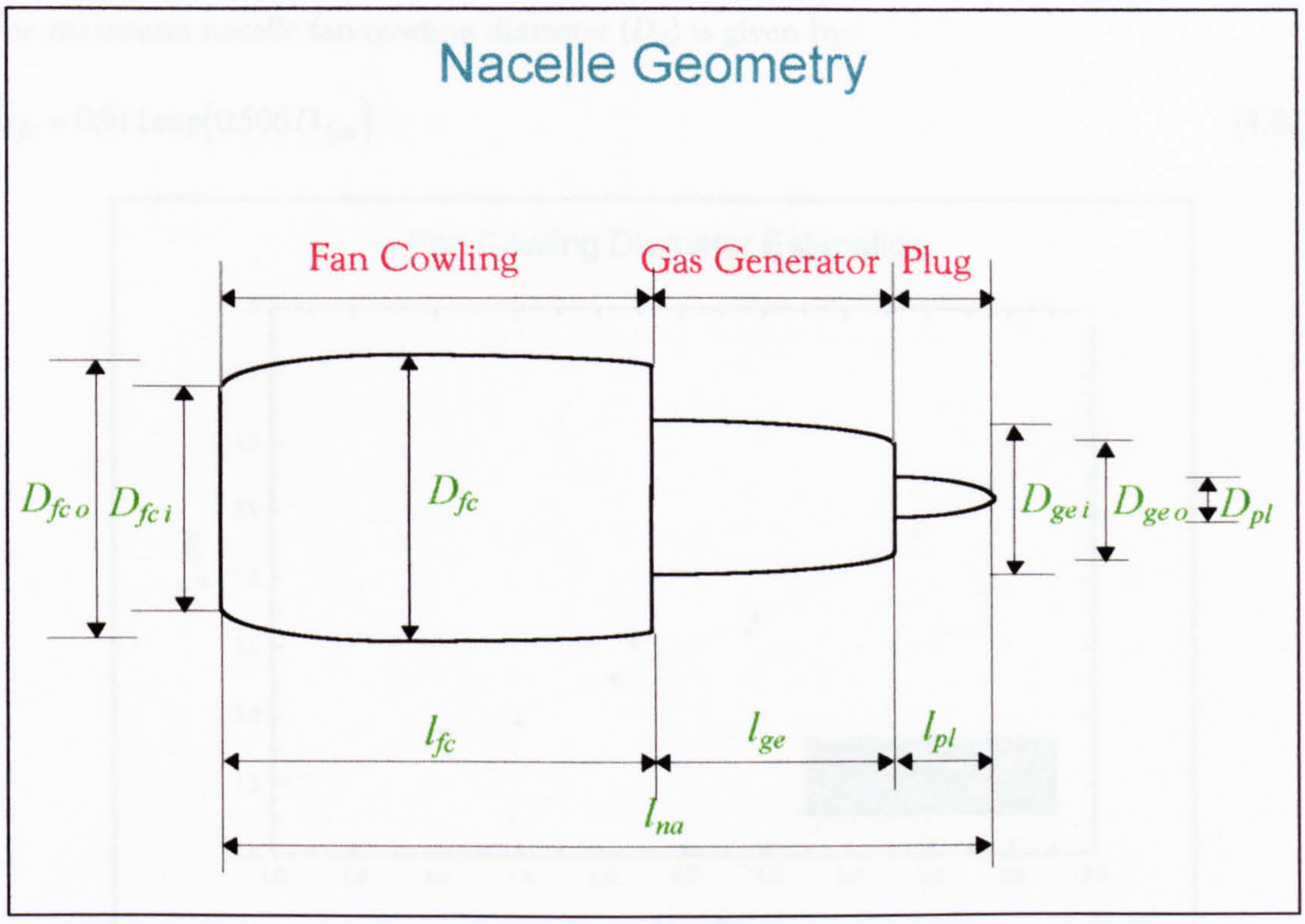


Figure 8.12 - Assumed nacelle geometry

The expressions for the component lengths and diameters are shown below, along with the data from which they were derived.

The total nacelle length (l_{na}) is given by:-

$$l_{na} = 3.74 \exp\left(\frac{4.35 \times 10^{-6} T_{nominal}}{\sqrt{BPR}}\right) \tag{4.81}$$

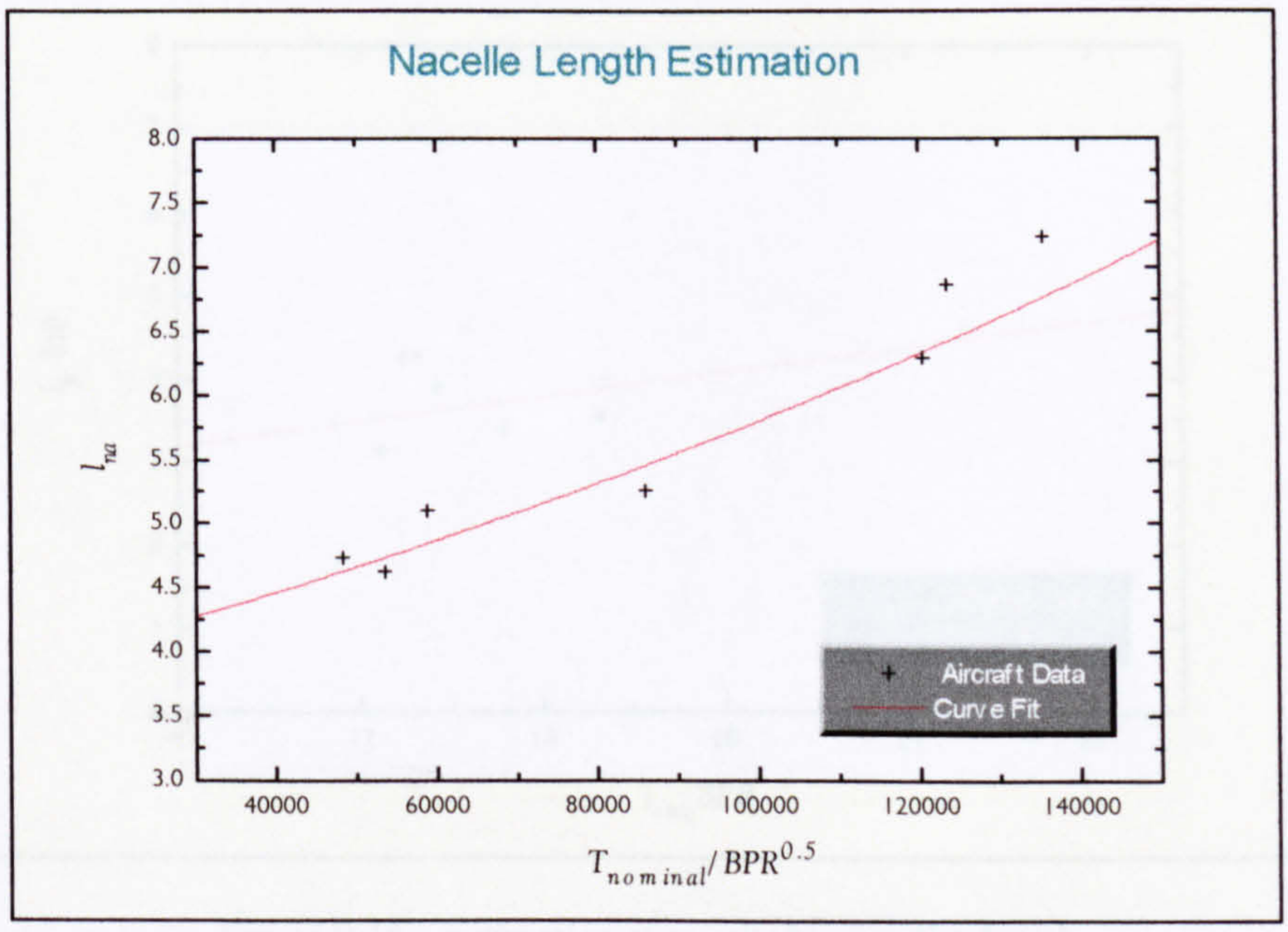


Figure 8.13- Estimation of the total nacelle length

The maximum nacelle fan cowling diameter (D_{fc}) is given by:-

$$D_{fc} = 0.911 \exp\left(0.506 D_{fan}\right) \tag{4.82}$$

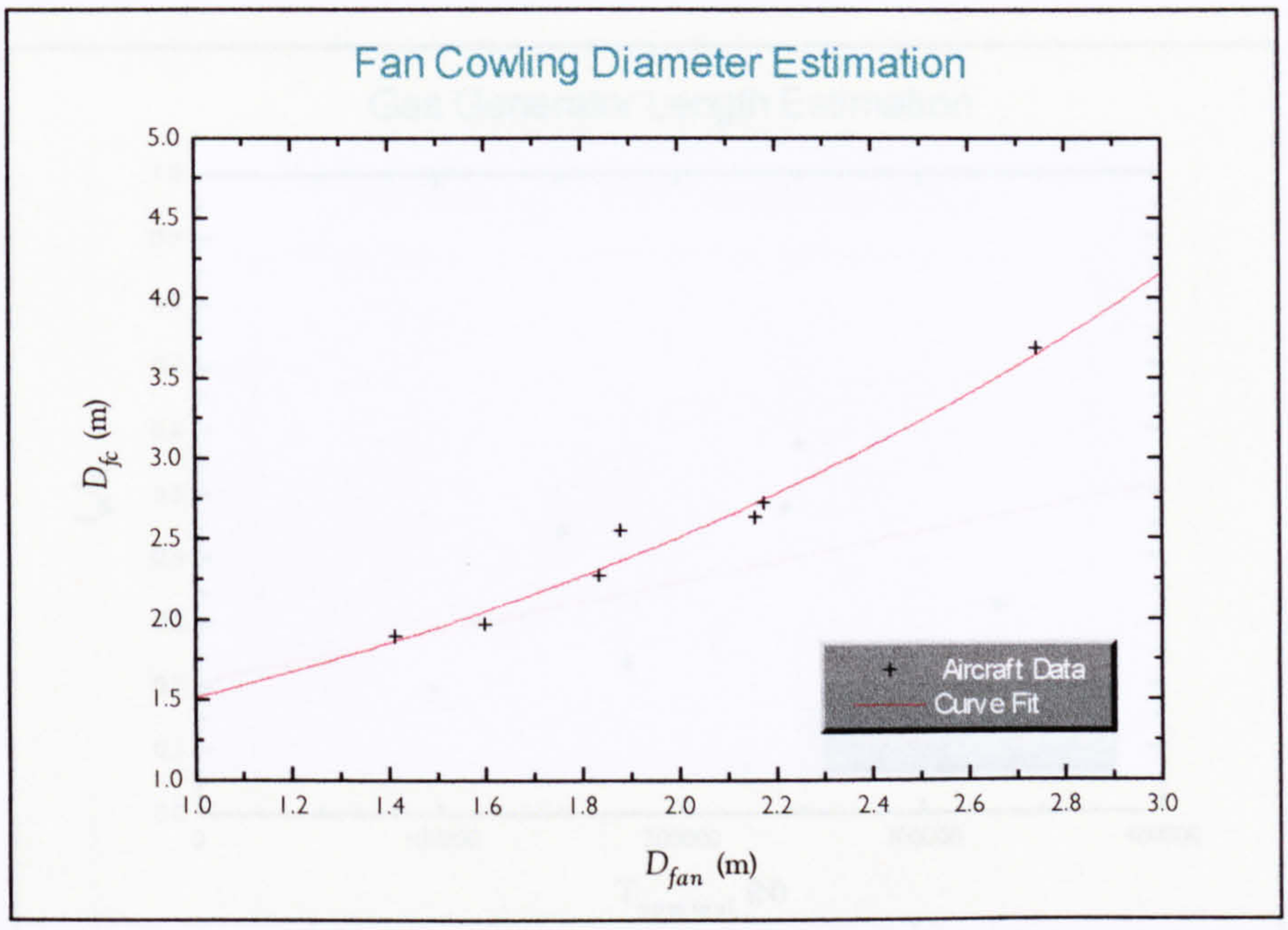


Figure 8.14- Estimation of maximum nacelle fan cowling diameter

The fan cowling length (l_{fc}) is given by:-

$$l_{fc} = 0.0739\left(l_{eng} BPR\right) + 2.5975 \tag{4.83}$$

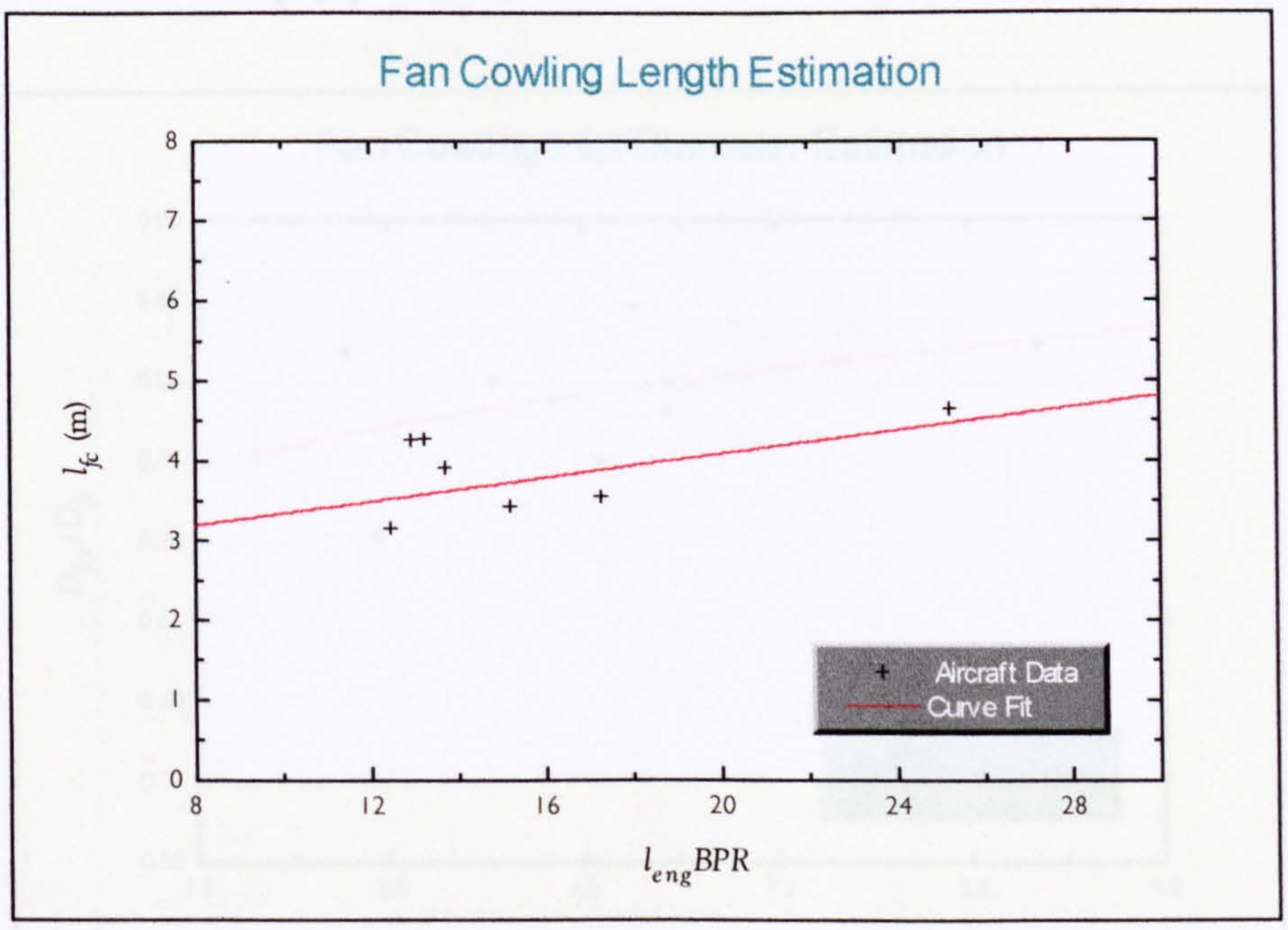


Figure 8.15 - Estimation of nacelle fan cowling length

The gas generator length (l_{ge}) is given by:-

$$\frac{l_{ge}}{l_{fc}} = 7.67 \times 10^{-7} T_{nominal} + 0.2076 \tag{4.84}$$

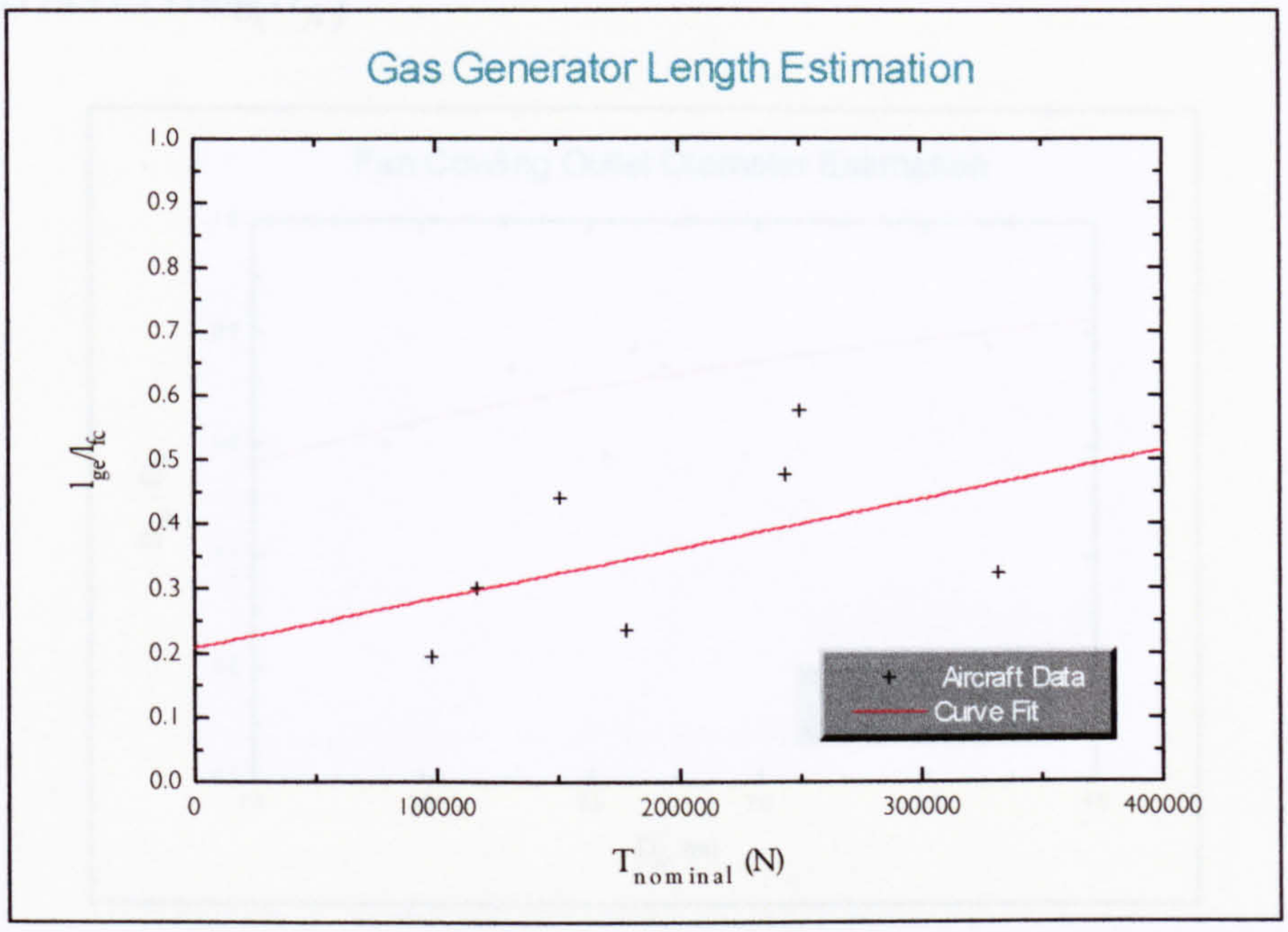


Figure 8.16- Estimation of nacelle gas generator length

The fan cowling inlet diameter ($D_{fc\,i}$) is given by:-

$$\frac{D_{fc_i}}{D_{fc}} = 0.711 + 0.0874 \log\left(D_{fc}\right) \tag{4.85}$$

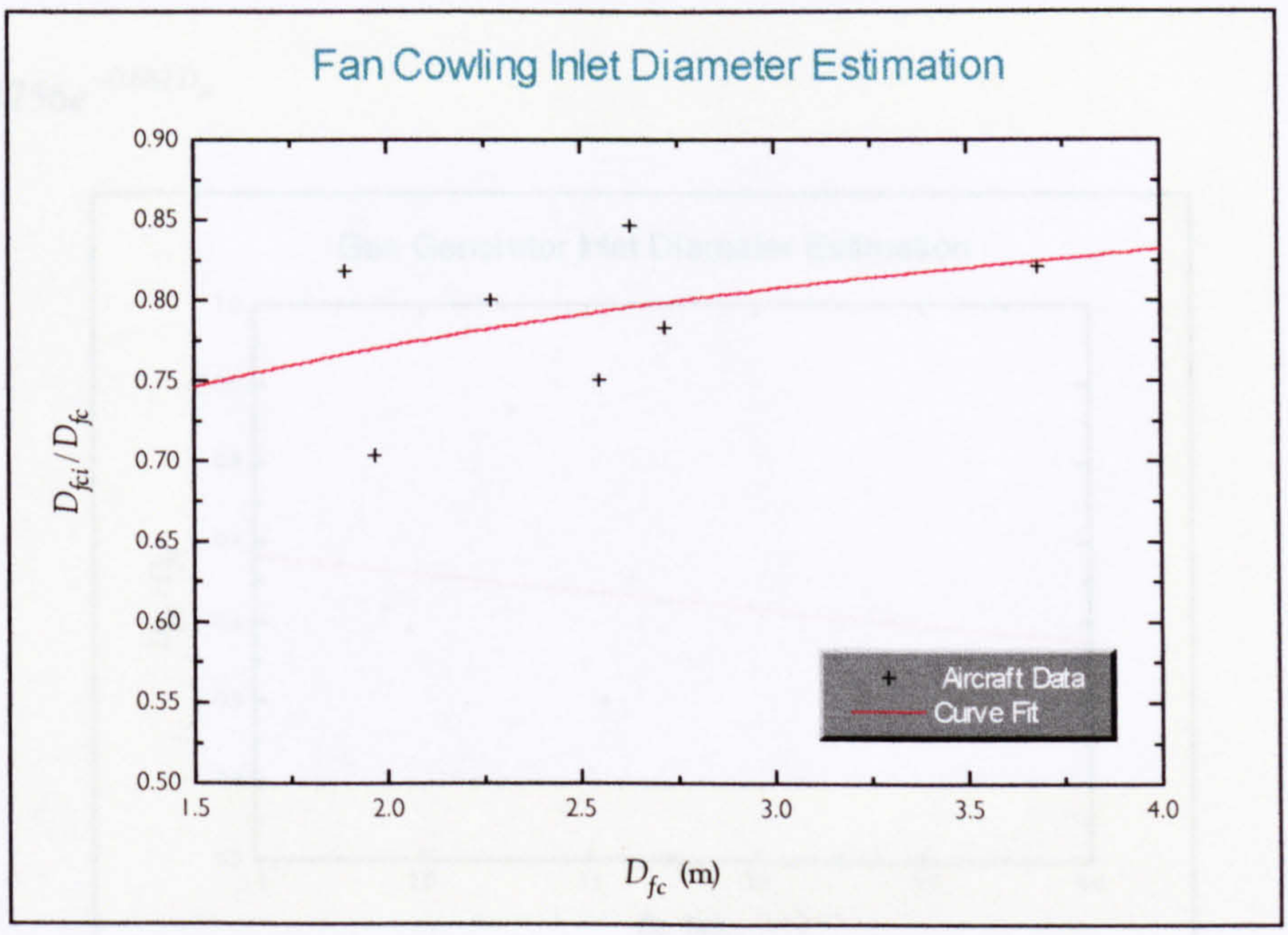


Figure 8.17- Estimation of nacelle fan cowling inlet diameter

The fan cowling outlet diameter ($D_{fc\,o}$) is given by:-

If $D_{fc} < 6$ then

$$\frac{D_{fc_o}}{D_{fc}} = 0.728 + 0.133\log\left(D_{fc}\right) \tag{4.86}$$

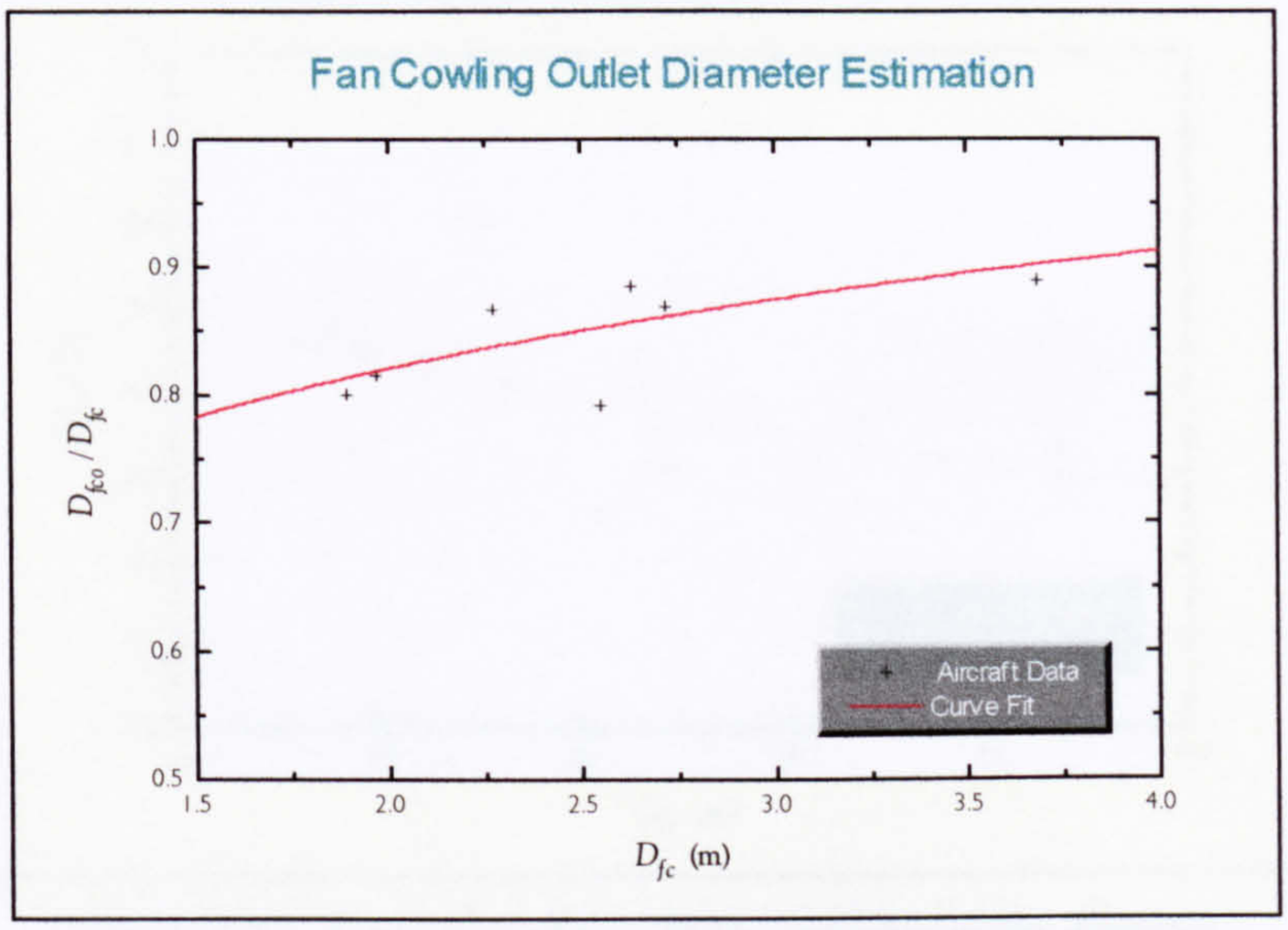


Figure 8.18 - Estimation of nacelle fan cowling outlet diameter

else

$$\frac{D_{fc_o}}{D_{fc}} = 0.966 \tag{4.87}$$

The inlet gas generator diameter ($D_{ge\,i}$) is given by:-

$$\frac{D_{ge_i}}{D_{fc}} = 0.756e^{-0.682 D_{fc}} \tag{4.88}$$

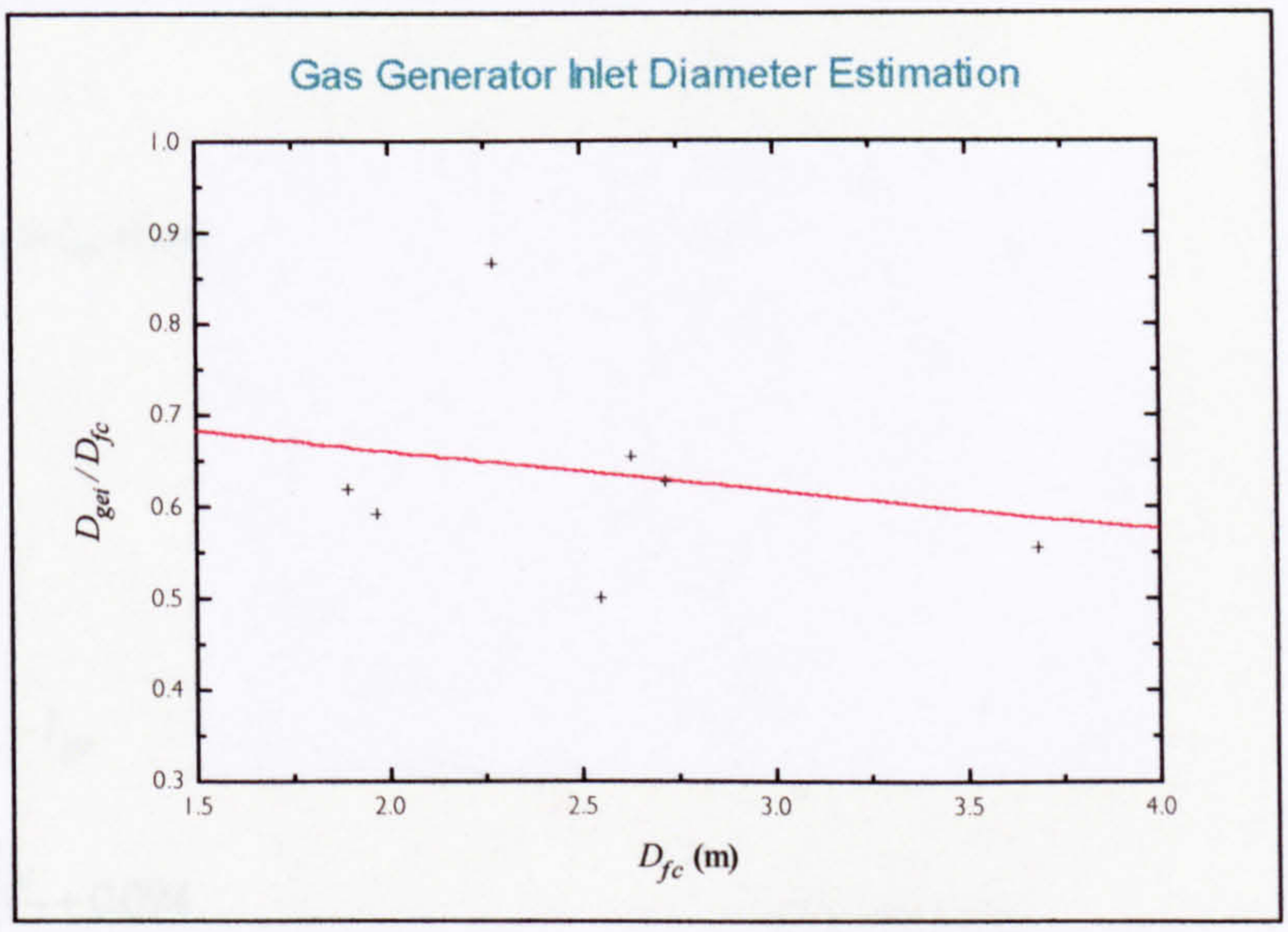


Figure 8.19 - Estimation of nacelle gas generator inlet diameter

The outlet gas generator diameter ($D_{ge\,o}$) is given by:-

$$\frac{D_{ge_o}}{D_{fc}} = 0.756e^{-0.682D_{fc}} \tag{4.89}$$

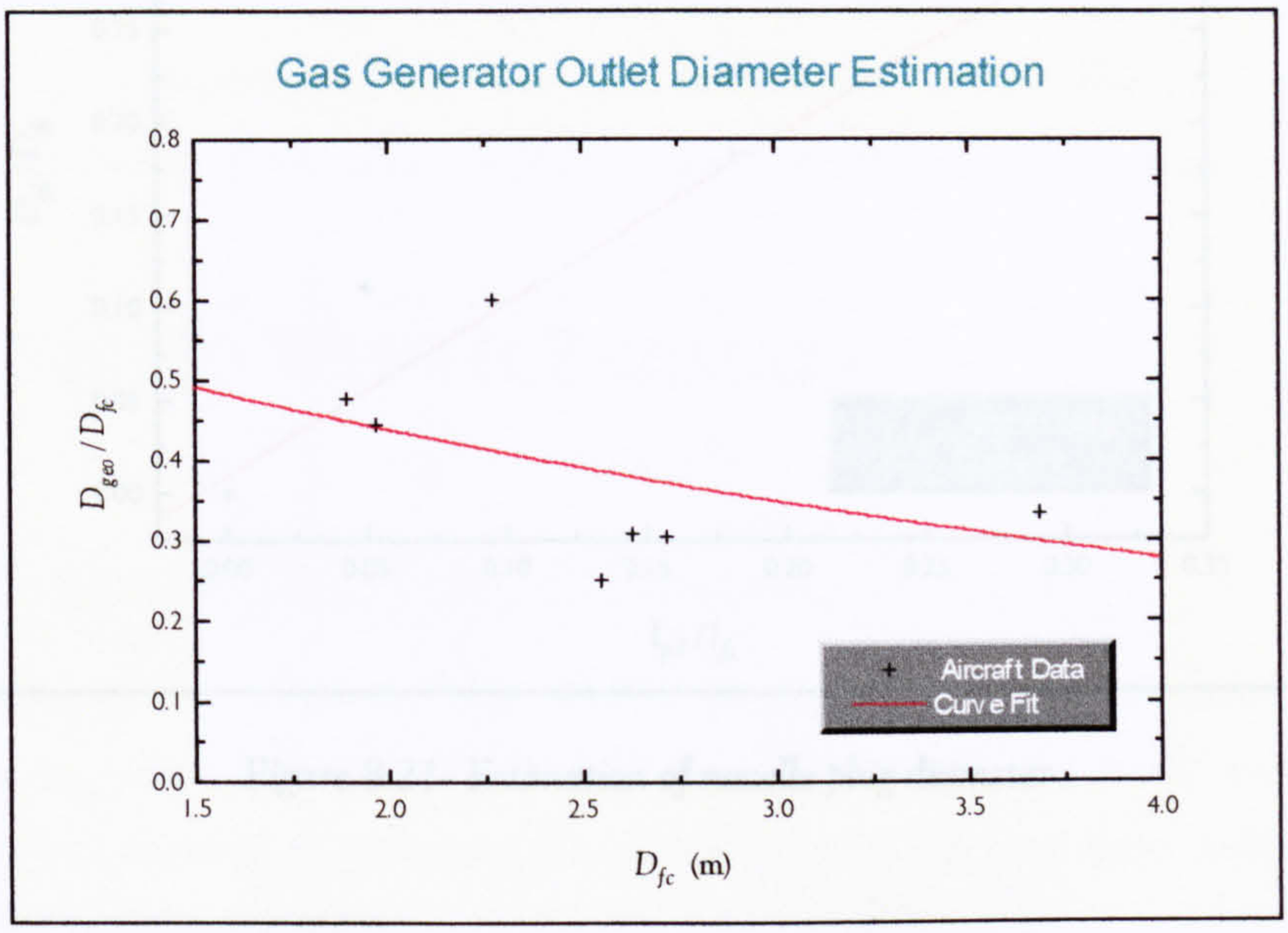


Figure 8.20 - Estimation of nacelle gas generator outlet diameter

The component lengths then need to be adjusted such that they sum exactly to the total nacelle length.

If $l_{fc} > l_{na}$ then

$$l_{fc} = 0.792 l_{fc} \tag{4.90}$$

$$l_{ge} = l_{na} - l_{fc} \tag{4.91}$$

and

$$l_{pl} = 0 \tag{4.92}$$

Also , if $l_{fc}+l_{ge} > l_{na}$ then

$$l_{ge} = l_{na} - l_{fc} \tag{4.93}$$

$$l_{pl} = 0 \tag{4.94}$$

Otherwise

$$l_{pl} = l_{na} - l_{fc} - l_{ge} \tag{4.95}$$

$$\frac{D_{pl}}{D_{fc}} = 0.929\frac{l_{pl}}{l_{fc}} + 0.094 \tag{4.96}$$

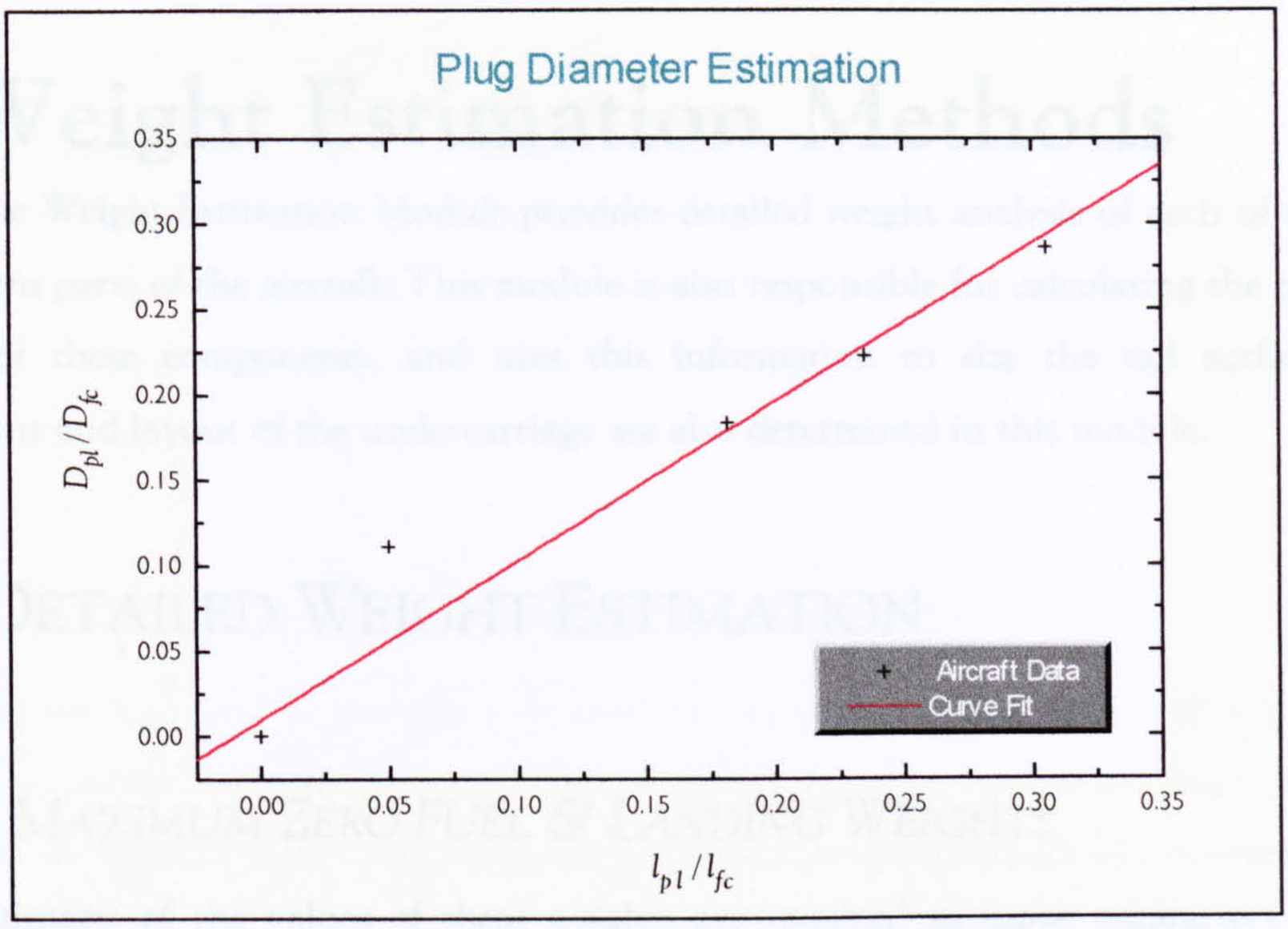


Figure 8.21- Estimation of nacelle plug diameter

9 .Weight Estimation Methods

The Weight Estimation Module provides detailed weight analysis of each of the main component parts of the aircraft. This module is also responsible for calculating the centres of gravity of these components, and uses this information to size the tail surfaces. The dimensions and layout of the undercarriage are also determined in this module.

9 .1 Detailed Weight Estimation

9 .1 .1 *Maximum Zero Fuel & Landing Weights*

Estimates of the values of these weights are required as input parameters for later calculations, so rough initial evaluations of these parameters are made using empirical correlations from existing aircraft data. Equations 5.1 and 5.2 have been derived from the data presented below in figure 9.1.

$$W_{zero-fuel} = 1.08\left(W_{oew} + W_{payload}\right) + 1113 \tag{5.1}$$

$$W_{land-\max} = 1.25\left(W_{oew} + W_{payload}\right) - 6870 \tag{5.2}$$

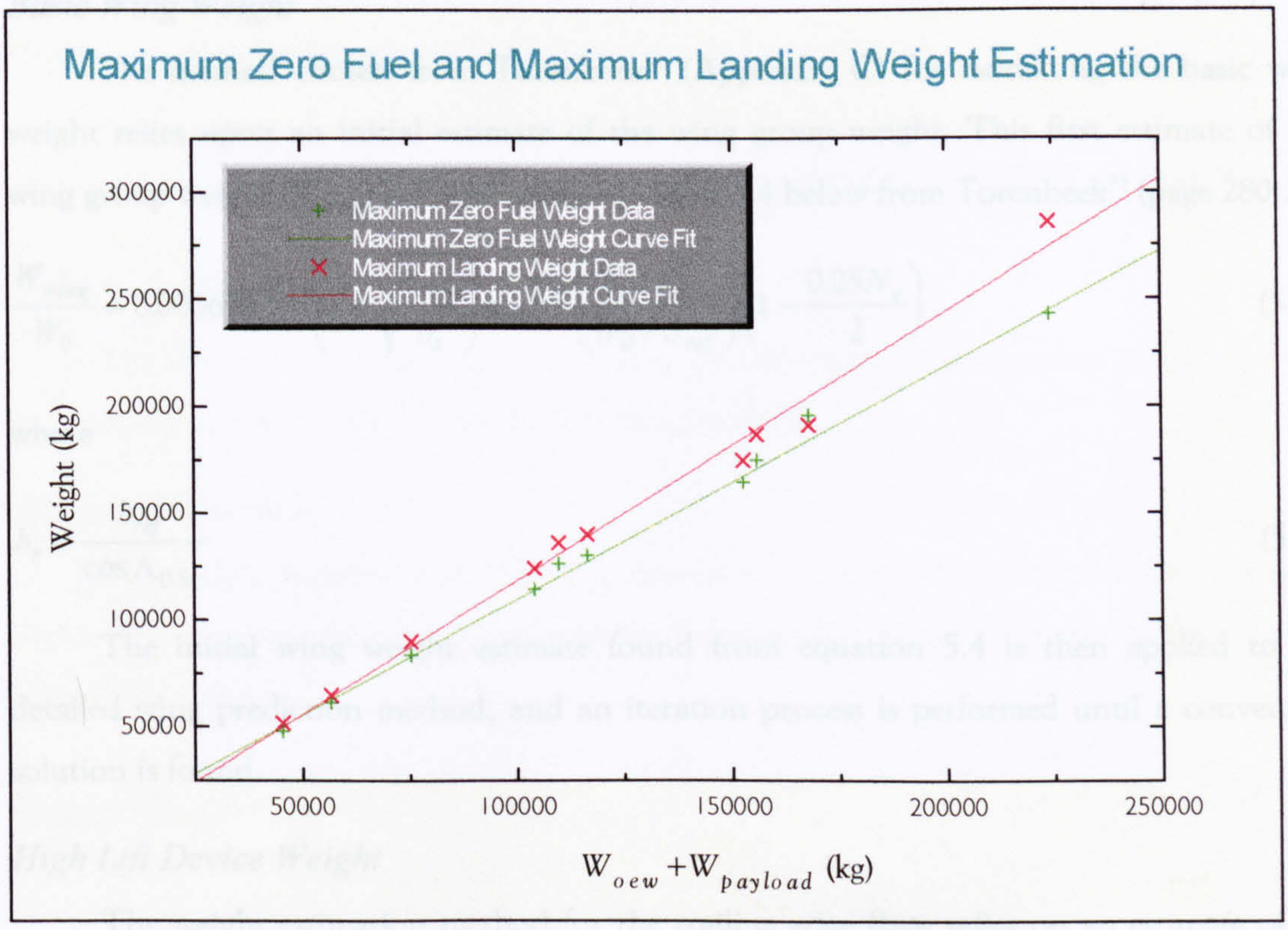


Figure 9.1- Estimation of maximum zero fuel and landing weights

9 .1 .2 ULTIMATE LOAD FACTOR

The ultimate load factor is calculated in accordance with the procedures laid out in the JAR-25[95] (Joint AirWorthiness Requirements). The manoeuvre and the gust load factors are calculated, and the ultimate load factor is taken to be 1.5 times the higher of these two values. For most civil aircraft this calculation ends up as $N_{ult}=1.5xN_{manoeuvre}$, where $N_{manoeuvre}=2.5$.

9 .1 .3 WING STRUCTURAL WEIGHT ESTIMATION

The method used to provide a detailed estimate of the wing structural weight is the method presented in Appendix C of Torenbeek[93]. A seemingly more thorough method is suggested in 'Development and application of a comprehensive design-sensitive weight prediction method for wing structures' by Torenbeek[96]. However, this method seemed to provide less reliable and accurate results than the ones from the more simple analysis. It was for this reason that the analysis of Torenbeek[93] (Appendix C) was chosen. The wing group weight is broken down into the main basic wing, the high lift devices, and any spoilers and air brakes. The wing group weight is given by:-

$$W_{wing} = W_{wing_{basic}} + 1.2\left(W_{hld} + W_{sp}\right) \tag{5.3}$$

Basic Wing Weight

The method chosen from Torenbeek[93] (Appendix C) for estimating the basic wing weight relies upon an initial estimate of the wing group weight. This first estimate of the wing group weight (W_{wing}) is found using equation 5.4 below from Torenbeek[93] (page 280).

$$\frac{W_{wing}}{W_0} = 0.00667 b_s^{0.75}\left(1+\sqrt{\frac{b_{ref}}{b_s}}\right) n_{ult}^{0.55}\left(\frac{b_s / t_{root}}{W_0 / S_{ref}}\right)\left(1-\frac{0.05N_e}{2}\right) \tag{5.4}$$

where

$$b_s = \frac{b_{ref}}{\cos\Lambda_{0.5c}} \tag{5.5}$$

The initial wing weight estimate found from equation 5.4 is then applied to the detailed wing prediction method, and an iteration process is performed until a convergent solution is found.

High Lift Device Weight

The weight estimation method for the trailing edge flaps relies on an estimate of the area that they occupy. This has been estimated as follows for the equivalent wing:-

$$c_{flap_o} = c_{root_e} - \left(c_{root_e} - c_{tip_e}\right)\frac{b_{flap_o}}{b_{ref}} \tag{5.6}$$

$$c_{flap_i} = c_{root_e} - \left(c_{root_e} - c_{tip_e}\right)\frac{b_{flap_i}}{b_{ref}} \tag{5.7}$$

$$S_{flap} = \frac{1}{2}\left(c_{flap_o} + c_{flap_i}\right)\left(b_{flap_o} - b_{flap_i}\right)\frac{c_{flap}}{c} \tag{5.8}$$

The area of the ailerons is calculated in the same manner and:-

$$S_{tef} = S_{flap} + S_{aileron} \tag{5.9}$$

The area of the leading edge devices must also be calculated, this has been approximated by making the assumption that they occupy the entire exposed leading edge region, and that the chord length of the leading edge devices is approximately 10% of the wing chord. These assumptions were made from studying wing designs of sample civil aircraft.

$$S_{lef} = 0.1c_{mean}\left(b_{ref} - b_{fuse}\right) \tag{5.10}$$

where c_{mean} is the mean geometric chord

The methods of Torenbeek[93] are then applied to calculate the weights of the trailing edge and leading edge high lift devices.

Spoilers & Speed Brakes

As the areas of the spoilers and the speed brakes are specified by the user, the weight of these devices is simply calculated using a specific weight of 12.2 kg/m^2 (Torenbeek[93]).

9 .1 .3 .1 Effect of advanced Technologies

The effect of any advanced technologies on the estimated wing group weight must be accounted for. This is done using the following methods.

Advanced Materials

The weight reduction of the wing due to the incorporation of advanced materials within the wing structure is known from the input section of the Component Specification Editor. Therefore:-

$$W_{wing} = W_{wing}\left(1 - \frac{\Delta W_{wing}}{W_{wing}}\right) \tag{5.11}$$

Variable Camber Wings

The change in wing weight due to the incorporation of variable camber wings is specified by the user. So:-

$$W_{wing} = W_{wing}\left(1 - \frac{\Delta W_{wing\,v.camber}}{W_{wing}}\right) \tag{5.12}$$

Laminar Flow and Hybrid Laminar Flow Control

The weight increment due to the incorporation of laminar flow control or hybrid laminar flow control systems is calculated using a specific weight. The value of this specific weight is 6.786 kg per m^2 of suction, as suggested by Lockheed-Georgia Company [97]. The area of the suction panels is calculated using the following relationships.

$$c_{fuse} = c_{root\,e} + \left(c_{tip\,e} - c_{root\,e}\right)\frac{b_{fuse}}{b_{ref}} \tag{5.13}$$

$$S_{exposed} = S_{ref\,e} - \frac{1}{2}\left(c_{root\,e} + c_{fuse}\right)b_{fuse} \tag{5.14}$$

So

$$S_{lfc} = \left(S_{exposed} - S_{lef} - S_{tef}\right)N_{surfaces} \tag{5.15}$$

or

$$S_{hlfc} = 0.2\left(S_{exposed} - S_{lef} - S_{tef}\right)N_{surfaces} \tag{5.16}$$

Where $N_{surfaces}$ is 1 or 2 depending whether the technology is applied to the upper surface only, or to both upper and lower surfaces. Therefore:-

$$W_{wing} = W_{wing} + 6.786 S_{(h)lfc} K_{tune(h)lfc.weight} \tag{5.17}$$

Winglets

As no methods were found for the estimation of the weight of winglets, the weight has been estimated as a percentage of the total wing weight, where the percentages for each type of winglet are based on data from existing aircraft.

For upper and lower winglet surfaces:-

$$W_{wing} = W_{wing}\left(1 + 0.04 K_{tune\,winglet}\right) \tag{5.18}$$

where the value 0.04 has been taken from Taylor[38].

For upper winglet surfaces only:-

$$W_{wing} = W_{wing}\left(1 + 0.049 K_{tune\,winglet}\right) \tag{5.19}$$

where the value of 0.049 has been taken from Boeing Airplane Company[39]. Although it may seem contradictory that the winglet with both a lower and an upper surface gives a smaller weight increment than one with just an upper surface, this paradox may arise from the lack of data available on the weight of winglets, meaning that each estimate has been based on just one data point for an optimised winglet surface, and the fact that these two winglets are mounted on completely different wings and are of very different sizes. This means that although great trust cannot be placed in the actual values produced by the equations, one can assume that they provide reasonable estimates, and more importantly reflect the qualitative effect of the addition of winglets. The effect of the winglet efficiency parameter $K_{tune\,winglet}$ is accounted for by assuming that an increased efficiency means an increased span and therefore increased weight.

For wing tip fences it has arbitrarily assumed from size considerations that:-

$$W_{wing} = W_{wing}\left(1 + \frac{0.04 K_{tune\,winglet}}{10}\right) \tag{5.20}$$

9 .1 .4 Fuselage Structural Weight

The fuselage structural weight is estimated using the weight penalty method described in Appendix D of Torenbeek[93]. Modifications needed to be made to this method to accommodate the unconventional fuselage types that are available to the user. As little or no public domain material was available to assist in the weight estimation of fuselage shapes other than those of conventional circular or ovoid cross-section, judgement and common sense has to be applied to overcome this limitation. As above, this means that although the actual numeric values may not be exact, they are hopefully within the realistic bounds of error for this type of analysis, and will qualitatively reflect the changes in properties of different fuselage structures.

9 .1 .4 .1 Circular Single Deck

The weight penalty method can be applied to a conventional circular fuselage shapes with no modification. Some of the assumptions made in the application of this method are outlined below.

h_{max} – Maximum Operational Altitude (m)

Δp – Maximum Operational Differential Cabin Pressure (Pa)

The maximum operational altitude has been estimated from the study of aircraft performance data to be given by:-

$$h_{max} = h_{cr1} + 1500 \tag{5.21}$$

and from Torenbeek[93] chapter 11

$$\Delta p = \left(0.8 - \delta_{h\,\max}\right) P_0 \tag{5.22}$$

where δ is the atmospheric pressure ratio, and P_0 is the sea level atmospheric pressure.

The number of emergency exits is calculated in accordance with safety regulations. It has been assumed that the exits required for aircraft seating 178 passengers or less are Type 1 exits, and that subsequent exits required for additional passengers are Type A exits.

$$N_{exit} = 4 + \text{int}\left(\frac{N_{pass} - 178}{110}\right) \times 2 \tag{5.23}$$

Analysis of current fuselage layouts suggested that a rough estimate of the number of windows could be provided by equation 5.24 below, with each window assumed to have an area of 0.06m^2.

$$N_{windows} = \frac{2l_{windows}}{0.6} \tag{5.24}$$

where

$$l_{windows} = l_{fuse} - 0.4l_{nose} - 0.6l_{tail} \tag{5.25}$$

A similar analysis of cockpit windshield areas (A_{ws}) provided the estimation that:-

If $b_{fuse} < 7$ then

$$A_{ws} = 1.5 \times 0.8 b_{fuse} \tag{5.26}$$

else

$$A_{ws} = 8.4 \tag{5.27}$$

The weight of the cabin floor is assumed to be proportional to the fuselage planform area :-

$$W_{floor} = 7.5 S_{planform} \tag{5.28}$$

The bulkheads are assumed to occupy an area that is equal to:-

$$S_{bh} = 2\pi\left(\frac{2}{3}\frac{b_{fuse}}{2}\right)^2 \tag{5.29}$$

All of the weight contributions are combined, and an initial estimate of the fuselage weight W_{fuse} is found. This is then adjusted for the presence of advanced materials such that:-

$$W_{fuse} = W_{fuse}\left(1 - \frac{\Delta W_{fuse}}{W_{fuse}}\right) \tag{5.30}$$

9 .1 .4 .2 Elliptical Cross-Section

The analysis for an elliptical fuselage shape is performed exactly as that for a circular cross-section shown above, except that the fuselage weight is multiplied by a factor $K_{ellipse}$ to represent the increased structural inefficiency of non-circular pressurised cross-sections. This factor has been tailored to give some agreement with the limited data available. Again, this method will not provide complete numerical accuracy, but adds a degree of qualitative description that would otherwise not be present.

If $\left(\frac{b_{ellipse}}{a_{ellipse}}\right) \geq 1$ then

$$K_{ellipse} = \left(\frac{b_{ellipse}}{a_{ellipse}}\right)^{0.4} \tag{5.31}$$

else

$$K_{ellipse} = \frac{1}{\left(\frac{b_{ellipse}}{a_{ellipse}}\right)^{0.4}} \tag{5.32}$$

9 .1 .4 .3 Double Deck Fuselage

The analysis of a circular or elliptical double deck fuselage is carried out using the methods above, but with two additional weight contributions. These contributions represent the addition of another cabin floor, and the increased number of windows along the fuselage. Although a detailed analysis of the lengths of the decks could be implemented, it was felt that for this purpose a simple approximation would suffice, as the contribution of these parts to the overall fuselage weight is relatively insignificant. Therefore the original floor and window estimations are modified by:-

$$W_{floor} = 1.8W_{floor} \tag{5.33}$$

$$W_{window} = 1.8 W_{window} \tag{5.34}$$

9 .1 .4 .4 747-Type Fuselage

As discussed in Chapter 8, for the purposes of weight estimation this type of fuselage is split into two component fuselages. The first being the main fuselage without the upper deck 'bubble', and the second being an extrapolation of the upper 'bubble' into a full fuselage cross-section of the same length as the upper deck. These fuselages are then treated independently, and their weights calculated using the methods above. The contributions are then added to give the total fuselage weight. This technique gives good agreement with the actual weights of the 747-range. The following additional assumptions have been made, where the main fuselage is denoted by the subscript '*1*', and the upper '*bubble*' is denoted by the subscript '*2*'.

$$N_{exit1} = 4 + \text{int}\left(\frac{N_{pass} - 178}{110}\right) \times 2 \tag{5.35}$$

$$N_{exit2} = 2 \tag{5.36}$$

The length of windows on each fuselage is given by:-

$$l_{windows1} = l_{fuse} - 0.4 l_{nose} - 0.6 l_{tail} \tag{5.37}$$

$$l_{windows2} = \phi_{fuse} l_{fuse} - 0.3 l_{nose} \tag{5.38}$$

9 .1 .4 .5 Double Bubble Fuselage

Similarly, the weight of a double bubble fuselage is calculated as a function of the weights of its two component circular fuselages. The weights of the component fuselages are calculated using the methods described in 9.1.4.1. The total weight has not been assumed to be the direct sum of the two fuselages, as this would neglect the effect of the distance between the fuselages (ϕ_{db} from figure 8.9). The two limiting cases being if ϕ_{db}=0, the fuselage can be treated as one circular fuselage, and if ϕ_{db}=1, the fuselage would be treated as two distinct circular fuselages. Therefore the factor K_{join} by which the circular fuselage weight must be multiplied is given by:-

$$K_{join} = 1 + \phi_{db} \tag{5.39}$$

It would seem prudent to increase this factor further to take into account the weight of the fairings, and to allow for the structural complications involved in the construction of a double bubble fuselage. A reasonable estimate would be:-

$$W_{fuse} = 1.05 K_{join} W_{fuse_{circular}} \tag{5.40}$$

9 .1 .5 UNDERCARRIAGE WEIGHT

The undercarriage weight is predicted using the method presented in chapter 8 of Torenbeek[93]. The equation used for both the main and the nose undercarriage is shown below, with the coefficients being taken directly from Torenbeek[93] without modification.

$$W_{uc} = K_{uc}\left((A+B)W_0{}^{0.75} + CW_0 + DW_0{}^{1.5}\right) \tag{5.41}$$

The effect of advanced materials is then taken into account:-

$$W_{uc} = W_{uc}\left(1 - \frac{\Delta W_{uc}}{W_{uc}}\right) \tag{5.42}$$

9 .1 .6 SURFACE CONTROL WEIGHT

The method for estimating the surface controls is again based on the method presented in chapter 8 of Torenbeek[93]. However, another factor ($K_{tune\ sc}$) has been added to make the results more closely match the data values and data trends of existing transport aircraft taken from Roskam[82].

$$W_{sc} = 0.64 \times 1.15 \times 1.2 \times W_0{}^{2/3} \times K_{tune\,sc} \tag{5.43}$$

where from data fitting analysis:-

$$K_{tune\,sc} = 1.15\left(1 - \left(\frac{abs(300000 - W_0 lb)}{3000000}\right)^{0.55}\right) \tag{5.44}$$

Then accounting for advanced materials

$$W_{sc} = W_{sc}\left(1 - \frac{\Delta W_{sc}}{W_{sc}}\right) \tag{5.45}$$

9 .1 .7 NACELLE WEIGHT

The nacelle weight is estimated directly using the method of Torenbeek[93], with the appropriate adjustment for the use of advanced materials.

$$W_{nac} = 0.065 \frac{T_0 lbf}{lb} \tag{5.46}$$

$$W_{nac} = W_{nac}\left(1 - \frac{\Delta W_{nac}}{W_{nac}}\right) \tag{5.47}$$

9 .1 .8 Propulsion Group Weight

An unmodified Torenbeek[93] method is used to scale the dry weight of the engines to give the total weight of the propulsion system.

$$W_{pg} = 1.15 \times 1.18 \times N_e \times W_{eng} \tag{5.48}$$

9 .1 .9 Airframe Services & Equipment Weight

The airframe services and equipment (ASE) weight is made up of a number of components. The methods used to estimate the weights of these components are described below. Some of the methods have been modified from the text book methods and include 'tuning' factors, which fine tune the results to give values that are more closely matched to real data. These tuning factors have been based on data for existing transport aircraft taken from Roskam[82] and Torenbeek[93], and are intended to counteract any error produced by the original equation.

9 .1 .9 .1 Auxiliary Power Unit (APU) Weight

The weight of the auxiliary power unit has been estimated using the equation below, derived from data in Roskam[82].

$$W_{apu} = 2.5 \times 11.7 K_{tune\,apu}\left(0.6 N_{pass}\right)^{\frac{3}{5}} \tag{5.49}$$

where

$$K_{tune\,apu} = \left(\frac{130000}{W_0 lb}\right)^{0.3} \tag{5.50}$$

9 .1 .9 .2 Instrumentation, Avionics, & Electronics Weight

This is estimated using the method of Roskam[82] multiplied by a relevant tuning factor to give improved accuracy.

$$W_{iae} = K_{tune\,iae}\left(2\left(15 + 0.032\frac{W_0}{1000}\right) + N_e\left(5 + 0.006\frac{W_0}{1000}\right) + 0.15\frac{W_0}{1000} + 0.012\frac{W_0}{1000}\right) \tag{5.51}$$

$$K_{tune\,iae} = 0.5\left(\frac{5000}{W_0}\right)^{0.4} \tag{5.52}$$

9 .1 .9 .3 Hydraulics & Pneumatics Weight

Slight modification of an equation from Torenbeek[93] gives the weight of the hydraulics and pneumatics to be as shown below in equation 5.53. The modification was introduced to give increased agreement with actual data for medium/large transports.

$$W_{hyd} = 0.012 W_{des} + 181 \tag{5.53}$$

Adjustment for advanced technologies gives:-

$$W_{hyd} = W_{hyd}\left(1 - \frac{\Delta W_{hyd}}{W_{hyd}}\right) \tag{5.54}$$

9 .1 .9 .4 Electrical System Weight

The method used to estimate the weight of the electrical system is again based upon a method from Torenbeek[93]. The modifications have been made to give better agreement with existing data and to make the method more applicable to medium/large transport aircraft.

$$W_{el} = K_{tune\,el}\left(0.019 W_0 + 181\right) \tag{5.55}$$

If $W_0 > 300000$lb then

$$K_{tune\,el} = \left(\frac{300000}{W_0 lb}\right)^{0.7} \tag{5.56}$$

else

$$K_{tune\,el} = 1 \tag{5.57}$$

Adjustment for advanced technologies gives:-

$$W_{el} = W_{el}\left(1 - \frac{\Delta W_{el}}{W_{el}}\right) \tag{5.58}$$

9 .1 .9 .5 Furnishings Weight

The method for estimating the weight of the furnishings is based upon the method presented in Roskam[93]. The method has been extended to take more account of the range of the aircraft. Rather than using discrete values for 'short' and 'long' range, a parameter is calculated that will more accurately reflect the range of the aircraft. A tuning factor is also introduced to further increase the accuracy of this weight estimation. The furnishings weight is given by:-

$$W_{furn} = 1.3 K_{tune\,furn} \begin{pmatrix} 55N_{fdc} + 32N_{pass} + 15N_{cc} + K_{lav} N_{pass}^{1.33} + K_{buf} N_{pass}^{1.12} \\ +109\left(N_{pass}\frac{(1+P_c)}{100}\right)^{0.505} + 0.771\frac{W_0}{1000} \end{pmatrix} \quad (5.59)$$

The evaluation of the unknown parameters in this equation is described below.

The cabin pressure (P_c) is evaluated using the standard assumption that during cruise conditions:-

$$P_c = 0.8 P_0 \quad (5.60)$$

The three parameters that represent the toilet weight factor (K_{lav}), food equipment weight factor (K_{buf}), and the number of flight deck crew (N_{fdc}) are range dependant so the following assumptions have been made:-

$R_{short} = 2000$ (nm)

$R_{long} = 6500$ (nm)

If $R_{crl} < R_{short}$ then

$$N_{fdc} = 2 \quad (5.61)$$

$$K_{lav} = 0.31 \quad (5.62)$$

$$K_{buf} = 1.02 \quad (5.63)$$

else

$$N_{fdc} = 3 \quad (5.64)$$

$$K_{lav} = 0.31 + (1.11 - 0.31)\frac{R_{crl} - R_{short}}{R_{long} - R_{short}} \quad (5.65)$$

$$K_{buf} = 1.02 + (5.68 - 1.02)\frac{R_{crl} - R_{short}}{R_{long} - R_{short}} \quad (5.66)$$

An approximation of the number of cabin crew has been made from experience and is given by equation 5.67.

$$N_{cc} = \text{int}\left(\frac{N_{pass}}{25}\right) + 1 \quad (5.67)$$

The value of the tuning factor, included to give better agreement with existing data, is given by the equations below.

If $N_{pass} < 250$ then

$$K_{tune\ furn} = 1 \tag{5.68}$$

If $N_{pass} > 250$ and $N_{pass} < 450$ then

$$K_{tune\ furn} = \left(\frac{N_{pass}}{250}\right)^{0.45} \tag{5.69}$$

If $N_{pass} > 450$ then

$$K_{tune\ furn} = 1.3\left(\frac{N_{pass}}{450}\right)^{0.05} \tag{5.70}$$

Adjustment for advanced technologies gives:-

$$W_{furn} = W_{furn}\left(1 - \frac{\Delta W_{furn}}{W_{furn}}\right) \tag{5.71}$$

9 .1 .9 .6 Air conditioning Weight

The air-conditioning weight estimation is based upon the method of Torenbeek[93] shown below in equation 5.72. A simple approximation of the length of cabin for which air conditioning is appropriate is given by 5.73.

$$W_{ac} = 14 l_{ac}^{1.28} \tag{5.72}$$

where

$$l_{ac} \approx 0.75 l_{fuse} \tag{5.73}$$

and adjustment for advanced technologies gives:-

$$W_{ac} = W_{ac}\left(1 - \frac{\Delta W_{ac}}{W_{ac}}\right) \tag{5.74}$$

9 .1 .9 .7 Oxygen System Weight

Using a method taken from Roskam[82], the weight of the oxygen system is given by equation 5.75 below.

$$W_{ox} = \frac{7\left(N_{crew} + N_{pass}\right)^{0.702}}{lb} \tag{5.75}$$

9 .1 .10 Operational Items Weight

The weight of the operational items of the aircraft have been calculated using the following methods.

The weight of the crew, baggage, and flight equipment has been estimated using the values taken from Tornebeek[93].

$$W_{crew} = 85N_{crew} + 150N_{cc} \tag{5.76}$$

The weights of the passenger consumable supplies, and the toilet supplies will be dependent on range. Therefore using the weight values of meals, snacks, and toilet supplies for various ranges from Torenbeek[93], the following assumptions have been made. This approach should give more realistic values, rather than relying on a discrete 'short range' or 'long range' approach.

If $R_{crl} + 370 < 2500$ km then

$$W_{meal\,standard} = 6.35\text{kg}$$

$$W_{meal_{1st.class}} = (6.35 + 2.27)\text{kg}$$

$$W_{toilet.supply} = 1.36\text{kg}$$

If $R_{crl} + 370 > 2500$ km and $R_{crl} + 370 < 4000$ km then

$$W_{meal\,standard} = 8.62\text{kg}$$

$$W_{meal_{1st.class}} = (8.62 + 2.27)\text{kg}$$

$$W_{toilet.supply} = 2.95\text{kg}$$

If $R_{crl} + 370 > 4000$ nm then

$$W_{meal\,standard} = 8.62\left(\frac{R_{cr1} + 370}{4000}\right)\text{kg}$$

$$W_{meal_{1st.class}} = (8.62 + 2.27)\left(\frac{R_{cr1} + 370}{4000}\right)\text{kg}$$

$$W_{toilet.supply} = 2.95\left(\frac{R_{cr1} + 370}{4000}\right)\text{kg}$$

This means that weight of the passenger supplies, and toilet supplies can now be calculated:-

$$W_{pass_{supply}} = \left(N_{pass} - N_{1st.class}\right)W_{meal\,standard} + N_{1st.class}W_{meal_{1st.class}} \tag{5.77}$$

$$W_{wc\,supply} = W_{toilet\,supply}N_{pass} \tag{5.78}$$

The weight of the safety equipment is given below (from Torenbeek[93]).

$$W_{safety} = 3.4N_{pass} \tag{5.79}$$

The weight of residual fuel is estimated from Torenbeek[93] using:-

$$W_{residual} = 0.151\left(\frac{W_{fuel}}{0.78}\right)^{\frac{2}{3}} \tag{5.80}$$

From Torenbeek[93] the weight of oil is given by:-

$$W_{oil} = 0.045W_{fuel} \tag{5.81}$$

The components are then summed to find W_{ope}, and then this is adjusted for the effect of advanced technologies.

$$W_{ope} = W_{ope}\left(1 - \frac{\Delta W_{ope}}{W_{ope}}\right) \tag{5.82}$$

9 .2 Centres Of Gravity

The methods used to estimate the centres of gravity of the major components have been based on the data presented in Torenbeek[93], and are described below,

Fuselage

The distance of the centre of gravity of the fuselage structure from the fuselage nose is given by equation 5.83 below.

$$X_{cg\ fuse} = 0.45l_{fuse} \tag{5.83}$$

Wing

The centre of gravity of the wing is assumed to be at 35% semi-span from the aircraft centreline, and at 70% of the distance between the front spar and the rear spar, measured from the front spar. This information allows the spanwise location $Y_{cg_{wing}}$, and the streamwise location (measured from the apex of the wing) $X'_{cg_{wing}}$ to be easily calculated from the wing planform geometry data.

Nacelles & Engines

The location of the engines must first be calculated. The expressions that have been derived to describe the longitudinal and lateral locations of the engines have been based on data for the engine locations of current civil aircraft.

It is assumed that depending whether the aircraft has 2 or 4 engines, the engines are located at a certain spanwise distance that is a function of the exposed wing span. The exposed wing span can be calculated from geometric considerations. As the height of the wing at the wing/fuselage intersection is known (it is assumed to be directly beneath the cabin floor), and the fuselage cross-section is known, then the spanwise location of the wing/fuselage intersection can be calculated. The spanwise location of the lower wing/fuselage intersection is denoted by $Y_{wing/fuse_l}$.

For a twin-engined aircraft the spanwise engine location is given by:-

$$Y_e = Y_{wing/fuse_l} + \frac{bref/2 - Y_{wing/fuse_l}}{2.5} \tag{5.84}$$

For a four-engined aircraft the spanwise engine locations are given by:-

$$Y_{ei} = \frac{bref/2 - Y_{wing/fuse_l}}{4} \tag{5.85}$$

$$Y_{eo} = \frac{2\left(bref/2 - Y_{wing/fuse_l}\right)}{3} \tag{5.86}$$

The longitudinal locations of the engine front faces (measured from the apex of the wing) have been assumed to be given by:-

$$X'_e = Y_e \tan\Lambda_{le} - l_{fc} - 0.8 \tag{5.87}$$

This means that making the assumption that the centre of gravity of the engine is located at 35% of the length of the fan cowling, and that the centre of gravity of the nacelle is located at 40% of the total nacelle length, the following expressions can be used.

$$X'_{cg_{pg}} = X'_e + 0.35 l_{fc} \tag{5.88}$$

and

$$X'_{cg_{nac}} = X'_e + 0.4 l_{na} \tag{5.89}$$

In the case of a four-engined configuration, the contributions of the inboard and outboard engines are averaged, to give the total engine and nacelle centres of gravity.

Airframe Service & Equipment

The centre of gravity of the airframe services and equipment group (measured from the fuselage nose) is assumed to be given by:-

$$X_{cg_{ase}} = 0.43 l_{fuse} \tag{5.90}$$

Surface Controls

The centre of gravity of the surface controls is estimated using the expression below, which assumes that the centre of gravity of the surface controls will be related to the longitudinal position of the mean aerodynamic chord of the equivalent wing.

$$X'_{cg_{sc}} = y_{mac} \tan \Lambda_{le} + c_{mac\,e} \tag{5.91}$$

9 .3 Tail Sizing

The size of both the horizontal tail and vertical tail are estimated using an iterative tail volume coefficient approach. Firstly, the tail volume coefficients (C_{ht} and C_{vt}) are estimated using empirical correlations from existing aircraft designs.

9 .3 .1 Tail Volume Coefficients

The analysis of the data shown below in figures 9.2 and 9.3 gave the equations 5.92 and 5.93. The tuning factors have been added to these equations to allow greater flexibility, with the values of these factors being set by the user (the default value is 1.0),

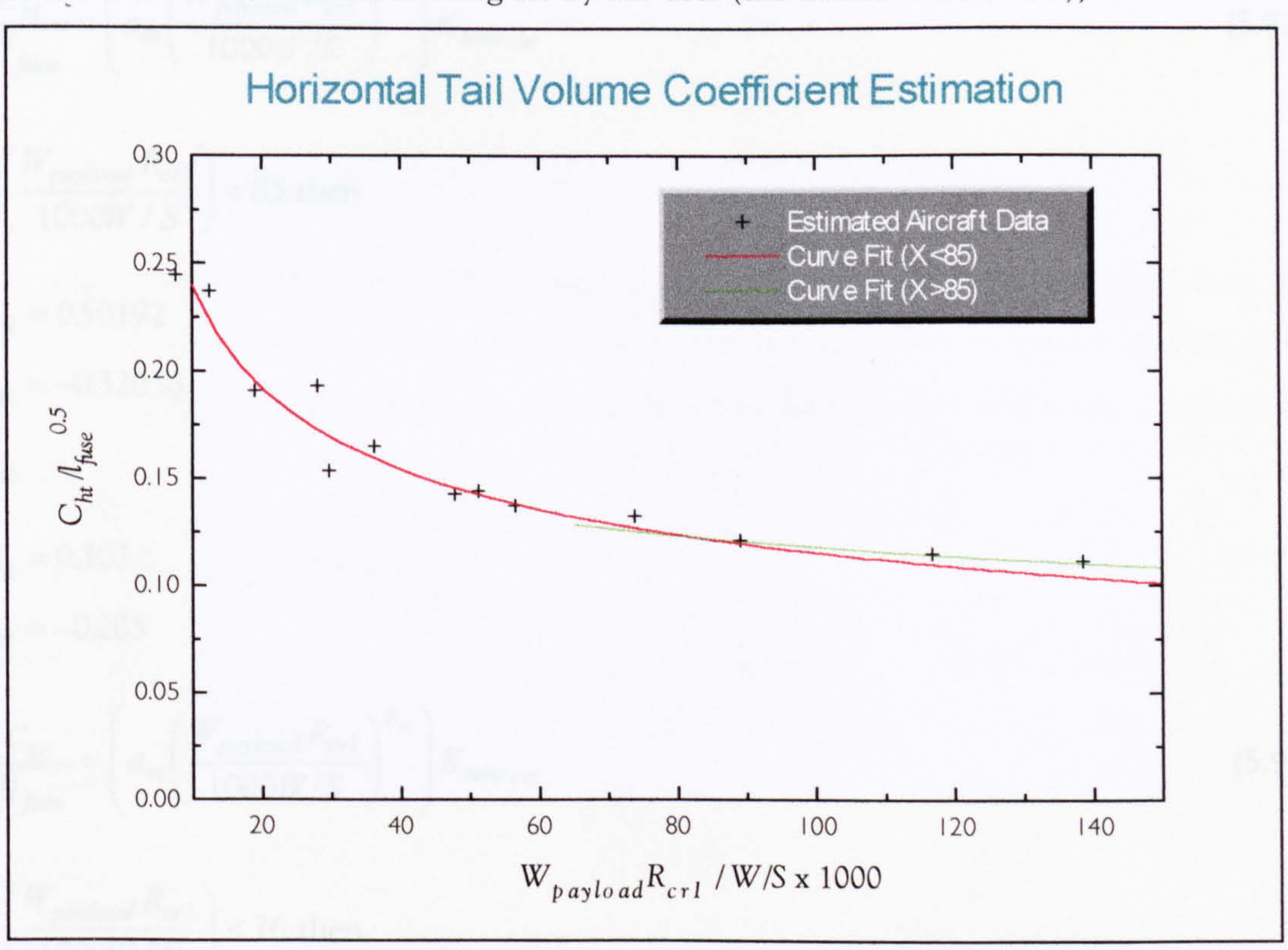


Figure 9.2 - Estimation of horizontal tail volume coefficient

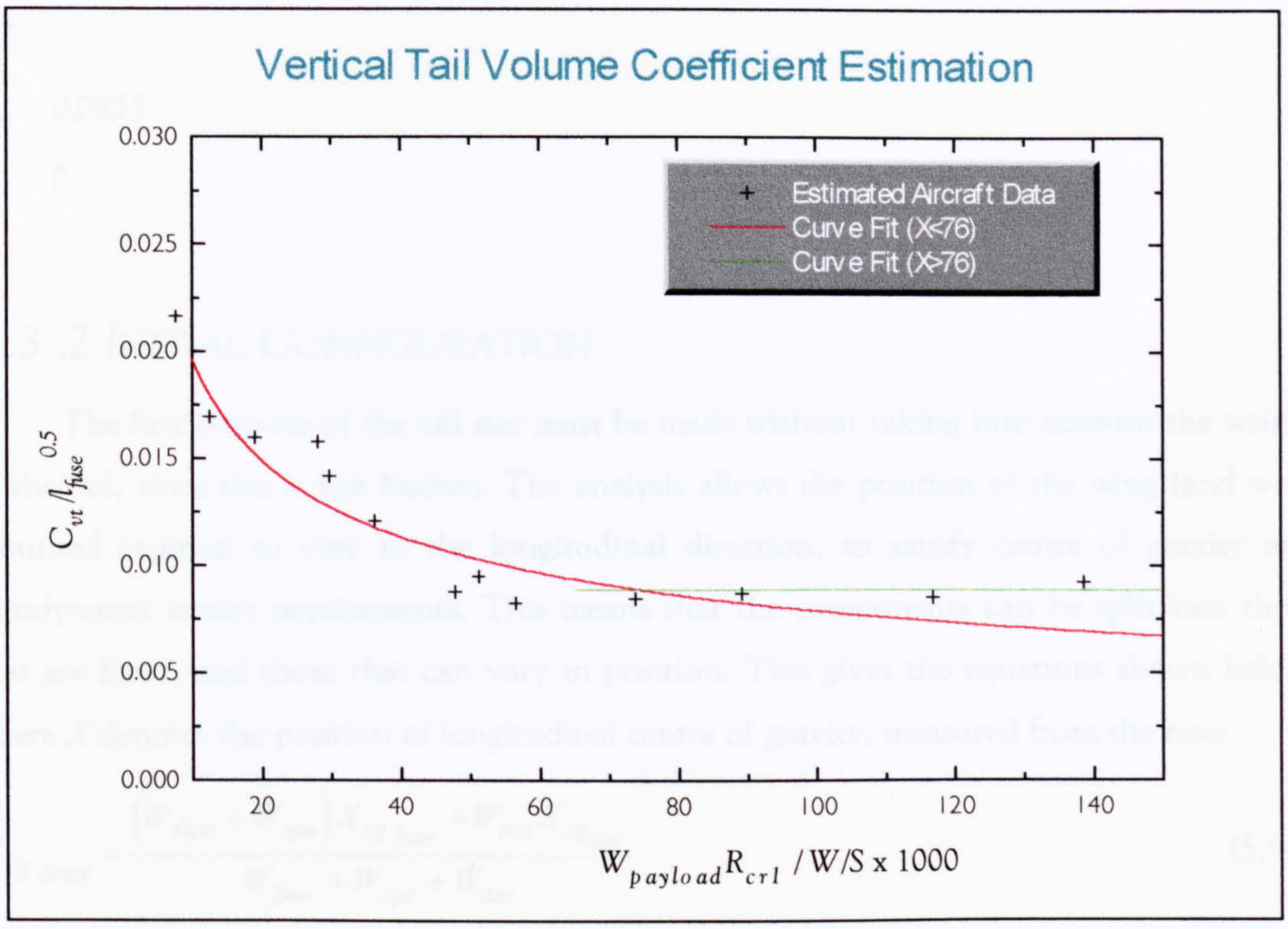


Figure 9.3 - Estimation of vertical tail volume coefficient

$$\frac{C_{ht}}{\sqrt{l_{fuse}}} = \left(a_{ht} \left(\frac{W_{payload} R_{cr1}}{1000 W/S} \right)^{b_{ht}} \right) K_{tune\,cht} \tag{5.92}$$

$$\text{if } \left(\frac{W_{payload} R_{cr1}}{1000 W/S} \right) < 85 \text{ then}$$

$$a_{ht} = 0.50192$$

$$b_{ht} = -0.32036$$

else

$$a_{ht} = 0.302$$

$$b_{ht} = -0.205$$

$$\frac{C_{vt}}{\sqrt{l_{fuse}}} = \left(a_{vt} \left(\frac{W_{payload} R_{cr1}}{1000 W/S} \right)^{b_{vt}} \right) K_{tune\,cvt} \tag{5.93}$$

$$\text{if } \left(\frac{W_{payload} R_{cr1}}{1000 W/S} \right) < 76 \text{ then}$$

$$a_{vt} = 0.04888$$

$$b_{vt} = -0.39643$$

else

$a_{vt} = 0.0855$

$b_{vt} = 0$

9 .3 .2 INITIAL CONFIGURATION

The first estimate of the tail size must be made without taking into account the weight of the tail, since this is not known. The analysis allows the position of the wing (and wing mounted engines) to vary in the longitudinal direction, to satisfy centre of gravity and aerodynamic centre requirements. This means that the components can be split into those that are fixed, and those that can vary in position. This gives the equations shown below, where X denotes the position of longitudinal centre of gravity, measured from the nose.

$$X_{cg\,fixed} = \frac{\left(W_{fuse} + W_{ope}\right)X_{cg\,fuse} + W_{ase}X_{cg\,ase}}{W_{fuse} + W_{ope} + W_{ase}} \tag{5.94}$$

$$W_{fixed} = W_{fuse} + W_{ope} + W_{ase} \tag{5.95}$$

$$X_{cg\,variable} = \frac{W_{wing}X_{cg\,wing} + W_{pg}X_{cg\,pg} + W_{nac}X_{cg\,nac} + W_{sc}X_{cg\,sc}}{W_{wing} + W_{pg} + W_{nac} + W_{sc}} \tag{5.96}$$

$$W_{variable} = W_{wing} + W_{pg} + W_{nac} + W_{sc} \tag{5.97}$$

It is important to note that by definition, in order for the user to have control over the value of the static margin, the distance between the aircraft centre of gravity and the wing aerodynamic centre is a fixed percentage of the mean aerodynamic chord ($\phi_{ac\,location}$) set by the user.

$$X_{ac\,wing} = X_{cg_{aircraft}} - X'_{ac.location} \tag{5.98}$$

where

$$X'_{ac\,location} = \frac{\phi_{ac\,location}c_{mac\,e}}{100} \tag{5.99}$$

and since

$$X_{cg_{wing}} = X_{ac\,wing} + X'_{cg_{wing}} - X'_{ac\,wing} \tag{5.100}$$

where X' indicates a distance measured from the wing apex, the other variable centres of gravity may be calculated by using this relationship.

$$X_{cg_{pg}} = X'_{cg_{pg}} + X_{cg_{wing}} - X'_{cg_{wing}} \tag{5.101}$$

$$X_{cg_{nac}} = X'_{cg_{nac}} + X_{cg_{wing}} - X'_{cg_{wing}} \tag{5.102}$$

$$X_{cg_{sc}} = X'_{cg_{sc}} + X_{cg_{sc}} - X'_{cg_{sc}} \tag{5.103}$$

Since an initial estimate of the aircraft centre of gravity can be calculated, the only unknown quantity is the location of the wing centre of gravity ($X_{cg\ wing}$). This can be found by iteration, to satisfy all the equations 5.94 to 5.103. This gives the baseline configuration from which an initial tail size estimate can be made.

9 .3 .3 Initial Tail Estimate

The surface areas of the tails can be estimated using their relationships with the tail volume coefficients from Raymer[90].

$$S_{ref_{ht}} = \frac{C_{ht} c_{mean} S_{ref}}{l_{ht}} \tag{5.104}$$

where l_{ht} is the horizontal tail arm (the distance between the wing and the horizontal tail aerodynamic centres).

$$S_{ref_{vt}} = \frac{C_{vt} b_{ref} S_{ref}}{l_{vt}} \tag{5.105}$$

l_{vt} is the vertical tail arm (the distance between the wing and the vertical tail aerodynamic centres).

The tail arm distances are calculated using the fact that it has arbitrarily been assumed that both the tails are longitudinally located such that their aft-most points are situated at the fuselage end.

From these initial estimates of the tail size it is possible to calculate detailed properties of the tail, which can be used to refine the tail size estimates. Since the aspect ratio, sweep, and taper ratio of the tail surfaces are known (as set by the user), every geometric property such as the chords and sweep at any particular point can easily be calculated.

9 .3 .4 Tail Weight Estimation

The weights of the tails are calculated using the equations of Roskam[82], with additional tuning factors to give better agreement with aircraft data.

$$W_{ht} = K_{tunewtail} \times 1.1 S_{ref\,ht}\left(\frac{3.81 {S_{ref\,ht}}^{0.2} V_{des}}{\sqrt{1000\cos\Lambda_{0.5c\,ht}}} - 0.287\right) \tag{5.106}$$

$$W_{vt} = K_{tunewtail} S_{ref\,vt}\left(\frac{3.81 {S_{ref\,vt}}^{0.2} V_{des}}{\sqrt{1000\cos\Lambda_{0.5c\,vt}}} - 0.287\right) \tag{5.107}$$

$$K_{tunewtail} = 0.7\left(\frac{370000}{W_0 lb}\right)^{0.15} \tag{5.108}$$

These weight estimates then need to be adjusted to take into account the effect of any advanced technologies. The weight reduction due to advanced materials is given by:-

$$W_{ht} = W_{ht}\left(1 - \frac{\Delta W_{ht}}{W_{ht}}\right) \tag{5.109}$$

$$W_{vt} = W_{vt}\left(1 - \frac{\Delta W_{vt}}{W_{vt}}\right) \tag{5.110}$$

For laminar flow control, the area that is assumed to be composed of laminar flow suction surface (S_{lfc}) for both upper and lower surface application is equal to 0.7 times the tail reference area. This area is assumed to be half this amount for the application of upper surface suction only.

For hybrid laminar flow control, this area (S_{hlfc}) is assumed to be 0.2 times the tail reference area when H.L.F.C. is applied to both the upper and lower surface, and half this amount for upper surface only. Using an equation of the form of equation 5.17:-

$$W_{(h\,or\,v)t} = W_{(h\,or\,v)t} + 6.786 S_{(h)lfc} K_{tune(h)lfc.wt.(h\,\text{or}\,\text{v})\text{t}} \tag{5.111}$$

9 .3 .5 TAIL CENTRES OF GRAVITY

The centres of gravity of the tails must now be calculated. For the horizontal tail and vertical tails, the following assumptions have been made about the location of their centres of gravity (from Torenbeek[93], chapter 8).

$$c_{cg\,ht} = c_{root\,ht} + 0.38\left(c_{tip\,ht} - c_{root\,ht}\right) \tag{5.112}$$

the distance of the centre of gravity along this chord is given by:-

$$X''_{cg\,ht} = 0.42 c_{cg\,ht} \tag{5.113}$$

For the vertical tail:-

$$c_{cg_{vt}} = c_{root_{vt}} + 0.55\left(c_{tip_{vt}} - c_{root_{vt}}\right) \tag{5.114}$$

the distance of the centre of gravity along this chord is given by:-

$$X''_{cg_{vt}} = 0.42 c_{cg_{vt}} \tag{5.115}$$

Therefore, as the geometry of the tails is known, and their location have been assumed such that their aft-most points are situated at the fuselage end, the exact locations of their centres of gravity can be calculated.

The mean aerodynamic chords and the aerodynamic centres of the tails are calculated using the same methods used for the wing (see chapter 7).

9 .3 .6 *Tail Iteration*

The addition of the tail causes a change in the aircraft centre of gravity, which in turn changes the desired location of the wing, and alters the tail arms of both the tail surfaces. This means that a complex iteration process must be undertaken to satisfy all of the above equations, and to produce a convergent solution.

The code first iterates for the location of the wing, and once this solution is found, the tail properties are calculated. The process is repeated until the tail reference areas are found to be convergent.

9 .4 Undercarriage Sizing

The number of main undercarriage bogeys, the number of wheels on each bogey, and the size of these wheels is calculated. The number of main bogeys is initially set to two, and the number of tyres on each bogey is also set to two. The number of tyres and the number of bogeys are gradually increased until a configuration is found that is capable of supporting the required aircraft loads. It is assumed throughout that the main undercarriage carries 90% of the aircraft weight. Using data from Raymer[90], the configurations are evaluated using the following methods.

The weight on each wheel is given by:-

$$W_{wheel} = \frac{0.9 W_0}{N_{bogey} N_{wheel}} \tag{5.116}$$

This infers a tyre diameter given by:-

$$D_{main} = 1.07\left(1.63 W_{wheel}{}^{0.315}\right) \tag{5.117}$$

The number of bogeys and tyres is increased until D_{main} can be satisfied by a standard tyre size. A relevant set of tyre data values for a range of tyre sizes (from Raymer[90]) is included in the program. So once the tyre size has been selected its detailed properties are known. This allows the footprint area and the tyre pressure to be easily calculated. It has been assumed from the study of aircraft configurations, and for the sake of simplicity, that the nose undercarriage consists of one bogey containing two wheels of the same size as the main undercarriage.

The stroke of the undercarriage is calculated using:-

$$S_{uc} = \frac{V_{vertical}{}^2}{2g\eta N_{gear}} - \frac{\eta_t}{\eta} S_T \tag{5.118}$$

where

$V_{vertical} = 10 \text{ ft/s}$

$\eta = 0.8$

$\eta_t = 0.47$

$N_{gear} = 2.5$

$S_T = 4.75 \text{ in}$

An estimation of the oleo diameter can then be calculated using the equation below, from Torenbeek[93].

$$D_{oleo} = 1.3 + 0.11\sqrt{\frac{0.9 W_0}{N_{bogey}}} \quad \text{(cm)} \tag{5.119}$$

The layout of the undercarriage is then calculated in accordance with guidelines laid out in Torenbeek[93] and Raymer[90].

9 .5 Undercarriage Drag

A simple estimation of the drag increment due to the deployment of the undercarriage is made using the landing gear component drags presented in chapter 12 of Raymer[90]. This gives:-

$$\left(\frac{D}{q}\right)_{tyre_{nose}} = (0.15 + 0.15) b_{tyre_{nose}} d_{outer\,nose} \tag{5.120}$$

$$\left(\frac{D}{q}\right)_{tyre_{main}} = (0.15 + 0.15) N_{bogey} b_{tyre_{main}} d_{outer\,main} \tag{5.121}$$

$$\left(\frac{D}{q}\right)_{strut\,nose} = (0.05) 3 S_{uc} D_{oleo} \tag{5.122}$$

$$\left(\frac{D}{q}\right)_{strut\,main} = (0.05) 3 S_{uc} D_{oleo} N_{bogey} \tag{5.123}$$

These components are then summed to find the actual drag.

10 .Drag Prediction Methods

The function of this module is to accurately predict the magnitude of all of the main contributions to the aircraft drag. The parasite drag is estimated using a component build-up method, and the drag due to lift is added to this. Other drag components, such as drag due to the deployment of flaps and undercarriage are also included. The effect of any advanced technologies on the aircraft are also estimated. The first step in the drag estimation process is to calculate the wetted areas of the major components.

10 .1 Wetted Area Calculation

The fuselage wetted area is calculated in the Geometry Module, the wetted area of the wing, tails, pylons, and nacelles, are calculated using the techniques described below.

10 .1 .1 Wing Wetted Area

The wetted area of the wing is computed using the results of Torenbeek[93] chapter 11. The equation used is shown below.

$$S_{wet\,wing} = 2S_{exposed}\left(1+0.25\left(\frac{t}{c}\right)_{root}\frac{1+\tau\lambda_e}{\lambda_e}\right) \tag{6.1}$$

where

$$\tau = \frac{\left(t/c\right)_{tip}}{\left(t/c\right)_{root}} \tag{6.2}$$

and $S_{exposed}$ is found from equation 5.14

10 .1 .2 Tail Wetted Areas

Both the horizontal and vertical tail areas are calculated using the same equation (6.1) as for the wing wetted area. The ratio of thickness to chord ratios (τ) is assumed to be equal to 1.

10 .1 .3 Pylon Wetted Area

The location of the engines is known from chapter 9. This means that the wing chord at these locations can be calculated:-

$$c_{pylon} = c_{root_e} + \left(c_{tip_e} - c_{root_e}\right)\frac{2y_{pylon}}{b_{ref}} \tag{6.3}$$

where $y_{pylon} = y_{e_i}$ or y_{e_o}

From analysis of current aircraft pylons, the pylon is assumed to approximate to a parallelogram with the length given by:-

$$l_{pylon=} 0.64 c_{pylon} \tag{6.4}$$

Assuming the height of the pylon to be approximately half of the fan cowling diameter, and that the pylon has negligible thickness, the wetted area is then calculated using:-

$$S_{wet\,pylon} = 2\frac{D_{fc}}{2} l_{pylon} \tag{6.5}$$

10 .1 .4 Nacelle Wetted Area

The wetted area of the nacelle is calculated using the methods in Appendix B of Torenbeek[93] for the calculation of fan cowling, gas generator, and plug wetted areas.

$$S_{wet\,fc} = l_{fc} D_{fc}\left(2 + 0.35\beta_{fc} + 0.8\beta_{fc} + 1.15\left(1-\beta_{fc}\right)\frac{D_{fc_o}}{D_{fc}}\right) \tag{6.6}$$

$$S_{wet\,ge} = \pi l_{ge} D_{ge_i}\left(1 - \frac{1}{3}\left(1 - \frac{D_{ge_o}}{D_{ge_i}}\right)\left(1 - 0.18\left(\frac{D_{ge_i}}{l_{ge}}\right)^{\frac{5}{3}}\right)\right) \tag{6.7}$$

$$S_{wet\,pl} = 0.7\pi l_{pl} D_{pl} \tag{6.8}$$

10 .2 Parasite Drag Components

These drag contributions are estimated using a standard component build up method (equation 6.9).

$$C_{D0_{component}} = \frac{C_{f_{component}} FF_{component} Q_{component} S_{wet\,component}}{S_{ref}} \tag{6.9}$$

The calculation of the fully laminar and fully turbulent skin friction coefficients is described in section 6.4.2.3, where the Reynolds number length parameter is the representative length of the particular component. For all components, transition from laminar flow to turbulent

flow is assumed to take place, in the absence of advanced technology, at a Reynolds number of 500,000. This gives rise to the transition location parameter $X_{transition}$, for each component:-

$$X_{transition} = \frac{500000}{Re_{component}} \tag{6.10}$$

The actual skin friction coefficient is then assumed to be given by equation 6.11 (the transition parameter cannot be lower than zero or greater than 1).

$$C_{f\,component} = X_{transition} C_{f\,laminar\,component} + (1 - X_{transition}) C_{f\,turbulent\,component} \tag{6.11}$$

The drag of each component is in fact calculated over a wide range of altitudes and Mach numbers. The total component drag values at these altitudes and Mach numbers are then stored in an array, so that the component drag may be evaluated at any particular condition. Also, the component drag value with and without any effect of laminar flow technologies are stored separately, so that they can be evaluated independently. The equations used for each aircraft component are described briefly below.

10 .2 .1 Wing Component Drag

The wing form factor is evaluated using the equation below. The airfoil maximum thickness parameter $(x/c)_m$ is known for both the root and tip airfoils from the airfoil data. The average of the root and tip value is taken.

$$FF_{wing} = \left(1 + \frac{0.6}{(x/c)_m}\frac{t}{c} + 100\left(\frac{t}{c}\right)^4\right)\left(1.34\,Ma^{0.18}(\cos\Lambda_m)^{0.28}\right) \tag{6.12}$$

The sweep at the maximum thickness (Λ_m) is easily calculated. The average thickness to chord ratio is given below, bearing in mind that the thickness to chord ratio distribution is assumed to vary from the root value to the tip value along the cranked portion, then to be constant along the remainder.

$$\frac{t}{c} = \frac{1}{2}\left(\left(\frac{t}{c}\right)_{root} + \left(\frac{t}{c}\right)_{tip}\right)\phi_{crank} + \left(\frac{t}{c}\right)_{tip}(1 - \phi_{crank}) \tag{6.13}$$

The wing interference factor $Q_{wing/fuse}$ is estimated from the data presented in figure 4.1 of Roskam[82]. The data has been put into an array and can be evaluated for any value of fuselage Reynolds number and Mach Number.

The effect of any advanced technologies on the aerodynamic performance of the wing must then be calculated.

10 .2 .1 .1 Natural Laminar Flow

The amount of natural laminar flow achievable at a given Reynolds number and sweep is calculated using the graph of figure 3.10 (Blanchard[50]). This graph has been converted into a data file, and the laminar flow limit can be interpolated for any value of Reynolds number and quarter chord sweep. The laminar flow limit is evaluated at 11 spanwise stations, and an average value is taken. This value is then assumed to be the upper surface transition limit at the design Mach number (cruise Mach number).

The results of the Boeing 757 N.L.F. flight test experiment published by Runyan et al.[51], suggest that the lower surface transition point is approximately 2/3 of the upper surface transition point. The effect of off-design Mach number is then estimated, also utilising the results of Runyan et al.[51], which show that the transition location moves to the leading edge once the flight Mach number falls approximately 0.2 below the design Mach number. These assumptions are shown below.

$X_{trlimit\ upper}$ – Upper surface design transition limit from Blanchard[50]

$X_{trlimit\ lower}$ – Lower surface transition limit

$$X_{trlimit\ lower} = \frac{2}{3} X_{trlimit\ upper} \tag{6.14}$$

if $Ma \le Ma_{cr1} - 0.2$ then the off - design Mach number transition points are:-

$$X_{tr\ upper} = 0$$

$$X_{tr\ lower} = 0$$

if $Ma > Ma_{cr1}$ then

$$X_{tr\ upper} = X_{trlimit\ upper}$$

$$X_{tr\ lower} = X_{trlimit\ lower}$$

if $Ma_{cr1} - 0.2 < Ma < Ma_{cr1}$ then

$$X_{tr\ upper} = X_{trlimit\ upper}\left(1 - \frac{Ma_{cr1} - Ma}{0.2}\right)$$

$$X_{tr\ lower} = X_{trlimit\ lower}\left(1 - \frac{Ma_{cr1} - Ma}{0.2}\right)$$

The average transition limit used in the determination of the drag must then also take into account the fact that the upper wing surface is responsible for approximately 2/3 of the wing drag (Morris[98]). Therefore:-

$$X_{transition\,wing} = \frac{2X_{tr\,upper} + X_{tr\,lower}}{3} \tag{6.15}$$

The location of transition is also limited by the location of the trailing edge flaps, which will cause transition if it has not already occurred.

$$if\ X_{transition} \geq 1 - \frac{c_f}{c}\ \text{then}$$

$$X_{transition} = 1 - \frac{c_f}{c} \tag{6.16}$$

The natural laminar flow tuning parameter, set in the Component Specification Editor, is used as a multiplier to the Reynolds number, in order to give the user some control of the transition limits. If the parameter is set to below 100% then more laminar flow will occur, and a value of greater than 100% will inhibit laminar flow.

10 .2 .1 .2 Laminar Flow Control

The chordwise location of transition is calculated using the following assumptions that have been based on experimental and flight test results of laminar flow control systems.

If $h < 4000$ ft the ice/insect shield will be deployed so:-

$$X_{tr\,upper} = 0$$

If $h > 4000$ ft then:-

If $Ma < 0.6$ then

$$X_{tr\,upper} = 1 - \frac{c_f}{c}$$

else

$$X_{tr\,upper} = 1 + X_{tr\,cr1}\frac{Ma - 0.6}{Ma_{cr1} - 0.6}$$

where $X_{tr\,cr1}$ is the cruise transition location specified by the user.

It is assumed that if lower surface suction is provided then $X_{tr\,lower} = X_{tr\,upper}$. Equations 6.15 and 6.16 are then used to calculate the effective transition location, and to ensure that the transition does not appear to be beyond the wing/flap interface.

10 .2 .1 .3 Hybrid Laminar Flow Control

The assumptions made in the calculation of the transition location for a hybrid laminar flow control system are similar to those for a full chord laminar flow control system. If $h < 4000$ ft the ice/insect shield will be deployed so:-

$$X_{tr\,upper} = 0$$

else

$$X_{tr\,upper} = X_{tr\,cr1}$$

If lower surface suction is included then $X_{tr\,lower} = \frac{4}{5} X_{tr\,upper}$. Equations 6.15 and 6.16 are then applied.

10 .2 .1 .4 Riblets

The application of riblets on the wing is assumed not to be practical on the area of the wing occupied by the trailing edge flaps or the leading edge slats. Therefore an estimate of the area occupied by the riblets is given by the equation below, assuming that the leading edge devices occupy approximately one tenth of the wing chord:-

$$S_{riblets} = S_{ref}\left(1 - 0.1 - \frac{c_f}{c}\right) \tag{6.17}$$

and

$$C_{f\,wing_{riblets}} = C_{f\,wing}\left(1 - \frac{\Delta C_{D\,riblets}}{C_D}\right) \tag{6.18}$$

where $\frac{\Delta C_{D\,riblets}}{C_D}$ is specified in the Component Specification Editor (default value 0.06).

This allows an estimate of the revised skin friction coefficient to be given by:-

$$C_f{}'_{wing} = C_{f\,wing} + \left(C_{f\,wing_{riblets}} - C_{f\,wing}\right)\frac{S_{riblet}}{S_{ref}} \tag{6.19}$$

10 .2 .2 TAIL COMPONENT DRAG

The estimation of the drag contributions of both the horizontal and vertical tails are calculated using exactly the same methods and equations as for the wing contribution. The length parameter used in Reynolds number equations is assumed to be the mean

aerodynamic chord of each surface, and the wing/flap interface for each surface is assumed to occur at 70% of the chord length. The interference factors are assumed to be equal to 1.0.

10 .2 .3 Pylon Component Drag

Again, the method used to estimate the pylon drag contribution is the same as for the wing drag contribution. The form factor is given by equation 6.12, where X_m is assumed to be equal to 0.5, and the pylon thickness to chord ratio is assumed to be equal to 0.05. The interference factor for the pylon is assumed to be equal to 1.0. The effect of advanced technologies is not applicable to the drag of the pylon.

10 .2 .4 Fuselage Component Drag

The fuselage zero-lift drag is assumed to consist of two components (Roskam[82]), which represent the drag of the fuselage neglecting base drag, and the base drag itself. The first component ($C_{D0\,fuse-base}$)is calculated using the equation 6.9, where the fuselage form factor is given by the equation below, taken from Raymer[90]. The fuselage interference factor is assumed to be equal to $Q_{wing/fuse}$ (see 10.2.1).

$$FF_{fuse} = 1 + \frac{60}{f^3} + \frac{f}{400} \tag{6.20}$$

where

$$f = \frac{l_{fuse}}{\sqrt{\frac{4}{\pi} S_{frontal}}} \tag{6.21}$$

The second component, the fuselage base drag, is calculated using the method of Roskam[82].

$$C_{Db\,fuse} = \frac{0.029\left(\frac{d_{base}}{b_{fuse}}\right)^3}{\sqrt{C_{D0\,fuse-base}\frac{S_{ref}}{S_{frontal}}}}\frac{S_{frontal}}{S_{ref}} \tag{6.22}$$

where d_{base} is the fuselage height calculated from equation 4.21.

Summing the two components gives:-

$$C_{D0\,fuse} = C_{D0\,fuse-base} + C_{Db\,fuse} \tag{6.23}$$

The application of riblets is dealt with using the methods of 10.2.1.4, where $S_{riblets}$=$S_{wet\,fuse}$

10 .2 .5 NACELLE DRAG

The drag of each nacelle is split into three components, and each component is evaluated using the techniques of Roskam[82]. The three components represent the nacelle zero lift drag, plus the additional interference drags due to the proximity of the wing and of the fuselage.

$$C_{D0_{nac}} = C_{D0_{nac}}{}' + C_{D_{wing/nac}} + C_{D_{fuse/nac}} \tag{6.24}$$

The first component is evaluated using the method of equation 6.9, where the nacelle form factor is calculated using equation 6.25 (from Raymer[90]).

$$FF_{nac} = 1 + \frac{0.35}{f_{nac}} \tag{6.25}$$

where

$$f_{nac} = \frac{l_{na}}{D_{fc}} \tag{6.26}$$

The wing/nacelle interference factor ($Q_{wing/nac}$) is calculated using the same technique used for the wing/fuselage interference factor (See 10.2.1).

The second component which represents an additional interference drag between the wing and the nacelle is calculated using:-

$$C_{D_{wing/nac}} = F_{a1} C_{D0_{nac}}{}' \frac{\Delta C_{D_{nac}}}{C_{D_{nac}}} \tag{6.27}$$

where Fa_1 is assumed to be equal to 0.75 (Roskam[82]).

The value of $\frac{\Delta C_{D_{nac}}}{C_D}$ can be seen to tend toward one for the nacelle locations assumed within this design methodology (fig 4.41 of Roskam[82]). Therefore the value of this parameter is assumed to be equal to 1. The additional drag due to the nacelle/fuselage interference is given by:-

$$C_{D_{fuse/nac}} = F_{a2}\left(Q_{fuse/nac} - 0.05\right)\frac{S_{wet_{nac}}}{S_{ref}} \tag{6.28}$$

where Fa_2 is assumed to be equal to 0.5 (Roskam[82]).

The interference factor ($Q_{fue/nac}$) is evaluated using figure 4.42 of Roskam[82], and a value of 0.1 is assumed for all designs.

10 .2 .5 .1 Natural Laminar Flow

The effect of natural laminar flow design is evaluated using similar techniques to those of section 10.2.1.1, assuming that laminar flow is only feasible over the fan cowling section of the nacelle. Therefore:-

$$X_{transition} = X_{tr\,cr1}\frac{l_{fc}}{l_{na}} \tag{6.29}$$

where Xtr_{cr1} (the cruise transition location) for the nacelle is set by the user in the Component Specification Editor (the default value being 0.60).

10 .2 .5 .2 Riblets

The effect of riblets is calculated using the methods of 10.2.1.4 where the riblet application area is assumed to be equal to the nacelle wetted area.

10 .3 Compressibility Drag

The increase in drag due to transonic effects is calculated using a modified version of the method from Raymer[90]. Each calculation described below is performed at a number of Mach numbers, altitudes, and lift coefficients, which provide enough data to estimate the transonic drag rise at any flight condition. The first step in calculating the drag rise is to estimate the drag divergence Mach number of the wing

10 .3 .1 Drag Divergence Mach Number

The estimation of the value of the drag divergence is done using the following equation, where the design lift coefficient is assumed to be the mid-cruise lift coefficient.

$$M_{DD} = M_{DD\,L=0}LF_{DD} - 0.05C_{L_{cr1}} \tag{6.30}$$

The lift factor LF_{DD} is calculated using a data array based on fig 12.27 of Raymer[90]. The wing is assumed to be supercritical, and therefore the thickness to chord ratio used in this evaluation is 0.6 times the value estimated from equation 6.13.

The drag divergence Mach number at zero lift ($M_{DD\,L=0}$) is estimated using data from figure 12.26 of Raymer[90]. The effective thickness to chord ratio used in this estimation has been evaluated using a number of assumptions. It would seem reasonable to assume that the airfoil of a modern aircraft designed to cruise at a Mach Number of 0.85 would have a higher drag divergence Mach number than an airfoil of the same thickness to chord ratio of an aircraft designed to cruise at a Mach Number of 0.8. Therefore, the effect of cruise Mach

number has been incorporated into the effective thickness to chord ratio of the wing. From an extrapolation of the graph it can be seen that for the condition of zero sweep, a 0.055 decrement in thickness to chord ratio approximately corresponds to a 0.05 increase in drag divergence Mach number. It would therefore seem reasonable to approximate the effective thickness to chord ratio, to take into account the supercritical design of wings for different cruise Mach number, by the following expression:-

$$\left(\frac{t}{c}\right)' = 0.6\frac{t}{c} - \left(Ma_{cr1} - 0.8\right)\frac{0.055}{0.05} \tag{6.31}$$

10 .3 .2 TRANSONIC DRAG RISE ESTIMATION

The drag rise through the transonic regime is estimated using the Boeing assumption that the drag divergence Mach number is the point where the drag reaches 20 'counts' (0.002) above its subsonic level, and that the critical Mach number is 0.08 below this point. Further assumptions taken from Raymer[90] suggest that the drag at $Ma=1.2$ is equal to the drag at $Ma=1.05$, and that the drag at $Ma=1.05$ is twice the drag at $Ma=1.0$. These assumptions allow the creation of a drag rise profile of the form shown below in figure 10.1.

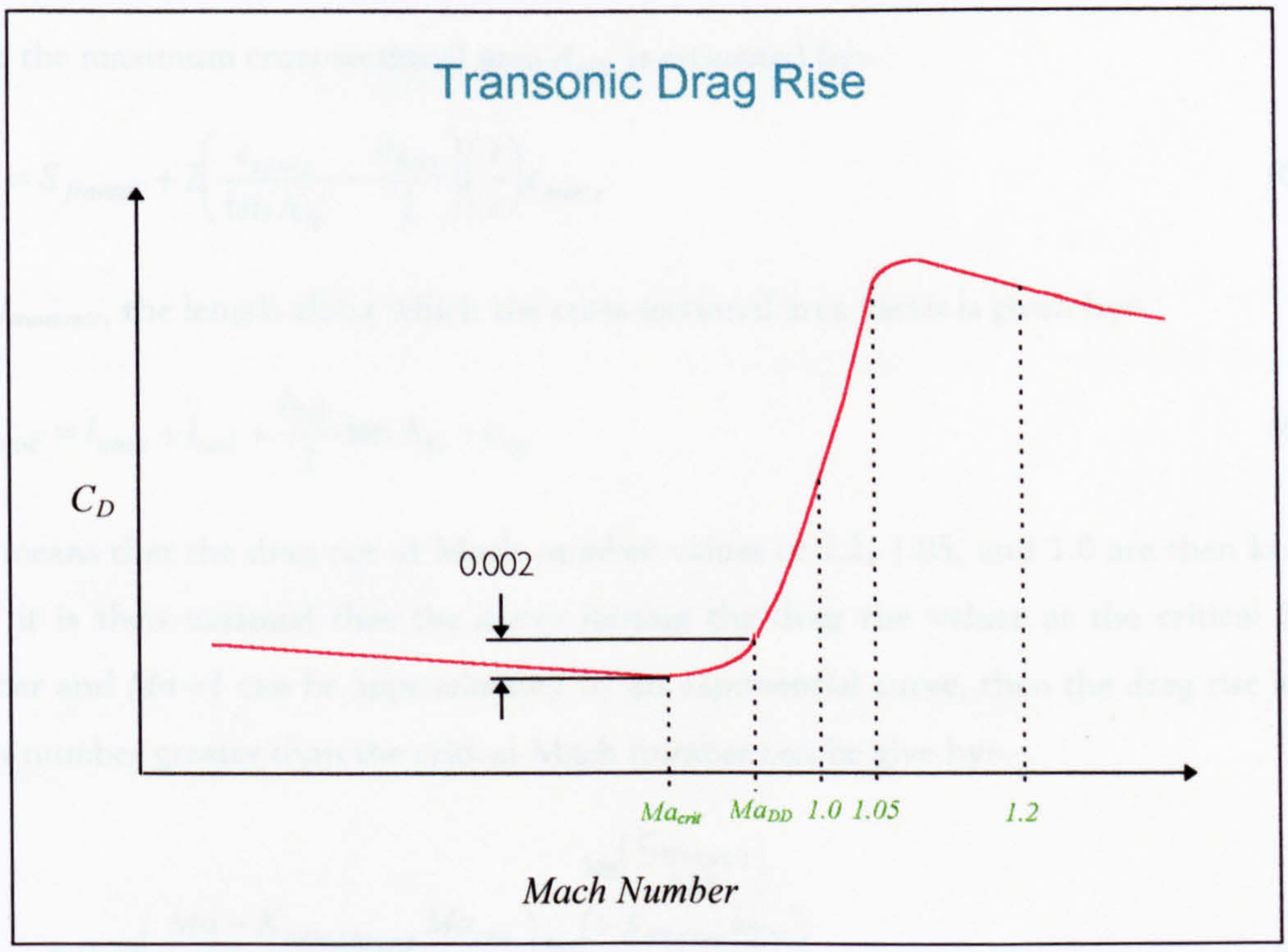


Figure 10.1- Transonic drag rise profile

To allow this process a greater degree of flexibility, a 'tuning' factor has been introduced ($K_{tune\ Ma\ crit}$) that is a multiplier to the critical Mach number. The value of this factor is by

default set to 100%, however the user may change this to explore the effect of changing the value of Ma_{crit}, to simulate possible advances in airfoil design.

The supersonic wave drag at $Ma=1.2$, is estimated using the method below taken from Raymer[90].

$$\left(\frac{D}{q}\right)_{wave} = E_{wd}\left[1-0.386\left(Ma-1.2\right)^{0.57}\left(1-\frac{\pi\Lambda_{le}{}^{0.77}}{100}\right)\right]\left(\frac{D}{q}\right)_{sears-hack} \tag{6.32}$$

which at $Ma=1.2$ reduces to:-

$$\left(\frac{D}{q}\right)_{wave} = E_{wd}\left(\frac{D}{q}\right)_{sears-hack} \tag{6.33}$$

where it has been assumed that

$$E_{wd} = 2 \tag{6.34}$$

and

$$\left(\frac{D}{q}\right)_{sears-hack} = \frac{9\pi}{2}\left(\frac{A_{max}}{l_{transonic}}\right)^2 \tag{6.35}$$

where the maximum cross-sectional area A_{max} is estimated by:-

$$A_{max} = S_{frontal} + 2\left(\frac{c_{root\,e}}{\tan\Lambda_{le}} - \frac{b_{fuse}}{2}\right)\left(\frac{t}{c}\right)c_{mac\,e} \tag{6.36}$$

and $l_{transonic}$, the length along which the cross-sectional area varies is given by:-

$$l_{transonic} = l_{nose} + l_{tail} + \frac{b_{ref}}{2}\tan\Lambda_{le} + c_{tip} \tag{6.37}$$

This means that the drag rise at Mach number values of 1.2, 1.05, and 1.0 are then known. So if it is then assumed that the curve joining the drag rise values at the critical Mach number and $Ma=1$ can be approximated by an exponential curve, then the drag rise at any Mach number greater than the critical Mach number can be give by:-

$$C_{D\,wave} = 0.02\left(\frac{Ma - K_{tune\,Ma\,crit}\,Ma_{crit}}{0.08}\right)^{\frac{\log\left(\frac{C_{DWave\,Ma=1}}{0.02}\right)}{\log\left(\frac{1-K_{tune\,Ma\,crit}\,Ma_{crit}}{0.08}\right)}} \tag{6.38}$$

10 .3 .3 Zero Lift Drag Increment Due To High Lift Devices

The zero lift drag increments due to the deployment of trailing edge flaps, ailerons, and leading edge slats are evaluated using the methods of Roskam[82]. For all high lift devices used during approach and takeoff, the zero lift drag increment is given by:-

$$C_{D0_{hld}} = C_{D\,profile_{flap}} + C_{D\,int\,flap} + C_{D\,profile_{aileron}} + C_{D\,int\,aileron} + C_{D\,profile_{lef}} + C_{D\,int\,lef} \quad (6.39)$$

The profile drag increment of the flaps and ailerons is given by equation 6.40.

$$C_{D\,profile_{flap}} = \Delta C_{d\,profile} \cos\Lambda_{0.25c} \frac{S_{flap}}{S_{ref}} \quad (6.40)$$

where the 2-d flap profile drag increment depends upon the flap type and the flap chord, and has been calculated using a set of data arrays based on figures 4.44 to 4.48 of Roskam[82].

The profile drag increment due to the deployment of leading edge slats is also calculated using equation 6.40, and the 2-d profile drag increment is given by:-

$$\Delta C_{d\,profile_{lef}} = \frac{c_{slat}}{c} C_{D0Wing} \quad (6.41)$$

where c_{slat}/c is assumed to be equal to 1.1.

The interference drag of the flaps is given by:-

$$C_{D\,int\,flap} = K_{int} C_{D\,profile_{flap}} \quad (6.42)$$

where the value of K_{int} depends on the flap type, and is taken from the list of suggested values in Roskam[82]. The interference drag of the leading edge slats is calculated using the same method.

10 .4 Windmilling Engine Drag

The extra drag due to a stopped or windmilling engine is estimated using the method presented in Raymer[90].

$$C_{D_{engine}} = \frac{0.3\pi\left(\frac{D_{fan}}{2}\right)^2}{S_{ref}} \quad (6.43)$$

10 .5 Lift Induced Drag

The drag due to lift is calculated assuming that the only relevant contribution comes from the wing lift. Exploratory calculations showed that contributions from the lift of the fuselage and nacelle were difficult to quantify, and were of negligible magnitude as far as the overall drag and its expected error for this kind of analysis were concerned. The drag due to the tail lift (trim drag) is dealt with at a later stage.

The induced drag of the wing is calculated using the methods of Roskam[82] where it has been split into three component parts.

$$C_{Di} = \frac{C_L^{\,2}}{\pi A e} + 2\pi C_L \varepsilon_t v_{twist} + 4\pi^2 \varepsilon_t^{\,2} w_{twist} \tag{6.44}$$

The first component is proportional to the square of the lift coefficient and is the component normally associated with wing induced drag calculations. The second component is derived from the induced drag due to linear twist, and the third component is from the zero lift drag due to linear twist. It has been assumed for these calculations that the wing lift coefficient is equal to the aircraft lift coefficient. This should be a good approximation for all trimmed conditions, especially during cruise, where the tail lift should be negligible.

10 .5 .1 The Span Efficiency Factor (e)

The span efficiency factor (e) from Roskam[82] is given by:-

$$e = \frac{1.1\dfrac{C_{L\alpha\,wing}}{A}}{R_{les}\left(\dfrac{C_{L\alpha\,wing}}{A}\right) + (1 - R_{les})\pi} K_{tune\,aero.effic} \tag{6.45}$$

where the wing lift curve slope ($C_{L\alpha\,wing}$) is found using the methods of Raymer[90] shown below:-

$$C_{L\alpha\,wing} = \frac{2\pi A}{2 + \sqrt{4 + \dfrac{A^2\beta^2}{\eta^2}\left(1 + \dfrac{\tan^2 \Lambda_m}{\beta^2}\right)}} \left(\frac{S_{exposed}}{S_{ref}}\right)(F) \tag{6.46}$$

where

$$\beta^2 = 1 - Ma^2 \tag{6.47}$$

$$\eta = \frac{C_{l\alpha}}{2\pi / \beta} \tag{6.48}$$

the 2-d lift curve slope ($C_{l\alpha}$) can be estimated from the airfoil data.

$$F = 1.07\left(1 + \frac{b_{fuse}}{b_{ref}}\right)^2 \tag{6.49}$$

The parameter R_{les} in equation 6.45 is the leading edge suction parameter defined in figure 4.7 of Roskam[82]. The data from this graph can be described by the equation 6.50 below:-

$$R_{les} = 0.972 - 0.0857\exp\left(-\frac{A_e\lambda_e}{2.48\cos\Lambda_{le}}\right) - 0.0265\exp\left(-\frac{A_e\lambda_e}{3.14\cos\Lambda_{le}}\right) \tag{6.50}$$

The factor $K_{tune\,aero.effic}$ is a user set aerodynamic tuning parameter (default value 100%).

10 .5 .2 Wing Twist Parameters

The parameters v_{twist} and w_{twist} are estimated using data arrays based on figures 4.9 and 4.10 of Roskam[82]. These parameters can then be estimated using interpolation for any value of taper ratio, Mach number, and corrected sweep angle.

10 .5 .3 Variable Camber Wings

It has been assumed that an aircraft equipped with variable camber wings will operate in the appropriate state such that minimum drag is achieved at every flight condition. Although this is not strictly true, as manoeuvre conditions will require a minimum bending moment rather than minimum drag. However, the detailed flight analysis of the Performance Module does not examine manoeuvres of much greater than 1g where low bending moment would be critical.

It is important to note that because a variable camber system would operate at lower incidences than a fixed wing, it provides reductions in profile drag as well as induced drag. These are estimated using the following methods.

If the drag is expressed using equation 6.51 (from Yates & Donaldson[99])

$$C_{Di} = \left(\frac{1}{\pi A e_{th}} + C_{d\,profile_{wing}}\right)C_L{}^2 \tag{6.51}$$

where e_{th} is a theoretical spanwise efficiency, and $Cd_{profile\,wing}$ is the 2-d airfoil profile drag.

Equating this to the expression of equation 6.44 gives:-

$$\frac{1}{\pi A e_{th}} + C_{d\,profile} = \frac{\frac{C_L{}^2}{\pi A e} + 2\pi C_L \varepsilon_t v_{twist} + 4\pi^2 \varepsilon_t{}^2 w_{twist}}{C_L{}^2} \tag{6.52}$$

and for an ideal 'elliptical' lift distribution ($e=1$)

$$\left(\frac{1}{\pi A e_{th}} + C_{d\,profile}\right)_{ideal} = \frac{\frac{C_L{}^2}{\pi A} + 2\pi C_L \varepsilon_t v_{twist} + 4\pi^2 \varepsilon_t{}^2 w_{twist}}{C_L{}^2} \tag{6.53}$$

It has been assumed that that a 'conventional' airfoil has a 2-d profile drag of 0.012, and that the average profile drag of a variable camber airfoil is 0.008 (from the data provided by Rao[74]) . The lift distribution provided by the variable camber wing is assumed to be some proportion of the ideal distribution away from the straight tapered equivalent, as specified by the user. The default value of this parameter ($K_{efficieny\ v.camber}$) is 60%, which means a lift distribution 60% between the straight tapered equivalent, and the ideal elliptical one for that planform. Therefore:-

$$\left(\frac{1}{\pi A e_{th}}\right)_{v.camber} = \left(\frac{C_{D_i}}{C_L{}^2} - 0.012\right) + \left(\left(\frac{C_{D_i\,ideal}}{C_L{}^2} - 0.012\right) - \left(\frac{C_{D_i}}{C_L{}^2} - 0.012\right) K_{efficiency\ v.camber}\right) \tag{6.54}$$

Therefore the induced drag of the variable camber wing is given by:-

$$C_{Di\,v.camber} = \left(\left(\frac{1}{\pi A e_{th}}\right)_{v.camber} + 0.008\right) C_L{}^2 \tag{6.55}$$

10 .6 Ground Effect

The effect of the proximity of the ground to the aircraft wing is to reduce the induced drag. The magnitude of this effect is evaluated using the methods of Torenbeek[93]. The reduction in drag is given by the equation:-

$$\Delta C_{D\,ge} = \frac{4\pi\sigma\, h/c_{mean} - \beta C_L}{4\pi\, h/c_{mean} - \beta C_L} C_{Di} - \frac{\beta C_L}{4\pi\, h/c_{mean}} C_{D\,profile_{wing}} \tag{6.56}$$

where

h – height of wing above ground

$$\sigma = -2.48\left(2\frac{h_{eff}}{b_{ref}}\right)^{0.768} \tag{6.57}$$

$$\beta = \sqrt{1 + \left(\frac{2h_{eff}}{b_{ref}}\right)^2} - \frac{2h_{eff}}{b_{ref}} \tag{6.58}$$

h_{eff} is the average of the height of the wing aerodynamic centre and of the trailing edge.

It has been assumed that $C_{D\,profile_{wing}} \approx C_{D0_{wing}}$

10 .7 Effect of Winglets

As no detailed theoretical or empirical methods for the estimation of the drag reduction effect of winglets were available, the magnitude of the drag reduction had to be estimated from the scant flight test and experimental data that was found to be relevant. The results were based on data from the DC-10 flight test program (Taylor[38], Shollenberger et al.[100], Gikey[101], and Douglas Aircraft Company[102]), the KC-135 flight tests (Lux[103] and Dodson[104]), and Boeing 747 winglet flight data (Boeing Airplane Company[39]). All of these results tended to be consistent in trend and roughly of the same magnitude as each other, and all showed that the percentage drag reduction due to the winglets was relatively insensitive to Mach number. The main factor in the determination of the drag reduction for all of the results was the lift coefficient. The data verified that in all configurations there was a particular lift coefficient where the drag reduction was a maximum.

10 .7 .1 Upper And Lower Winglets

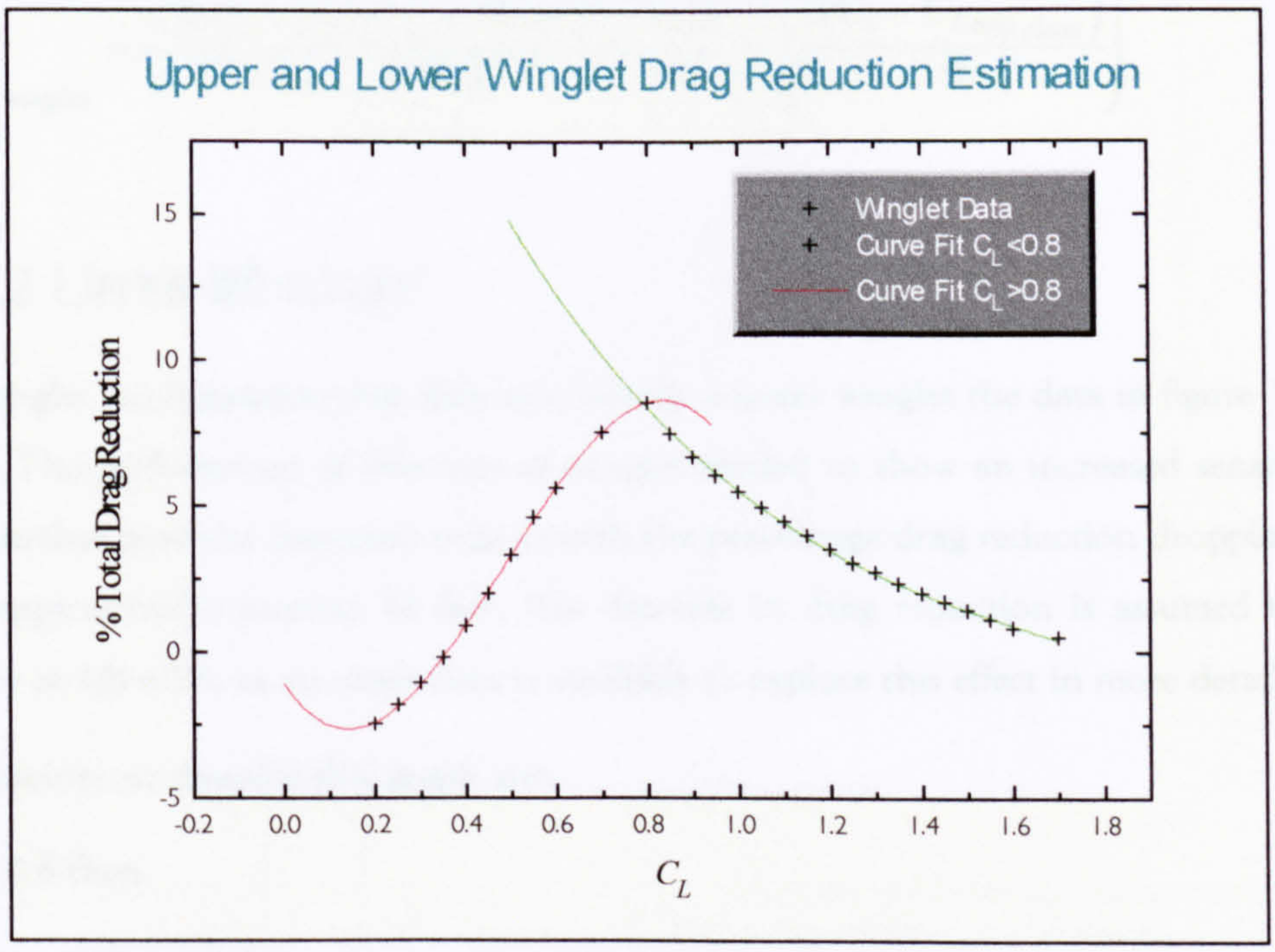


Figure 10.2 - Estimation of drag reduction due to upper and lower winglets

Figure 10.2 above was constructed from the data to show average values of the percentage drag reduction against lift coefficient, for a winglet configuration that includes a lower winglet. This data is based upon a clean wing configuration and maximum drag reduction can be seen to occur at a lift coefficient of approximately 0.8.

Data from Taylor[38] and Shollenberger et al.[100] quantify the effect of flap and slat deflection on the percentage drag reduction. The general trend that could be drawn from the data is that the lift coefficient at which the maximum drag reduction occurs increases slightly with increasing flap deflection, while the magnitude of the reduction decreases.

This leads to the equations below that describe the percentage drag reduction due to upper and lower winglet installation.

For clean configuration:-

If $C_L < 0.8$ then

$$\left(\frac{\Delta C_D}{C_D}\right)_{winglet} = \frac{-1.091 - 23.37C_L + 97.78C_L{}^2 - 66.92C_L{}^3}{100} \tag{6.59}$$

else

$$\left(\frac{\Delta C_D}{C_D}\right)_{winglet} = \frac{-36.01 - 48.11C_L + 25.63C_L{}^2 - 5.07C_L{}^3}{100} \tag{6.60}$$

If flaps and slats are deployed then a best estimate of the data average is given by:-

$$\left(\frac{\Delta C_D}{C_D}\right)_{winglet} = \frac{-36.01 - 48.11C_L + 25.63C_L{}^2 - 5.07C_L{}^3}{100}\left(\frac{7\left(C_L - C_{L\,max\,clean}\right)}{8}\right) \tag{6.61}$$

10 .7 .2 UPPER WINGLET

For a winglet configuration that does not include a lower winglet the data in figure 10.3 was plotted. The performance of this type of winglet tended to show an increased sensitivity to Mach number near the transonic region, with the percentage drag reduction dropping as the speeds approached transonic. In fact, this decrease in drag reduction is assumed to occur suddenly at $Ma = 0.8$, as no exact data is available to explore this effect in more detail.

The equations to describe this graph are:-

If $Ma < 0.8$ then

For clean configuration:-

If $C_L < 0.8$ then

$$\left(\frac{\Delta C_D}{C_D}\right)_{winglet} = \frac{-0.185 - 17.06C_L + 66.77C_L{}^2 - 37.95C_L{}^3}{100} \tag{6.62}$$

else

$$\left(\frac{\Delta C_D}{C_D}\right)_{winglet} = \frac{-45.80 - 79.35C_L + 52.68C_L{}^2 - 13.23C_L{}^3}{100} \tag{6.63}$$

If flaps and slats are deployed then a best estimate of the data average is given by:-

$$\left(\frac{\Delta C_D}{C_D}\right)_{winglet} = \frac{-45.80 - 79.35C_L + 52..68C_L{}^2 - 13.23C_L{}^3}{100}\left(\frac{7\left(C_L - C_{L_{max\,clean}}\right)}{8}\right) \tag{6.64}$$

else if $Ma >= 0.8$

$$\left(\frac{\Delta C_D}{C_D}\right)_{winglet} = \frac{-0.779 - 10.42C_L + 45.98C_L{}^2 - 27.37C_L{}^3}{100} \tag{6.65}$$

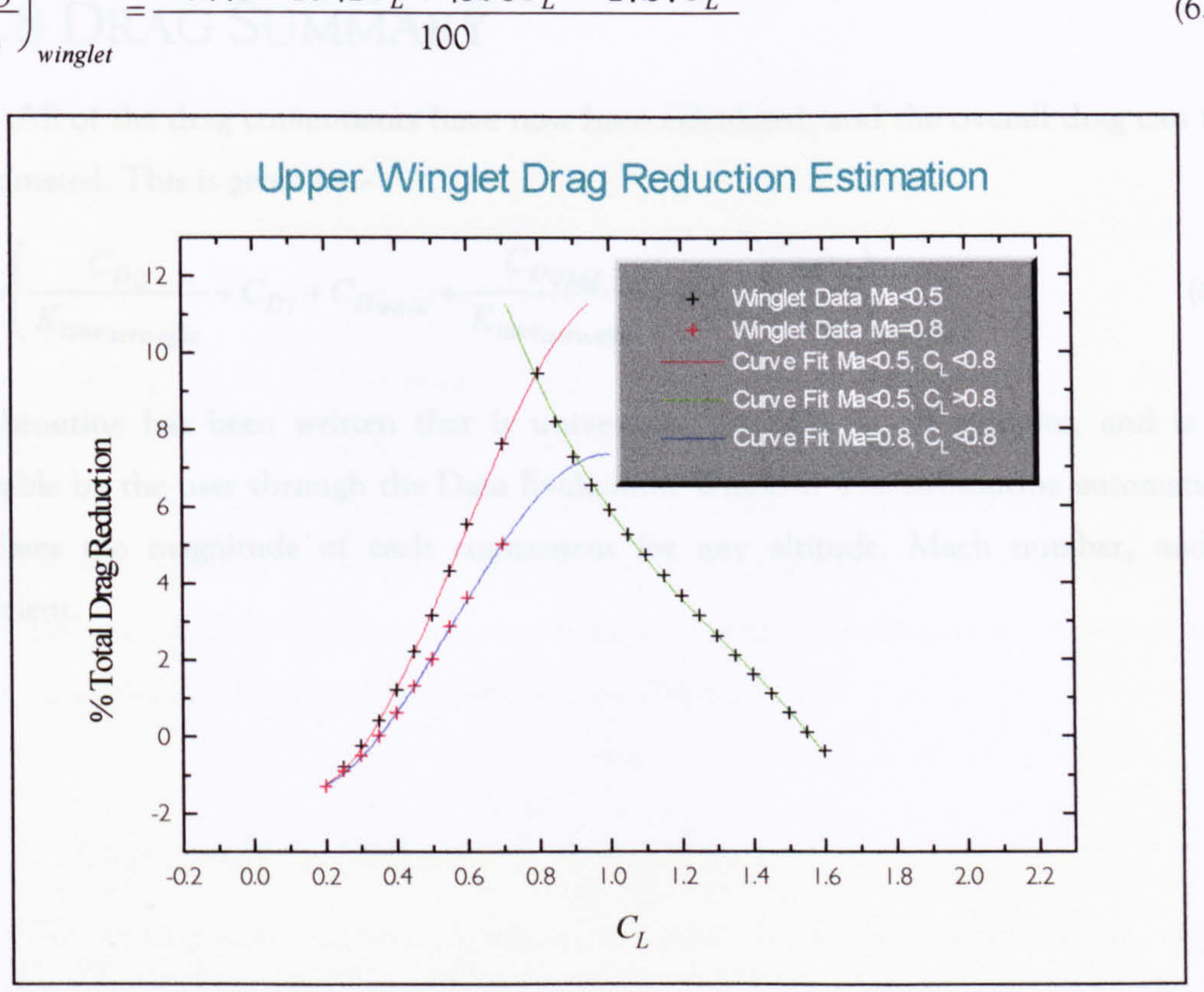


Figure 10.3- Estimation of drag reduction due to upper winglet

10 .7 .3 WING TIP FENCES

The drag reduction behaviour of wing tip fences is assumed to follow the same pattern as the upper and lower winglet. The magnitude of the drag reduction however will obviously be

smaller. Data from Poisson-Quiton[42] suggests that the drag reduction of wing tip fences may be of the order of a half of the value of that from upper and lower winglets. Therefore, the assumption has been made that the drag reduction of a wing tip fence is half that of an upper and lower winglet combination.

10 .7 .4 WINGLET EFFICIENCY

The drag reduction for each type of winglet is then corrected for the user defined winglet efficiency, which is a parameter that has been defined as a function of the efficiency of the winglet design, and the size of the winglet.

$$\left(\frac{\Delta C_D}{C_D}\right)_{winglet} = K_{tune\,winglet}\left(\frac{\Delta C_D}{C_D}\right)_{winglet} \tag{6.62}$$

10 .8 DRAG SUMMARY

All of the drag components have now been calculated, and the overall drag can then be estimated. This is given by:-

$$C_D = \left(\frac{C_{D0}}{K_{tune\,aero.effic}} + C_{Di} + C_{Dwave} + \frac{C_{D0hld}}{K_{tune\,aero.effic}} + C_{Dge}\right)\left(\frac{\Delta C_D}{C_D}\right)_{Winglet} \tag{6.63}$$

A subroutine has been written that is universally available to all modules, and is also accessible by the user through the Data Evaluation Window. The subroutine automatically calculates the magnitude of each component for any altitude, Mach number, and lift coefficient.

11 .Stability Analysis Methods

This module is responsible for calculating the longitudinal stability characteristics of the aircraft. The static margin is calculated for a range of conditions, and a trim plot is produced that covers a range of flight conditions.

11 .1 Aircraft Trim Condition

For each considered value of altitude, Mach number, and lift coefficient, the correct incidence of the aircraft and tail incidence angle must be found that keeps the aircraft in a steady state 'trimmed' condition. In this condition the total of the pitching moments about the centre of gravity is zero. Therefore using the methods and notation of Raymer[90], this trim condition is described by the equation below.

$$C_{m_{cg}} = 0 = C_{L_{wing}}\left(\overline{X}_{cg} - \overline{X}_{ac\,wing}\right) + C_{m_{wing}} + C_{m_{flap}} + C_{m_{fuse}} + \eta_h \frac{S_{ref\,ht}}{S_{ref}} C_{L_{ht}}\left(\overline{X}_{cg} - \overline{X}_{ac\,ht}\right) - \frac{T}{qS_{ref}}\overline{Z}_t + \frac{F_p}{qS_{ref}}\left(\overline{X}_{cg} - \overline{X}_{pg}\right) \tag{7.1}$$

where $\overline{X}$ and $\overline{Z}$ denote lengths normalised by the mean wing chord, and F_p is the force at the engine front face due to the turning motion of the inlet air.

The right hand side of this equation is evaluated in order to produce the trim plot. It is evaluated for a number of values of lift coefficient, altitude, and tail incidence angle, and the trim condition can then be found from the the particular tail incidence angle which gives zero pitching moment for a given lift coefficient and altitude. The first step in each evaluation is an iteration to find the correct angle of aircraft incidence (α), at a number tail incidence angles (i_{ht}), which will maintain the total desired lift.

11 .1 .1 Aircraft Incidence Solution

The starting point of this iteration is the aircraft incidence without the tail, and the iteration is performed using the knowledge of the wing and tail characteristics described below.

For a particular value of aircraft incidence (α) and tail incidence angle (i_{ht}):-

$$C_{L_{wing}} = C_{L\alpha_{wing}}\left(\alpha + i_{wing_{mac}} - \alpha_{0_{mac}}\right) \tag{7.2}$$

$$C_{L_{ht}} = C_{L\alpha_{ht}}\left(\alpha + i_{ht} - \alpha_{0_{ht}} - \varepsilon\right) \tag{7.3}$$

where ε represents the downwash angle, which is calculated using data taken from the graphs of fig 16.12 of Raymer[90]. The data is interpolated for the relevant values of aspect ratio, taper ratio, and geometric properties, which are all known, and the downwash derivative ($d\varepsilon/d\alpha$) is then found. It is assumed that the downwash is halved in the presence of ground effect. The 3-d lift curve slopes of the wing and horizontal tail are calculated using the methods outlined in Chapter 10. It is assumed that the lift curve slope increases by 10% in the presence of ground effect.

This then means that:-

$$\varepsilon = \frac{d\varepsilon}{d\alpha}\left(\alpha + i_{wing_{mac}}\right) \tag{7.4}$$

The incidence is then found such that:-

$$C_L = C_{L_{wing}} + \eta_h \frac{S_{ref_{ht}}}{S_{ref}} C_{L_{ht}}$$

where C_L is the desired aircraft lift coefficient.

Once this iteration is complete and the aircraft incidence is known, the evaluation of each of the components of equation 7.1 is carried out using the methods below.

11 .1 .2 Wing Pitching Moment

The contribution of the wing to pitching moment is made up of two parts. These are the moment due to the lift of the wing acting away from the aircraft centre of gravity, and the moment due to the pitching moment of the wing itself. As the total wing lift contribution is known from equation 7.2, the wing pitching moment can be calculated. First the amount of the wing lift neglecting any flap contribution is found, then the 2-d lift coefficient is calculated using equation 3.23. Once the 2-d lift is known, the 2-d pitching moment can be calculated from the 2-d airfoil data. This is converted into a 3-d pitching moment using the equation below from Raymer[90].

$$C_{m_{wing}} = \left(C_{m_{wing_{2d}}} \left(\frac{A\cos^2 \Lambda_{1/4c}}{A + 2\cos\Lambda_{1/4c}} \right) - 0.01\varepsilon_t \right) K_{pm} \tag{7.6}$$

where $K_{pm}=1.3$ for $Ma>0.8$, or $K_{pm}=1$ for $Ma<0.8$.

11 .1 .3 FLAP PITCHING MOMENT

The contribution of the flaps to the wing pitching moment is calculated using the methods given below.

$$C_{m\,flap} = C_{L\,flap}\left(\bar{X}_{cp\,flap} - \bar{X}_{cg}\right) \tag{7.7}$$

where $C_{L\,flap}$ is known from the overall lift coefficient, and the centre of pressure of the flap system is calculated using the graph of fig. 16.9 from Raymer[90]. This graph suggests that the centre of pressure to chord ratio is equal to 0.44 for all slotted flaps. Therefore as the wing chord at the flap inboard and outboard locations (c_{flapo} and c_{flapi}) are known:-

$$\lambda_{flap} = \frac{c_{flap_o}}{c_{flap_i}} \tag{7.8}$$

and assuming that

$$y_{mac\,flap} = \frac{b_{flap_o} - b_{flap_i}}{6}\left(\frac{1+2\lambda_{flap}}{1+\lambda_{flap}}\right) \tag{7.9}$$

so the wing chord at the flap m.a.c. location can be calculated ($c_{mac\,flap}$). Therefore:-

$$X_{cp\,flap} = y_{mac\,flap}\tan\Lambda_{le} + 0.44c_{mac\,flap} + X_{ac\,wing} - X'_{ac\,wing} \tag{7.10}$$

The same procedures are then used to calculate the aileron centre of pressure ($X_{cp_{aileron}}$).

The centre of pressure of the combined flap system is then found from amalgamating the centres of pressure of the main trailing edge flaps and the ailerons (which can be used for lift augmentation). The ratio of the lift from the flaps and ailerons is estimated using the relationship below:-

$$\frac{C_{L\,aileron}}{C_{L\,flap}} = \frac{\delta_{aileron}/\delta_{flap}}{\left(K_{flap.lift}\dfrac{b_{flap_o} - b_{flap_i}}{b_{aileron_o} - b_{aileron_i}}\right)} \tag{7.11}$$

where $K_{flap.lift}$ takes the value shown below, depending on the type of flaps in use. These values have been selected from the results of the lift coefficient ratios of various flap systems.

Single Slotted Fixed Hinge Flaps	-1.0
Single Slotted Fowler Flaps	-4.0
Double Slotted Fixed Vane Flaps	-3.2
Double Slotted Variable Geometry	-4.8
Double Slotted Fowler Flaps	-6.7
Triple Slotted Fowler Flaps	-7.0

Then the total centre of pressure is given by:-

$$X_{cp\,flaps} = X_{cp\,flap} + \left(X_{cp\,ailerons} \frac{C_{L\,aileron}}{C_{L\,flap}} \right) \Bigg/ \left(1 + \frac{C_{L\,aileron}}{C_{L\,flap}} \right) \tag{7.12}$$

11 .1 .4 FUSELAGE PITCHING MOMENT

The fuselage pitching moment is given by the relationship below from Raymer[90], where $Cm_{a\,fuse}$ is the fuselage pitching moment derivative with respect to aircraft incidence.

$$C_{m\,fuse} = C_{m\alpha\,fuse}\alpha \tag{7.13}$$

where

$$C_{m\alpha\,fuse} = \frac{K_f W_{fuse} l_{fuse}}{c_{mean} S_{ref}} \tag{7.14}$$

The value of K_f is found from the interpolation of a data array based on fig. 16.14 of Raymer[90].

11 .1 .5 HORIZONTAL TAIL PITCHING MOMENT

This contribution is simply the product of the lift from the horizontal tail and the distance between its aerodynamic centre and the aircraft centre of gravity.

$$C_{m\,ht} = \eta_h \frac{S_{ref\,ht}}{S_{ref}} C_{L\,ht} \left(\bar{X}_{ac\,ht} - \bar{X}_{cg} \right) \tag{7.15}$$

11 .1 .6 THRUST PITCHING MOMENT

The contributions of the engine thrust and the inlet air to the aircraft pitching moment are calculated using the following methods.

$$C_{m\,thrust} = \frac{T}{qS_{ref}} \frac{z_t}{c_{mean}} \tag{7.16}$$

where the distance z_t is the perpendicular distance between the engine thrust line and the aircraft centre of gravity, which is known from geometry considerations.

$$C_{m\,inlet} = \frac{F_p}{qS_{ref}} \left(\frac{X_{cg\,pg} - X_{cg}}{c_{mean}} \right) \tag{7.17}$$

The only unknown in this equation is the force magnitude F_p which is given by:-

$$F_p = F_{p_\alpha}\left(\alpha + \alpha_{inlet} + \alpha\frac{d\varepsilon_p}{d\alpha}\right) \tag{7.18}$$

The inlet incidence α_{inlet} is set by the user, and the upwash derivative ($d\varepsilon_p/d\alpha$) is assumed to be equal to 1.2 from consideration of fig. 16.11 of Raymer[90]. The force vs. incidence slope ($F_{p\alpha}$) is calculated from mass flow considerations (Raymer[90]) shown below:-

$$F_{p_\alpha} = \rho V A_{inlet} N_e \tag{7.19}$$

11 .2 Neutral Point

Once the total aircraft pitching moment and its contributions have been calculated, the neutral point may be evaluated using the equation below (Raymer[90]) for the 'power on' conditions.

$$\bar{X}_{np} = \frac{C_{L\alpha wing}\bar{X}_{ac\,wing} - C_{m\alpha\,fuse} + \eta_h \frac{S_{ref\,ht}}{S_{ref}} C_{L\alpha\,ht}\frac{d\alpha_{ht}}{d\alpha}\bar{X}_{ac\,ht} + \frac{F_{p_\alpha}}{qS_{ref}}\frac{d\alpha_{pg}}{d\alpha}\bar{X}_{cg\,pg}}{C_{L\alpha wing} + \eta_h \frac{S_{ref\,ht}}{S_{ref}} C_{L\alpha\,ht}\frac{d\alpha_{ht}}{d\alpha} + \frac{F_{p_\alpha}}{qS_{ref}}} \tag{7.20}$$

where

$$\frac{d\alpha_{ht}}{d\alpha} = 1 - \frac{d\varepsilon}{d\alpha} \tag{7.21}$$

and

$$\frac{d\alpha_{pg}}{d\alpha} = 1 + \frac{d\varepsilon_p}{d\alpha} \tag{7.21}$$

The remainder of the variables in this equation are known from previous analysis.

11 .3 Static Margin

Once the neutral point has been calculated, the static margin can be evaluated using the equation below. The static margin has been specifically calculated at the cruise, takeoff, and landing conditions.

$$SM = \left(\bar{X}_{np} - \bar{X}_{cg}\right)\frac{c_{mean}}{c_{mac\,e}} \times 100\% \tag{7.22}$$

11 .4 TRIM DRAG

The tail incidence required to trim the aircraft at a particular flight condition can be calculated from the trim data calculated previously. This can then be used to provide an estimate of the trim drag at cruise, takeoff, and landing conditions. The following equation (from Raymer[90]) is used to evaluate the trim drag.

$$C_{D\,trim} = \eta_h \frac{S_{ref\,ht}}{S_{ref}} \frac{1}{\pi A_{ht} e_{ht}} C_{L\,ht}{}^2 \tag{7.23}$$

Where the lift of the horizontal tail ($C_{L\,ht}$) is known from the trim analysis, and the span efficiency factor of the horizontal tail (e_{ht}) can be estimated using the equation below from Raymer[90].

$$e_{ht} = 4.61\left(1 - 0.045 A_{ht}^{0.68}\right)\left(\cos \Lambda_{le\,ht}\right)^{0.15} - 3.1 \tag{7.24}$$

12 .Performance Prediction Methods

The purpose of this module is to numerically simulate a realistic flight profile, from take-off to landing, evaluating the flight properties at every point during the flight. This gives a detailed insight into the behaviour of the aircraft, and provides accurate estimates of the range, takeoff length, landing length, and balanced field length of the aircraft. The flight profile that is executed is created by the user from the Performance Profile Editor.

12 .1 Calculation Process

The flight is assumed to begin with takeoff, and then climb to an initial altitude of 1500ft. The program then interprets the profile set by the user, and carries out a simulation of each segment of the specified flight profile. Normally, the flight profile should end with an 'approach' segment, which will automatically be followed with a landing segment. The balanced field length is subsequently calculated.

The fuel reserves procedure for each cruise segment is set by the user, by giving the 'Reserves' parameter a value between 0 and 2. These values correspond to no reserves, an extra 10% cruise, or an extra 1 hours cruise time, and are automatically accounted for in the range calculations.

The whole flight process must then be iterated such that either the range of the aircraft exactly equals a specified input range, or so that the total mass of fuel consumed is exactly equal to the initial fuel mass. The choice of iteration type is set by the user from the 'Iteration Mode' parameter within the 'Performance' section of input variables, which must be given the value '1' or '2' depending on which mode is required.

The iteration for range requires that the mass of fuel is changed accordingly as to whether the range has been exceeded or whether all of the fuel has been consumed. The iteration for fuel requires that the range of the aircraft is altered such that it is the exact range travelled for the set fuel mass. This is achieved by increasing or decreasing the range of the first cruise segment (assumed to be the main cruise segment) depending whether there is a fuel deficit or surfeit.

Another parameter which must be found by iteration is the range of the descent from cruise. The number of segments which define the descent from cruise is specified by the user, and the descent range is found by the iteration of the length of the cruise range before the descent, such that the range up to the cruise segment plus the range travelled during descent is exactly equal to the desired cruise range.

The calculation of the properties of each flight segment is described in detail below, bearing in mind that the thrust and drag of the aircraft at any altitude, Mach number, and lift coefficient have been calculated previously.

The number of steps into which each segment is divided depends on the value of the accuracy parameters set by the user. The greater the value of the accuracy parameter, then the greater the number of steps.

Another consideration in the performance calculation is the proportion of time for which a laminar flow system is assumed to be effective. The proportion of the flight time for which laminar flow is attainable is set by the user. During the performance calculations the drag is estimated using the assumptions that the laminar flow system is effective, until such a time is reached that the estimated proportion of the flight time for which the system is effective has passed, and then the drag for the remainder of the flight is calculated assuming that the system is inoperative.

12 .2 Common Procedures

For each segment there are a number of methods and procedures that are common to each. The thrust, fuel consumption, and drag, can be estimated for any flight condition using the universal sub-routines derived from the methods of Chapter 5 and Chapter 10.

For the calculation of thrust during the climb and acceleration segments a variable throttle approach has been used. This means that if the climb or acceleration rate falls below a critical value, then the engine throttle setting will be increased to counteract this. The maximum throttle setting is 110%. The following equations can be applied to each step of the performance evaluation.

The mass of fuel consumed in each step (of duration Δt) is given by:-

$$Q_{fuel} = T \times C \times N_e \times \Delta t \tag{8.1}$$

with the total mass of fuel consumed given by:-

$$W_{fuel} = W_{fuel} + Q_{fuel} \tag{8.2}$$

and the total aircraft mass:-

$$W_{total} = W_{total} - Q_{fuel} \tag{8.3}$$

The calibrated airspeed is converted to Mach number, and vice-versa, using the methods of Roskam[91]:-

$$Ma^2 = \frac{2}{\gamma - 1}\left\{\left[\left(\frac{P_0}{P}\right)\left\{\left(1 + \frac{\gamma - 1}{2}\left(\frac{V_c}{Va_0}\right)^2\right)^{\frac{\gamma}{\gamma-1}} - 1\right\} + 1\right]^{\frac{\gamma-1}{\gamma}} - 1\right\} \tag{8.4}$$

where $\gamma = 1.4$, and $Va_0 = 661$ knots

12 .3 TAKEOFF ANALYSIS

The takeoff segment is split into four portions. These are the ground roll, the rotation, the transition, and the initial climb. The takeoff distance is the distance required to reach an altitude of 35ft. The methods used in these segments are described separately below.

12 .3 .1 GROUND ROLL

The ground roll is the portion in which the aircraft accelerates along the ground from zero velocity up to the takeoff velocity. This portion has arbitrarily been split into 21 steps, and the following methods have been used to calculate the range, fuel consumption, etc., at each step.

At *i*th step

$$V_i = V_{to}\frac{(i-1)}{21} \tag{8.5}$$

As suggested in Raymer[90], the thrust at each step is calculated at V_t which is given by:-

$$V_t = V_i + 0.7(V_{i+1} - V_i) \tag{8.6}$$

The distance travelled is found using equation 17.99 from Raymer[90].

$$\Delta R = \frac{1}{2gK_A}\log\left(\frac{K_T + K_A V_{i+1}^2}{K_T + K_A V_i^2}\right) \tag{8.7}$$

where

$$K_A = \frac{\rho}{2W_{total}/S_{ref}}\left(\mu C_L - C_{D0} - C_{Di}\right) \tag{8.8}$$

μ is assumed to be equal to 0.03, and C_L equals C_{Lgr}

and

$$K_T = \left(\frac{T}{W_{total}}\right) - \mu \tag{8.9}$$

The time for each step is given by:-

$$\Delta t = \frac{2R}{V_{i+1} + V_i} \tag{8.10}$$

The contributions from each step are added and the ground roll calculations are complete.

12 .3 .2 ROTATION

The rotation segment is assumed to take 2.5 seconds. During which time the aircraft is assumed not to accelerate, and therefore remains at the velocity V_{to}. The distance travelled and the fuel consumed are easily calculated.

12 .3 .3 TRANSITION

In this segment the aircraft accelerates from takeoff velocity ($1.1V_{stall}$) to $1.2V_{stall}$ as it climbs, and the flight path angle increases from zero to some value γ_{max}. Again, this segment is split into 21 steps. The aircraft has been assumed to follow a circular path during each step, with the radius of the path in each step increasing as the load factor diminishes. The following assumptions describe the motion of the aircraft during this transition segment.

$$C_{L initial} = C_{L to max} = \frac{W_0}{\frac{1}{2}\rho\left(\frac{V_{to}}{1.1}\right)^2 S_{ref}} \qquad (C_{L to max} \text{ known from equation 3.26}) \tag{8.11}$$

$$C_{L final} = 0.95 C_{L initial} \tag{8.12}$$

and

$$V_{stall initial} = \frac{V_{to}}{1.1} \tag{8.13}$$

$$V_{stall final} = \frac{W_{total}}{\sqrt{C_{L final} 0.5 \rho S_{ref}}} \tag{8.14}$$

so

$$V_{initial} = 1.1 V_{stall initial} \tag{8.15}$$

$$V_{final} = 1.2 V_{stall final} \tag{8.16}$$

at the ith step

$$C_{Li} = C_{L\,initial} + \left(C_{L\,final} - C_{L\,initial}\right)\frac{i-1}{21} \tag{8.17}$$

$$V_i = V_{initial} + \left(V_{final} - V_{initial}\right)\frac{(i-1)}{21} \tag{8.18}$$

The maximum flight path angle (γ_{max}) at each step is given by:-

$$\gamma_{max\,i} = \sin^{-1}\left(\frac{T-D}{W_{total}}\right) \tag{8.19}$$

It has been assumed that the increase in flight path angle during transition is given by:-

$$\gamma_i = \left(\frac{i-1}{20}\right)^{1.1}\gamma_{max\,i} \tag{8.20}$$

the load factor (n) is assumed to be equal to:-

$$n = \frac{C_{Li}}{C_{L\,initial}}\left(\frac{(V_i + V_{i+1})/2}{V_{stall\,initial}}\right) \tag{8.21}$$

and from Raymer[90], the radius of the circular path is:-

$$r_i = \frac{V_i + V_{i+1}}{2}\frac{1}{g(n-1)} \tag{8.22}$$

This gives a flight path as shown below in figure 12.1. Geometric analysis of this diagram allows the step increments in range and height to be evaluated with the expressions shown below.

The overall flight distance x is found from:-

$$x_i = \sqrt{2r^2\left(1-\cos\left(\gamma_i - \gamma_{i-1}\right)\right)} \tag{8.23}$$

so

$$\Delta R_i = x_i \cos\left(\frac{\gamma_i + \gamma_{i-1}}{2}\right) \tag{8.24}$$

$$\Delta h_i = x_i \sin\left(\frac{\gamma_i + \gamma_{i-1}}{2}\right) \tag{8.25}$$

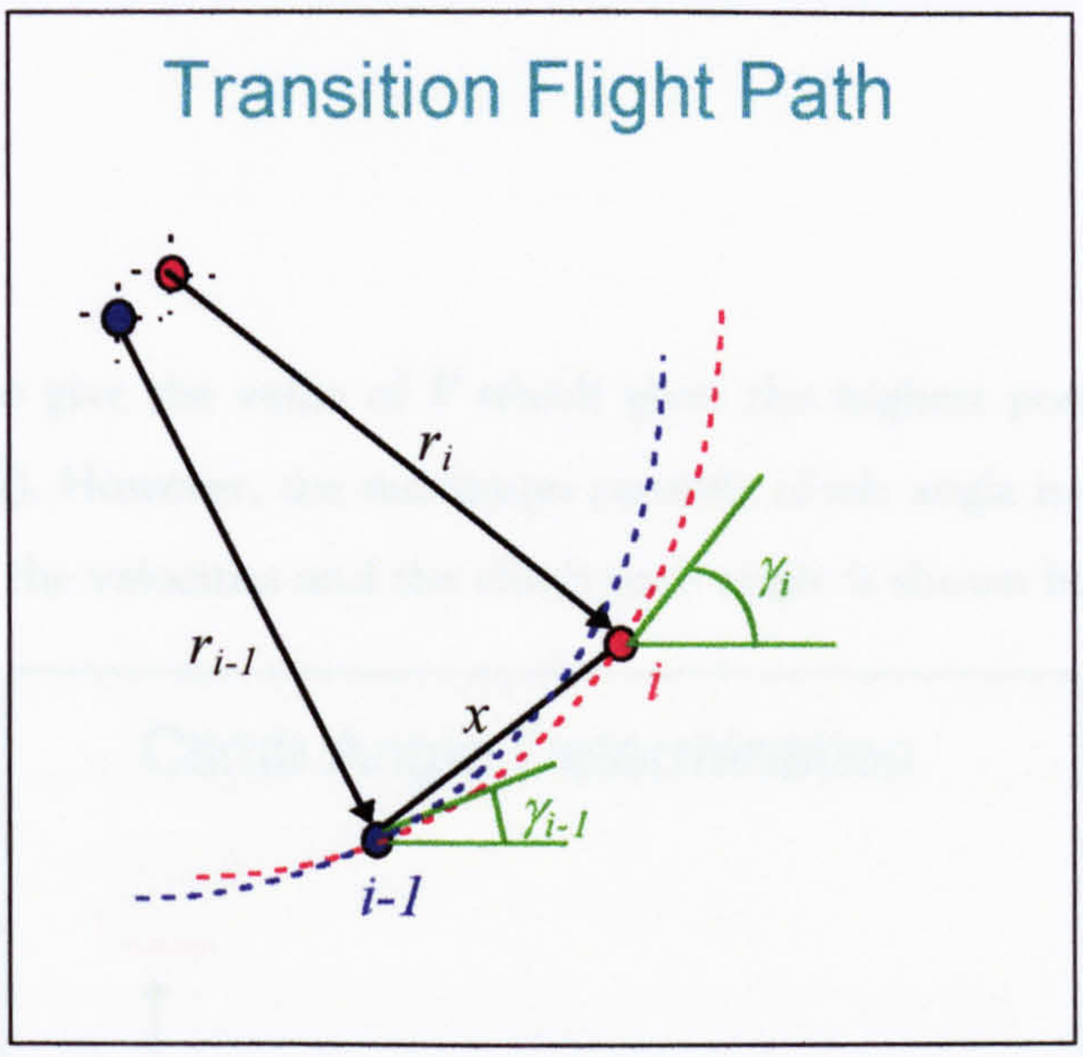


Figure 12.1- Construction of transition flight path

12 .3 .4 INITIAL CLIMB

The aircraft then climbs from the altitude reached at the end of the transition segment to an eventual altitude of 1500ft. This climb is split into three separate climb portions, the first being a climb up to 35ft, the second a climb to 400ft, and the third is the final climb to 1500ft. The performance through these sections is calculated using the assumption that the climb occurs at the maximum possible path angle, and hence the methods described in section 12.4 are used.

12 .4 CLIMB AT MAXIMUM GAMMA (γ)

This is a climb profile in which the velocity is optimised such that the flight path angle is a maximum, and therefore the steepest possible climb is achieved. In order to climb the aircraft must produce an excess power, greater than the power required for steady level flight. This excess power can be used to gain altitude or to accelerate the aircraft, or a combination of both, as expressed by the equation below.

$$P_s = \frac{V(T-D)}{W} = V\sin\gamma + \frac{V}{g}\frac{dV}{dt} \tag{8.26}$$

solving for the vertical velocity V_v and making substitutions gives:-

$$V_v = V\frac{T}{W} - \frac{\rho V^3 C_{D0}}{2W/S} - \frac{2K}{\rho V}\frac{W}{S} \tag{8.27}$$

where

$$K = \frac{C_{Di}}{C_L{}^2} \tag{8.28}$$

This can be solved to give the value of V which gives the highest possible vertical velocity (Raymer[90] Chapter 17). However, the maximum possible climb angle is of more interest. The relationship between the velocities and the climb path angle is shown below in figure 12.2.

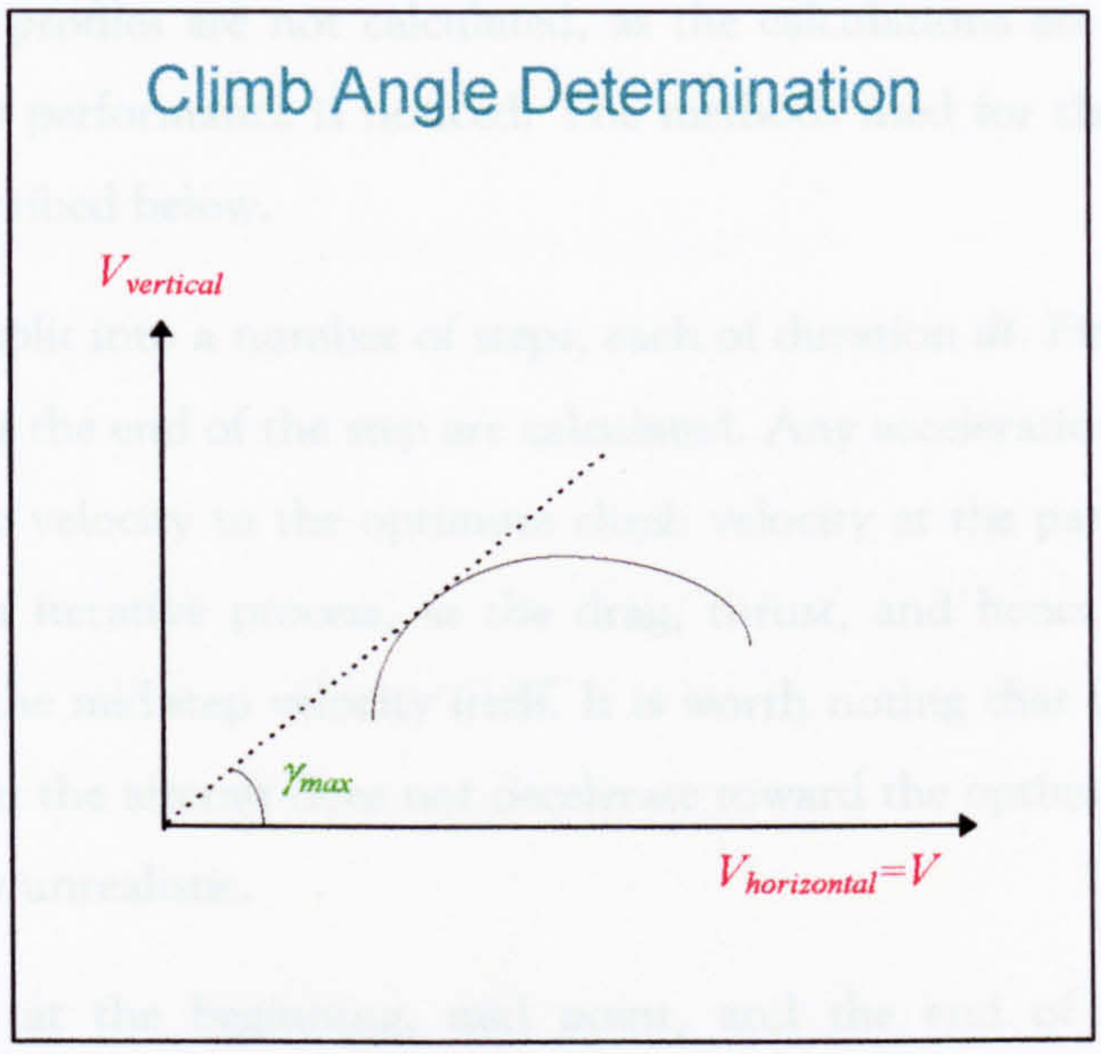


Figure 12.2 - Determination of maximum climb angle

This diagram illustrates that the solution of the maximum climb angle is found from the straight line of gradient γ_{max} which intercepts the plot of the vertical velocity versus horizontal velocity at a tangent. Using the fact that $V_v = V\sin\gamma$, this can be substituted into equation 8.26 and this can be solved to find an expression for V which provides convergent roots. This expression for V gives the velocity at which the climb angle is a maximum:-

$$V_{\gamma\,max} = \frac{2W}{\rho S_{ref}}\sqrt{\frac{K}{C_{D0}}} \tag{8.29}$$

The fact that there is a particular velocity for each flight condition that gives an optimum climbing velocity suggests that the best climb rate may in some cases be achieved when the aircraft is allowed some acceleration so that it can achieve this optimum velocity. Therefore a number of profiles are calculated, each with a different proportion of the excess power being applied for acceleration rather than climb. The best profile is then chosen as the desired climb profile. Twenty profiles are calculated using the following relationship:-

$$\frac{dV}{dt} = \phi_{acc\,j} \frac{T - D}{W} \tag{8.30}$$

where

j=1 to 21

$$\phi_{acc\,j} = \frac{j-1}{20} \tag{8.31}$$

In reality all twenty profiles are not calculated, as the calculations are ceased as soon as a degradation in climb performance is noticed. The methods used for the evaluation of each climb profile are described below.

The climb profile is split into a number of steps, each of duration *dt*. Firstly, the velocities at the start-point and at the end of the step are calculated. Any acceleration potential is used to guide the end of step velocity to the optimum climb velocity at the particular condition for that step. This is an iterative process, as the drag, thrust, and hence the optimum climb velocity depend on the mid-step velocity itself. It is worth noting that the method has been constrained such that the aircraft does not decelerate toward the optimum climb velocity, as this would be wholly unrealistic.

Once the velocities at the beginning, mid point, and the end of the step have been determined, this means that the range and altitude increment of each step can then be calculated using the following equations, where the lift force has been assumed to be equal to the aircraft weight.

$$\gamma_i = \sin^{-1}\left(\frac{T - D}{W} - \frac{1}{g}\frac{dV}{dt}\right) \tag{8.32}$$

where dV/dt is the acceleration over the step

$$\Delta R_i = V_{mid\,i} \cos\gamma_i dt \tag{8.33}$$

$$\Delta h_i = V_{mid\,i} \sin\gamma_i dt \tag{8.34}$$

12 .5 Climb at Constant Calibrated Airspeed

This is an alternative climb profile, in which the aircraft is assumed to climb at a constant calibrated airspeed, and provides a much simpler approach than the climb profile of section 12.4. For each step there is an assumed altitude increment Δh based on the desired accuracy. Therefore:-

$$h_{i+1} = h_i + \Delta h \tag{8.35}$$

Since the calibrated airspeed is constant, the increase in altitude means an increase in Mach number, and hence true velocity. The maximum Mach number achievable during the climb is set by the user. Therefore, the climb path angle (γ) for each step is given by equation 8.36, where the drag has been calculated on the basis of the lift force being approximately equal the aircraft weight.

$$\gamma = \sin^{-1}\left(\frac{T-D}{W} - \frac{1}{g}\frac{dV}{dt}\right) \tag{8.36}$$

however, since the time increment for each step is given by:-

$$dt = \frac{\Delta h}{V \sin\gamma} \tag{8.37}$$

the equations must be iterated to find a convergent solution of γ and dt. Once these parameters are known, then the range increment, and the fuel consumed over each step can be calculated.

12 .6 Acceleration

The aircraft is assumed to accelerate at a constant altitude. The final target velocity can be expressed as either a calibrated airspeed, or as a Mach number, and will automatically be identified. The lift is assumed to equal the weight, and the drag is calculated accordingly. The calculation is performed over a discrete number of steps with time increment Δt .This means that at each step the acceleration is given by:-

$$\frac{dV}{dt} = \left(\frac{T-D}{W}\right)g \tag{8.38}$$

Therefore

$$V_{i+1} = V_i + \frac{dV}{dt}\Delta t \tag{8.39}$$

12 .7 Cruise

The cruise portions are split into a number of time steps, and are assumed to occur at constant altitude and Mach number. The lift is assumed to equal the weight, and the drag is calculated accordingly. The thrust is given by:-

$$T = D \tag{8.40}$$

The fuel consumption can then be determined, and the range increment is calculated using the Breguet equation:-

$$\Delta R = \frac{V}{C}\frac{L}{D}\ln\left\{\frac{W_{total}}{W_{total} - \Delta W_{fuel}}\right\} \tag{8.41}$$

12 .8 Deceleration

The deceleration segment for the aircraft uses the same approach as the acceleration segment, but with the thrust set to an idle value rather than a maximum thrust value. For the deceleration segment it is possible to specify the final target velocity in terms of calibrated airspeed, Mach number, or in terms of a multiple of a stall velocity. When the user specifies the velocity in terms of a multiple of a stall velocity, the user also specifies the stall velocity, and the altitude at which this velocity is valid, which allows the descent lift coefficient to be calculated. This allows the descent/deceleration portion of the flight to be controlled so that it conforms to the approach and landing regulations, and gives more realistic values of lift coefficient.

This means that the lift value for the deceleration is assumed to be equal to the weight, unless the stall velocity approach has been specified, in which case the lift coefficient is determined from the stall velocity using:-

$$C_L = \frac{W_{total}}{0.5\rho_{h\,stall} S_{ref} V_{stall}^{\,2}} \tag{8.42}$$

The drag and the idle thrust are then calculated, and the deceleration is calculated using equation 8.38. This means that the range, fuel consumption, and velocity decrement over each step are known.

12 .9 Descent

The analysis of the descent segment is performed in a similar manner to the climb at constant calibrated airspeed. The descent is split into a number of discrete steps of height Δh. The upper limit of calibrated airspeed during the descent is set by the user, either directly, or indirectly via a multiple of a stall velocity. If the multiple of a stall velocity is specified, then the stall velocity itself is also specified, and the altitude at which the stall velocity occurs is assumed to be the final descent altitude. As in the deceleration segment, the specification of the velocity in this way infers a value of descent lift that would otherwise

be assumed equal to the weight. When the velocity is specified in this way, the calibrated airspeed which corresponds to the multiple of the stall velocity can be calculated, and this is used as the calibrated airspeed upper limit.

As with the climb at constant calibrated airspeed, the change in altitude over the step means a change in Mach number. The calibrated airspeed is calculated such that if the initial value was below the specified limit, then its allowed to increase until the limit is reached, whereupon it is held constant at that limit.

The calculation of the descent path depends whether the user has specified a constrained or an unconstrained descent path angle. For an unconstrained descent, the engine thrust is assumed to be idle and the minimum path angle can be calculated accordingly from the relevant thrust, drag, and weight values in the same manner as the climb path angle (see 12.5). If however, the user has specified a particular descent path angle (as specified in approach regulations), then it is possible to calculate the required thrust to maintain this angle of descent using equation 8.36.

As many of the variables are inter-dependant, it is necessary in both cases to iterate the equations to find the convergent solution. Once this has been done, the range, fuel, and time increments over each step can be calculated.

12 .10 LOITER

The calculation of the aircraft loiter performance is done using exactly the same methods as the cruise performance, the only difference being that the duration of the segment is limited by time rather than distance.

12 .11 ABORTED LANDING

The only calculations that need to be made to simulate an aborted landing are to predict the change in fuel that occurs as a result of this type of manoeuvre. From analysis of the detailed landing calculations it was found that a reasonable approximation could be given by:-

$$\frac{\Delta W_{fuel}}{W_{fuel}} = 0.03 \tag{8.43}$$

12 .12 LANDING

For the correct calculation of the landing distance, the segment preceeding the 'approach' segment should be a descent to 50ft, at a velocity of 1.3 times the landing stall velocity. This gives the correct initial conditions for the final approach. The calculation of the landing segment is essentially analogous to the reverse of the takeoff segment. The landing is split into four segments which are described below:-

12 .12 .1 FINAL APPROACH

This is the final descent of the aircraft to a height h_{min} as specified by the user in the 'approach' segment. The descent angle is assumed to be limited to -3 degrees, and the descent velocity is 1.3 times the stall velocity. The descent performance is then calculated using the methods of 12.8.

12 .12 .2 FLARE

The 'flare' portion of the landing is the reverse of the 'transition' portion of the takeoff segment and a similar method is used. For this analysis the lift coefficient throughout this segment is assumed to be constant, and equal to the landing lift coefficient.

$$C_{L\,flare} = C_{L\,la} \tag{8.44}$$

and

$$V_{stall} = \frac{V_{initial}}{1.3} \tag{8.45}$$

and using the fact that the landing velocity must be at least 1.15 times the stall velocity

$$V_{final} = \frac{V_{initial}}{1.3} 1.15 \tag{8.46}$$

at the ith step

$$V_i = V_{initial} + \left(V_{final} - V_{initial}\right)\frac{(i-1)}{21} \tag{8.47}$$

It has been assumed that the flight path angle during flare is given by:-

$$\gamma_i = -3 + 3\left(\frac{i-1}{20}\right)^{0.95} \quad \text{(deg)} \tag{8.48}$$

the load factor (n) is assumed to be equal to:-

$$n = \left(\frac{(V_i + V_{i+1})/2}{V_{stall\ initial}} \right) \tag{8.49}$$

and from Raymer[90], the radius of the circular path is given by equation 8.22. This means that the height decrement and range increment can be calculated using equations 8.24 and 8.25.

12 .12 .3 FREE ROLL

It is assumed that once the aircraft has touched down it will roll freely for 2 seconds (Raymer[90]) before the brakes or thrust reversers are applied. The velocity over this period is assumed to be constant, the additional distance travelled and time taken are added to the cumulative values for these parameters.

12 .12 .4 GROUND ROLL (WITH THRUST REVERSAL)

It has been assumed the thrust reversal (where applicable) is used to slow the aircraft down from its landing velocity to a velocity of 26m/s (Raymer[90]). The equations used are the exact equations used to describe the takeoff ground roll (eqns. 8.7 and 8.8) with μ=0.4 (the ground roll resistance with the brakes applied). The segment is split into 21 steps where the velocity at each step is given by:-

for the *i*th step

$$V_i = V_{la} + (26 - V_{la}) \frac{(i-1)}{21} \tag{8.50}$$

The thrust with thrust reversers is given by the equation below (Raymer[90]).

$$T = -\frac{T_0}{2.5} N_e \tag{8.51}$$

The thrust without thrust reversers is assumed to be idle.

It has been assumed that the spoilers and air-brakes are deployed 1.5 seconds into this segment of the ground roll. The resulting drag increment and reduced lift are given by equations 8.52 and 8.53 below. Before the spoilers and air-brakes are deployed the lift coefficient is assumed to be equal to the ground roll lift coefficient.

$$C_{D\,spoiler} = \frac{1.6\left(S_{spoiler} + S_{airbrake}\right)}{S_{ref}} \tag{8.52}$$

$$C_L = 0.1 C_{L_{gr}} \tag{8.53}$$

This information allows the range, time, and fuel increments, to be calculated for each step.

12 .12 .5 Ground Roll (without thrust Reversal)

The final portion of the ground roll where the velocity reduces from 26m/s to zero is assumed to occur without the application of thrust reversal. The same method as described above is used, with the thrust assumed to be idle. The landing distance is then the sum of the four component distances.

12 .13 FAR Landing Distance

The FAR landing distance is calculated using the method above, with the weight at the beginning of the approach being equal to 85% of the takeoff weight, which represents the maximum allowable landing weight of the aircraft. This landing distance is then multiplied by a safety factor of 1.666.

12 .14 Balanced Field Length

The balanced field length is defined as the takeoff distance required to reach an altitude of 35ft, when an engine fails at the 'decision' speed V_{dec}. This speed is defined as the speed at which the distance required to takeoff exactly equals the distance to brake to a halt. The balanced field length is calculated using the following technique.

An initial estimate is made of the decision speed V_{dec}. The ground roll distance up to the engine failure is calculated using the takeoff ground roll method (12.3.1). The ground roll distance required to reach the takeoff velocity after the engine has failed is also calculated using the takeoff ground roll method (12.3.1), but with the thrust of the aircraft reduced accordingly. It has been assumed that after the engine fails there is a transient period where the thrust of that engine dies off linearly to zero over a period of four seconds. The rotation, transition, and initial climb to 35ft, of the aircraft are then calculated at the reduced thrust conditions, using the methods of 12.3.

The distance required to brake to a halt is estimated using similar methods as used for the landing distance. It is assumed that the brakes are applied at decision speed, with the spoilers and air brakes being applied 1.5 seconds later. The engine thrust is again assumed to die away from its takeoff value to its idle value over a period of four seconds, the regulations specify that the use of thrust reversal is not applicable for this calculation.

Once the two distances for the takeoff to 35ft and the brake to a halt have been calculated, an iteration for the correct decision speed is carried out. This decision speed is varied until the two distances are exactly equal. The balanced field length is then equal to this length. The balanced field length and 1.15 times the takeoff length are then compared, and the greater of the two is considered to be the FAR takeoff distance.

13 .Design Tool Methods

The methods used within the fuselage sizing tool, the optimisation routines, and the correlation routines, are described within this chapter.

13 .1 Fuselage Sizing

The fuselage sizing routines which perform the necessary calculations for the Fuselage Sizing Window can be split into those that are concerned with the 2-dimensional cross-section layout, and those that are concerned with the 2-dimensional seating plan layout.

13 .1 .1 Cross-section Layout

The physical dimensions of the fuselage cross-section is mainly determined by the chosen seating arrangements, seat sizes, aisle widths, and cabin heights. The way in which these choices influence the cross-section, and any pertinent assumptions are described below for each type of cross-section.

13 .1 .1 .1 Elliptical Single Deck

The elliptical (ovoid) fuselage cross-section is assumed to be of the form shown below in figure 13.1.

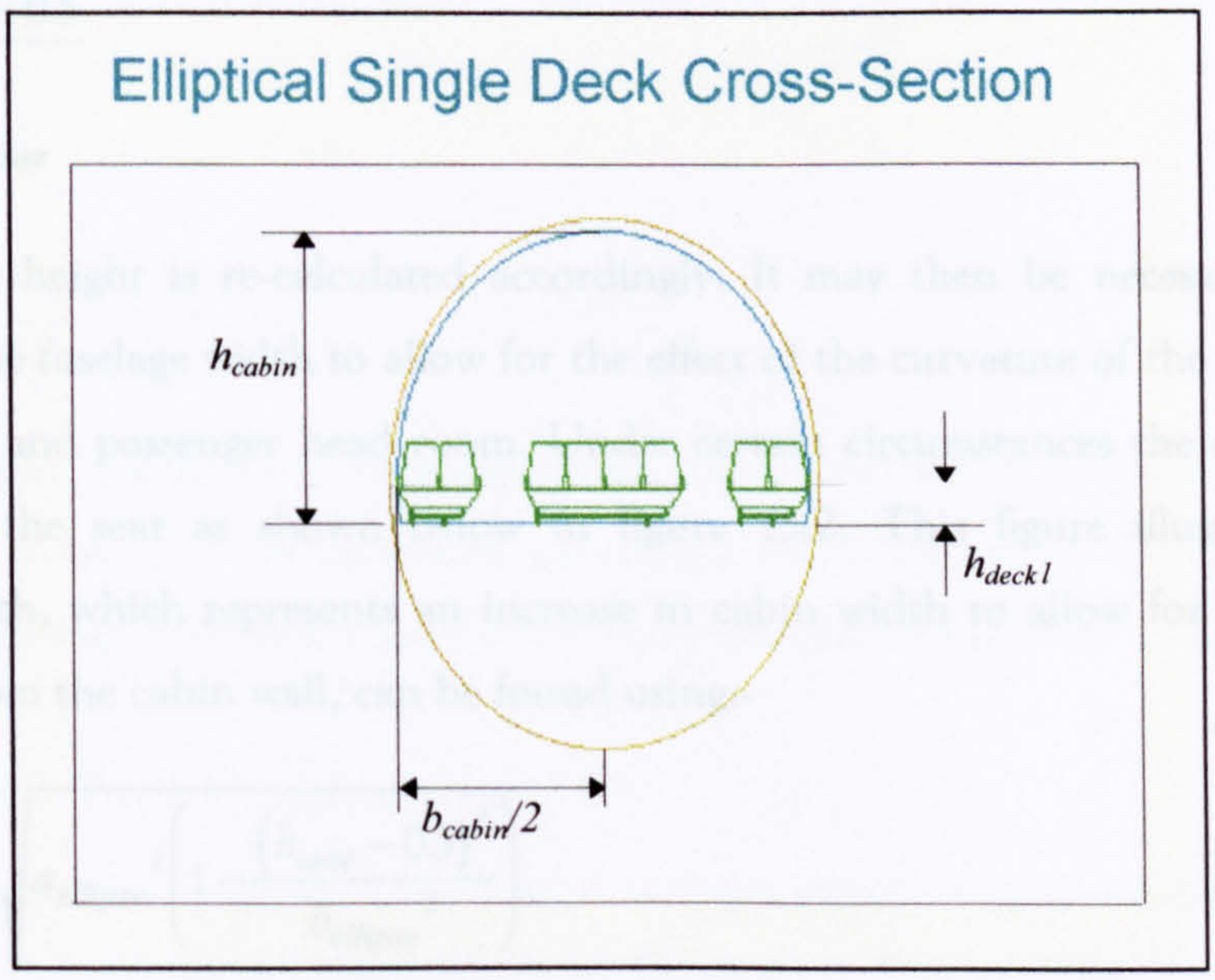


Figure 13.1- Layout of elliptical single deck fuselage cross-section

The methods and assumptions used in the determination of the fuselage cross-section are described below. The most important assumptions being that the vertical location of the

widest part of the cabin is along the centre line of the ellipse, and that this maximum width occurs at a height h_{deck1} from the bottom of the cabin floor. This means that h_{deck1} is defined as the vertical distance between the cabin floor and the centre line of the main ellipse. Analysis of the seat geometry shows that the value of this height is approximately equal to the height of the midpoint of the armrests above the cabin floor, and is assumed to be equal to 0.5m.

For each class, the cabin width necessary to accommodate the chosen layout is calculated by summing the widths of the selected number of seats for the particular seat sizes, and adding the necessary aisle widths. The maximum of these widths is then taken to be the initial estimate of the cabin width (b_{cabin}). This means that the initial estimate of the cabin ellipse coefficients ($a_{ellipse}$ and $b_{ellipse}$) can be estimated:-

$$a_{ellipse} = \frac{b_{cabin}}{2} \tag{9.1}$$

$$b_{ellipse} = a_{ellipse}\left(\frac{b}{a}\right)_{fuse} \tag{9.2}$$

These initial estimates must first be checked to ensure that they provide adequate cabin height.

If $b_{ellipse} < h_{cabin} - 0.5$ then

$$a_{ellipse} = \frac{h_{cabin} - 0.5}{\left(\frac{b}{a}\right)_{fuse}} \tag{9.3}$$

and the ellipse height is re-calculated accordingly. It may then be necessary to make a correction to the fuselage width to allow for the effect of the curvature of the fuselage on the seat placement and passenger head room. Under certain circumstances the cabin wall may intersect with the seat as shown below in figure 13.2. This figure illustrates that the correction length, which represents an increase in cabin width to allow for the seats to be placed away from the cabin wall, can be found using:-

$$l_{h\,seat} = a_{ellipse} - \sqrt{{a_{ellipse}}^2\left(1 - \frac{(h_{seat} - 0.5)^2}{{b_{ellipse}}^2}\right)} \tag{9.4}$$

From the geometry of the seats, it is known that:-

$$l_{correct} = l_{h\,seat} - 2b_{armrest} \tag{9.5}$$

where the armrest width ($b_{armrest}$) is known.

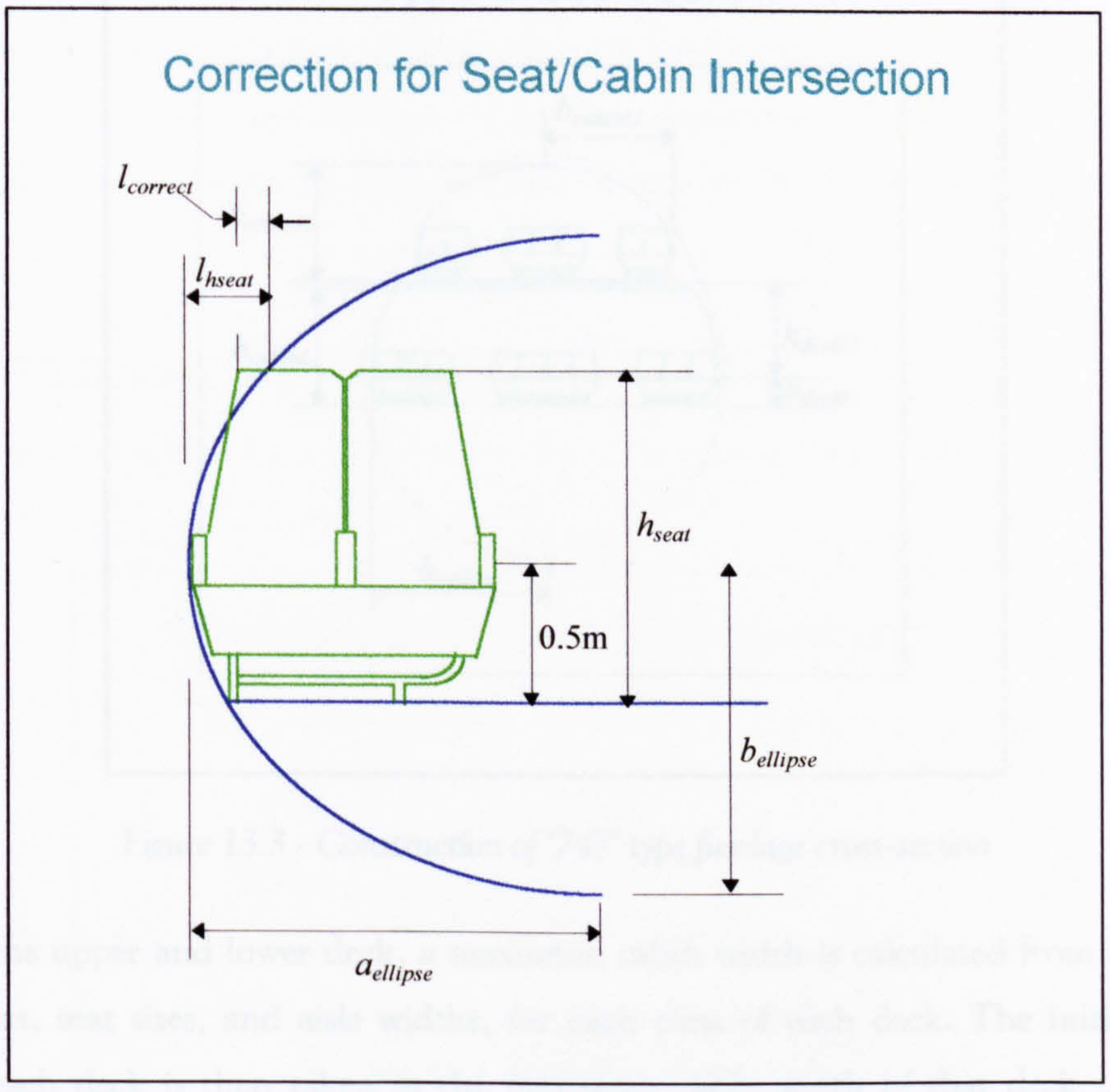


Figure 13.2 - Determination of correction length for cabin/seat intersection

Therefore, the cabin can be re-sized to allow for this extra distance between the cabin wall and the end seats.

if $b_{cabin} + 2l_{correct} > 2a_{ellipse}$ then

$$a_{ellipse} = \frac{\left(b_{cabin} + 2l_{correct}\right)}{2} \tag{9.6}$$

The ellipse height coefficient is then calculated using equation 9.3. The external fuselage ellipse coefficients can then be calculated assuming a wall thickness of 12.5cm. As the cabin and therefore fuselage dimensions are known, the cross-section can then be drawn.

13 .1 .1 .2 747-Type Cross-section

An example of a 747-type cross-section with an upper 'bubble' smoothly attached to the main elliptical section is shown below in figure 13.3. The external dimensions of this type of fuselage are illustrated in figure 8.8.

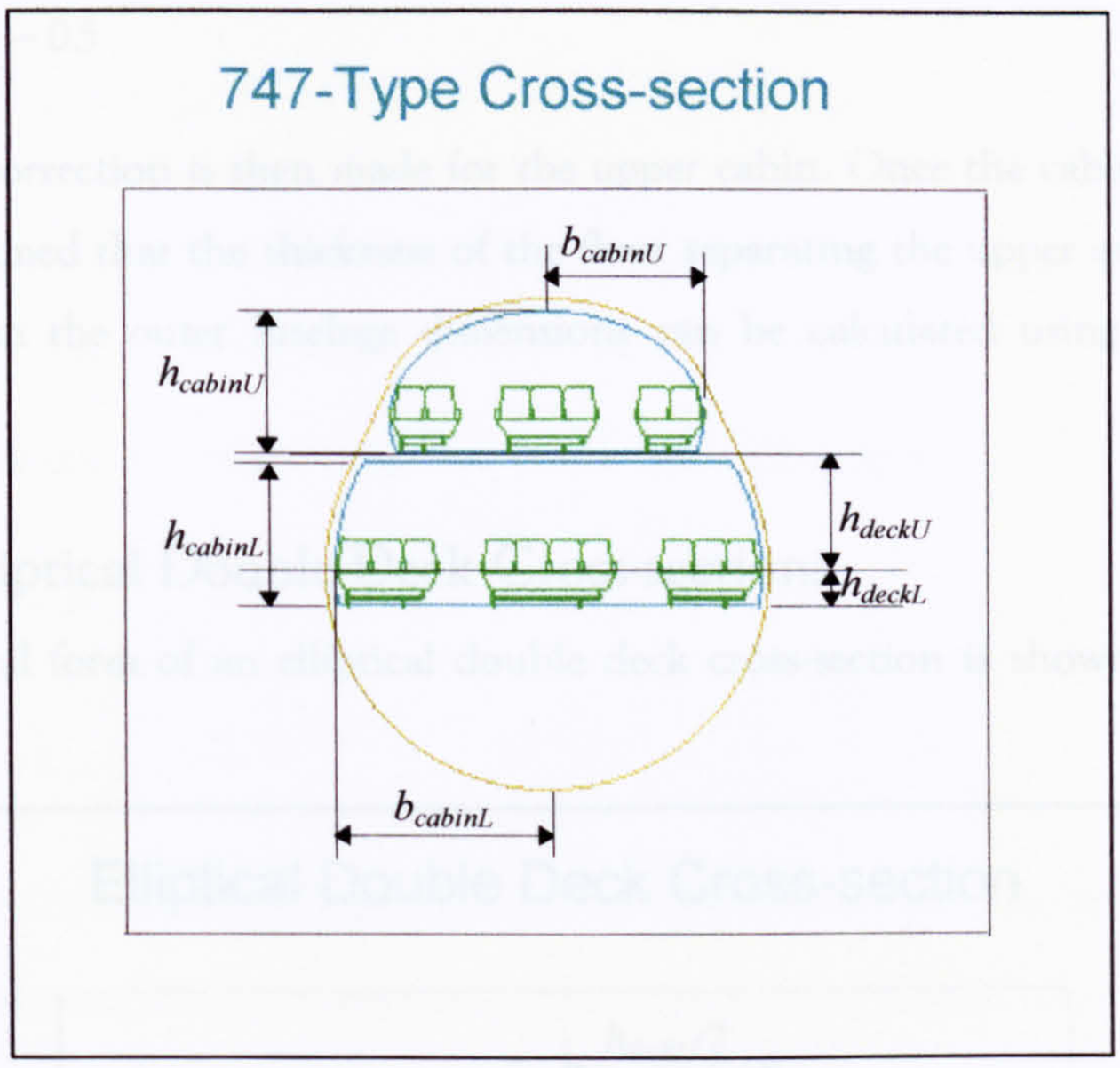


Figure 13.3 - Construction of '747' type fuselage cross-section

For both the upper and lower deck, a maximum cabin width is calculated from the seating arrangement, seat sizes, and aisle widths, for each class of each deck. The initial baseline width of each deck is then taken as the maximum cabin width of that deck. Again it is assumed that for each deck the floor is vertically situated a distance of 0.5m below the line of maximum width. From these initial estimates of maximum cabin width ($b_{cabin\,L}$ and $b_{cabin\,U}$) the following assumptions can be made-

$$a_{ellipse_L} = \frac{b_{cabin\,L}}{2} \tag{9.7}$$

$$b_{ellipse_L} = a_{ellipse_L}\left(\frac{b}{a}\right)_{fuse} \tag{9.8}$$

checking that this is compatible with the desired lower cabin height:-

If $b_{ellipse_L} < h_{cabin\,L} - 0.5$ then

$$a_{ellipse_L} = \frac{h_{cabin\,L} - 0.5}{\left(\frac{b}{a}\right)_{fuse}} \tag{9.9}$$

A correction is then made for any seat/cabin intersection using the equations of 9.4 and 9.5. The dimensions of the upper cabin are then calculated assuming that:-

$$a_{ellipse_U} = \frac{b_{cabinU}}{2} \tag{9.10}$$

$$b_{ellipse_U} = h_{cabin_U} - 0.5 \tag{9.11}$$

The seat/cabin correction is then made for the upper cabin. Once the cabin dimensions are known, it is assumed that the thickness of the floor separating the upper and lower cabin is 12.5cm, and then the outer fuselage dimensions can be calculated using the methods of 8.2.2.

13 .1 .1 .3 Elliptical Double Deck Cross-sections

The general form of an elliptical double deck cross-section is shown below in figure 13.4.

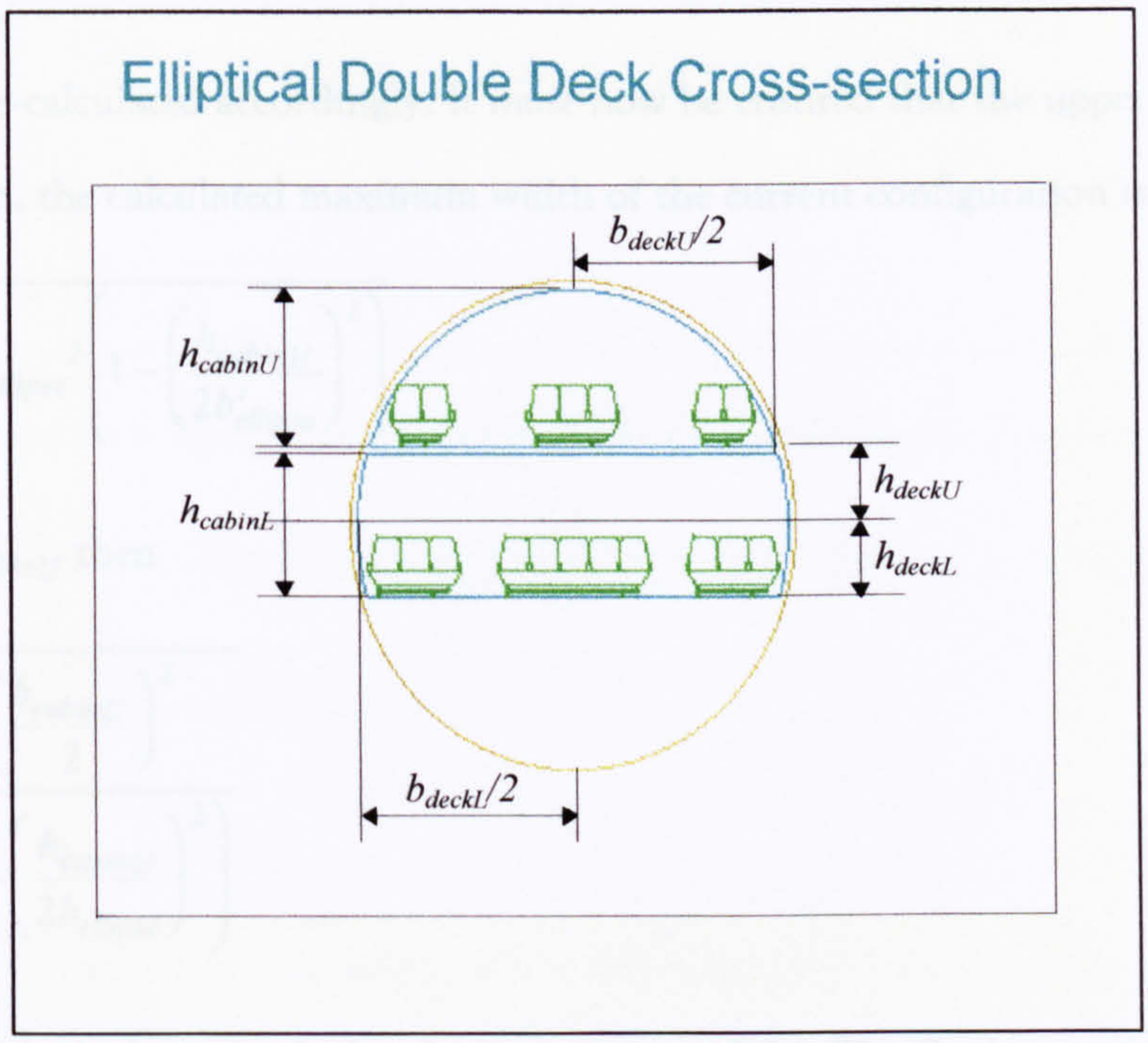


Figure 13.4 - Construction of elliptical double deck fuselage cross-section

Again, initial estimates of the maximum cabin widths for both the upper and lower deck are made (b_{cabinL} and b_{cabinU}), based upon the selected seat arrangement, seat sizes, and aisle widths for each class. The location of the lower cabin for this configuration is such that its centre line is coincident with the ellipse centre line.

$$h_{deck\,L} = \frac{1}{2} h_{cabin\,L} \tag{9.12}$$

This means that an initial estimate of the internal cabin ellipse parameters is given by the equations below, noting that the perimeters of both the lower and upper cabins lie on the path of the same ellipse.

$$a_{ellipse} = \sqrt{\left(\frac{b_{cabin\,L}}{2}\right)^2 + h_{deck\,L}{}^2\left(\frac{b}{a}\right)^2_{fuse}} \tag{9.13}$$

$$b_{ellipse} = a_{ellipse}\left(\frac{b}{a}\right)_{fuse} \tag{9.14}$$

Checking that this gives enough height for the desired upper deck:-

If $b_{ellipse} < \frac{h_{cabin\,L}}{2} + h_{cabinU} + 0.125$ then

$$b_{ellipse} = \frac{h_{cabin\,L}}{2} + h_{cabinU} + 0.125 \tag{9.15}$$

and $a_{ellipse}$ is re-calculated accordingly. It must now be ensured that the upper deck provides sufficient width, the calculated maximum width of the current configuration is given by:-

$$b'_{cabinU} = 2\sqrt{a'_{ellipse}{}^2\left(1 - \left(\frac{h_{cabinU}}{2b'_{ellipse}}\right)^2\right)} \tag{9.16}$$

If $b'_{cabinU} < b_{cabinU}$ then

$$a_{ellipse} = \sqrt{\frac{\left(\frac{b_{cabinU}}{2}\right)^2}{\left(1 - \left(\frac{h_{cabinU}}{2b_{ellipse}}\right)^2\right)}} \tag{9.17}$$

The ellipse height is then re-calculated using equation 9.14. The final part of the calculation is to include the correction for any seat/cabin intersection as described previously. This is done for the upper deck using the methods of section 13.1.1.1. The final geometry is then known and can be drawn as necessary.

13 .1 .1 .4 Horizontal Double Bubble

The general form of the horizontal double bubble cross-section is illustrated below. The details of the external geometry are described in section 8.2.3. The initial estimate of the cabin width (b_{cabin}) is once again based upon the sum of the seat and aisle widths across the cross-section. It has been assumed that the external fuselage skin and the internal partition are all of thickness 12.5cm, and that again h_{deck}=0.5m. This means that an initial estimate of the diameter of each fuselage component is given by:-

$$D_{fuse} = \frac{\left(2b'_{cabin} + \left(3 \times 0.125\right)\right)}{1 + \phi_{db}} \tag{9.18}$$

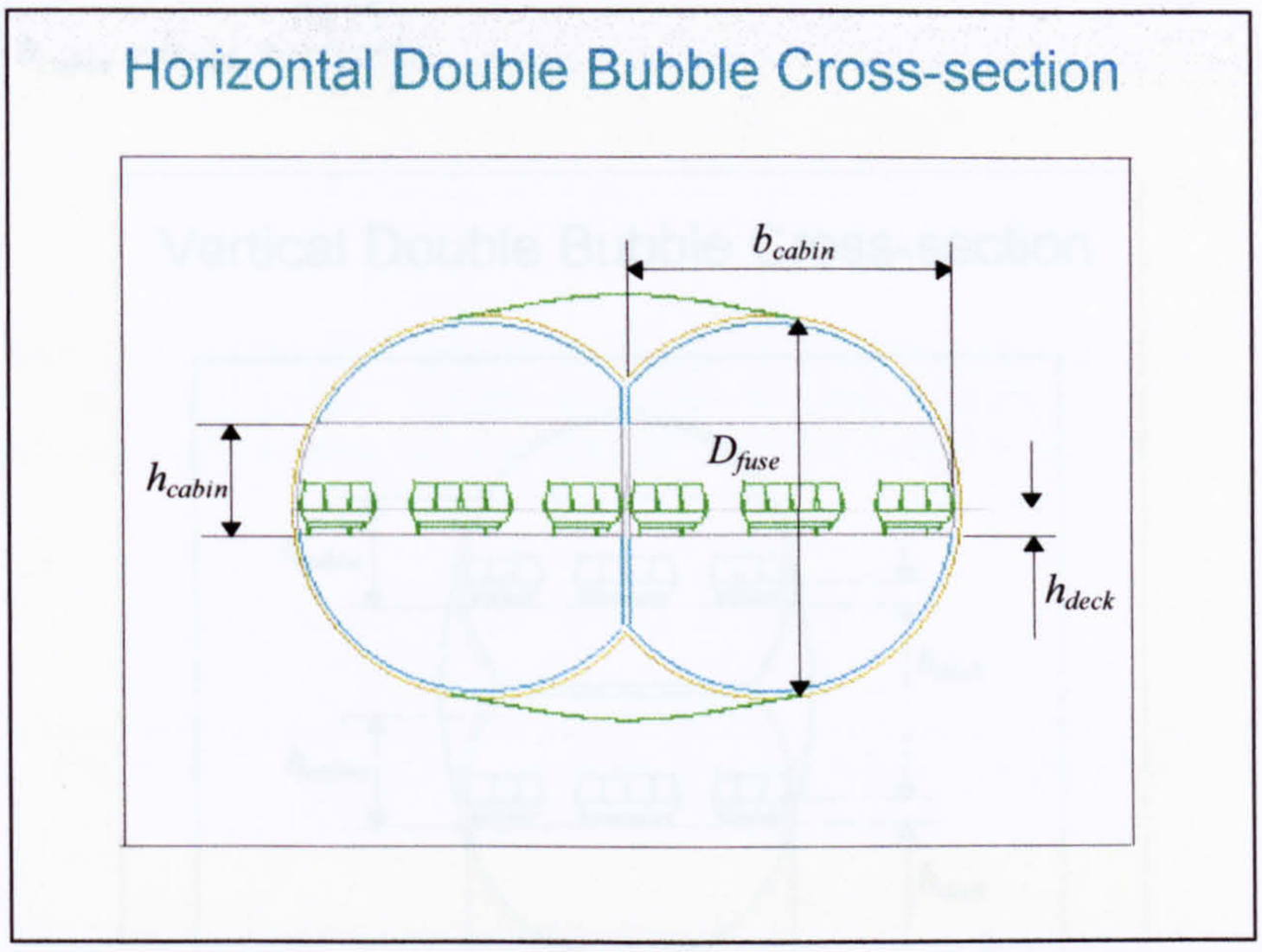


Figure 13.5- Construction of horizontal double bubble fuselage cross-section

This estimation must be checked to ensure that it provides adequate cabin height.

$$\text{If } h_{cabin} - h_{deck} > \frac{D_{fuse}}{2} - 0.125 \text{ then}$$

$$D_{fuse} = 2\left(h_{cabin} - h_{deck} + 0.125\right) \tag{9.19}$$

No cabin/seat intersection is possible, since the cabin wall at the height of the seats is practically vertical. Now that the diameter of each fuselage portion is known, and since the join ratio (ϕ_{db}) is set by the user, then the external geometry can be calculated using the methods of 8.2.3.

13 .1 .1 .5 Vertical Double Bubble Cross-section

Figure 13.6 below illustrates the general geometry of the vertical double bubble cross-section. The initial cabin width estimate (b_{cabin}) is calculated from the maximum of the sum of the seat and aisle widths for each class. Again, it has been assumed that h_{deck}=0.5m and the thickness of the cabin walls is 12.5cm. The initial estimate for the diameter of each fuselage is calculated using the following expression:-

$$D_{fuse} = b_{cabin} + \left(2 \times 0.125\right) \tag{9.20}$$

This estimate is then checked to ensure that it provides adequate cabin height.

$$\text{If } h_{cabin} - h_{deck} > \frac{D_{fuse}}{2}\phi_{db} - \frac{0.125}{2} \text{ then}$$

$$D_{fuse} = \frac{2}{\phi_{db}}\left(h_{cabin} - h_{deck} + \frac{0.125}{2}\right) \tag{9.21}$$

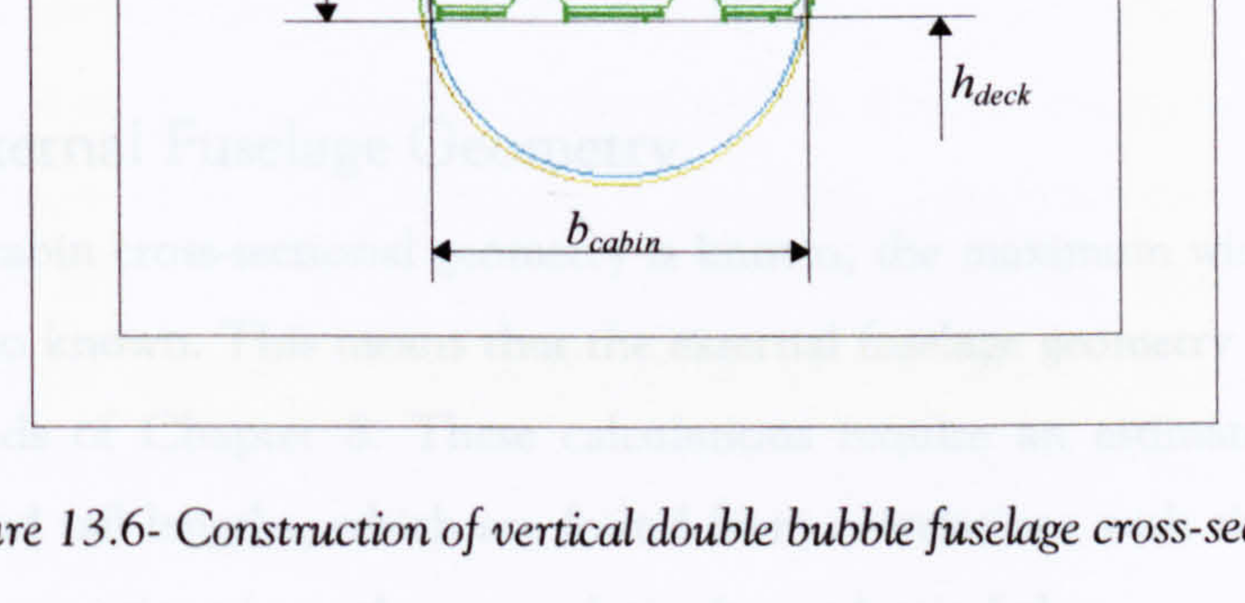


Figure 13.6- Construction of vertical double bubble fuselage cross-section

As for the horizontal double bubble, the diameter of each fuselage is now known and the complete external geometry can be calculated (using the methods of 8.2.4). No correction is made for any seat/cabin intersection as any intersection is not possible due to the circular nature of each fuselage portion.

13 .1 .2 SEATING PLAN

Once the fuselage cross-section has been determined, it is possible to calculate the detailed seating plan of the aircraft, including toilets, galleys, and emergency exits, an example of which is shown below in figure 13.7. Deriving methods for the description of the internal arrangement proved to be a challenging task. The methods needed to be flexible enough to deal with all fuselage types, and to successfully deal with the enormous range of possible configurations that could be entered by the user. The final method provides excellent results, yet as this is a very complex and laborious process it needed to be optimised to operate as swiftly as possible. This has meant that rather than indulging in an iterative approach which would ultimately provide the most accurate layout, an inventive 'single execution' approach has been used which does not need iteration, yet provides results

that are only marginally less reliable. The main steps carried out for this calculation are described below for a single deck elliptical fuselage. Modifications to these methods for other fuselage types are discussed later.

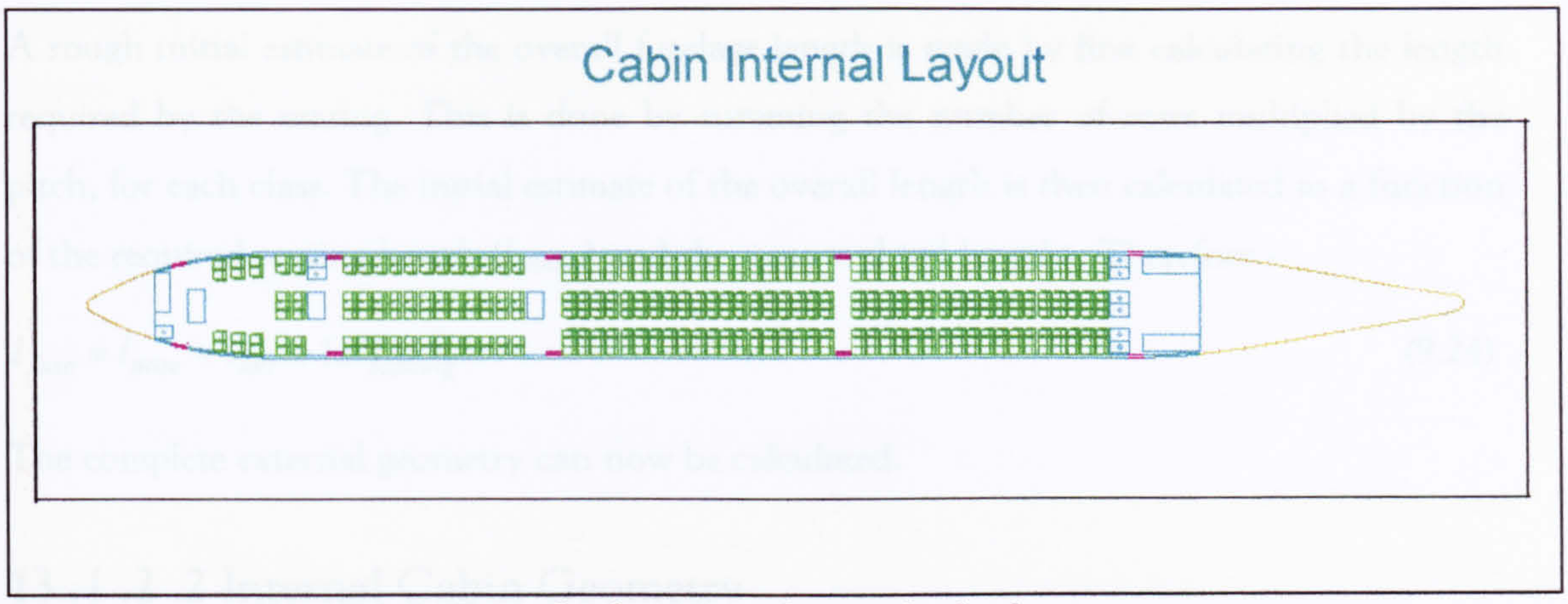


Figure 13.7 - Example of automated internal cabin layout generation

13 .1 .2 .1 External Fuselage Geometry

Since the cabin cross-sectional geometry is known, the maximum width and height of the fuselage is also known. This means that the external fuselage geometry can be calculated using the methods of Chapter 8. These calculations require an estimate of the fuselage planform nose and tail lengths, which are found from correlations with the fuselage width. The data and the equations from these correlation's are shown below.

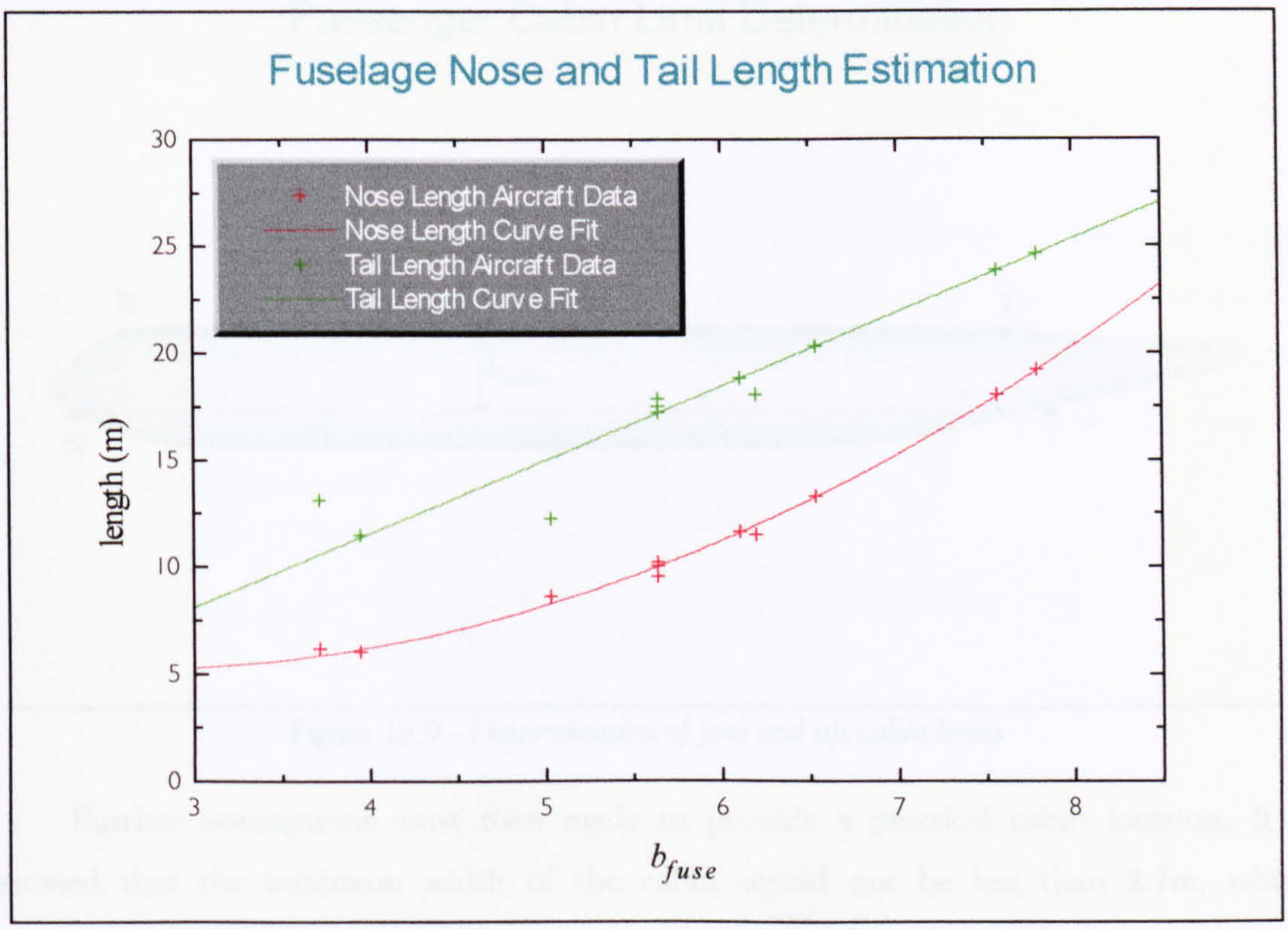


Figure 13.8 - Estimation of nose and tail lengths of the fuselage

$$l_{nose} = 0.517 b_{fuse}^{\ 2} - 2.68 b_{fuse} + 8.67 \quad (9.22)$$

$$l_{tail} = 3.45 b_{fuse} - 2.26 \quad (9.23)$$

A rough initial estimate of the overall fuselage length is made by first calculating the length required by the seating. This is done by summing the number of rows multiplied by the pitch, for each class. The initial estimate of the overall length is then calculated as a function of the required seating length ($l_{seating}$) and the nose and tail lengths. Therefore:-

$$l_{fuse} = l_{nose} + l_{tail} + 1.1 l_{seatimg} \quad (9.24)$$

The complete external geometry can now be calculated.

13 .1 .2 .2 Internal Cabin Geometry

Since the fuselage geometry is now known, and the vertical position and height of the passenger cabin is also known, then the forward and aft limits of the passenger cabin can be calculated (see figure 13.9). The solutions of the lines describing the upper and lower longitudinal cabin limits (the green and red lines below) and the curves making up the fuselage nose and tail sections are found (Point 'N' and 'T' below). For the forward cabin limit the furthest aft of these solutions (Points 'N') is used, and for the aft limit the most forward of these solutions (Points 'T') is used.

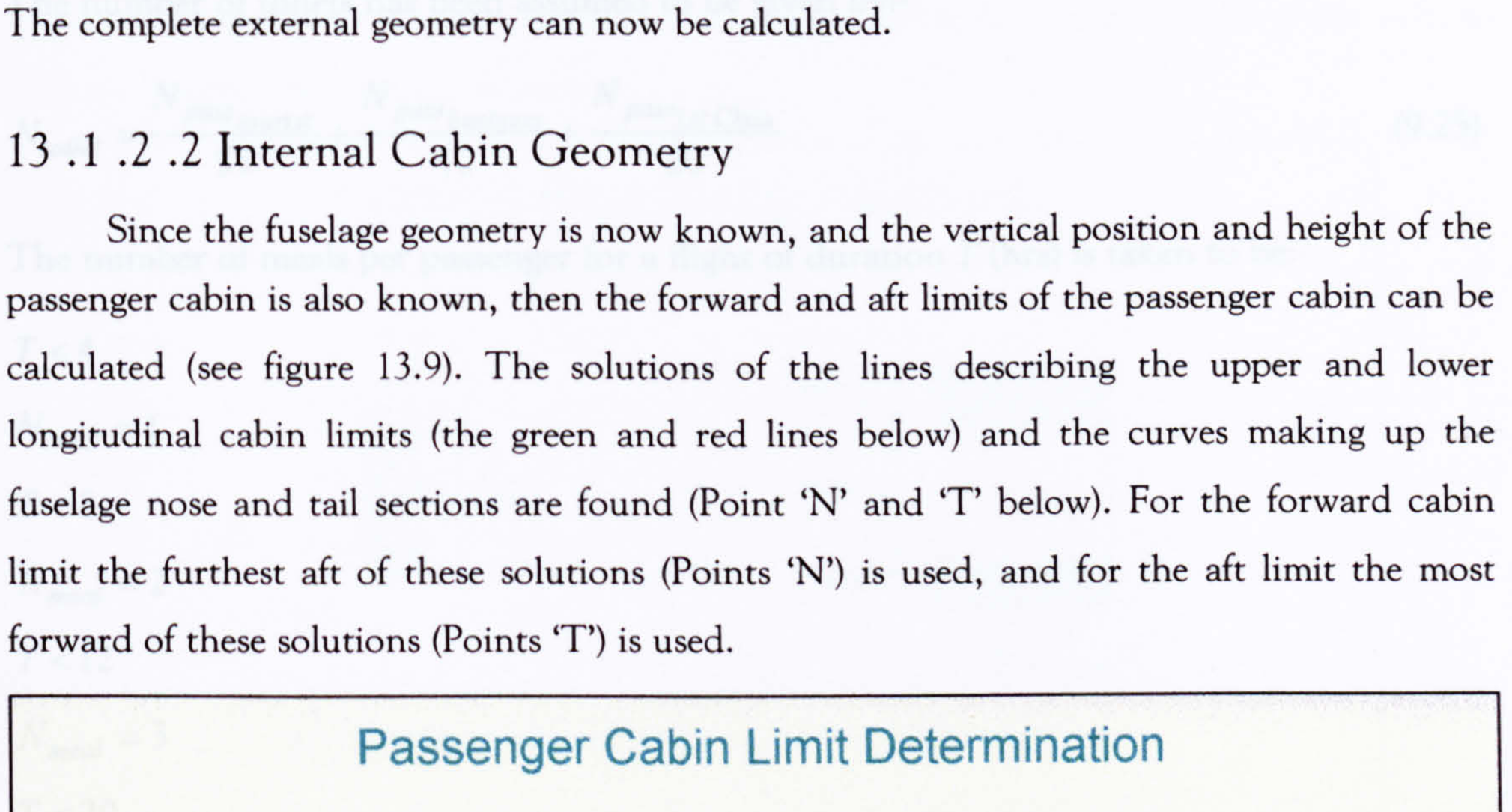


Figure 13.9 - Determination of fore and aft cabin limits

Further assumptions must then made to provide a practical cabin location. It is assumed that the minimum width of the cabin would not be less than 2.7m, which represents a reasonable lower bound for the fuselage width of a medium to large civil aircraft. So if the current fore or aft locations infer a width less than this value, then the

cabin is moved to a limit where the width is exactly equal to 2.7m. It has also been assumed that due to cockpit requirements the cabin will never be located less than a distance of 3.5m from the nose. Similarly, the tail limit of the cabin is chosen to allow adequate room for the integration of the horizontal and vertical tail surfaces into the fuselage. The cabin geometry is now known and the internal details can be estimated.

13 .1 .2 .3 Amenity Evaluation

The number of required amenities such as galleys, toilets, and emergency exits, is evaluated using the techniques described below.

The number of toilets has been assumed to be given by:-

$$N_{toilet} = \frac{N_{pass_{tourist}}}{55} + \frac{N_{pass_{business}}}{40} + \frac{N_{pass_{1st\ Class}}}{20} \tag{9.25}$$

The number of meals per passenger for a flight of duration T (hrs) is taken to be:-

$T < 4$

$N_{meal} = 1$

$T < 8$

$N_{meal} = 2$

$T < 12$

$N_{meal} = 3$

$T < 20$

$N_{meal} = 4$

The values of the average galley volume required for a single meal for a passenger of each class are taken from Roskam[82]. A correction is applied to the number of meals per passenger to account for the fact that due to the volume of fixed equipment, the total galley volume will not be absolutely proportional to the number of meals. The final expression for the total volume of galley required (ft^3) is then:-

$$\begin{aligned} V_{galley} = {} & 0.22 N_{pass_{tourist}} \left(1 + \frac{5}{6}(N_{meal} - 1)\right) + 0.45 N_{pass_{business}} \left(1 + \frac{5}{6}(N_{meal} - 1)\right) \\ & + 0.7 N_{pass_{1st\ Class}} \left(1 + \frac{5}{6}(N_{meal} - 1)\right) \end{aligned} \tag{9.26}$$

The number of emergency exits is calculated in line with the FAR regulations, and assumes that the first four exits are of type 1, and that subsequent exits required for passenger capacities of greater than 178 are of type A (see equation 5.23).

13 .1 .2 .4 Rear Galley Arrangement

The arrangement of the amenities at the rear of the cabin has been determined such that it provides a good usage of the available space, and is compatible with the layouts of existing aircraft. It is assumed that the very rear portion of the cabin is occupied by a galley, the planform of which depends on a number of factors, and is selected from the galley planforms shown below. The height of all the galleys is assumed to be 1.5m.

The planform chosen for the rear galley depends on a number of criteria such as the cabin width at this point, and the galley volume required. If the cabin width is less than 3.4m then a rectangular galley is used. The length of this galley (l_{galley}) will be the maximum value possible such that it does not exceed the cabin width, and such that the galley volume does not exceed the required volume.

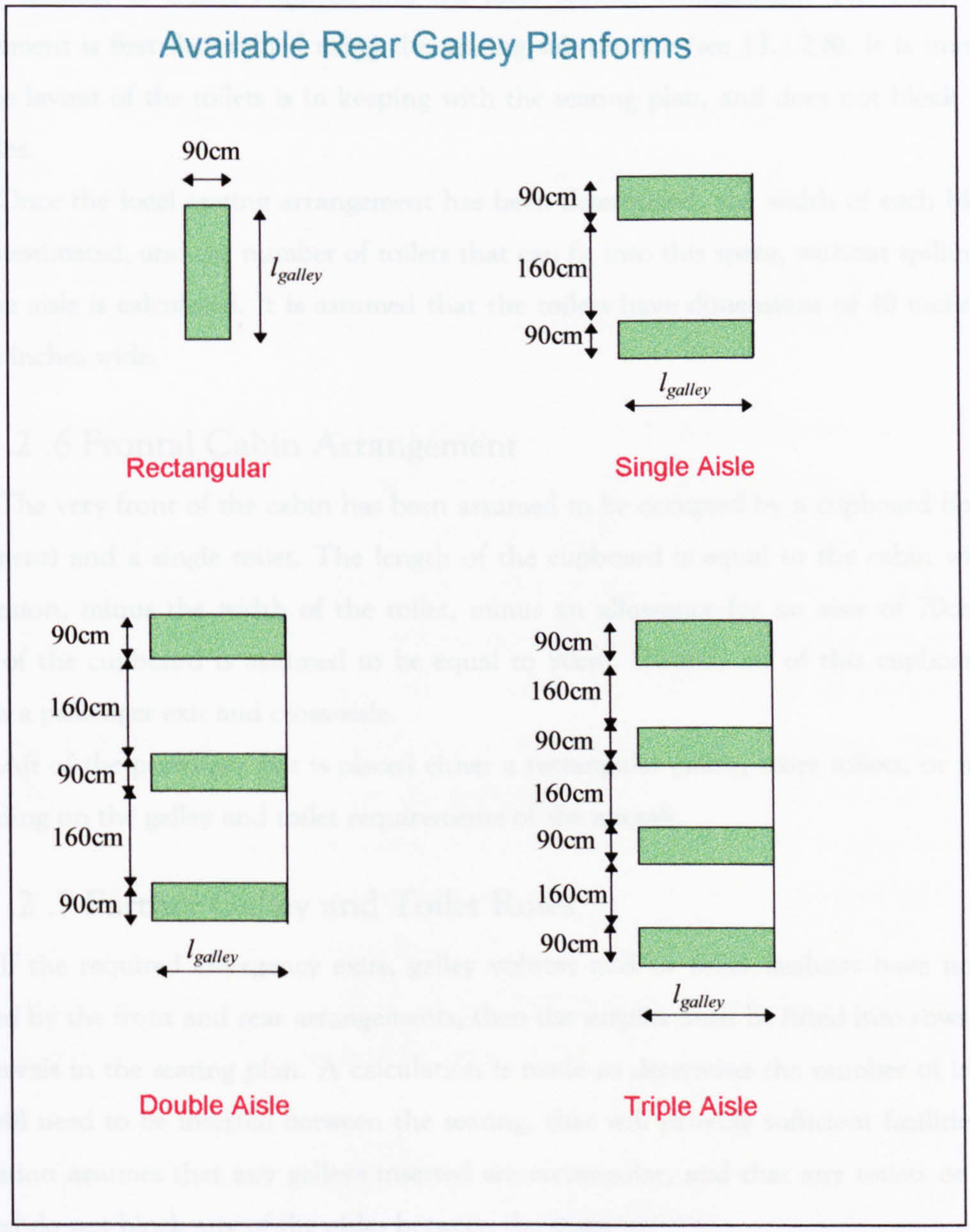


Figure 13.10 - Possible galley arrangements

If the cabin width is capable of supporting a galley with aisles, then the planform is selected that provides the maximum galley volume for this cabin width. The length of this type of galley is calculated from the galley volume required, but is limited to a value of 3m.

Once the rear galley geometry has been calculated, it is assumed that there is a passenger exit and cross-aisle directly forward of this galley. Forward of this cross-aisle there is assumed to be a row of toilets.

13 .1 .2 .5 Toilet Arrangement

The arrangement of the toilets at the rear of the aircraft uses the same procedures as for the arrangement of the toilets in any other part of the aircraft. The toilets are set in rows across the cabin width, with the number of toilets and their layout in these rows depending on the number of toilets required and the local seating arrangement. The local seating arrangement is first determined using the seating sub-routine (see 13.1.2.8). It is important that the layout of the toilets is in keeping with the seating plan, and does not block any of the aisles.

Once the local seating arrangement has been determined, the width of each block of seats is estimated, and the number of toilets that can fit into this space, without spilling over into the aisle is calculated. It is assumed that the toilets have dimensions of 40 inches long and 26 inches wide.

13 .1 .2 .6 Frontal Cabin Arrangement

The very front of the cabin has been assumed to be occupied by a cupboard (for crew equipment) and a single toilet. The length of the cupboard is equal to the cabin width at this station, minus the width of the toilet, minus an allowance for an aisle of 70cm. The width of the cupboard is assumed to be equal to 90cm. Directly aft of this cupboard and toilet is a passenger exit and cross-aisle.

Aft of the passenger exit is placed either a rectangular galley, more toilets, or neither, depending on the galley and toilet requirements of the aircraft.

13 .1 .2 .7 Further Galley and Toilet Rows

If the required emergency exits, galley volume and/or toilet facilities have not been satisfied by the front and rear arrangements, then the surplus must be fitted into rows placed at intervals in the seating plan. A calculation is made to determine the number of intervals that will need to be inserted between the seating, that will provide sufficient facilities. This calculation assumes that any galleys inserted are rectangular, and that any toilets or galleys inserted do not block any of the aisles between the seats.

13 .1 .2 .8 Seating Arrangement

As the cross-section of the fuselage is not constant along its length, the arrangement of the seats will also vary along its length to ensure the best use of available space. As the cabin width at any longitudinal station is known, the best seating arrangement at this point can be determined.

It has been assumed that the number of aisles within a particular class of seating cannot vary, and that the correction length to avoid seat/cabin intersection calculated in section 13.1.1 is constant along the fuselage. This means that for a given cabin width, number of aisles, and correction length, the configuration can be determined which provides the maximum number of seats of the set size along the particular width.

As the nose and tail portions of the cabin are already defined, the seating arrangements in these areas are determined first using this technique. The first class seats are positioned at the front of the aircraft, and the seats are positioned row by row in the nose until it is full. Once the required number of first class seats have been positioned, then the business class seats are positioned behind them. The tourist class seats are then positioned once the business class seating is completed.

Once the seating in the nose has been arranged, the seating in the tail portion is set. The seating is again positioned row by row, assuming however that all seating in the tail is tourist class.

The remaining seats are then positioned in the main section of the fuselage. This is the portion of the fuselage that has constant cross-section. The seats are positioned row by row, ensuring that any cross-aisles required for further galleys, toilets, or emergency exits, are inserted at regular intervals. As the length of this portion is not known before hand, and the spacing of cross-aisles must be based on an estimated length, then the cross-aisles can sometimes be placed somewhat irregularly. Although this will appear as an inconsistency in the drawing, it does not affect the fuselage length, or any other important aspect of the fuselage layout. The only way to solve this problem would be to adapt an iterative approach, however, as these calculations are some of the most time consuming within the Aircraft Design program, and as this problem does not impinge on any quantitative aspect of the design, it was decided against doing this.

Once all of the seats, and all of the facilities have been positioned, then the seating plan is complete, and the fuselage length is now known.

13 .1 .3 747-Type Fuselage Methods

The methods used to calculate the layout of both the upper and lower decks of this type of fuselage are identical in principle to those described above for a single deck fuselage.

The main difference in this case, is the fact that the length of the upper deck is a function of the overall length, which is not known until the layout is complete. Hence it is vital that the initial guess of the fuselage length in this case is as accurate as possible, as no iterations are applied. The equation shown below provides a more than adequate first estimate of the fuselage length:-

$$l_{fuse} = l_{nose} + l_{tail} + \frac{0.9 l_{seating}}{1 + \frac{b_{cabinU}}{b_{cabinL}} \phi_{fuse}} \tag{9.27}$$

The length of the upper cabin is calculated from this, and the external geometry is calculated using the methods of Chapter 8. The internal cabin geometry of each cabin is calculated using the method described in section 13.1.2.2.

The overall provisions for the aircraft are split between the upper and lower decks by assuming an estimated passenger split given by:-

$$N'_{pass_L} = \frac{N_{pass_{tourist}} + N_{pass_{business}} + N_{pass_{1st\ class}}}{1 + 0.8 \frac{b_{cabinU}}{b_{cabinL}} \phi_{fuse}} \tag{9.28}$$

$$N'_{pass_U} = N_{pass_{tourist}} + N_{pass_{business}} + N_{pass_{1st\ class}} - N'_{pass_L} \tag{9.29}$$

The number of toilets, galleys, and emergency exits can then be calculated for each deck. The layout of each deck is then estimated using the methods described in sections 13.1.2.3 to 13.1.2.7, with the addition of a staircase toward the front of the cabin. To give a correct layout, and corresponding fuselage length, the positioning of seats in the main fuselage seating area (the area of constant cross-section) is carried out row by row on alternate decks, to ensure that each deck is filled completely and contains no gaps.

13 .1 .4 Double Deck Fuselage Methods

The methods used to determine the layout of a double deck fuselage are exactly the same as the methods described above in section 13.1.3, with the only major difference being the assumed split of amenities between the lower and upper deck. For the purpose of assigning toilets, galleys, and emergency exits, the upper deck is assumed to house approximately three seventh's of the total number of passengers, with the remainder being seated on the lower deck. The detailed layout, and the actual passenger arrangement can then be calculated. The initial fuselage length estimate is given by:-

$$l_{fuse} = l_{nose} + l_{tail} + \frac{0.7 l_{seating}}{2} \tag{9.30}$$

13 .1 .5 Horizontal Double Bubble Methods

Again, the methods used to calculate the layout of this type of fuselage are based upon the methods described is section 13.1.2. The main difference being that apart from the very front and rear portions of the cabin where no partition is assumed, the layout is symmetrical across the partition joining the two fuselage portions. This fact can be used to reduce the number of calculations made, and therefore speed up the process.

13 .1 .6 Vertical Double Bubble Methods

This is treated exactly like a double deck fuselage, and the methods of section 13.1.4 are used.

13 .2 Optimisation Methods

The user has a choice of optimisation algorithms that can be applied to studies within the Optimisation Window. The two available algorithms are based upon a 'Hook-Jeeves' method and a 'Rosenbrock' method (Shoup and Mistree[105]), and are briefly described below. Both methods are pattern search rather than gradient search methods, which was thought more appropriate for the kind of analysis undertaken, as the gradients of many functions will be far from continuous. Both methods also assume that the design space is unimodal i.e. it consists of one global optimum, rather than any number of local optima, it is thought that this is a reasonable assumption for the kind of design space dealt with here. The application of these methods is carried out using a penalty function, which provides a undesirable value of the merit function (the expression that is being minimised or maximised) if any of the constraints are breached, or if the independent variables are outside their limits.

13 .2 .1 Hooke & Jeeves Method

This is a straightforward pattern search method. An initial design point is taken, and an exploration is made from this initial point. The exploration involves evaluating the merit function for design points above and below the initial design point. If the value of the merit function at one of these exploration points is more desirable than the value of the merit function at the initial point, then this exploration point is taken as the new base point. This kind of exploration is carried out in turn for each of the independent design variables. If a

more desirable design point is found then the exploration is continued in the same direction, and the size of the exploration step is increased. If however, a more desirable design point is not found then the size of the exploration step is decreased, and the process is repeated to see if a better design point can be found.

Once this analysis has been performed for each independent variable, the whole process is repeated. Repeating this analysis a number of times eventually leads to the discovery of the optimum value of the merit function for the given independent variables. The optimum value of the merit function is identified as the design point at which no further improvement can be detected, even by very small changes in the values of the independent variables.

The limitations of this method are that it can be relatively slow, it is not foolproof when it comes to following boundaries and constraints, and that it assumes that the design space is unimodal. However, as this method is relatively simple, it is very reliable and robust, and produces quick results for simple optimisation analyses.

13 .2 .2 ROSENBROCK METHOD

This is a more complex analysis technique that attempts to provide better ridge following capabilities than those of the Hooke & Jeeves method. The method is very similar to the Hooke & Jeeves method, however, rather than perturbing the independent variables separately, the co-ordinate system is rotated so that one axis points along a ridge or boundary.

Again, an initial design point is chosen and an exploration about this point is undertaken. If the merit function at this new exploration is improved then the exploration step size is increased, if the merit function is not improved then an exploration is made on the other side of the design point. This is repeated for each variable until one success and one failure has been achieved for each variable. The path in the design space to the current best design point from the previous best design point gives the current direction of the search.

The co-ordinate axes of the design space are then rotated using matrix manipulation, such that they are aligned with the direction of the current search. Then rather than increment or decrement the variables independently, the variables are changed with respect to the new co-ordinate axes. This is all repeated until no further improvements in the merit function can be detected and convergence is achieved. The optimum value of the merit function is then found.

13 .3 CORRELATION METHOD

The correlation between data sets in the Correlation Window is carried out using Gauss-Jordan Elimination to find the least squares fit between the two data sets. The fitting function that expresses the relationship between the two data sets can be of the form of a polynomial up to the 7th degree, a logarithmic expression, an exponential expression, or a power law expression (See Appendix A). Gaussian elimination is applied to the data matrix, and the coefficients of the particular fitting function are estimated.

14 .Design Method Validation

Before any UHCA or advanced technology design examples could be created, the design methods must be validated, and the accuracy of these methods evaluated for existing aircraft. A total of 24 designs were evaluated, 19 of the designs being based on existing aircraft and their variants, and 5 of the designs being based on UHCA concepts proposed by Boeing or Airbus.

Many of the main design input parameters could be taken from data presented in Janes 'All the World's Aircraft'[106], or from the Flight International 'Aircraft of the World' Directory[107]. In the absence of any numeric data, geometric parameters could be measured from drawings of the aircraft. If the relevant data or drawing was not available, then an educated guess, using common sense and judgement was used to estimate parameters. The data for the Deutsche Airbus 502, 602, and 702 UHCA concept aircraft was taken from Oelkers[9].

It proved more difficult to find data that could be used to compare the output values of the modules with the actual design values. The output of the Sizing and the Performance Modules was easily comparable, however detailed data on the airfoil and engine performance, wing characteristics, weight breakdown, aerodynamic drag, and stability properties, proved almost impossible to obtain. This means that some of this output data must be assessed indirectly, or must be assessed in general order of magnitude terms.

The results proved to be highly accurate and consistent for this type of analysis. As some of the methods were in fact based on existing aircraft data, this may appear to be no major achievement. However, the results of the thirteen designs that had no involvement in the derivation of the design methods showed an equally good accuracy as those that were used to derive some methods. Even more encouraging was the fact that this accuracy could be maintained over a wide scope of aircraft designs, ranging from the 124 passenger Airbus A319 to the double deck 850 seat Airbus A3XX concept.

The results produced from each design module are outlined below. Some of the main design parameters have been incorporated into the tables shown within this chapter. The complete set of design parameters for each example aircraft can be found within the design files that are included with the Aircraft Design program.

14 .1 Airfoil & Engine Results

Due to a lack of data, as discussed above, there is no way of directly assessing the accuracy of the data produced from the Airfoil and Engine Module. However, the accuracy

of the data produced from this module is discussed below, in terms of its qualitative properties.

14 .1 .1 AIRFOIL DATA

As the data produced from the airfoil routines is directly chosen from the airfoil data library, with only minor adjustments to the thickness to chord ratio, then a high degree of confidence can be placed in the validity of this data. The only question mark that could be placed over these results relates to the actual validity of the original data in the data library. Although this data is not from state of the art commercial airfoils, it is based on the best available public domain subsonic and transonic airfoil data, and can therefore be assumed to be accurate enough for this type of conceptual design work.

14 .1 .2 ENGINE DATA

Qualitatively, the module can be seen to produce results that correctly reflect the expected trends that a change in bypass ratio, thrust rating, or certification year would yield. The changes in specific fuel consumption and weight of the engine due to increases in bypass ratio can be compared to values presented by Eccleston and Metcalfe[15] from a study conducted by Rolls-Royce. A similar trade off study was carried out using the Aircraft Design program to evaluate a number of engines with an identical cruise thrust rating, at a number of bypass ratios. The results of this study and the Eccleston and Metcalfe[15] study are compared below.

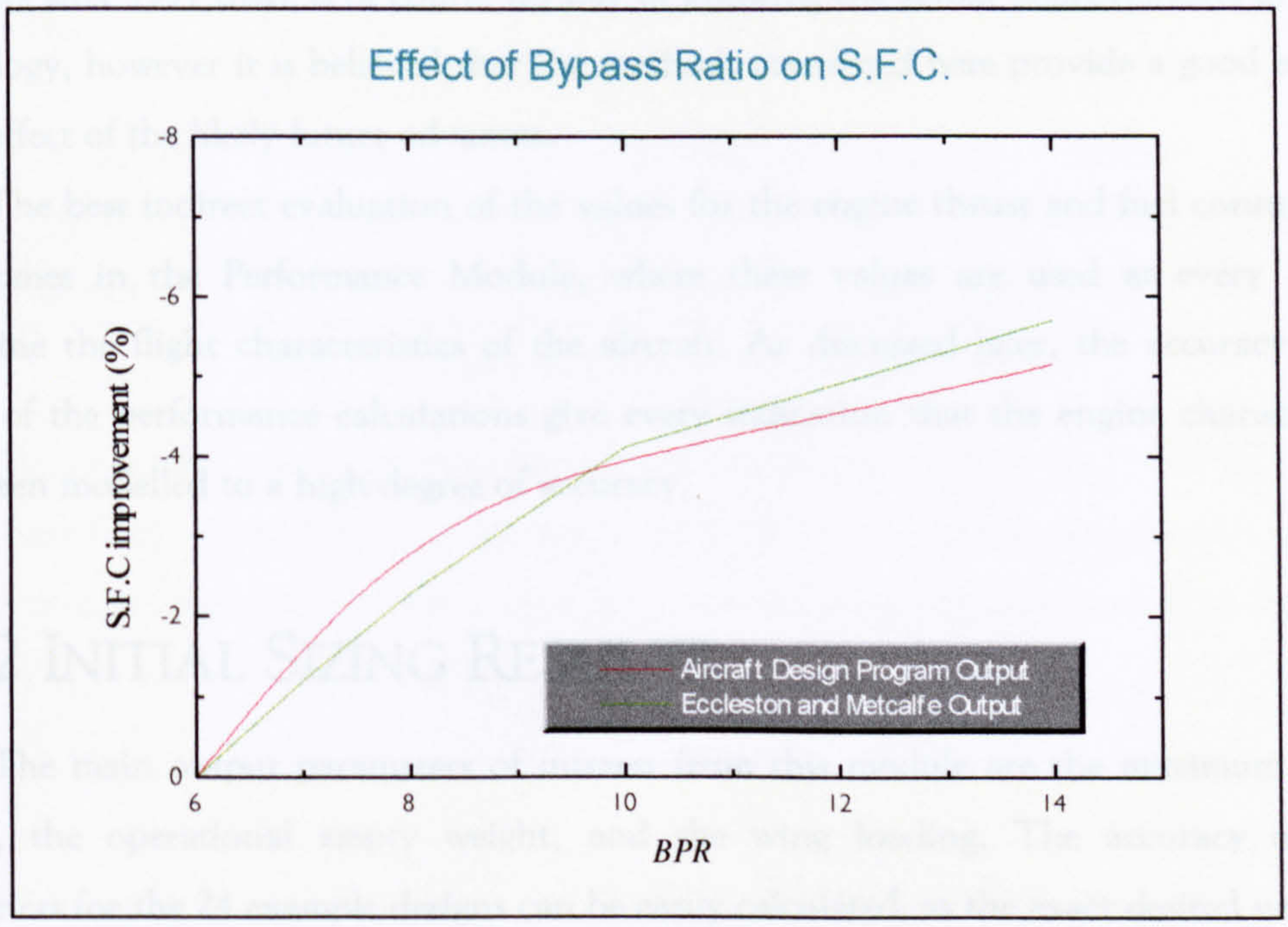


Figure 14.1- The effect of bypass ratio on engine specific fuel consumption

The graph above shows that the two studies give good agreement, both in a qualitative and quantitative sense. The graph below of the engine dry weight versus bypass ratio shows a similar level of agreement. These graphs show that the modelling of the effect of bypass ratio can be deemed to be of sufficient accuracy.

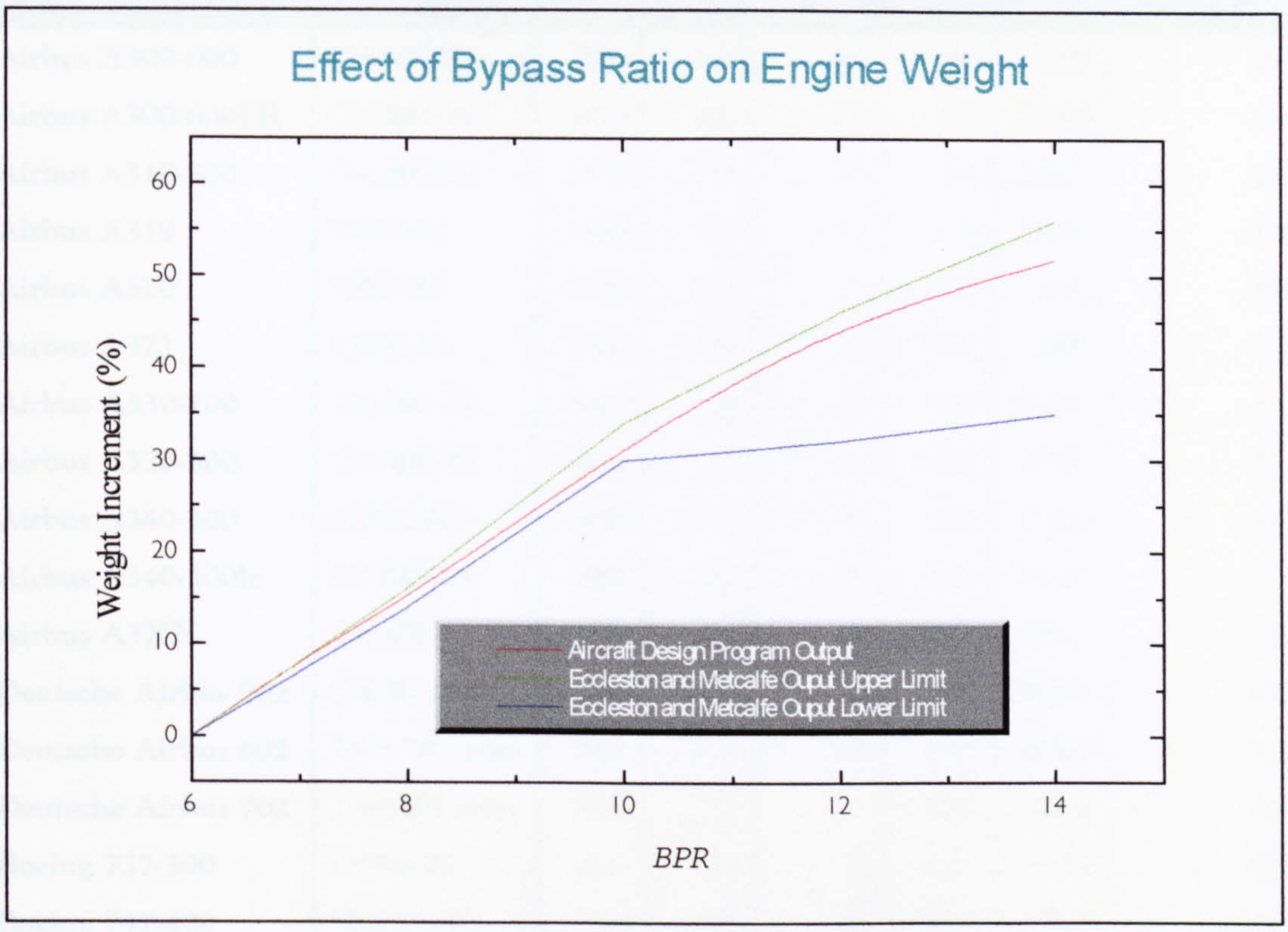


Figure 14.2 - Effect of bypass ratio on engine weight

The effect of certification year can be assumed to be accurate for up to the year 1997. For years after 1997 there is of course no way of knowing the actual improvements in engine technology, however it is believed that the methods contained here provide a good estimate of the effect of the likely future advances.

The best indirect evaluation of the values for the engine thrust and fuel consumption data comes in the Performance Module, where these values are used at every step to determine the flight characteristics of the aircraft. As discussed later, the accuracy of the results of the performance calculations give every indication that the engine characteristics have been modelled to a high degree of accuracy.

14 .2 Initial Sizing Results

The main output parameters of interest from this module are the maximum takeoff weight, the operational empty weight, and the wing loading. The accuracy of these parameters for the 24 example designs can be easily calculated, as the exact desired values for each example design is known.

The main input parameters involved in these calculation for each example design are shown in the table below.

Aircraft Name	*Engine*	R_{cr1} (nm)	N_{pass}	$N_{1st\ cl.}$	Ma_{cr1}	h_{cr1} (ft)	$\Delta W_{oew\ composite}$ (%)
Airbus A300-600	CF6-80C2A2	3600	266	26	0.8	31000	2.91
Airbus A300-600ER	CF6-80C2A5	3950	266	26	0.8	31000	2.91
Airbus A310-300	CF6-80C2A5	5170	218	20	0.8	36000	2.37
Airbus A319	V2522-A5	2650	124	12	0.78	31000	2.37
Airbus A320	V2527-A5	2700	150	12	0.78	31000	2.37
Airbus A321	V2530-A5	2300	185	12	0.78	31000	2.37
Airbus A330-200	CF6-80E1A2	6400	256	30	0.82	37500	3.11
Airbus A330-300	CF6-80E1A2	4500	335	30	0.82	37500	3.11
Airbus A340-300	CFM56-5C4	6600	295	40	0.82	37500	3.11
Airbus A340-300lr	CFM56-5C4	7300	295	40	0.82	37500	3.11
Airbus A3XX	CF6-80E1	7500	530	80	0.85	35000	5.60
Deutsche Airbus 502	CF6-80 series	7000	476	34	0.85	35000	5.93
Deutsche Airbus 602	Trent 700 series	7000	611	40	0.85	35000	5.61
Deutsche Airbus 702	Trent 800 series	7000	727	51	0.85	35000	5.61
Boeing 737-300	CFM56-2B	1600	140	0	0.75	35000	0.59
Boeing 747-400	RB211-524G	7100	420	50	0.83	35000	0.59
Boeing 747-600X	PW4062	7200	550	0	0.855	39000	1.85
Boeing 757-200	RR-535E4	2980	186	16	0.8	39000	0.65
Boeing 757-300	RR-535 series	2980	250	0	0.8	39000	0.69
Boeing 767-200	CF6-80A	3160	270	0	0.8	35000	0.67
Boeing 767-300ER	CF6-80C2B4	5760	210	24	0.8	35000	0.67
Boeing 777-200IW	PW4084	6300	305	40	0.83	39000	1.52
Boeing 777-300	PW4098	5700	368	40	0.83	39000	1.52
Boeing MD-11	PW4460	6984	293	40	0.82	35000	1.52

Table 14.1- Main sizing parameters of sample aircraft

The calculated takeoff weights, operational empty weights, and wing loadings (with all tuning parameters set to 100%) are shown in table 14.2 below, along with the actual values for each aircraft, and the calculation error (in terms of percentage difference from the actual value).

Aircraft	W_0 calc. (kg)	$W_{0\,ref}$ Actual (kg)	Error (%)	W_{oew} calc. (kg)	W_{oew} Actual (kg)	Error (%)	W\S calc. (kg/m²)	$W\S_{ref}$ Actual (kg/m²)	Error (%)
A300-600	152156	165000	-7.8	81305	90115	-9.8	595.9	634.6	-6.1
A300-600ER	164125	170500	-3.7	86809	90339	-3.9	607.0	655.8	-7.4
A310-300	167840	164000	2.3	87758	82488	6.4	645.5	748.9	-13.8
A319	66180	68400	-3.2	37579	39200	-4.1	565.9	558.8	1.3
A320	76254	73500	3.7	43656	42069	3.8	567.5	600.5	-5.5
A321	81721	83000	-1.5	46081	47966	-3.9	554.9	678.1	-18.2
A330-200	222703	230000	-3.2	115020	120170	-4.3	684.4	633.4	8.0
A330-300	208992	212000	-1.4	115725	120285	-3.8	624.4	583.9	6.9
A340-300	263336	257000	2.5	134260	126873	5.8	690.7	707.8	-2.4
A340-300lr	287789	275000	4.7	142108	129806	9.5	712.8	757.4	-5.9
A3XX	484368	495000	-2.1	239546	253600	-5.5	719.1	647.1	11.1
DA 502	411530	410000	0.4	204390	200000	2.2	703.3	700.7	0.4
DA 602	518304	519000	-0.1	260711	256000	1.8	703.3	704.3	-0.1
DA 702	603254	614000	-1.8	310859	298000	4.3	703.3	715.9	-1.8
B.737-300	56822	56470	0.6	31717	31895	-0.6	532.8	529.5	0.6
B.747-400	400953	394625	1.6	187086	182775	2.4	706.5	695.3	1.6
B.747-600X	460450	467200	-1.4	217004	-	-	709.7	720.1	-1.4
B.757-200	97842	99790	-2.0	52669	57180	-7.9	576.4	587.8	-2.0
B.757-300	123311	122470	0.7	66807	65980	1.3	576.4	572.4	0.7
B.767-200	138022	136080	1.4	74963	74750	0.3	582.0	573.9	1.4
B.767-300ER	182367	175540	3.9	90302	89130	1.3	664.2	639.3	3.9
B.777-200IW	264429	267620	-1.2	130593	138120	-5.4	681.2	689.4	-1.2
B.777-300	286788	299370	-4.2	146236	157215	-6.9	662.3	618.0	7.2
B.MD-11	285430	273289	4.4	133766	129680	3.2	702.9	673.0	4.4

Table 14.2 - Initial sizing results of sample aircraft

The results for the maximum takeoff weight show a high degree of accuracy, with an average error of 2.85%, and a maximum error of 7.8%. The operating empty weight calculation provides an average error of 4.1%, and a maximum error of -9.8%. The wing loading, which is notoriously difficult to calculate, gives good agreement with actual data, an average error of 5.3% and a maximum error of -18.2% are observed.

It is important to note that some degree of error will always be present in this kind of calculation, especially when dealing with aircraft that have been designed with more than one configuration in mind, and where the design may take into account the future stretch or shrink requirements of the aircraft. This is especially true of wing loading calculations, where

the actual wing of the aircraft may be determined from a number of factors, such as commonality with other aircraft made by the same manufacturer, and also where the wing is often sized such that it is capable of supporting future growth in range, payload, or size of the particular aircraft.

14 .3 Wing Design Results

14 .3 .1 Wing Planform

Since the taper ratio, aspect ratio, and crank geometry are specified by the user, then the accuracy of the wing planform geometry depends entirely on the accuracy of the calculated wing reference area. As the wing reference area is calculated from the takeoff weight and the wing loading, then the error of the wing reference area is strongly related to the errors accumulated from the Initial Sizing Module. The results of the wing sizing calculation are shown below:-

Aircraft	S_{ref} *calc.* (m^2)	S_{ref} *Actual* (m^2)	*Error* (%)	b_{ref} *calc.* (m)	b_{ref} *Actual* (m)	*Error* (%)
Airbus A300-600	255.3	260.0	-1.8	44.4	44.8	-0.9
Airbus A300-600ER	270.4	260.0	4.0	45.7	44.8	2.0
Airbus A310-300	260.0	219.0	18.7	47.8	43.9	9.0
Airbus A319	116.9	122.4	-4.4	33.1	33.9	-2.3
Airbus A320	134.4	122.4	9.8	35.5	33.9	4.7
Airbus A321	147.3	122.4	20.3	37.2	33.9	9.7
Airbus A330-200	325.4	363.1	-10.4	57.1	60.3	-5.4
Airbus A330-300	334.7	363.1	-7.8	57.9	60.3	-4.0
Airbus A340-300	381.3	363.1	5.0	61.8	60.3	2.4
Airbus A340-300lr	403.7	363.1	11.2	63.6	60.3	5.4
Airbus A3XX	673.5	-	-	76.1	77.1	-1.3
Deutsche Airbus 502	585.1	592.0	-1.2	71.0	74.3	-4.4
Deutsche Airbus 602	736.9	765.0	-3.7	79.6	84.0	-5.2
Deutsche Airbus 702	857.7	902.0	-4.9	85.9	91.5	-6.2
Boeing 737-300	106.7	105.4	1.2	29.0	28.9	0.6
Boeing 747-400	567.5	524.9	8.1	67.0	64.4	4.0
Boeing 747-600X	648.8	-	-	71.6	73.8	-2.9
Boeing 757-200	169.8	185.3	-8.4	36.4	38.1	-4.2

Aircraft	S_{ref} calc. (m^2)	S_{ref} Actual (m^2)	Error (%)	b_{ref} calc. (m)	b_{ref} Actual (m)	Error (%)
Boeing 757-300	214.0	185.3	15.5	40.9	38.1	7.5
Boeing 767-200	237.1	283.3	-16.3	43.2	47.6	-9.1
Boeing 767-300ER	274.6	283.3	-3.1	46.5	47.6	-2.2
Boeing 777-200IW	388.2	427.8	-9.3	58.0	60.9	-4.7
Boeing 777-300	433.0	427.8	1.2	61.3	60.9	0.6
Boeing MD-11	406.1	338.9	19.8	56.6	51.7	9.6

Table 14.3- Wing design results of sample aircraft

The average error of the calculated wing area is 8.3%, which is a good level of accuracy for this type of aircraft, especially when one considers the proprietary nature of many of the wings on these aircraft and their derivatives. The maximum error of 20.3% for the Airbus A321 is somewhat disappointing, but is almost certainly due to the fact that the Airbus A321 is in fact a stretched version of the A320, and has been designed to provide maximum compatibility with the A320, so includes a wing design that is taken directly from the Airbus A320. However, with judicious use of the wing loading tuning factor, this and all other errors can be reduced or eliminated. The wing span calculation appears to be less sensitive to errors, with an average error of 4.4%, and a maximum error of 9.7%.

The remaining geometric properties of the wing such as the location of the mean aerodynamic chord and the equivalent wing are theoretically based and there is no data or method available to check the accuracy of these parameters. Although, as they are calculated using tried and tested methods one can assume that they are correct.

14 .3 .2 Wing Lift Distribution

In the absence of any detailed data for the lift distributions of these aircraft, a visual inspection shows that the methods used provide adequate results, and produce the kind of distribution that one would expect for this type of aircraft, i.e. almost elliptical. An example distribution is shown below, along with the expected ideal elliptical distribution, for a design based on the Boeing 747-400.

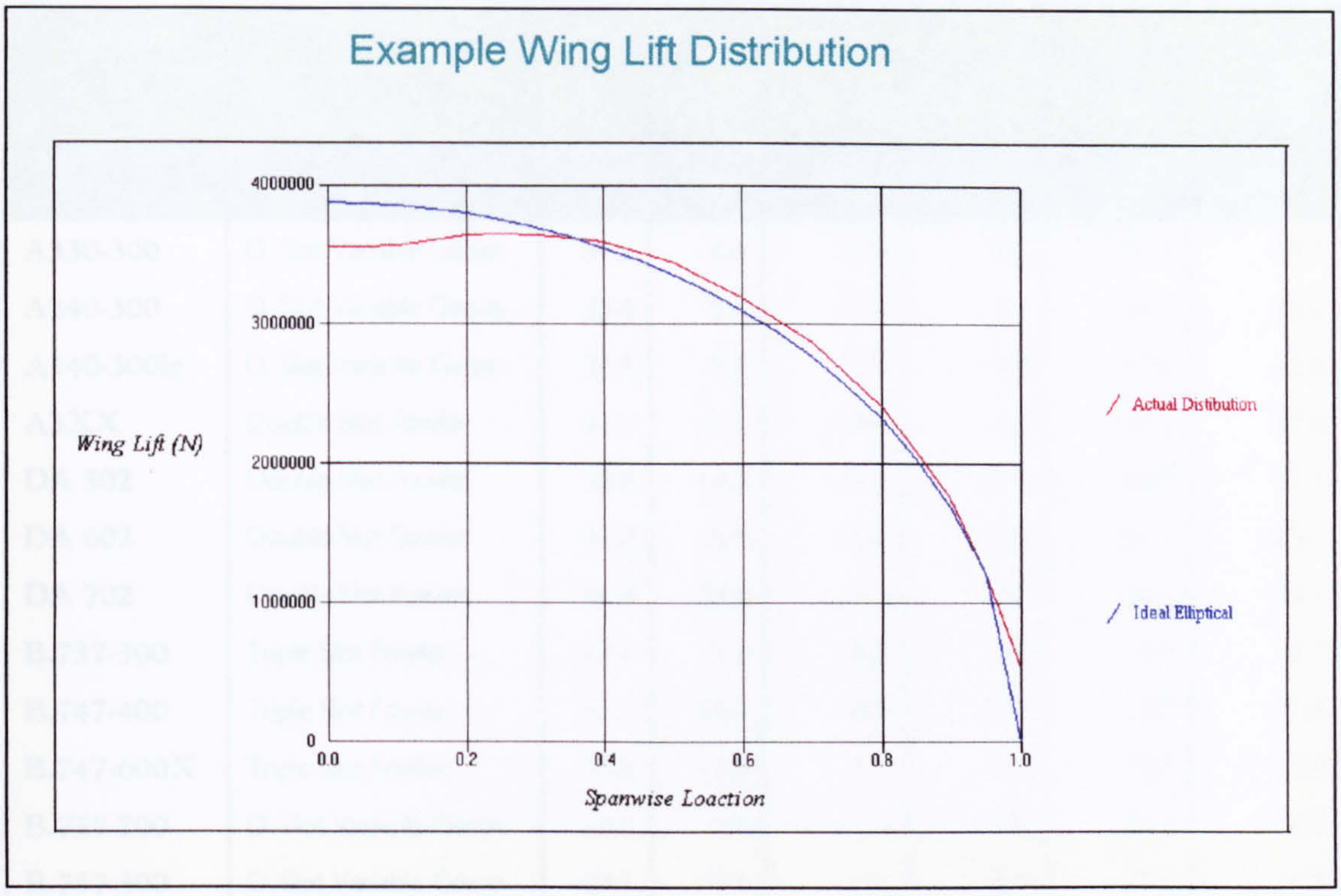


Figure 14.3 - Example wing lift distribution

14 .3 .3 FLAP PERFORMANCE

The other main results of interest from the Wing Design Module are those pertaining to the performance of the high lift systems. Although no exact data is available for the flap and aileron deflections, the results below illustrate that with the correct flap type, and with the correct inboard and outboard flap and aileron locations (non-dimensionalised with respect to span), the resulting deflections are of the magnitude that one would expect for this type of aircraft. In the absence of any information to the contrary, the ailerons have been used for lift augmentation in all cases.

Aircraft	*Flap Type*	b_{flap} (m)	$b_{aileron}$ (m)	δ_{flap} *Takeoff* (deg)	$\delta_{aileron}$ *Takeoff* (deg)	δ_{flap} *Landing* (deg)	$\delta_{aileron}$ *Landing* (deg)
A300-600	Double Slot Fixed Vane	26.1	5.3	13.7	10.9	28.4	22.7
A300-600ER	Double Slot Fixed Vane	26.8	5.5	13.9	11.1	28.6	22.9
A310-300	Double Slot Fowler	25.6	8.2	16.3	9.8	44.3	26.6
A319	Single Slot Fowler	21.4	4.8	11.5	6.9	32.2	19.3
A320	Single Slot Fowler	22.8	5.1	11.7	7.0	32.7	19.6
A321	Double Slot Fixed Vane	23.9	5.3	12.4	7.4	27.6	16.5
A330-200	D. Slot Variable Geom.	30.9	8.5	14.9	12.0	42.7	34.1

Aircraft	Flap Type	b_{flap} (m)	$b_{aileron}$ (m)	δ_{flap} Takeoff (deg)	$\delta_{aileron}$ Takeoff (deg)	δ_{flap} Landing (deg)	$\delta_{aileron}$ Landing (deg)
A330-300	D. Slot Variable Geom.	31.3	8.6	11.0	8.8	30.2	24.2
A340-300	D. Slot Variable Geom.	33.4	9.2	15.5	12.4	44.0	35.2
A340-300lr	D. Slot Variable Geom.	34.4	9.5	15.9	12.7	44.5	35.6
A3XX	Double Slot Fowler	41.1	15.2	14.5	11.6	34.5	27.6
DA 502	Double Slot Fowler	38.4	14.2	14.2	11.3	33.9	27.1
DA 602	Double Slot Fowler	43.0	15.9	13.6	10.8	31.4	25.1
DA 702	Double Slot Fowler	46.4	24.9	13.3	10.7	30.1	24.1
B.737-300	Triple Slot Fowler	17.1	5.3	6.3	3.8	14.4	8.7
B.747-400	Triple Slot Fowler	33.5	16.2	8.9	7.2	19.5	15.6
B.747-600X	Triple Slot Fowler	35.8	17.3	9.5	7.6	19.7	15.8
B.757-200	D. Slot Variable Geom.	24.2	7.4	11.4	6.9	31.3	18.8
B.757-300	D. Slot Variable Geom.	27.1	8.3	11.5	6.9	31.3	18.8
B.767-200	Double Slot Fixed Vane	16.0	21.8	17.2	10.3	42.0	25.2
B.767-300ER	Double Slot Fowler	17.3	23.4	15.1	9.0	41.3	24.8
B.777-200IW	Double Slot Fowler	27.2	22.8	15.5	9.3	37.6	22.6
B.777-300	Double Slot Fowler	33.2	13.4	14.4	11.5	32.2	25.8
B.MD-11	Double Slot Fowler	28.7	24.1	9.3	5.6	20.3	12.2

Table 14.4- Flap deflection results for sample aircraft

14 .4 Geometry Results

14 .4 .1 Fuselage Geometry

The calculations of the fuselage wetted area, frontal area, and planform area, appear to give consistent and reliable results. There is however no data available for the example aircraft which enables a direct comparison of the accuracy of the calculated values. The only parameter for which data is available is the bulk freight volume. A comparison of actual and calculated freight volumes is given below. It must be remembered that the calculated freight volume provides only a very rough indication of the cargo capacity, and is only included for completeness, as it does not impinge on the design itself in any way. Nevertheless the results shown below are reasonably accurate given the simplicity of the method employed.

Aircraft	$V_{freight}$ calc. (m^3)	$V_{freight}$ Actual (m^3)	Error (%)
Airbus A300-600	150.7	147.4	2.7
Airbus A300-600ER	150.7	147.4	1.3
Airbus A310-300	96.2	102.1	-5.7
Airbus A319	35.3	-	-
Airbus A320	44.6	38.8	14.9
Airbus A321	62.5	52.0	20.1
Airbus A330-200	206.9	-	-
Airbus A330-300	206.9	-	-
Airbus A340-300	206.9	-	-
Airbus A340-300lr	206.9	-	-
Airbus A3XX	253.9	-	-
Deutsche Airbus 502	374.1	-	-
Deutsche Airbus 602	374.5	-	-
Deutsche Airbus 702	422.1	-	-
Boeing 737-300	27.4	30.2	-9.3
Boeing 747-400	211.6	-	-
Boeing 747-600X	375.8	-	-
Boeing 757-200	50.5	50.69	-0.4
Boeing 757-300	63.2	-	-
Boeing 767-200	101.8	111.3	-8.5
Boeing 767-300ER	134.5	147.0	-8.5
Boeing 777-200IW	176.9	160.2	9.4
Boeing 777-300	244.2	200.5	22.0
Boeing MD-11	163.9	194.0	-15.5

Table 14.5- Results of freight volume estimation for sample aircraft

For the data that was available, the average error is 9.9%, which appears to be reasonable for this calculation. The maximum error of 22.0% is disappointing, however, as stated above these figures are only intended for 'ball park' estimations of the bulk freight volume.

14 .4 .2 Nacelle Dimensions

This is another area where it is very difficult to make exact assumptions about the nature of the geometry for a particular aircraft. A choice of engines is often offered to the

airlines, and the nacelle design can depend on the particular engine manufacturer used for that particular aircraft. It is therefore the aim of these calculations to provide a good estimate which will reflect the general qualities of the nacelle, and will provide reasonable dimensions for the basis of the nacelle drag and weight calculations. The calculations are performed using the methods described in chapter 8, using data derived from drawings of a relatively small number of aircraft. Since this limited data remains the only data available, there seems little point in comparing the results of these methods to the data from which they were derived. Some results are presented below, along with typical nacelle dimensions for the particular aircraft, to illustrate that the methods provide sensible values, characteristic of nacelles for that size of engine.

Aircraft	T_{max} (lbf)	*BPR*	l_{fc} *calc.* (m)	l_{na} *calc.* (m)	D_{na} *calc.* (m)	l_{fc} *typical* (m)	l_{na} *typical* (m)	D_{na} *typical* (m)
Airbus A300-600ER	61500	5.05	3.9	6.1	3.0	3.9	6.6	2.8
Airbus A320	26500	4.75	3.7	4.7	2.0	3.4	4.6	2.0
Airbus A340-300	34600	6.60	3.9	4.8	2.3	3.5	5.0	2.3
Boeing 737-300	22000	6.00	3.9	4.5	2.1	3.3	4.7	2.0
Boeing 747-400	58000	4.10	3.6	6.2	2.8	3.4	5.6	2.8
Boeing 777-300	84600	4.80	4.2	7.9	3.4	4.6	7.7	3.7

Table 14.6 - Results of nacelle sizing for sample aircraft

14 .5 Weight Estimation Results

14 .5 .1 Operating Empty Weight

The main result of the weight estimation module is the detailed estimate of the operational empty weight. This is built up of many individual components, but as no detailed information is available pertaining to the values of these component weights, then the best indication of the accuracy of these weights is the resulting operational empty weight found from summing the components. The table below compares the calculated and the actual operational empty weights for the example designs. The results from each design have been presented for two different cases. The first case has been calculated with all the tuning factors set to 100%, and the weight calculation is therefore based on a design that already includes errors from the previous four modules. The second case has been calculated such that the tuning factors have been adjusted such that the weights from the Initial Sizing

Module, the wing reference area, and the tail reference areas are exactly equal to the actual values. This second case gives a better indication of the isolated performance of the Weight Estimation Module. For each case, the deviation of the detailed operational empty weight value from both the value predicted from the Initial Sizing Module (error 1) and from the actual value (error 2) are shown.

Aircraft	W_{oew} *actual* (kg)	W_{oew} *calc.* (kg)	*Error 1* (%)	*Error 2* (%)	W_{oew} *calc.* (kg)	*Error 1* (%)	*Error 2* (%)
		Case 1			Case 2		
Airbus A300-600	90115	82433	1.4	-8.5	84519	-6.2	-6.2
Airbus A300-600ER	90339	85575	-1.4	-5.3	86090	-4.7	-4.7
Airbus A310-300	82488	85815	-2.2	4.0	83355	1.1	1.1
Airbus A319	39200	36057	-4.1	-8.0	36516	-6.9	-6.8
Airbus A320	42069	40751	-6.7	-3.1	40372	-4.1	-4.0
Airbus A321	47966	43829	-4.9	-8.6	43274	-9.7	-9.8
Airbus A330-200	120170	113367	-1.4	-5.7	116818	-2.9	-2.8
Airbus A330-300	120285	114220	-1.3	-5.0	115881	-3.6	-3.7
Airbus A340-300	126873	127267	-5.2	0.3	125026	-1.4	-1.5
Airbus A340-300lr	129806	134422	-5.4	3.6	131398	1.1	1.2
Airbus A3XX	253600	224108	-6.4	-11.6	230397	-9.2	-9.1
Deutsche Airbus 502	200000	207721	1.6	3.9	207546	3.9	3.8
Deutsche Airbus 602	256000	248229	-3.1	-3.0	248376	-3.0	-3.0
Deutsche Airbus 702	298000	307571	3.3	3.2	308151	3.5	3.4
Boeing 737-300	31895	34618	9.1	8.5	34532	8.5	8.3
Boeing 747-400	182775	194763	4.1	6.6	191322	4.7	4.7
Boeing 747-600X	182754	224188	3.3	-	41347	-0.2	-0.3
Boeing 757-200	57180	52097	-1.1	-8.9	53143	-7.1	-7.1
Boeing 757-300	65980	64065	-4.1	-2.9	63643	-3.5	-3.5
Boeing 767-200	74750	74141	-1.1	-0.8	75930	1.6	1.6
Boeing 767-300ER	89130	88235	-2.3	-1.0	87438	-2.0	-1.9
Boeing 777-200IW	138120	132069	1.1	-4.4	134657	-2.5	-2.5
Boeing 777-300	157215	147699	1.0	-6.1	149890	-4.7	-4.7
Boeing MD-11	129680	142472	6.5	9.9	139002	7.2	7.2

Table 14.7- Results of detailed weight estimation for sample aircraft

The O.E.W. results of case 1 show an average error of magnitude 3.4% from the initial sizing estimate, and 5.3% from the actual operating empty weight of each design. The figures of case 2 display an average error of 4.5% from both the initial sizing estimate and

the actual O.E.W. (since the actual O.E.W. and the initial sizing estimate of the O.E.W. are equal for the case 2 results). The improved accuracy of the case 2 results over case 1 is to be expected, since the accumulation of errors from other modules is reduced. These results illustrate that the weight estimation methods provide a high degree of accuracy and consistency.

14 .5 .2 TAIL SURFACE SIZING

The task of finding a suitable method to accurately size the tail surfaces proved to be a difficult one. The method used is based upon a tail volume coefficient approach and provides reasonable results that appear to be more accurate than those from other methods. Part of the problem in estimating the tail surfaces of existing aircraft is the use of the same tail surfaces for more than one aircraft of different size and weights by aircraft manufacturers in order to reduce component cost and to provide manufacturing commonality. This means that the tail surfaces on some aircraft are not exactly optimal, but rather based on economic or production considerations. The results below illustrate that the method used provides a reasonably good estimate of the kind of tail surface areas that one would expect for that particular aircraft. Again the results are presented for two cases as above. The first case is the results of the calculations performed with all tuning factors set to 100%, and therefore the calculations incorporate errors from the previous four modules. The second case is with the initial sizing weights and the wing reference area set to the exact values (by the use of tuning factors), and aims to isolate the performance of the tail sizing calculations, neglecting any error from previous modules.

For the horizontal tail surface:-

Aircraft	$S_{ref\,ht}$ *Actual* (m^2)	$S_{ref\,ht}$ *calc.* (m^2)	*Error* (%)	$S_{ref\,ht}$ *calc.* (m^2)	*Error* (%)
		Case 1		Case 2	
Airbus A300-600	64.0	67.1	4.9	70.6	10.3
Airbus A300-600ER	64.0	71.8	12.2	69.1	8.0
Airbus A310-300	64.0	69.4	8.5	55.1	-13.9
Airbus A319	31.0	28.9	-6.7	30.5	-1.5
Airbus A320	31.0	32.1	3.6	28.2	-9.1
Airbus A321	31.0	33.4	7.8	26.8	-13.5
Airbus A330-200	73.0	62.8	-14.0	73.2	0.3
Airbus A330-300	73.0	65.5	-10.3	73.2	0.3

Aircraft	$S_{ref\,ht}$ Actual (m^2)	$S_{ref\,ht}$ calc. (m^2)	Error (%)	$S_{ref\,ht}$ calc. (m^2)	Error (%)
		Case 1		Case 2	
Airbus A340-300	73.0	76.7	5.1	71.4	-2.2
Airbus A340-300lr	73.0	82.5	13.1	70.7	-3.1
Airbus A3XX	-	166.4	-	204.3	-
Deutsche Airbus 502	140.0	134.6	-3.8	136.8	-2.3
Deutsche Airbus 602	182.0	178.6	-1.9	178.6	-1.9
Deutsche Airbus 702	232.0	217.9	-6.1	217.8	-6.1
Boeing 737-300	31.3	32.1	2.6	31.6	0.9
Boeing 747-400	136.6	147.9	8.3	131.2	-3.9
Boeing 747-600X	-	151.0	-	29.9	-
Boeing 757-200	50.4	44.3	-11.9	50.1	-0.6
Boeing 757-300	50.4	53.8	6.8	44.6	-11.4
Boeing 767-200	75.8	65.4	-13.8	83.6	10.2
Boeing 767-300ER	75.8	69.3	-8.5	71.3	-5.9
Boeing 777-200IW	101.3	89.3	-11.8	101.5	0.2
Boeing 777-300	101.3	92.6	-8.5	92.5	-8.6
Boeing MD-11	85.5	106.8	25.0	83.9	-1.9

Table 14.8 - Horizontal tail sizing results for sample aircraft

The average error for the case 1 calculations is 8.9%, while the average error for the case 2 calculations is 5.3%.

For the vertical tail surface:-

Aircraft	$S_{ref\,vt}$ Actual (m^2)	$S_{ref\,vt}$ calc. (m^2)	Error (%)	$S_{ref\,vt}$ calc. (m^2)	Error (%)
		Case 1		Case 2	
Airbus A300-600	48.0	40.0	-16.6	42.3	-11.8
Airbus A300-600ER	48.0	42.6	-11.3	41.2	-14.1
Airbus A310-300	48.8	47.7	-2.3	38.1	-20.7
Airbus A319	21.5	23.1	7.6	24.3	13.1
Airbus A320	21.5	25.2	17.4	22.2	3.1
Airbus A321	21.5	25.9	20.6	21.1	-2.1
Airbus A330-200	46.5	47.9	3.0	55.8	19.9
Airbus A330-300	46.5	50.0	7.6	55.8	20.0

Aircraft	$S_{ref\,vt}$ Actual (m^2)	$S_{ref\,vt}$ calc. (m^2)	Error (%)	$S_{ref\,vt}$ calc. (m^2)	Error (%)
		Case 1		Case 2	
Airbus A340-300	50.5	58.1	15.1	54.1	7.0
Airbus A340-300lr	50.5	62.3	23.4	53.4	5.8
Airbus A3XX	-	108.3	0.0	137.0	-
Deutsche Airbus 502	95.0	91.9	-3.2	93.9	-1.2
Deutsche Airbus 602	118.0	119.0	0.8	119.0	0.8
Deutsche Airbus 702	163.0	151.0	-7.3	151.0	-7.4
Boeing 737-300	23.1	22.2	-4.2	21.8	-5.8
Boeing 747-400	77.1	92.1	19.5	82.3	6.8
Boeing 747-600X	-	96.2	0.0	23.9	-
Boeing 757-200	34.4	27.9	-19.0	31.4	-8.8
Boeing 757-300	34.4	33.0	-4.1	27.6	-19.8
Boeing 767-200	46.0	41.5	-9.8	52.8	14.8
Boeing 767-300ER	46.0	42.9	-6.9	43.9	-4.7
Boeing 777-200IW	53.2	57.5	8.0	65.0	22.2
Boeing 777-300	53.2	58.8	10.6	59.0	10.9
Boeing MD-11	56.2	62.4	10.9	49.3	-12.3

Table 14.9 - Vertical tail sizing results for sample aircraft

The average error for the case 1 calculations is 10.4%, while the average error for the case 2 calculations is 10.6%.

These results demonstrate that for the horizontal tail surface the calculations are accurate to within approximately 5%, and within approximately 10% for the vertical tail surface. While the vertical tail results are disappointing, a number of factors have contributed to this margin of error that could not be avoided. Many of the values for the actual tail areas have been measured from drawings, which is a potential source of error, plus the assumption of a static margin of approximately 5% has been arbitrarily made in the absence of any other information, and is also a potential source of error.

14 .5 .3 Undercarriage Sizing

The results of the main undercarriage sizing calculations are shown below. They give reasonably accurate results compared to the actual undercarriage layouts of the example aircraft. Although the exact layout is not always identical, the number of tyres, and the general requirements of the undercarriage are well matched. The non-integer values for the

actual average number of tyres per bogey of some aircraft stems from the use of a smaller central bogey on some aircraft.

Aircraft	N_{tyres} *(main)* *Calc.*	N_{tyres} *(main)* *Actual*	N_{bogeys} *(main)* *Calc.*	N_{bogeys} *(main)* *Actual*	*Tyres per bogey (average)* *Calc.*	*Tyres per bogey (average)* *Actual*
Airbus A300-600	8	8	2	2	4	4
Airbus A300-600ER	8	8	2	2	4	4
Airbus A310-300	8	8	2	2	4	4
Airbus A319	4	4	2	2	2	2
Airbus A320	4	4	2	2	2	2
Airbus A321	4	4	2	2	2	2
Airbus A330-200	12	8	2	2	6	4
Airbus A330-300	12	8	2	2	6	4
Airbus A340-300	12	10	2	3	6	3.3
Airbus A340-300lr	12	10	2	3	6	3.3
Airbus A3XX	24	-	3	-	8	-
Deutsche Airbus 502	18	20	3	5	6	4
Deutsche Airbus 602	24	24	3	5	8	4.8
Deutsche Airbus 702	32	30	4	5	8	6
Boeing 737-300	4	4	2	2	2	2
Boeing 747-400	18	16	3	4	6	4
Boeing 757-200	8	8	2	2	4	4
Boeing 757-300	8	8	2	2	4	4
Boeing 767-200	8	8	2	2	4	4
Boeing 767-300ER	8	8	2	2	4	4
Boeing 777-200IW	12	12	2	2	6	6
Boeing 777-300	12	12	2	2	6	6
Boeing MD-11	12	12	2	3	6	4

Table 14.10 - Results of undercarriage sizing for sample aircraft

14 .6 Drag Prediction Results

Unfortunately, as sufficient quantities of reliable data were not found to be available for the aerodynamic drag of any of the example aircraft, the results from this module cannot be directly compared. A degree of confidence in the results from this module comes from the general trends and values of the results that can be seen to be of the form and of the

magnitude that would be expected for this type of aircraft (see figures below). A large amount of confidence of the drag data comes indirectly from the results of the Performance Module.

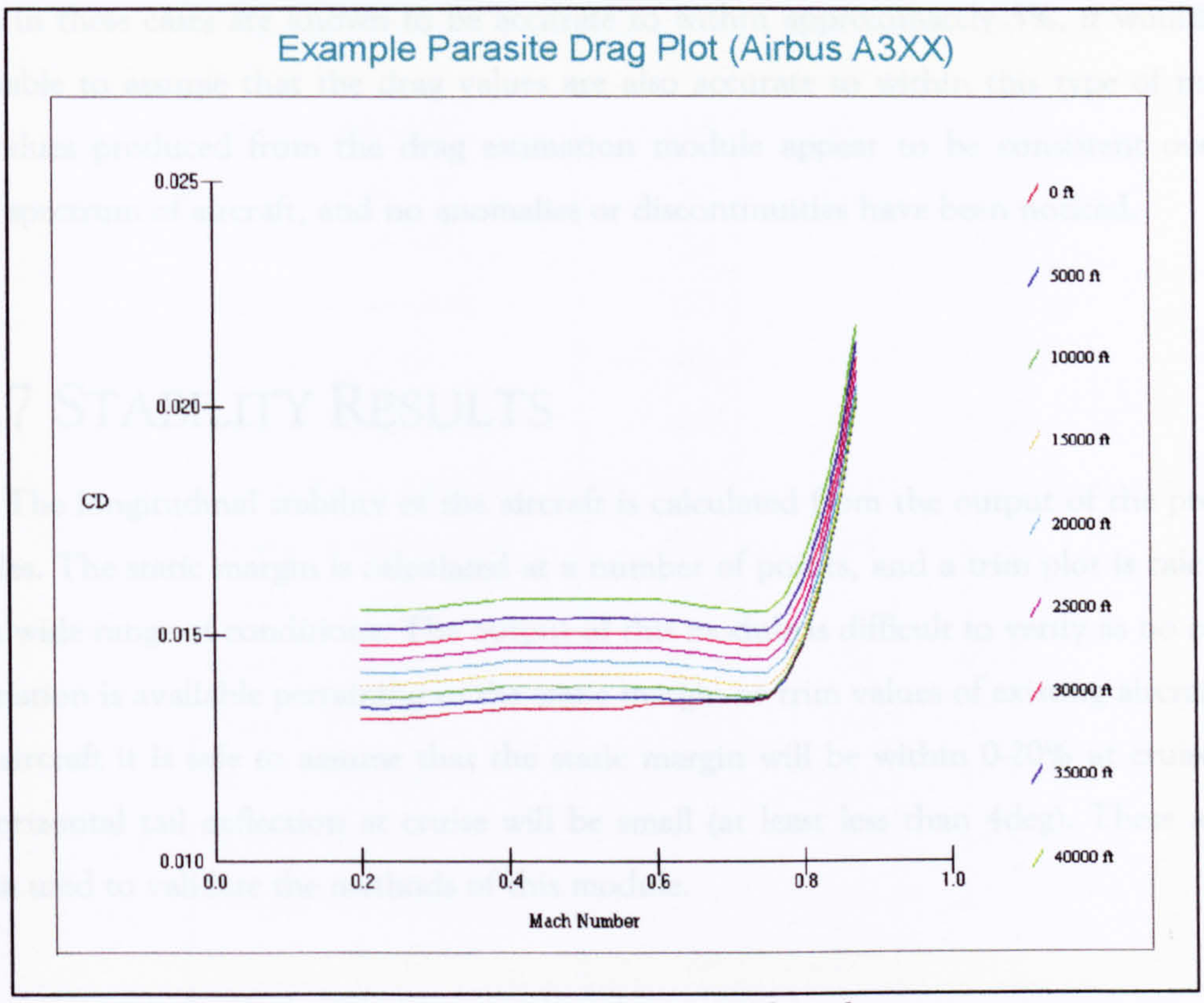


Figure 14.4 - Example parasite drag plot

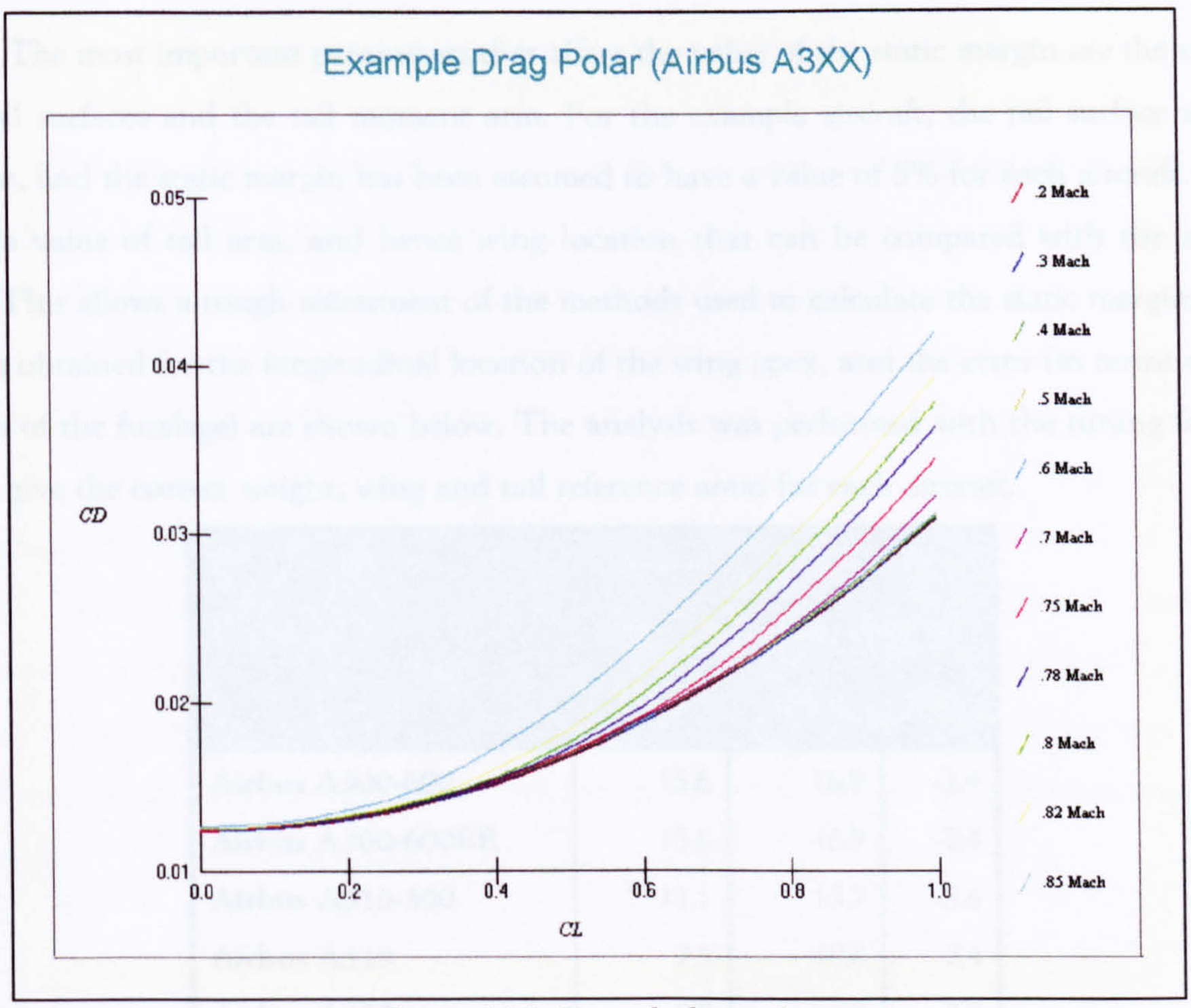


Figure 14.5- Example drag polar

The main contributors to the final results of the Performance Module are the thrust, s.f.c., and the drag values. In certain instances the thrust and fuel consumption data is known almost exactly from the data supplied by Rolls-Royce. Therefore, as the performance results in these cases are known to be accurate to within approximately 5%, it would seem reasonable to assume that the drag values are also accurate to within this type of margin. The values produced from the drag estimation module appear to be consistent over the whole spectrum of aircraft, and no anomalies or discontinuities have been noticed.

14 .7 Stability Results

The longitudinal stability of the aircraft is calculated from the output of the previous modules. The static margin is calculated at a number of points, and a trim plot is calculated over a wide range of conditions. The output of this module is difficult to verify as no reliable information is available pertaining to the static margin or trim values of existing aircraft. For most aircraft it is safe to assume that the static margin will be within 0-20% at cruise, and the horizontal tail deflection at cruise will be small (at least less than 4deg). These are the criteria used to validate the methods of this module.

14 .7 .1 Static Margin

The most important parameters that affect the value of the static margin are the size of the tail surfaces and the tail moment arm. For the example aircraft, the tail surface size is known, and the static margin has been assumed to have a value of 5% for each aircraft. This gives a value of tail arm, and hence wing location that can be compared with the actual data. This allows a rough assessment of the methods used to calculate the static margin. The values obtained for the longitudinal location of the wing apex, and the error (in terms of the length of the fuselage) are shown below. The analysis was performed with the tuning factors set to give the correct weight, wing and tail reference areas for each aircraft.

Aircraft	X_{wing} (m) *Calc.*	X_{wing} (m) *Actual*	*Error* (%)
Airbus A300-600	15.6	16.9	-2.4
Airbus A300-600ER	15.6	16.9	-2.4
Airbus A310-300	11.1	13.7	-5.6
Airbus A319	7.5	10.0	-7.4
Airbus A320	9.0	11.9	-7.8

Aircraft	X_{wing} (m) *Calc.*	X_{wing} (m) *Actual*	*Error* (%)
Airbus A321	12.1	16.2	-9.1
Airbus A330-200	15.4	18.5	-4.8
Airbus A330-300	15.4	20.6	-8.2
Airbus A340-300	15.3	21.0	-8.9
Airbus A340-300lr	15.3	21.0	-8.9
Airbus A3XX	14.0	18.3	-6.3
Deutsche Airbus 502	18.0	23.5	-7.2
Deutsche Airbus 602	17.2	23.2	-7.6
Deutsche Airbus 702	18.7	23.8	-6.1
Boeing 737-300	8.7	11.4	-8.1
Boeing 747-400	14.5	17.6	-4.7
Boeing 757-200	14.2	16.8	-5.5
Boeing 757-300	17.1	20.3	-5.9
Boeing 767-200	11.8	14.0	-4.6
Boeing 767-300ER	13.7	17.1	-6.2
Boeing 777-200IW	15.4	19.7	-6.8
Boeing 777-300	19.3	23.0	-5.1
Boeing MD-11	14.5	18.0	-5.9

Table 14.11- Results of wing location for sample aircraft

The figures shown above illustrate that there is reasonable agreement between the calculated and the actual data. The average error is 6.3%, while the maximum error is 9.1%. However the data does illustrate that in each case, the calculated location of the wing is fore of the actual location. This pattern has been investigated and a number of conclusions have been drawn. The likely cause of this trend is a combination of errors in the centre of gravity location calculation and in the neutral point calculation, associated with the basic assumption of a 5% static margin, and a neglect to include any active centre of gravity control calculations. Possible remedies to this situation where evaluated, including adjustments to the centre of gravity calculation, however these adjustments had knock on effects which degraded the performance of other calculations. It was decided that due to the complete lack of relevant data on the subject, a 6% error in the wing location could be tolerated.

14 .7 .2 TRIM CALCULATIONS

An example trim plot for an A300-600 aircraft at cruise conditions is shown below. The plot can be seen to include the main features one would expect from this kind of diagram.

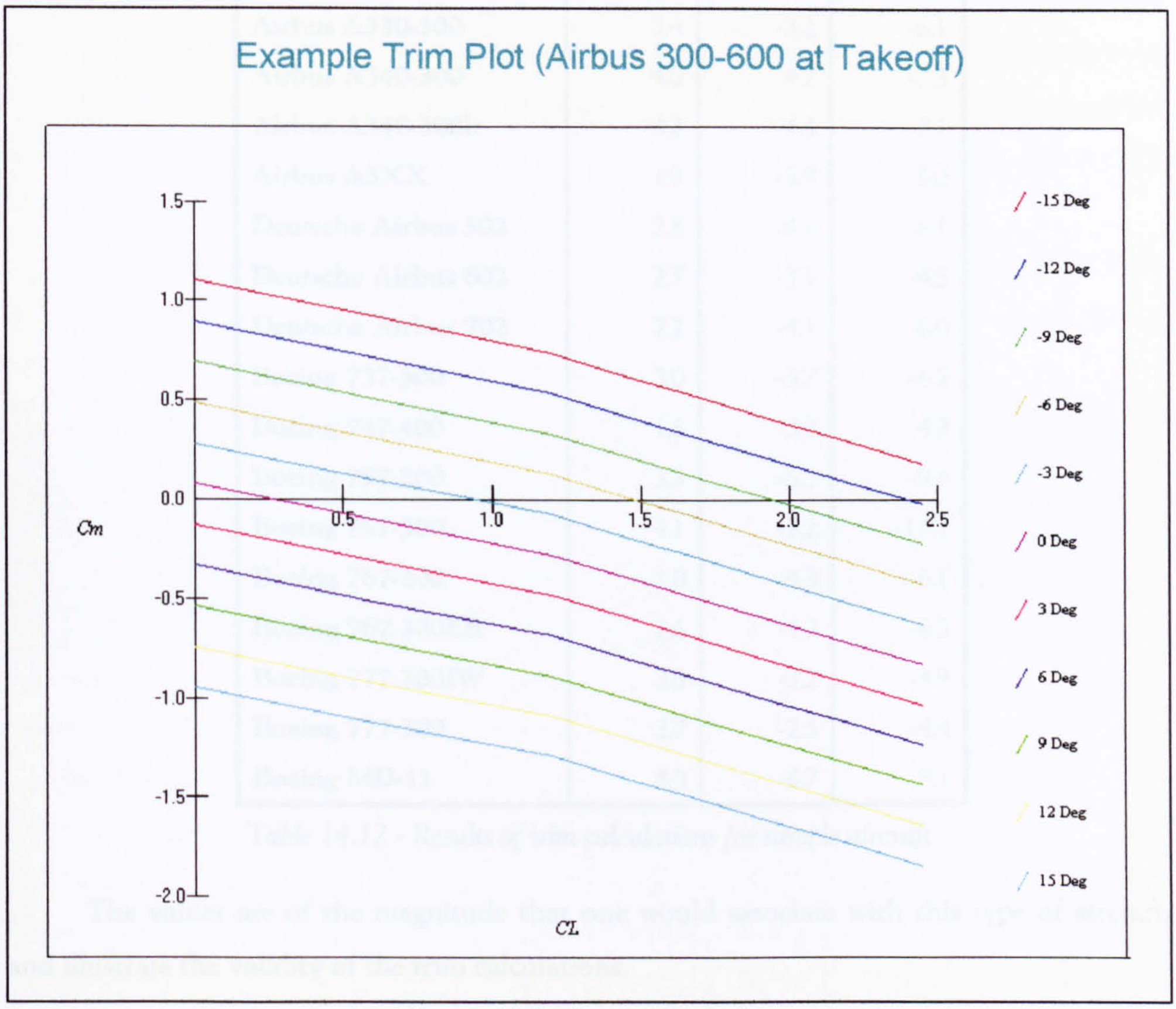


Figure 14.6 - Example trim plot

The module provides detailed results of the trim calculations for the aircraft at cruise, takeoff, and landing conditions. The values of the horizontal tail incidence angle required to trim the aircraft at these conditions are given in the table below.

Aircraft	i_{ht} (deg) *Cruise*	i_{ht} (deg) *Takeoff*	i_{ht} (deg) *Landing*
Airbus A300-600	1.9	-7.6	-11.8
Airbus A300-600ER	2.0	-7.7	-12.0
Airbus A310-300	3.5	-4.1	-5.2
Airbus A319	2.4	-4.0	-7.1
Airbus A320	2.6	-4.0	-7.4
Airbus A321	2.8	-3.6	-5.8

Aircraft	i_{ht} (deg) Cruise	i_{ht} (deg) Takeoff	i_{ht} (deg) Landing
Airbus A330-200	3.5	-3.8	-7.0
Airbus A330-300	3.4	-3.2	-6.1
Airbus A340-300	4.0	-4.2	-7.3
Airbus A340-300lr	4.2	-4.4	-7.1
Airbus A3XX	1.9	-3.9	-5.0
Deutsche Airbus 502	2.8	-4.3	-6.1
Deutsche Airbus 602	2.7	-3.1	-4.5
Deutsche Airbus 702	2.2	-4.1	-6.0
Boeing 737-300	3.0	-3.7	-6.2
Boeing 747-400	1.6	-3.3	-4.3
Boeing 757-200	3.3	-5.3	-9.4
Boeing 757-300	4.1	-7.2	-11.1
Boeing 767-200	1.8	-4.3	-6.1
Boeing 767-300ER	2.6	-4.2	-6.5
Boeing 777-200IW	3.0	-3.2	-4.9
Boeing 777-300	3.7	-2.5	-4.4
Boeing MD-11	4.3	-6.7	-8.1

Table 14.12 - Results of trim calculations for sample aircraft

The values are of the magnitude that one would associate with this type of aircraft, and illustrate the validity of the trim calculations.

14 .8 Performance Module results

This is the final calculation module, and brings together the output from all the other modules to predict the performance of the aircraft. The main output of this module is the range of the aircraft for a given fuel load and flight profile. The other parameters of interest are the takeoff and landing field lengths.

14 .8 .1 Flight Range

The methods used to calculate the detailed performance of the aircraft over the given flight profile have undergone extensive validation processes. The best indicator of the accuracy of these methods is the final predicted range of the aircraft for a given fuel load. The results could alternatively be presented in terms of the fuel required for a given range,

but this introduces further inaccuracies due to the takeoff weight of the aircraft being an unknown in the iteration process. Most aircraft designs were tested for a number of flight profiles, taken from a number of sources, and modelled as accurately as possible.

The range values taken from 'Janes' are assumed to occur at the design payload, and include reserves for a cruise to alternate airport and loiter as appropriate. The data taken from 'Flight International' occur at a specified payload, and does not include any reserves. Supplemental data for the Boeing 767 was supplied by British Airways, and includes loiter and diversion. The range values for the Deutsche Airbus conceptual designs also include loiter and diversion reserves.

The flight profiles were modelled to include any reserve policy by simulating the flight during the diversion and loiter portions, and then assuming that the remaining fuel at landing is zero. The resulting values of the calculated range are shown below:-

Aircraft	$W_{payload}$	*Range Data Source*	R_{cr1} actual (nm)	R_{cr1} calc (nm)	*Error* (%)	R_{cr1} calc (nm)	*Error* (%)
				Case 1		Case 2	
Airbus A300-600	26177	Janes	3600.0	3444.3	-4.3	3599.7	-0.0
Airbus A300-600R	26177	Janes	3950.0	3821.1	-3.3	3949.7	-0.0
Airbus A300-600R	41100	Flight	3283.1	3424.0	4.3	3355.6	2.2
Airbus A300-600R	27100	Flight	4697.8	4851.8	3.3	4762.2	1.4
Airbus A310	21441	Janes	5150.0	5093.6	-1.1	5150.3	0.0
Airbus A310	34350	Flight	4643.8	4716.2	1.6	4644.2	0.0
Airbus A319	12202	Janes	2650.0	2649.6	-0.0	2701.5	1.9
Airbus A320	14737	Janes	2700.0	2765.1	2.4	2648.8	-1.9
Airbus A320	14737	Janes	2700.0	2620.3	-3.0	2467.0	-8.6
Airbus A320	20000	Flight	2257.1	2107.2	-6.6	2152.6	-4.6
Airbus A320	13500	Flight	3671.9	3365.6	-8.3	3439.6	-6.3
Airbus A321	18151	Janes	2300.0	2433.5	5.8	2303.9	0.2
Airbus A321	22800	Flight	2078.9	2200.8	5.9	2161.3	4.0
Airbus A321	18050	Flight	3072.5	3085.7	0.4	3072.9	0.0
Airbus A330-200	25238	Janes	6400.0	6270.1	-2.0	6425.4	0.4
Airbus A330-300	32942	Janes	4500.0	4517.3	0.4	4401.8	-2.2
Airbus A330-300	46300	Flight	3995.9	4032.3	0.9	4033.6	0.9
Airbus A330-300	16500	Flight	7127.8	7260.6	1.9	7235.2	1.5
Airbus A340-300	29132	Janes	6600.0	6527.8	-1.1	6775.7	2.7
Airbus A340-300	51300	Flight	5831.8	5754.1	-1.3	5873.1	0.7
Airbus A340-300	21240	Flight	8693.7	8549.0	-1.7	8782.3	1.0

Aircraft	$W_{payload}$	Range Data Source	R_{crl} actual (nm)	R_{crl} calc (nm)	Error (%)	R_{crl} calc (nm)	Error (%)
				Case 1		Case 2	
Airbus A340-300lr	29132	Janes	7300.0	7255.9	-0.6	7514.3	2.9
Airbus A3XX	52413	Janes	7500.0	7203.0	-4.0	6846.9	-2.2
Deutsche Airbus 502	46729	Oelkers[9]	7000.0	6610.6	-5.6	7275.7	3.9
Deutsche Airbus 602	59949	Oelkers[9]	7000.0	7000.4	0.0	7613.2	8.8
Deutsche Airbus 702	71361	Oelkers[9]	7000.0	7471.4	-6.7	7406.0	-5.8
Boeing 737-300	13653	Janes	1600.0	1691.4	5.7	1590.1	-0.6
Boeing 737-300	8705	Flight	3187.0	3455.2	8.4	1720.2	9.0
Boeing 747-400	41413	Janes	7100.0	7404.6	4.3	7334.5	3.3
Boeing 747-400	63870	Flight	6949.6	7247.3	4.3	7263.1	4.5
Boeing 747-400	40840	Flight	8321.1	8677.5	4.3	8710.1	4.7
Boeing 747-600X	53637	Janes	7200.0	7361.4	2.2	-	-
Boeing 757-200	18284	Janes	2980.0	2947.5	-1.1	2490.2	-16.4
Boeing 757-300	24381	Janes	2980.0	3002.8	0.8	2883.0	-3.3
Boeing 757-300	29470	Flight	2926.7	3173.8	8.4	3033.9	3.7
Boeing 767-300	26331	Janes	3160.0	3173.0	0.4	3128.2	-1.0
Boeing 767-300Er	20697	Janes	5760.0	5975.5	3.7	5575.4	-3.2
Boeing 767-300Er	20843	B.A.	5150.0	5273.8	2.4	4947.3	-3.9
Boeing 767-300Er	30000	B.A.	3703.7	4069.6	9.9	3813.9	3.0
Boeing 767-300Er	3400	B.A.	7150.0	7466.6	4.4	7007.7	-2.0
Boeing 777-200IGW	30107	Janes	6300.0	6094.6	-3.3	5795.9	-8.0
Boeing 777-200IGW	54450	Flight	5000.2	5000.6	0.0	4984.1	-0.3
Boeing 777-200IGW	29050	Flight	7052.2	7169.3	1.7	7123.5	1.0
Boeing 777-300	36251	Janes	5700.0	5454.7	-4.3	5197.1	-8.8
Boeing MD-11	28937	Janes	7250.0	7250.3	0.0	6628.5	-8.6
Boeing MD-11	51272	Flight	5993.8	6672.6	11.3	6534.1	9.0

Table 14.13- Results of range calculations for sample aircraft

The results can be seen to give excellent agreement with the actual data. For case 1 the average error is 3.4%, with a maximum error of 11.3%. For case 2 the average error is 3.5%, with a maximum error of 16.4%. These results provide full validation of not only the Performance Module calculations, but of the results from all of the modules, especially the drag prediction and engine performance modules.

14 .8 .2 TAKEOFF AND LANDING DISTANCES

For the performance profiles given above, the resultant takeoff field lengths and landing field lengths are shown. These are compared to the actual values for the particular aircraft where possible. In many cases, data on the field lengths were conflicting depending on the source of the data, in these cases an average value has been chosen. Again, the results are presented for the two cases of the tuning factors set to 100%, and for the tuning factors adjusted to give correct weight and aerodynamic surface reference areas.

The takeoff field length results are:-

Aircraft	$W_{payload}$ (kg)	*Range Data Source*	FAR_{to} actual (m)	FAR_{to} calc (m)	*Error* (%)	FAR_{to} calc (m)	*Error* (%)
				Case 1		Case 2	
Airbus A300-600	26177	Janes	2280	2109	-7.5	2239	-1.8
Airbus A300-600R	26177	Janes	2290	2197	-4.0	2259	-1.3
Airbus A300-600R	41100	Flight	2290	2224	-2.9	2259	-1.3
Airbus A300-600R	27100	Flight	2290	2224	-2.9	2259	-1.3
Airbus A310	21441	Janes	2423	2242	-7.5	2194	-9.4
Airbus A310	34350	Flight	2423	2256	-6.9	2193	-9.5
Airbus A319	12202	Janes	1970	2303	16.9	2367	20.1
Airbus A320	14737	Janes	2336	2375	1.7	2304	-1.4
Airbus A320	14737	Janes	2336	2375	1.7	2304	-1.4
Airbus A320	20000	Flight	2336	2354	0.8	2309	-1.2
Airbus A320	13500	Flight	2336	2347	0.5	2302	-1.5
Airbus A321	18151	Janes	2328	2249	-3.4	2259	-3.0
Airbus A321	22800	Flight	2328	2261	-2.9	2283	-1.9
Airbus A321	18050	Flight	2328	2264	-2.7	2287	-1.8
Airbus A330-200	25238	Janes	--	2621	--	2700	--
Airbus A330-300	32942	Janes	2300	2464	7.1	2507	9.0
Airbus A330-300	46300	Flight	2300	2452	6.6	2511	9.2
Airbus A330-300	16500	Flight	2300	2452	6.6	2511	9.2
Airbus A340-300	29132	Janes	2870	3032	5.6	2963	3.3
Airbus A340-300	51300	Flight	2870	3043	6.0	2964	3.3
Airbus A340-300	21240	Flight	2870	3043	6.0	2964	3.3
Airbus A340-300lr	29132	Janes	3000	3409	13.6	3259	8.6
Airbus A3XX	52413	Janes	--	2943	--	3016	--
Deutsche Airbus 502	46729	Oelkers	--	3019	--	3036	--
Deutsche Airbus 602	59949	Oelkers	--	3029	--	2946	--

Aircraft	$W_{payload}$ (kg)	Range Data Source	FAR_{to} actual (m)	FAR_{to} calc (m)	Error (%)	FAR_{to} calc (m)	Error (%)
				Case 1		Case 2	
Deutsche Airbus 702	71361	Oelkers	--	2948	--	3006	--
Boeing 737-300	13653	Janes	2286	2146	-6.1	2136	-6.6
Boeing 737-300	8705	Flight	2286	2133	-6.7	2134	5.3
Boeing 747-400	41413	Janes	3220	3191	-0.9	2587	-2.4
Boeing 747-400	63870	Flight	3220	3193	-0.8	3141	-1.9
Boeing 747-400	40840	Flight	3220	3191	-0.9	3158	-2.0
Boeing 747-600X	53637	Janes	-	3370	-	3155	--
Boeing 757-200	18284	Janes	1720	1891	9.9	1917	11.5
Boeing 757-300	24381	Janes	2044	2098	2.6	2082	1.8
Boeing 757-300	29470	Flight	2044	2098	2.6	2081	1.8
Boeing 767-300	26331	Janes	1798	2215	23.2	2209	22.9
Boeing 767-300Er	20697	Janes	2545	2578	1.3	2498	-1.8
Boeing 767-300Er	20843	B.A.	2545	2315	-9.0	2419	-4.9
Boeing 767-300Er	30000	B.A.	2545	2304	-9.5	2408	-5.4
Boeing 767-300Er	3400	B.A.	2545	2304	-9.5	2408	-5.4
Boeing 777-200IGW	30107	Janes	2652	2520	-5.0	2546	-4.0
Boeing 777-200IGW	54450	Flight	2652	2486	-6.2	2546	-4.0
Boeing 777-200IGW	29050	Flight	2652	2486	-6.2	2546	-4.0
Boeing 777-300	36251	Janes	2652	2701	1.9	2791	5.3

Table 14.14 - Results of takeoff field length calculations for sample aircraft

For this type of calculation, and considering the unreliable nature of some of the available data, these results give good agreement, and definitely provide a more accurate method of estimating the takeoff field length than empirical methods provided in standard text books. For case 1 the average error is 5.7% and the maximum error is 23.2%, while for case 2 the average error is 5.4% and the maximum error is 22.9%.

The results of the FAR landing field length calculations are:-

Aircraft	$W_{payload}$ (kg)	Range Data Source	FAR_{ta} actual (m)	FAR_{ta} calc (m)	Error (%)	FAR_{ta} calc (m)	Error (%)
				Case 1		Case 2	
Airbus A300-600	26177	Janes	1536	1573	2.4	1589	3.4
Airbus A300-600R	26177	Janes	1555	1596	2.7	1604	3.1
Airbus A300-600R	41100	Flight	1555	1599	2.8	1604	3.1
Airbus A300-600R	27100	Flight	1555	1548	-0.4	1553	-0.1
Airbus A310	21441	Janes	1500	1609	7.3	1603	6.9
Airbus A310	34350	Flight	1500	1610	7.3	1603	6.9
Airbus A319	12202	Janes	1420	1555	9.5	1562	10.0
Airbus A320	14737	Janes	1470	1562	6.3	1555	5.8
Airbus A320	14737	Janes	1470	1562	6.3	1555	5.8
Airbus A320	20000	Flight	1470	1560	6.2	1556	5.8
Airbus A320	13500	Flight	1470	1560	6.1	1555	5.8
Airbus A321	18151	Janes	1587	1558	-1.8	1562	-1.6
Airbus A321	22800	Flight	1587	1559	-1.8	1564	-1.4
Airbus A321	18050	Flight	1587	1559	-1.7	1564	-1.4
Airbus A330-200	25238	Janes	--	1680	--	1687	--
Airbus A330-300	32942	Janes	1760	1673	-5.0	1674	-4.9
Airbus A330-300	46300	Flight	1760	1672	-5.0	1674	-4.9
Airbus A330-300	16500	Flight	1760	1672	-5.0	1674	-4.9
Airbus A340-300	29132	Janes	1926	1709	-11.2	1704	-11.5
Airbus A340-300	51300	Flight	1926	1710	-11.2	1704	-11.5
Airbus A340-300	21240	Flight	1926	1710	-11.2	1704	-11.5
Airbus A340-300lr	29132	Janes	1964	1758	-10.5	1749	-11.0
Airbus A3XX	52413	Janes	--	1696	--	1699	--
Deutsche Airbus 502	46729	Oelkers	--	1698	--	1697	--
Deutsche Airbus 602	59949	Oelkers	--	1704	--	1703	--
Deutsche Airbus 702	71361	Oelkers	--	1701	--	1701	--
Boeing 737-300	13653	Janes	1433	1573	9.8	1572	9.7
Boeing 737-300	8705	Flight	1433	1571	9.6	1572	-9.8
Boeing 747-400	41413	Janes	2073	1868	-9.9	1865	-10.1
Boeing 747-400	63870	Flight	2073	1868	-9.9	1866	-10.0
Boeing 747-400	40840	Flight	2073	1868	-9.9	1865	-10.0
Boeing 747-600X	53637	Janes	-	1892	-	1892	-
Boeing 757-200	18284	Janes	1494	1513	1.2	1518	1.6
Boeing 757-300	24381	Janes	1700	1549	-8.9	1546	-9.0

Aircraft	$W_{payload}$ (kg)	Range Data Source	FAR_{la} actual (m)	FAR_{la} calc (m)	Error (%)	FAR_{la} calc (m)	Error (%)
				Case 1		Case 2	
Boeing 757-300	29470	Flight	1700	1549	-8.9	1546	-9.0
Boeing 767-300	26331	Janes	1463	1610	10.0	1606	9.8
Boeing 767-300Er	20697	Janes	1646	1698	3.1	1689	2.6
Boeing 767-300Er	20843	B.A.	1646	1671	1.5	1684	2.3
Boeing 767-300Er	30000	B.A.	1646	1670	1.5	1683	2.2
Boeing 767-300Er	3400	B.A.	1646	1670	1.5	1683	2.2
Boeing 777-200IGW	30107	Janes	1661	1642	-1.2	1646	-0.9
Boeing 777-200IGW	54450	Flight	1661	1639	-1.3	1646	-0.9
Boeing 777-200IGW	29050	Flight	1661	1639	-1.3	1646	-0.9
Boeing 777-300	36251	Janes	1860	1799	-3.3	1811	-2.6

Table 14.15 - Results of landing field length calculations for sample aircraft

As with the takeoff field length results, the values of the FAR landing field distance give good agreement to the actual values, and illustrates the validity of the method used. For case 1 the average error is 5.6% and the maximum error is 11.2%. For case 2 the average error is also 5.6% and the maximum error is 15.2%.

14 .9 Fuselage Sizing Results

The results of the fuselage sizing tool are presented below for a variety of existing and concept aircraft.

14 .9 .1 Fuselage Cross Section

Based upon data of the actual type of cross section, the seating layout, the seat sizes, and the aisle widths of the aircraft, an estimate of the fuselage cross-section could be made. The design size of the fuselage is assumed to depend on the tourist class layout. If the actual seat size or aisle width was unknown then an educated guess was taken. The agreement of these estimates with the actual fuselage cross-section is shown below. In the table below, values separated by a slash indicate lower deck and upper deck values.

Aircraft	Seat No.	Seat Size (w x h x d) (cm)	Aisle Width (cm)	b_{fuse} actual (m)	b_{fuse} calc. (m)	Error (%)	h_{fuse} actual (m)	h_{fuse} calc. (m)	Error (%)
A300/310	8	46x104x66	60	5.64	5.68	0.7	5.64	5.68	0.7
A320/319/321	6	46x104x66	50	3.95	3.91	1.0	3.95	3.91	1.0
A330/340	9	42x98x66	50	5.64	5.63	0.2	5.64	5.63	0.2
A3XX	8/10	42x98x66	50/50	6.95	6.81	-2.0	8.47	8.51	-0.5
DA 502	11	46x104x66	64	7.82	7.80	-0.3	7.82	7.80	-0.3
DA 602	9/6	46x104x66	50/63	6.54	6.77	3.5	8.76	8.80	0.5
DA 702	11/7	46x104x66	51/51	7.70	7.57	-1.7	8.94	8.70	-2.7
B. 737-300	6	43.5x104x66	55	3.85	3.82	-0.8	3.85	3.82	-0.8
B. 747	10/6	43.5x104x66	50/43	6.11	6.25	2.3	6.85	6.88	0.4
B. 757	6	43.5x104x66	55	3.72	3.82	2.6	3.72	3.82	2.6
B. 767	7	43.5x104x66	55	5.03	4.92	2.2	5.03	4.92	2.2
B. 777	10	43.5x104x66	55	6.20	6.36	2.5	6.20	6.36	2.5
B. MD-11	9	46x104x66	48	6.02	5.98	-0.7	6.02	5.98	-0.7

Table 14.16 - Results of fuselage cross-section sizing for sample aircraft

These results show a high degree of accuracy, even for double deck and 747-type fuselage shapes. The average error for the fuselage width is 1.6%, with a maximum error of 2.6%. The height calculation has an average error of 1.2%, with a maximum error of 2.7%.

14 .9 .2 FUSELAGE LENGTH

Once the cross-section of the fuselage is known, then the fuselage length can be estimated for a given class distribution of seating. The results of this calculation are shown below. The letters T (tourist), B (business), and 1st (1st class), indicate the values for each of these classes. The cross-sectional seating number for each class (and for each deck), the overall seating distribution for each class, and the seat pitch values for each class are the main values involved in determining the fuselage length, and are displayed below.

Aircraft	*Seat No.* T-B-1st	*Seat Distribution* T-B-1st	*Seat Pitch* T-B-1st (in)	l_{fuse} actual (m)	l_{fuse} calc. (m)	*Error* (%)
A300	8 - 0 - 6	240 - 0 - 26	32 - 0 - 40	53.3	53.1	0.4
A310	9 - 0 - 0	280 - 0 - 0	30 - 0 - 0	45.1	47.1	4.4
A319	6 - 0 - 4	112 -0 - 12	32 - 0 - 36	33.8	34.1	0.9
A320	6 - 0 - 4	138 -0 - 12	32 - 0 - 36	38.5	38.2	-0.8
A321	6 - 0 - 4	169 -0 - 16	32 - 0 - 36	44.5	43.3	-2.7
A330/340	9 - 0 - 0	444 - 0 - 0	28 - 0 - 0	63.6	63.6	0.0
A3XX	10 - 0 - 0 (l) 8 - 0 - 0 (u)	854 - 0 - 0	30 - 0 - 0	68.3	70.5	3.2
DA 502	11 - 10 - 6	309 - 133 - 34	34 - 36- 60	75.7	79.7	5.3
DA 602	9 - 8 - 6 (l) 6 - 0 - 0 (u)	399 - 172 - 40	34 - 36- 60	78.8	71.8	-8.9
DA 702	11 - 10 -6 (l) 7 - 0 - 0 (u)	474 -202 - 51	34 - 36- 60	84.1	77.6	-7.7
B. 737-300	6 - 0 - 4	120 - 0 - 8	32- 0 - 36	33.4	34.5	3.3
B. 747-400	10 - 6 - 0 (l) 6 - 0 - 0 (u)	482 - 42 -0	32 - 38 - 0	68.6	70.4	2.6
B. 747-600X	10 - 0 - 0 (l) 6 - 0 - 0 (u)	700 - 0 -0	32 - 0 - 0	73.8	77.0	4.3
B. 757-200	6 - 4 - 0	196 - 0 - 12	32 - 38 - 0	47.0	49.2	4.7
B. 757-300	6 - 4 - 0	238 - 0 - 12	32 - 38 - 0	54.0	54.8	1.5
B. 767-200	7 - 6 - 0	206 - 0 - 18	32 - 38 - 0	47.2	49.2	4.2
B. 767-200	7 - 6 - 0	245 - 0 - 25	32 - 38 - 0	53.7	54.9	1.2
B. 777-200	10 - 0 - 0	440 - 0 - 0	28 - 0 - 0	62.8	61.8	-1.6
B. 777-300	10 - 0- 0	550- 0 - 0	28 - 0 - 0	72.9	71.5	-1.4
B. MD-11	9 - 0 - 0	410 - 0 - 0	28 - 0 - 0	58.7	62.4	6.3

Table 14.17 - Results of fuselage length estimation for sample aircraft

These results show excellent agreement for all aircraft, including double deck concept aircraft. The average error is 3.3%, and the maximum error is 8.9%. This illustrates that the fuselage sizing tool can be used with a high degree of confidence.

15 .Design Study Results

The results of the design studies into UHCA aircraft and aircraft incorporating advanced technologies are presented here. The first study concentrates on comparing four possible fuselage configurations for an 800 seat concept aircraft, all based on the same technology level.

15 .1 800 Seat Concept Designs

Four designs based on a double deck fuselage, a '747' type fuselage, a horizontal double bubble fuselage, and a vertical double bubble fuselage, were evaluated bearing in mind the design goals and constraints described below.

15 .1 .1 Design Goals and Constraints

Each aircraft has been designed to carry 800 passengers in an all economy layout (a seat pitch of 32in) for a range of 7000nm (excluding reserves). The main physical dimensions of the aircraft have been constrained in line with the values suggested in Chapter 2 for new UHCA regulations. This means that the wing span must be less than or equal to 90 metres, and that the fuselage length is also limited to 90m. The cruise is assumed to occur at a Mach number of 0.85, and at an altitude that is chosen to be optimal for each aircraft. The technology level of the aircraft is assumed to be of the type anticipated for the year 2000. A summary of the design constraints are given in figure 15.1 below.

Passenger Load	- 800 (economy)
Seat Pitch	- 32in
Range	- 7000nm
Cruise Mach Number	- 0.85
Length	- 90m
Wing Span	- 90m
Engine Year of Service	- Year 2000
Advanced Material Level	- Year 2000

Figure 15.1- UHCA design example constraints

These values were chosen to give an aircraft of greater payload-range capacity than any concept aircraft produced by the major aircraft manufacturers. In comparison, the Airbus A3XX-200 is designed to carry approximately 660 passengers a distance of 7500nm, whereas the Boeing-747-600X is designed to carry only 550 passengers a distance of 7200nm.

The Deutsche Airbus 702 concept described by Oelkers[9] is possibly the aircraft that is most similar to the concept aircraft designed here. It is capable of carrying 727 passengers with a range of 7000nm, however this passenger load is contained within a very spacious three class layout, which results in a much larger and heavier aircraft.

15 .1 .2 Design Assumptions

For each design a number of common assumptions were made, mainly relating to the design input parameters. These are summarised below:-

Parameter Name	Value	Unit
Engine Bypass Ratio	8.0	-
Root Airfoil T\C ratio	14.1	%
Tip Airfoil T\C ratio	11.0	%
Tail Airfoil T\C ratio	11.0	%
Airfoil Critical Mach Number TF	100	%
Overall Aerodynamic Efficiency TF	103	%
Wing AMWS	10.5	%
Fuselage AMWS	6.0	%
Vertical Tail AMWS	27.0	%
Horizontal Tail AMWS	22.5	%
Nacelle AMWS	19.5	%
Surface Control AMWS	24.8	%
Undercarriage AMWS	3.0	%
Hydraulic AMWS	5.0	%
Electrics AMWS	5.0	%
Air Conditioning AMWS	5.0	%
Furnishing AMWS	5.0	%
Operational Items AMWS	2.0	%
Wing Taper Ratio	0.25	-
Wing Quarter Chord Sweep	35.0	deg
Wing Twist	3.0	deg
Crank Span / Wing Span	0.25	-
Landing Lift Coefficient	2.4	-
Landing Velocity	145	Knots
Wing Spoiler Area	20	m^2
Wing Airbrake Area	30	m^2
Horizontal Tail Aspect Ratio	5.0	-
Vertical Tail Aspect Ratio	1.8	-
Horizontal Tail Taper Ratio	0.2	-
Vertical Tail Taper Ratio	0.3	-
Horizontal Tail Quarter Chord Sweep	27.0	deg
Vertical Tail Quarter Chord Sweep	30.0	deg

Table 15.1- UHCA design example assumptions

15 .1 .3 Design Procedure

Given the design constraints and the design assumptions shown above, each design can then be evaluated. This initial evaluation will be carried out with all initial sizing and tail sizing tuning factors set to 100%. Subsequent evaluations will then be carried out, with a number of parameters being modified in order to find the correct design point. The wing aspect ratio, the engine thrust, the L/D ratio tuning factor, the takeoff weight tuning factor, the flap layout and location parameters, the cruise altitude, and the wing location parameter, are all set such that the final design is the optimal design that satisfies the given constraints, and provides consistent results. This means that as well as satisfying the main design requirements, these parameters are set such that the estimate of the operational empty weight from the Initial Sizing Module exactly equals the detailed operational empty weight estimate, the range predicted from the performance module exactly equals the design range, and the cruise static margin is equal to 10%.

This procedure was carried out for each of the fuselage concepts, and the final design point was found in each case. Each aircraft satisfied all the design requirements, and the results produced appear to be of the magnitude that one would associate with this type of aircraft.

A study was carried out to assess the effect of varying the wing loading of the designs, and although some performance benefit could be gained by increasing the wing loading up to a point, this benefit was found to be negligible (a maximum takeoff weight reduction of approximately 2%), and so optimisation for wing loading was not performed.

15 .1 .4 Design Results

The four concept aircraft are shown as three dimensional models on the following four pages. These models were produced automatically from the design data, and illustrate the main features of the aircraft, including the chosen seating arrangements.

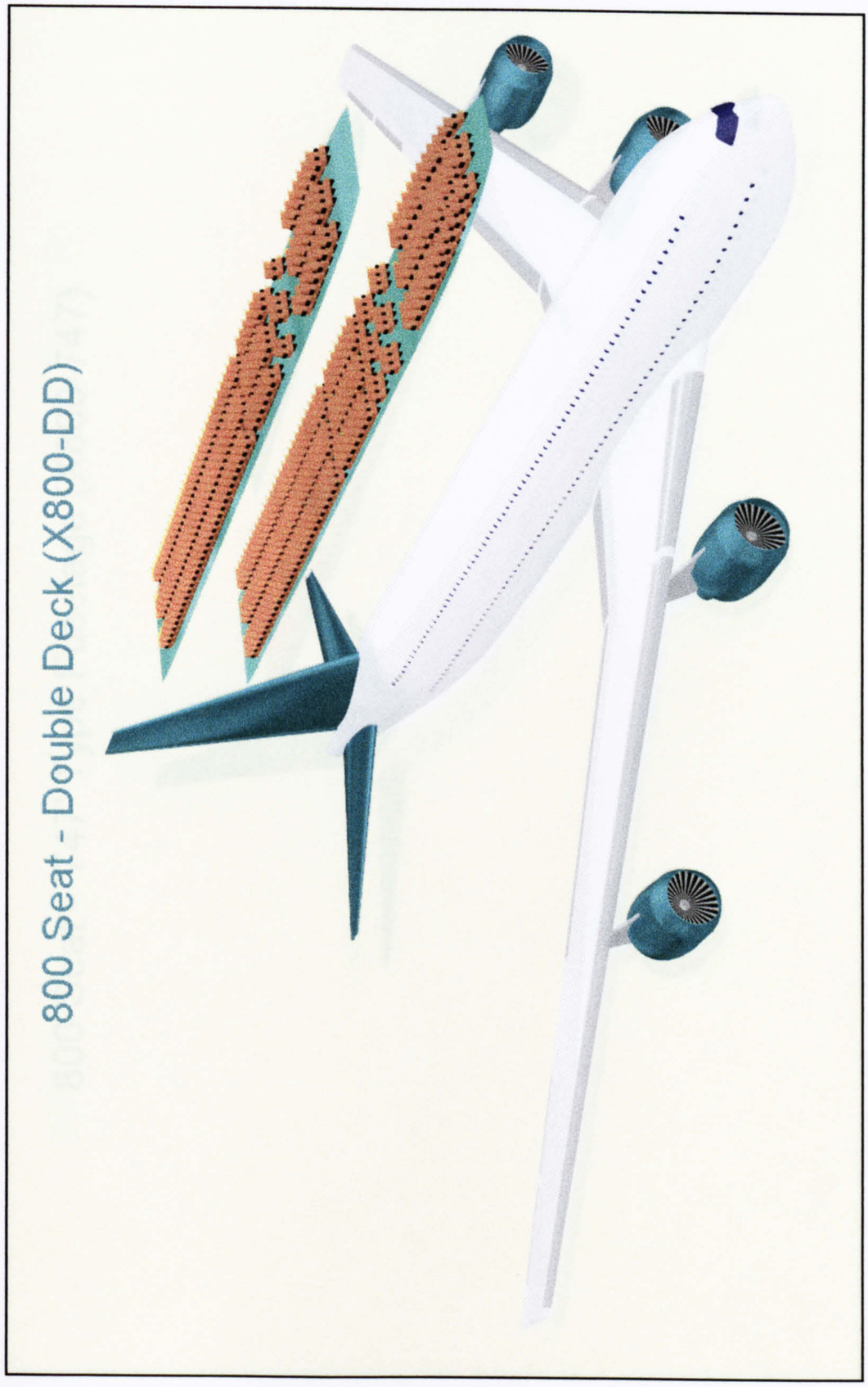


Figure 15.2



Figure 15.3

Figure 15.4

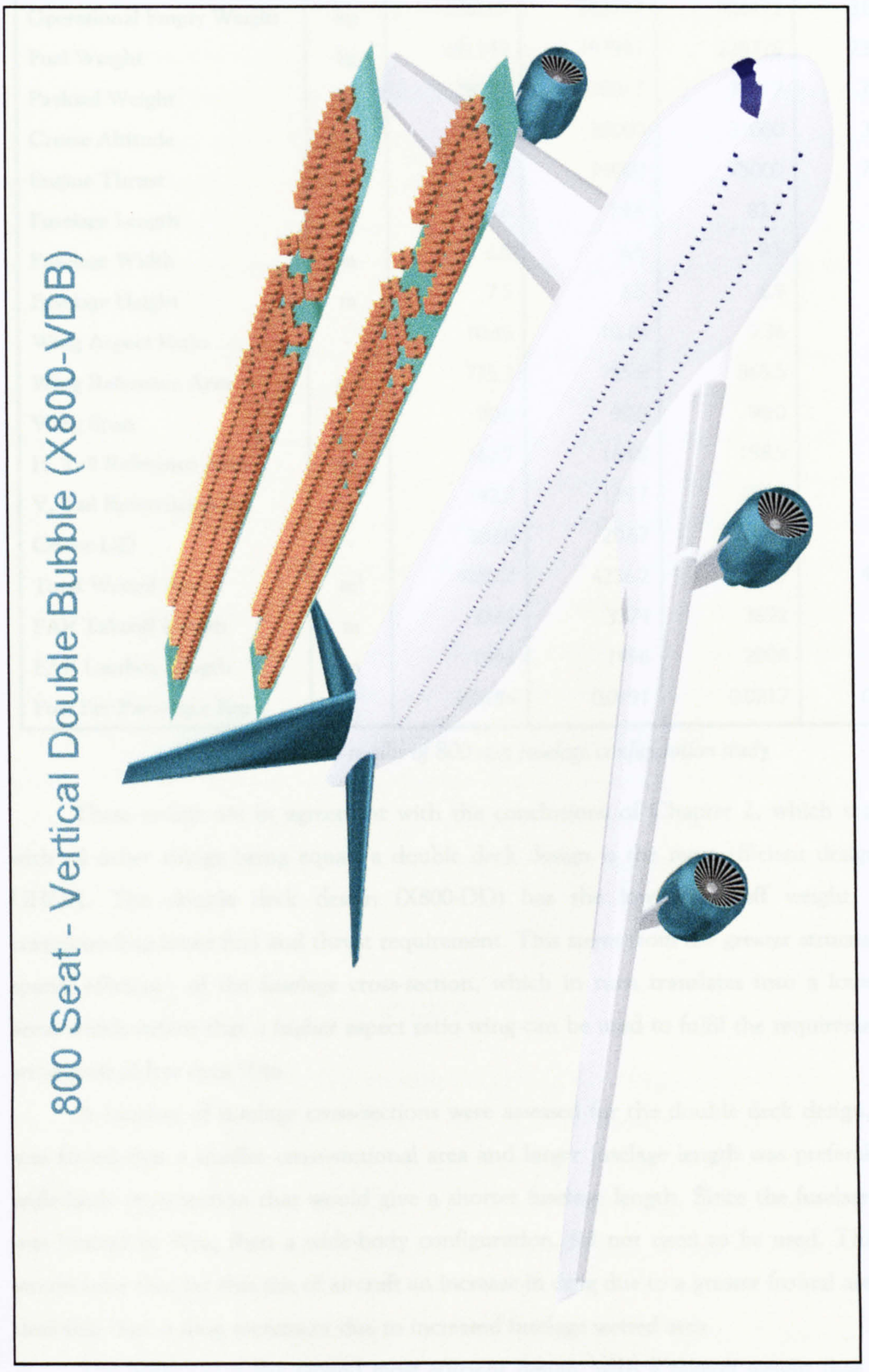


Figure 15.5

The main output parameters for each design concept are shown in the table below:-

Parameter Name	Unit	X800-DD	X800-747	X800-HDB	X800-VDB
Takeoff Weight	kg	545281	559799	608719	621135
Operational Empty Weight	kg	276119	283787	305472	310681
Fuel Weight	kg	191143	197993	225228	232436
Payload Weight	kg	78017	78017	78017	78017
Cruise Altitude	ft	35000	35000	31000	31000
Engine Thrust	LBF	73000	74000	75000	75000
Fuselage Length	m	73.6	79.4	82.7	85.0
Fuselage Width	m	6.5	6.5	9.5	7.1
Fuselage Height	m	7.5	6.5	6.9	9.8
Wing Aspect Ratio	-	10.45	10.18	9.36	9.17
Wing Reference Area	m^2	775.3	795.9	865.5	883.1
Wing Span	m	90.0	90.0	90.0	90.0
H. Tail Reference Area	m^2	162.7	164.8	198.5	192.1
V. Tail Reference Area	m^2	142.7	139.7	154.5	145.3
Cruise L\D	-	20.88	20.67	19.55	19.28
Total Wetted Area	m^2	4057.7	4236.2	4766.3	4995.8
FAR Takeoff Length	m	3345	3374	3692	3771
FAR Landing Length	m	1995	1996	2008	2008
Fuel Per Passenger-Km	-	0.0184	0.0191	0.0217	0.0224

Table 15.2- Main results of 800 seat fuselage configuration study

These results are in agreement with the conclusions of Chapter 2, which state that with all other things being equal, a double deck design is the most efficient design for a UHCA. The double deck design (X800-DD) has the lowest takeoff weight, and a corresponding lower fuel and thrust requirement. This stems from the greater structural and spatial efficiency of the fuselage cross-section, which in turn translates into a lower wing area, which means that a higher aspect ratio wing can be used to fulfil the requirement of a wing span of less than 90m.

A number of fuselage cross-sections were assessed for the double deck design, and it was found that a smaller cross-sectional area and larger fuselage length was preferable to a wide-body cross-section that would give a shorter fuselage length. Since the fuselage length was limited to 90m, then a wide-body configuration did not need to be used. This result would infer that for this size of aircraft an increase in drag due to a greater frontal area is less desirable than a drag increment due to increased fuselage wetted area.

The X800-747 is the second most efficient design, with a takeoff weight that is 2.7% greater than that of the X800-DD. This is a result of the larger fuselage length required to fit

the 800 passengers, and the structural inefficiencies related to the construction of an upper 'bubble'.

The X800-HDB has a takeoff weight that is 11.6% greater than that of the X800-DD. Again this is due to the large fuselage length and the inefficient use of space, which results in a heavier fuselage structure and a larger wetted area.

The takeoff weight of the X800-VDB is 13.9% greater than that of the X800-DD. The reasons for this are mainly related to the inefficient use of space within the fuselage cross-section, which results in a heavier fuselage, and in turn increases the wetted area of the aircraft. These facts mean that a larger wing is required, the aspect ratio must be reduced, and the engine thrust requirement is increased. These all conspire to increase the takeoff weight of the aircraft.

Although the X800-DD has a slightly greater payload-range than the Deutsche Airbus 702 concept aircraft, the X800-DD takeoff weight is 12.6% smaller than that of the DA702. The main reasons for this are a much smaller fuselage, derived by specifying an all economy class layout with 32in pitch, rather than the more luxurious 3-class arrangement of the DA702. This, combined with a greater use of advanced materials, and the incorporation of engines of higher bypass ratio allow the takeoff weight to be reduced, and hence the wing area can be reduced accordingly. This means that the X800-DD can have a wing of aspect ratio 10.45, compared to 8.6 for the DA702. This higher aspect ratio wing increases the aerodynamic efficiency of the aircraft, and further reduces the takeoff weight.

These results indicate that presuming the environmental and noise issues, and the airport compatibility issues raised in chapter 2 can be resolved, then this type of aircraft could be built using today's technology, or very near future technology. Importantly, the predicted weight of the X800-DD aircraft is well below the proposed 635 ton limit (see chapter 2).

15 .2 1000 Seat Concept

A greater challenge to the aviation industry is the design of an aircraft capable of carrying 1000 passengers up to a range of 7000nm. It is envisaged that this kind of aircraft would need to rely heavily on advanced technologies to increase the efficiency of the aircraft, and to reduce its size to an acceptable level. It is for this reason that a 1000 seat aircraft concept designed around year 2000 technology has also been chosen as a baseline for the advanced technology studies

The design constraints, assumptions, and procedures, are exactly as described for the 800 seat concept aircraft described in sections 15.1.1 to 15.1.3. The fuselage cross-section used was of the same dimensions as the cross-section of the 800 seat double deck aircraft, but

the fuselage was stretched to accommodate the extra passengers. The resulting design is shown below in figure 15.6.

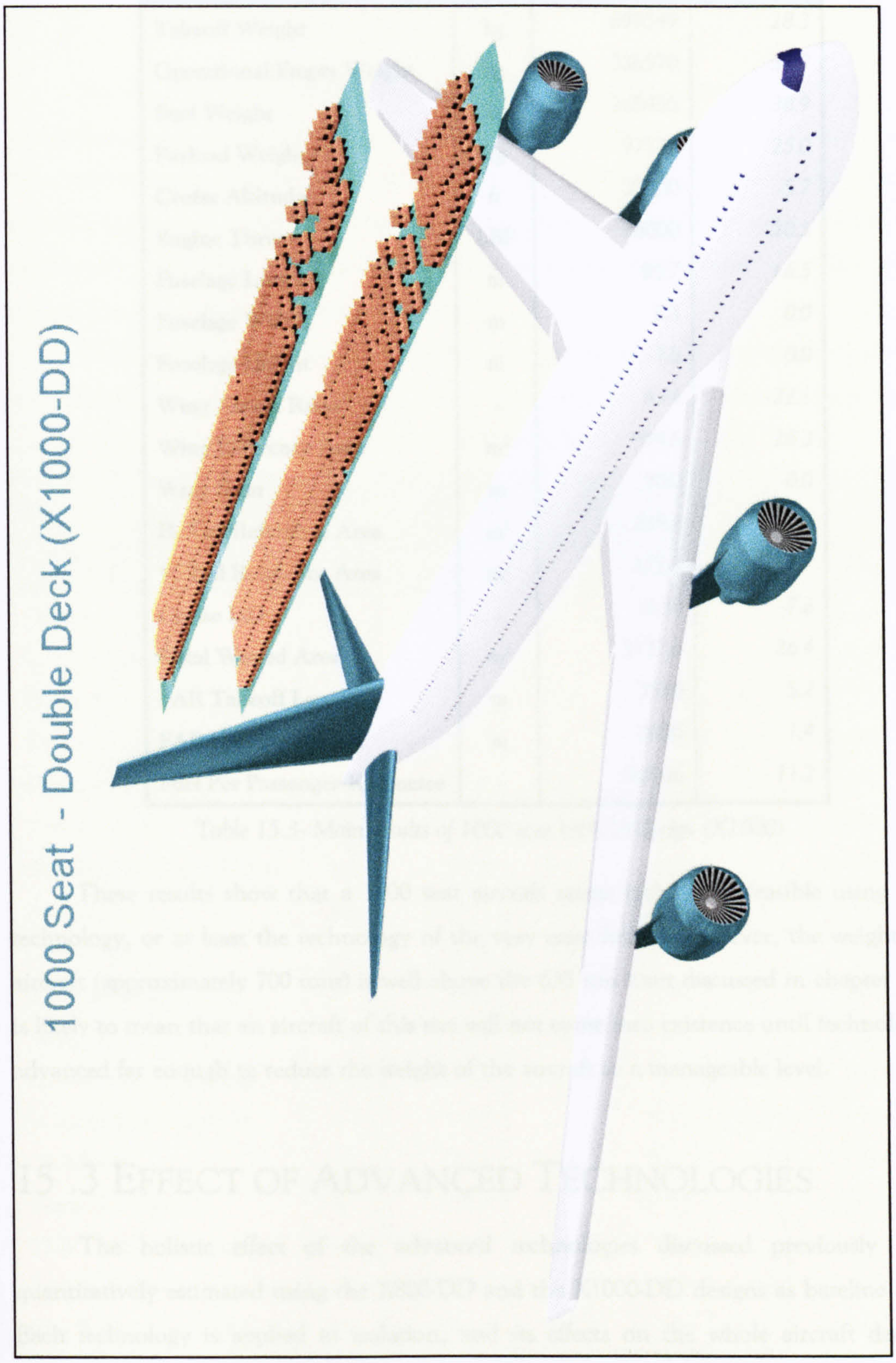


Figure 15.6

The main output parameters of the design are presented below in table 15.3, along with a comparison to the 800 seat double deck design. The comparative value of each parameter (Δx) is expressed in terms of (X1000-X800)/X800 x 100%.

Parameter Name	*Unit*	*X1000-DD*	*Δx (%)*
Takeoff Weight	kg	699549	*28.3*
Operational Empty Weight	kg	336570	*21.9*
Fuel Weight	kg	265455	*38.9*
Payload Weight	kg	97522	*25.0*
Cruise Altitude	ft	33000	*-5.7*
Engine Thrust	LBF	88000	*20.5*
Fuselage Length	m	85.7	*16.5*
Fuselage Width	m	6.5	*0.0*
Fuselage Height	m	7.5	*0.0*
Wing Aspect Ratio	-	8.14	*-22.1*
Wing Reference Area	m^2	994.6	*28.3*
Wing Span	m	90.0	*0.0*
H. Tail Reference Area	m^2	248.2	*52.6*
V. Tail Reference Area	m^2	175.2	*22.7*
Cruise L\D	-	19.38	*-7.2*
Total Wetted Area	m^2	5127.6	*26.4*
FAR Takeoff Length	m	3520	*5.2*
FAR Landing Length	m	2020	*1.4*
Fuel Per Passenger-Kilometre	-	0.0205	*11.2*

Table 15.3- Main results of 1000 seat UHCA design (X1000)

These results show that a 1000 seat aircraft seems technically feasible using today's technology, or at least the technology of the very near future. However, the weight of the aircraft (approximately 700 tons) is well above the 635 ton limit discussed in chapter 2. This is likely to mean that an aircraft of this size will not come into existence until technology has advanced far enough to reduce the weight of the aircraft to a manageable level.

15 .3 Effect of Advanced Technologies

The holistic effect of the advanced technologies discussed previously is now quantitatively estimated using the X800-DD and the X1000-DD designs as baseline aircraft. Each technology is applied in isolation, and its effects on the whole aircraft design are appraised. This means that the design procedure discussed in 15.1.3 is followed for each design, but with the particular advanced technology present. The only difference in design

procedure being that rather than varying the aspect ratio to maintain a wing span of 90m, the aspect ratio of the wings is kept constant, so as to better isolate the effect of the technology itself.

15 .3 .1 ADVANCED ENGINES

The effect of three proposed advanced propulsion concepts are evaluated. The first is a turbofan engine with a bypass ratio of 12, designed for entry into service in the year 2005. This represents the limit to which current turbofan engine technology can be pushed. The second engine is an advanced ducted propeller of bypass ratio 15, estimated to enter service in the year 2010. The most advanced engine is a contrafan engine of bypass ratio 20, designed to enter service in the year 2020.

The effect of these engines on the 800 seat design is shown in the table below. The main design parameters are presented, along with their percentage displacements from the baseline design (which incorporates a year 2000 turbofan of bypass ratio 8).

Parameter Name	*Unit*	*X800-DD*	*Δx (%)*	*X800-DD*	*Δx (%)*	*X800-DD*	*Δx (%)*
		Engine 1		**Engine 2**		**Engine 3**	
Engine Type	-	Turbofan	-	A.D.P.	-	Contrafan	-
Year of Service	-	2005	-	2010	-	2020	-
Bypass Ratio	-	12	*50.0*	15	*87.5*	20	*150.0*
Thrust	LBF	72000	*-1.4*	73000	*0.0*	74000	*1.4*
Cruise s.f.c.	hr^{-1}	0.498	*-6.2*	0.425	*-18.9*	0.363	*-31.6*
Takeoff Weight	kg	538579	*-1.2*	498315	*-8.6*	459789	*-15.7*
Operational Empty Weight	kg	275084	*-0.4*	262676	*-4.9*	244408	*-11.5*
Fuel Weight	kg	185477	*-3.0*	157621	*-17.5*	137364	*-28.1*
Cruise Altitude	ft	35000	*0.0*	35000	*0.0*	35000	*0.0*
Wing Reference Area	m^2	765.7	*-1.2*	708.5	*-8.6*	653.7	*-15.7*
Wing Span	m	89.5	*-0.6*	86.0	*-4.4*	82.7	*-8.2*
H. Tail Reference Area	m^2	157.6	*-3.1*	137.3	*-15.6*	120.3	*-26.0*
V. Tail Reference Area	m^2	138.0	*-3.3*	119.5	*-16.3*	104.3	*-27.0*
Cruise L\D	-	20.16	*-3.4*	19.12	*-8.4*	17.54	*-16.0*
Total Wetted Area	m^2	4070.9	*0.3*	3972.9	*-2.1*	3974.6	*-2.0*
FAR Takeoff Length	m	3402	*1.7*	3119	*-6.7*	2873	*-14.1*
FAR Landing Length	m	1993	*-0.1*	1989	*-0.3*	1983	*-0.6*
Fuel Per Passenger-Km	-	0.0179	*-3.0*	0.0152	*-17.5*	0.0132	*-28.2*

Table 15.4 - Effect of advanced technology engines on X800 aircraft

The results of the study for the 1000 seat concept aircraft are given below in table 15.5.

Parameter Name	Unit	X1000-DD	Δx (%)	X1000-DD	Δx (%)	X1000-DD	Δx (%)
		Engine 1		Engine 2		Engine 3	
Engine Type	-	Turbofan	-	A.D.P.	-	Contrafan	-
Year of Service	-	2005	-	2010	-	2020	-
Bypass Ratio	-	12	*50.0*	15	*87.5*	20	*150.0*
Thrust	LBF	90000	*2.3*	88000	*0.0*	93000	*5.7*
Cruise s.f.c.	hr^{-1}	0.519	*-5.5*	0.442	*-19.5*	0.376	*-31.4*
Takeoff Weight	kg	692178	*-1.1*	626063	*-10.5*	580016	*-17.1*
Operational Empty Weight	kg	336629	*0.0*	314751	*-6.5*	295114	*-12.3*
Fuel Weight	kg	258027	*-2.8*	213790	*-19.5*	187381	*-29.4*
Cruise Altitude	ft	33000	*0.0*	33000	*0.0*	33000	*0.0*
Wing Reference Area	m^2	984.1	*-1.1*	890.1	*-10.5*	824.7	*-17.1*
Wing Span	m	89.5	*-0.5*	85.1	*-5.4*	82.0	*-8.9*
H. Tail Reference Area	m^2	240.4	*-3.1*	200.3	*-19.3*	175.9	*-29.1*
V. Tail Reference Area	m^2	169.4	*-3.3*	140.3	*-19.9*	122.8	*-29.9*
Cruise L\D	-	18.69	*-3.6*	17.77	*-8.3*	16.25	*-16.1*
Total Wetted Area	m^2	5153.8	*0.5*	4921.7	*-4.0*	4945.0	*-3.6*
FAR Takeoff Length	m	3446	*-2.1*	3208	*-8.9*	2853	*-18.9*
FAR Landing Length	m	2021	*0.0*	2017	*-0.2*	2014	*-0.4*
Fuel Per Passenger-Km	-	0.0199	*-2.8*	0.0165	*-19.4*	0.0145	*-29.4*

Table 15.5- Effect of advanced technology engines on X1000 aircraft

These results show the kinds of trend that one would expect with the application of advanced technology engines. The results from both designs show good agreement, and are consistent with the mechanisms involved in bringing about any performance benefit. It is clear from the results that as the fuel consumption of the engine improves, the fuel weight of the aircraft decreases, as does the takeoff weight. The operational empty weight of the aircraft also decreases, but the decrease is proportionally less, as one would expect.

It is also important to note that the increase in bypass ratio of the engines means that the effect of thrust lapse at higher altitudes is greater, and in some cases the engine thrust must be increased, or the cruise altitude decreased, to overcome this.

The high bypass ratio turbofan engine, while providing a significant reduction in s.f.c., also provides a relatively large drag increment. This means that overall it only provides a small performance benefit. The reduction of takeoff weight for the 800 and 1000

seat aircraft is 1.2% and 1.1% respectively, while the fuel burned per passenger-kilometre improvement is 3.0% and 2.8% respectively.

The greater fuel efficiency of the A.D.P. engine, and its later year of service provides both fuel burn and engine dry weight benefits. The results show an estimated takeoff weight reduction of 8.6% and 10.5% for the 800 and 1000 seat concepts, and a reduction in fuel burn per passenger-kilometre of 17.5% and 19.4%.

The contrafan engine provides even greater fuel efficiency and dry weight savings. These result in an approximate 15.7% and 17.1% takeoff weight reduction for the 800 and 1000 seat aircraft, and a 28.2% and 29.4% reduction in fuel burned per passenger-kilometre.

This illustrates the vitally important role that the fuel efficiency of the aircraft engines plays in determining the overall characteristics of the aircraft. The use of a year 2020 contrafan engine of bypass ratio 20, which combines the increased overall efficiency of the contrafan engine concept with improved component efficiencies and higher bypass ratios, achieves a reduction in cruise s.f.c. of approximately 32% over the X800-DD turbofan engine, and in turn produces a takeoff weight reduction of approximately 16%.

15 .3 .2 Wing Tip Devices

Although winglets are currently used on many aircraft, their potential benefit for the use on UHCA is debatable. Most current large aircraft concepts do not include winglets, as extra span is preferred, and the beneficial drag reduction effects of winglets tend to decrease with increasing span and aspect ratio. Both the X800 and the X1000 baseline design were modified to incorporate each of the available winglet types (with the efficiency set to the default value of 100%), and the aircraft were resized to evaluate the effect of the technology. The wing span in each case was kept constant at 90m by means of changing the wing loading rather than the aspect ratio, so as to better isolate the effect of the wing tip devices. The results of each study are shown in tables 15.6 and 15.7 below.

Parameter Name	*Unit*	X800	*Δx* (%)	X800	*Δx* (%)	X800	*Δx* (%)
		Upper & Lower		Upper Only		Tip Fences	
Takeoff Weight	kg	547520	*0.4*	548195	*0.5*	544856	*-0.1*
Operational Empty Weight	kg	281330	*1.9*	281187	*1.8*	277371	*0.5*
Fuel Weight	kg	188172	*-1.5*	188991	*-1.1*	189468	*-0.9*
Cruise L\D	-	21.46	*2.8*	21.25	*1.8*	21.15	*1.3*
Fuel Per Passenger-Km	-	0.01809	*-1.8*	0.01822	*-1.1*	0.01821	*-0.9*

Table 15.6 - Effect of wing tip devices on X800 aircraft

Parameter Name	Unit	X1000	Δx (%)	X1000	Δx (%)	X1000	Δx (%)
		Upper &	Lower	Upper	Only	Tip	Fences
Takeoff Weight	kg	700942	*0.2*	703121	*0.5*	699747	*0.0*
Operational Empty Weight	kg	340709	*1.2*	341641	*1.5*	338003	*0.4*
Fuel Weight	kg	262710	*-1.0*	263958	*-0.6*	264222	*-0.5*
Cruise L\D	-	19.65	*1.4*	19.56	*1.0*	19.51	*0.7*
Fuel Per Passenger-Km	-	0.02026	*-1.0*	0.02036	*-0.5*	0.02036	*-0.5*

Table 15.7- Effect of wing tip devices on X1000 aircraft

The results show that despite an increase in takeoff weight and operational empty weight, directly attributable to the weight of the wing tip device, the wing tip devices give an overall improved fuel efficiency. As would be expected for a large wing of high aspect ratio, the percentage increase in fuel efficiency is small. The upper and lower winglet combination gives the greatest reduction in fuel consumption of approximately 1.55% for the X800 and 1.03% for the X1000, while the case with the upper winglet only gives a reduction of approximately 1.13% for the X800 and 0.56% for the X1000. The wing tip fences give a fuel consumption reduction of 0.88% for the X800 and 0.46% for X1000.

The disparity between the sizes of the fuel weight reductions is almost certainly due to the fact that the X800 has a higher cruise lift coefficient than the X1000, and hence the wing tip devices are more effective. A similar study carried out on an Airbus A340 type design, which has a smaller span and larger cruise lift coefficient than either design, exhibited fuel weight reductions of approximately 2.5%.

These results can be compared with the case below, where extra span is added to the wing instead of a wing tip device. The total span of the winglet was assumed to be approximately 3 metres, therefore for the purpose of this study the wing span was increased to 93m. The results of the UHCA designs with an extra 3 metre wing span are given below.

Parameter Name	Unit	X800	Δx (%)	X1000	Δx (%)
		93m	Span	93m	Span
Takeoff Weight	kg	544778	*-0.1*	698748	*-0.1*
Operational Empty Weight	kg	278775	*1.0*	340185	*1.1*
Fuel Weight	kg	188005	*-1.6*	261039	*-1.7*
Wing Reference Area	m^2	788.4	*1.7*	1009.6	*1.5*
Cruise L\D	-	21.25	*1.8*	19.73	*1.8*
Fuel Per Passenger-Km	-	0.01812	*-1.6*	0.02013	*-1.6*

Table 15.8- Effect of extra span on X800 and X1000 aircraft

These results indicate that an increase in wing span of similar magnitude to the total span of the wing tip device provides a greater increase in fuel efficiency. For the X800 design the fuel weight is reduced by 1.64%, compared to 1.55% for the best winglet, whilst for the X1000 design the fuel weight is reduced by 1.66% compared to 1.03% for the best winglet. This agrees with the conclusions of chapter 3, and reinforces the idea that winglets are best used as retrofit devices.

15 .3 .3 Advanced Materials

The effect of future advances in material technology is quantified for aircraft designs estimated to be based on year 2010 and year 2020 material technology. The material strategies assumed for these two years are shown in the table below.

Parameter Name	Unit	Year 2010	Year 2020
Wing Composite Amount	%	55.0	75.0
Wing Al-Li Amount	%	10.0	20.0
Fuselage Composite Amount	%	35.0	50.0
Fuselage Al-Li Amount	%	5.0	20.0
Vertical Tail Composite Amount	%	95.0	100.0
Horizontal Tail Composite Amount	%	90.0	100.0
Nacelle Composite Amount	%	75.0	80.0
Surface Control Composite Amount	%	95.0	100.0
Undercarriage Weight Savings	%	10.0	15.0
Hydraulics Weight Savings	%	10.0	15.0
Electrics Weight Savings	%	10.0	15.0
Air Conditioning Weight Savings	%	10.0	15.0
Furnishings Weight Savings	%	10.0	15.0
Operational Items Weight Savings	%	10.0	15.0

Table 15.9 - Advanced material strategy (Years 2010 and 2020)

The results of these studies are given below in tables 15.10 and 15.11, for both the 800 seat concept aircraft and the 1000 seat concept aircraft.

Parameter Name	Unit	X800	Δx (%)	X1000	Δx (%)
		Year	2010	Year	2010
Takeoff Weight	kg	505238	-7.3	644796	7.8
Operational Empty Weight	kg	247291	-10.4	301413	-10.4
Fuel Weight	kg	179929	-5.9	245861	-7.4
Thrust	ft	66000	-9.6	82000	-6.8
Wing Reference Area	m^2	718.3	-7.3	916.8	-7.8
Wing Span	m	86.6	-3.7	86.4	-4.0
H. Tail Reference Area	m^2	143.1	-12.0	214.2	-13.7
V. Tail Reference Area	m^2	124.9	-12.5	150.4	-14.1
Cruise L\D	-	20.67	-0.9	19.24	-0.7
Total Wetted Area	m^2	3830.3	-5.6	4811.5	-6.2
FAR Takeoff Length	m	3424	2.4	3489	-0.9
FAR Landing Length	m	1989	-0.3	2017	-0.2
Fuel Per Passenger-Km	-	0.0174	-5.9	0.0190	-7.4

Table 15.10 - Effect of year 2010 materials on X800 and X1000 aircraft

Parameter Name	Unit	X800	Δx (%)	X1000	Δx (%)
		Year	2020	Year	2020
Takeoff Weight	kg	474829	-12.9	594659	-15.0
Operational Empty Weight	kg	225783	-18.2	271134	-19.4
Fuel Weight	kg	171027	-10.5	226001	-14.9
Thrust	ft	63000	-13.7	78000	-11.4
Wing Reference Area	m^2	675.1	-12.9	845.5	-15.0
Wing Span	m	84.0	-6.7	83.0	-7.8
H. Tail Reference Area	m^2	128.7	-20.9	186.6	-24.8
V. Tail Reference Area	m^2	111.9	-21.6	130.5	-25.5
Cruise L\D	-	20.46	-2.2	19.02	-1.9
Total Wetted Area	m^2	3668.9	-9.6	4539.6	-11.5
FAR Takeoff Length	m	3360	0.5	3411	-3.1
FAR Landing Length	m	1984	-0.5	2013	-0.4
Fuel Per Passenger-Km	-	0.0165	-10.5	0.0174	-14.8

Table 15.11- Effect of year 2020 materials on X800 and X1000 aircraft

The tables above indicate the kinds of trends that one would expect with the application of advanced materials. The year 2010 materials give a 10.4% reduction in the operational empty weight for both aircraft, with smaller reductions of 7.3% and 7.8% in the

takeoff weight for the X800 and X1000 respectively. The fuel weight shows an improvement of 5.9% for the X800, and 7.4% for X1000.

The year 2020 material strategy provides an 18.2% reduction in operating empty weight of the X800 design, with the X1000 having a 19.4% reduction. The reductions in takeoff weight and fuel weight are again proportionally smaller, as one would expect. The X800 design shows a 12.9% takeoff weight reduction, while the X1000 has a 15.0% reduction. The fuel weight reductions are 10.5% for the X800, and 14.9% for the X1000.

The values of these weight improvements are of the magnitude that one would expect for this type of analysis, and show good consistency between the designs, as well as reflecting the expected attributes involved with the application of advanced materials. These results indicate that although the operational empty weight improvements for each aircraft are almost identical, the larger aircraft benefits more in terms of improved fuel efficiency and reduced takeoff weight.

15 .3 .4 VARIABLE CAMBER WINGS

The effect of the implementation of variable camber wings, of varying efficiencies (the default efficiency is 60%), is estimated for both of the baseline UHCA. The results of the studies are shown for each aircraft in the tables 15.12 and 15.13 below.

Parameter Name	*Unit*	*X800*	*Δx (%)*	*X800*	*Δx (%)*	*X800*	*Δx (%)*
		Efficiency	20%	Efficiency	60%	Efficiency	100%
Takeoff Weight	kg	520291	-4.6	513291	-5.9	506170	-7.2
Operational Empty Weight	kg	260031	-5.8	258096	-6.5	256042	-7.3
Fuel Weight	kg	173848	-9.0	168845	-11.7	163845	-14.3
Thrust	ft	62000	-15.1	60000	-17.8	59000	-19.2
Wing Reference Area	m^2	739.7	-4.6	729.8	-5.9	719.7	-7.2
Wing Span	m	87.9	-2.3	87.3	-3.0	86.7	-3.7
H. Tail Reference Area	m^2	151.0	-7.2	147.7	-9.2	144.4	-11.3
V. Tail Reference Area	m^2	132.1	-7.4	129.1	-9.6	126.1	-11.7
Cruise L\D	-	22.04	5.6	22.53	7.9	23.01	10.2
Total Wetted Area	m^2	3894	-4.0	3852	-5.1	3813	-6.0
Takeoff Field Length	m	3700	10.6	3762	12.5	3767	12.6
FAR Landing Length	m	1978	-0.9	1977	-0.9	1976	-1.0
Fuel Per Passenger-Km	-	0.01676	-9.0	0.01628	-11.7	0.0158	-14.3

Table 15.12- Effect of variable camber wing efficiency parameter for X800 aircraft

Parameter Name	Unit	X1000	Δx (%)	X1000	Δx (%)	X1000	Δx (%)
		Efficiency	20%	Efficiency	60%	Efficiency	100%
Takeoff Weight	kg	658215	-5.9	643116	-8.1	628575	-10.1
Operational Empty Weight	kg	315685	-6.2	310201	-7.8	305500	-9.2
Fuel Weight	kg	233540	-12.0	224125	-15.6	214455	-19.2
Thrust	ft	79000	-10.2	76000	-13.6	73000	-17.0
Wing Reference Area	m^2	935.8	-5.9	914.4	-8.1	893.7	-10.1
Wing Span	m	87.3	-3.0	86.3	-4.1	85.3	-5.2
H. Tail Reference Area	m^2	222.9	-10.2	214.5	-13.5	206.6	-16.8
V. Tail Reference Area	m^2	156.7	-10.5	150.7	-14.0	144.9	-17.3
Cruise L\D	-	20.28	4.7	20.70	6.8	21.15	9.2
Total Wetted Area	m^2	4870	-5.0	4781	-6.8	4694	-8.5
FAR Takeoff Length	m	3673	4.3	3760	6.8	3868	9.9
FAR Landing Length	m	1989	-1.6	1988	-1.7	1986	-1.8
Fuel Per Passenger-Km	-	0.0180	-12.0	0.0173	-15.6	0.0165	-19.2

Table 15.13- Effect of variable camber wing efficiency parameter for X1000 aircraft

These values illustrate that an increase in efficiency of the variable camber wing produces a steady improvement in takeoff weight, operational empty weight, and fuel weight of the aircraft. The relative values of these weights (relative to the baseline design) have been plotted against the variable camber efficiency parameter in the graphs below.

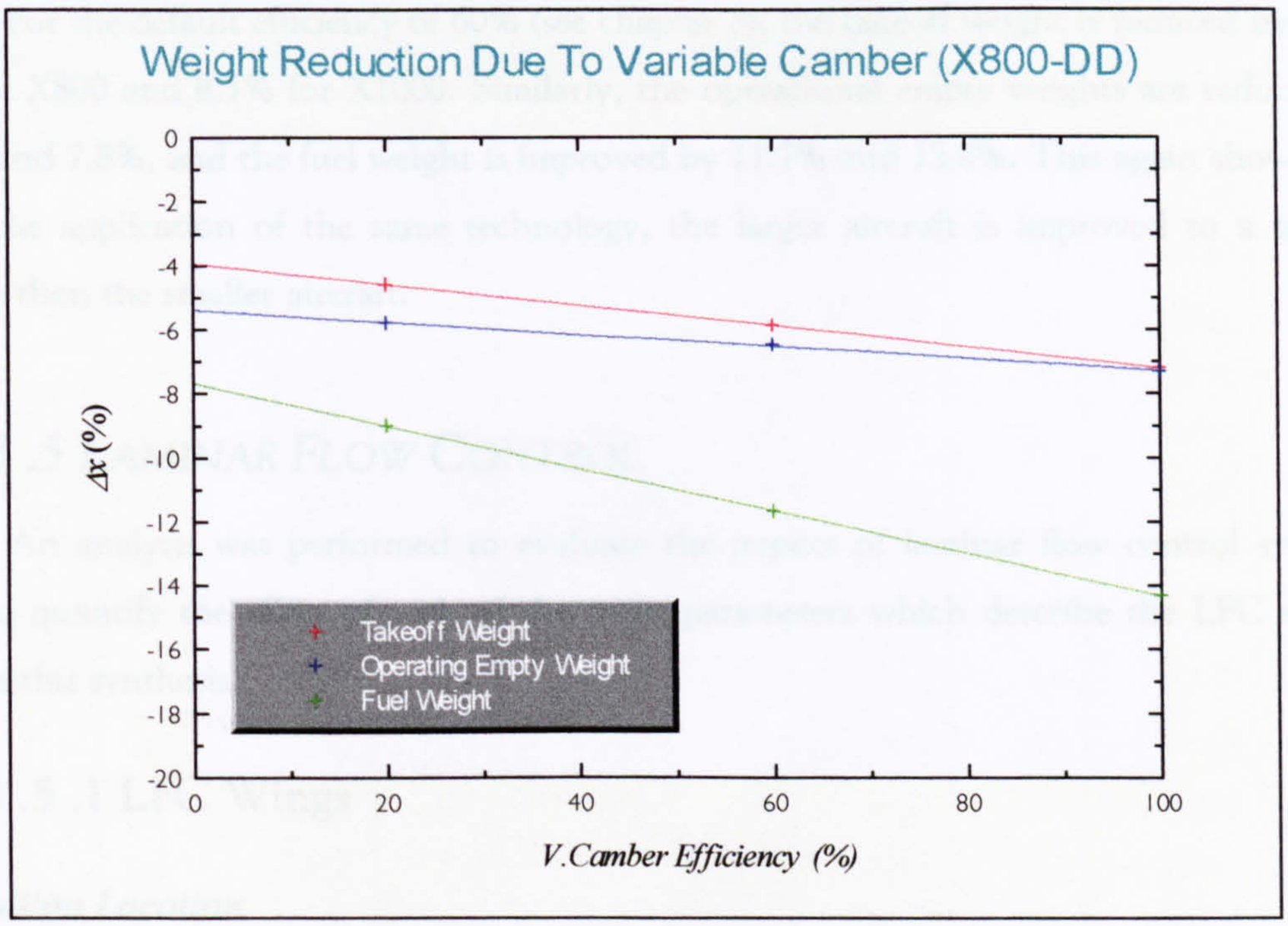


Figure 15.7- Weight reduction due to variable camber wing (X800)

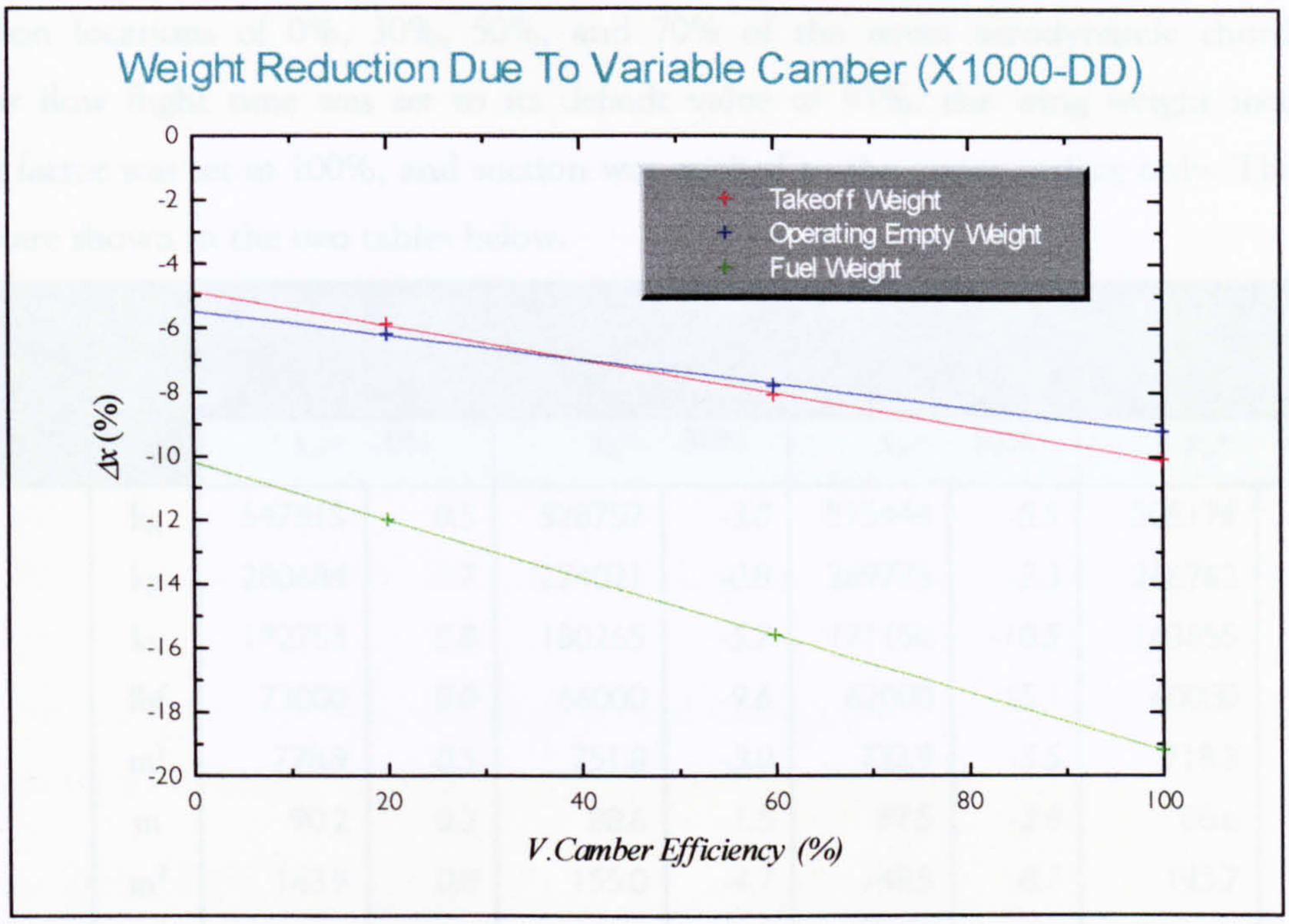


Figure 15.8 - Weight reduction due to variable camber wing (X1000)

These graphs indicate that the weight reductions are directly proportional to the variable camber wing efficiency parameter. The weight reduction at zero efficiency is due to the assumption throughout this study that the variable camber wing affects a 10% reduction in wing weight. Comparing the weight reductions at 0% efficiency and 100% efficiency illustrates that approximately half of the improvements are due to the wing weight reduction potential of the wing rather than the aerodynamic benefits.

For the default efficiency of 60% (see chapter 3), the takeoff weight is reduced by 5.9% for the X800 and 8.1% for X1000. Similarly, the operational empty weights are reduced by 6.5% and 7.8%, and the fuel weight is improved by 11.7% and 15.6%. This again shows that with the application of the same technology, the larger aircraft is improved to a greater degree than the smaller aircraft.

15 .3 .5 Laminar Flow Control

An analysis was performed to evaluate the impact of laminar flow control systems, and to quantify the effect of each of the main parameters which describe the LFC system within this synthesis.

15 .3 .5 .1 LFC Wings

Transition Location

The effect of the assumed cruise transition location on the overall aircraft was estimated for each design. The synthesis was performed for the cases of assumed cruise

transition locations of 0%, 30%, 50%, and 70% of the mean aerodynamic chord. The laminar flow flight time was set to its default value of 93%, the wing weight increment tuning factor was set to 100%, and suction was applied to the upper surface only. The main results are shown in the two tables below.

Parameter Name	Unit	X800	Δx (%)	X800	Δx (%)	X800	Δx (%)	X800	Δx (%)
		x_{tr}= 0%		x_{tr}= 30%		x_{tr}= 50%		x_{tr}= 70%	
W_0	kg	547815	0.5	528752	-3.0	515444	-5.5	505176	-7.4
W_{oew}	kg	280684	1.7	274021	-0.8	269775	-2.3	266762	-3.4
W_{fuel}	kg	192753	0.8	180265	-5.7	171150	-10.5	163855	-14.3
T_0	lbf	73000	0.0	66000	-9.6	62000	-15.1	60000	-17.8
S_{ref}	m^2	778.9	0.5	751.8	-3.0	732.9	-5.5	718.3	-7.4
b_{ref}	m	90.2	0.2	88.6	-1.5	87.5	-2.8	86.6	-3.7
$S_{ref\,ht}$	m^2	163.9	0.8	155.0	-4.7	148.5	-8.7	143.7	-11.7
$S_{ref\,vt}$	m^2	143.9	0.8	135.7	-4.9	129.9	-9.0	125.5	-12.1
L/D_{crl}		20.85	-0.1	22.01	5.4	22.81	9.3	23.64	13.2
S_{wet}	m^2	4070	0.3	3950	-2.7	3869	-4.6	3811	-6.1
FAR_{to}	m	3381	1.1	3600	7.6	3713	11.0	3749	12.1
FAR_{la}	m	1995	0.0	1992	-0.1	1991	-0.2	1989	-0.3
W_{fuel}/NR	-	0.0186	0.8	0.0174	-5.7	0.0165	-10.4	0.0158	-14.3

Table 15.14 - Effect of LFC transition location on X800 aircraft

Parameter Name	Unit	X1000	Δx (%)	X1000	Δx (%)	X1000	Δx (%)	X1000	Δx (%)
		x_{tr}= 0%		x_{tr}= 30%		x_{tr}= 50%		x_{tr}= 70%	
W_0	kg	705586	0.9	671974	-3.9	648539	-7.3	622558	-11.0
W_{oew}	kg	344107	2.2	332560	-1.2	326321	-3.0	316730	-5.9
W_{fuel}	kg	268949	1.3	246717	-7.1	229431	-13.6	212901	-19.8
T_0	lbf	90000	2.3	83000	-5.7	79000	-10.2	74000	-15.9
S_{ref}	m^2	1003.2	0.9	955.4	-3.9	922.1	-7.3	885.1	-11.0
b_{ref}	m	90.4	0.4	88.2	-2.0	86.7	-3.7	84.9	-5.7
$S_{ref\,ht}$	m^2	251.9	1.5	231.9	-6.6	217.7	-12.3	203.3	-18.1
$S_{ref\,vt}$	m^2	177.9	1.6	163.3	-6.8	153.0	-12.7	142.6	-18.6
L/D_{crl}	-	19.33	-0.2	20.38	5.2	21.12	9.0	21.87	12.9
S_{wet}	m^2	5168	0.8	4963	-3.2	4822	-6.0	4668	-9.0
FAR_{to}	m	3494	-0.7	3616	2.7	3686	4.7	3834	8.9
FAR_{la}	m	2022	0.0	2020	-0.1	2019	-0.2	2016	-0.3
W_{fuel}/NR	-	0.0208	1.3	0.0190	-7.0	0.0177	-13.6	0.0164	-19.8

Table 15.15 - Effect of LFC transition location on X1000 aircraft

These results show that the increase in transition location brings about a steady, almost linear improvement in the weight and performance characteristics of the aircraft. The case where the transition location is assumed to be 0% of the chord gives a performance reduction due to the weight of the LFC system, and due to the completely turbulent wing. This shows up as a 0.5% takeoff weight increase for the X800 aircraft, and 0.9% increase for the X1000.

The results at the default transition value of 50% show takeoff weight decreases of 5.5% and 7.3% for the X800 and X1000 respectively, while the operational empty weight decrements are 2.3% and 3.0%. The fuel weight improvements for the two aircraft are 10.5% and 13.6%.

This again indicates that the larger aircraft shows a greater proportional benefit when an advanced technology is applied to both the baseline aircraft.

Laminar Flow Flight Time

The effect of the flight time for which laminar flow can be maintained was investigated for both the baseline designs, with the transition location set to the default value of 50%, and with suction applied only to the upper surface. The laminar flow flight time was reduced to 46.5% (a 50% reduction), and the following results were obtained.

Parameter Name	*Unit*	*X800*	*Δx (%)*	*X1000*	*Δx (%)*
		flight time	46.5%	flight time	46.5%
Takeoff Weight	kg	530927	-2.6	677510	-3.2
Operational Empty Weight	kg	274210	-0.7	333900	-0.8
Fuel Weight	kg	182256	-4.7	250932	-5.5
Thrust	ft	64000	-12.3	83000	-5.7
Wing Reference Area	m^2	754.9	-2.6	963.3	-3.2
Wing Span	m	88.8	-1.3	88.6	-1.6
H. Tail Reference Area	m^2	156.1	-4.0	235.2	-5.2
V. Tail Reference Area	m^2	136.8	-4.2	165.8	-5.4
Cruise L\D Ratio	-	22.90	9.7	21.18	9.3
Total Wetted Area	m^2	3954	-2.6	4992	-2.6
FAR Takeoff Length	-	3718	11.1	3648	3.6
FAR Landing Length	-	1992	-0.1	2020	-0.1
Fuel Per Passenger-Km	-	0.0176	-4.6	0.0194	-5.4

Table 15.16 - Effect of LFC flight time on X800 and X1000 aircraft

This table shows that the effect of halving the laminar flow flight time is to almost exactly halve the percentage weight reductions.

Upper and Lower Surface Suction

The effect of additional suction on the lower surface of the wing is illustrated by the results in table 15.17. These results are based on designs which incorporate LFC on both upper and lower surfaces, with an assumed cruise transition location of 50%, a laminar flow flight time of 93%, and the wing weight increment tuning factor set to 100%.

Parameter Name	Unit	X800	Δx (%)	X1000	Δx (%)
		lower	suction	lower	suction
Takeoff Weight	kg	502391	-7.9	622086	-11.1
Operational Empty Weight	kg	268596	-2.7	320664	-4.7
Fuel Weight	kg	162653	-14.9	213071	-19.7
Thrust	ft	59000	-19.2	74000	-15.9
Wing Reference Area	m^2	714.3	-7.9	884.5	-11.1
Wing Span	m	86.4	-4.0	84.9	-5.7
H. Tail Reference Area	m^2	142.4	-12.5	203.1	-18.1
V. Tail Reference Area	m^2	124.2	-13.0	142.5	-18.7
Cruise L\D Ratio	-	23.87	14.3	22.08	14.0
Total Wetted Area	m^2	3794	-6.5	4666	-9.0
FAR Takeoff Length	-	3814	14.1	3862	9.7
FAR Landing Length	-	1989	-0.3	2016	-0.3
Fuel Per Passenger-Km	-	0.0157	-14.9	0.0164	-19.7

Table 15.17 - Effect of additional LFC lower surface suction on X800 and X1000 aircraft

These results indicate that the application of lower suction increases the benefits of LFC by approximately a further 50%. This would appear to be a result of the assumption that only one third of the wing drag is related to the flow over its lower surface.

Wing LFC Summary

An analysis of the results shows that the percentage reductions in takeoff weight, operating empty weight, and fuel weight are almost exactly proportional to the amount of laminar flow present on the wing. The graphs shown below in figures 15.9 and 15.10 illustrate this point by plotting the weight reductions against a laminar flow parameter. This laminar flow parameter is the product of the assumed cruise transition location, the laminar flow flight time, and a constant which equals 1 for upper surface suction only or 1.5 for upper and lower surface suction.

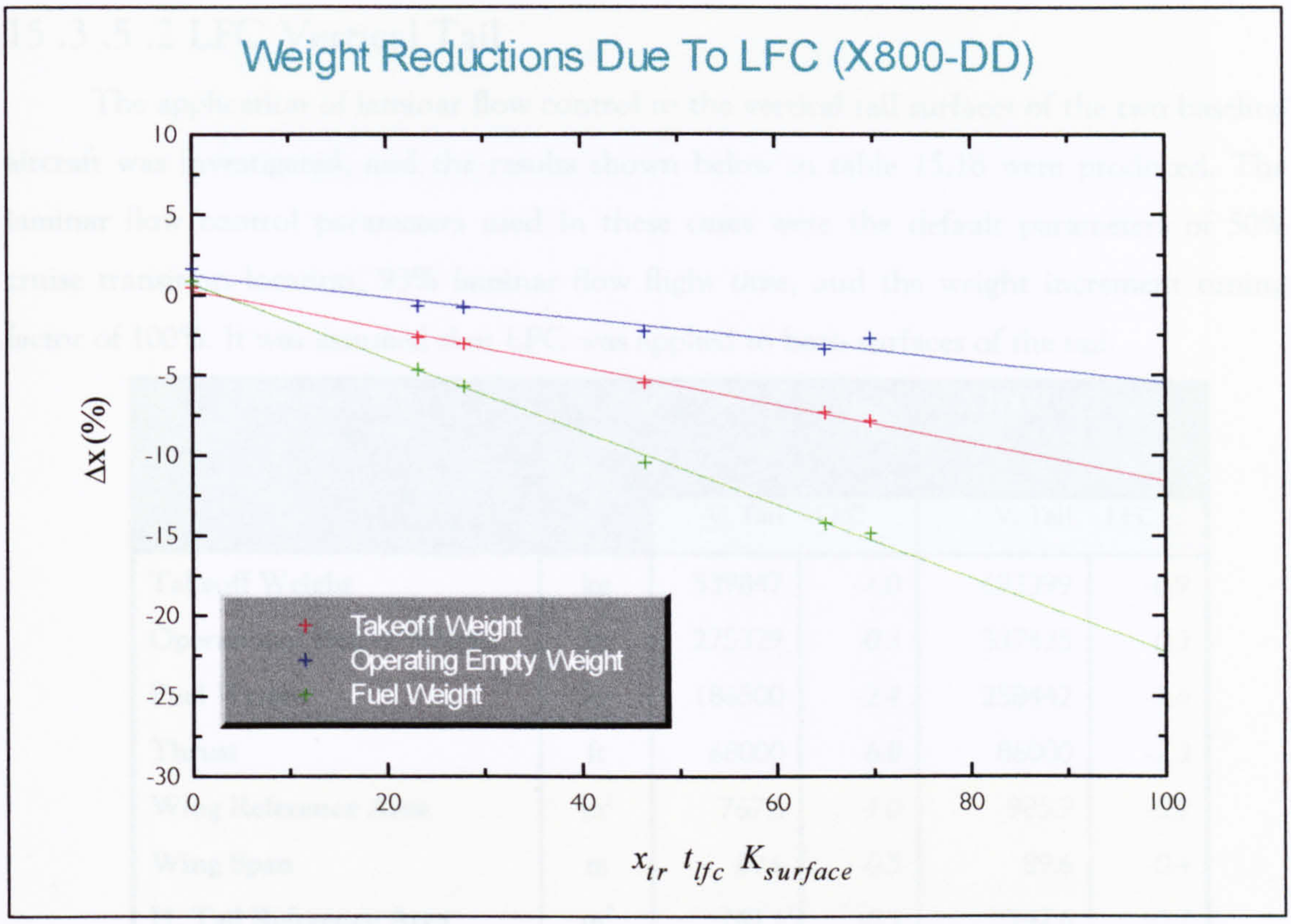


Figure 15.9 - Weight reductions due to LFC wing on X800 aircraft

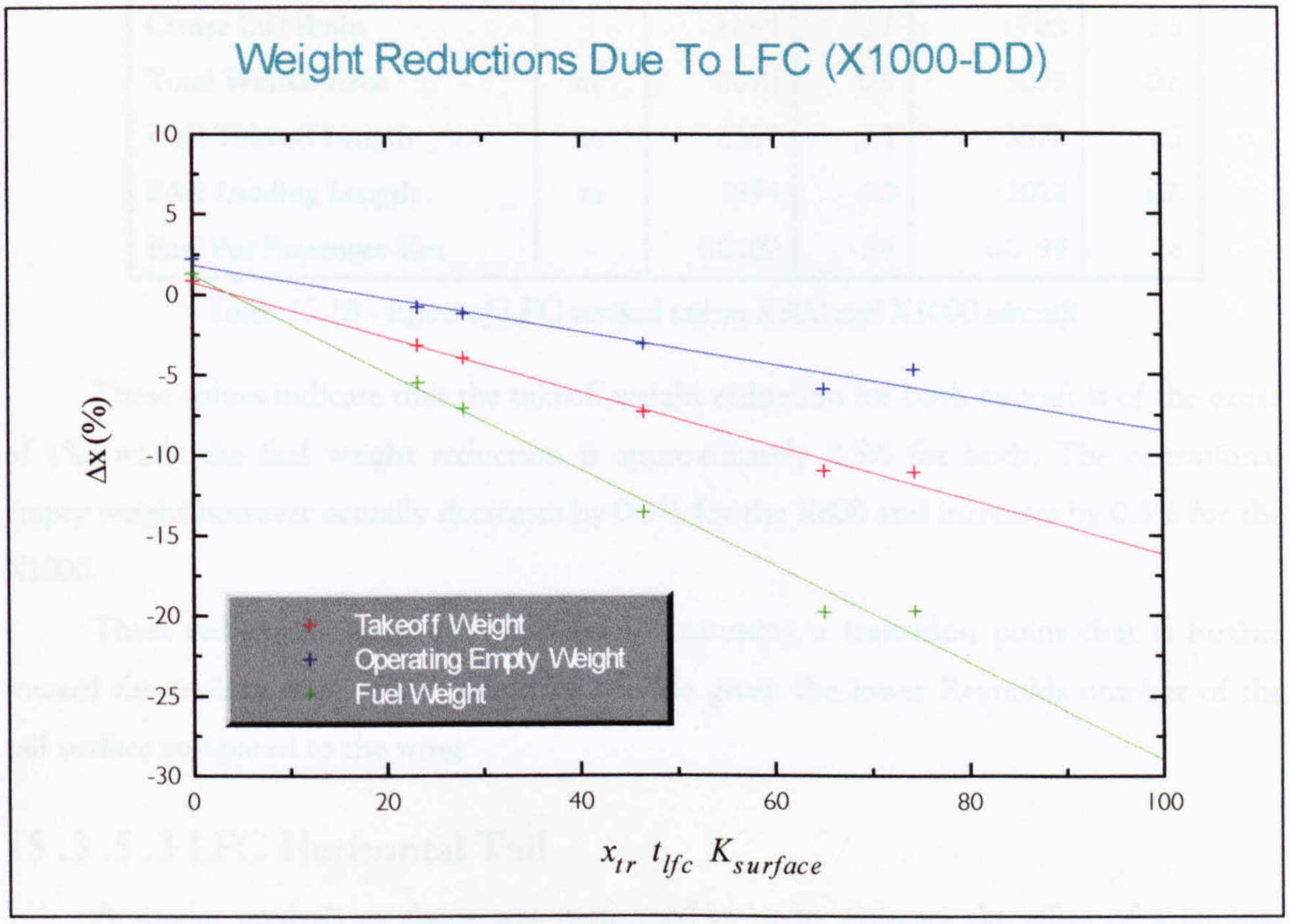


Figure 15.10 - Weight reductions due to LFC wing on X1000 aircraft

15 .3 .5 .2 LFC Vertical Tail

The application of laminar flow control to the vertical tail surfaces of the two baseline aircraft was investigated, and the results shown below in table 15.18 were produced. The laminar flow control parameters used in these cases were the default parameters of 50% cruise transition location, 93% laminar flow flight time, and the weight increment tuning factor of 100%. It was assumed that LFC was applied to both surfaces of the tail.

Parameter Name	*Unit*	*X800*	*Δx (%)*	*X1000*	*Δx (%)*
		V. Tail LFC		V. Tail LFC	
Takeoff Weight	kg	539847	*-1.0*	693399	*-0.9*
Operational Empty Weight	kg	275329	*-0.3*	337435	*0.3*
Fuel Weight	kg	186500	*-2.4*	258442	*-2.6*
Thrust	ft	68000	*-6.8*	86000	*-2.3*
Wing Reference Area	m^2	767.6	*-1.0*	985.9	*-0.9*
Wing Span	m	89.6	*-0.5*	89.6	*-0.4*
H. Tail Reference Area	m^2	162.1	*-0.3*	247.6	*-0.2*
V. Tail Reference Area	m^2	142.4	*-0.3*	174.9	*-0.2*
Cruise L\D Ratio	-	21.44	*2.7*	19.83	*2.3*
Total Wetted Area	m^2	4020	*-0.9*	5099	*-0.6*
FAR Takeoff Length	m	3557	*6.3*	3572	*1.5*
FAR Landing Length	m	1994	*0.0*	2022	*0.0*
Fuel Per Passenger-Km	-	0.0180	*-2.4*	0.0199	*-2.6*

Table 15.18 - Effect of LFC vertical tail on X800 and X1000 aircraft

These values indicate that the takeoff weight reduction for both aircraft is of the order of 1%, while the fuel weight reduction is approximately 2.5% for both. The operational empty weight however actually decreases by 0.3% for the X800 and increases by 0.3% for the X1000.

These reductions could be increased by assuming a transition point that is further toward the trailing edge, which could be feasible given the lower Reynolds number of the tail surface compared to the wing.

15 .3 .5 .3 LFC Horizontal Tail

A similar analysis as above was performed in order estimate the effect of a laminar flow control horizontal tail surface. The LFC system was confined to the upper surface, and the default parameters of 50% transition location, 93% laminar flight time, and a 100% weight tuning factor were assumed. The results are presented below in table 15.19.

Parameter Name	Unit	X800	Δx (%)	X1000	Δx (%)
		H. Tail	LFC	H. Tail	LFC
Takeoff Weight	kg	540453	-0.9	690629	-1.3
Operational Empty Weight	kg	274830	-0.5	335973	-0.2
Fuel Weight	kg	187606	-1.9	257134	-3.1
Thrust	ft	68000	-6.8	86000	-2.3
Wing Reference Area	m^2	768.4	-0.9	981.9	-1.3
Wing Span	m	89.6	-0.4	89.4	-0.6
H. Tail Reference Area	m^2	161.7	-0.6	245.0	-1.3
V. Tail Reference Area	m^2	141.9	-0.6	172.9	-1.3
Cruise L\D Ratio	-	21.33	2.2	19.80	2.2
Total Wetted Area	m^2	4020	-0.9	5080	-0.9
FAR Takeoff Length	m	3561	6.5	3557	1.1
FAR Landing Length	m	1994	0.0	2022	0.0
Fuel Per Passenger-Km	-	0.0181	-1.9	0.0198	-3.1

Table 15.19 - Effect of LFC horizontal tail on X800 and X1000 aircraft

The takeoff weight reduction is of the same order of that achieved with an LFC vertical tail. The X800 exhibits a 0.9% reduction while the X1000 reduction is 1.3%. The improvement in operational empty weight is marginally greater than the improvement gained with an LFC vertical tail, with 0.5% and 0.2% reductions for the X800 and X1000. The average decrement in fuel weight is 2.5% and is exactly the same as that achieved for the LFC vertical tail, with the two designs showing 1.9% and 3.1% improvements.

15 .3 .6 Hybrid Laminar Flow Control

The analysis performed for the implementation of laminar flow control was repeated for the case of hybrid laminar flow control systems. Each design study is evaluated using the same parameter values as for the equivalent LFC study, with the exception of the upper & lower surface suction analysis which is not applicable to a hybrid LFC system.

15 .3 .6 .1 HLFC Wing

Transition Location

The tables 15.20 and 15.21 below illustrate the results of the transition location analysis for a hybrid laminar flow control system.

Parameter Name	Unit	X800	Δx (%)	X800	Δx (%)	X800	Δx (%)	X800	Δx (%)
		x_{tr}= 0%		x_{tr}= 30%		x_{tr}= 50%		x_{tr}= 70%	
W_0	kg	547341	0.4	528230	-3.1	515301	-5.5	504046	-7.6
W_{oew}	kg	277893	0.6	271377	-1.7	267399	-3.2	264099	-4.4
W_{fuel}	kg	192297	0.6	179682	-6.0	170718	-10.7	162753	-14.9
T_0	lbf	73000	0.0	66000	-9.6	62000	-15.1	60000	-17.8
S_{ref}	m^2	778.2	0.4	751.0	-3.1	732.7	-5.5	716.6	-7.6
b_{ref}	m	90.2	0.2	88.6	-1.6	87.5	-2.8	86.5	-3.9
$S_{ref\,ht}$	m^2	163.7	0.6	154.7	-4.9	148.5	-8.7	143.1	-12.0
$S_{ref\,vt}$	m^2	143.7	0.6	135.5	-5.1	129.8	-9.1	125.0	-12.5
L/D_{cr}		20.85	-0.1	22.00	5.4	22.81	9.3	23.63	13.2
S_{wet}	m^2	4068	0.3	3947	-2.7	3868	-4.7	3805	-6.2
FAR_{to}	m	3362	0.5	3578	7.0	3693	10.4	3720	11.2
FAR_{la}	m	1995	0.0	1992	-0.1	1991	-0.2	1989	-0.3
W_{fuel}/NR	-	0.0185	0.6	0.0173	-6.0	0.0165	-10.7	0.0157	-14.8

Table 15.20 - Effect of HLFC transition location on X800 aircraft

Parameter Name	Unit	X1000	Δx (%)	X1000	Δx (%)	X1000	Δx (%)	X1000	Δx (%)
		x_{tr}= 0%		x_{tr}= 30%		x_{tr}= 50%		x_{tr}= 70%	
W_0	kg	706834	1.0	670452	-4.2	643561	-8.0	622477	-11.0
W_{oew}	kg	341534	1.5	329173	-2.2	321224	-4.6	313959	-6.7
W_{fuel}	kg	268970	1.3	244907	-7.7	225937	-14.9	212093	-20.1
T_0	lbf	90000	2.3	83000	-5.7	77000	-12.5	74000	-15.9
S_{ref}	m^2	1005.0	1.0	953.2	-4.2	915.0	-8.0	885.0	-11.0
b_{ref}	m	90.5	0.5	88.1	-2.1	86.3	-4.1	84.9	-5.7
$S_{ref\,ht}$	m^2	252.5	1.8	230.7	-7.0	215.0	-13.3	203.1	-18.1
$S_{ref\,vt}$	m^2	178.4	1.8	162.5	-7.3	151.1	-13.8	142.5	-18.7
L/D_{crl}	-	19.34	-0.2	20.38	5.2	21.13	9.1	21.87	12.9
S_{wet}	m^2	5174	0.9	4954	-3.4	4788	-6.6	4667	-9.0
FAR_{to}	m	3481	-1.1	3587	1.9	3752	6.6	3811	8.3
FAR_{la}	m	2023	0.0	2020	-0.1	2018	-0.2	2017	-0.3
W_{fuel}/NR	-	0.0208	1.4	0.0189	-7.7	0.0174	-14.9	0.0164	-20.1

Table 15.21- Effect of HLFC transition location on X1000 aircraft

The results display exactly the same trends as the data describing the laminar flow control results. The main difference is the slightly improved performance that is obtained through using a smaller area of suction and a subsequently lighter mechanism.

This performance improvement is realised as an average extra 0.1% takeoff weight reduction for the X800, and an average extra 0.2% for the X1000. The operational empty weight improvement over the laminar flow control case is on average 1.0% for both aircraft, and the extra reduction of fuel weight is 0.3% for X800 and 0.5% for the X1000.

Laminar Flow Flight Time

The effect of the laminar flow flight time on performance is investigated for the HLFC wing aircraft. As for the LFC aircraft, the laminar flow flight time is halved from 93% to 46.5%, and the effect is evaluated with an assumed cruise transition location of 50%, and weight tuning factor of 100%. These results are given below:-

Parameter Name	*Unit*	*X800*	*Δx (%)*	*X1000*	*Δx (%)*
		flight time	46.5%	flight time	46.5%
Takeoff Weight	kg	531045	-2.6	671219	-4.0
Operational Empty Weight	kg	271990	-1.5	330291	-1.9
Fuel Weight	kg	181886	-4.8	244560	-7.9
Thrust	ft	64000	-12.3	81000	-8.0
Wing Reference Area	m^2	755.0	-2.6	954.3	-4.0
Wing Span	m	88.8	-1.3	88.2	-2.0
H. Tail Reference Area	m^2	156.2	-4.0	231.0	-6.9
V. Tail Reference Area	m^2	136.8	-4.1	162.7	-7.1
Cruise L\D Ratio	-	22.90	9.7	21.20	9.4
Total Wetted Area	m^2	3955	-2.5	4949	-3.5
FAR Takeoff Length	-	3700	10.6	3688	4.8
FAR Landing Length	-	1992	-0.1	2020	-0.1
Fuel Per Passenger-Km	-	0.0175	-4.8	0.0189	-7.8

Table 15.22- Effect of HLFC flight time on X800 and X1000 aircraft

As with the LFC analysis, reducing the laminar flow flight time by a half approximately cuts the weight improvements in the takeoff weight, operational empty weight, and fuel weight by a half.

Summary

The graphs shown below in figures 15.11 and 15.12 illustrate that the weight decrements are proportional to the amount of laminar flow obtained over the wing surface (as found in the LFC analysis). The weight decrements are plotted against the assumed cruise transition location multiplied by the laminar flow flight time fraction.

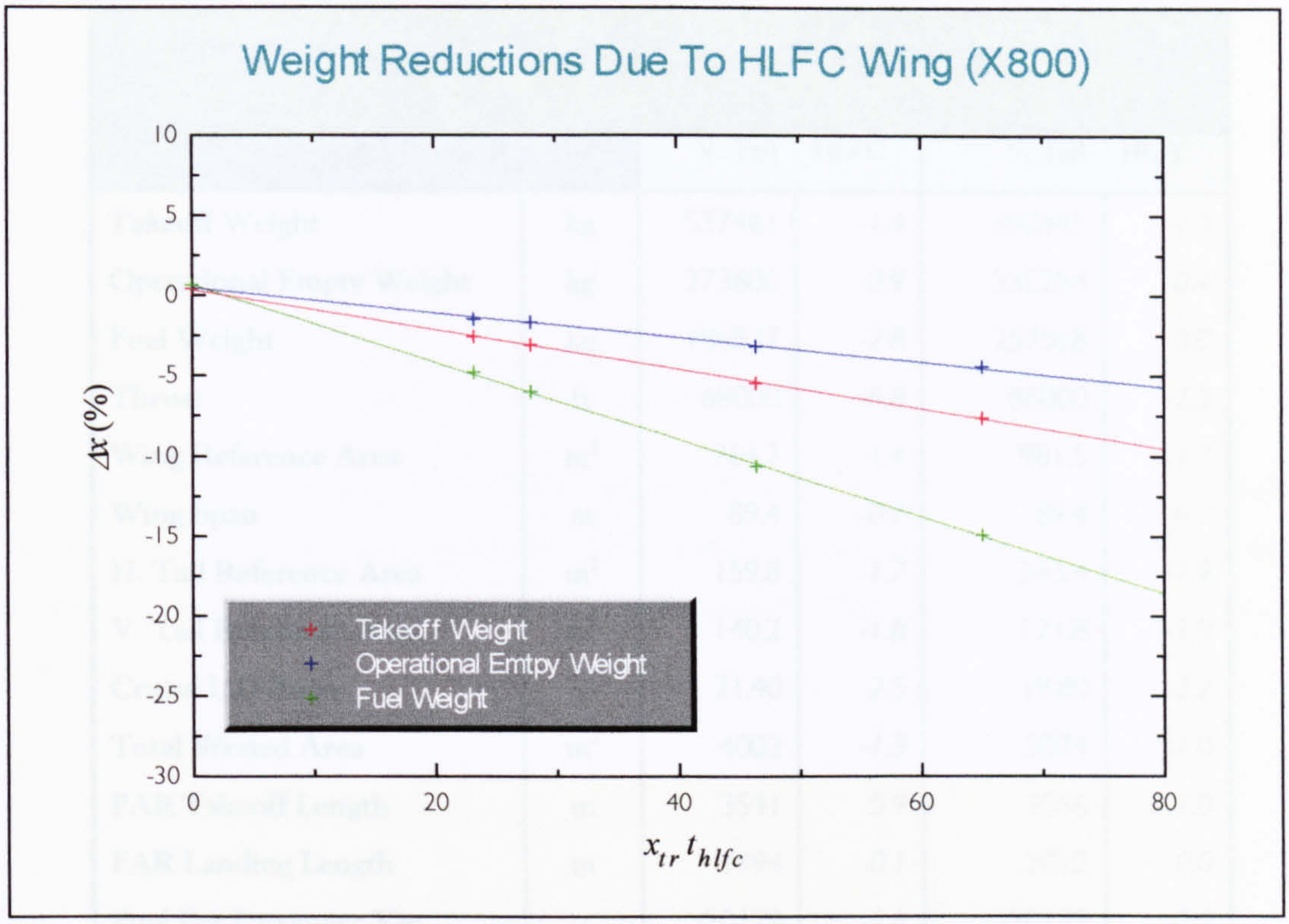


Figure 15.11 - Weight reductions due to HLFC wing on X800 aircraft

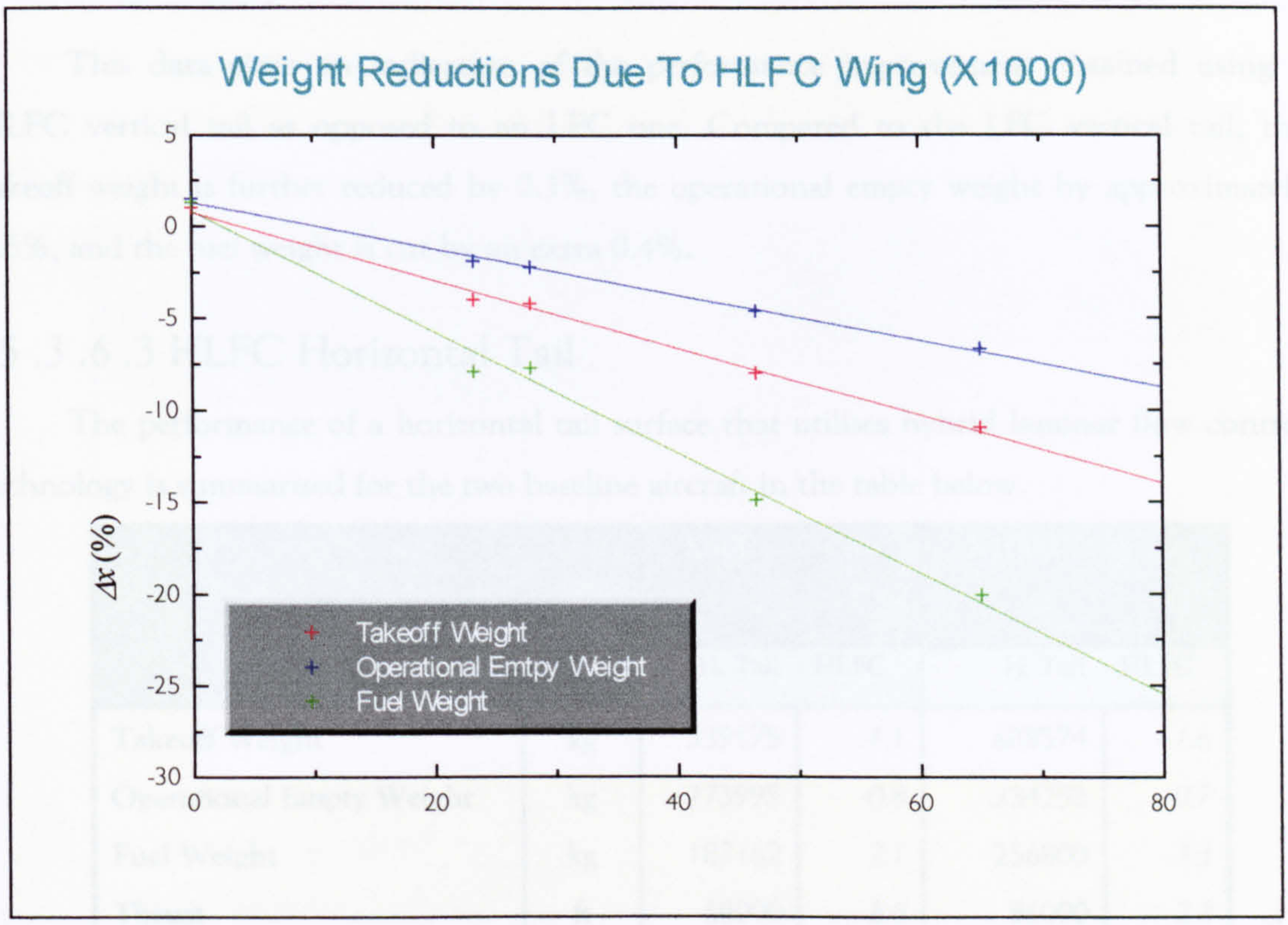


Figure 15.12 - Weight reductions due to HLFC wing on X1000 aircraft

15 .3 .6 .2 HLFC Vertical Tail

The results of the design studies for the baseline aircraft with hybrid laminar flow control vertical tail surfaces are given below.

Parameter Name	Unit	X800	Δx (%)	X1000	Δx (%)
		V. Tail	HLFC	V. Tail	HLFC
Takeoff Weight	kg	537461	-1.4	690345	-1.3
Operational Empty Weight	kg	273606	-0.9	335254	-0.4
Fuel Weight	kg	185837	-2.8	257568	-3.0
Thrust	ft	68000	-6.8	86000	-2.3
Wing Reference Area	m^2	764.2	-1.4	981.5	-1.3
Wing Span	m	89.4	-0.7	89.4	-0.7
H. Tail Reference Area	m^2	159.8	-1.7	243.4	-1.9
V. Tail Reference Area	m^2	140.2	-1.8	171.8	-1.9
Cruise L\D Ratio	-	21.40	2.5	19.80	2.2
Total Wetted Area	m^2	4003	-1.3	5074	-1.0
FAR Takeoff Length	m	3541	5.9	3556	1.0
FAR Landing Length	m	1994	-0.1	2022	0.0
Fuel Per Passenger-Km	-	0.0179	-2.8	0.0199	-2.9

Table 15.23 - Effect of HLFC vertical tail on X800 and X1000 aircraft

This data gives an indication of the performance improvement obtained using a HLFC vertical tail as opposed to an LFC one. Compared to the LFC vertical tail, the takeoff weight is further reduced by 0.3%, the operational empty weight by approximately 0.6%, and the fuel weight is cut by an extra 0.4%.

15 .3 .6 .3 HLFC Horizontal Tail

The performance of a horizontal tail surface that utilises hybrid laminar flow control technology is summarised for the two baseline aircraft in the table below.

Parameter Name	Unit	X800	Δx (%)	X1000	Δx (%)
		H. Tail	HLFC	H. Tail	HLFC
Takeoff Weight	kg	539175	-1.1	688574	-1.6
Operational Empty Weight	kg	273995	-0.8	334252	-0.7
Fuel Weight	kg	187162	-2.1	256800	-3.3
Thrust	ft	68000	-6.8	86000	-2.3
Wing Reference Area	m^2	766.6	-1.1	979.0	-1.6
Wing Span	m	89.5	-0.6	89.3	-0.8
H. Tail Reference Area	m^2	160.4	-1.4	242.1	-2.4
V. Tail Reference Area	m^2	140.7	-1.4	170.8	-2.5
Cruise L\D Ratio	-	21.33	2.2	19.80	2.2

Parameter Name	Unit	X800	Δx (%)	X1000	Δx (%)
Total Wetted Area	m^2	4011	-1.2	5063	-1.2
FAR Takeoff Length	m	3552	6.2	3546	0.8
FAR Landing Length	m	1994	-0.1	2022	0.0
Fuel Per Passenger-Km	-	0.0181	-2.1	0.0198	-3.2

Table 15.24- Effect of HLFC horizontal tail on X800 and X1000 aircraft

The improved design of the HLFC system provides an extra takeoff weight reduction of approximately 0.25% compared to the LFC system. This is in conjunction with a further operational empty weight reduction of approximately 0.4%, and an extra fuel weight decrement of 0.2%

15 .3 .7 Natural Laminar Flow (NLF)

15 .3 .7 .1 Nacelles

It was possible to demonstrate that noticeable performance improvements could be achieved by the introduction of NLF nacelles. Assuming a transition point that is 60% along the length of the fan cowling (see chapter 3), the following results were obtained for the X800 and the X1000 aircraft.

Parameter Name	Unit	X800		Δx (%)	X1000		Δx (%)
		NLF	Nacelle		NLF	Nacelle	
Takeoff Weight	kg	535134		-1.9	684516		-2.1
Operational Empty Weight	kg	272790		-1.2	332556		-1.2
Fuel Weight	kg	184325		-3.6	254437		-4.2
Thrust	ft	68000		-6.8	85000		-3.4
Wing Reference Area	m^2	760.9		-1.9	973.2		-2.1
Wing Span	m	89.2		-0.9	89.0		-1.1
H. Tail Reference Area	m^2	158.0		-2.9	239.2		-3.6
V. Tail Reference Area	m^2	138.4		-3.0	168.6		-3.7
Cruise L\D Ratio	-	21.52		3.1	19.88		2.6
Total Wetted Area	m^2	3988		-1.7	5036		-1.8
FAR Takeoff Length	m	3525		5.4	3568		1.4
FAR Landing Length	m	1993		-0.1	2021		0.0
Fuel Per Passenger-Km	-	0.0178		-3.6	0.0196		-4.1

Table 15.25 - Effect of NLF nacelles on X800 and X1000 aircraft

These values indicate a takeoff weight reduction of approximately 2%, an operational empty weight reduction of 1.2%, and a reduction in fuel weight of approximately 4%.

15 .3 .7 .2 Wing & Tail Surfaces

Calculations performed on the two baseline aircraft indicated that it was not possible to maintain any significant portions of laminar flow on either the wings or the tail surfaces by using natural laminar flow techniques. This is a direct result of the high Reynolds numbers of these flows, and the relatively large sweep angles required to cruise at Mach 0.85. Therefore, it can be concluded that NLF techniques are not applicable to the wing and tail surfaces of UHCA.

15 .3 .8 RIBLETS

The beneficial effect of riblets on the wing, tail, and fuselage surfaces have been investigated for both baseline UHCA. The results of these studies are presented in tables 15.26 and 15.27 for the X800 and X1000 respectively. The addition of riblets to the nacelle surfaces was found to produce little significant effect on the overall performance of the aircraft.

Parameter Name	*Unit*	X800	*Δx (%)*	X800	*Δx (%)*	X800	*Δx (%)*	X800	*Δx (%)*
		Wing	Riblets	V. Tail	Riblets	H. Tail	Riblets	Fuselage	Riblets
W_0	kg	540271	-0.9	544175	-0.2	544159	-0.2	543397	-0.3
W_{oew}	kg	273955	-0.8	275258	-0.3	275264	-0.3	275199	-0.3
W_{fuel}	kg	188298	-1.5	190898	-0.1	190877	-0.1	190180	-0.5
T_0	lbf	68000	-6.8	70000	-4.1	70000	-4.1	70000	-4.1
S_{ref}	m^2	768.2	-0.9	773.7	-0.2	773.7	-0.2	772.6	-0.3
b_{ref}	m	89.6	-0.5	89.9	-0.1	89.9	-0.1	89.9	-0.2
$S_{ref\,ht}$	m^2	160.6	-1.3	162.5	-0.1	162.5	-0.1	162.0	-0.4
$S_{ref\,vt}$	m^2	140.9	-1.3	142.6	-0.1	142.6	-0.1	142.2	-0.4
L/D_{crl}		21.20	1.5	20.99	0.5	21.00	0.6	21.08	1.0
S_{wet}	m^2	4014	-1.1	4041	-0.4	4041	-0.4	4037	-0.5
FAR_{to}	m	3558	6.4	3496	4.5	3495	4.5	3490	4.4
FAR_{la}	m	1993	-0.1	1994	0.0	1994	0.0	1994	0.0
W_{fuel}/NR	-	0.0182	-1.5	0.0184	-0.1	0.0184	-0.1	0.0183	-0.5

Table 15.26 - Effect of riblets on X800 aircraft

Parameter Name	Unit	X1000	Δx (%)	X1000	Δx (%)	X1000	Δx (%)	X1000	Δx (%)
		Wing	Riblets	V. Tail	Riblets	H. Tail	Riblets	Fuselage	Riblets
W_0	kg	694653	-0.7	698149	-0.2	697939	-0.2	695855	-0.5
W_{oew}	kg	336030	-0.2	336265	-0.1	336344	-0.1	335711	-0.3
W_{fuel}	kg	261101	-1.6	264361	-0.4	264072	-0.5	262621	-1.1
T_0	lbf	87000	-1.1	88000	0.0	88000	0.0	88000	0.0
S_{ref}	m^2	987.7	-0.7	992.6	-0.2	992.3	-0.2	989.4	-0.5
b_{ref}	m	89.7	-0.4	89.9	-0.1	89.9	-0.1	89.8	-0.3
$S_{ref\ ht}$	m^2	245.2	-1.2	247.3	-0.4	247.1	-0.4	245.9	-0.9
$S_{ref\ vt}$	m^2	173.0	-1.2	174.5	-0.4	174.4	-0.4	173.5	-0.9
L/D_{cr1}	-	19.61	1.2	19.42	0.2	19.44	0.3	19.49	0.6
S_{wet}	m^2	5097	-0.6	5120	-0.1	5118	-0.2	5108	-0.4
FAR_{to}	m	3534	0.4	3512	-0.2	3510	-0.3	3499	-0.6
FAR_{la}	m	2021	0.0	2021	0.0	2021	0.0	2021	0.0
W_{fuel}/NR	-	0.0201	-1.6	0.0204	-0.4	0.0204	-0.5	0.0203	-1.0

Table 15.27- Effect of riblets on X1000 aircraft

These results clearly indicate that the most potential for drag reduction by the use of riblets occurs on the wing surface, followed by the fuselage surface, and then by the tail surfaces.

The application of riblets to the wing surface causes an average takeoff weight improvement of 0.8%, and an average fuel weight improvement of 1.55%. The fuselage riblets are responsible for an average takeoff weight decrement of 0.4%, and the fuel weight is decreased by approximately 0.8%. The riblets applied to the vertical and horizontal tail surfaces produce almost identical performance gains, with a 0.2% takeoff weight reduction, and an average 0.3% fuel weight reduction.

15 .3 .9 Summary of Advanced Technologies

A summary of the benefits of the application of various advanced technologies is given in the tables below, ranked in order of greatest fuel efficiency benefit, along with an anticipated year of entry into service. Tables 15.28 and 15.29 give the values found with the advanced technology parameters set to their default values for the X800 and the X1000 concept aircraft respectively, while table 15.30 gives the average values for the two aircraft.

Technology Name (X800)	Year	ΔW_0 (%)	ΔW_{oew} (%)	ΔW_{fuel} (%)	$\Delta L/D_{cr1}$ (%)
Contrafan Engine	2020	-15.7	-11.5	28.1	-16.0
Advanced Ducted Propeller	2010	-8.6	-4.9	-17.5	-8.4
Variable Camber Wings	2020	-5.9	-6.5	-11.7	7.9
HLFC Wings	2010	-5.5	-3.2	-10.7	9.3
Advanced Materials (2020)	2020	-12.9	-18.2	-10.5	-2.2
LFC Wings	2015	-5.5	-2.3	-10.5	9.3
Advanced Materials (2010)	2010	-7.3	-10.4	-5.9	-0.9
NLF Nacelles	2000	-1.9	-1.2	-3.6	3.1
High Bypass Ratio Turbofan	2005	-1.2	-0.4	-3.0	-3.4
HLFC Vertical Tail	2010	-1.4	-0.9	-2.8	2.5
LFC Vertical Tail	2015	-1.0	-0.3	-2.4	2.7
HLFC Horizontal Tail	2010	-1.1	-0.8	-2.1	2.2
LFC Horizontal Tail	2015	-0.9	-0.5	-1.9	2.2
Winglets (Upper & Lower)	-	0.4	1.9	-1.5	2.8
Wing Riblets	2000	-0.9	-0.8	-1.5	1.5
Winglets (Upper)	-	0.5	1.8	-1.1	1.8
Wing Tip Fences	-	-0.1	0.5	-0.9	1.3
Fuselage Riblets	2000	-0.3	-0.3	-0.5	1.0
Vertical Tail Riblets	2000	-0.2	-0.3	-0.1	0.5
Horizontal Tail Riblets	2000	-0.2	-0.3	-0.1	0.6

Table 15.28 - Summary of advanced technologies applied to X800

Technology Name (X1000)	Year	ΔW_0 (%)	ΔW_{oew} (%)	ΔW_{fuel} (%)	$\Delta L/D_{cr1}$ (%)
Contrafan Engine	2020	-17.1	-12.3	-29.4	-16.1
Advanced Ducted Propeller	2010	-10.5	-6.5	-19.5	-8.3
Variable Camber Wings	2020	-8.1	-7.8	-15.6	6.8
Advanced Materials (2020)	2020	-15.0	-19.4	-14.9	-1.9
HLFC Wings	2010	-8.0	-4.6	-14.9	9.1
LFC Wings	2015	-7.3	-3.0	-13.6	9.0
Advanced Materials (2010)	2010	-7.8	-10.4	-7.4	-0.7
NLF Nacelles	2000	-2.1	-1.2	-4.2	2.6
HLFC Horizontal Tail	2010	-1.6	-0.7	-3.3	2.2
LFC Horizontal Tail	2015	-1.3	-0.2	-3.1	2.2
HLFC Vertical Tail	2010	-1.3	-0.4	-3.0	2.2
High Bypass Ratio Turbofan	2005	-1.1	0.0	-2.8	-3.6
LFC Vertical Tail	2015	-0.9	0.3	-2.6	2.3
Wing Riblets	2000	-0.7	-0.2	-1.6	1.2
Fuselage Riblets	2000	-0.5	-0.3	-1.1	0.6

Technology Name (X1000)	Year	ΔW_0 (%)	ΔW_{oew} (%)	ΔW_{fuel} (%)	$\Delta L/D_{cr1}$ (%)
Winglets (Upper & Lower)	-	0.2	1.2	-1.0	1.4
Winglets (Upper)	-	0.5	1.5	-0.6	1.0
Wing Tip Fences	-	0.0	0.4	-0.5	0.7
Horizontal Tail Riblets	2000	-0.2	-0.1	-0.5	0.3
Vertical Tail Riblets	2000	-0.2	-0.1	-0.4	0.2

Table 15.29 - Summary of advanced technologies applied to X1000

Technology Name	Year	ΔW_0 (%)	ΔW_{oew} (%)	ΔW_{fuel} (%)	$\Delta L/D_{cr1}$ (%)
Contrafan Engine	2020	-16.4	-11.9	-28.8	-16.1
Advanced Ducted Propeller	2010	-9.5	-5.7	-18.5	-8.3
Variable Camber Wings	2020	-7.0	-7.2	-13.7	7.3
HLFC Wings	2010	-6.8	-3.9	-12.8	9.2
Advanced Materials (2020)	2020	-14.0	-18.8	-12.7	-2.1
LFC Wings	2015	-6.4	-2.7	-12.1	9.2
Advanced Materials (2010)	2010	-7.5	-10.4	-6.7	-0.8
NLF Nacelles	2000	-2.0	-1.2	-3.9	2.8
High Bypass Ratio Turbofan	2005	-1.2	-0.2	-2.9	-3.5
HLFC Vertical Tail	2010	-1.3	-0.7	-2.9	2.3
HLFC Horizontal Tail	2010	-1.3	-0.8	-2.7	2.2
LFC Vertical Tail	2015	-1.0	0.0	-2.5	2.5
LFC Horizontal Tail	2015	-1.1	-0.3	-2.5	2.2
Wing Riblets	2000	-0.8	-0.5	-1.5	1.3
Winglets (Upper & Lower)	-	0.3	1.6	-1.3	2.1
Winglets (Upper)	-	0.5	1.7	-0.8	1.4
Fuselage Riblets	2000	-0.4	-0.3	-0.8	0.8
Wing Tip Fences	-	-0.0	0.5	-0.7	1.0
Vertical Tail Riblets	2000	-0.2	-0.2	-0.3	0.3
Horizontal Tail Riblets	2000	-0.2	-0.2	-0.3	0.4

Table 15.30 - Summary of advanced technologies (average values)

These tables show that by far the largest performance gains can be achieved through the use of advanced engine technologies. The other areas of technology which provide the greatest potential are the use of advanced materials, variable camber wings, LFC wings, and HLFC wings, all of which show a similar level of performance improvement.

The main surprise is the relatively large impact of the NLF nacelles, which provide greater benefits than the use of LFC or HLFC tails and riblets.

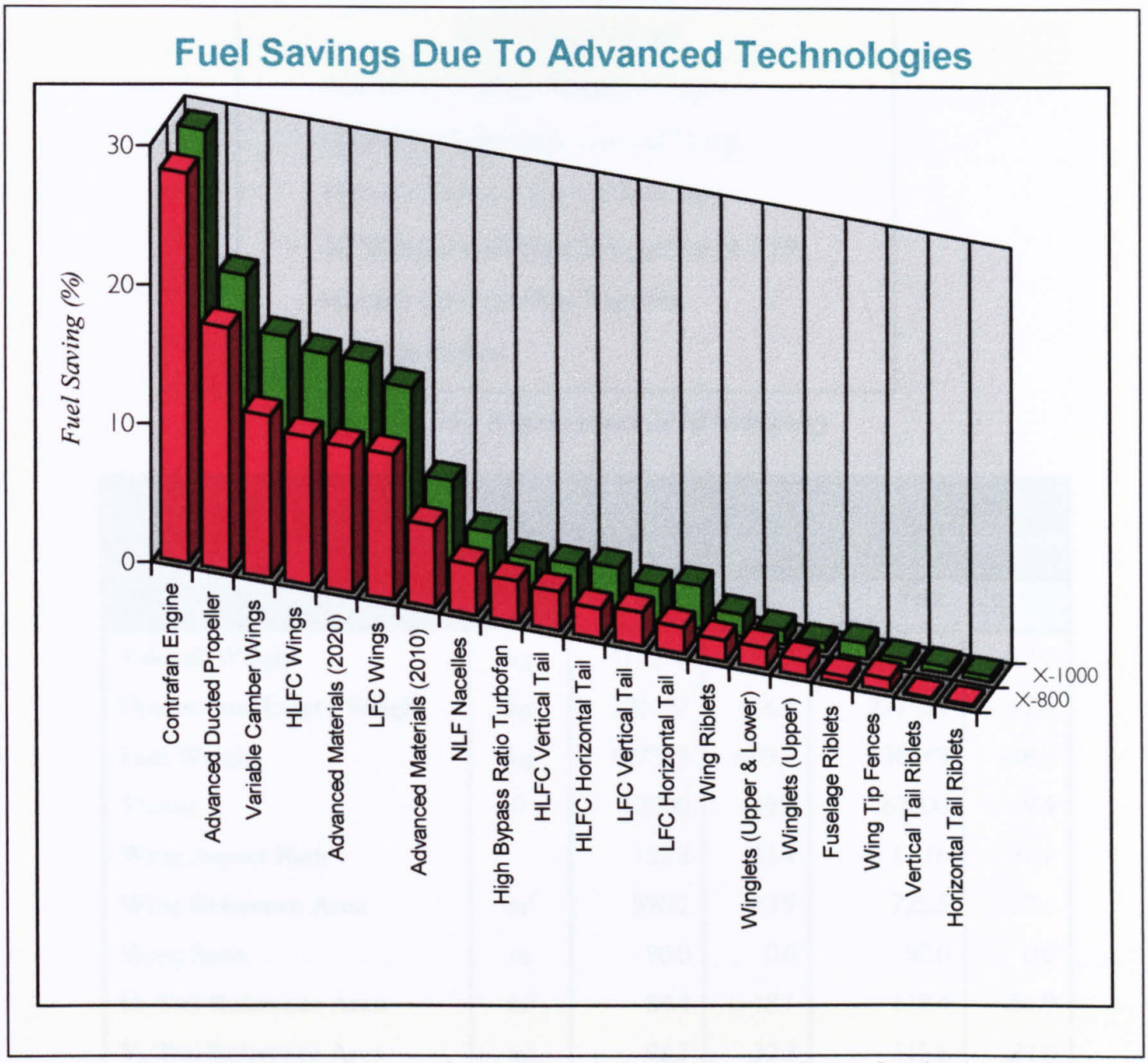


Figure 15.13 - Fuel savings for X-800 and X-1000 due to advanced technologies

15 .4 Future Designs

With the above data in mind, the 800 seat and 1000 seat concept aircraft have been modified to reflect the impact of possible year 2010 and year 2020 technologies. The year 2010 technology is summarised in figure 15.14, and the assumed 2020 technology level is shown in figure 15.15. These strategies have been chosen to simulate the likely state of development of cutting-edge advanced technologies at these two times. The results of table 15.30 have been used to chose the best available technologies within the time frame being considered.

2010 Technology

Advanced Ducted Propeller Engine

Hybrid Laminar Flow Control Wing

Hybrid Laminar Flow Control Tails

2010 Advanced Materials (see table 15.9)

Natural Laminar Flow Nacelles

Fuselage Riblets

Figure 15.14 - Assumed year 2010 technology

Parameter Name	*Unit*	*X800*	*Δx (%)*	*X1000*	*Δx (%)*
		Year	2010	Year	2010
Takeoff Weight	kg	415078	-23.9	510283	-27.1
Operational Empty Weight	kg	230197	-16.6	277480	-17.6
Fuel Weight	kg	107579	-43.7	136249	-48.7
Thrust	ft	52000	-28.8	62000	-29.5
Wing Aspect Ratio		13.73	31.4	11.16	37.1
Wing Reference Area	m^2	590.2	-23.9	725.5	-27.1
Wing Span	m	90.0	0.0	90.0	0.0
H. Tail Reference Area	m^2	84.4	-48.1	119.4	-51.9
V. Tail Reference Area	m^2	96.7	-32.3	115.6	-34.0
Cruise L\D Ratio	-	24.58	17.7	23.58	21.7
Total Wetted Area	m^2	3429	-15.5	4165	-18.8
FAR Takeoff Length	m	3609	7.9	3745	6.4
FAR Landing Length	m	1977	-0.9	1986	-1.8
Fuel Per Passenger-Km	-	0.0104	-43.7	0.0105	-48.7

Table 15.31 - Effect of year 2010 technology applied to X800 and X1000 aircraft

2020 Technology

Contrafan Engine

Variable Camber Wing

Hybrid Laminar Flow Control Tails

2020 Advanced Materials (see table 15.9)

Natural Laminar Flow Nacelles

Fuselage Riblets

Figure 15.15 - Assumed year 2020 technology

Parameter Name	Unit	X800	Δx (%)	X1000	Δx (%)
		Year	2020	Year	2020
Takeoff Weight	kg	360807	-33.8	451232	-35.5
Operational Empty Weight	kg	190537	-31.0	236098	-29.9
Fuel Weight	kg	86100	-55.0	109035	-58.9
Thrust	ft	48000	-34.2	57000	-35.2
Wing Aspect Ratio		15.00	43.5	12.63	55.1
Wing Reference Area	m^2	513.0	-33.8	641.6	-35.5
Wing Span	m	87.7	-2.5	90.0	0.0
H. Tail Reference Area	m^2	65.9	-59.5	88.1	-64.5
V. Tail Reference Area	m^2	82.4	-42.3	96.2	-45.1
Cruise L\D Ratio	-	22.64	8.4	22.05	13.8
Total Wetted Area	m^2	3298	-18.7	3983	-22.3
FAR Takeoff Length	m	3392	1.4	3589	2.0
FAR Landing Length	m	1952	-2.1	1968	-2.6
Fuel Per Passenger-Km	-	0.0083	-55.0	0.0084	-58.9

Table 15.32 - Effect of year 2020 technology applied to X800 and X1000 aircraft

These values indicate the vast potential that exists for the application of future advanced technologies to UHCA. The year 2010 technology strategy exhibits an average takeoff weight reduction of 25%, an average operating empty weight reduction of approximately 17%, and a potentially massive improvement in fuel weight of an average 46%.

The year 2020 strategy shows significantly greater benefits, with an average 35% takeoff weight reduction, an average 31% operating empty weight reduction, and an average fuel weight decrement of 57%.

It is important to note that these kind of improvement margins are not stated as predictions for the next 20 to 25 years, but as the results of an investigation into the effect of realising the full potential of possible candidate technologies. The above results do not take into account the financial limitations associated with the technologies, and do not make adjustments for the practical day to day operational necessities of each technology.

Even with these facts in mind, these results are still valid and provide an excellent insight into the potential directions of future aerospace technologies research, and the kind of improvements that may take place in the aerospace industry over the next 25 years.

16 .Discussion

To fulfil the goals of the research programme a number of essential steps had to be successfully completed in the right sequence. The first aim was to investigate the reasons behind the need for UHCA, the problems that could be faced in their development, and to explore the likely configurations for this type of aircraft. This was followed by a thorough review of candidate advanced technology concepts, the merits and possible drawbacks of each technology were assessed, and methods of incorporating these technologies into a design synthesis were identified. It was then possible to create the software package that would provide the environment for the conceptual design and analysis of these aircraft. The design methods were carefully chosen and new methods were created to give added accuracy for current medium to large aircraft. Once these methods had been validated using existing aircraft data, then it was possible to develop methods that would provide suitable means of assessing UHCA designs incorporating advanced technologies. The final Aircraft Design program could then be used to investigate advanced technology UHCA designs.

16 .1 Ultra High Capacity Aircraft

Various predictions for the growth in air traffic agree that the world wide airline revenue is likely to increase by approximately 6% annually over the next 20 years. There are three main possible strategies that can be employed to avoid over congestion in the future air transport markets. It is unlikely that any single solution will be followed in isolation, but a combination of these three will be used where appropriate to ease possible traffic congestion. The idea of building more local airports (route dispersion) could be a valid approach for a number of situations, but requires the construction of an extensive network of local airports and does not solve congestion problems on certain hub routes which will always encourage a disproportionate amount of traffic. There are also a number of major obstacles which could be prohibitive to the suggestion of the expansion of existing airports. The environmental pollution, the procurement of the necessary land, and the safety aspects associated with handling more aircraft movements, are the main issues that would need to be resolved for any airport before it could consider increasing its capacity. The third potential remedy is the manufacture of aircraft capable of carrying many more passengers than any passenger aircraft currently available. These ultra high capacity aircraft (UHCA) would be particularly welcome in Europe and Japan, where there is already a shortage of runway slots, and the ability to carry more passengers per flight might ease some of the pressure on runway activities.

The worlds current largest passenger aircraft, the Boeing 747, was originally designed in the 1960's, and since its inception we have seen only small growth in the size of passenger aircraft, due to stretched versions of the Boeing 747. This is contrary to many predictions made in the 1960's, 70's, and 80's, of large increases in the size of aircraft for the late 1990's and the turn of the century, and is also contrary to what we have seen is technically achievable with the 600 ton Antonov 225. This would suggest that one of the main reasons we have not seen UHCA as yet is the unwillingness of the aircraft manufacturers to invest in the enormous development cost of such an aircraft without a guaranteed market (a conservative estimate of the development cost would be $12 Billion).

As the market for this kind of aircraft has matured, Boeing and Airbus in particular have begun to invest in the early stages of programmes aimed at developing these type of aircraft. The main obstacles currently in the way of UHCA development appear to be those of airport compatibility and environmental compatibility. Although it seems that plans are already afoot to increase the maximum allowable wing span and aircraft length to 90m, the issues of passenger embarkation/disembarkation, suitable maintenance hangars, and the separation of aircraft on both the ground and in the air have yet to be fully resolved. It would seem that the introduction of UHCA would require fairly extensive changes in both airport legislation and facilities. The environmental compatibility of these aircraft is also under question, with studies showing that such aircraft could have difficulties meeting current regulation noise limits, and would find further difficulties if the current limits are reduced as expected.

Studies on unconventional configurations have shown that while there may be operational and compatibility benefits, the performance benefits of canard configured and blended wing body aircraft are debatable. When one considers the immense financial and technological risks involved in the development of such unconventional concepts, it is easy to see why aircraft manufacturers continue to concentrate on conventional aircraft. For these reasons it was decided that this research would concentrate on conventionally configured aircraft, but with the possible selection of unconventional fuselage cross-sections and advanced technologies.

16 .2 Advanced Technologies

The effect of advanced technologies on possible future aircraft designs has also been considered very carefully. A review of past and current literature led to the choice of a number of candidate technologies, ranging from near future derivative technologies to experimental prototypes.

Propulsion

Current thinking seems to indicate that the recent trends of turbofan engines will continue for the near future, with bypass ratios increasing up to a possible limit of approximately 13, giving an approximate fuel consumption decrease of 6% due to the increase in bypass ratio alone. Increased component efficiencies and the use of advanced materials are likely to give total fuel burn reductions over mid 90's engines of between 15-20% by the year 2005, and 30% by the year 2015. It has also been suggested that the use of advanced materials will reduce the weight of turbofan engines by approximately 20% over the next ten year period.

The need to achieve bypass ratios greater than fifteen has led to a number of advanced engine concepts. The propfan engine uses two rows of contra-rotating blades to produce bypass ratios of the order of 40, and to reduce the fuel efficiency by approximately 30%. However, the noise generated by this type of engine, and problems of blade certification mean that the propfan is unlikely to be used on large civil aircraft. The advanced ducted propeller is a compromise between a turbofan and a propfan, and through the use of a reduction gear box it can produce bypass ratios of greater than 15, and hence has the potential of reducing fuel consumption by approximately 10% over current turbofans. A less established alternative solution is the contrafan engine which uses a directly driven counter rotating fan, and hence eliminates the need for a reduction gearbox, this provides the potential for possible fuel savings of 15% over current turbofans.

Materials & Structures

The role of advanced materials, especially composites, in the construction of modern aircraft has been investigated thoroughly. On average the use of a composite material in place of a conventional metal can give a weight reduction of approximately 30%, however the use of composites in current aircraft has been somewhat limited to secondary structure. Part of the reason for this slow uptake of composite materials has been the fact that all current materials of this type have been thermoset composites. Although thermosets provide tremendous strength and stiffness, along with good corrosion and fatigue properties, they need to be produced using complex labour intensive production techniques, which can make them less cost effective than metals, and unsuitable for large components. Due to the complex nature of the material there is also a lack of adequate analytical methods, as well as a shortage of maintenance and repair data.

It is for these reasons that research has been directed towards new materials such as thermoplastic, metal matrix, and ceramic matrix composites. Although these technologies are still at an early stage of development, the thermoplastic and metal matrix composites in

particular could provide the potential weight benefits of composite materials, while retaining many of the fabrication techniques of existing metals, such as welding, drilling and milling.

The other main area of research into aviation materials has been centred on Aluminium-Lithium alloys, which are approximately 10% lighter than conventional aluminium alloys and 5% stronger.

Aerodynamics

The use of supercritical airfoils has made a significant contribution to improvements in aircraft efficiency over the last 20 years. The development of this type of airfoil has been reviewed, and it would seem that this technology has reached a suitably mature level whereby further improvements of major significance seem unlikely. It would appear that a possible 2-3% drag reduction over the next 25 years is the kind of refinement that we could expect to see in this area.

The use of winglets has been carefully explored and the mechanism by which they produce drag reductions has been investigated. The addition of these winglets does tend to increase the wing bending moment, but has little effect on any other stability or aerodynamic characteristics of the wing. Flight test data has illustrated that the magnitude of the drag reduction, for both upper winglet and combined upper and lower winglet configurations, is strongly dependant on the wing lift coefficient. A summary of this data was produced and used within the Aircraft Design program to estimate the drag reduction effect due to the application of optimised winglets. The main debate on the use of winglets appears to revolve around the question of whether increasing the wing span actually gives better performance than adding a winglet of the same size. Evidence does tend to suggest that increased span is preferable, and it is very likely that in future we will see winglets mainly used as retrofit devices on large aircraft, rather than being incorporated into the original design concept.

Natural laminar flow wings have been the subject of much research and effort over the last decade or so. Many successful 2-d airfoil designs have been tested that demonstrated significant portions of laminar flow at transonic Mach numbers. However, the effect that increasing the Reynolds number and the sweep has in reducing the amount of laminar flow achievable has meant that natural laminar flow wings, or indeed tail surfaces, cannot be considered an appropriate technology for large aircraft cruising at transonic Mach numbers.

The design of NLF nacelles does however seem more promising. It has been demonstrated that laminar flow can be maintained over large areas of the nacelles by the use of appropriate streamwise shaping. Results from CFD analysis, wind tunnel tests, and flight tunnel tests have all indicated that it seems very reasonable to expect laminar flow to be maintained for approximately 60% of the nacelle length, even at transonic Mach numbers.

The massive potential drag reductions that are obtainable by maintaining laminar flow over the wing surface (of the order of 80% for the upper surface, and 60% for the lower surface), have led to a large quantity of research effort being aimed at developing Laminar Flow Control (and Hybrid Laminar Flow Control) systems for use on the wing surfaces of transport aircraft. Tests with full chord and partial chord LFC systems have shown encouraging results. However, recently attention has been turned to the more promising concept of HLFC, which only uses suction up to the front spar of the wing, combined with favourable airfoil shaping aft of the suction region to achieve similar quantities of laminar flow on the wing upper surface. The use of suction only up to the wing front spar means that the weight of the suction systems is smaller, and the wing can be designed using a conventional wing box approach. The available data on LFC and HLFC tests indicate that an average value of laminar flow length would be 50% of the clean wing chord at cruise conditions, and that this value is likely to be closer to 100% for speeds below Mach 0.6. The main issues in the use of such active drag control systems are the operational concerns, particularly insect and ice contamination. Devices such as leading edge insect shields and nozzles for ejecting freezing point depressant liquid have been tested with a high degree of success, but the use of these devices on a day to day basis is still very questionable. Another concern is the effect of loss of laminar flow during flight and its implications on fuel reserve policy, and aircraft stability in the case of an asymmetric loss of laminar flow. Flight tests have shown that laminar flow is temporarily lost during travel through clouds, and it is this kind of unpredictability that might make LFC and HLFC technologies unpopular with airlines and regulatory authorities.

The use of riblets to alter the structure of the turbulence near the surface of the aircraft have been proven to reduce skin friction drag by approximately 7%. The main obstacle to their commercial usage has been the difficulty of their application, and the high degree of precision with which they must be applied. There are also concerns over their life span, and their vulnerability to damage from fluids used in aircraft maintenance. It would seem that current riblet technology is not suitably advanced for the rigours of commercial application, but this may change in the years to come.

Large eddy breakup devices are small airfoils or thin plates immersed in the turbulent boundary layer and have a similar drag reduction effect as riblets, but are still as yet an experimental technology.

The use of variable camber wings to optimise the wing lift distribution for all flight conditions has been an idea that has been investigated for a number of years. Two approaches have been suggested as methods for achieving this variable camber. A flexible wing skin which can deform the wing shape seems an ideal solution, however the technology to achieve this appears to be a long way off. A compromise solution is the use of multi-

element airfoils which can be used to change the wing camber at a number of independent spanwise stations, without drastically changing the conventional structural design of the wing. Results of wind tunnel tests show that the cruise wing lift could be significantly altered closer to its ideal elliptical distribution, with an approximate 60% improvement compared to an analogous conventional wing lift distribution. It was also demonstrated that the manoeuvre lift distribution could be manipulated to give large wing root bending moment reductions, and hence reduce the overall wing structural weight by approximately 10%. Although these findings are encouraging, there remain a number of complex problems regarding geometry and reliability which need to be resolved before a variable camber wing becomes a realistic prospect.

Other miscellaneous technologies that have been identified include the use of active control to further reduce the static margin of the aircraft, giving rise to drag reductions of the order of 4%, the use of fibre optics to reduce the avionics weight by a possible 50%, and the use of advanced electrical systems to replace hydraulic and pneumatic secondary power systems, with a takeoff weight saving of approximately 5%.

16 .3 The Aircraft Design Program

The objectives that were chosen for the Aircraft Design program have been met and perhaps surpassed in most aspects. The completed program is available as a Windows package compatible with both Windows 95 and Windows 3.11, and provides a completely integrated and interactive environment from which conceptual aircraft design and analysis can be performed.

The package is operated via standard user friendly Windows controls and commands, incorporates a comprehensive context sensitive on-line help facility, and uses a document structure to store each aircraft design, rather than text based data files. Up to twenty documents may be opened simultaneously, and features are available that allow for the contents of the documents to be compared both graphically or numerically. The environment supports copy, cut, and paste functions that allow the easy transfer of data, and also gives the user the flexibility to express values of parameters in a variety of units.

The program itself contains up to nineteen sub windows that can be opened at will and each have a specific purpose, such as displaying a particular type of output data, input data, drawing, or for the analysis of the aircraft design data. Each window is fully integrated into the design process, and the data in each window is automatically updated after each calculation execution. For the purpose of analysing the aircraft design results, a specially written language has been incorporated into the environment which allows the user to evaluate any mathematical expression involving design parameters and mathematical

functions. This mathematical language proves to be particularly useful when using the optimisation, correlation, trade-off and sensitivity studies functions. The program also includes the ability to automatically generate a highly detailed 3-d mesh, incorporating both external and internal features of the aircraft. This can then be imported into AutoCAD versions 12 and above, where it may be viewed and rendered.

The design calculations themselves have been conveniently split into eight separate modules, each of which can be run independently, and have their own input and output parameters. The number of input parameters that is required to be set by the user has been minimised, with only 88 parameters being used to specify the entire aircraft design. A fuselage sizing tool is also incorporated, which in the absence of detailed geometric knowledge helps provide an accurate estimate of the fuselage dimensions based upon the passenger layout.

Once the design has been calculated, it may be further analysed using the Optimisation, Correlation, Trade-off Studies, or Sensitivity Studies Windows. The Optimisation Window allows the user to optimise a design for any valid expression, with up to 10 independent variables, and 10 constraints. The Correlation Window enables the user to plot the results of up to 15 user-defined expressions for all the open documents, and to use the curve fitting functions to derive a line of best fit to the data. The Trade-off Studies window allows the user to simultaneously vary up to two design parameters and to then evaluate the effect that this has on any aspect of the aircraft design. The Sensitivity Window can be used to quantitatively estimate the dependency of user defined expressions on up to 10 independent variables.

The Aircraft Design program has succeeded in providing a totally integrated and flexible environment in which the conceptual design process of subsonic civil transports can be performed. The program is not only intuitive and easy to use but provides the user with complete freedom, especially in the area of design analysis, where there are no limitations on the types of analysis that may be performed. The minimisation of the number of input parameters has meant that the program can be used by all levels of designers, and reduces much of the guesswork associated with conceptual design. The completed program certainly stands out as a valid educational and professional tool for use in the conceptual aircraft design process.

Although there are a number of computerised design syntheses already available in both the commercial and educational world, such as AAA, ACSYNT, CAPDA, OPDOT, CASP, and CACAD, the Aircraft Design program does bring a unique approach to conceptual aircraft design. While having many features in common with the programs mentioned above, Aircraft Design is the only package which incorporates a fully integrated user-friendly Windows interface, with a complete synthesis and detailed performance

prediction model, along with flexible design analysis tools, and the ability to evaluate UHCA designs incorporating advanced technologies.

16 .4 Design Methods

Many new design methods were created, and existing methods modified in order to both improve the accuracy of these methods when applied to existing aircraft, and to extend their applicability to UHCA incorporating advanced technologies. Most of the equations derived with the goal of improving the accuracy of existing methods were based on data correlations. These data correlations were made using the Correlation Windows of Aircraft Design, and were either based upon exact data of existing aircraft or data for existing aircraft that was estimated using the Aircraft Design program itself. In this way, the development of the methods used within the design synthesis was an evolutionary process, with the final design program being the result of many modifications and improvements.

The methods employed to describe the effect of advanced technologies were entirely based upon the results of published research. The complexity of the methods used was dependent on the availability of adequate data, which varied considerably between technologies. For each case, a broad spectrum of literature was critically reviewed, and the results distilled into equations which would give adequate quantitative description of the main physical effects of the technology.

The main methods of each module, and their measured accuracies are described below.

Airfoil & Engine Module

The data supplied in the airfoil data library is directly taken from published values of the lift, drag, and moment performance of existing NACA 6-series and RAE supercritical airfoils, and hence can be regarded as being highly accurate. The airfoils cover both a wide range of thickness to chord ratios and maximum lift coefficients, and should be sufficient for most applications, although further airfoils can be added at any time by the user.

The engine data library currently consists of 7 engines covering a thrust range from approximately 20,000lbs to 80,000lbs, although this can be added to at any time by the user. This data was kindly supplied by Rolls-Royce and can therefore be considered to be of a very high accuracy. In order to create the performance data for an engine of any thrust level, bypass ratio, and year of service, the data from the engines in the engine data library is modified and interpolated appropriately. The methods used to do this have been based upon a combination of empirical and semi-empirical correlations, and have been proven to give the correct qualitative results. Although there is insufficient data available to validate

all of these methods, the results of a trade-off study to show the effect of varying the bypass ratio on the specific fuel consumption and the engine weight has been shown to give excellent agreement with the results of a similar study performed on behalf of Rolls-Royce.

Initial Sizing

The maximum takeoff weight, operating empty weight, and fuel weight, are estimated using a much modified weight fraction method. The expressions for each weight fraction have been modified to more accurately reflect the flight parameters for this kind of aircraft, with these modifications being based on the detailed output of flight profiles from the performance module for a number of sample aircraft. The estimation of weight fractions has also been made more accurate by providing detailed initial estimates of such parameters as lift to drag ratios, wing loading, lift coefficients, and thrust settings at the first possible opportunity. Most of these estimates have been based on correlations of sample data and provide a higher degree of accuracy than most existing methods. The effect on these parameters of any advanced technologies such as winglets, laminar flow control, and riblets is also estimated at this early stage to improve the overall quality of the results.

An important feature of the maximum takeoff weight estimation is the creation of an equation which relates the estimated takeoff weight of the aircraft without advanced materials to its range, payload, cruise lift to drag ratio, cruise specific fuel consumption, and its cruise Mach number. This equation can then be linked to estimates of weight savings due to advanced materials, and the weight fractions discussed above, to provide accurate estimates of the aircraft weights.

The final results illustrate the high degree of accuracy that has been achieved using this method. The maximum takeoff weight displays an average error of 2.85%, while the operating empty weight has an average error of 4.1%, and the wing loading gave an average error of 5.3%.

Wing Design

The Wing Design Module calculates the geometric and lift properties of the wing and its flap systems. An innovative approach was used to calculate the geometry of the cranked wing, which involved iterating for the tip chord and crank length until a planform was found that satisfied the area requirements and all the constraints set by the user. An equivalent wing could then also be calculated by assuming a wing of equal area and tip chord, but without the cranked section.

The aerodynamic properties of the wing were then found using standard techniques, and its lift distribution was calculated using the Diedrich and Anderson method. The maximum clean lift coefficient of the wing at all conditions was calculated from airfoil data with appropriate corrections, and the lift contributions of the trailing edge flaps, and

ailerons (when being used to augment lift) could be evaluated for a range of deflections. Although no data was available on the exact flap deflections for the sample aircraft, the calculated flap deflections were all of the order of magnitude that one would expect for both the takeoff and landing conditions.

Geometry

The Geometry Module successfully produces accurate mathematical models of the fuselage shape for each of the fuselage geometries, including the '747' type fuselage and the double bubble fuselages. A combination of ellipses, cubic splines, and linear segments was used to describe the fuselage geometry in such a way that the cross-sectional shape at any longitudinal section could be calculated, and the overall wetted area, planform area, and frontal area could be calculated using this fact.

An estimate of the fuselage freight volume is also calculated, based upon the geometric properties of the fuselage cross-section, and the available length for freight storage. This estimate was shown to give an average error of 9.9%.

The geometry of the nacelle is calculated from correlations of sample data, and from consideration of the dry engine dimensions. These calculations were found to give values that were of the correct magnitude for typical engine installations over a wide range of engine specifications.

Weight Estimation

The detailed weight estimate relies upon calculations of the weights of each of the main components of the aircraft, and incorporates any correction for the inclusion of advanced technologies. The techniques for estimating the weights of the components are based upon text book methods, with some modification to improve agreement with sample component data, and with new methods based upon published research which account for the weight of advanced technologies such as variable camber wings and laminar flow control. The estimation of the fuselage weight includes new methods to describe the weight of '747' type fuselages, double-deck, horizontal double bubble, and vertical double bubble fuselages.

The centres of gravity of each component are also estimated, and the size of the tail surfaces are calculated from tail volume coefficient and centre of gravity considerations. The tail volume coefficients are estimated using new equations derived from correlations of data from a number of sample aircraft. The average error of the horizontal tail sizing calculation was found to be 5.3%, while the average error of the vertical tail sizing was 10.6%.

The undercarriage of the aircraft is then configured, and its drag contribution estimated. The assumed configuration of the undercarriage gave very good agreement with the actual undercarriage layouts of the sample aircraft

With all of the components of the aircraft sized, the weight contributions of each can be added, and the detailed estimate of the operational empty weight can be found. The average error of the operating empty weight from the actual value of the sample aircraft was found to be 4.5%, which is an excellent degree of accuracy for this type of calculation.

Drag Prediction

The wetted area of each of the major components is calculated from geometric considerations, and the parasite drag of the aircraft for a range of altitudes and Mach numbers is then calculated using a component build up method. The form factors and interference factors of each component have been calculated using text book equations.

In the absence of advanced technology, the flow transition location is assumed to occur at a Reynolds number of 500,000, however the application of NLF, LFC, of HLFC, requires that the revised transition location be calculated for the particular component at the particular Mach number and altitude. These calculations have been based upon the results of published research in these areas. The application of riblets is assumed to have the effect of reducing the skin friction coefficient by a fixed percentage at all flight conditions.

The compressibility drag is then calculated over a wide range of altitudes, Mach numbers, and lift coefficients. The drag divergence Mach number is calculated using a standard method, however a new correction factor was introduced to take into account the improved design of new airfoils for higher cruising speeds. The transonic drag rise can then be estimated by calculating the drag at $Ma=1.05$ and $Ma=1.0$, and creating an appropriate graph, which was approximated as an exponential curve.

The induced drag was calculated using a standard method, but was modified for the case of variable camber wings, in order to reflect the improvement in the lift distribution of such wings. The effect of winglets was quantified from the published results of flight tests and wind tunnel tests, and was assumed to be a percentage reduction in the total aircraft drag that was dependant on lift coefficient and Mach number.

The complete drag polars give the kind of trend one would expect for this kind of aircraft, and the results of the performance module, which rely heavily on the data from this module, suggest that the drag predictions are accurate to within at least 5%.

Stability Analysis

The static longitudinal stability is calculated, and a trim plot is produced for a range of flight conditions. The pitching moment contributions and derivatives are calculated using standard text book methods. The results of the static margin, tail incidence angle, and trim drag calculations for the cruise, takeoff, and landing conditions, all give the magnitude of values expected for such aircraft. In fact, assuming that the sample aircraft each have a cruise static margin of 5%, and since in this analysis the static margin is controlled by the wing

location parameter, an evaluation of the accuracy of these calculations can be made by comparing the wing location of the sample aircraft with the location calculated by the program. Such a comparison shows an average error of 6.3%.

Performance Prediction

The Performance Module provides an excellent tool for estimating the flight range, fuel consumption, takeoff field length, and landing field length of an aircraft. The approach used was to allow the user to enter the desired flight profile in terms of segments such as 'climb', 'cruise', 'descent', 'loiter', etc. The range of allowable segments and their parameters means that almost any reasonable flight profile can be set by the user. This profile is then followed by the Performance Module, with each segment being split into a number of steps, and the main flight parameters, such as thrust, lift, drag, fuel consumption, being estimated at each step in the flight. A number of iterations are performed such that the goals specified by the user, such as a particular overall range, or a particular fuel mass are met exactly.

The takeoff analysis has been split into the ground roll, the rotation, the transition, and the initial climb. Each segment (except the rotation) has been split into a number of steps, and the behaviour of the aircraft at each point carefully modelled. The landing analysis is analogous with an initial descent, flare, and ground roll stages that include the use of spoilers, airbrakes, and thrust reversers. These calculations allow the estimation of the takeoff field length, the landing field length, and the balanced field length. The average error of the takeoff field length calculation was found to be 5.4%, while the average error of the landing field length was found to be 5.6%.

The cruise, loiter, acceleration, deceleration, and climb at constant calibrated airspeed segments were carried out using straightforward consideration of the flight mechanics involved. The climb at maximum flight path angle involved some analysis of the equations involved to come up with a new approach for modelling this kind of flight. This climb segment now performs a number of calculations, which guide the aircraft velocity toward the optimum climb velocity, and which optimise the amount of acceleration of the aircraft, in order to find the best overall climb profile.

The descent profile has also been tailored to give a more realistic approach, by including the option of limiting the glide path angle, and by specifying the descent velocity in terms of a multiple of a stall velocity, a stated in FAR regulations.

All of these factors have combined to give excellent results from the Performance Module. For a sample of 49 calculations for which the range was the objective for a given fuel load, the average error observed was 3.5%. This level of error means that full confidence can be placed in the content of these calculations.

Fuselage Sizing

In the absence of any detailed knowledge of the main fuselage dimensions, it is possible to estimate both the cross-sectional and planform layouts and dimensions of a wide variety of fuselage styles by using the fuselage sizing tool which has been integrated into Aircraft Design.

The fuselage cross-sectional layout for each fuselage type has been defined by a few simple geometric relationships, found from studying existing fuselage cross-sections. These relationships together with the seating layout, seat size, and aisle size for each deck, specified by the user, allow the program to automatically generate realistic fuselage cross-sections that satisfy all the necessary constraints. For both single deck and double deck fuselage layouts these calculations displayed an average error of 1.6% for the fuselage width, and 1.2% for the fuselage height.

By specifying the number of passengers per class, and the level of seating comfort for each class, the fuselage sizing tool is also capable of automatically generating an accurate internal fuselage layout, which includes the location of seats, toilets, galleys, and emergency exits. A unique approach was adopted for the calculation of the internal arrangement. A relationship was found between the nose and tail lengths of the fuselage and the fuselage width, this meant that the nose and tail geometries could be immediately known, and therefore the length of the main 'cylindrical' portion of the fuselage is the only unknown. The number of toilets and the galley volume required could be calculated from the number of passengers present, and inconjunction with a set of suitable rules, the seats, toilets, galleys, and emergency exits could be placed at suitable locations, and the overall fuselage length can be determined. The average error for the calculation of the fuselage length for both single deck and double deck aircraft was found to be 3.3%.

16 .5 Design Results

The completed program could then be used to investigate the properties and relative merits of UHCA aircraft, and the application of advanced technologies to UHCA. The design process adopted involved specifying a desired range for a given payload. This meant that each design was found from an iterative process, in which the initial sizing tuning factors were adjusted such that the range performance was met exactly, and the difference between the initial and the detailed operational empty weight estimates was less than 0.1%. There may also have been some adjustment of the wing aspect ratio, and the wing location, in order to set the values of the wing span and the static margin respectively.

16 .5 .1 UHCA CONFIGURATION

The first study was concerned with determining the most advantageous fuselage configuration for a UHCA capable of carrying 800 passengers a distance of 7000nm (a higher payload-range than any existing aircraft), with both the fuselage length and wing span confined to 90 metres. The four fuselage concepts that were evaluated were the double deck fuselage, the '747' type fuselage, the horizontal double bubble, and the vertical double bubble. The technology level assumed for each design was that of a year 2000 aircraft.

The results of the analysis clearly showed that the double deck fuselage aircraft (the X800-DD) was the most efficient in terms of fuel per passenger-kilometre, it was also found to be more aerodynamically efficient, and was also lighter than the other three aircraft. The '747' type aircraft was the second most fuel efficient aircraft (3.6% behind the X800-DD), while the horizontal double bubble aircraft was 17.9% less fuel efficient than the X800-DD, and the vertical double bubble aircraft was 21.6% less fuel efficient than the X800-DD. The fuel efficiency of the X800-DD was in fact estimated to be approximately 38% improved over that of a current day Boeing 747-400.

These results concur with the assumptions made in Chapter 2, that the double deck design is the most efficient fuselage design, and is almost certain to be the configuration of first generation UHCA, for both design and economic reasons.

The efficiency of this type of fuselage shape stems from its good use of internal space and its structural efficiency. The '747' type fuselage would appear to be a compromise design, which by including a small double deck region increases the frontal area of the aircraft over a similar single deck design yet does not appreciably reduce the length, while also introducing structural complications due to the construction of an upper 'bubble'. Both the double bubble designs exhibit a poor use of internal space, and also introduce structural complexities which mean that both the drag and the weight of these aircraft are greater than that of a double deck design.

Although the differences between these designs may have been exaggerated by the use of a 90 metre span limit, which allows the aspect ratio of the wings to be increased for the lighter designs, and hence further increase the overall efficiencies of the lighter aircraft, the trends shown between the designs are clearly correct.

The other main conclusion that can be draw from this study is that the technology for the design of an 800 seat aircraft is already established, and that such an aircraft could be constructed that would be well within the 635 ton weight limit, and the 90 metre length and wing span limits that are likely to be proposed for UHCA.

16 .5 .2 The Impact of Advanced Technologies

Each advanced technology and its overall effect on the aircraft design and performance was assessed by first applying each technology in isolation to the X800-DD baseline design and to a new 1000 seater baseline design (the X1000). Although the technologies were applied in isolation, the whole aircraft was redesigned in each case to take full advantage of the possible benefits from each technology. The X1000 design was based on the same technology level and assumptions as the X800-DD design, only with a longer fuselage to accommodate the extra passengers. The results of the analysis showed that such an aircraft would weigh approximately 700 tons and, would hence be unlikely to become reality without the use of advanced technologies to reduce its weight to a more manageable level.

Advanced Engines

Out of all the candidate technologies, the application of a year 2020 contrafan engine of bypass ratio 20 gave the greatest increases in fuel efficiency and improvements in all areas of the aircraft performance. The efficiency (fuel per passenger-km) was improved by 28.1% for the X800, and by 29.4% for X1000.

Similarly, the application of a year 2010 advanced ducted propeller of bypass ratio 15 improved the efficiency of the X800 by 17.5%, and the X1000 by 19.5%. A year 2005 turbofan engine of bypass ratio 12 improved the efficiency of the X800 by only 3.0%, and the X1000 by only 2.8%.

These results indicate that the biggest potential for the improvement in the efficiency of civil aircraft comes from the application of advanced engine concepts. The improvement in fuel efficiency of nearly 30% due to the application of the contrafan engine compares to an improvement of only approximately 15% due to the best aerodynamic device (variable camber wings).

The small benefit gained from increasing the bypass ratio of the turbofan engine to 12 may appear to be somewhat surprising, but when one considers that this engine is designed for entry into service in the year 2000, and hence does not include any of the improvements in thermal efficiencies or weight reductions that have been assumed for the other engines, as well as the increase in drag due to the larger frontal area, then this small improvement is understandable.

Wing Tip Devices

The inclusion of upper & lower winglets in the designs gave a 1.5% improvement in fuel efficiency for the X800, and 1.0% for the X1000, while the inclusion of only upper winglets gave improvements of 1.1% and 0.6% for the X800 and X1000 respectively. The

application of wing tip fences to both designs gave fuel savings of 0.9% and 0.5% for the X800 and for the X1000. These results are of the order of magnitude that one would expect, and show that as the size of the wing tip device increases, so does its potential for improving the fuel efficiency of the aircraft.

An analysis of these results also found that the magnitude of the fuel saving was heavily dependent on the cruise lift coefficient, which is not surprising given that the method used to evaluate the drag reduction of the wing tip devices relates the drag decrement to the Mach number and to the lift coefficient.

More importantly however, were the results of study which aimed to estimate the effect of an increase in wing span equivalent to the span of the winglets. These results showed an increase in efficiency of 1.6% for both the X800 and the X1000. This would suggest that extra span is indeed preferable to wing tip devices at the design stage, and that the use of wing tip devices is likely to be limited to applications as retrofit devices on existing wing designs.

Advanced Materials

The study into the effect of introducing more composite materials and advanced aluminium alloys into the aircraft structure was based around the application of two material strategies. The first strategy attempted to define the likely material content of the aircraft in the year 2010, and the second for the year 2020.

The year 2020 strategy exhibited a 10.5% improvement in fuel efficiency, and a massive 18.2% reduction in operating empty weight of the X800 aircraft. Similarly, the X1000 aircraft showed a 14.9% improvement in fuel efficiency and a 19.4% reduction in operating empty weight.

The results of the year 2010 study showed 5.9% and 10.4% improvements in the fuel efficiency and the operating empty weight of the X800 respectively, while the X1000 results showed 7.4% and 10.4% improvements.

These results illustrate the kinds of trends that one would expect, and clearly follow the mechanism of the weight reduction, with the reduction in operating empty weight being of greater magnitude than the reductions in fuel or takeoff weights.

Variable Camber Wings

The application of a 60% efficient variable camber wing to the baseline designs produced fuel efficiency improvements of 11.7% for the X800 and 15.6% for the X1000.

An investigation into the effect of the efficiency parameters, which controls the efficiency of the wing in creating an ideal elliptical lift distribution, concluded that the improvements in fuel, takeoff, and operational empty weight were all proportional to this parameter. However, because all these studies were conducted under the assumption that the

variable camber wing will bring about a 10% reduction in structural weight due to its reduced bending moment, then even an efficiency of 0% brought about significant benefits due to this weight reduction effect. In fact it could be concluded that the weight reduction due to bending moment relief is of equal if not greater significance in increasing the aircraft efficiency than the reduction of drag due to an improved lift distribution.

Laminar Flow Control

The inclusion of a typical laminar flow control system on the wings of the X800 and X1000 aircraft brought about improvements in fuel efficiency of 10.5% and 13.6% respectively. The inclusion of a similar system on the horizontal tail surfaces of these aircraft brought about fuel improvements of 1.9% and 3.1%, while its inclusion on the vertical tail surfaces gave improvements of 2.4% and 2.6%.

Studies on the effect of transition location, laminar flow flight time, and the addition of lower surface suction, concluded that the reductions in fuel, takeoff, and operational empty weights were directly proportional to the amount of laminar flow obtained during the flight. This is to say that these weight reductions were proportional to the product of the transition location, the amount of time for which laminar flow could be maintained, and a constant representing the number of surfaces to which laminar flow control is applied.

These results indicate that there are large potential benefits associated with the application of LFC to aerodynamic surfaces, especially the wing surface, although many of the operational issues discussed previously have yet to be resolved, and it would seem that hybrid laminar flow control is a much more realistic proposition.

Hybrid Laminar Flow Control

The studies carried out for the inclusion of LFC devices on aerodynamic surfaces of both the X800 and X1000 aircraft were repeated for HLFC devices. The results for typical HLFC wing surfaces indicated a 10.7% fuel efficiency improvement for the X800, and 14.9% for the X1000. Application of HLFC to the horizontal tail surfaces showed potential fuel savings of 2.1% for the X800 and 3.3% for the X1000, while its application to the vertical tail surfaces gave fuel savings of 2.8% and 3.0%.

These results clearly illustrate the higher efficiency of a HLFC system compared to a LFC system, with the fuel improvements of the HLFC system being greater in every case. This is mainly due to the reduced weight of a HLFC system because of its use of suction only up to the leading edge spar, and because of the assumption in the calculations that both systems operate with the same transition location.

As with the LFC systems, the potential benefits are large, although a number of operational difficulties must be overcome before they can be realised.

Natural Laminar Flow

By assuming a transition location that was a distance of 60% of the fan cowling length (as taken from published flight test and wind tunnel results), it was discovered that improvements in fuel efficiency of 3.6% for the X800 and 3.9% for X1000 resulted. This would suggest that this kind of technology could have enormous potential benefit for comparatively small development cost and risk.

An investigation into the possibility of obtaining significant amounts of natural laminar flow on any of the aerodynamic surfaces of these aircraft concluded that it would not be possible due to the combination of the high sweep angles and the high Reynolds numbers of these surfaces.

Riblets

The application of riblets to the wing surface was responsible for a 1.5% improvement in fuel efficiency in the X800, and 1.6% in the X1000. Similarly fuselage riblets gave improvements of 0.5% and 1.1%, while horizontal tail riblets showed improvements of 0.1% and 0.5%, and vertical tail riblets improved the fuel efficiency of the X800 and the X1000 by 0.1% and 0.4% respectively.

These results indicate that significant fuel savings can be achieved through the use of riblets, especially in the wing and fuselage areas, however, the logistics and the economics behind their use are still debatable.

Summary

All of the technologies described above gave some degree of improvement over the original baseline designs (with the exception of NLF aerodynamic surfaces). The physical mechanisms behind the performance improvements appeared to have been modelled correctly, and the resulting values of the improvements to the main parameters of the aircraft design appear to reflect this.

One further observation that can be made from these results is the fact that the larger aircraft (the X1000) consistently tended to show greater improvements, especially in fuel efficiency, than the smaller aircraft (the X800) for the application of a given technology. The reasons for this phenomenon cannot be directly explained, since the design synthesis is a complex model containing many variables. However it could prove to be an important observation that was made entirely possible by the automated design synthesis created specifically for this research.

16 .6 FUTURE DESIGNS

The final task of the research was to assimilate all of the previous knowledge and results, and to use this to design concept UHCA aircraft of the future. Four aircraft were designed in total, with these being both 800 seat and 1000 seat concepts, with versions based on assumed technology levels of both the year 2010 and the year 2020.

From consideration of the results of the technology assessment, the year 2010 technology level was assumed to be comprised of ADP engines of bypass ratio 15, HLFC wings, HLFC tails, 2010 advanced materials, NLF nacelles, and fuselage riblets.

The year 2020 technology was improved by the introduction of a contrafan engine of bypass ratio 20, the replacement of the HLFC wing with a variable camber wing, and more advanced structural materials.

The results of these studies showed that for the year 2010 designs, fuel efficiency improvements of 43.7% for the X800 and 48.7% for the X1000 were achievable. This was in-conjunction with takeoff weight reductions of 23.9% and 27.1%, and operational empty weight reductions of 16.6% and 17.6% for the X800 and X1000 respectively.

For the year 2020 study, these fuel improvements were assessed as being 55.0% and 58.9% for the X800 and X1000, while the takeoff weight reductions were 33.8% and 35.5%, and the operating empty weight reductions were 31.0% and 29.9% for the X800 and X1000 respectively.

These results would suggest that through the application of advanced technologies, the size of a 1000 seat aircraft, or in fact an aircraft of even greater capacity, could be reduced to an acceptable level over the next 10 or 20 years.

Comparing the estimated fuel efficiencies of these aircraft to current aircraft shows an approximate improvement over a Boeing 747-400 of 65% for both year 2010 designs, and an approximate 72% improvement for both year 2020 designs.

Although fuel efficiency is a very good measure of overall improvement from an engineering perspective, as well from an operational one, the main note of caution to be associated with these results would be the lack of regard for the financial and in some cases operational risks associated with the application and development of some of the technologies. The synthesis has dealt mainly with the potential benefits associated with the technologies, and although increases in weight and perhaps drag have been included, increases in complexity, maintenance, unit cost, and development cost have not been present. This would mean that the results of the studies above indicate what would perhaps be achievable in a world where development and maintenance costs where not of significance, which is why the enormous improvements predicted above should be tainted with a note of financial and operational reality.

Conclusions

It is without doubt that the development of Ultra High Capacity Aircraft will be part of the strategy adopted to combat possible congestion of the future air transport system. It has been demonstrated that these aircraft are technically feasible, even based on current technology levels. However, the main problem areas for these aircraft are the issues of airport and environmental compatibility, as well as the economic burden of their development costs. The use of advanced technologies will certainly play a significant part in increasing the efficiencies of these aircraft and reducing their sizes to more practical levels, and hence make them more attractive commercial prospects by alleviating the above limitations.

The investigation into UHCA concepts and the influence of advanced technologies has been made possible through the development of a state of the art Windows based software package, specifically written to perform the process of conceptual design and analysis for medium to large advanced civil transports.

Aircraft Design incorporates new methods that have been created in order to improve the accuracy of conceptual design work for conventional types of civil aircraft, and to extend their applicability to UHCA and advanced technology aircraft. These new methods have been developed during the research programme, and have largely been based on data from a broad sample of modern existing and concept aircraft, as well as published research. Validation of these methods was carried out with additional aircraft designs not included in the original sample, demonstrating an average accuracy of the order of 5% from real flight data. This confirms that the program provides a reliable platform for extensive investigations into the effects of advanced technologies on the overall aircraft design.

Investigations carried out using the Aircraft Design program indicate that the double deck concept is one of the most efficient designs for a UHCA, and is almost certain to be the first generation UHCA configuration. It was also possible to demonstrate that an 800 seat aircraft could be built using year 2000 technology that would fulfil the requirements of the new aircraft regulations governing airport compatibility that are likely to be introduced in the near future. Similarly, it was concluded that an aircraft capable of carrying 1000 passengers for a range of 7000nm would not be practically feasible without the extensive use of advanced technologies.

Results of the study into the effect of candidate advanced technologies clearly show that proposed future propulsion concepts such as the advanced ducted propeller and the contrafan engine have the greatest potential for improvements in fuel efficiency. These are closely followed by such concepts as variable camber wings, advanced materials, and laminar

flow technologies, which all show a significant performance benefit. Other technologies such as riblets and winglets also show some fuel savings, but of a smaller magnitude than those associated with the above technologies. It is interesting to note that results from Aircraft Design indicate that the benefits of applying advanced technologies to UHCA tend become greater as the aircraft size increases.

Future UHCA's will contain combinations of suitable advanced technology concepts. The assumption that aircraft flying in the year 2010, utilising cutting-edge technologies of the time such as hybrid laminar flow wings and tails, ADP engines, NLF nacelles, and fuselage riblets, led to designs exhibiting fuel savings of approximately 46% over year 2000 aircraft. Similarly, aircraft flying in the year 2020 with further advances such as contrafan engines, variable camber wings, and more advanced materials, achieved fuel savings of approximately 57% over the same year 2000 aircraft.

Although this work has provided an excellent design program with correspondingly good results, there is still scope for extending this research program. Further work could include the broadening of the design program to include a wider range of configurational options, such as T-tails, 3-engine configurations, and perhaps more unconventional layouts. The analysis itself could benefit from the inclusion of more detailed calculations, particularly in the areas of undercarriage design and stability analysis, and it may be possible to make the program even more user friendly.

References

1. Sutton O. , *Regional airlines census*, Interavia/Aerospace World, April 1993, p. 52.

2. Acton R. , *British Airways requirements for a new large airliner*, The new large aircraft: Proceedings of the conference, London, U.K, Oct. 6, 1993, Royal Aeronautical Society, 1993.

3. Orlowski W.J. & Callaghan J.T. , *A phased approach to introduce new high capacity aircraft*, The new large aircraft: Proceedings of the conference, London, U.K, Oct. 6, 1993, Royal Aeronautical Society, 1993.

4. Airbus Industrie, *New large aircraft*, Flight International, 24-30 Nov. 1993, p. 36.

5. Schriever B.A. & Seifert W.W. , *Air transportation 1975 and beyond: A systems approach*, Report of the transportation workshop, 1967, The M.I.T. Press.

6. Yeger S. , *Aircraft of the future*, NASA TM-77952 (N86-13318).

7. Whitford R. , *Design of an ultra-high capacity aircraft*, Royal Military College of Science, Cranfield Institute of Technology, (AIAA-93-3953).

8. Serghides V.C. , *Ultra high capacity airliner design concepts*, 2nd International Symposium on Aeronautical Science and Technology of Indonesia, ISATI '96, Jakarta, June 24-27, 1996.

9. Oelkers W. , *High capacity aircraft*, Deutsche Airbus, ICAS 18th Congress, Beijing, China, 1992, Proceedings vol. 2. pp. 1979-1988.

10. Knowles K. & Martinez-Val R. , *Conventional and unconventional configurations for ultra-high capacity aircraft*, ICAS 19th Congress, Anheim, California, Sept. 18-23 1994, Proceedings vol. 1 (A94-31534, 10-01), 1994, pp. 656-663.

11. Ritchie G. , *The new large aircraft physical separations at airports*, The new large aircraft: Proceedings of the conference, London, U.K, Oct. 6, 1993, Royal Aeronautical Society, 1993.

12. Critchley J.B. & Greenwood J.S. , *The new large aircraft: Separations in flight*, The new large aircraft: Proceedings of the conference, London, U.K, Oct. 6, 1993, Royal Aeronautical Society, 1993.

13. Russell R.E. & Streckenback J.M. , *Aircraft noise reduction*, International symposium on transportation noise, Pretoria, South Africa, 21-23 Oct. 1981, (N83-12080).

14. Jagger D.H. , *Design considerations for new large aircraft*, The new large aircraft: Proceedings of the conference, London, U.K, Oct. 6. 1993, Royal Aeronautical Society, 1993.

15. Eccleston A. & Metcalfe M. , *Environmental implications of engines on very large aircraft*, The new large aircraft: Proceedings of the conference, London, U.K, Oct. 6. 1993, Royal Aeronautical Society, 1993.

16. Haberland Ch. et al. , *Impact of operational and environmental aspects on commercial aircraft design*, ICAS 19th Congress, Anheim, California, Sept. 18-23 1994, Proceedings vol. 1 (A94-31602), 1994, pp. 646-655.

17. Callaghan J.T. & Liebeck R.H. , *Some thoughts on the design of subsonic transport aircraft for the 21st century*, Cockpit (ISSN 0742-1508), Oct.-Dec. 1990, pp. 5-13.

18. Martinez-Val R. et al. , *Design constraints in the payload-range diagram of ultrahigh capacity transport airplanes*, Journal of Aircraft, vol. 31, No. 6, Nov.-Dec. 1994.

19. Webb W.L. , *Advancements in aircraft gas turbine engines past and future*, ICAS 18th Congress, Beijing, China, 1992, Proceedings vol. 2, pp. XLII-LIII.

20. Pickerell D.J. , *Future trends in aviation propulsion*, The 1987 Australian aviation symposium, Canberra, 18-20 Nov. 1987. PNR 90443 (N88-28068).

21. Peackock N.J. & Sadler H.R. , *Advanced propulsion systems for large subsonic transports*, Journal of Propulsion and Power, vol. 8, No. 3, May-June 1992.

22. Aeronautics and Space Engineering Board - National Research Council (NAS-NRC), *Aeronautical technologies for the twenty-first century*, NASA CR-190918.

23. Stryker H.Y. , *Twenty-first century commercial transport engines*, 30th aircraft symposium, Tsukuba, Japan, Sep. 30 - Oct. 2, 1992, Proceedings (A94-28718, 09-01).

24. Knip G. , *Analysis of an advanced technology subsonic turbofan incorporating revolutionary materials*, TM-89868 (N87-22860).

25. Shaiu B.J. & Chen H. , *Al-Li-X alloys for aircraft application: An overview* , (N89-18548).

26. Bartlett D.W. et al. , *Application of advanced technologies to very large subsonic transports*, SAE Aerotech '92 conference, Anaheim, California, Oct. 5-8 1992, SAE Paper 92193.

27. Vogelesang L.B. & Gunnink J.W. , *ARALL, a material for the next generation of aircraft, a state of the art*, Delft University of Technology, Department of Aerospace Engineering, Report LR-400 (1984).

28. Resetar S.A. et al. , *Advanced airframe structural materials: A primer and cost estimating methodology*, AD-A253371 (N92-3418).

29. Jackson et al. , *Study of utilization of advanced composites in fuselage structures of large transports*, NASA CR-172404 (N87-28619).

30. Austin F. et al. , *Active rib experiment for adaptive conformal wing*, The third international conference on adaptive structures. Nov. 9-11, 1992, San Diego, California, Proceedings (A94-20579 04-63).

31. Harris C.D. , *NASA supercritical airfoils: A matrix of family-related airfoils*, NASA TP-296 (N90-16710).

32. Conner D.W. et al. , *Technology requirements and readiness for very large aircraft*, NASA TM-81783 (N80-20223).

33. Merkl C.S. & Marsden D.J. , *Winglet forward thrust quantified and the mechanism of induced drag reduction*, CASI 5th aerodynamics symposium, Montreal, Canada, May 9,10, 1995 (A95-43126 12-02).

34. Thomas A.S.W. , *Aircraft drag reduction technology- A summary*, AGARD Report No. 273, Paper 1.

35. Barber M.R. & Selegan D. , *KC-135 winglet program overview*, NASA CP-2211 (N84-27687).

36. Flechner S.G. , *Effect of winglets on a first generation jet transport wing*, NASA TP-1330 (N80-10101).

37. Douglas Aircraft Co. , *DC-10 winglet flight evaluation*, NASA CR-3704 (N85-29949).

38. Taylor A.B. , *Development of selected advanced aerodynamics and active control concepts for commercial transport aircraft*, NASA CR-3781 (N87-17659).

39. Boeing Airplane Company, *Selected advanced aerodynamics and active controls technology concepts development on a derivative B-747*, NASA CR-3295 (N83-26831).

40. Sweetman B. & Gregory W.H. , *Boeing 777:Breaking the habits of a lifetime*, Interavia Aerospace Review 12, 1990.

41. Körner H. , *Tendencies in the development of subsonic transport aircraft with special consideration of aerodynamics*, European Space Agency ESA-TT-705 1981 (N82-18214).

42. Poisson-Quinton Ph. , *Parasitic and interference drag prediction and reduction*, AGARD-R-723, Paper 6.

43. Spillman J.J. , *The use of wingtip sails to reduce vortex drag*, Aeronautical Journal, Paper No. 618, p. 387, 1978.

44. Schmitt D. , *Advanced technology - constant challenge and evolutionary process*, Aeronautical Journal, December 1990, pp. 335-340.

45. Patterson J.C. , *Wingtip vortex propeller*, Patent application, NASA-Case-LAR-13019-1 (N84-20495).

46. Mineck R.E. , *Assessment of potential aerodynamic benefits from spanwise blowing at the wing tip*, NASA TM-107847 (N92-25261).

47. Viken J.K. et al. , *Design of the low-speed NLF(1)-0414F and the high-speed HSNLF(1)-0213 airfoils with high-lift systems*, Research in natural laminar flow and laminar flow-control part 3, NASA CP-2487, pp. 637-672.

48. Khalid M. & Jones D.J. , *A summary of transonic natural laminar flow airfoil development at NAE*, National Aeronautical Establishment, Canada, AD-A221702, (N91-11679).

49. Boeing Airplane Co. , *Selected advanced aerodynamic and active control concepts development*, NASA CR-3220 (N82-15033).

50. Reneaux J. & Blanchard A. , *The design and testing of an airfoil with hybrid laminar flow control*, ONERA TP no. 1992-22 (A92-48585).

51. Runyan L.J. et al. , *757 NLF glove flight test results*, Research in natural laminar flow and laminar flow-control part 3, NASA CP-2487, pp. 795-818.

52. Meyer R.R. et al. , *F-14 VSTFE and results of the cleanup flight test program*, Research in natural laminar flow and laminar flow-control part 3, NASA CP-2487, pp. 819-844.

53. Viken J.K. , *Boundary-layer stability and airfoil design*, Laminar flow aircraft certification, NASA CP-2413, pp. 1-30 (N88-23738).

54. Pfenninger W. ,*Long-range LFC transport*, Research in natural laminar flow and laminar flow-control part 1, NASA CP-2487, pp. 89-116.

55. Faust G.K. & Munger P. , *Nacelle design*, Research in natural laminar flow and laminar flow-control part 3, NASA CP-2487, pp. 891-907.

56. Radespiel R. et al. , *Feasibility study on the design of a laminar flow nacelle*, Journal of Aircraft, vol. 27, No. 11, November 1990.

57. Lamb M. et al. , *Natural laminar flow nacelle for transport aircraft*, Langley symposium on aerodynamics, Hampton, Virginia, April 23-25, 1985, vol. 1, pp. 445-460, NASA CP-2397.

58. Obara C.J. & Dodbele S.S. , *Nacelle aerodynamic performance*, Research in natural laminar flow and laminar flow-control part 3, NASA CP-2487, pp. 908-913.

59. Mullender A.J. et al., *The application of natural laminar flow to aero-engine nacelles*, ISABE-International symposium on air breathing engines, 12th, Melbourne, Australia, Sep. 10-15 ,1995 Proceedings vol.2 (A95-44654 12-07), ISABE 95-711.

60. Brooks C.W. & Harris C.D. , *Results of LFC experiment on slotted swept supercritical airfoil in Langley's 8-foot transonic pressure tunnel*, Research in natural laminar flow and laminar flow-control part 2, NASA CP-2487, pp. 453-470.

61. Fisher D.F. & Fischer M.C. , *Development flight tests of jetstar LFC leading-edge flight test experiment*, Research in natural laminar flow and laminar flow-control part 1, NASA CP-2487, pp. 117-140.

62. Maddalon D.V. et al. , *Simulated airline service experience with laminar-flow control leading-edge systems*, Research in natural laminar flow and laminar flow-control part 1, NASA CP-2487, pp. 195-218.

63. Attar A.M. , *Problems of laminar flow control and the use of suction air in determining aircraft performance*, Analysis and Evaluation of an Integrated Laminar Flow Control Propulsion System, NASA CR-192162 (N93-20268).

64. Thibert J.J. et al. , *The A320 laminar fin programme*, ONERA TP no 1992-23 (A92-48586).

65. Collier F.S. , *Recent progress in the development of laminar flow aircraft*, ICAS 19th Congress, Anheim, California, Sep. 18-23, 1994, Proceedings vol. 1, 1994, pp. 2436-2455B.

66. Green S.J. , *Industry Perspective (of laminar flow aircraft)*, Laminar flow aircraft certification, NASA CP-2413, pp. 267-268 (N88-23748).

67. Lynch F.T. & Klinge M.D. , *Some practical aspects of viscous drag reduction concepts*, SAE Paper 912129 (A92-39976).

68. Walsh M.J. , Riblets for aircraft skin-friction reduction, Langley symposium on aerodynamics, Hampton, Virginia, April 23-25, 1985, vol.1, pp. 557-572, NASA CP-2397.

69. Viswanath P.R. & Mukund R. , *Turbulent drag reduction using riblets on a supercritical airfoil at transonic speeds*, AIAA Journal, vol. 33, no.5, May 1995.

70. Stockman N.O. et al. , *Scale model test of an isolated turbofan nacelle with riblets*, SAE Paper 912128.

71. Hefner J.N. , *An overview of the Langley drag reduction program*, Langley symposium on aerodynamics, Hampton, Virginia, April 23-25, 1985, vol. 1, pp. 393-400, NASA CP-2397.

72. Anders J.B. , *Airfoil large eddy breakup devices for turbulent drag reduction*, Langley symposium on aerodynamics, Hampton, Virginia, April 23-25, 1985, vol. 1, pp. 573-586, NASA CP-2397.

73. Austin F. & Van Nostrand W. , *Shape control of an adaptive wing for transonic drag reduction*, Industrial and commercial applications of smart structures technologies: Proceeding of conference, San Diego, California, March 2, 3, 1995 (A95-38480).

74. Rao A.J. , *Variable camber wings for transport aircraft*, PhD Thesis, Department of Aerodynamics, Cranfield Institute of Technology, 1989.

75. Spillman J.J. , *The use of variable camber to reduce drag, weight and costs of transport aircraft*, Aeronautical Journal, vol. 96, Jan. 1992 pp. 1-9.

76. Fielding J.P. et al. , *The aerodynamic and structural design of a variable camber wing*, ICAS 18th Congress, Beijing, China, 1992, pp. 1098a-1098k.

77. Hilbig R. & Koerner H. , *Aerodynamic design trends for commercial aircraft*, NASA TM-77976 (N86-17338).

78. MBB, *MBB studies variable camber wing for Airbus*, JPRS WST-85-024, N86-15447.

79. Rising J.J. et al. , *Demonstration of relaxed static stability on a commercial transport*, AGARD CP-384, Paper 14.

80. Murray W.E. et al. , *Evaluation of all-electric secondary power for transport aircraft*, NASA CR-189977 (N95-27999).

81. DAR Corporation, World wide web:- http://www.darcorp.com

82. Roskam J. , Airplane design, Roskam Aviation and Engineering Corp., Ottawa. KS. USA, 1985.

83. Mason W.H. & Arledge T.K. , *ACSYNT aerodynamic estimation - an examination an validtation for the use in conceptual design*, AIAA Paper 93-0973.

84. Haberland C. et al. , *A computer augmented procedure for commercial aircraft preliminary design and optimization*, ICAS 14th Congress, Toulouse, France, Sept. 9-14, 1984, Proceedings vol. 2, pp. 943-953.

85. Arbuckle P.D. & Silwa S.M. , *Experiences performing conceptual design optimisation of transport aircraft*, Recent experiences in multidisciplinary analysis and optimization; Proceedings of a symposium held at NASA Langley Research Centre, Hampton, Virginia, April 24-26, 1984, pp. 87-102.

86. Sieron T.R. et al. , *Procedures and design data for the formulation of aircraft configurations*, AD-A270150 (WL-TR-93-3068) (N94-18779).

87. Vaziry-Z M.A.F. & Fielding J.P. , *Computer aided conceptual aircraft design (CACAD) for transport aircraft*, College of Aeronautics, Cranfield University, COA Report No. 9608, April 1996.

88. Ruijgrok G.J.J. *Lecture notes on the principles and practice of airplane performance*, Tech. Hogeschool, Delft, VTH-LR-385 vol. 1 (N84-19345).

89. Mattingly J.D. et al. , *Aircraft engine design*, AIAA Education Series, AIAA, Washington DC, USA, 1987.

90. Raymer D.P. , *Aircraft design: A conceptual approach*, Second Edition, AIAA Education Series, AIAA, Washington DC, USA, 1992.

91. Roskam J. & Lan C.E. , *Airplane aerodynamics and performance*, Roskam Aviation and Engineering Corp., Ottawa, Kansas, USA.

92. ESDU, *Geometrical properties of cranked and straight tapered wing planforms*, Item No. 76003, ESDU International, London, Jan. 1976.

93. Torenbeek E. , *Synthesis of subsonic airplane design*, Delft University Press, Holland, 1982.

94. Scott C.A. , *Cartesian plan geometry part 1-analytical cones*, Dent's Mathematical & Scientific text books for Schools, 1907.

95. JAR-25, *Joint airworthiness requirements - large aeroplanes*, Airworthiness Authority Steering Committee, Civil Aviation Authority, Cheltenham, England.

96. Torenbeek E. , *Development and application of a comprehensive, design-sensitive weight prediction method for wing structures of transport aircraft*, Technische Univ., Delft, Netherlands, LR-693 (N94-13687).

97. Lockheed-Georgia Company, *Evaluation of laminar flow control system concepts for subsonic commercial transport aircraft*, NASA CR-159254 (N80-31384).

98. Morris J. , *LFC- a maturing concept*, Research in natural laminar flow and laminar flow-control part 1, NASA CP-2487, pp. 45-52.

99. Yates J.E. & Donaldson C. du P. , *A fundamental study of drag and an assessment of conventional drag-due-to-lift reduction devices*, NASA CR-4004, 1986.

100. Shollenberger C.A. et al. , *Results of winglet development studies for DC-10 derivatives; Final report*, NASA CR-3677 (N85-10936).

101. Gikey R.D. , *Design and wind tunnel tests of winglets in a DC-10 wing; Final report*, NASA CR-3119 (N81-27046).

102. Douglas Aircraft Company, *DC-10 winglet flight evaluation; Final report*, NASA CR-3704 (N85-29949).

103. Lux D.P. , *In-flight lift and drag measurements on a first generation jet transport equipped with winglets*, KC-135 Winglet Program Review, Proceedings of a symposium held at Dryden Flight Research Center, Edwards, California, Sep. 16, 1981, NASA CP-2211 pp. 103-116.

104. Dodson R.O. , *Comparison of flight measured, predicted, and wind tunnel measured winglet characteristics on a KC-135 aircraft*, KC-135 Winglet Program Review, Proceedings of a symposium held at Dryden Flight Research Center, Edwards, California, Sep. 16, 1981, NASA CP-2211 pp. 145-170.

105. Shoup T.E & Mistree F. , *Optimisation methods with applications for personal computers*, Prentice-Hall Inc. Englewood Cliffs, New Jersey 07632.

106. *Janes 'All the Worlds Aircraft'*.

107. *Flight International 'Aircraft of the World' Directory*, Flight International 3-9 Sept. 1997

USER GUIDE

A .1 General.....381

A .2 Setup 382

A .3 Document Manipulation.....383

A .3 .1 Multiple File Sessions.....383

A .3 .2 Document Selection.....384

A .3 .3 Document Comparison.....384

A .3 .3 .1 Text Comparisons.....384

A .3 .3 .2 Graphical Comparisons 384

A .4 Code Execution 386

A .5 Common Features Of All Windows 388

A .5 .1 General.....388

A .5 .2 Units 388

A .5 .2 .1 Parameter Units 388

A .5 .2 .2 Available Units.....389

A .5 .3 Graph Facilities 389

A .6 Library Files 391

A .6 .1 .1 Airfoil Data File Format 392

A .6 .1 .2 Engine Data File Format.....393

A .7 Parameter Input Windows.....394

A .7 .1 Main Design Parameter Window 394

A .7 .1 .1 Parameter Selection.....394

A .7 .1 .2 Setting Parameter Value 395

A .7 .1 .3 Copy, Cut, and Paste Functions.....395

A .7 .1 .4 Launching Peripheral Windows.....396

A .7 .2 Component Selection Editor.....396

A .7 .2 .1 Technology Selection 397

A .7 .2 .2 Airfoil Setup 398
A .7 .2 .3 Engine Setup 398
A .7 .2 .4 Wing Tip Device Setup 399
A .7 .2 .5 Advanced Material Setup 400
A .7 .2 .6 Drag Reduction Technology Setup 402

A .7 .3 Fuselage Sizing Window 404
A .7 .3 .1 Estimating Fuselage Dimensions 405
A .7 .3 .2 Inputting Fuselage Dimensions 407

A .7 .4 Performance Profile Editor 409
A .7 .4 .1 Constructing The Flight Profile 410
A .7 .4 .2 Flight Segment Parameters 410

A .8 Parameter Output Windows 414

A .8 .1 Airfoil Data Window 414

A .8 .2 Engine Data Window 415
A .8 .2 .1 Thrust Graph 416
A .8 .2 .2 Fuel Consumption Graph 417

A .8 .3 Wing Lift Distribution Window 418

A .8 .4 Drag Data Window 419
A .8 .4 .1 Parasite Drag Graph 420
A .8 .4 .2 Total Drag Graph 421

A .8 .5 Data Evaluation Window 421

A .8 .6 Stability Data Window 424
A .8 .6 .1 The Trim Plot 425
A .8 .6 .2 Static Margin Graph 426

A .8 .7 3-View Drawing Window 426

A .8 .8 Performance Data Window 428

A .8 .9 Performance Graph Window 431

A .8 .10 Performance Summary Window 433

A .9 Data Manipulation 436

A .9 .1 Mathematical Expression Evaluations 436

A .9 .2 Correlation Window 437
A .9 .2 .1 Setting and Evaluating Expressions 438
A .9 .2 .2 Plotting Expressions 439
A .9 .2 .3 Curve Fitting 440
A .9 .2 .4 Comparing Correlation Data 442
A .9 .3 Optimisation Window 442
A .9 .3 .1 Optimisation Setup 444
A .9 .3 .2 Setting The Merit Function 445
A .9 .3 .3 Setting Independent Variables 445
A .9 .3 .4 Setting Constraints 445
A .9 .3 .5 Optimisation Method 447
A .9 .3 .6 Optimisation Controls 447
A .9 .3 .7 Optimisation Progress Diagram 448
A .9 .3 .8 Analysis of Optimisation Results 448
A .9 .4 Sensitivity Studies Window 449
A .9 .4 .1 Sensitivity Study Setup 450
A .9 .4 .2 Setting Variables 451
A .9 .4 .3 Executing Sensitivity Study 451
A .9 .4 .4 Viewing Sensitivity Data 451
A .9 .5 Trade-Off Studies Window 451
A .9 .5 .1 Trade-Off Setup 452
A .9 .5 .2 Setting Independent Variables 453
A .9 .5 .3 Executing Trade-Off Study 453
A .9 .5 .4 Analysis of Trade Off Results 454
A .10 Reference Data 457
A .10 .1 Design Parameter Names & Description 457

A .1 GENERAL

The layout of Aircraft Design will be familiar to all Windows users, the windows can be moved, sized, minimised, and maximised in the usual manner. The menu commands should also be easily navigated, as they follow a similar pattern to most Windows applications.

While the program is certainly designed for use with a mouse, every function of the program can be accessed by the use of the keyboard, using the arrow keys, the [tab], [enter], and [space] keys appropriately, as well as making use of alphabetic shortcuts.

A .2 SETUP

The user may change certain attributes of the program to suit individual preferences, these changes are then stored in the file '*acdesign.dfl*'. The attributes which may be altered are:-

- Height and width of the application window on screen. This is changed from the '*Setup*' menu on the initial Aircraft Design screen.
- Default units of the parameters in the Main Design Parameter Window.
- Default units of the Performance Output parameters.
- Default document(s).
- Default module execution options.
- Default 3-d model generation options.

A .3 DOCUMENT MANIPULATION

Each aircraft design is saved as a document with the '*.acd*' extension. These aircraft design documents are analogous to Microsoft Word documents ('*.doc*'), or Microsoft Excel documents ('*.xls*'), and can be manipulated in similar ways from within the Aircraft Design program.

Single documents can be opened/saved/closed/created using the standard '*Open*'/'*Save*' (or '*Save As*')/'*Close*'/'*New*' commands from the '*File*' menu on the menu bar of each window. Once a document has been opened its Main Design Parameter Window will appear, it is from this that subsequent windows (child windows) of that design can be opened. Since the program runs a multiple document interface (MDI), it is possible to have more than one document (and its child windows) open at the same time within the same Aircraft Design Window. These windows can be arranged within the main Aircraft Design Window by clicking the '*Tile*' (vertical or horizontal) command from the '*Window*' menu.

A .3 .1 MULTIPLE FILE SESSIONS.

It is possible to open more than one document at a time, and for these documents to be contained within the same Main Design Parameter (MDP) Window. This is called a 'Multiple File Session'. A Multiple File Session can be initiated by clicking the '*New Multiple File Session*' command on the '*File*' menu. A File List Window will appear, and the files to be included in the session can be chosen. A file is added to the session by double clicking on its name in the 'files' list, or by selecting it from this list and pressing the  button. A file is removed from a session by either double clicking on its name in the 'Multiple file session' list or by selecting it from this list and pressing the  button.

The documents contained within a multiple file session can be changed at any time by clicking the '*Edit File List*' command on the '*File*' menu. The File List Window will appear, and files can be added or removed at will.

A multiple file session can be saved at any time by selecting the '*Save Session*' command from the '*File*' menu. The relevant data will be written to a file with the '*.acs*' extension, with trade-off data being written to a '*.act*' file. These files contain comprehensive information about the names of the documents, any correlation, optimisation, sensitivity, and trade-off data contained within the session. The session can then be resumed at a later date by selecting the '*Open Multiple File Session*' command from the '*File*' menu.

A .3 .2 DOCUMENT SELECTION



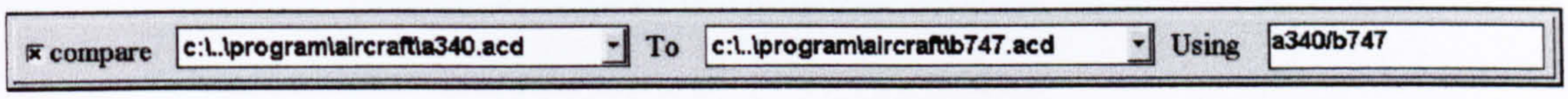
The above figure is typical of the top region of most of the windows in Aircraft Design. This area is used for controlling the selection and comparison of documents in multiple file sessions. In the above case the compare check box is inactive and the document '*a340.acd*' is selected. This means that any operations performed by the window, such as calculations, plotting, printing, or editing, will be performed on the parameters of the '*a340.acd*' document. This will be referred to later as 'single document' mode.

A .3 .3 DOCUMENT COMPARISON

If the 'compare' check box of a window is active, then the parameters of two or more documents from a multiple file session will be compared in that window. This will be referred to later as 'compare' mode. Depending whether the window is graphically based or text based the controls for comparing documents are slightly different:-

A .3 .3 .1 Text Comparisons

If the window is a text based one, then the top region of the window will look similar to the picture below:-



In the case above, the user is comparing the parameter values of a document '*a340.acd*' to a those of a document '*b747.acd*'. The values shown in the window will be the value of the '*a340*' parameter divided by the '*b747*' parameter, expressed as a percentage. Alternatively, by clicking on the box situated at the top right, the mode of comparison can be altered. The other possible modes would be '*a340-b747*' ('*b747*' values subtracted from '*a340*' values), '*b747-a340*' ('*a340*' values subtracted from '*b747*' values), and '*b747/a340*' ('*b747*' values divided by '*a340*' values). When in 'compare' mode, it is not possible to edit the input values of a document.

A .3 .3 .2 Graphical Comparisons

If the window is graphically based, activating the 'compare' mode will cause a change to the options listed in the document selection box. The first available option will be '*All Files*', this will plot the details of all the documents simultaneously. The remaining options will be the document file names preceded by the letters '*TO:*'. Selecting one of these options will

replot the graph(s) using the parameters of the selected file as a baseline for all the y-axis values. This creates a visual tool for estimating the deviation of one document's parameters from the chosen baseline document's parameters.

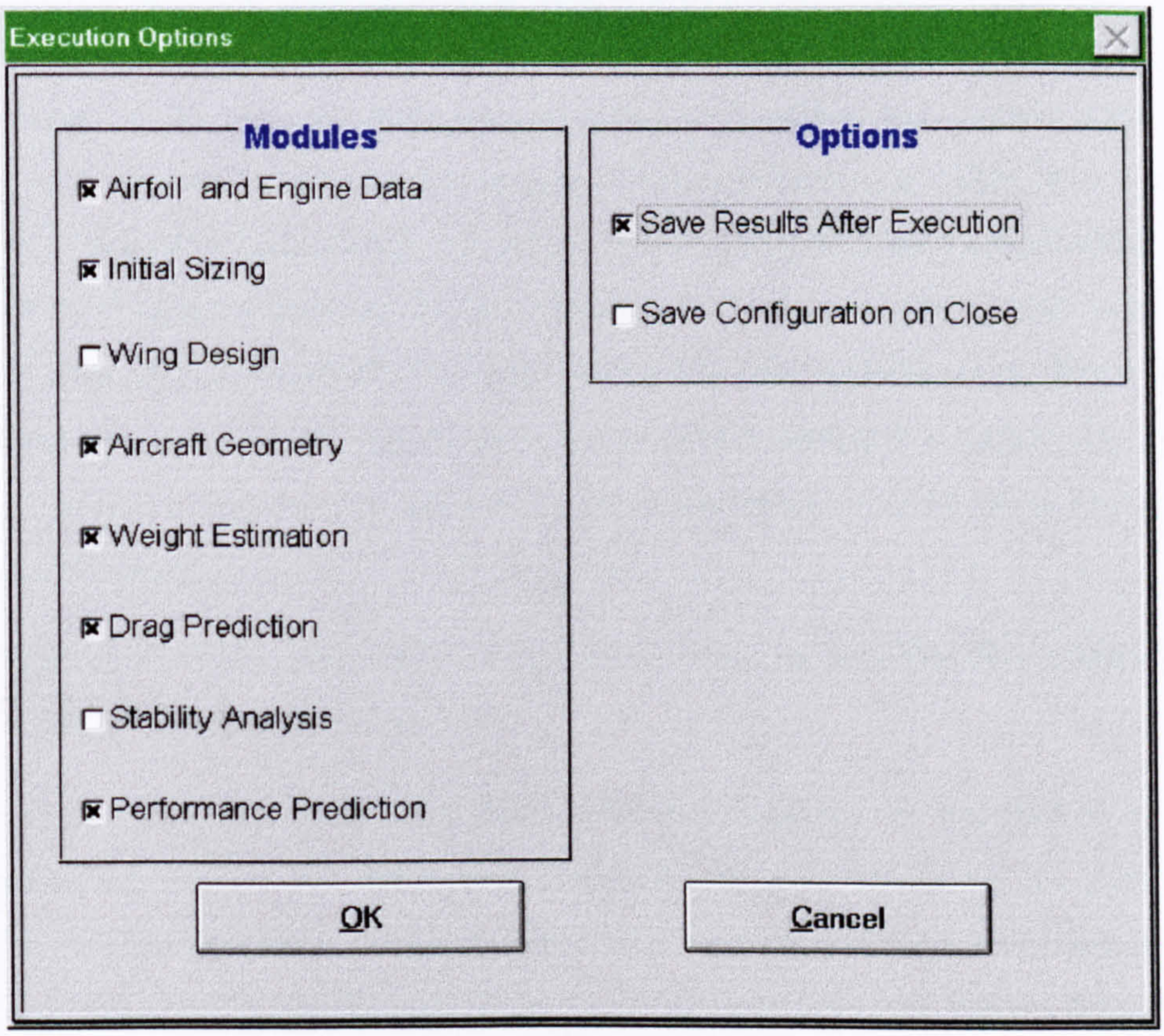
A .4 CODE EXECUTION

The code for the calculation of the design parameters has been spilt into eight separate modules. These modules are responsible for distinct areas of the design process, and are designed to be run successively. The input parameters for these modules have also been split into groups accordingly.

Firstly, before any modules can be executed, the design configuration must be specified using the Component Specification Editor and the parameters in the 'General Configuration' section. In general, a module cannot be executed before the input parameters for that module have been set to within the prescribed limits. It also follows that a module cannot be executed if any parameters for a module preceding it have not been correctly specified as each module relies on input and output data from preceding modules.

For the performance calculations to be successful it is necessary that a pertinent flight profile has been chosen using the Performance Profile Editor.

Once the design variables have been set satisfactorily, an analysis of the design can be performed. This can be done by clicking the '*Execute*' command on the '*Calculations*' menu, ensuring first that the required modules have been selected for execution from the Execution Options Window, as pictured below. This is accessed from the '*Options*' command on the '*Calculations*' menu.



Other options available on the Execution Options Window are those of saving the design automatically after execution, and saving the chosen options as default.

While the code is running, the Calculation Progress box will appear on the screen showing the current status of the code execution. During a performance iteration the box will give the values of the main performance iteration variables (Fuel Weight, Total Range, and Main Cruise Descent Range). It is possible to abort the calculations at any time by selecting '*Abort*' from the '*Execute*' menu on the Calculation Progress box. It is also possible to run the calculations in the background by minimising the Calculation Progress box.

A .5 COMMON FEATURES OF ALL WINDOWS

A .5 .1 GENERAL

All windows within the Aircraft Design environment are designed for ease of use and to have as much commonality as possible. Each window has a '*File*' menu from which documents can be opened, closed or saved, as described previously. A '*Window*' menu is also present on every main design page, it is from this menu that it possible to arrange the windows on the screen, to switch to another window, and where appropriate, to call up a list of variables and their labels. Calculations can be executed, or the calculation options changed from the '*Calculation*' menu included on most windows. It is possible to obtain a printout of the window as it appears on screen, print design details, or depending on the window, print some other aspect of the design by clicking the appropriate option on the '*Print*' menu.

As well as these common menu commands, each window may have commands unique to that window. These are described individually in the detailed explanation of each window.

A .5 .2 UNITS

A .5 .2 .1 Parameter Units

All parameters in the program have been assigned a dimension (e.g. length, time, weight, etc.), and each dimension has a corresponding selection of units (e.g. meter, foot, inch, etc.). Whenever a parameter is displayed, its value is shown along with its corresponding units. It is possible to change its units by double clicking on them or selecting them and pressing [enter]. Double clicking repeatedly will cycle through all the possible units. When the units are changed, the value of the parameter is automatically changed to reflect the change in units. It is worth noting that the units of an input parameter have no effect on the output parameters of a design.

The default units of the parameters in the MDP Window and the Performance Output Windows can be saved, as stated in A.2.

When two or more parameters have been combined together by the user to produce a mathematical expression, the dimensions and units of this expression are automatically calculated. If the dimensions of the function are inconsistent then 'inconsistent' will be displayed as the units. If the dimensions are consistent but are of no known form, then the

units will be displayed in the form $m^a kg^b sec^c$. If however the units are recognised, then these can be changed as described above.

A .5 .2 .2 Available Units

Below is a summary of units recognised by the program.

Dimension	Units
Length	Meter(m), Foot(ft), Kilometre(Km), Nautical Mile(nm), Mile(Mile), Inch(in)
Mass	Kilogram(kg), Pound(lb)
Time	Second(sec), Minute(min), Hour(hr)
Angle	Radians(rad), degrees(deg)
Velocity	Metric(m/s), Knots(knots), English(ft/s)
Area	Metric(m^2), English(ft^2)
Thrust	Metric(N), Metric(KN.), English(LBF)
Fuel Consumption	Metric(Sec^{-1}), English(hr^{-1})
Force	Metric(N), English(LBF)
Density	Metric(kgm^{-3}), English($lbft^{-3}$)
Viscosity	Metric(m^2sec^{-1}),English(ft^2sec^{-1})
Temperature	Kelvin (K)
Pressure	Metric(Pa), Metric(Kpa), English(PSI)
Acceleration	Metric($msec^{-2}$)
Wing Loading	Metric(kgm^{-2}), English($lbft^{-2}$)
Mach Number	Mach Number(Mach)
Volume	Metric(m^3), English(ft^3)

A .5 .3 GRAPH FACILITIES

Graphs can expanded by double clicking on them or by selecting the graph and pressing [enter]. Depending on the graph there will be 1 or 2 levels of expansion. Once the graph is fully expanded, double clicking on it will return it to its normal size.

It is also possible to fine tune the appearance of the graphs by selecting the '*Graph Setup*' command from the '*Options*' menu that appears on a window with one or more graphs. Once this option is selected the Graph Setup Window will appear, giving choices of graph style (lines, lines & symbols, lines & sticks etc..), y-axis style, and axes units. The y-axis can be one of three types:

- Best Fit - Automatically sized for best fit with zero origin
- Variable - Automatically sized for best fit without zero origin
- User Defined - User sets minimum and maximum values

Graphs may also be printed out by clicking the '*Print Graph*' command on the '*Print*' menu. This will initiate the Print Preview Window where the graph can be resized using the '*Size*' command on the '*Graph*' menu. Clicking this will initiate the graph height and width scroll bars. Once satisfied with the size of the graph, it can be printed by clicking 'OK' and selecting '*Print*' from the '*Graph*' menu. The default size of the graph on the Print Preview screen is automatically set to the height and width of the selected paper size on the current printer.

It must be noted that when there is more than one graph in the window, the graph chosen for the Setup or Print Preview Window is the graph which was the most recently selected. A graph is selected by single clicking on it, or using the [tab] key to make it the active object.

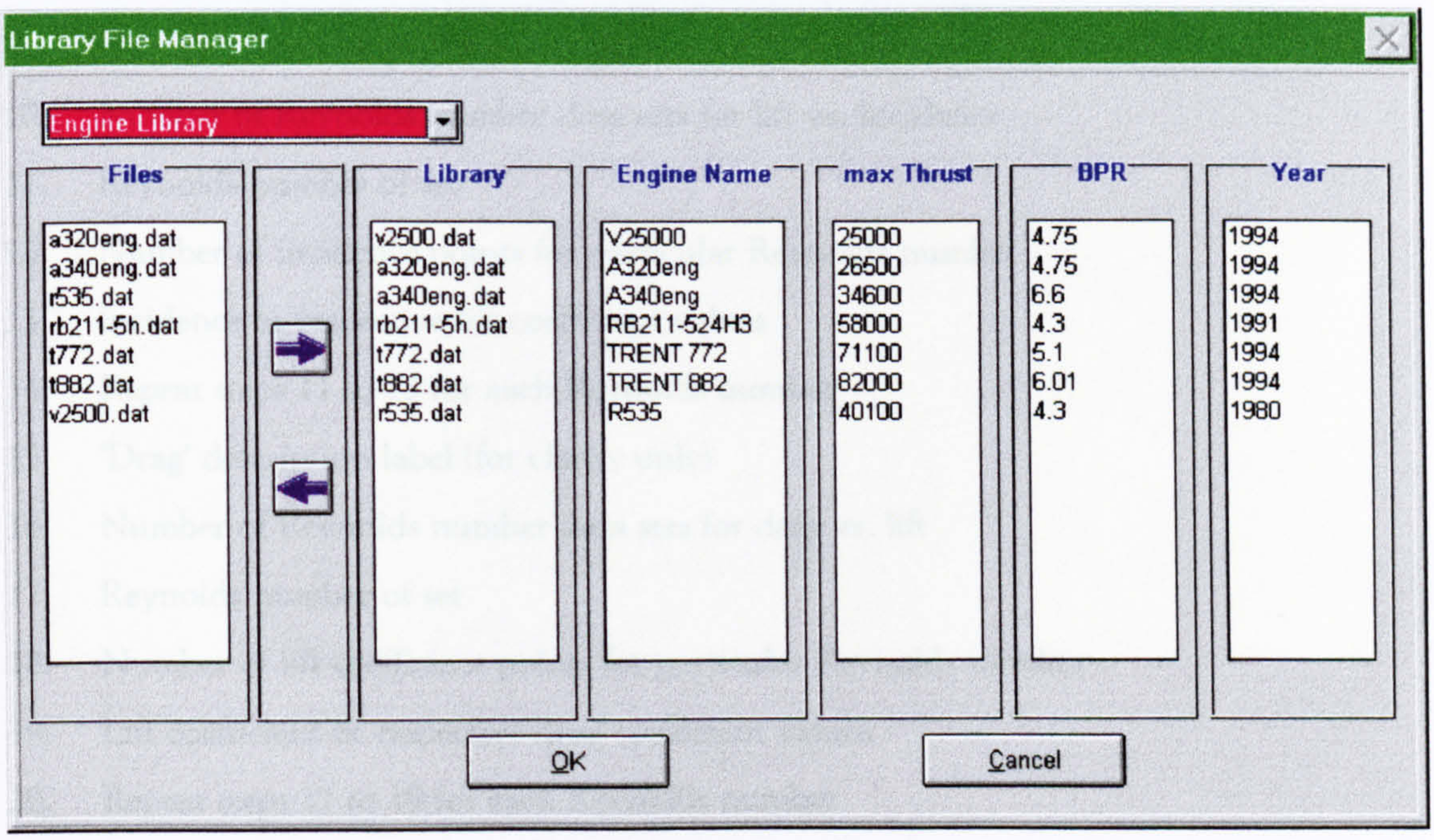
A .6 LIBRARY FILES

Data to describe the properties of airfoils and engines is stored in files with the '**.dat*' extension in the '*/airfoils*' and the '*/engines*' subdirectories.

Each airfoil data file gives details of the lift, drag, and pitching moment, at given Reynolds numbers for a particular airfoil, in accordance with the format laid out in A.6.1.

Each engine data file consists of detailed data to describe the thrust performance of the engine with respect to Mach number and altitude for various modes of flight. Values of specific fuel consumption for various Mach number and thrust settings are also included in each engine data file.

It is possible to edit the list of available data files by launching the Library File Manager from the Main Design Parameter Window. This is done by clicking the '*Library File Manager*' command on the '*Setup*' menu, the window shown below will appear.



The list box in the top left-hand corner of the window is used to select whether the airfoil or the engine file library is to be edited. All the files in the relevant subdirectory are listed in the 'Files' box. The files chosen to be included in the library are listed in the 'Library' box, and the main properties of the airfoils or engines are listed in the subsequent boxes.

A file can be added to the library by double-clicking on its name in the 'Files' list, or by highlighting the file and pressing the ➡ button. A file is removed by double clicking on the file in the 'Library' list, or by highlighting it and pressing the ⬅ button. The listed files are then available for use from the Component Specification Editor.

The format of the files is not crucial, provided that all the required data is present. The files must text based, with commas between values, but with no comma at the end of a line.

A .6 .1 AIRFOIL DATA FILE FORMAT

Any files used to provide airfoil information must contain the following data:-

1. Airfoil name
2. Thickness to chord ratio
3. Maximum lift coefficient
4. Zero incidence lift coefficient
5. Zero lift coefficient incidence
6. Chord location of maximum thickness
7. Ratio of perimeter to chord
8. Leading edge sharpness parameter (Δy)
9. 'Lift' description label (for clarity only)
10. Number of Reynolds number data sets for lift vs. incidence
11. Reynolds number of set
12. Number of incidence points for particular Reynolds number
13. Incidence & respective lift coefficient values
14. Repeat steps 11 to 13 for each Reynolds number
15. 'Drag' description label (for clarity only)
16. Number of Reynolds number data sets for drag vs. lift
17. Reynolds number of set
18. Number of lift coefficient points for particular Reynolds number
19. Lift coefficient & respective drag coefficient values
20. Repeat steps 17 to 19 for each Reynolds number
21. 'Pitching Moment' description label (for clarity only)
22. Number of Reynolds number data sets for pitching moment vs. lift
23. Reynolds number of set
24. Number of lift coefficient points for particular Reynolds number
25. Lift coefficient & respective pitching moment coefficient values
26. Repeat steps 23 to 25 for each Reynolds number

A .6 .2 ENGINE DATA FILE FORMAT

Files used to provide engine data must contain the following information, noting that δ and θ refer to the atmospheric pressure and temperature ratios.

1. Engine name
2. Maximum sea level static thrust
3. Installed sea level static thrust ($T_{nominal}$)
4. Bypass ratio
5. Year of entry into service
6. Dry weight
7. Fan diameter
8. Engine length
9. 'Takeoff' segment label (for clarity only)
10. Number of altitude data sets for segment
11. Number of Mach number points at each altitude
12. Altitude of particular data set
13. Mach number & respective installed thrust ratio ($T/T_{nominal}$) values
14. Steps 12-13 should be repeated for each altitude set
15. Repeat steps 9-14 for 'Climb', 'Cruise', 'Idle' and 'Continuous' segments
16. 'S.F.C' segment label (for clarity only)
17. Theta (value of θ_{sfc}, in equation of step 21)
18. Number of Mach number data sets
19. Number of thrust ratio points of each data set
20. Mach number of particular data set
21. Non-dimensionalised thrust ratio $\left(\frac{T}{T_{nominal} \times \delta}\right)$ and respective non-dimensionalised S.F.C. $\left(\frac{c}{\theta^{\theta_{sfc}}}\right)$ values
22. Steps 20-21 should be repeated for each mach number data set
23. 'Idle Fuel Flow' segment label (for clarity only)
24. Number of altitude data sets for segment
25. Number of Mach number points at each altitude
26. Altitude of particular data set
27. Mach Number and respective idle fuel flow (actual idle fuel flow divided by $T_{nominal}$) values
28. Steps 26-27 should be repeated for each altitude Set

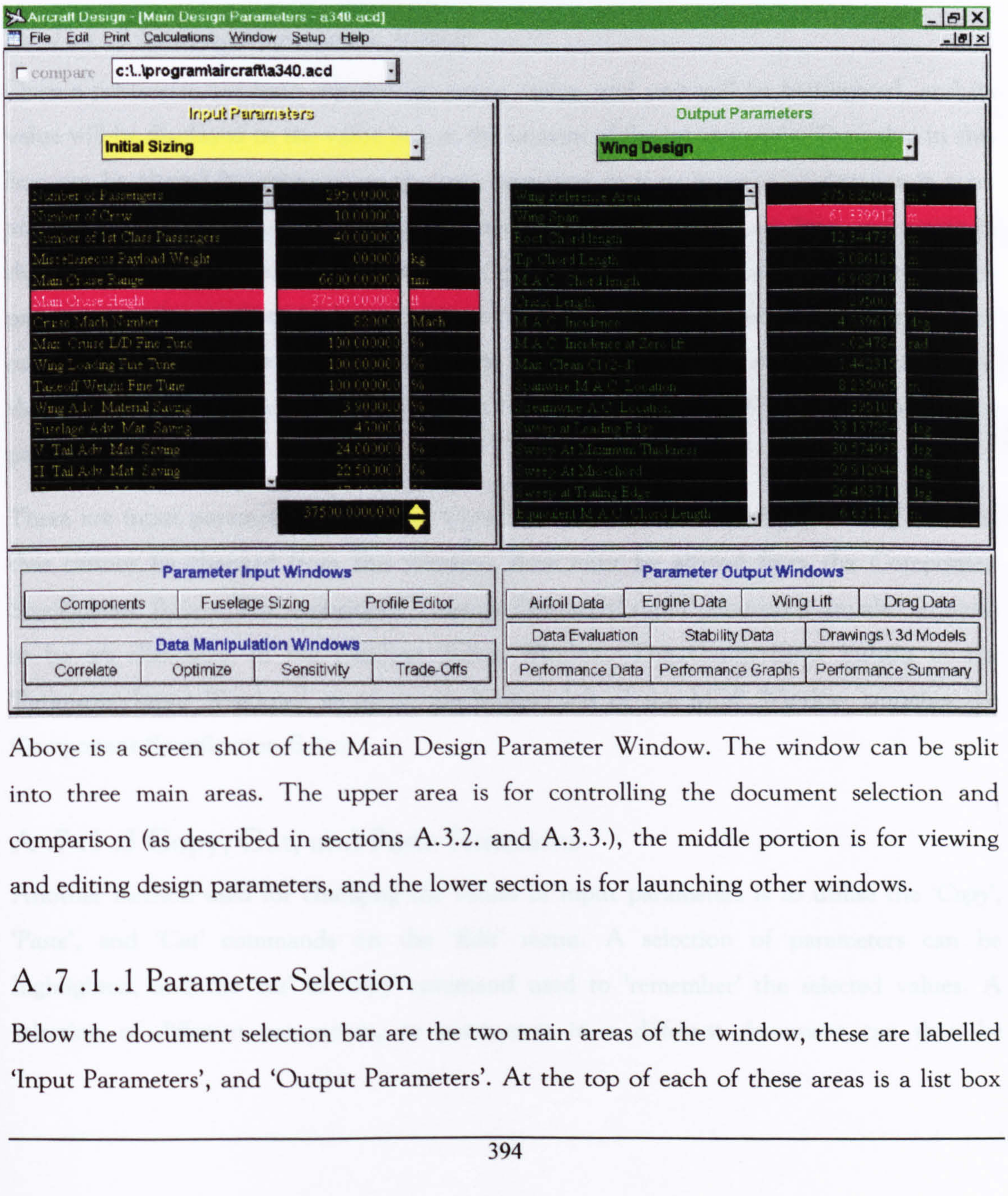
A .7 Parameter Input Windows

A .7 .1 Main Design Parameter Window

Function

This is the window that first appears when you open a document, and is the window from which all others are opened. The main function of this window is to set the values of the majority of the input parameters, and to display the values of many of the output parameters.

Description



Above is a screen shot of the Main Design Parameter Window. The window can be split into three main areas. The upper area is for controlling the document selection and comparison (as described in sections A.3.2. and A.3.3.), the middle portion is for viewing and editing design parameters, and the lower section is for launching other windows.

A .7 .1 .1 Parameter Selection

Below the document selection bar are the two main areas of the window, these are labelled 'Input Parameters', and 'Output Parameters'. At the top of each of these areas is a list box

which controls the type of parameter displayed in each area. The list box allows the user to chose a selection of parameters associated with a particular design area. In the example above, the input parameters are those concerned with the Initial Sizing of the aircraft, and the output parameters are the results from the Wing Design Module. It is important to note that the grouping of the parameters corresponds to their use in the calculation code. That is to say, that an input parameter in the Initial Sizing group will only have an effect on the output of the Initial Sizing Module, and the modules that succeed it. The output parameters are a direct result of the calculation module associated with it.

To change the value of an input parameter one must first select that parameter, either using the mouse or arrow keys. When the value box is the active control, it is possible to use the up and down arrow keys to select parameters without leaving the box.

A .7 .1 .2 Setting Parameter Value

Once a parameter has been selected, its name, value, and unit will be highlighted, and its value will be displayed in the value box at the bottom of the input panel. The value in this box can be altered by either using the spin box next to it to increase or decrease it a set amount (the amount depends on the parameter itself), or by selecting the box, and typing in the desired value. Once set, the user must press the [enter] key to actually change the parameter to the value in the box. Once the [enter] key is pressed the user is prompted for confirmation. If however, the value is outside a sensible range of values for that parameter, the parameter cannot be set. The value that is set, is in the units of the parameter at that particular time.

There are input parameters within the 'General Configuration' and 'Initial Sizing' sections that cannot be changed from this window, they must be altered from the Component Specification Editor. The majority of 'Fuselage Geometry' input parameters are also required to be set elsewhere, in the Fuselage Sizing Window. The Components button in the 'Parameter Input Windows' group at the bottom left of the MDP Window launches the Component Specification Editor.

A .7 .1 .3 Copy, Cut, and Paste Functions

Another method used for changing the values of input parameters is to utilise the '*Copy*', '*Paste*', and '*Cut*' commands on the '*Edit*' menu. A selection of parameters can be highlighted, and the '*cut*' or '*copy*' command used to 'remember' the selected values. A selection of different parameters, or parameters in a different document can then be

highlighted, and the values pasted in. If the number of parameters copied is smaller than the number selected for pasting then the excess parameters will be unchanged.

A .7 .1 .4 Launching Peripheral Windows

The bottom part of the MDP Window is the area from which all other main windows are launched. The window names are grouped accordingly, and clicking on a button will launch that window. Clicking on the button once the window has been launched will bring that window to the front of the screen.

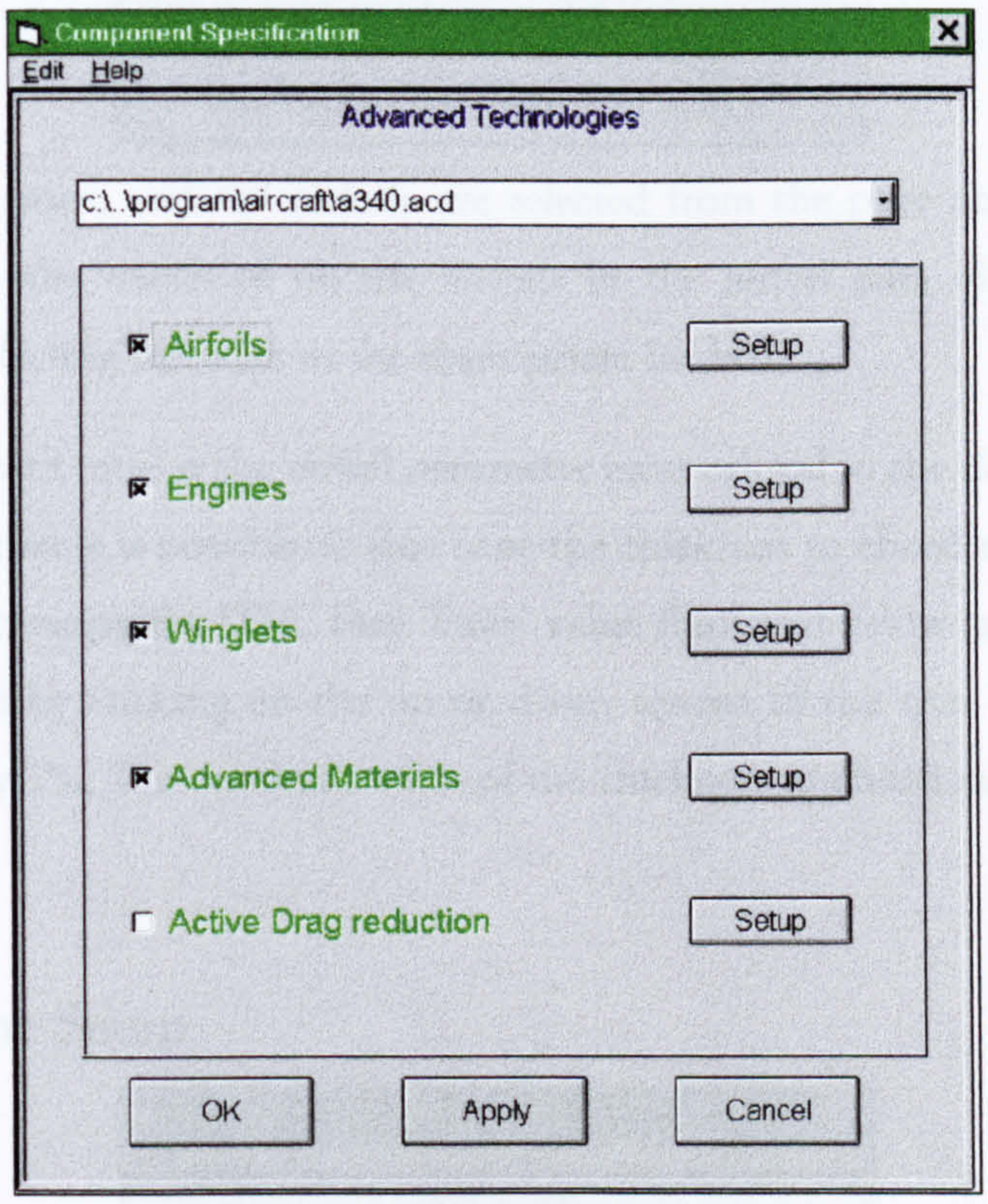
A .7 .2 Component Specification Editor

Function

The type of engines, airfoils, materials, and drag reduction technologies to be incorporated into the aircraft design are selected from the Component Specification Editor. It is from this window that it is also possible to fine tune the properties and efficiencies of each of the technologies.

Description

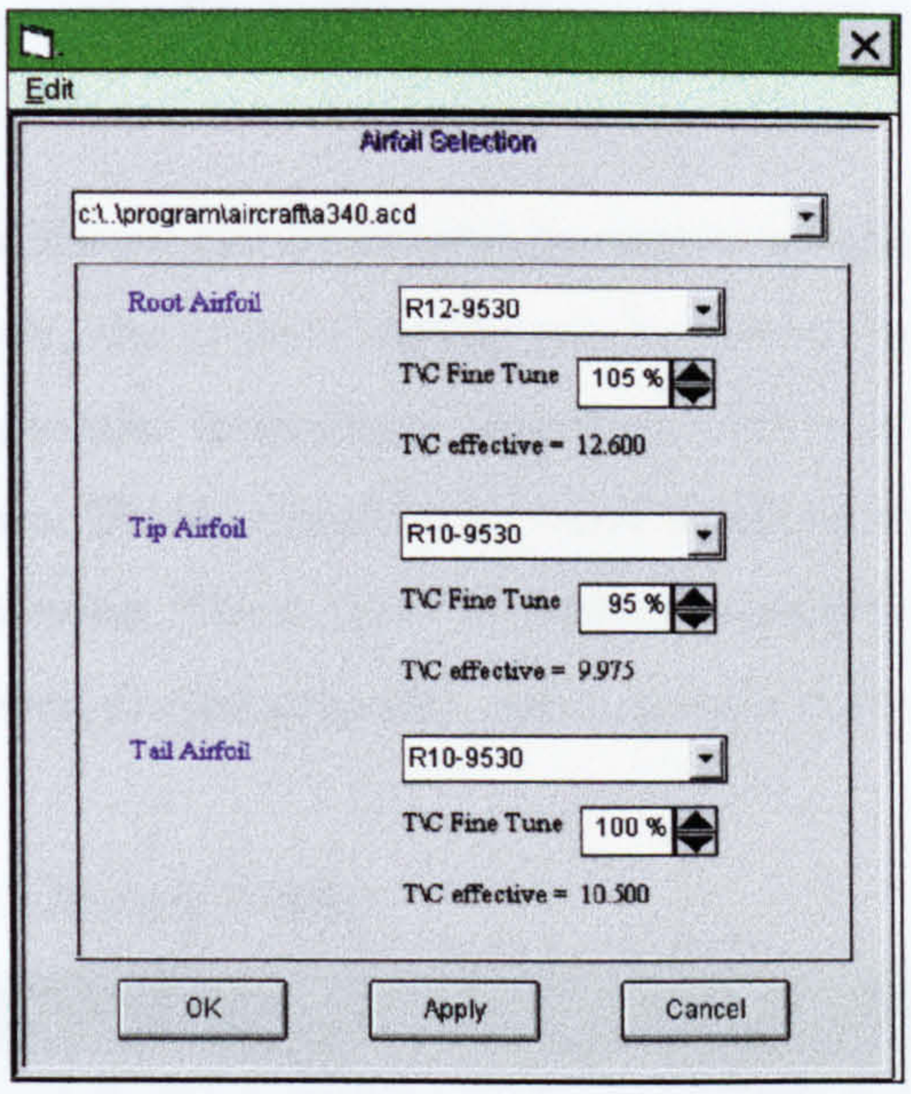
A .7 .2 .1 Technology Selection



The main technology selection screen is shown above. It is from this screen that the user can chose to include winglets, advanced materials, and active drag reduction technologies (airfoils, and turbofan engines must be included in a design). A technology is selected by activating the relevant check box, and once the technology has been chosen it can be configured by clicking on the '*setup*' button.

The document to which the technology is to be applied is selected from the list box at the top. It is possible to copy and paste selections between documents using the commands on the '*Edit*' menu. This is applicable to all pages within the Component Specification Editor.

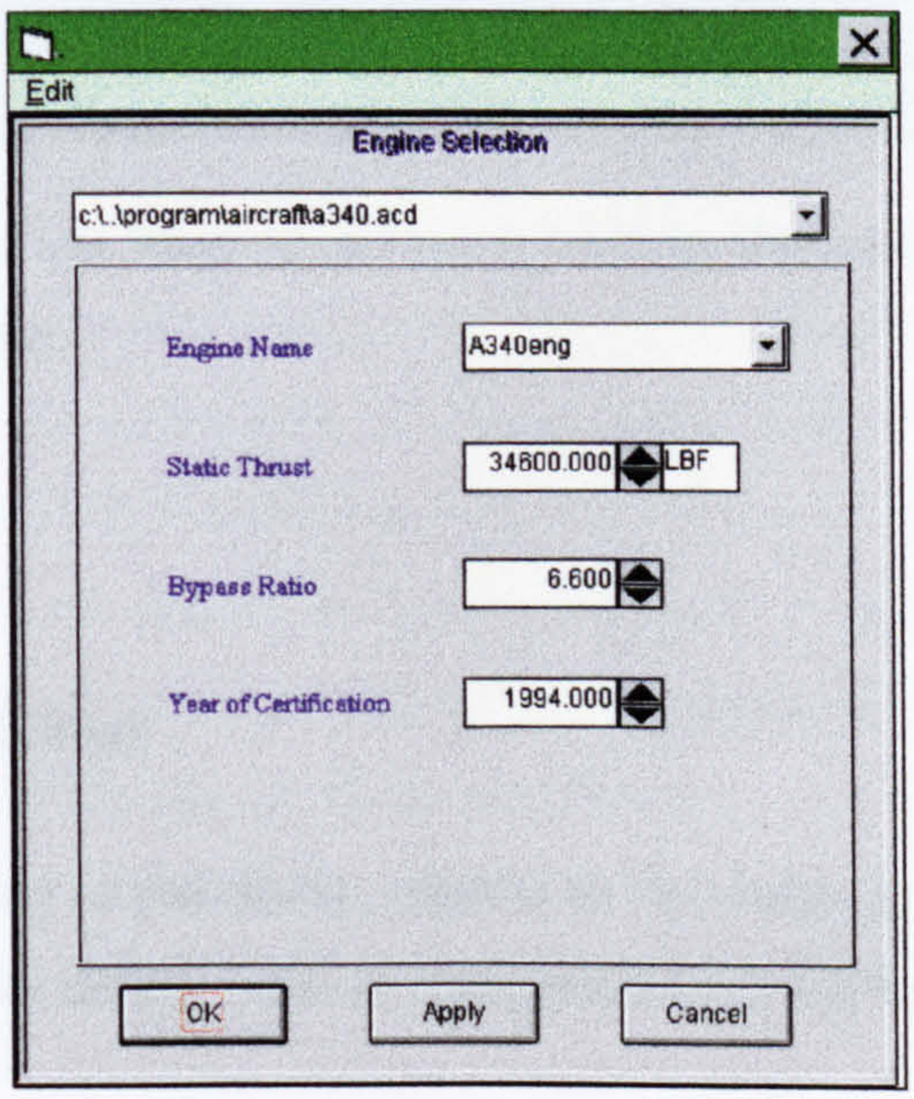
A .7 .2 .2 Airfoil Setup



The wing tip, wing root, and tail airfoils are selected from the page above. The three list boxes each contain the names of all the airfoils in the airfoil data library. An airfoil is chosen by simply selecting its name in the appropriate list box.

The thickness to chord ratio is the airfoil parameter most critical in the design synthesis. It is for the this reason that it is possible to fine tune the thickness to chord ratio of each airfoil, by decreasing or increasing the 'T\C Fine Tune' value displayed below each airfoil selection. The value is altered by clicking on the up or down arrows of the spin box, to increase or decrease its value by 1%. The resultant value of the thickness to chord ratio is printed below the tuning value.

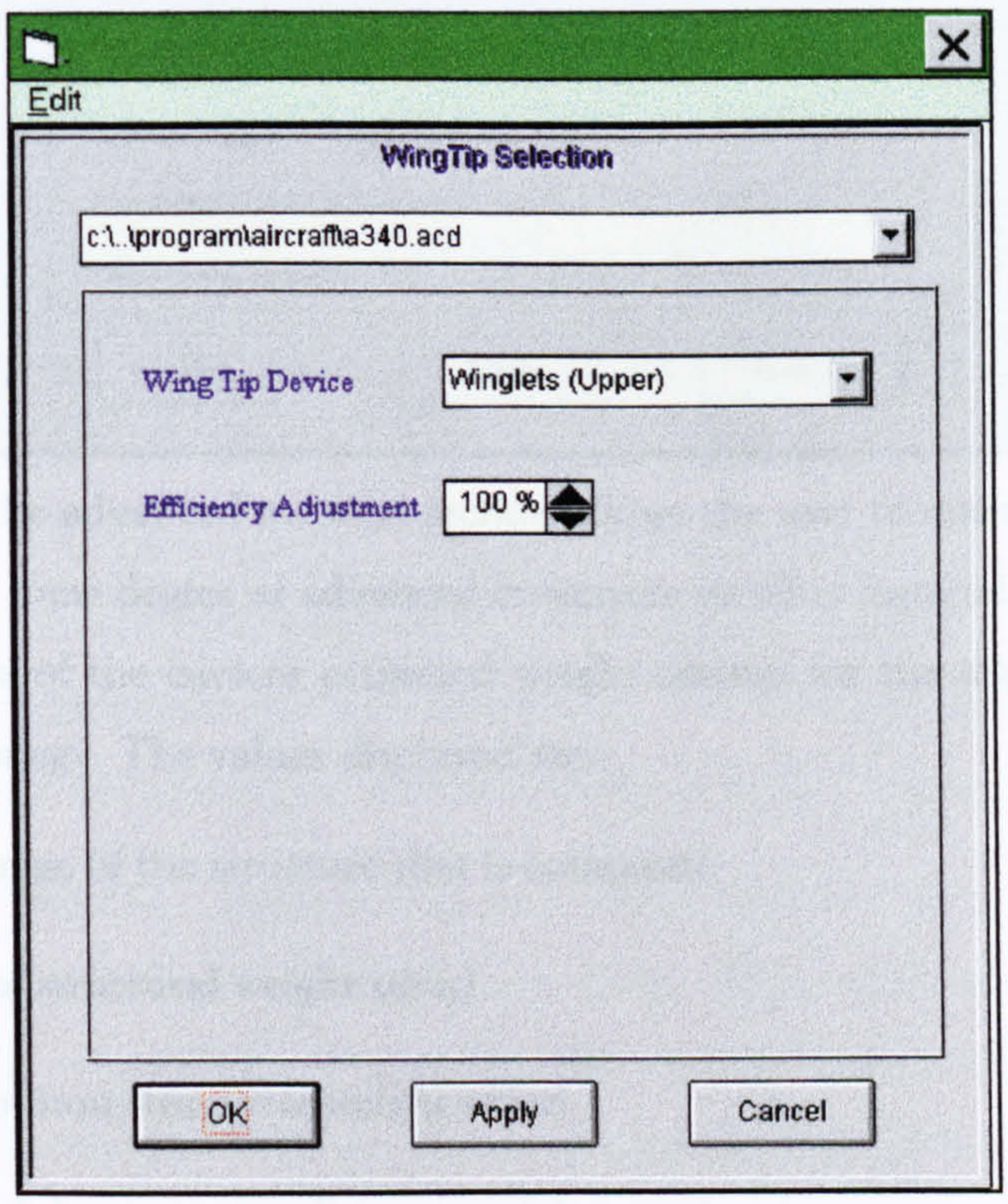
A .7 .2 .3 Engine Setup



The properties of the aircraft powerplant are selected from the page above. The engine can be one chosen directly from the Engine Data Library, or it can be one tailored to suit the design requirements.

An engine from the data library can be chosen by simply selecting its name in the engine name list box. Alternatively, the 'custom' option can be chosen from the list box. Choosing a 'custom' engine allows the user to enter the engine takeoff thrust, the engine bypass ratio, and the year of certification. These values can be input using either the keyboard or the spin boxes at the side of each value. Three types of custom powerplant are available, a custom turbofan, a custom advanced ducted propeller, and a custom contrafan.

A .7 .2 .4 Wing Tip Device Setup

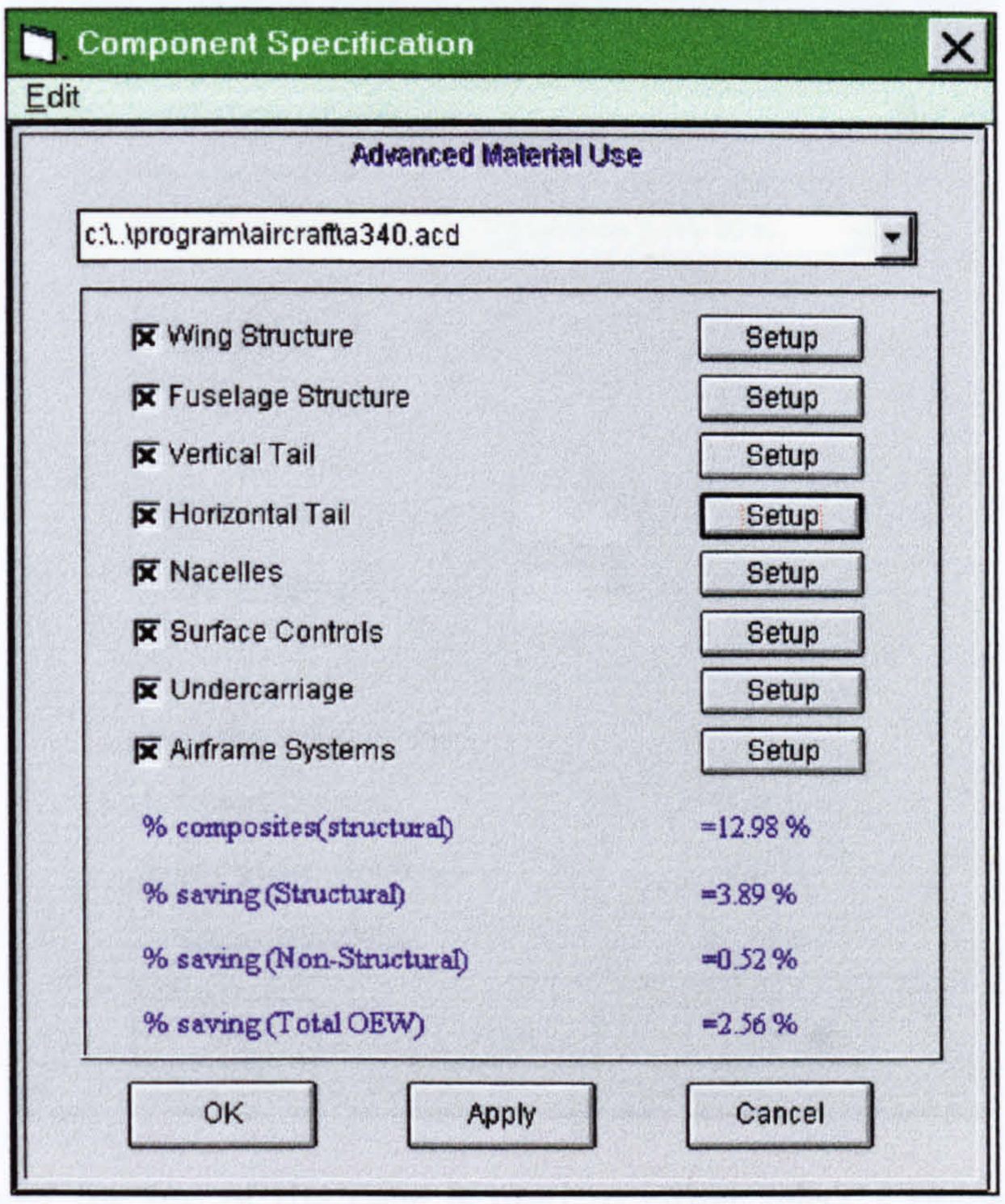


The type and efficiency of any wing tip devices is set from the page above. A choice of three wing tip devices is available:-

- Wing tip fences
- Winglets (Upper)
- Winglets (Upper and Lower)

The aerodynamic efficiency of the device, relative to the design synthesis baseline device, is set using the spin box. The default value of this parameter is 100%.

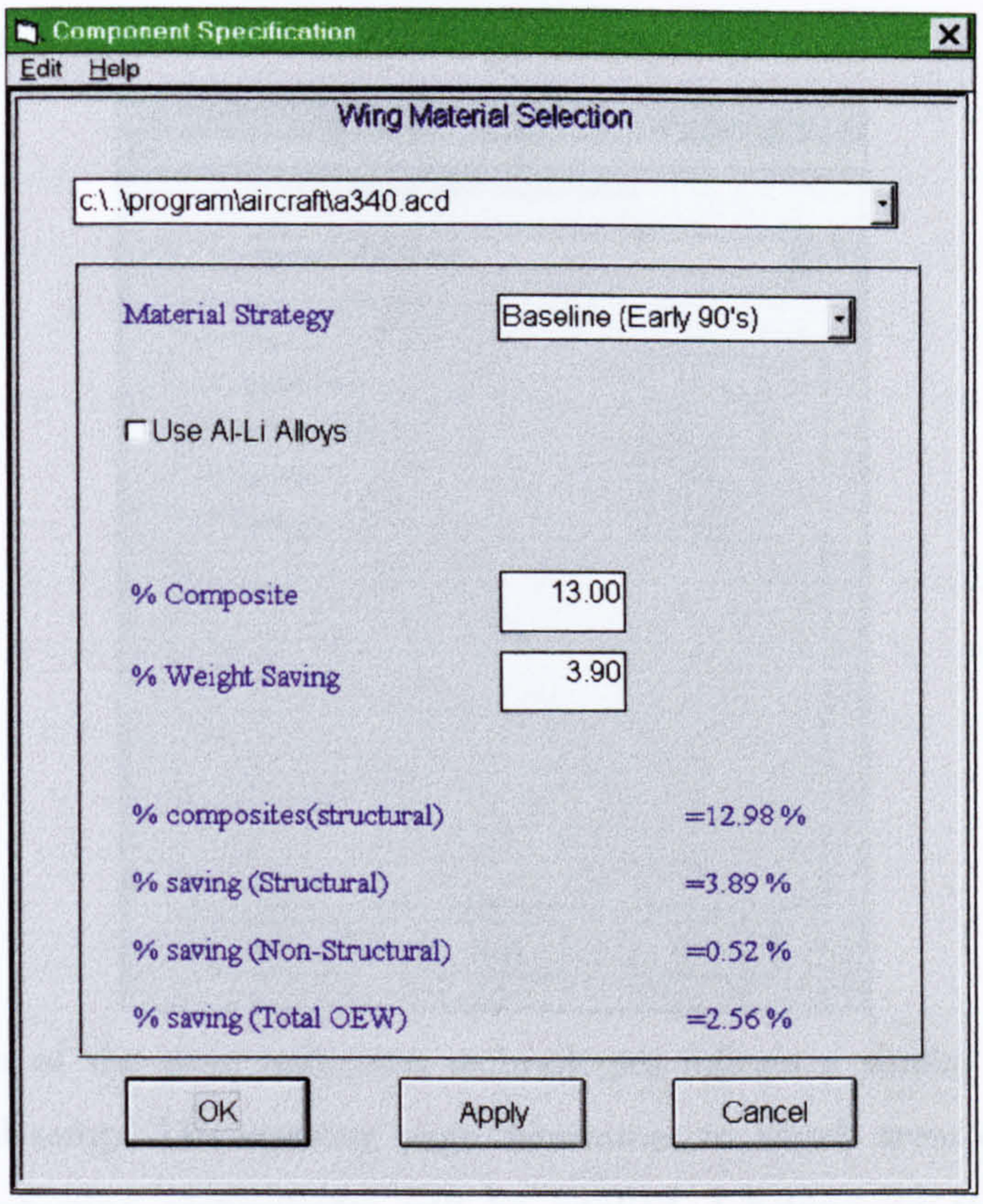
A .7 .2 .5 Advanced Material Setup



The initial page of the advanced material section allows the user to select which areas of the aircraft will contain some degree of advanced composite or alloy material. The bottom of the window gives details of the current projected weight savings for the selected design and its selected material strategy. The values displayed are:-

- The total percentage of the structure that is composite
- The percentage of structural weight saved
- The percentage of non-structural weight saved
- The percentage of the operational empty weight saved

If an area is to include advanced materials the check box adjacent to the name of that area should be checked, and then clicking on the '*Setup*' button (with the exception of 'Airframe Systems') will open the detailed material selection page. When the 'Airframe Systems' area is being considered, clicking on the '*Setup*' button will open a more in-depth area selection page, similar to the main area selection page above. The detailed material selection page for each area will be of a similar format to that shown below.



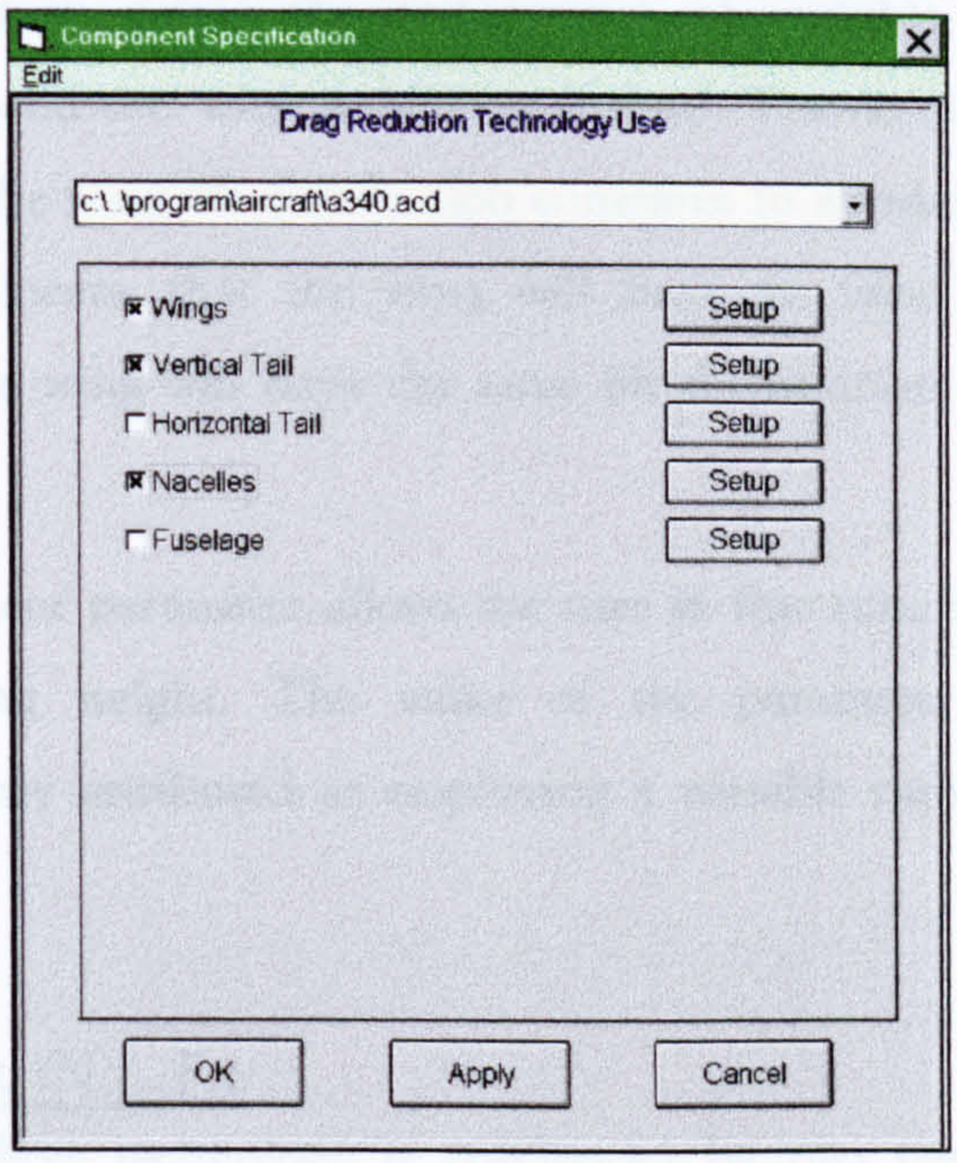
The list box toward the top of the page is used to either select a predetermined material strategy or to select a 'user specified' strategy. A predetermined strategy automatically computes an estimate of the percentage amount of composite material to be included in the chosen area, for that particular strategy description. The 'user specified' strategy allow the user to manually enter the amount of composite material in the '% composite' box.

In some cases, the 'Use Al-Li Alloys' check box will be visible. This is used to incorporate some degree of advanced alloy material into the design. When this option is selected a box appears to the right, containing the value for the estimated percentage by weight of the component which is composed from the advanced alloy. The amount of alloy can be altered from its default value by using the spin box next to it.

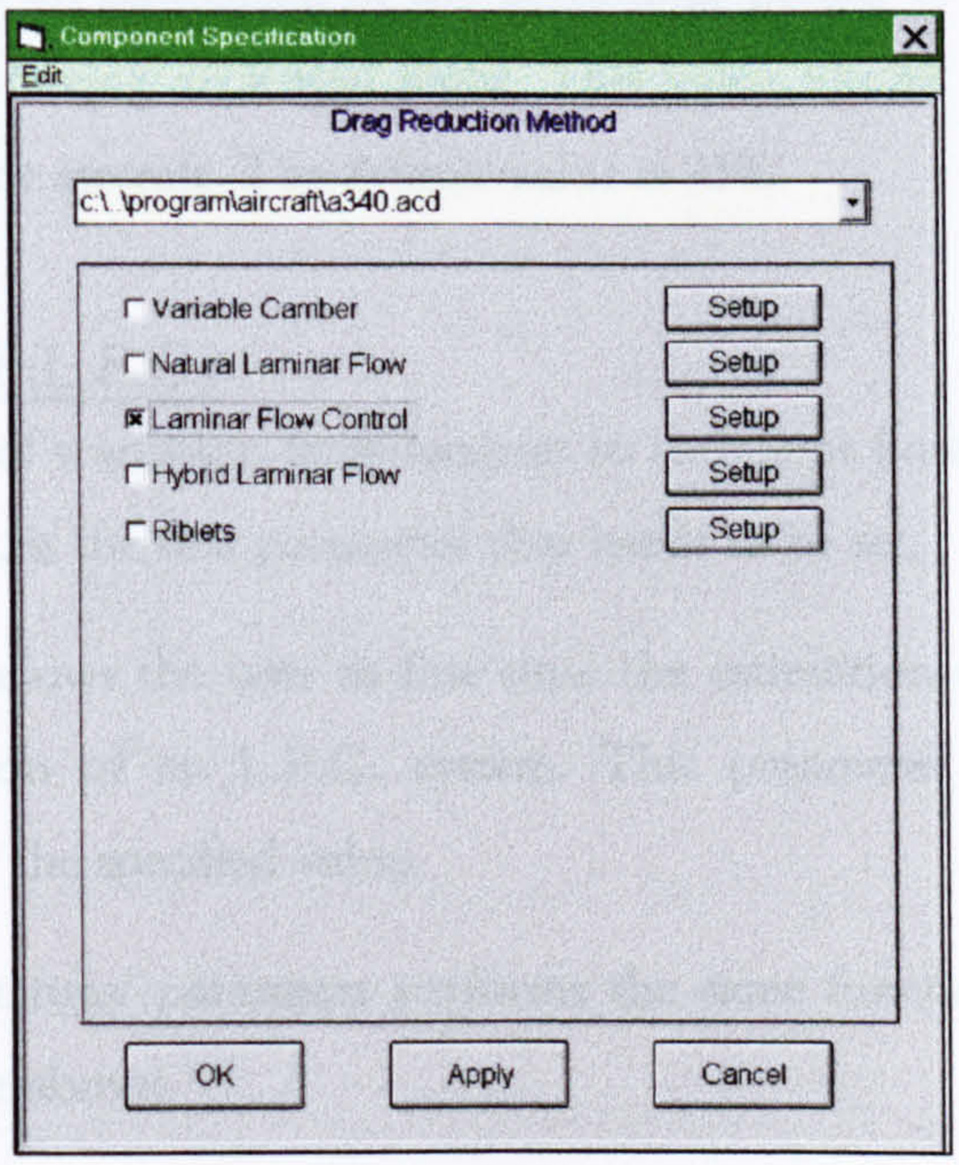
The information toward the bottom of the page, and the value of weight saved for the particular component (printed in '% weight saving' box), are automatically updated when any change is made to the material strategy.

For some areas or components the material selection page will differ from that above, in that the advanced alloy options will not be available, and that the material strategy will be input in terms of weight saved, rather than in terms of the amount of composites used.

A .7 .2 .6 Drag Reduction Technology Setup



The configuration of the drag reduction technologies follows a similar procedure to the advanced material setup. The opening page determines to which areas of the aircraft the advanced drag reduction technologies will be applied. Clicking on the relevant '*Setup*' button progresses the user to a more detailed configuration screen (below).



This page allows the user to select one of the technologies for incorporation into the chosen area. The list of available technologies is dependant on the area of the aircraft that is being considered. Once the technology has been chosen, its detailed configuration page can be opened by clicking the '*Setup*' button. The layout of the detailed configuration will vary, depending on which technology has been selected. The parameters for each technology are outlined below.

Variable Camber Wings

The two parameters which define the performance of variable camber wings are the 'aerodynamic efficiency' and the 'wing weight increment'. The aerodynamic efficiency is the measure of how closely the wing lift distribution compares to an ideal elliptical one. A 100% aerodynamic efficiency means that the wing will have an ideal lift distribution, a 0% efficiency means that the wing will have the same lift distribution as the equivalent swept tapered wing.

The wing weight increment parameter allows the user to fine tune the effect of the variable camber system on wing weight. The value of the parameter is simply the weight increase/reduction directly attributed to employing a variable camber system. The default value is -10 %.

Natural Laminar Flow (N.L.F.)

The natural laminar flow technology is configured by two parameters. The first is a 'Reynolds number correction' parameter, this is used as a multiplier for the Reynolds number in the N.L.F. equations. This allows the user to decrease or increase the effective Reynolds number, making laminar flow more or less likely.

The second parameter is an estimation of the percentage period of time for which laminar flow can be maintained during an actual flight. This value has an important effect on the overall performance of the aircraft. The default value is 93%.

Laminar Flow Control (L.F.C.)

The chordwise location of transition from laminar to turbulent flow along the wing surface, during cruise conditions, is the first parameter that needs to be set.

The second parameter allows the user to fine tune the estimation of the weight increment due to the incorporation of an L.F.C. system. This parameter multiplies the weight increment estimation by the specified value.

The 'laminar flow flight time' parameter performs the same function as that described for natural laminar flow (see above).

The final configuration parameter determines whether the L.F.C. system is employed on both upper and lower surfaces, or on the upper surface only.

Hybrid laminar Flow Control (H.L.F.C.)

The configuration parameters for the hybrid laminar flow control system are exactly the same as for the laminar flow control system described above.

Riblets

The only configuration parameter that describes the performance of riblets estimates the percentage reduction in cruise drag of the component due to the application of riblets. The default value is 7%.

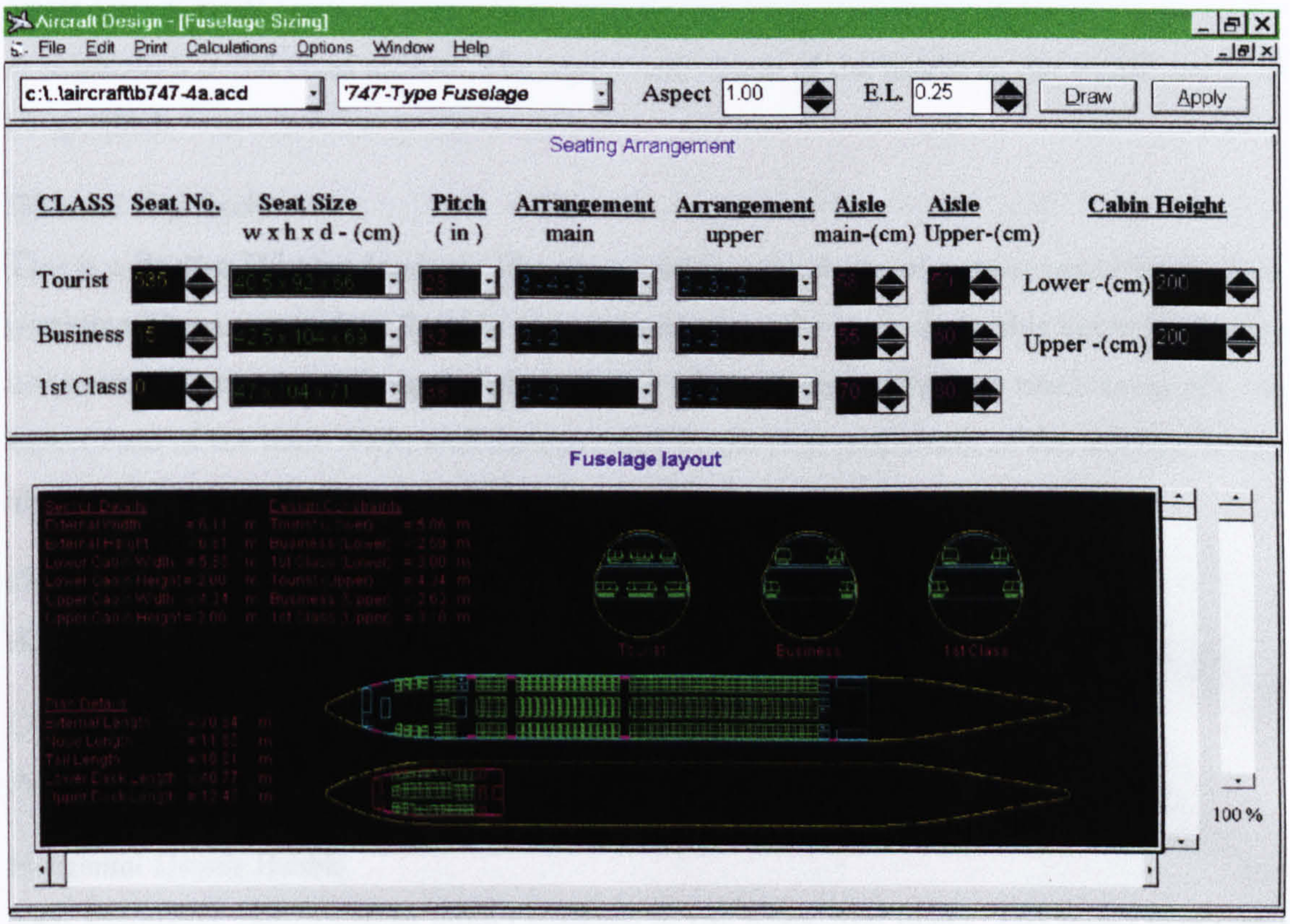
A .7 .3 FUSELAGE SIZING WINDOW

Function

The values of the parameters within the 'Fuselage Geometry' section of input variables are set from this window. The values can be input manually, or they can be estimated using the sophisticated fuselage sizing tool, which estimates the detailed geometry of the fuselage from the selected cabin and seating arrangement.

Description

A .7 .3 .1 Estimating Fuselage Dimensions



The above picture illustrates how the fuselage tool can be used to accurately estimate the fuselage dimensions of a Boeing 747-400 aircraft, using only a few simple input parameters.

The user selects the document that is to be considered using the File list box in the top left corner of the window. The fuselage drawing may be updated at any time by clicking the '*draw*' button, and the resultant fuselage dimensions may be pasted directly into the 'Fuselage Geometry' input parameter section by clicking the '*Apply*' button. Both buttons are located in the top right of the window.

Fuselage Style

To estimate the fuselage dimensions, firstly the type of fuselage to be incorporated into the design is chosen from the Fuselage Style list box, located next to the File list box. Depending on the style of fuselage chosen, up to two parameters may have to be set that further describe the style of fuselage. In the above example the 'aspect ratio' of the fuselage and the 'extended fuselage length' must be set, using the '*Aspect*' and '*E.L.*' boxes to the right of the Fuselage Style list box. The available fuselage styles, and any descriptive parameters are described below:-

Single Deck (Circular)

A single deck cylindrical cross section. No parameters need to be specified.

Single Deck (Ovoid)

A single deck ovoid cross section. The aspect ratio (ratio of the height to the width) needs to be specified.

Extended Top Deck

This is a Boeing 747 type fuselage. The cross section is made up of a main ovoid single deck portion with an upper deck 'bubble' that is built on to the main deck, this upper deck does not necessarily continue along the whole length of the fuselage. The user needs to specify the aspect ratio of the main deck, and the extended length (the proportion of the fuselage length along which the upper deck is included).

Double Deck (Circular)

A double deck cylindrical cross-section. No parameters need to be specified.

Double Deck (Ovoid)

A double deck ovoid cross-section. The aspect ratio needs to be specified.

Horizontal Double Bubble

Two cylindrical cross-sections joined together in the horizontal plane. The Join Length (the value of the length from the centre of each circle to the join, divided by the radius of each circle) must be specified.

Vertical Double Bubble

Two cylindrical cross-sections joined together in the vertical plane. The join Length must be specified.

Seating Plan

The total number of passengers seated in the fuselage is set from the M.D.P. Window, and corresponds to the value of the '*Max. Passenger Number*' parameter in the '*General*

Configuration' input parameter section. It is important to note that this value may differ from the '*Number of Passengers*' parameter in the '*Initial Sizing*' section, because the initial sizing parameter imposes an operational payload limit at a particular range, whereas the '*Max. Passenger Number*' imposes a structural payload limit at any range.

The class distribution of the passengers is set using the three boxes under the '*Class*' heading. The number of passengers in '*Tourist*', '*Business*', or '*1st class*' may be increased or decreased by using the spin box to the right of the particular value. The total number of passengers is automatically kept constant by adding passengers or reducing passengers to or from another class as appropriate.

The seat size, seat pitch, seating arrangement, and aisle width, can be set independently for each class. The top values refer to '*Tourist class*', the middle to '*Business class*', and the bottom to '*1st Class*'. The seating arrangement and aisle width of an upper deck, for each class, may also be set independently when appropriate.

The physical size of the seats in terms of width, height, and depth, is chosen from a selection of sizes under the '*Seat Size*' heading. The lengthways separation of the seats is determined from the values of '*Pitch*'. The way in which the seats are arranged across the fuselage cross-section is selected using the '*Seating Arrangement*' list boxes. The width of the aisle(s) for each particular class is set from the boxes under the '*Aisle*' heading, and the minimum height for each cabin is set from the boxes under the '*Cabin Height*' heading.

The calculation of the seating layout usually takes into account the estimated intersection of the tail surfaces with the internal cabin. This calculation can be bypassed by checking '*Ignore Tail Clearances*' from the '*Options*' menu.

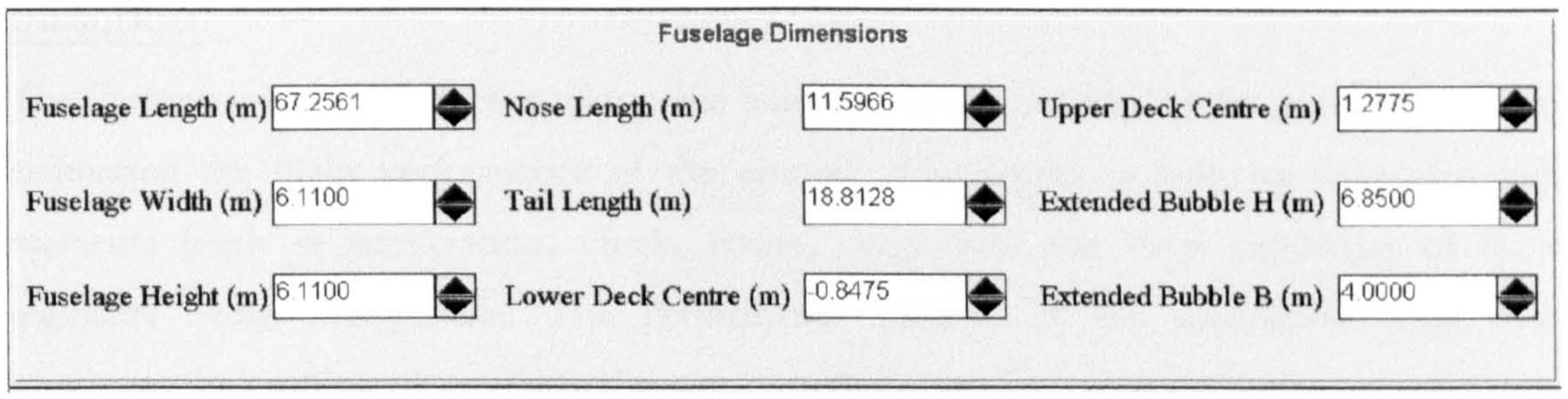
Fuselage Drawings

Once the parameters have been set, they can be processed and a drawing generated. The drawing shows cross sections of all three class layouts, and an internal plan of the fuselage that includes toilets, galleys, cupboards, and stairs. The text to the left of the drawing gives the values for the fuselage and cabin dimensions. The '*design constraints*' are the minimum cabin widths allowable for each class that will satisfy the constraints imposed by the input parameters. The maximum value of the constraints for each deck is taken to be the actual width of that deck.

A .7 .3 .2 Inputting Fuselage Dimensions

If the user wishes to ignore the estimates from the fuselage sizing routines, then clicking '*Override*' on the '*Options*' menu allows the user to do so. A panel as shown below will

appear in place of the '*Seating Arrangement*' panel, and values for the main fuselage dimensions may be entered manually.



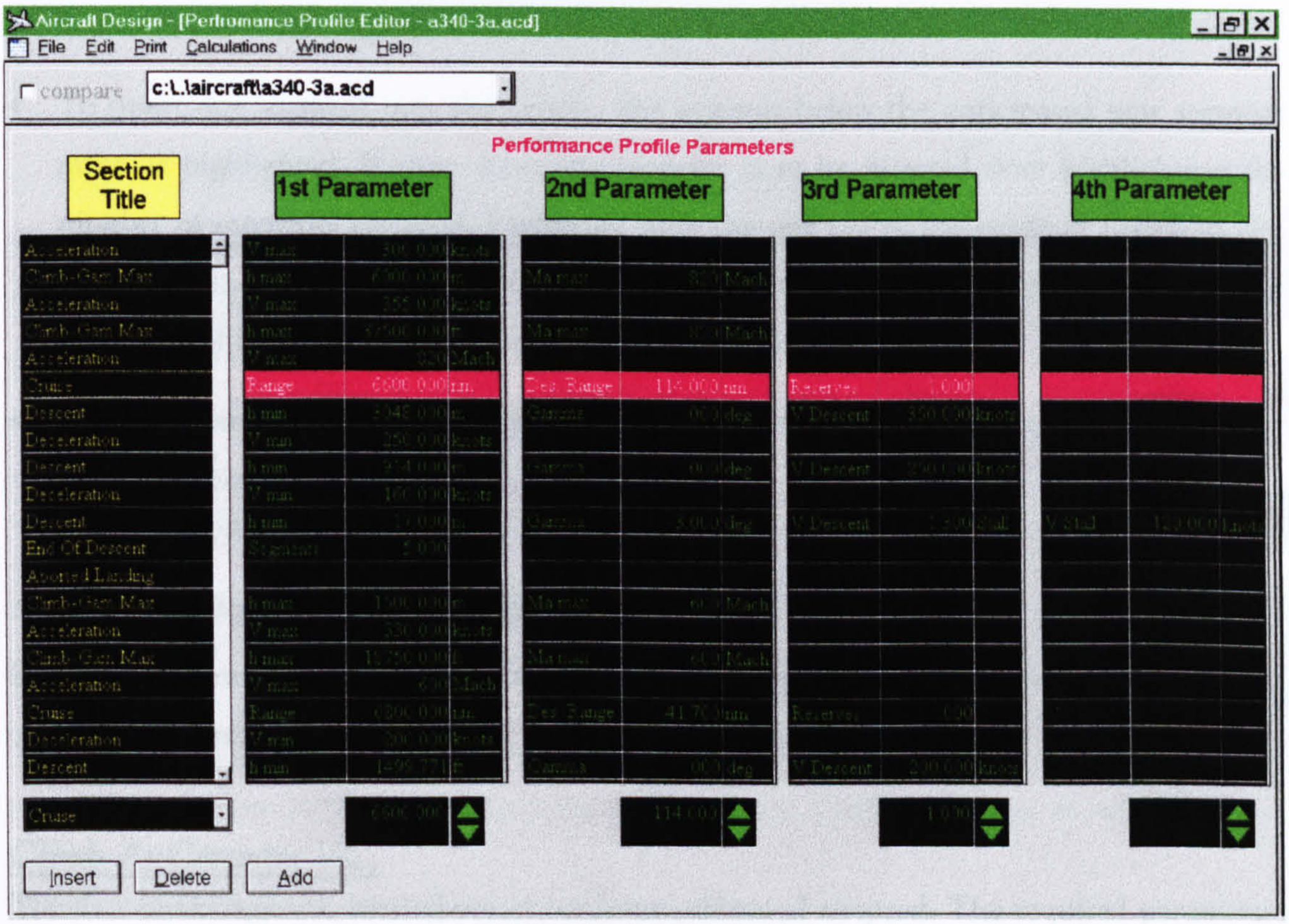
Parameters can be set using the spin boxes to increase or decrease the values in the boxes, or they can be typed in using the keyboard.

A .7 .4 PERFORMANCE PROFILE EDITOR

Function

The Performance Profile Editor allows the user to create a detailed flight profile for use in estimating the flight performance of the aircraft. The profile is built up from standard segments (such as acceleration, climb, cruise, etc.), with the main properties of these segments being configurable. The Performance Module of the calculation code then interprets the profile and simulates the necessary flight conditions accordingly.

Description



The layout of the Performance Profile Editor is shown above. Selection and comparison of documents is carried out using the procedures described previously (A.3). The comparison of documents within this window, does however differ in one aspect. When comparing one document to another, only the values of flight segments of the same type are compared. If no segment of the same type can be matched, then the boxes will contain the '****' symbol. If two velocities, expressed in different ways are attempted to be compared, then the 'mismatch' message will appear in the value box.

Setting the parameter values in the Performance Profile Editor is achieved using the same methods described for setting the parameter values in the MDP Window (See A.7.1.2)

A .7 .4 .1 Constructing The Flight Profile

There are a number of methods available for placing the flight segments in the required order:-

- To change the highlighted segment (be it blank or occupied), the required segment type must first be selected from the segment list box situated at the bottom left of the window. Pressing the [enter] key, and answering 'OK' to the confirmation prompt completes the change.

- To add a segment to the end of the current profile, the type of segment to be added should be selected from the list box, and then clicking on the '*Add*' button will append that segment to the flight profile.

- To insert one segment into the profile, the segment below the anticipated new segment must be highlighted. If more than one segment is to be inserted then highlighting the number of segments required, beginning with the one below the point of insertion will indicate this. Clicking on the '*Insert*' button will then insert the relevant number of segments, of the type set from the list box, at the point selected.

- Segments can be removed by highlighting the unwanted segments and clicking on the '*Delete*' button.

A .7 .4 .2 Flight Segment Parameters

Below is a summary of the available types of flight segments, and the parameters required to correctly configure them.

Climb At Constant VC.

This is a climb segment, carried out at constant calibrated airspeed. The required parameters are:-

1) Climb Altitude (h_{max})

The final altitude of the climb segment, expressed in any unit of length.

2) Calibrated Airspeed (V_c)

The airspeed that is maintained throughout the climb segment, expressed in any unit of velocity (not Mach number).

3) Maximum Mach No. (Ma_{max})

The maximum Mach number possible during the climb.

Climb At Maximum Gamma

This is an alternative climb segment, where the climb is performed such that the overall climb angle (γ) is a maximum for the given conditions. The required parameters are:-

1) Climb Altitude (h_{max})

The final altitude of the climb segment, expressed in any unit of length.

2) Maximum Mach No. (Ma_{max})

The maximum Mach number possible during the climb.

Acceleration

The Acceleration segment simply increases the speed of the aircraft. The required parameter is:-

1) Final Velocity (V_{max})

The velocity of the aircraft at the end of the segment. The velocity V_{max} can be input either in terms of airspeed (knots, m/s, or ft/s), or can be input in terms of Mach number. The format of the input is automatically recognised.

Cruise

The cruise portion of the flight is assumed to be carried out at constant altitude and constant Mach number. The cruise parameters are:-

1) Cruise Range (Range)

The distance reached at the end of cruise, or at the end of the descent from the cruise, depending whether an 'End of Descent' segment is placed after the descent section.

2) Descent Range (Des. Range)

A first estimation of the range travelled in descending, so that the cruise requirement is met exactly. If the contribution of the descent is not to be included in the cruise range (no 'End of Descent' segment in the descent section), then the descent range will be zero.

3) Reserve Policy (Reserves)

This parameter specifies the reserve fuel policy applicable to the Cruise segment. Setting the parameter to zero indicates that there is no reserve fuel policy. A value of one for the parameter means that a long-range fuel reserve policy is adopted (continuation of cruise for an extra 10% of cruise time). A short range fuel reserve policy (an extra one hour cruise time) is employed if the parameter value is two.

Descent

The aircraft loses altitude in the manner defined by the descent parameters. The number of parameters entered depends on the type of descent chosen:-

1) Descent Altitude (h_{min})

The altitude at the end of the Descent segment, expressed in any unit of length.

2) Descent Angle (Gamma)

It is possible to impose a constraint on the angle of descent by setting this parameter to any value smaller than zero. Setting the value to zero will lead to an unconstrained descent for this segment. The descent angle can expressed in angles or radians.

3) Descent Velocity ($V_{descent}$)

The velocity of the descent can be expressed in one of two ways. If the velocity is expressed as an airspeed (knots, m/s, or ft/s), then it is assumed that this value is a calibrated airspeed, to which the descent velocity will be constrained (i.e. a constant calibrated airspeed descent). If the velocity is a value smaller than two, then it is assumed the velocity is being expressed in terms of a multiple of the stall velocity at h_{min}.

4) Stall Velocity (V_{stall})

If the descent velocity has been specified in terms of a multiple of the stall velocity, then the value of the stall velocity at h_{min} must be set. The stall velocity is expressed as a true airspeed (knots, m/s, or ft/s). The main purpose of expressing parameters in terms of the stall velocity, is to simulate a real life descent where the regulations specify approach velocities in terms of stall velocities. The other reason for doing this is to give the descent more realistic flight settings, in terms of lift and drag coefficients.

Deceleration

The Deceleration segment simply decreases the speed of the aircraft. The required parameters are:-

1) Final Velocity (V_{min})

This is the speed of the aircraft at the end of the Deceleration segment. The speed can be expressed as a true airspeed, as a Mach number, or as a multiple of a stall velocity. The nature of the parameter is detected automatically from its value.

2) Stall Velocity (V_{stall})

If the final deceleration velocity has been expressed as a multiple of a stall velocity, then the value of the stall velocity is set using this parameter. It is expressed as a true airspeed.

3) Stall Altitude (h_{stall})

This is the height at which the stall velocity is referred to, should the final velocity be expressed as a multiple of a stall velocity.

Approach

An Approach segment should normally be the last segment of the flight profile. It indicates that the aircraft has finished its flight and is about to land. There is one parameter that needs to be set.

1) Final Altitude (h_{min})

The final height of this segment is the height at which the flare section of the landing is initiated. A value of 1-6 metres is appropriate.

Aborted Landing

This segment can be inserted to simulate an aborted or missed approach landing. No parameters need be specified for this segment.

Loiter

The Loiter segment is similar to the Cruise segment, in that it takes place at constant altitude and velocity. The difference however, is that the length of the Loiter segment is specified by a time rather than a distance. One parameter needs to be set:-

1) Loiter Time (time)

The length of time that the aircraft holds at the same altitude and speed, specified in hours, minutes, or seconds.

End of Descent

The 'End of Descent' segment is placed after one or more Descent/Deceleration segments that follow a Cruise segment. The purpose is to indicate the amount of descent range to be included in the cruise range. If for example a cruise range of 3000nm is specified, and there are 5 segments of mixed Descent and Deceleration segments succeeding the Cruise segment, the range travelled during the descent could be 100nm. This would mean that the aircraft would only need to travel 2900nm during the cruise phase. Adding an End of Descent segment after the 5 Descent/Deceleration segments, instructs the performance code to deduct the 100nm from the cruise distance. There is only one parameter to be specified:-

1) Number of Segments (segments)

This is the total number of segments that make up the relevant descent phase.

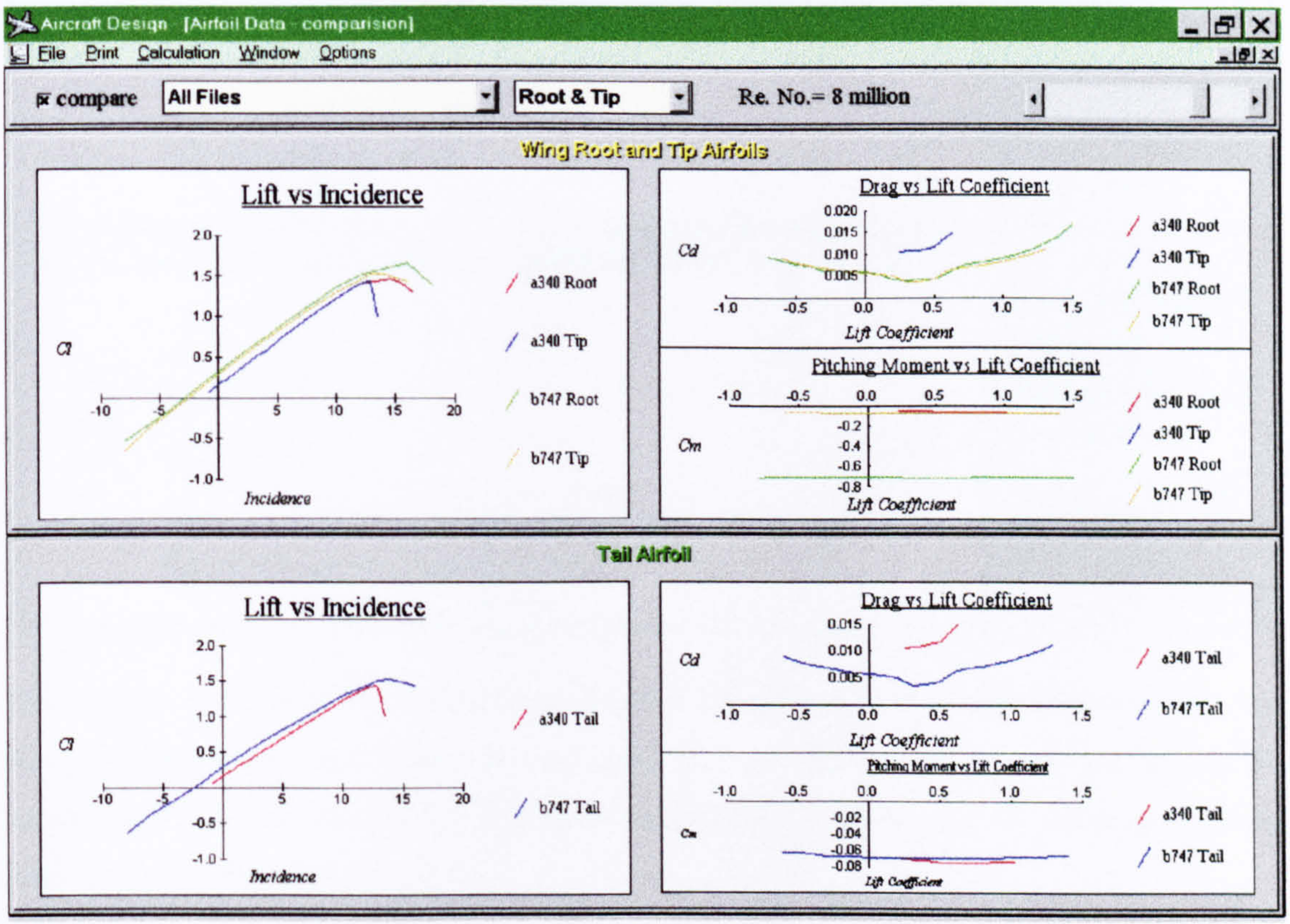
A .8 Parameter Output Windows

A .8 .1 Airfoil Data Window

Function

The Airfoil Data Window displays the lift, drag, and pitching moment data for the root, tip, and tail airfoils selected for the aircraft design. It is possible to configure the graphs to display the required data in a useful format, and to compare the data of one or more documents.

Description



The above screen shot shows the Airfoil Data Window being used to compare the airfoil data of two different documents ('*a340*' and '*b747*').

The top portion of the window contains the 'compare' check box and the document selection list box. These function as previously described in section A.3.3.2, with the exception that when the window is in 'compare' mode, the document list box gives the user no option other than to compare all the currently opened documents. When one or more documents are being compared, the Reynolds number scroll bar appears. The Reynolds

number at which the airfoil data is to be compared is selected by moving the scroll bar appropriately. Outside of 'compare' mode the scroll bar disappears, and the data is displayed at all available Reynolds numbers.

To the right of the document selection list box is the airfoil selection list box. This allows the user to elect to display the data for either the root, the tip, or both airfoils, in the graph below it.

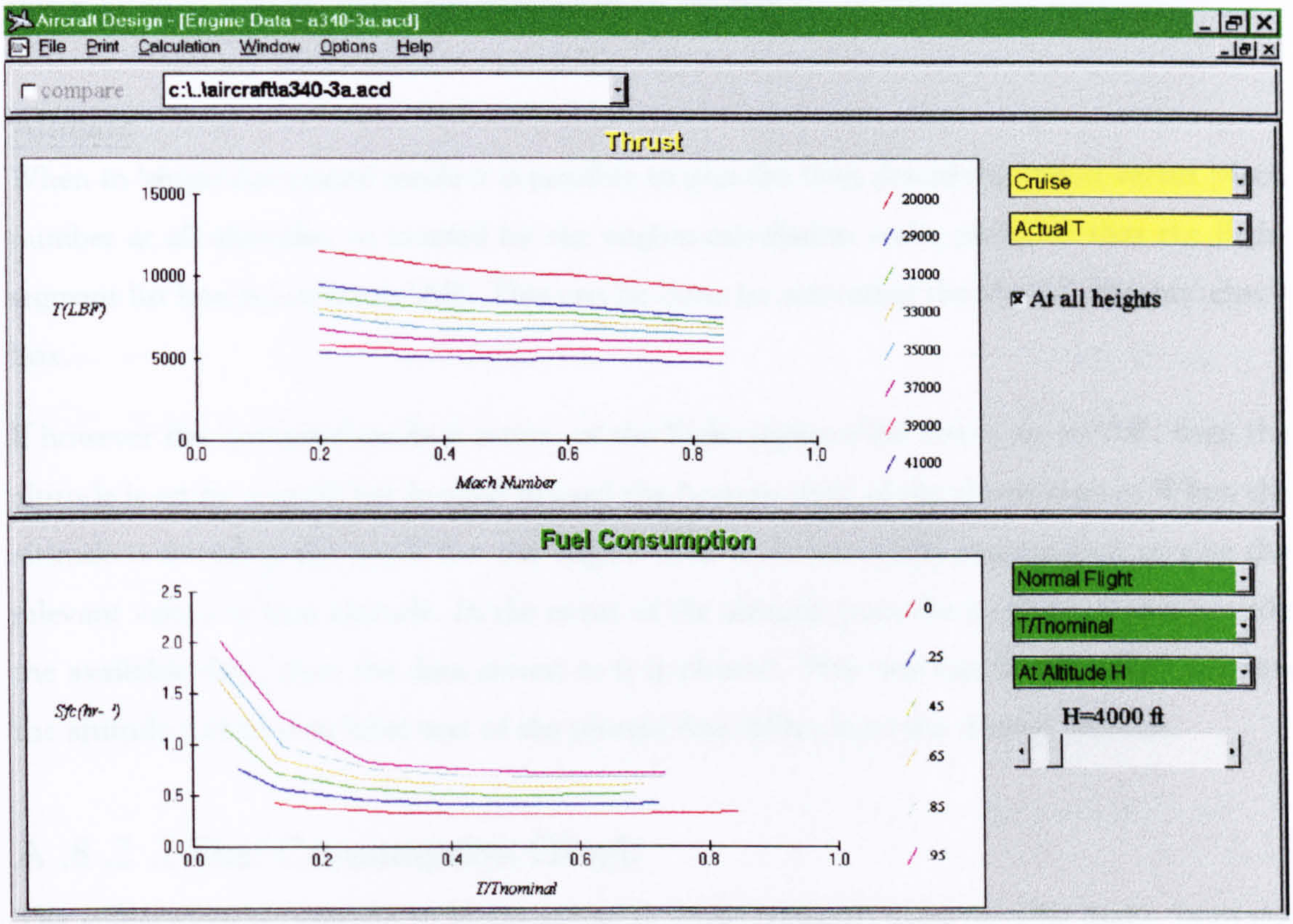
The main part of the window is split into two parts. The upper part contains the graphs pertaining to the root and tip airfoils, while the lower portion contains the graphs related to the tail airfoil. Each graph can be expanded and customised as described in section A.5.3.

A .8 .2 ENGINE DATA WINDOW

Function

The thrust and fuel consumption data for the aircraft's engines are displayed graphically. Thrust values can be displayed for various altitudes, and flight segments, whereas the fuel consumption graph values are dependant on altitude, flight segment, and Mach number.

Description



Above is an example of the Engine Data Window being used to display thrust and s.f.c. data from the '*a340.acd*' design. The 'compare' check box and the document selection list box are located at the top of the window. Comparison of designs can be carried out in accordance with the guidelines of A.3.3.2

Both the thrust graph and the fuel consumption graph can be expanded and customised using the techniques described in A.5.3.

A .8 .2 .1 Thrust Graph

The maximum available thrust of a single engine, for particular altitudes, Mach numbers, and types of flight (takeoff, climb, cruise, continuous, and idle) are plotted on this graph.

Flight Segment

The type of flight is selected from the list box located at the top right of the thrust area. By selecting 'All' it is possible to simultaneously plot the data for all of the flight segments.

Thrust Values

The values of thrust plotted on the graph can be plotted as either the actual numerical thrust value, or as a normalised thrust value. The normalised thrust value is the actual thrust divided by the installed sea level static thrust ($T/T_{nominal}$). The choice is made from the thrust list box, situated below the flight segment list box.

Altitude

When in 'single document' mode it is possible to plot the lines describing thrust versus Mach number at all altitudes, as created by the engine calculation code, provided that the flight segment list box is not set to 'All'. This can be done by activating the 'At All Heights' check box.

If however the 'compare' mode is active, or the flight segment list box is set to 'All', then the altitude is set by a scroll bar located toward the bottom right of the thrust region. When the altitude is set using the scroll bar the engine data is automatically interpolated to give the relevant values at that altitude. In the event of the altitude from the scroll bar being outside the available data, then the data closest to it is plotted. This case can be identified as when the altitude included in label text of the plotted line differs from the desired altitude.

A .8 .2 .2 Fuel Consumption Graph

The engines can be selected to be operating in either 'normal' flight or 'idle' flight, from the flight type list box situated toward the top right of the fuel consumption region. The fuel consumption of the engines for 'normal' flight is plotted against thrust, whilst the fuel consumption of the engines when idle is plotted against Mach number. For 'normal' flight the following options are available:-

Thrust Values

As above, the thrust can be plotted in terms of actual thrust value, or in terms of a non-dimensionalised thrust value. The type of value to be plotted is selected from the thrust list box situated below the flight type list box.

S.F.C Values

Values of specific fuel consumption can be plotted in the non-dimensionalised format used in the engine data files, or can be converted to an actual s.f.c. value that is dependant on altitude. The s.f.c. list box beneath the thrust list box allows the user to choose the format.

Altitude

If the format of the s.f.c. values is specified to be 'At Altitude h', then the altitude scroll bar will appear underneath the s.f.c. list box. The value of the altitude is set by moving the scroll bar to the left or to the right.

Mach Number

When the window is in 'single document' mode, then a line will be plotted for each Mach number on which data is available. If the 'compare' mode is active, a scroll bar will appear toward the bottom right of the fuel consumption area, the flight Mach number of interest can be set using this scroll bar. The interpolation for Mach number is carried out in a similar manner to the interpolation of altitude for the thrust graph, as described above.

For engine idle flight the following options are available:-

Fuel Consumption Values

The fuel consumption may be plotted as a specific fuel consumption (s.f.c.) or as a fuel flow rate. The choice may be made using the list box situated beneath the flight type list box.

Altitude

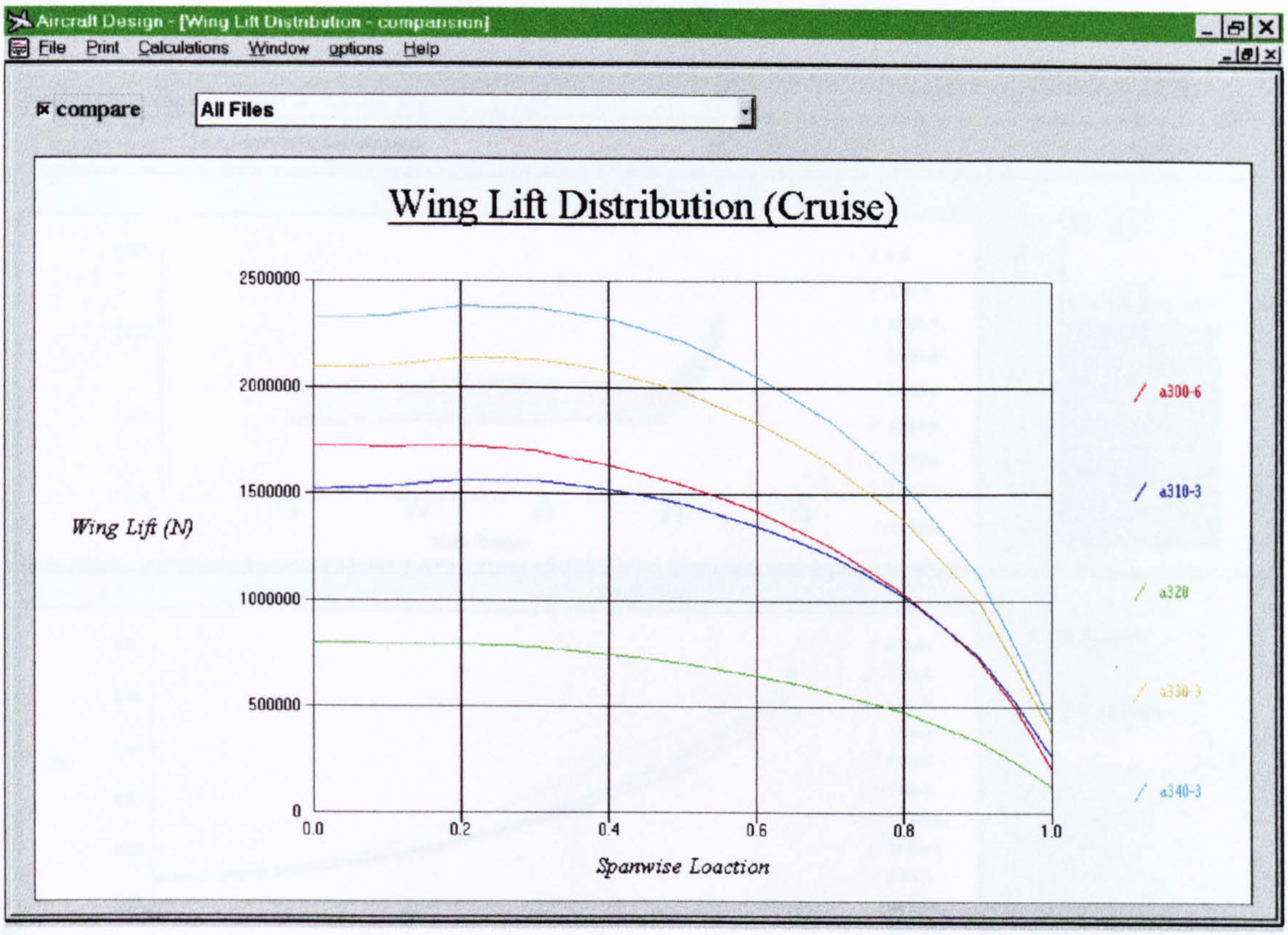
In 'single document' mode, fuel consumption lines are plotted for all the available altitude data. When the 'compare' mode is being used, a scroll bar will appear from which the altitude may be set. The fuel consumption data is interpolated in a similar manner to the thrust data described above.

A .8 .3 WING LIFT DISTRIBUTION WINDOW

Function

The results of the 3-d wing lift distribution calculations, carried out in the Wing Design Module, are graphically presented in this window.

Description



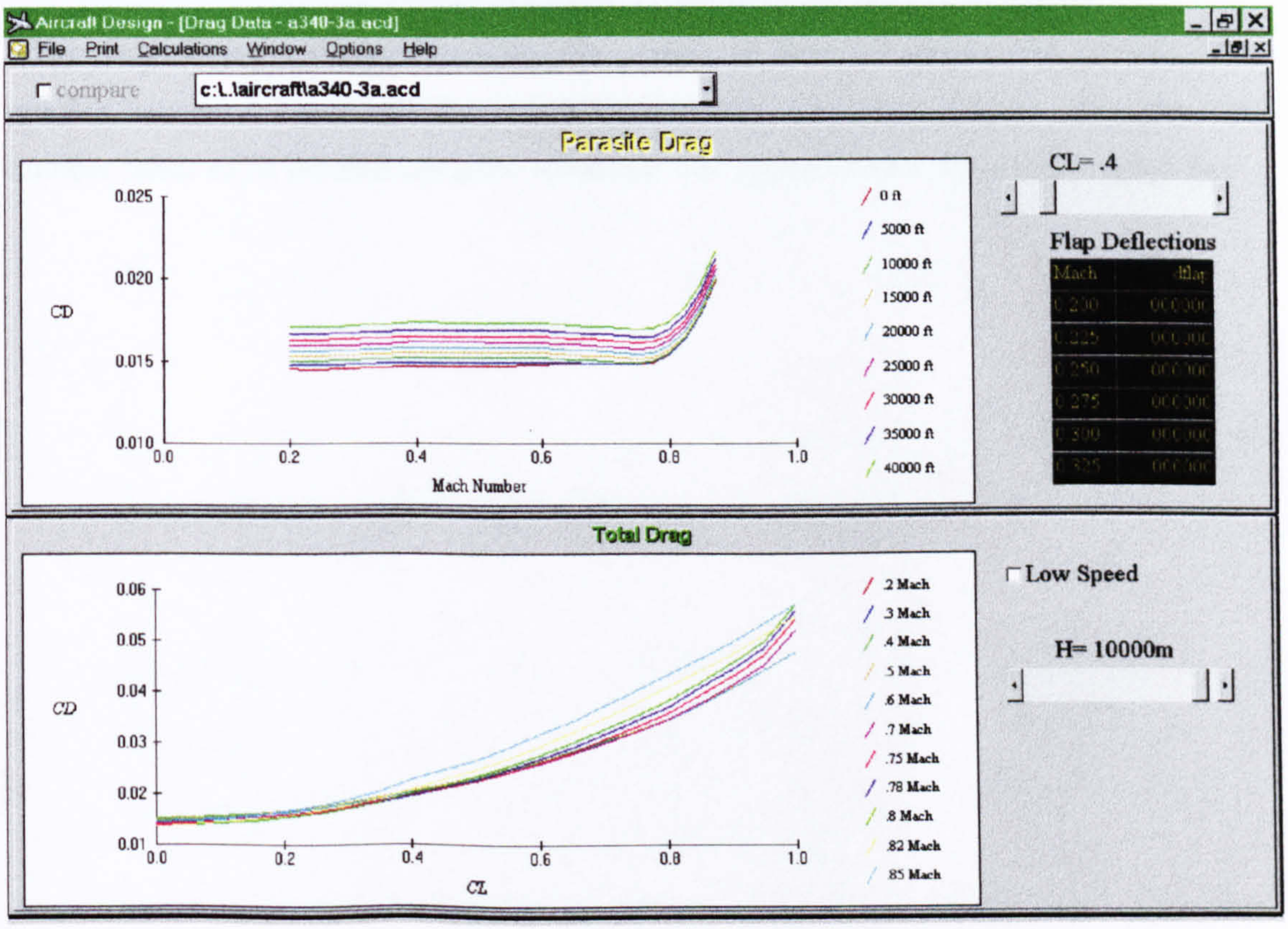
The graph describes the variation of local lift with spanwise position during cruise. The window supports multiple document comparison (shown in the example above), as explained in A.3.3.2

A .8 .4 DRAG DATA WINDOW

Function

The first graph in this window plots the parasite (zero lift) drag versus Mach number. The other, plots the aircraft drag polar (the total aircraft drag versus lift coefficient). The amount of flap deflection required to achieve the selected lift coefficient is also displayed.

Description



The top region of the window is responsible for document selection and comparison as outlined in A.3.3, and both graphs can be expanded and customised as explained in A.5.3.

A .8 .4 .1 Parasite Drag Graph

In 'single document' mode the parasite drag is plotted against Mach number for a variety of altitudes between 0ft and 40000ft, at the lift coefficient set by the scroll bar situated in the top right of the 'parasite drag' area. The text box beneath the scroll bar gives the amount of flap deflection required to achieve that lift coefficient at various Mach numbers.

In 'compare' mode the altitude must be specified, using the scroll bar that appears in place of the flap deflection box.

For both cases, the Mach number axis is automatically scaled to reflect any change in lift coefficient, keeping the graph data regime within sensible values.

A .8 .4 .2 Total Drag Graph

The drag polar consists of total aircraft drag values plotted against lift coefficient. The 'low speed' check box allows the graph to be toggled between low Mach number/high lift, and high Mach number/low lift scenarios. The altitude is set from the scroll bar located toward the top right of the 'total drag' region

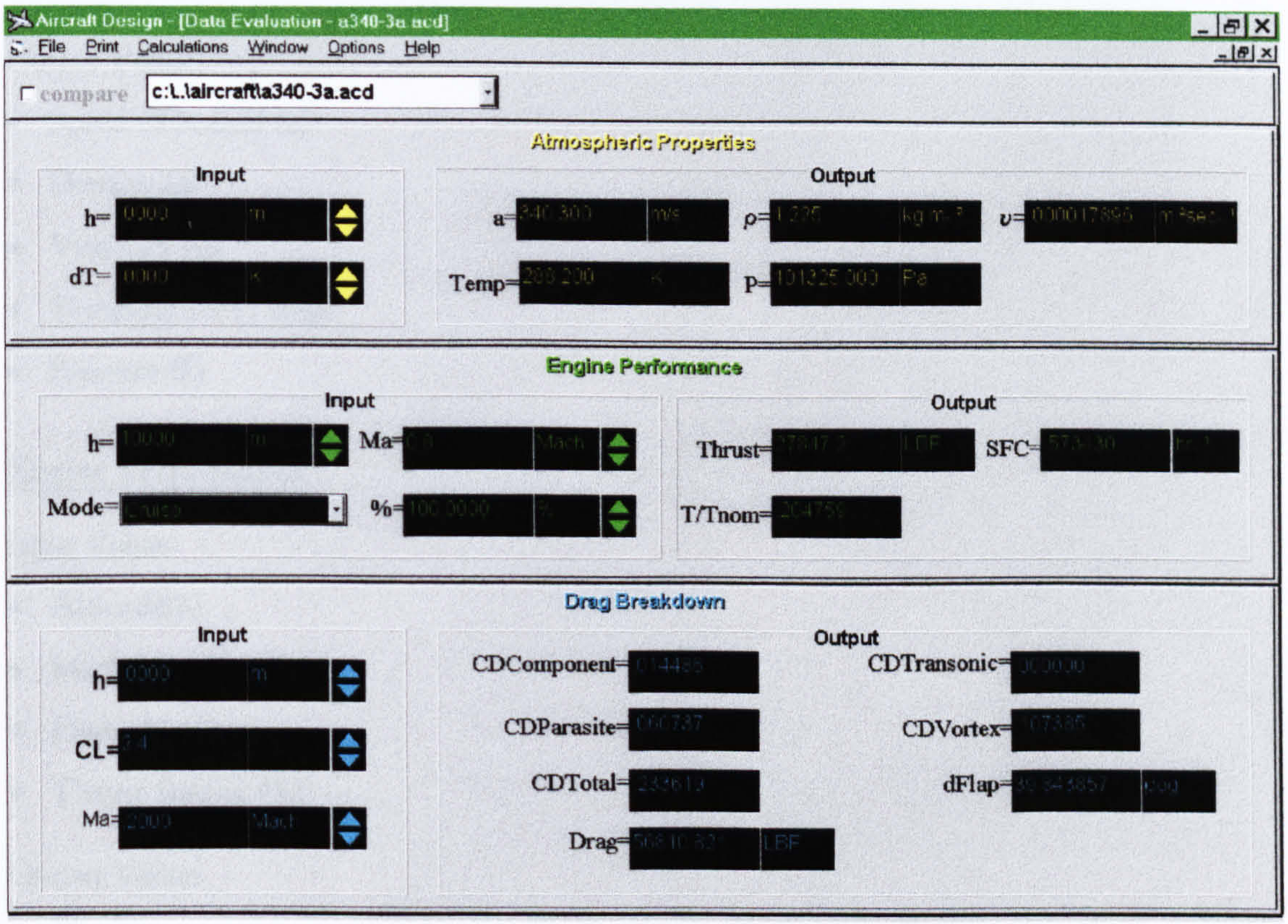
When considering a single document, the values of drag are plotted for various Mach number between 0.2 and 0.85. If however the 'compare' check box is active, then the Mach number needs to be selected using the scroll bar that appears below the altitude scroll bar.

A .8 .5 DATA EVALUATION WINDOW

Function

This window allows the user direct access to the standard atmosphere, engine performance, and aircraft drag evaluation routines. Detailed breakdowns of the output from these routines are provided, at the specific input conditions.

Description



The selection and comparison of documents within the window is controlled using identical techniques to those described in A.3.3.1. There is however one additional feature unique to this window. The output of the evaluation routines can be either compared between documents for different input conditions, or the input conditions can be locked so that changing them for one document automatically changes them for all others within the same session. This is done by clicking '*All files same input*' on the '*Options*' menu.

All input values can be entered numerically and confirmed using the [enter] key, or they can be increased and decreased a small amount using the spin boxes. When the spin boxes are used to change the parameter value, the output is automatically updated without the need to press the [enter] key. When documents are being compared it is not possible to change the values of the input parameters.

Below the document selection and comparison region, the window is split into three distinct areas, these are for the evaluation of atmospheric properties, engine performance, and drag breakdown respectively.

Atmospheric Properties

Input Values

- Altitude (h)
- Temperature Deviation from international standard (dT)

Output Values

- Speed of Sound (a)
- Density (ρ)
- Viscosity (υ)
- Temperature (Temp)
- Pressure (P)

Engine Performance

Input Values

- Altitude(h)
- Mach Number (Ma)
- Flight Mode
- Thrust Rating (%)

Output Values

- Thrust
- Specific Fuel Consumption (s.f.c.)
- Non-dimensionalised thrust ($T/T_{nominal}$, $T_{nominal}$=Installed static sea level thrust)

Drag Breakdown

Input Values

- Altitude (h)
- Lift Coefficient (CL)
- Mach Number (Ma)

Output Values

- Total Component Drag Coefficient (CdComponent)
- Transonic Wave Drag Coefficient(CdTransonic)

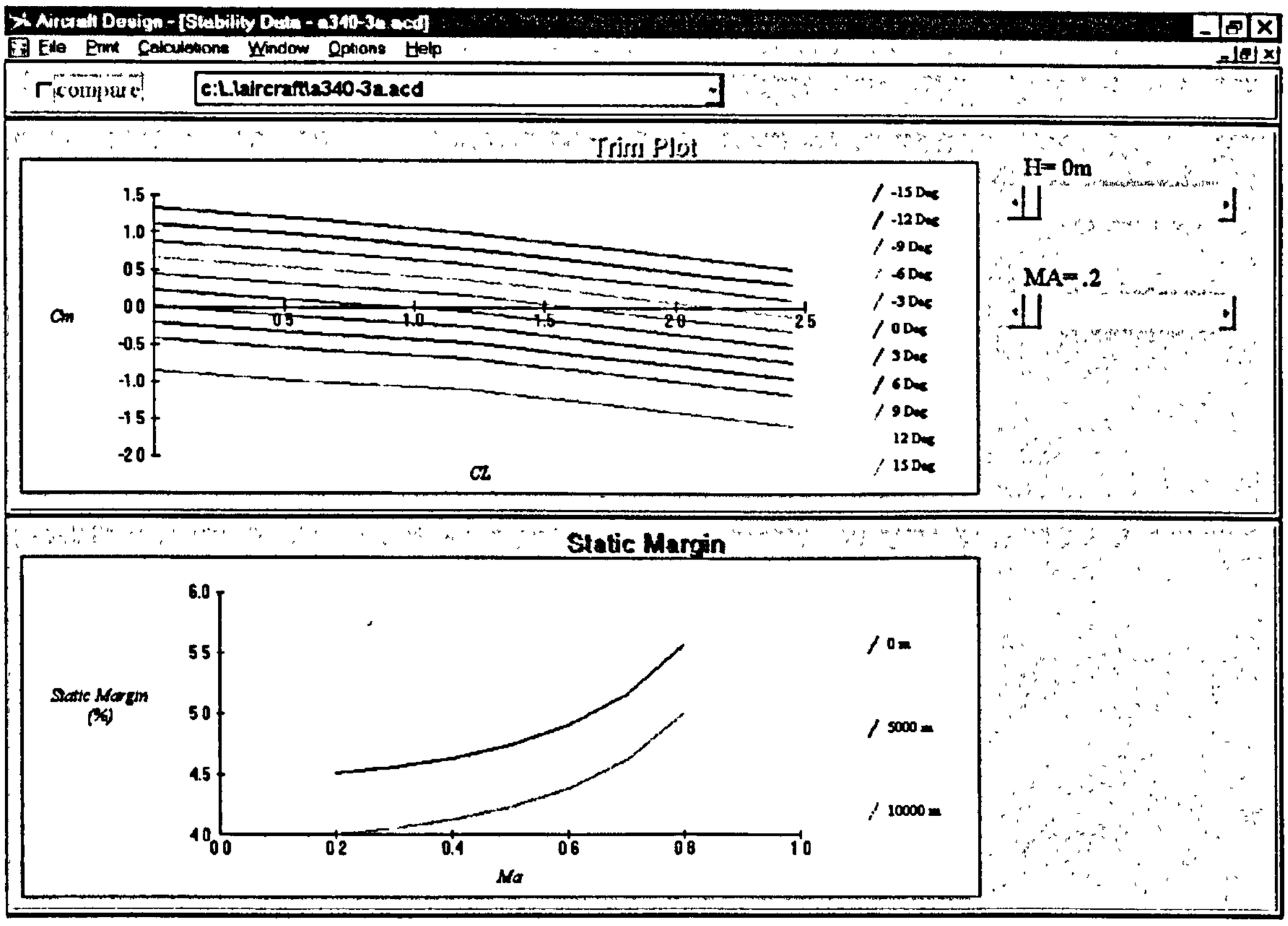
- Total Parasite Drag Coefficient(CdParasite)
- Lift Induced Drag Coefficient (CdVortex)
- Total Drag Coefficient (CdTotal)
- Flap Deflection (dFlap)
- Total Drag Force (Drag)

A .8 .6 STABILITY DATA WINDOW

Function

The aircraft trim plot, and the variation of the static margin with altitude and Mach number are plotted in this window.

Description



The window supports all graphical comparison and graph customisation features. The two graphs displayed in the window are described below:-

A .8 .6 .1 The Trim Plot

The upper part of the window contains the trim plot and its controls. In 'single document' mode the value of the pitching moment C_m is plotted against the lift coefficient C_L for a range of tail incidence angles i_{ht}. The altitude and Mach number of the plot are set using the two scroll bars situated to the right of the plot

If the window is in 'compare' mode, a single value of elevator angle i_{ht} is plotted, this value is set from the scroll bar which appears below the altitude and Mach number scroll bars.

A .8 .6 .2 Static Margin Graph

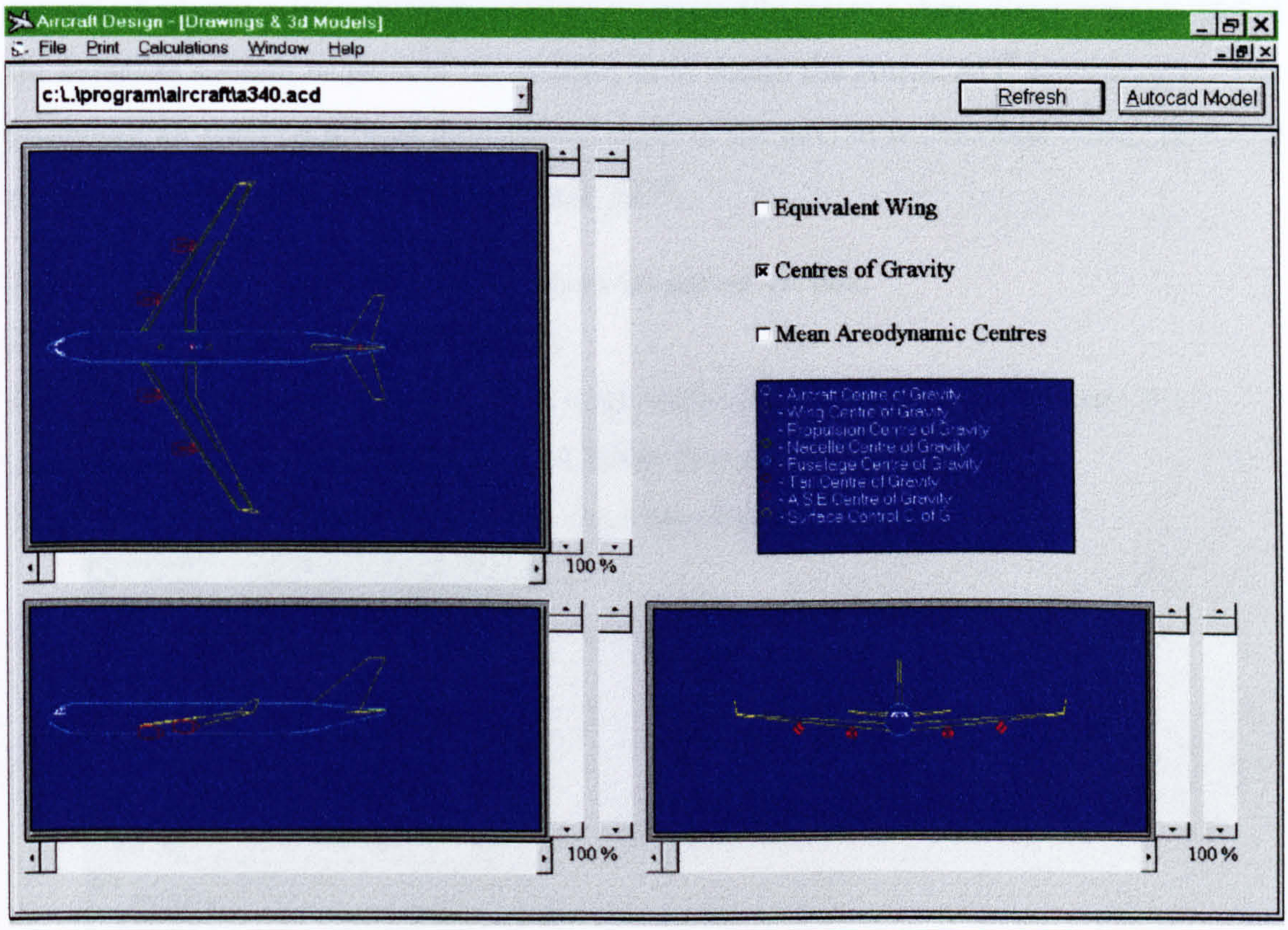
The magnitude of the static margin is plotted against Mach number. In 'single document' mode the graph is plotted for three values of altitude. In 'compare' mode the altitude is set from a scroll bar to the right of the graph.

A .8 .7 DRAWING / 3D MODEL WINDOW

Function

This window contains 2-d drawings of the designed aircraft which can be zoomed and panned to suit the user. A detailed three dimensional model of the aircraft may also generated from this window.

Description



The active document is selected from the list box at the top of the window. No compare features are available in this window.

A .8 .7 .1 2-d Drawings

The window consists of three sub-windows, these contain a plan view, a side view and a frontal view of the aircraft. These drawings can be refreshed at any time by clicking the '*Refresh*' button at the top right of the window.

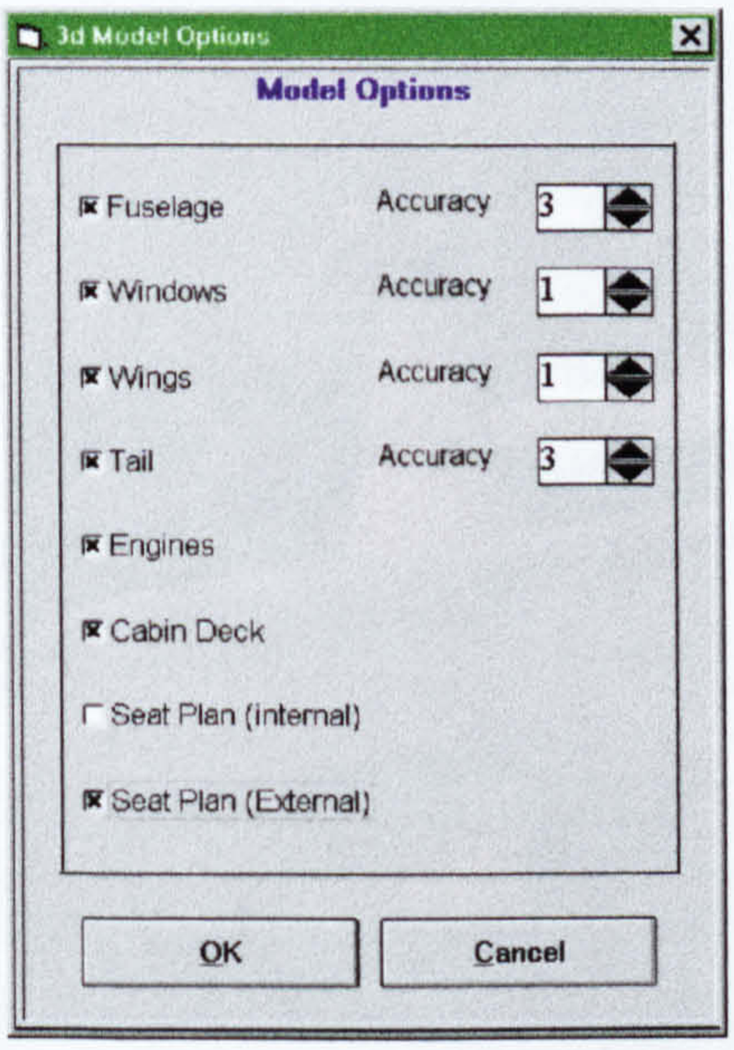
The plan drawing can include an outline of the equivalent wing planform, the centres of gravity of the aircraft components, and the longitudinal position of the wing aerodynamic centre. These are selected by activating the relevant check boxes.

Each drawing can be expanded by double clicking on it, or by selecting it and pressing the [enter] key. It is also possible to zoom in on a particular part of the drawing, by increasing the magnification using the scroll bar to the far right of the drawing. The drawing may then be panned to the left/right and up/down using the scroll bars to the bottom and to the right of the drawing.

A .8 .7 .2 3-d Models

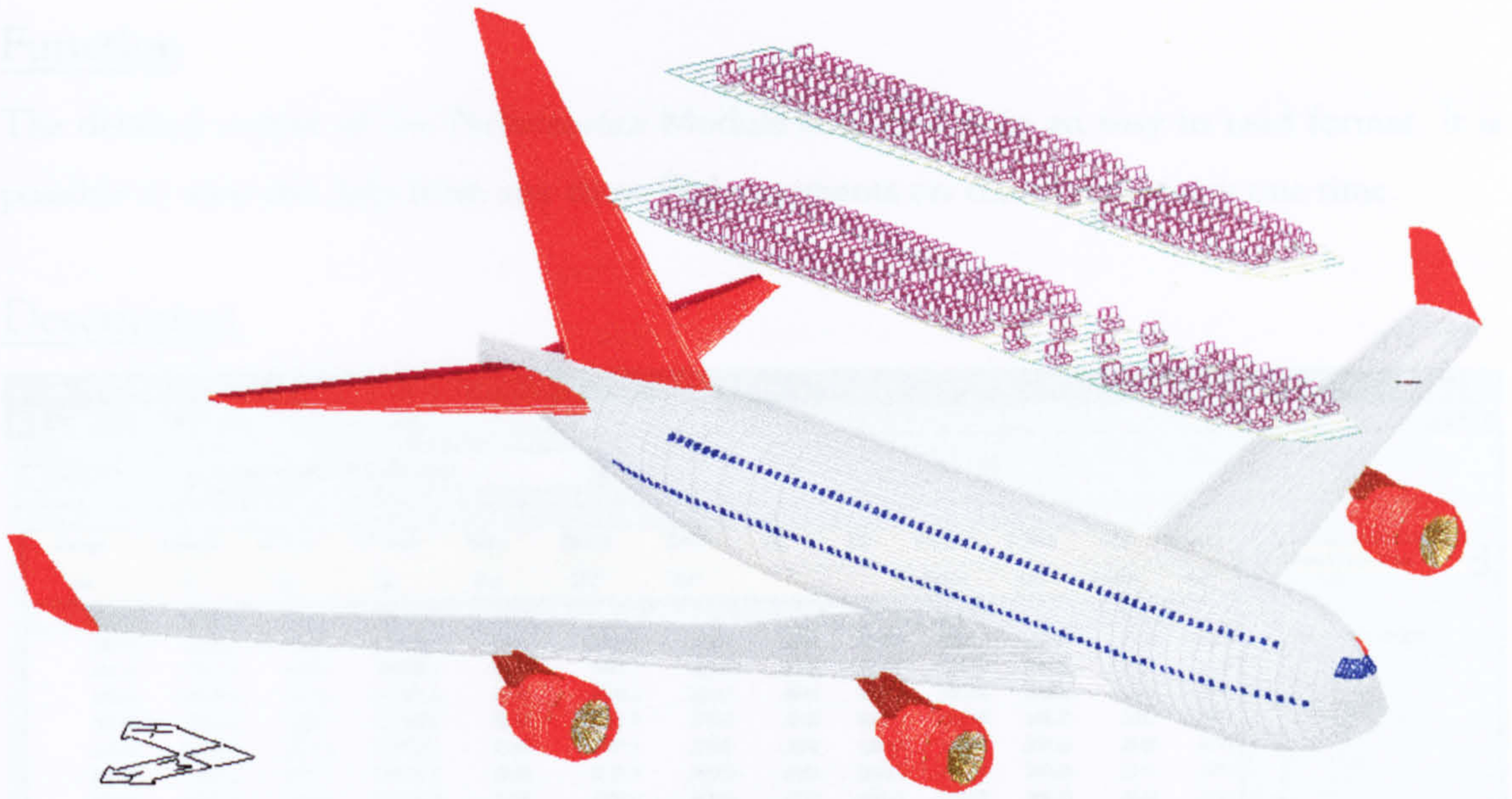
By clicking the '*AutoCAD Model*' button in the top right corner of the window, a data file is created which can subsequently be used to automatically create a three dimensional model of the complete aircraft, or parts of the aircraft, from within the AutoCAD® environment. The procedure for creating a three dimensional mesh of the aircraft is described below, provided that the user has access to a copy of AutoCAD®.

1. Select the appropriate document from document list box.
2. Click the '*AutoCAD Model*' button
3. Select the name for the data file (The provided Auto Lisp routine must read the data from a file '*Model.dat*', situated in the AutoCAD root directory).
4. Select the 3-d Model options from the screen below.



5. Start AutoCAD.
6. Load the application '*Model.lsp*', contained in the '*models*' directory of the Aircraft Design program.
7. Enter the '(draw)' command at the AutoCAD command prompt.
8. The drawing will automatically be generated.

An example mesh is show below, along with an example of a fully rendered model.





A .8 .8 PERFORMANCE DATA WINDOW

Function

The detailed output of the Performance Module is tabulated in an easy to read format. It is possible to view the data from any three flight segments on the screen at any one time.

Description

Aircraft Design - [Performance Data - a340-3a.acd]

File Print Calculations Window Help

compare c:\..\aircraft\a340-3a.acd

Range nm	Altitude ft	W fuel kg	W Total kg	Time min	Thrust LBF	S.F.C hr-1	CL	CD	V Callib. knots	V True m/s	Ma Mach	Gamma deg
264.78	37500.0	7392.2	255944.2	39.86					261.77		.8141	
108.75	23941.4	4331.6	259004.9	19.81	10539.8	.59352	.3800	.01832	332.17	240.25	.7724	1.4568
136.32	27311.9	4928.1	258408.4	23.35	9493.7	.58640	.4369	.02027	314.52	240.25	.7833	1.1527
163.89	29910.9	5472.9	257863.6	26.90	8749.3	.58115	.4844	.02224	301.18	240.25	.7921	.8889
191.47	32832.4	6030.3	257306.1	30.44	9015.3	.57714	.5246	.02413	286.46	240.25	.8023	.9991
219.05	35444.4	6581.4	256755.1	33.98	8999.1	.57149	.5881	.02815	273.56	240.25	.8118	.8933
246.62	36810.5	7077.3	256259.1	37.53	8133.9	.56904	.6454	.03183	265.98	240.25	.8141	.4672
274.20	37857.6	7555.5	255780.9	41.07	7856.0	.56815	.6714	.03315	259.62	240.25	.8141	.3581

Climb-Gam Max.

in sequence

Range nm	Altitude ft	W fuel kg	W Total kg	Time min	Thrust LBF	S.F.C hr-1	CL	CD	V Callib. knots	V True m/s	Ma Mach
267.15	37500.0	7425.7	255910.7	40.16					263.89		.8200
265.24	37500.0	7398.7	255937.8	39.92	7854.0	.56815	.6708	.03312	262.20	240.59	.8153
265.70	37500.0	7405.2	255931.3	39.98	7854.0	.56857	.6688	.03309	262.61	240.93	.8165
266.16	37500.0	7411.7	255924.8	40.03	7854.0	.56898	.6669	.03306	263.02	241.27	.8176
266.62	37500.0	7418.1	255918.3	40.09	7854.0	.56939	.6650	.03303	263.43	241.60	.8187
267.08	37500.0	7424.6	255911.8	40.15	7854.0	.56979	.6632	.03300	263.82	241.93	.8198
267.15	37500.0	7425.7	255910.7	40.16	7854.0	.57018	.6614	.03298	263.89	241.98	.8200

Range km	Altitude ft	W fuel kg	W Total kg	Time hr	Thrust LBF	S.F.C hr-1	CL	CD	V Callib. m/s	V True m/s	Ma Mach	L\D
13043.11	37500.0	93702.8	169633.7	14.54					135.82		.8200	
1146.35	37500.0	12813.5	250523.0	1.39	7230.0	.57024	.6611	.03297	135.82	241.98	.8200	20.0485
1797.98	37500.0	18079.1	245257.3	2.11	7066.2	.57024	.6472	.03223	135.82	241.98	.8200	20.0824
2449.63	37500.0	23227.2	240109.2	2.83	6908.5	.57024	.6336	.03151	135.82	241.98	.8200	20.1099
3101.28	37500.0	28262.2	235074.3	3.55	6756.6	.57024	.6203	.03081	135.82	241.98	.8200	20.1309
3752.94	37500.0	33188.1	230148.3	4.27	6610.3	.57024	.6073	.03014	135.82	241.98	.8200	20.1453
4404.61	37500.0	38008.9	225327.5	4.99	6469.3	.57024	.5945	.02950	135.82	241.98	.8200	20.1533
5056.28	37500.0	42728.5	220607.9	5.71	6333.4	.57024	.5821	.02888	135.82	241.98	.8200	20.1545

The Performance Module computes the output variables for the flight profile entered in the Performance Profile Editor. Each flight segment is calculated using a step by step analysis, the number of steps depending on the level of accuracy set by the user. For each step the values of the main twelve flight variables are output. These are:-

1. Range
2. Altitude
3. Weight of fuel consumed
4. Total Aircraft Weight
5. Flight Time
6. Engine Thrust
7. Engine s.f.c.
8. Lift Coefficient
9. Drag Coefficient

10. Calibrated Airspeed

11. True Airspeed

12. Mach Number

For climb and cruise segments a thirteenth variable is output, this is the value of the climb angle, and the lift to drag ratio respectively.

The main portion of the window contains three data viewing areas, each capable of viewing the data of one flight segment. Each area contains a title bar, displaying the names and units of the twelve output variables of each flight step, and any other variables peculiar to the selected segment.

The segment that is to be displayed in each particular area is selected using the list box located to the right of the title bar of each area. If the '*in sequence*' check box is activated, then the three areas are automatically locked so that the segments displayed in each of the three areas are sequential. This means that only the segment for the top area needs to be selected, and the other areas will automatically follow.

The first line of data in the tables, the line with the grey background, is the data at the end of the segment that has been interpolated using the data of the final two steps, to give a more accurate answer. The remainder of the data in the tables are the raw values of each step in the performance calculation.

Units of the parameters can be changed in accordance with the procedures of A.5.2. Documents are selected and compared using the methods of A.3.3. When comparing one or more documents there is one important consideration unique to the performance data output windows. It is possible to compare output values from the segments of two documents on a strictly numerical basis, where the first segment of one is compared to the first segment of the other and so on. Alternatively, the segments can be compared using a more tactical approach, whereby only segments of the same type are compared, ignoring segments that do not match. If no match can be found for a segment then the '****' message will appear in the segment list box. The mode of comparison is toggled using the '*compare alike*' check box.

A .8 .9 PERFORMANCE GRAPH WINDOW

Function

This window allows the user to analyse data from the Performance Module in a graphical context. The axes of three graphs in the window can each be independently set to a variety of parameters.

Description



As for all of the input and output parameter windows, the upper portion of the window is used to control document selection and comparison. In this window an accuracy box is also present, this controls the amount of data that is plotted on the graphs. A accuracy setting of 5 means that the data for every step of the performance calculations is plotted, this can in some cases be time consuming. It is for this reason that it is possible to reduce the amount of data used, and therefore expedite the plotting process. A '*refresh*' button is also included to enable the user to redraw the graphs at any time.

To the right hand side of each graph is an *x*-axis list box, and a *y*-axis list box below it. The nature of the data plotted on the *x*-axis and the *y*-axis is selected using these boxes.

Each graph can be expanded horizontally by double clicking on it (or pressing [enter]). Once expanded a scroll bar below the *y*-axis list box becomes active, which can be used to scroll the graph to the left or to the right. The graph can be restored to its original size by double

clicking on it once more. The units and the style of the graphs can be altered from the '*graph setup*' command on the '*options*' menu.

A .8 .10 PERFORMANCE SUMMARY WINDOW

Function

A summary is provided of the data from the Performance Module. The detailed data from each step of the calculation is ignored, and only the data at the end of each segment is considered. The changes in range, weight, and time over each segment are also displayed.

Description

Aircraft Design - [Performance summary - a340-3a.acd]

File Print Calculation Window Help

compare c:\..\aircraft\a340-3a.acd

Flight Summary

Section	Range	Altitude	W Fuel	W Total	W Fract.	Time	V Callib	Ma	DRange	DFuel	DTime	DWfract.
	km	ft	kg	kg		min	knots	Mach	nm	kg	sec	
Acceleration	13375.19	18750.0	96303.9	167032.6	.6342934	904.75	282.272	.600	.99	30.0	9.9	.999821
Cruise	13494.59	18750.0	97200.8	166135.6	.6308872	914.92	282.272	.600	64.47	897.0	610.3	.994630
Deceleration	13509.77	18750.0	97202.6	166133.8	.6308805	916.47	200.000	.430	8.20	1.8	93.2	.999989
Descent	13681.75	1499.8	97229.9	166106.5	.6307767	939.36	200.000	.330	92.87	27.3	1373.6	.999835
Loiter	13877.54	1499.8	99755.5	163581.0	.6211862	969.36	200.000	.310	105.72	2525.5	1800.0	.984796
Deceleration	13882.84	1499.8	99760.0	163576.4	.6211689	970.30	160.000	.248	2.86	4.6	56.0	.999972
Descent	13892.92	55.8	99995.7	163340.7	.6202738	972.35	155.945	.237	5.44	235.7	123.0	.998559
Approach	13893.24	9.8	100002.0	163334.5	.6202501	972.41	156.048	.236	.17	6.2	4.0	.999962
Flare	.38	4.9	100049.4	163287.0	.6200698	972.43	138.431	.209	.21	47.5	.8	.999709
LA. Ground Roll1	.96	0	100138.2	163198.2	.6197328	972.61	51.774	.078	.31	88.8	10.8	.999456
LA. Ground Roll2	1.05	0	100142.9	163193.6	.6197151	972.72	.722	.001	.05	4.7	6.8	.999971
FAR Approach	.27	9.8	14.3	223821.7	.8499458	.06	156.048	.236	.15	14.3	3.4	.999936
FAR Flare	.34	4.9	61.8	223774.2	.8497655	.07	138.450	.209	.03	47.5	.8	.999788
FAR Ground	.94	0	156.4	223679.6	.8494061	.26	51.774	.078	.33	94.6	11.4	.999577
FAR Ground	1.03	0	161.0	223674.9	.8493885	.37	.722	.001	.05	4.6	6.7	.999979
BFL-TO Roll1	1.75	0	247.2	263089.2	.9990612	.73	146.338	.221	.95	247.2	43.7	.999061
BFL-TO Roll2	2.30	0	279.6	263056.8	.9989381	.84	163.078	.247	.29	32.4	6.8	.999877
BFL-Rotation	2.51	0	280.7	263055.7	.9989339	.88	163.078	.247	.11	1.1	2.5	.999996
BFL-Transition	2.62	7.8	286.3	263050.1	.9989128	.90	182.204	.276	.06	5.5	1.3	.999979
BFL-Climb	2.76	35.0	291.5	263044.9	.9988929	2.40	182.203	.276	.08	5.3	89.6	.999980
BFL-Abort Roll1	1.75	0	248.1	263088.3	.9990578	.73	145.406	.220	.95	248.1	43.9	.999058
BFL-Abort Roll2	2.73	0	331.6	263004.8	.9987406	1.08	2.121	.003	.53	83.5	20.8	.999682

The document selection and comparison of the window functions in exactly the same way as for the Performance Data Window (see A.8.8). The values displayed in the table correspond to the values of the parameters at the end of each segment. The twelve parameters are:-

1. Range
2. Altitude
3. Weight of Fuel Consumed
4. Total Aircraft Weight
5. Weight Fraction (Total Weight divided by Initial Takeoff Weight)
6. Flight Time
7. Calibrated Airspeed
8. Mach Number
9. Range Increment

10. Fuel Weight Used Increment
11. Time Increment
12. Segment Weight Fraction (Final segment weight divided by initial segment weight)

The units of the parameters can be changed by double clicking the relevant column on the title bar.

A .9 DATA MANIPULATION

A .9 .1 MATHEMATICAL EXPRESSION EVALUATIONS

Function

When analysing data in the Optimisation, Correlation, Sensitivity, and Trade-Off Windows, it is important to be able to evaluate mathematical expressions and functions that involve the aircraft design parameters. A self-contained mathematical language has been created for the program, which allows the user to evaluate these type of functions from within the data manipulation windows.

Description

The nature of the language will be familiar to those with experience of computer languages such as FORTRAN and BASIC. Each parameter within the Aircraft Design environment is given an abbreviated variable name or label, for example the fuselage length has the label 'lfuse'. These labels, combined with the appropriate mathematical notation can produce a limitless number of functions for analysis. A list of variables, constants, conversions factors, and their appropriate labels can be opened by clicking the '*Variable List*' command on the '*Window*' menu, whilst in any of the data manipulation windows.

The expression or function may contain up to 16 levels of parenthesis, with up to ten variables in each parenthesis level. The dimensions and units of the function are automatically calculated, and if the dimensions of the function are of a recognisable format the appropriate units will be assigned to it.

A summary of notations recognised by the expression interpreter, and their mathematical functions are shown below:-

Command	*Description*	*Function*
a+b	- Addition	a+b
a - b	- Subtraction	a - b
*a*b*	- Multiplication	a x b
a/b	- Division	$\left(\frac{a}{b}\right)$
a^b	- Raised to the power	a^b
sin(a)	- Sine function	sin(a)

cos(a)	- Cosine function	cos(a)
tan(a)	- Tangent function	tan(a)
asin(a)	- Arc sine function	asin(a)
acos(a)	- Arc cosine function	acos(a)
atan(a)	- Arc Tangent function	atan(a)
sinh(a)	- Hyperbolic Sine function	sinh(a)
cosh(a)	- Hyperbolic Cosine function	cosh(a)
tanh(a)	- Hyperbolic Tangent function	tanh(a)
asinh(a)	- Inverse Hyperbolic Sine function	asinh(a)
acosh(a)	- Inverse Hyperbolic Cosine function	acosh(a)
atanh(a)	- Inverse Hyperbolic Tangent function	atanh(a)
ln(a)	- Natural logarithm	$\log_e(a)$
exp(a)	- exponential function	e^a
log(a)	- Base 10 logarithm function	$\log_{10}(a)$
abs(a)	- Returns Absolute value	abs(a)

An example of this type of notation would be:-

' *(lfuse*(1+(lnose/ltail)^2)*sin(SweepLE/2))* '

This would evaluate the function:-

$$l_{fuse}\left(1+\left(\frac{l_{nose}}{l_{tail}}\right)^2\right)\times\sin\left(\frac{Sweep_{le}}{2}\right)$$

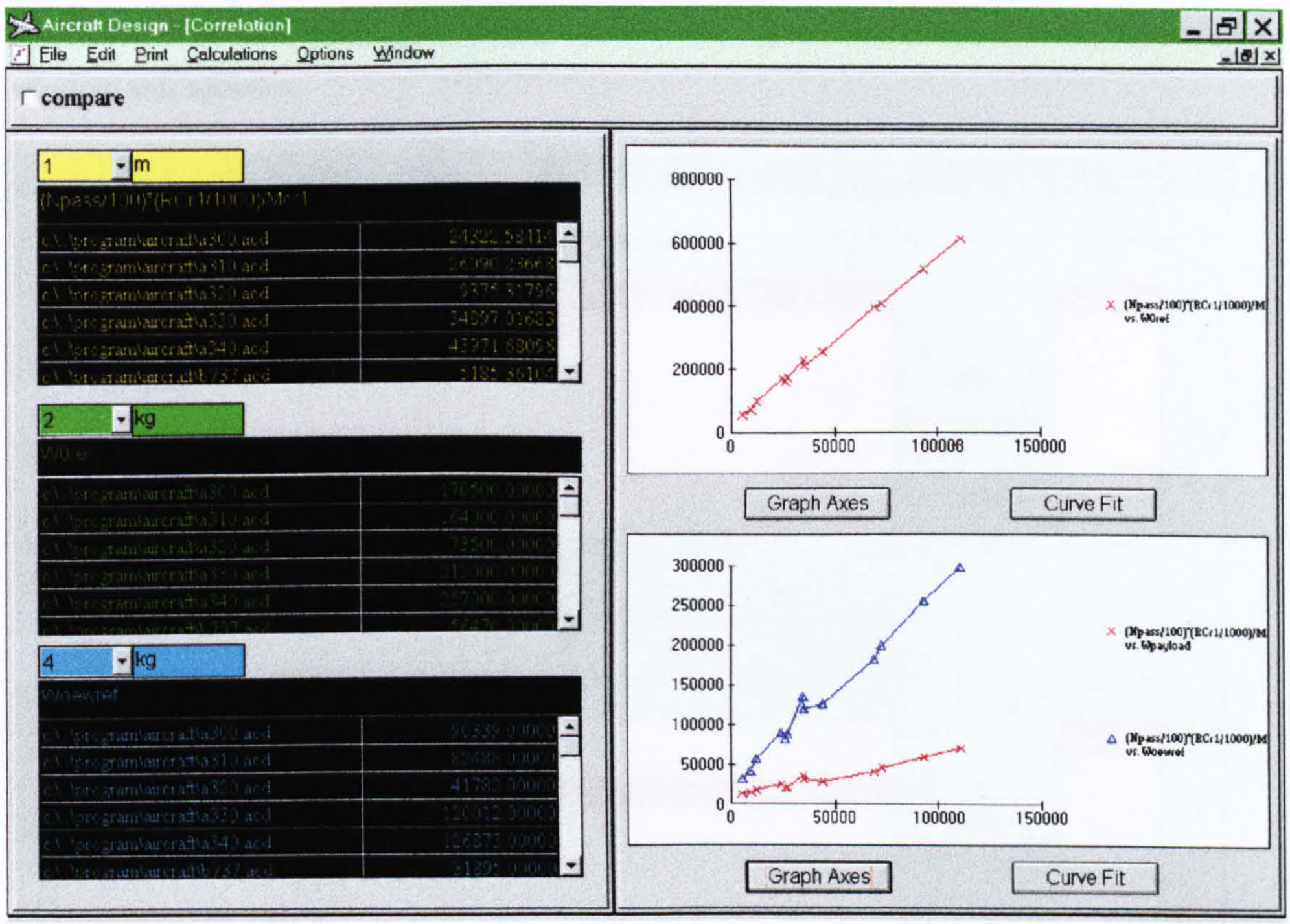
The interpreter is fully error trapped, and gives warning messages of unmatched parenthesis, unrecognised syntax errors, and any occurrence of a division by zero. A full list of recognised parameters, and their variable names are given in section A.10.

A .9 .2 CORRELATION WINDOW

Function

The relationship between design parameters, or functions of design parameters, can be explored using this window. The values of user specified functions are calculated for each design in the session, creating a set of data values for that function. These data sets can then be plotted against each other to illustrate any relationship between the functions, and a suitable curve then fitted to the data to approximate this relationship.

Description



The window can be split into three main areas, the document comparison area at the top, the expression evaluation area on the left, and the expression plotting and curve fitting area on the right.

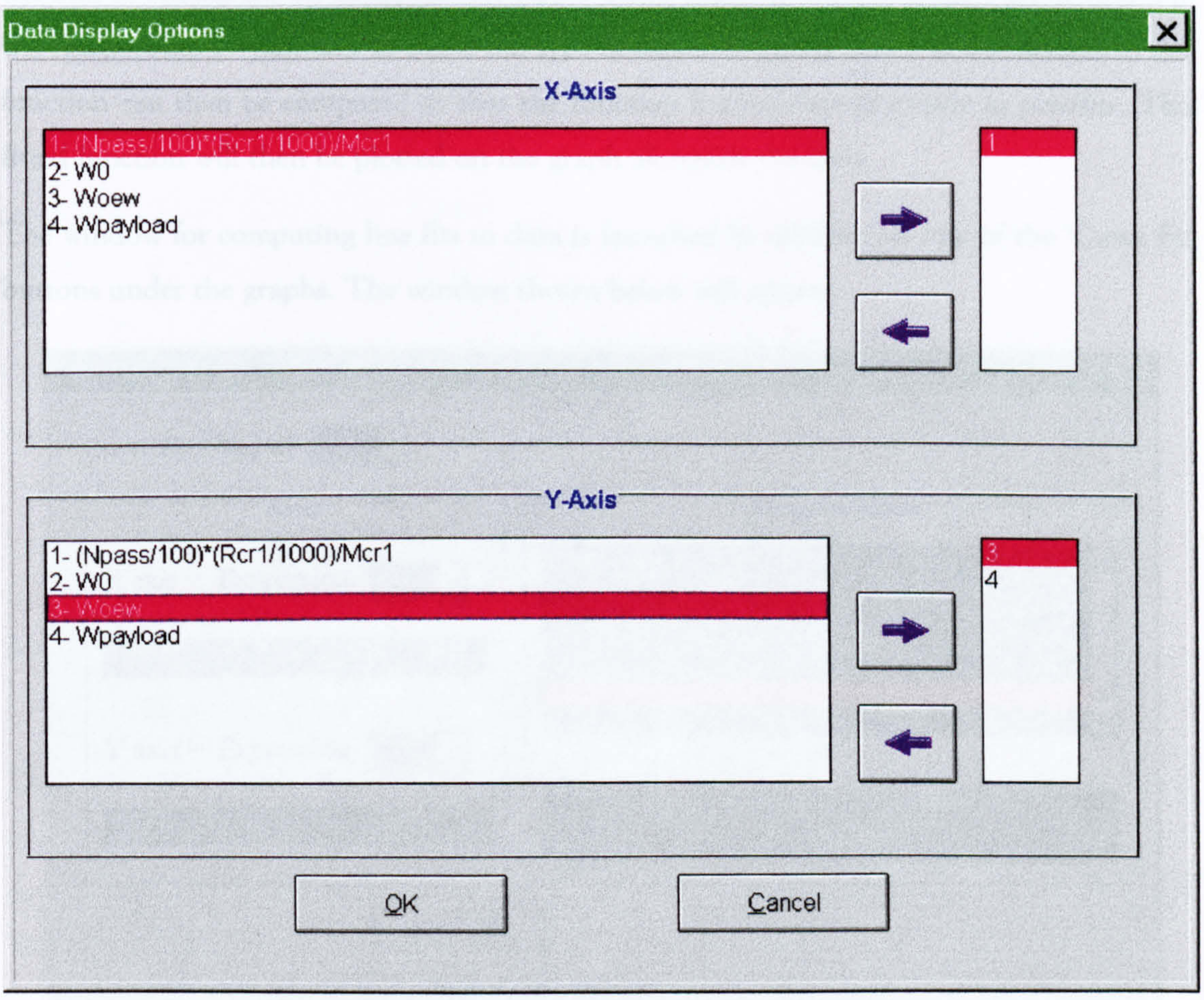
A .9 .2 .1 Setting and Evaluating Expressions

The expression evaluation panel contains three areas that are each responsible for selecting an expression, entering an expression, changing the units of an expression, and displaying the results of an expression. The expression that is being referred to in a particular area is set by using the list box at the top left of each area to select a 'slot' number between 1 and 15. There are 15 slots available for storing mathematical expressions.

The expression is typed in the box below the expression selection list box, using the notation described in A.9.1. The expression is evaluated when the [enter] key is pressed. It can be evaluated at any time by selecting the expression text box and pressing the [enter] key. The values of the expression for each document are displayed in the table below the expression text box. The units of the displayed values can be changed, when appropriate, by double clicking or pressing [enter] on the box to the right of the selection box.

A .9 .2 .2 Plotting Expressions

There are two graphs in the expression plotting panel. Each graph can be configured to be a multi-line two dimensional plot of any combination of the 15 expressions. The axes of the graph are set by clicking on the '*Graph Axes*' button below the relevant graph. The following window will appear:-



For each axis there is a box listing all the expressions that have been set, ignoring any slots yet to be filled. To the right of this is a box listing the number(s) of the expression(s) to be plotted on the relevant axis.

An expression can be included on either the *x* or *y* axes by double clicking it in the relevant expression listing box, or by selecting it in the relevant expression listing box and pressing

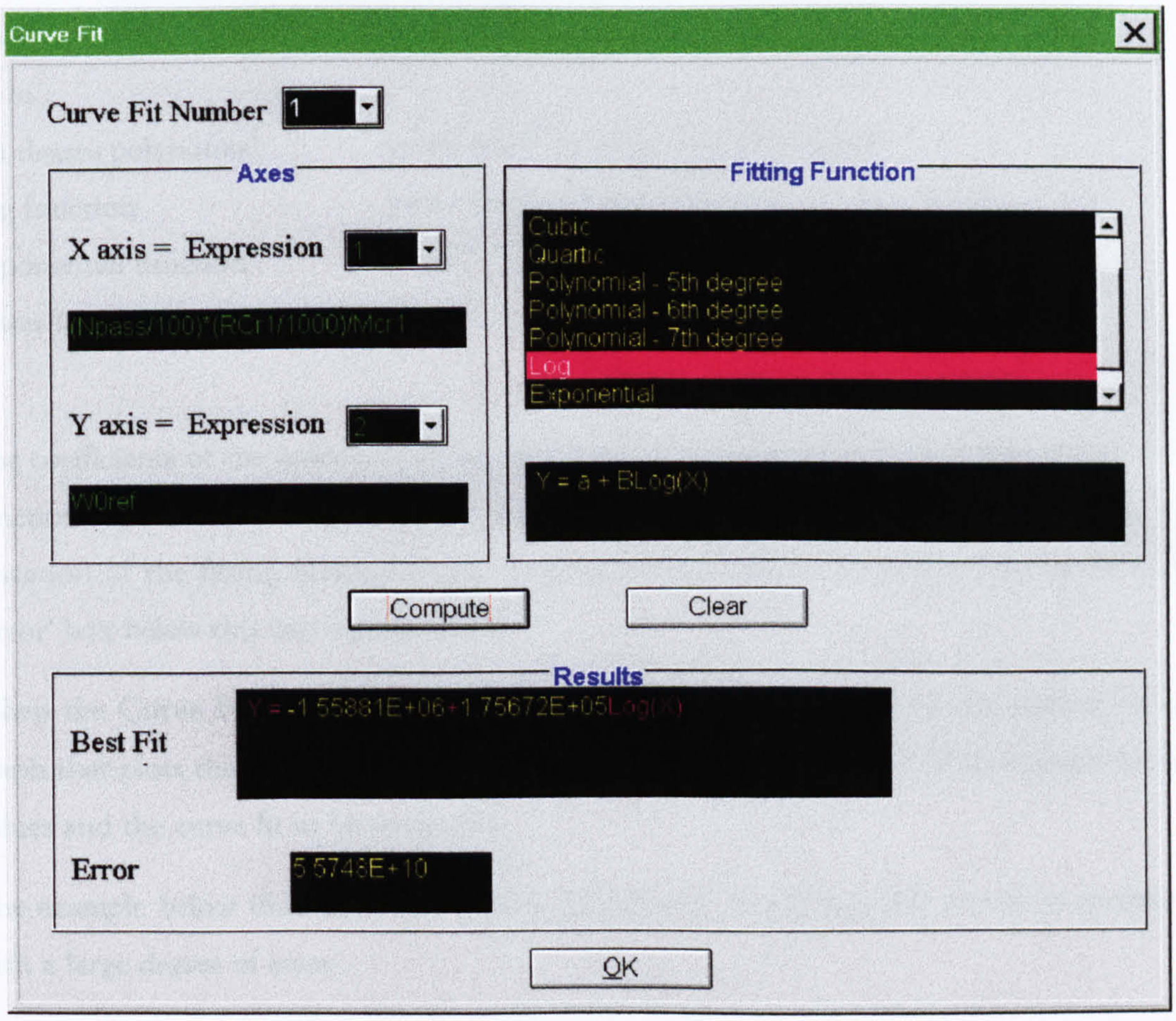
the ➡ button. An expression may be removed from the axis by double clicking its number in the relevant axis list box, or by selecting its number in the relevant axis list box and pressing the ⬅ button.

Once the axes have been set and the '*OK*' button pressed the graph is automatically updated. The graph is also updated whenever a expression included on the graph is re-evaluated. The graphs can be expanded and configured as explained in section A.5.3.

A .9 .2 .3 Curve Fitting

For any two expressions it is possible to use data correlation techniques to approximate the relationship between the two data sets of the expressions, as a curve of best fit passing through the points of a graph of these two expressions. The techniques available here allow the user to choose the set of expression values which make up the x and the y set of values in the relationship $y=f(x)$, and to chose the type of function that is f(x). The coefficients of this function can then be computed so that the function fits the data as closely as possible. This fitted function will then be plotted on the graph alongside the data.

The window for computing line fits to data is launched by clicking on one of the '*Curve Fit*' buttons under the graphs. The window shown below will appear.



There are 10 curve fit 'slots' available, each slot stores the number of the expression used for the x and for the y axis of the particular curve fit, the type of fitting function used, and the values of the function coefficients. The slot that is currently selected is chosen using the 'Curve Fit Number' list box.

The set of x-axis values and the corresponding y-axis values for the active curve fit are chosen from the 'x axis' and 'y axis' list boxes. The number of the expression from which the relevant set of values originated should be selected in these list boxes.

The desired method of curve fitting should then be highlighted in the 'fitting function' list box. If there are insufficient data points (i.e. insufficient documents) to use a particular method, the message '**Unavailable**' will appear in the box below the 'fitting function' list when that method is highlighted. If the method can be used, the form of the function selected is displayed in mathematical notation.

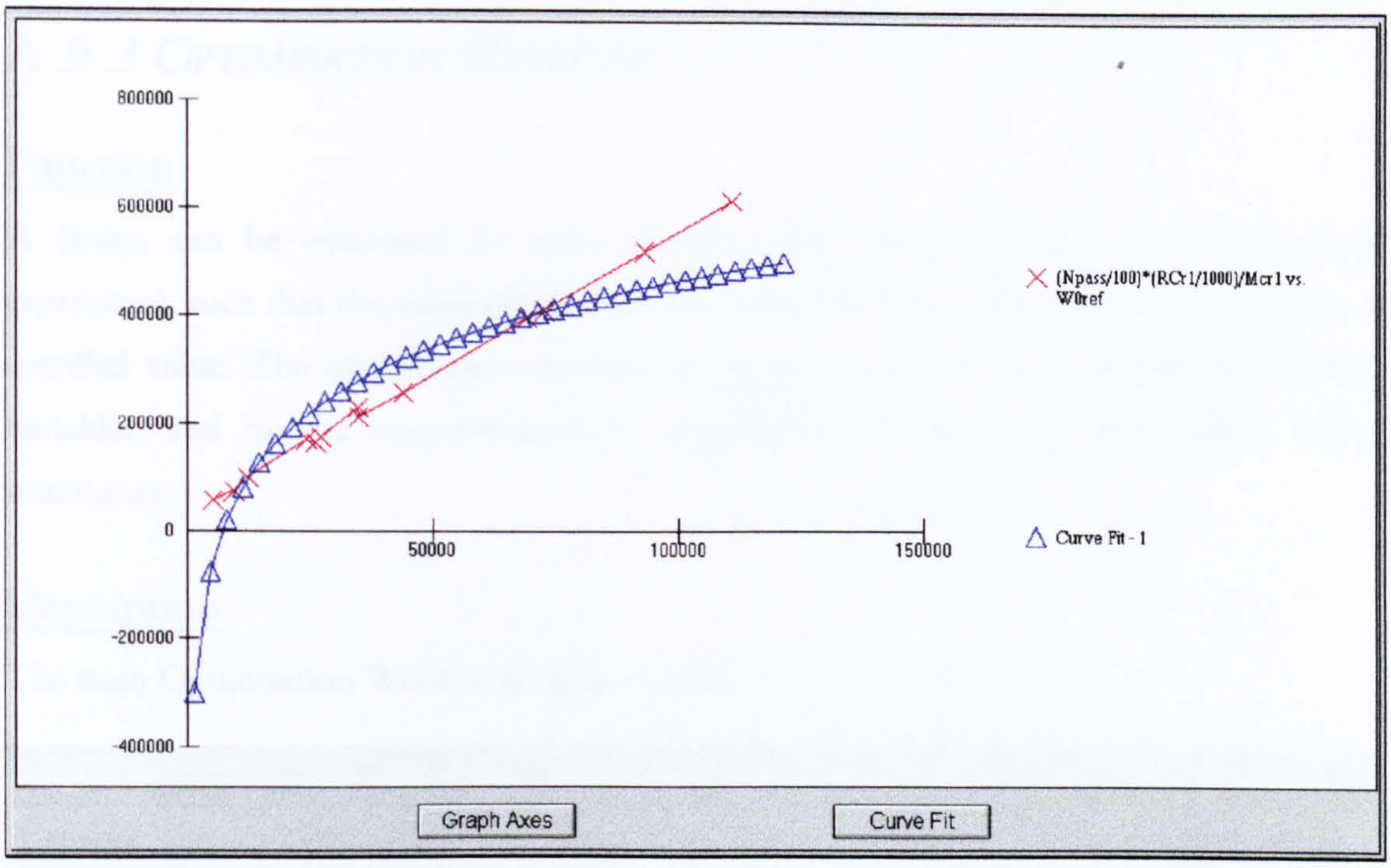
The available fitting functions are:-

description	*Formula*
Linear	$y=ax+b$
Quadratic	$y=ax^2+bx+c$
Cubic	$y=ax^3+bx^2+cx+d$
up to...	
7th degree polynomial	$y=ax^7+bx^6+cx^5+dx^4+ex^3+fx^2+gx+h$
Log function	$y=a+b\log(x)$
Exponential function	$y=ae^{bx}$
Power law	$y=ax^b$

The coefficients of the function can be calculated by clicking the '*compute*' button below the function list box. The coefficients will appear in the 'Best Fit' box in the 'Results' panel. The deviation of the fitting function from the data is displayed as a standard deviation in the 'Error' box below this (see equation 0.1).

When the Curve Fitting Window is closed, the curve fit will automatically appear on any graph that plots the x and y data of the curve fit along its x and y axes. This enables the data values and the curve fit to be compared.

The example below illustrates how a poor selection of fitting function results in a curve fit with a large degree of error.



The curve fit can be removed from the graph by clicking the '*Clear*' button when the curve fit is selected in the Curve Fitting Window.

A .9 .2 .4 Exporting Correlation Data

The data displayed in the actively selected graph, including any curve fits, can be exported to a text based data file by clicking '*Export data*' on the '*File*' menu. This data file can then be imported into a spreadsheet or text editor type package.

A .9 .2 .5 Comparing Correlation Data

The data values for all of the documents can be compared to the data values of one particular document for each expression, using methods similar to those outlined in section A.3.3.1. The compare check box should be activated, and the document to which all the values are to be compared selected in the document list box. The data values in the tables and the values plotted on the graph are then automatically updated to reflect the nature of the comparison method chosen.

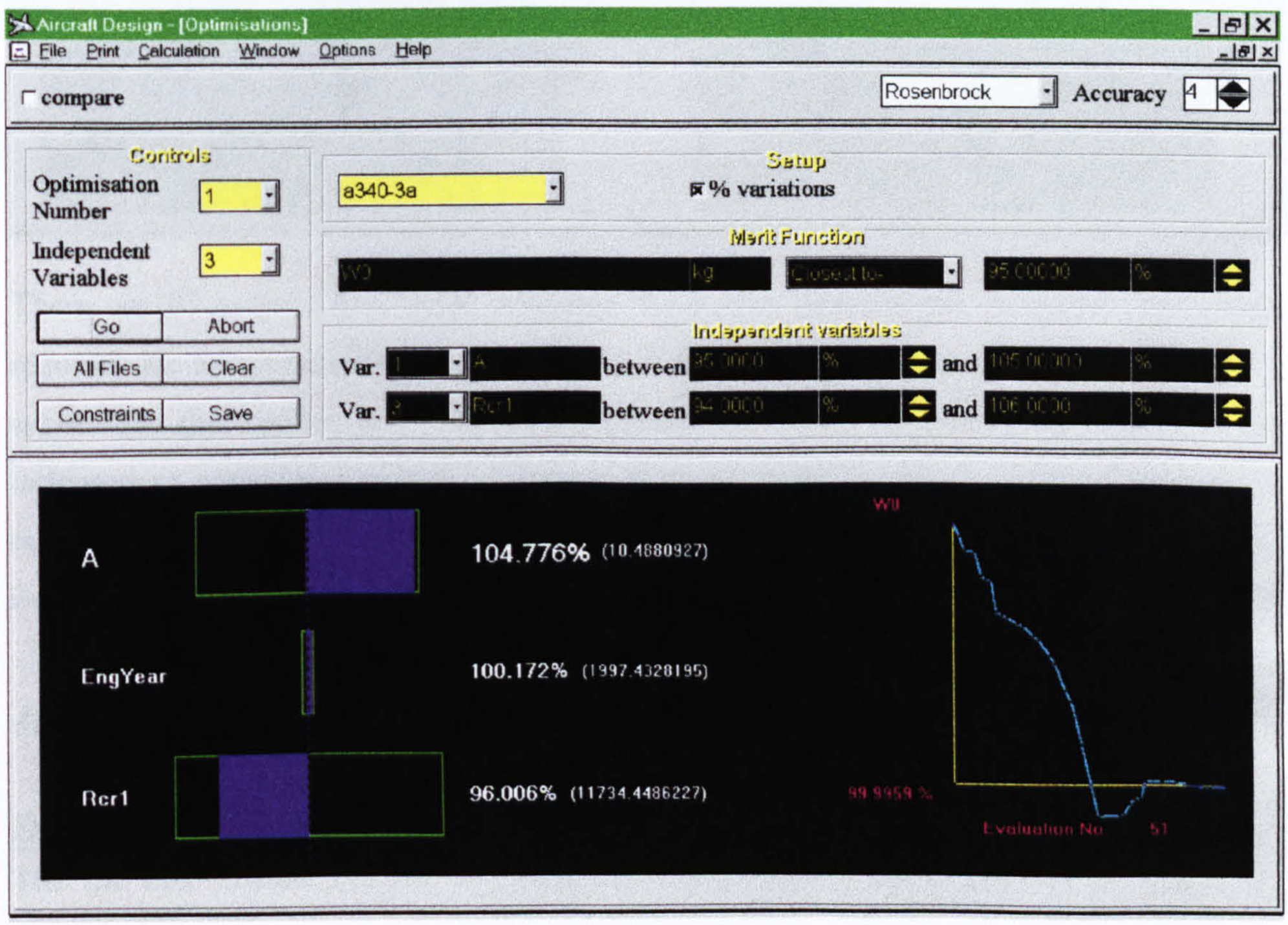
A .9 .3 Optimisation Window

Function

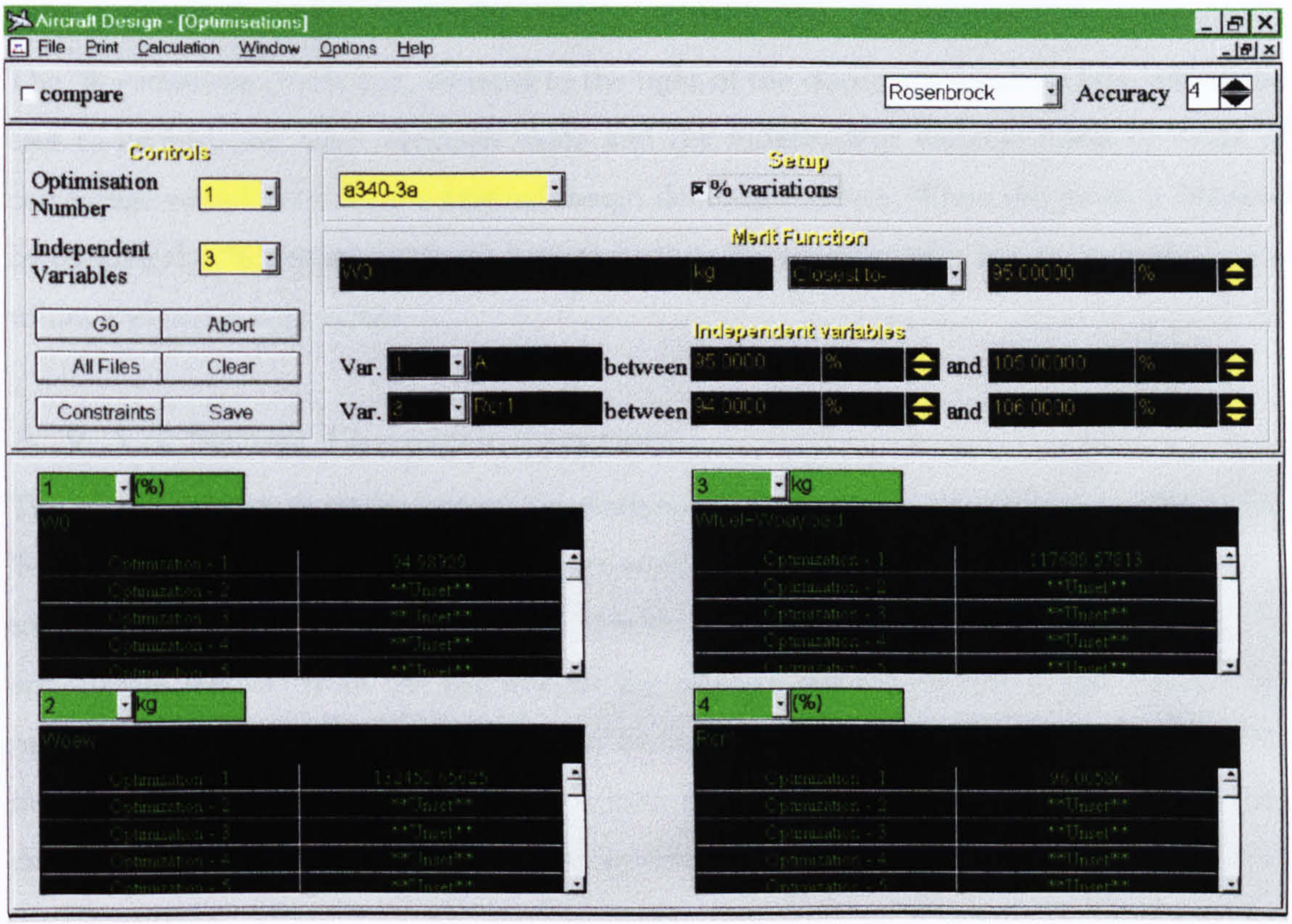
A design can be optimised in terms of any merit function (any valid mathematical expression), such that the value of this function is a maximum, a minimum, or is closest to a specified value. The optimisation process can be reliant on up to 10 independent design variables, and can be unconstrained, or constrained by up to 10 independent logical statements.

Description

The main Optimisation Window is shown below:-



The bottom panel that is visible in the window depends on which part of the optimisation process is being considered. The bottom portion of the screen may alternatively display the controls shown in the picture below. One panel graphically displays the progress of an optimisation, while the other is used for analysis of all the optimisation results. The two views may be toggled by double clicking on the bottom panel.



There are 10 optimisation 'slots' available. Each slot contains the complete information required for an optimisation strategy. This information comprises of the merit function expression, the manner in which this expression is to be optimised, the names of the independent variables, the limits imposed on these variables, the document that is to be optimised, and any constraint data. The optimisation slot that is currently active is selected from the 'Optimisation Number' list box situated in the 'Controls' panel.

A .9 .3 .1 Optimisation Setup

Document Selection

The list box toward the left of the 'Setup' panel selects the document on which the optimised design is to be based. It is important to note that when an optimisation is performed the original document is not altered, the program creates a temporary skeleton document for each optimisation slot. This means that when an optimisation has been completed, the main design parameters for that optimised design are saved so that they can be evaluated and analysed using the four expression boxes in the bottom half of the screen. The detailed drag and performance data of the optimised design is not however saved, as these cannot be evaluated from the expression boxes, and to include it would be inefficient from both a memory and a time point of view. The optimised skeleton design can be saved as a complete design by using the '*Save*' button as described later.

Percentage Variations

The '% variations' check box, situated to the right of the document selection box, allows the user to express any merit function value and the independent variable limits in terms of percentage variations from the original design document values. When the mode is changed by clicking the '% variations' check box, the values are automatically toggled between actual values and percentage values.

A .9 .3 .2 Setting The Merit Function

The merit function is set by entering a mathematical expression in the box located in the 'Merit Function' panel, using the notation outlined in A.9.1. The design can be optimised toward a maximum, a minimum, or a specific value of this expression, by selecting the appropriate method from the list box to the right of the expression. If the 'Closest To' method is selected, then a value needs to be entered in the box that appears next to the method list box. This value can be entered using the keyboard or the spin box and determines the value of the merit function to which the optimisation is aimed.

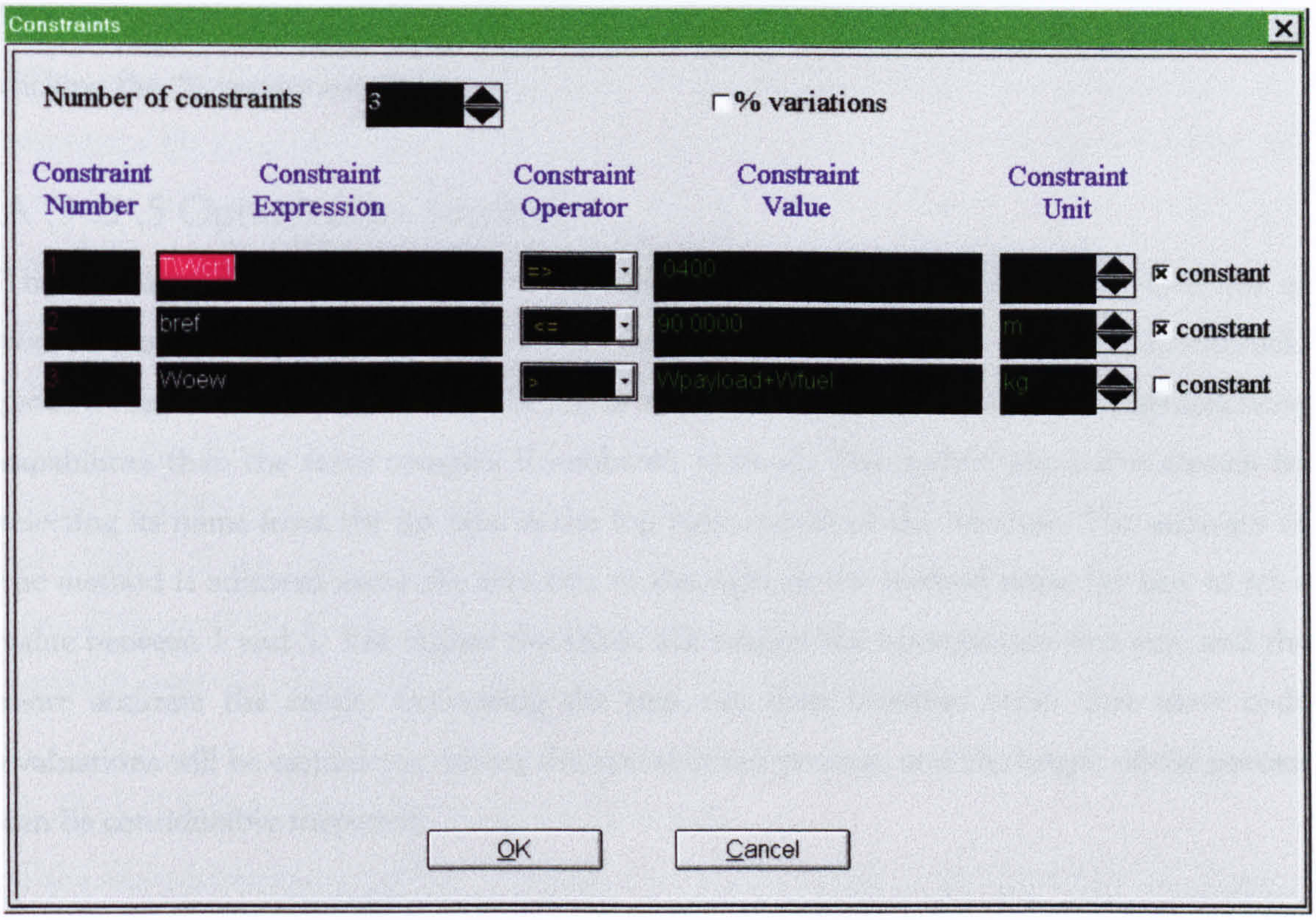
A .9 .3 .3 Setting Independent Variables

The design input parameters that are to be varied independently, and the limits between which they may be varied are set using the controls in the 'Independent Variables' Panel. The number of independent variables for the selected optimisation is chosen from the 'Independent Variables' list box, located in the 'Controls' panel of the window. Although the design may be optimised for up to 10 independent variable, the details of only 2 variables can be viewed at any one time. The number of the variable, of which the name and limits are being viewed, is selected from the appropriate list box to the left of the area in which its details are to be displayed.

The name of the input variable must be typed in the box to the right of the variable number list box, and the [enter] key pressed. Both the upper and the lower limit of the variable will set by default to be the actual value of that variable in the chosen design. These limit values may then be altered by entering a new value from the keyboard, or by using the spin box to increase or decrease its value. The units of the independent variable limits may be changed by double clicking them (unless the '% variation' mode is active).

A .9 .3 .4 Setting Constraints

Clicking the '*Constraints*' button situated in the 'Controls' panel opens the window shown below.



Up to 10 constraints may be placed on each optimisation process. The number of constraints is shown in the top left of the window, this value can be increased or decreased by clicking the up or down arrows to the right of the box containing the constraint number.

Each constraint is in the form of an inequality, and comprises of a constraint expression, a constraint operator, and a constraint value. During the optimisation process the constraint expressions are evaluated after each code evaluation, and checked to see if they remain within the bounds set by the constraint operator and the constraint value. If the bounds on one or more of the constraints have been breached then that particular evaluation is deemed to be a failure.

The constraint expression is entered using the notation of A.9.1. The type of inequality that governs the constraint is chosen from the constraint operator list box. This provides a choice between the 'greater or equal to', 'greater than', 'less or equal to', or 'less than' operators. The constraint value can be expressed as either a constant numeric value, or in terms of the value of a mathematical expression containing design variables. The method used to describe the constraint value is toggled using the 'constant' check box to the right of the constraint value box. When the value has been expressed in terms of a function of design variables, changing the mode of the constraint value to 'constant' causes the expression to be replaced with the value of the expression at that time. During the optimisation process the constraint values expressed as functions are re-evaluated after every code evaluation.

The constraint values may be expressed as percentages of the constraint expression value by clicking the '% variations' check box.

A .9 .3 .5 Optimisation Method

The technique that is used to control the optimisation process can be selected from one of two methods. The two methods available are the 'Hook & Jeeves' and the 'Rosenbrock' pattern search methods. The Hook & Jeeves method is simpler, but with less ridge-following capabilities than the more complex Rosenbrock method. The desired method is chosen by selecting its name from the list box in the top right corner of the window. The accuracy of the method is adjusted using the spin box to the right of the method name list box to set a value between 1 and 5. The higher the value, the smaller the optimisation step size, and the more accurate the result. Decreasing the step size does however mean that more code evaluations will be carried out during the optimisation process, and the length of the process can be considerably increased.

A .9 .3 .6 Optimisation Controls

Beginning The Optimisation Process

Once the optimisation details have been set, it is possible to run the optimisation process by clicking the '*Go*' button on the 'Controls' panel. It may be aborted at any time by clicking the '*Abort*' button situated next to the '*Go*' button.

The amount and content of design data calculated for each design evaluation depends on the number and type of modules that are executed each time. These can be customised by clicking the '*Execution Setup*' command on the '*Options*' menu. The Execution Options Window will appear, with the modules that need to be run to satisfy the data requirements of the variables and constraints of the optimisation being disabled. The user can elect to run any other modules, which although do not have a direct effect on the optimisation, will provide data that can be used to analyse the optimised design.

Copying Optimisation Strategies

An optimisation slot based on one document may be copied so that it can perform the same optimisation on all documents. This is done by selecting the relevant slot and clicking the '*All Files*' button. This will automatically copy the data from the selected slot to the successive slots, changing only the document on which the optimisation is performed.

The data from an optimisation slot may be deleted by pressing the '*Clear*' button when the slot is active.

Saving The Optimal Design

The optimised design may be saved as a document by clicking the '*Save*' button and choosing a file name from the subsequent prompt. As explained in 'Optimisation Setup', the data that is saved during an optimisation does not include highly detailed wing, drag, stability and performance data. This must be created by running these modules using the optimised design parameters. After the user selects a file name for the document, the Execution Options Window will appear, from which it is possible to select the modules that will be executed to provide data for the document. Modules whose names appear grey in the Execution Options Window cannot be deselected, as they are necessary requirements, due to the reliance of the merit function, independent variables, or constraint variables on data from these modules. Once the desired modules have been chosen, the calculations will be executed using the optimal input parameters, and the document will be saved.

A .9 .3 .7 Optimisation Progress Diagram

When the optimisation is being processed the bottom panel of the Optimisation Window displays the progress of the calculations. The left hand portion of the progress display has a green rectangular bar to represent each independent variable. The distance of each side of the bar from the vertical origin (dotted blue line), is proportional to the percentage variation of the lower and upper limits of the variable from its original value. During the optimisation, areas of the bars become filled with blue, this is used to indicate the value of the variable in the current optimal state. The value of the variable is printed alongside each bar, both in terms of percentage deviation from the original value and the actual value.

The right hand side of the progress window shows a graph of the merit function plotted against the number of evaluations. For maximum and minimum optimisations the *y*-axis of the graph is plotted in terms of percentage deviations from the original document value, with the origin at 100%. For optimisations toward a specific value the *y*-axis points are percentage deviations from the specified value, the origin is again 100%.

A .9 .3 .8 Analysis of Optimisation Results

The resultant data from optimised designs can be analysed by making use of up to 10 mathematical expression slots. The bottom panel of the Optimisation Window can be used to enter these expressions, and to view the data of up to four of them simultaneously. This area works in much the same way as the 'Expression Evaluation' area in the Correlation Window, with the exception that the results are listed in terms of optimisation slot rather than document. The number of the desired expression is selected from the list box, the expression is entered in the box below, and the value of the expression for each of the

optimised designs is listed below that. The units of the results can be changed by double clicking the box displaying the units name. It is possible to view the values in terms of percentage variation from the original document value by selecting the '(%)' unit.

The results of optimisations can be compared in the same way as documents, by clicking the 'compare' check box, selecting the optimisation to which the others are to be compared to, and the method with which the data is compared.

A .9 .4 SENSITIVITY STUDIES WINDOW

Function

The effect that the value of specified input variables have on a particular expression or function can be quantified and analysed using this window.

Description



The Sensitivity Studies Window has many features in common with Optimisation Window.

A .9 .4 .1 Sensitivity Study Setup

The document on which the sensitivity study is being carried out is selected from the list box located at the top left of the 'Dependent Variable' panel.

There are 10 sensitivity study 'slots' which store all the data required for a particular strategy. The active slot is chosen from the 'Sensitivity Number' list box in the 'Controls' panel. The data from a slot can be deleted using the '*Clear*' button in the 'Controls' panel, and data can be copied to create identical studies for all documents by clicking the '*All files*' button.

A .9 .4 .2 Setting Variables

The dependent variable can be any mathematical expression or function containing at least one design output parameter. The expression is entered using the notation described in A.9.1.

There may be up to ten independent variables. The number of variables required is set from the 'Independent Variables' list box in the 'Controls' panel. The names of only four of the variables can be viewed at any one time, the list boxes on the left of the four variable name boxes control which ones are displayed. The independent variables are set by entering the name of the desired design input parameter.

A .9 .4 .3 Executing Sensitivity Study

The sensitivity values are calculated by clicking the '*Go*' button. The modules necessary to compute the required data are automatically selected and then executed. A status bar will appear in the top right corner of the window indicating the percentage of the calculations that have been completed. The process can be stopped at any time by clicking the '*Abort*' button.

A .9 .4 .4 Viewing Sensitivity Data

The results of the sensitivity studies are displayed in the table in the bottom half of the window.

The value of the sensitivity parameter for each independent variable is calculated by executing the necessary modules a number of times, each time with a small deviation in the value of the independent variable. The resultant value of the dependent variable is noted, and the sensitivity parameter is calculated as an average percentage deviation of the dependent variable divided by the percentage deviation of the independent variable. This means that a sensitivity value of 0.00 signifies that the independent variable has no effect on the dependent variable expression, whereas a value of 1.00 would indicate that for a particular percentage change in that independent variable, the value of the dependent variable expression changes the same percentage amount.

These sensitivity values are tabulated, with the sensitivity slots along the columns of the table, and the independent variables down the rows.

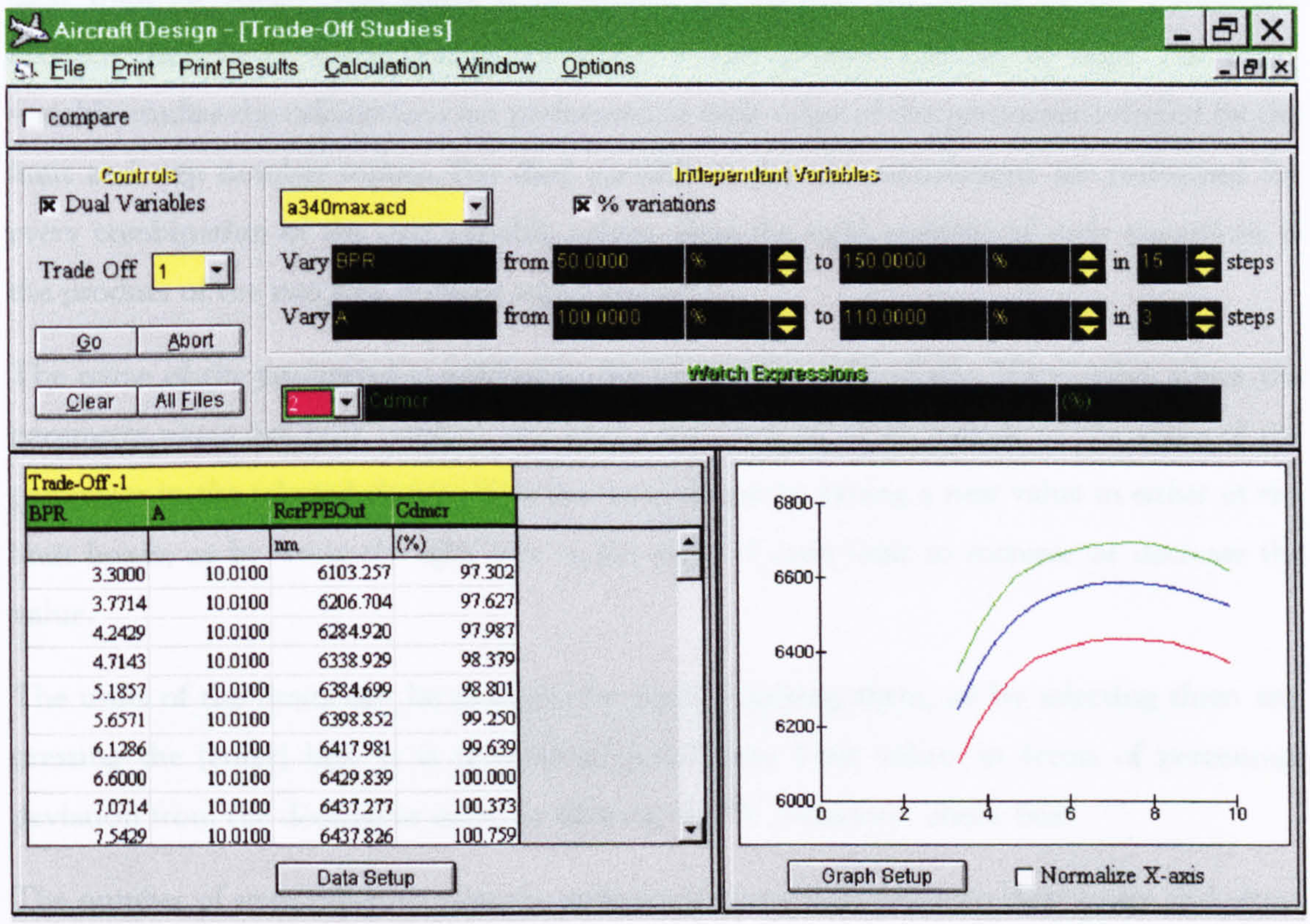
A .9 .5 TRADE-OFF STUDIES WINDOW

Function

This window is used to assess the impact of varying one or two design input parameters simultaneously through a number of discrete steps. A 'map' of design output parameters can be built up, and the values of expressions can be tabulated and plotted for each point on the map. This leads to a multi-line plot showing the effect of continuous variation of the input parameter(s).

Description

The window below shows an example analysis of the variation of aircraft range with engine bypass ratio and wing aspect ratio, for constant takeoff weight.



Many of the controls of the Trade-Off Studies Window exhibit similarities to those of the Optimisation and Sensitivity Windows.

A .9 .5 .1 Trade-Off Setup

As with other data manipulation windows, there are 10 'slots', each of which can be used independently to store data relating to a particular study strategy. The number of the active slot is selected from the 'Trade Off' box in the 'Controls' panel. When the desired slot is active, the data in that slot can be deleted by pressing the '*Clear*' button, or pressing the '*All*

files' button creates identical copies of that study for all open documents. When creating studies using the '*All Files*' command, the trade-off input data will be copied into the successive slots, appropriately changing the document on which the trade-off calculations are to be made.

The document to which a trade-off study applies is selected from the list box situated toward the top left of the 'Independent Variables' panel.

The Trade-Off Studies Window can be chosen to operate in either single variable or dual variable mode by clicking the 'Dual Variables' check box in the 'Controls' panel (see below).

A .9 .5 .2 Setting Independent Variables

There may be up to two design input parameters chosen as the independent variables of each trade-off study. The study is performed by varying the values of the parameters between the selected lower and upper limits, in the specified number of steps. For single variable studies the calculations are performed at each value of the parameter inferred by the limit and step number inputs. For dual variable studies the calculations are performed for every combination of the two variable values, thus the total number of code executions is the product of the two step number input values.

The name of the parameter is entered in the box to the right of the 'Vary' label. Once the parameter name has been entered, the limit values will be set as default to the value of the parameter in the selected design. This can be changed by typing a new value in either of the limit boxes, or by using the spin box to the right of each limit to increase or decrease the value.

The units of the limits can be changed by double-clicking them, or by selecting them and pressing the [enter] key. It is possible to specify the limit values in terms of percentage deviation from the document value by clicking the '% variations' check box.

The number of steps taken to vary the independent variables between their lower and upper limits are entered in boxes to the left of the 'steps' label, the value may be entered from the keyboard or using the spin box.

A .9 .5 .3 Executing Trade-Off Study

The modules which are to be executed for each evaluation in the trade-off study can be selected by clicking the '*Execution Setup*' command from the '*Options*' menu. The modules which appear greyed out in the subsequent Execution Options Window cannot be deselected

as they are the minimum requirement for consistent results, based on which modules have the independent variables as input parameters.

When analysing the results of the trade-off, it is only possible to refer to output variables of modules that have been executed in the study. It is therefore important to execute any modules from which it is anticipated that the output data may be of interest.

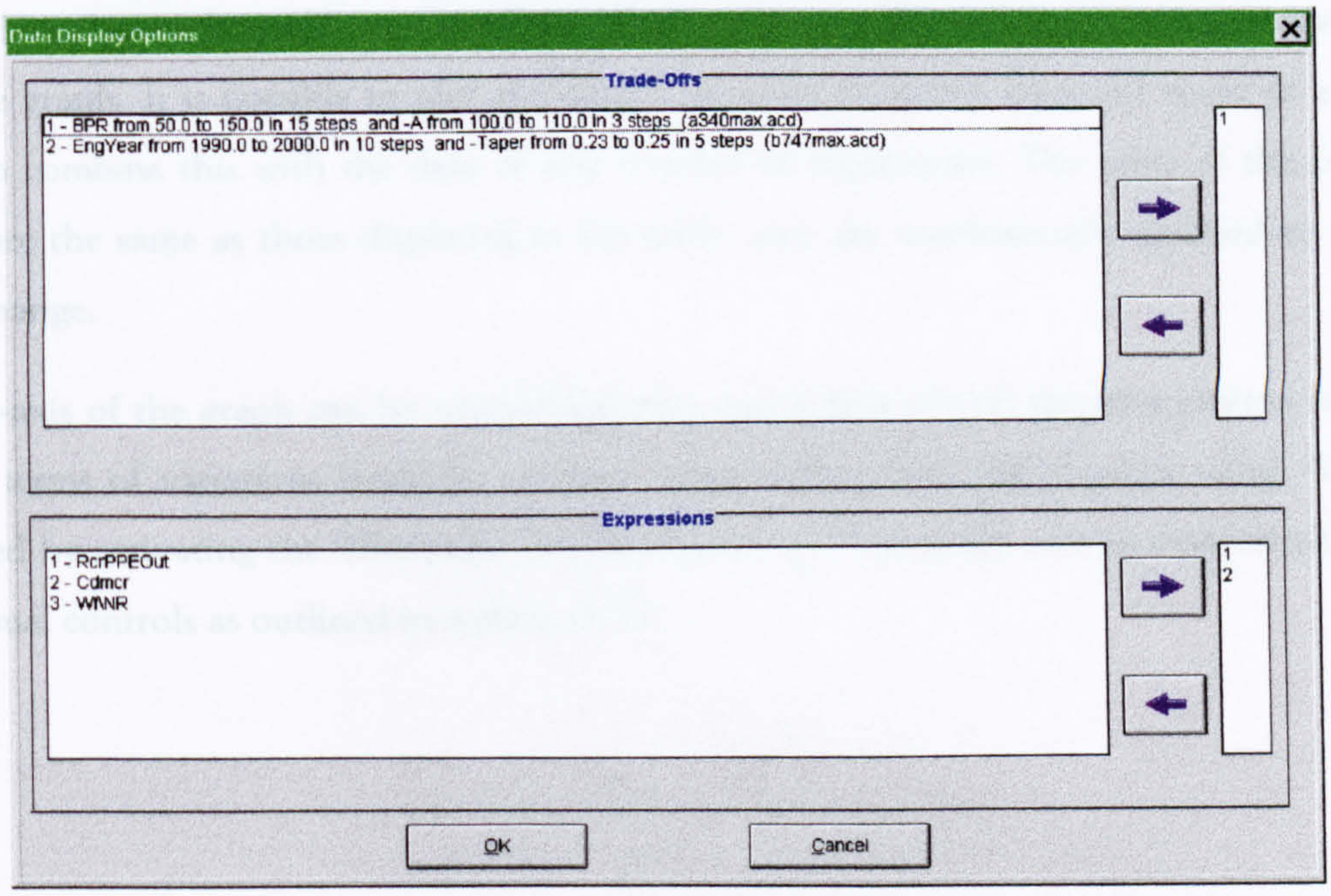
The calculations are started by clicking the '*Go*' button in the 'Controls' panel, they may be aborted at any time by clicking the adjacent '*Abort*' button. During the calculation process a gauge will appear in the top right of the window, this will indicate the proportion of the calculations that have been completed.

A .9 .5 .4 Analysis of Trade-Off Results

Once the trade-off calculations have been completed, the output data for each executed module at each variable state is stored in a temporary file on the hard disk. This data can be analysed by creating 'Watch Expressions', the values of these expressions at each variable state can then be tabulated and plotted as required.

There are 10 available slots for entering expressions, the number of the expression slot is selected form the list box at the left of the 'Watch Expressions' panel. The expression itself is entered in the box adjacent to this using the notation of A.9.1. The units of the expression are displayed alongside.

The bottom half of the screen contains a data table and a graph. The values displayed in these are chosen independently using the '*Setup*' buttons beneath them. Clicking either of the '*setup*' buttons will open a window similar to the one shown below:-



Descriptions of all the valid trade-off studies are listed in the 'Trade-offs' list box. The ones that are to be displayed are listed by number in the box to the right. A trade-off is added by double clicking it in the description box (or selecting it and pressing the ➡ button), and it is removed by double clicking it in the displayed number box (or selecting it and pressing the ⬅ button).

The available 'Watch Expressions' are listed in the 'Expressions' box. These are added and removed from the displayed data in the same way as the trade-offs described above.

Once the data display options are set, clicking the '*OK*' button closes the window and automatically causes the data table/graph to be updated accordingly. Both the data table and graph may be expanded by double clicking on them, or by selecting them and pressing the [enter] key.

Data Table

Each selected trade-off study occupies a main column at the top of the table (shown as yellow). Each trade-off column is further split into columns displaying the values of the independent variable(s) and the selected 'Watch expressions' (shown as green). The rows correspond to the values of the independent variables and watch expressions for each variables state. The units of the columns can be changed by either double clicking the first row of the column, or by changing the units from the 'Watch Expression' panel. All values can be expressed as percentage deviations from their original values by selecting the '(%)' unit.

Data Plotting

The data chosen from the relevant Data Display Options Window is plotted automatically on the graph. It is possible to plot the data from more than one trade off study at a time, and to combine this with the data of any number of expressions. The units of the plotted data are the same as those displayed in the table, and are automatically updated to reflect any change.

The x-axis of the graph can be normalised, this means that the all the data plotted is done so in terms of variations from the original value, rather than the absolute value. This is selected by activating the 'Normalise X-axis' check box. The graph can be customised using the usual controls as outlined in section A.5.3.

Data Comparison

The data from one or more trade-offs can be compared to the data of another. The 'compare' check box should be activated, and the trade off slot to which the others are to be compared should be selected in the list box that appears next to it. Depending on which method of comparison is used, the data in each row of each column of the table is simply subtracted or divided by the value in the analogous column of the 'compare' trade-off study. In 'compare' mode, the graph displays the values of the selected 'compare' trade-off variables subtracted from all the other trade off variables.

For the compare data to be meaningful the independent variables and the number of steps in each trade-off should be identical.

A .10 REFERENCE DATA

A .10 .1 DESIGN PARAMETER NAMES & DESCRIPTIONS

The name, description, and the label of each parameter that can be addressed using the Aircraft Design expression interpreter is listed in this section. There are three types of parameter:-

Input Parameters

These are parameters required for the design of the aircraft. The input parameters are split into groups according to the calculation module to which they are relevant. The exception to this is the 'Reference Parameter' section of inputs, which are not used in the design calculation, but can be used to evaluate design accuracy when working on existing aircraft, or when certain design goals have been specified.

Output Parameters

The data values output from the calculation modules are referred to as output parameters. These parameters are ordered into groups, each group corresponds to the calculation module which is responsible for estimating the value of that parameter.

System Parameters

The expression interpreter can be used to reference the values of parameters created and set in other design and data manipulation windows, as well as the values of global constants. The input and output values of the Data Evaluation Window, the values of expressions created in the Correlation Window, and the output values from the Fuselage Sizing Window can all be addressed using the appropriate label. Universal constants and conversion factors may also be included in mathematical expressions.

General Configuration Input Parameters

Name	Description	Label
Aircraft Name	A text description of the aircraft design.	
Description 1	A text description.	
Description 2	A text description.	
Number of Engines	The total number of engines of the aircraft.	*Ne*
Wing Aspect Ratio	The aspect ratio of the wing.	*A*
Max. Passenger Number	The fuselage passenger limit.	*NpassMax*
Engine Takeoff Thrust	The takeoff thrust of each engine, as specified from the Component Specification Editor.	*T0*
Engine Bypass Ratio	The bypass ratio of each engine, as specified from the Component Specification Editor.	*BPR*
Engine Year In-Service	The approximate year of entry into service of the engines, specified in the Component Specification Editor.	*EngYear*
Root Airfoil T\C Fine Tune	The adjustment factor of the wing root thickness to chord ratio from its airfoil library file value.	*Kt\cRoot*
Tip Airfoil T\C Fine Tune	The adjustment factor of the wing tip thickness to chord ratio from its airfoil library file value.	*Kt\cTip*
Tail Airfoil T\C Fine Tune	The adjustment factor of the tail thickness to chord ratio from its airfoil library file value.	*Kt\cTail*
Wing Tip Device Efficiency	The relative efficiency of any wing tip device, as selected from the Component Specification Editor.	*KWinglet*
Airfoil Mcrit Fine Tune	The tuning factor of the critical Mach number for the wing airfoils.	*KMCrit*
Overall Aerodynamic Efficiency	The overall aerodynamic efficiency of the aircraft relative to mid-90's aircraft. This parameter allows for small intangible aerodynamic design details.	*KAeroeffic*

Initial Sizing Input Parameters

Name	Description	Label
Number Of Passengers	Number of passengers at the cruise conditions specified below.	*Npass*
Number Of Crew	Number of crew at the cruise conditions specified below.	*Ncrew*
Number of 1st Class Passengers	Number of first class passengers at the cruise conditions specified below.	*N1stClass*
Miscellaneous Payload Weight	Any extra payload, additional to passengers & baggage at cruise conditions specified below.	*Wpaymisc*
Main Cruise Range	Cruise range without diversion or loiter, for payload conditions stated above.	*Rcr1*
Main Cruise Height	Altitude at cruise conditions.	*hcr1*
Cruise Mach Number	Mach Number at cruise conditions.	*Macr1*
Max. Cruise L/D Fine Tune	Adjustment to the cruise lift to drag ratio estimate calculated in the Sizing Module.	*KL\D*
Wing Loading Fine Tune	Adjustment to the wing loading estimate calculated in the Sizing Module.	*KW\S*
Takeoff Weight Fine Tune	Adjustment to the takeoff weight calculated in the Sizing Module.	*KW0*
Wing Adv. Mat. Saving	Percentage of wing weight saved by use of advanced materials, as specified in the Component Specification Editor.	*AMWSwing*
Fuselage Adv. Mat. Saving	Percentage of fuselage weight saved by use of advanced materials, as specified in the Component Specification Editor.	*AMWSfuse*
V.Tail Adv. Mat. Saving	Percentage of vertical tail weight saved by use of advanced materials, as specified in the Component Specification Editor.	*AMWSvt*
H.Tail Adv. Mat. Saving	Percentage of horizontal tail weight saved by use of advanced materials, as specified in the Component Specification Editor.	*AMWSht*

Nacelle Adv. Mat. Saving	Percentage of nacelle weight saved by use of advanced materials, as specified in the Component Specification Editor.	*AMWSNac*
S.Control Adv. Mat. Saving	Percentage of surface control weight saved by use of advanced materials, as specified in the Component Specification Editor.	*AMWSsc*
U.Carriage. Adv. Mat. Saving	Percentage of undercarriage weight saved by use of advanced materials, as specified in the Component Specification Editor.	*AMWSuc*
Hydraulics Adv. Mat. Saving	Percentage of hydraulic equipment weight saved by use of advanced materials, as specified in the Component Specification Editor.	*AMWShyd*
Electrics Adv. Mat. Saving	Percentage of electrical equipment weight saved by use of advanced materials, as specified in the Component Specification Editor.	*AMWSelec*
Air Condit. Adv. Mat. Saving	Percentage of air conditioning weight saved by use of advanced materials, as specified in the Component Specification Editor.	*AMWSac*
Furnishing Adv. Mat. Saving	Percentage of furnishings weight saved by use of advanced materials, as specified in the Component Specification Editor.	*AMWSfur*
Oper. Items Adv. Mat. Saving	Percentage of operational items weight saved by use of advanced materials, as specified in the Component Specification Editor.	*AMWSope*

Wing Design Input Parameters

Name	Description	Label
Wing Taper Ratio	Ratio of wing tip chord to wing root chord.	*Taper*
Wing Quarter Chord Sweep	Angle of sweep of wing quarter chord line.	*Swp1\4C*
Wing Twist	Angular twist between wing root and wing tip.	*Twist*
Crank Span\ Wing Span	Ratio of the length of the cranked portion of the wing to the entire wing span.	*Lcrank*
Crank Trailing Edge Sweep	The trailing edge sweep of the cranked portion of the wing.	*SwpCrank*
Inboard Flap Span/ Span	The ratio of the span at the inboard station of the trailing edge flaps to the entire wing span.	*bfi\b*
Outboard Flap Span/ Span	The ratio of the span at the outboard station of the trailing edge flaps to the entire wing span.	*bfo\b*
Flap Type	The number representing the type of trailing edge flaps used.	*Flap*
Flapped/Unflapped chord	Ratio of the average flap chord to the average wing chord.	*cf\c*
Inboard Aileron Span/Span	The ratio of the span at the inboard station of the ailerons to the entire wing span.	*bai\b*
Outboard Aileron Span/ Span	The ratio of the span at the outboard station of the ailerons to the entire wing span.	*bao\b*
Aileron/Flap deflection ratio	Estimate of the average ratio of the aileron deflection to the trailing edge flap deflection.	*da\df*
Wing Spoiler Area	Estimate of the total wing spoiler surface area.	*Sspoiler*
Wing Airbrake Area	Estimate of the total wing airbrake surface area.	*Sairbrake*
Landing Lift Coefficient	Estimate of the maximum value of the landing lift coefficient.	*CLla*
Landing Velocity	Estimate of the minimum velocity at landing.	*Vla*
Horizontal Tail Aspect Ratio	Aspect ratio of the horizontal tail.	*Aht*
Vertical Tail Aspect Ratio	Aspect ratio of the vertical tail.	*Avt*
Horizontal Tail Taper Ratio	Taper ratio of the horizontal tail.	*Taperht*

Vertical Tail Taper Ratio	Taper ratio of the vertical tail.	*Tapervt*
Horizontal Tail 1\4 Chord Sweep	Quarter chord sweep of the horizontal tail.	*Swp1\4cht*
Vertical Tail 1\4 Chord Sweep	Quarter chord sweep of the vertical tail.	*Swp1\4cvt*
Horizontal Tail Size Fine Tune	Adjustment of horizontal tail size estimate.	*KCht*
Vertical Tail Size Fine Tune	Adjustment of vertical tail size estimate.	*KCvt*

Fuselage Geometry Input Parameters

Name	Description	Label
Fuselage Style	The type of fuselage cross section used.	*FuStyle*
Fuselage Length	The overall fuselage length.	*lfuse*
Fuselage Width	The overall width of the fuselage (the width of the main ovoid section of a '747'-type fuselage).	*bfuse*
Fuselage Height	The overall height of the fuselage (the height of the main ovoid section of a '747'-type fuselage).	*hfuse*
Fuselage Nose Length	The length of the nose portion of the fuselage.	*lnose*
Fuselage Tail Length	The length of the tail portion of the fuselage.	*ltail*
X-Section Aspect Ratio	The aspect ratio (Height/Width) of the fuselage cross section.	*FuAspect*
Join Length	The longitudinal length ratio of the extended deck of a '747'-type fuselage, or the ratio describing the distance between the two fuselage centres of a double bubble fuselage.	*FuJoin*
Lower Deck Position	The vertical position of the floor of the lower deck relative to the fuselage centre.	*HdeckL*
Upper Deck Position	The vertical position of the floor of the upper deck relative to the fuselage centre.	*HdeckU*
'747'- Fuselage Total Height	The total height of the cross section including the extended deck 'bubble' of a '747'-type fuselage.	*Hfusedsh*
'747'- Fuselage Bubble Width	The width of the extended deck bubble of a '747'-type fuselage.	*bbubble*
Wetted Area Accuracy	The accuracy of the fuselage wetted area & geometry calculations (The higher the value the more accurate).	*FuAccuracy*

Weight Estimation Input Parameters

Name	Description	Label
Wing A.C. relative to C.G.	The longitudinal position of the wing aerodynamic centre, relative to the aircraft centre of gravity. Specified in terms of % of the wing mean aerodynamic chord.	*PhiAClocation*
Maximum Design Speed	The maximum structural design speed, usually 450 knots.	*Vdes*

Stability Analysis Input Parameters

Name	Description	Label
Dynamic Head Ratio	The ratio of the tail to wing dynamic head.	*EtaH*
Engine Inlet Angle	The engine inlet angle about the horizontal plane (engine incidence).	*AlInlet*

Performance Prediction Input Parameters

Name	Description	Label
Fuel Mass Initial Guess	The initial estimate of the mass of fuel used for the performance profile. Setting this value to zero means the fuel mass calculated from the Initial Sizing Module is used.	*WfuelPPIn*
Payload Mass	The payload mass carried during the performance profile. Setting this value to zero means that the value calculated from the Initial Sizing Module is assumed.	*WpayPP*
Thrust Reversal Parameter	Determines whether thrust reversal is applied on landing. A value of one indicates that it is, whereas a value of zero indicates it is not.	*TReverse*
Iteration Mode	Specifies which is the iteration goal of the performance profile. A value of one means that the range is iterated to meet the fuel requirement, whereas a value of two means that the fuel is iterated to meet the range requirement.	*PPItmode*
Climb1 \ Descent Accuracy	The step size of the climb and descent at constant calibrated airspeed segments. A higher value indicates a smaller step size.	*Cl1Accuracy*
Climb Max. Gamma Accuracy	The step size of the climb for maximum gamma segments. A higher value indicates a smaller step size.	*Cl2Accuracy*
Acceleration Accuracy	The step size of the acceleration segments. A higher value indicates a smaller step size.	*AcAccuracy*
Cruise Accuracy	The step size of the cruise segments. A higher value indicates a smaller step size.	*CrAccuracy*
B.F.L. Accuracy	A higher value indicates a greater precision in the balance field length iteration.	*BFLAccuracy*
Main Cruise Range Initial Guess	The main cruise range, as specified from the Performance Profile Editor.	*Rcr1PPIn*

Reference Variables

Name	Description	Label
Takeoff Weight	Reference takeoff weight.	*W0Ref*
Operational Empty Weight	Reference operational empty weight.	*WoewRef*
Maximum Fuel Weight	Reference maximum possible fuel weight.	*WfuelRef*
Maximum Payload Weight	Reference maximum payload weight.	*WpayRef*
FAR Takeoff Field Length	Reference FAR takeoff field length.	*FARtoRef*
FAR Landing Field Length	Reference FAR landing field length.	*FARlaRef*
Performance Profile Payload	Reference payload weight for the performance profile.	*WpayPPRef*
Performance Profile Range	Reference range for the performance profile	*RcrPPRef*
Performance Profile Fuel	Reference fuel weight for the performance profile.	*WfuelPPRef*
Gross Wing Area	Reference wing planform area.	*SrefRef*
Gross Wing Span	Reference wing span.	*brefRef*
Gross H.Tail Area	Reference horizontal tail planform area.	*SrefHtRef*
Gross V.Tail Area	Reference vertical tail planform area.	*SrefVtRef*
Miscellaneous 1	Can be used for any relevant data.	*Misc1*
Miscellaneous 2	Can be used for any relevant data.	*Misc2*
"	"	"
Miscellaneous 23	Can be used for any relevant data.	*Misc23*

General Configuration Output Parameters

Name	Description	Label
Nominal Engine Thrust	Installed static sea level thrust of each engine.	*Tnominal*
Engine Bypass Ratio	Bypass ratio of engines.	*BPROut*
Engine Dry Weight	Dry weight of each engine.	*WEng*
Engine Fan Diameter	Diameter of engine fan.	*DFan*
Engine Length	Length of engine.	*Leng*
Root Airfoil t\c Ratio	Resultant thickness to chord ratio of root airfoil.	*t\cRoot*
Tip Airfoil t\c Ratio	Resultant thickness to chord ratio of tip airfoil.	*T\cTip*
Tail Airfoil t\c Ratio	Resultant thickness to chord ratio of tail airfoil.	*t\cTail*
Root Airfoil Clmax	Maximum 2-d lift coefficient of root airfoil.	*ClMaxRoot*
Tip Airfoil Clmax	Maximum 2-d lift coefficient of tip airfoil.	*ClMaxTip*
Tail Airfoil Clmax	Maximum 2-d lift coefficient of tail airfoil.	*ClMaxTail*
Root Incidence at Zero Cl	Root airfoil incidence at zero lift coefficient.	*Al0Root*
Tip Incidence at Zero Cl	Tip airfoil incidence at zero lift coefficient.	*Al0Tip*
Tail Incidence at Zero Cl	Tail airfoil incidence at zero lift coefficient.	*Al0Tail*
Root Lift at Zero Incidence	Root airfoil lift coefficient at zero incidence.	*Cl0Root*
Tip Lift at Zero Incidence	Tip airfoil lift coefficient at zero incidence.	*Cl0Tip*
Tail Lift at Zero Incidence	Tail airfoil lift coefficient at zero incidence.	*Cl0Tail*

Initial Sizing Output Parameters

Name	Description	Label
Takeoff Weight	Maximum weight at takeoff.	*W0*
Operational Empty Weight	Initial estimate of operational empty weight at selected range and payload.	*Woew*
Fuel Weight	Fuel mass for selected range and payload.	*Wfuel*
Payload Weight	Payload mass for selected number of passengers and miscellaneous payload.	*Wpayload*
End of Flight Weight Fraction	Ratio of the weight at the end of the flight to the weight at beginning of the flight.	*Wend\0*
Mid-Cruise Weight Fraction	Ratio of the weight at the mid-cruise point to the weight at beginning of the flight.	*Wmcr1\0*
Wtakeoff / Wwarmup	Ratio of the weight at the end of the takeoff to the weight at end of the warm-up.	*Wto\0*
Wclimb1 / Wtakeoff	Ratio of the weight at the end of the climb to cruise height, to the weight at end of the takeoff.	*Wcl1\to*
Wcruise1 / Wclimb1	Ratio of the weight at the end of the main cruise to the weight at end of the main climb.	*Wcr1\cl1*
Wdescent1 / Wcruise1	Ratio of the weight at the end of the main descent to the weight at end of the main cruise.	*Wde1\cr1*
Wabort.land./Wdescent1	Ratio of the weight at the end of an aborted landing to the weight at the end of the descent.	*Wal\de1*
Wclimb2 / Wabort.land.	Ratio of the weight at the end of a climb to diversion height, to the weight at end of the aborted landing.	*Wcl2\al*
Wcruise2 / Wclimb2	Ratio of the weight at the end of the diversion cruise to the weight at end of the diversion climb.	*Wcr2\cl2*
Wdescent2 / Wcruise2	Ratio of the weight at the end of the diversion descent to the weight at end of the diversion cruise.	*Wde2\cr2*

Wloiter / Wdescent2	Ratio of the weight at the end of the loiter to the weight at end of the diversion descent.	*Wlo\de2*
Wdescent3 / Wloiter	Ratio of the weight at the end of the final descent to the weight at end of the loiter.	*Wde3\lo*
Wlanding / Wdescent3	Ratio of the weight at the end of the landing to the weight at end of the final descent.	*Wla\de3*
Main Cruise Velocity	The velocity during the main cruise.	*Vcr1*
Main Cruise Thrust	The estimated main cruise average thrust.	*Tcr1*
Main Cruise T/W	The estimated main cruise average thrust to weight ratio.	*T\Wcr1*
Takeoff T/W	Takeoff thrust to weight ratio.	*T\Wto*
Speed of Sound at Main Cruise	Speed of sound at main cruise conditions.	*acr1*
Speed of Sound at Diversion	Speed of sound at diversion cruise conditions.	*acr2*
Air Density at Main Cruise	Air density at main cruise conditions.	*Rhocr1*
Air Density at Diversion	Air density at diversion cruise conditions.	*Rhocr2*
Air Viscosity at Main Cruise	Air viscosity at main cruise conditions.	*NuCr1*
Air Viscosity at Diversion	Air viscosity at diversion cruise conditions.	*NuCr2*
Estimated Main Cruise L/D	Initial estimation of the main cruise average lift to drag ratio.	*L\Dcr1*
Estimated W/S	The aircraft wing loading estimate.	*W\S*
Estimated Main Cruise S.F.C.	Estimate of the average main cruise s.f.c.	*sfcCr1*
Estimated Max. Cruise Thrust	Estimate of the maximum thrust available at main cruise conditions.	*Tcr1max*

Wing Design Output Parameters

Name	Description	Label
Wing Reference Area	Area of reference wing planform.	*Sref*
Wing Span	Span of reference wing.	*bref*
Root Chord Length	Length of reference wing root chord.	*Croot*
Tip Chord Length	Length of reference wing tip chord.	*Ctip*
M.A.C. Length	Length of ref. wing mean aerodynamic chord.	*Cmac*
Crank Length	Length of cranked portion of reference wing.	*bcrank*
M.A.C. Incidence	Incidence angle of the mean aerodynamic chord with respect to the fuselage.	*AlMAC*
M.A.C. Incidence at Zero Lift	Incidence of the m.a.c. at zero lift (2-d).	*Al0MAC*
Maximum Clean Cl (2-d)	Max. lift of the mean aerodynamic chord (2-d).	*ClMax*
Spanwise M.A.C. location	The location of the mean aerodynamic chord in the spanwise direction (Y-axis).	*Ymac*
Streamwise A.C. location	Distance of the aerodynamic centre from the wing leading edge in the streamwise direction (X-axis), as a ratio of the m.a.c. length.	*Xac\Cmac*
Sweep at Leading Edge	Sweep at the wing leading edge.	*SwpLE*
Sweep at Maximum Thickness	Sweep along line of wing airfoil max. thickness.	*SwpM*
Sweep at Mid-Chord	Sweep along mid-chord line of the wing.	*Swp0.5c*
Sweep at Trailing Edge	Sweep at the wing trailing edge.	*SwpTE*
Equivalent Wing M.A.C. Length	Length of the equivalent wing mean aerodynamic chord.	*CmacE*
Equivalent Wing Aspect Ratio	Aspect ratio of the equivalent wing.	*AE*
Equivalent Wing Taper Ratio	Taper ratio of the equivalent wing.	*TaperE*
Equivalent Wing Area	The planform area of the equivalent wing.	*SrefE*
Equivalent Wing 1/4C Sweep	Quarter chord sweep of the equivalent wing.	*Swp1\4cE*
Equivalent Wing Root Chord	Length of the equivalent wing root chord.	*CrootE*
Equivalent Wing Tip Chord	Length of the equivalent wing tip chord.	*CtipE*

Wing C.G. Distance From Apex	Streamwise distance of the wing centre of gravity from the wing apex.	*Xdshcg*
Equiv. Wing Streamwise A.C. location	The distance of the aerodynamic centre of the equivalent wing from the leading edge, in the streamwise direction (X-axis),expressed as a ratio of its mean aerodynamic chord length.	*Xac\CmacE*
Equiv. Wing A.C. distance from apex	Streamwise distance of the equivalent wing aerodynamic centre from the wing apex.	*XdshacE*
H.Tail Streamwise A.C. Location	The distance of the aerodynamic centre of the horizontal tail from the leading edge, in the streamwise direction (X-axis),expressed as a ratio of its mean aerodynamic chord length.	*Xac\cHT*
V. Tail Streamwise A.C. Location	The distance of the aerodynamic centre of the vertical tail from the leading edge, in the streamwise direction (X-axis),expressed as a ratio of its mean aerodynamic chord length.	*Xac\cVT*
Cruise CL (3-d)	Mid-cruise lift coefficient (3-d).	*CLCr1*
Cruise Max. Clean CL (3-d)	Mid-cruise maximum clean lift coefficient (3-d).	*CLCr1Cln*
Takeoff CL (3-d)	Takeoff lift coefficient (3-d).	*CLTo*
Takeoff Velocity	Takeoff Velocity.	*Vto*
Takeoff Max. Clean CL (3-d)	Takeoff maximum clean lift coefficient (3-d).	*CLToCln*
Takeoff Flap Deflection	Takeoff trailing edge flap deflection.	*dfto*
Takeoff Aileron Deflection	Takeoff aileron deflection.	*dato*
Landing CL (3-d)	Landing lift coefficient (3-d).	*CLLa*
Landing Max. Clean CL (3-d)	Landing maximum clean lift coefficient (3-d).	*CLLaCln*
Landing Flap Deflection	Landing trailing edge flap deflection.	*dfla*
Landing Aileron Deflection	Landing aileron deflection.	*dala*
Ground Roll CL (3-d)	Ground roll lift coefficient (3-d).	*CLGr*
Ground Roll Lift Curve Slope	Gradient of 3-d lift vs. incidence curve, during ground roll.	*CLalphaGr*
H. Tail Volume Coefficient	Estimated horizontal tail volume coefficient.	*Cht*
V. Tail Volume Coefficient	Estimated vertical tail volume coefficient.	*Cvt*

Aircraft Geometry Output Parameters

Name	Description	Label
Fuselage Wetted Area	Wetted area of the fuselage.	*SwetFuse*
Fuselage Plan Area	Area of the fuselage planform.	*Splanform*
Fuselage Frontal Area	Maximum area of the fuselage cross section	*Sfrontal*
Component Fuse.1 Wetted Area	The wetted area of one of the component fuselages, if the required fuselage is made up of more than one fuselage section.	*SwetFuse1*
Component Fuse.1 Plan Area	The planform area of one of the component fuselages, if the required fuselage is made up of more than one fuselage section.	*Splanorm1*
Component Fuse.2 Wetted Area	The wetted area of the other of the component fuselages, if the required fuselage is made up of more than one fuselage section.	*Swetfuse2*
Component Fuse.2 Plan Area	The planform area of the other of the component fuselages, if the required fuselage is made up of more than one fuselage section.	*SPlanform2*
Nacelle Fan Cowling Length (Lna)	The length of each nacelle fan cowling.	*lfc*
Nacelle Max. Diameter (Dfc)	The maximum diameter of each nacelle.	*Dfc*
Streamwise Location of Dfc	The streamwise location of the position of the maximum diameter, as a ratio of the nacelle length.	*BetaFc*
Diameter at Fan Inlet /Dfc	Ratio of the fan inlet diameter to the maximum nacelle diameter.	*Dfci\fc*
Diameter at Fan Exit / Dfc	Ratio of the fan exit diameter to the maximum nacelle diameter.	*Dfco\fc*
Gas Generator Length / Lfc	The ratio of gas generator length to nacelle fan cowling length.	*Lge\fc*
Gas Gen. Max. Diameter /Dfc	Ratio of the maximum gas generator diameter to the maximum nacelle diameter.	*Dgei\fc*

Gas Gen. Min. Diameter /Dfc	Ratio of the minimum gas generator diameter to the maximum nacelle diameter.	*Dgeo\fc*
Plug Length / Lfc	The ratio of nacelle plug length to the nacelle fan cowling length.	*Lpl\fc*
Plug Max. Diameter / Dfc	Ratio of the maximum nacelle plug diameter to the maximum nacelle diameter.	*Dpl\fc*
Vertical Wing-Fuse. Distance	Vertical distance from bottom of the fuselage to the wing mean aerodynamic chord.	*ZWingFuse*
Vertical Tail-Wing Distance	Vertical distance between the wing and tail mean aerodynamic chords.	*ZWingTail*
Vertical Engine-Wing Distance	Average vertical distance between the wing mean aerodynamic chord and the engine centres.	*ZWingEng*
Fuselage Width at Tail	The width of the fuselage at the apex of the horizontal tail.	*HFuseTail*
Estimated Freight Volume	An estimation of the volume available for freight in the cargo hold.	*Vcargo*

Weight Estimation Output Parameters

Name	Description	Label
Operational Empty Weight	Estimate of the operational empty weight, based on the detailed calculations of the component weights.	*WoewCalc*
Error (from sizing estimate)	The percentage difference between the Weight Estimation & the Initial Sizing operational empty weight estimates.	*WoewErr*
Total Wing Weight	The total weight of all wing components.	*WWingTot*
(Basic Wing Weight)	Weight of the basic wing components.	*WWingbas*
(Leading Edge Flap Weight)	Weight of the leading edge flap system.	*Wlef*
(Trailing Edge Flap Weight)	Weight of the trailing edge flap system.	*Wtef*
(Aileron Weight)	Weight of the ailerons.	*Waileron*
(Spoiler Weight)	Weight of wing mounted spoilers.	*Wspoiler*
Horizontal Tail Weight	The total weight of the horizontal tail.	*Wht*
Vertical Tail Weight	The total weight of the vertical tail.	*Wvt*
Fuselage Weight	The total weight of the fuselage structure.	*Wfuse*
Nacelle Weight	The total weight of all nacelles.	*Wnac*
Propulsion Group Weight	The total weight of all engines & systems.	*Wpg*
Airframe Services Weight	The total weight of all the airframe services and equipment components.	*Wase*
(Power Unit Weight)	Weight of the power unit.	*Wapu*
(Instrumentation Weight)	Weight of instrumentation equipment.	*Wiae*
(Hydraulics Weight)	Weight of hydraulic systems.	*Whyd*
(Electrics Weight)	Weight of electrical systems.	*Wel*
(Furnishings Weight)	Weight of fuselage furnishing.	*Wfurn*
(Air conditioning Weight)	Weight of air conditioning system.	*Wac*
(Miscellaneous Weight)	Weight of miscellaneous items	*Wasemisc*
Surface Control Weight	Weight of surface control systems.	*Wsc*

Undercarriage Weight	Weight of undercarriage.	*Wuc*
Operational Items Weight	Total weight of operational items.	*Wope*
(Crew Items Weight)	Weight of crew and crew luggage.	*Wcrew*
(Passenger Supplies Weight)	Weight of passenger food and drink supplies.	*Wfood*
(Toilet Supplies Weight)	Weight of toilet supplies.	*Wtoilet*
(Safety Supplies Weight)	Weight of safety supplies.	*Wsafety*
(Residual Fuel & Oil Weight)	Weight of residual fuel and oil.	*Wresid*
Wing Weight Fraction	Wing weight expressed as % of operational empty weight (OEW).	*Wwing\W*
Horizontal Tail Weight Fraction	Horizontal tail weight expressed as % of OEW.	*Wht\W*
Vertical Tail Weight Fraction	Vertical tail weight expressed as % of OEW.	*Wvt\W*
Fuselage Weight Fraction	Fuselage weight expressed as % of OEW.	*Wfuse\W*
Nacelle Weight Fraction	Nacelle weight expressed as % of OEW.	*Wnac\W*
Propulsion Weight Fraction	Propulsion weight expressed as % of OEW.	*Wpg\W*
Airframe Services Weight Fraction	Airframe services and equipment weight expressed as a % of OEW.	*Wase\W*
Surface Control Weight Fraction	Surface control weight expressed as % of OEW.	*Wsc\W*
Undercarriage Weight Fraction	Undercarriage weight expressed as % of OEW.	*Wuc\W*
Operational Items Weight Fraction	Operational items weight expressed as a % of OEW.	*Wope\W*
Ultimate Load Factor	The ultimate structural load factor	*nult*
Aircraft C. of G. Location	Streamwise location of aircraft centre of gravity, measured from fuselage nose.	*Xcg*
Wing A.C. Location	Streamwise location of wing aerodynamic centre, measured from fuselage nose	*Xacwing*
Wing C. of G. Location	Streamwise location of wing centre of gravity, measured from fuselage nose.	*Xcgwing*
Horizontal Tail A.C. Location	Streamwise location of horizontal tail aerodynamic centre, measured from fuselage nose.	*Xacht*
Vertical Tail Arm	Streamwise distance between vertical tail and wing aerodynamic centres.	*Lvt*

Tail C. of G. Location	Streamwise location of the centre of gravity of the vertical and horizontal tails, measured from the fuselage nose.	*Xcgtail*
Fuselage C. of G. Location	Streamwise location of the centre of gravity of the fuselage, measured from the fuselage nose.	*Xcgfuse*
Nacelle C. of G. Location	Streamwise location of the centre of gravity of the nacelles, measured from the fuselage nose.	*Xcgnac*
Propulsion C. of G. Location	Streamwise location of the centre of gravity of the engines, measured from the fuselage nose.	*Xcgpg*
A.S.E. C. of G. Location	Streamwise location of the centre of gravity of the A.S.E., measured from the fuselage nose.	*Xcgase*
Surface Control C. of G. Location	Streamwise location of the centre of gravity of the surface controls, measured from the fuselage nose.	*Xcgsc*
Horizontal Tail Ref. Area	Reference planform area of the horizontal tail.	*SrefHt*
Vertical Tail Ref. Area	Reference planform area of the vertical tail.	*SrefVt*
Horizontal Tail Span	Span of the horizontal tail.	*brefht*
Vertical Tail Span	Span of the vertical tail.	*brefvt*
Horizontal Tail Root Chord	Length of the horizontal tail root chord.	*CrootHt*
Vertical Tail Root Chord	Length of the vertical tail root chord.	*CrootVt*
Horizontal Tail Tip Chord	Length of the horizontal tail tip chord.	*CtipHt*
Vertical Tail Tip Chord	Length of the vertical tail tip chord.	*CtipVt*
Horizontal Tail M.A.C. Length	Length of the horizontal tail m.a.c.	*CmacHt*
Vertical Tail M.A.C. Length	Length of the vertical tail m.a.c.	*CmacVt*
H.Tail Leading Edge Sweep	Leading edge sweep of the horizontal tail.	SwpLeHt
V. Tail Leading Edge Sweep	Leading edge sweep of the vertical tail.	SwpLeVt
H. Tail Max. Thickness Sweep	Sweep along the line of maximum thickness of the horizontal tail.	SwpMht
V. Tail Max. Thickness Sweep	Sweep along the line of maximum thickness of the vertical tail.	SwpMvt
Main Undercarriage Bogey No.	Number of bogeys of the main undercarriage.	NBogey
Main Undercarriage Tyre No.	Number of tyres on each bogey.	Ntyre

Main Undercarriage Tyre Diameter	Diameter of each tyre on main undercarriage.	Dtyre
Main Undercarriage Tyre Pressure	Pressure of each tyre on main undercarriage.	Ptyre
Main Undercarriage Stroke Length	Length of the stroke of the main undercarriage bogeys.	Suc
Main Undercarriage Oleo Diameter	Diameter of the oleo of the main undercarriage bogeys.	Doleo
Total Undercarriage Height	Total Height of the main undercarriage.	Huc
Total Undercarriage Drag	Total drag of all of the undercarriage.	CDuc

Drag Prediction Output Parameters

Name	Description	Label
Mid-Cruise Component Drag	The mid-cruise parasite drag, not including compressibility effects.	*CDcmpnCr1*
Mid-Cruise Compressibility Drag	Mid-cruise drag due to compressibility effects.	*CDcmprCr1*
Mid-Cruise Parasite Drag	The total mid-cruise parasite drag value.	*CD0Cr1*
Mid-Cruise Drag	The total mid-cruise drag value, including drag due to lift.	*CDCr1*
Takeoff Component Drag	The takeoff parasite drag, not including flap deflection effects.	*CDcmpnTo*
Takeoff Flap Drag	Takeoff drag increment due to flap deflection.	*CDflapTo*
Undercarriage Drag	The drag increment due to undercarriage.	*CDUcdsh*
Takeoff Parasite Drag	The total takeoff parasite drag.	*CD0To*
Takeoff Drag	The total drag at takeoff	*CDTo*
Windmilling Jet Drag	The extra drag of an inoperative engine.	*CDengine*
Takeoff Engine Out Parasite Drag	The total parasite drag at takeoff with one engine inoperative.	*CD0ToEo*
Takeoff Engine Out Drag	Total takeoff drag with one engine inoperative.	*CDToEo*
Landing Component Drag	The landing parasite drag, not including flap deflection effects.	*CDcmpnLa*
Landing Flap Drag	Landing drag increment due to flap deflection.	*CDflapLa*
Landing Parasite Drag	The total landing parasite drag.	*CD0La*
Landing Drag	The total drag at landing conditions.	*CDLa*
Total Wetted Area	The total wetted area of the aircraft.	*Swet*
Wing Wetted Area	The total wetted area of the wing.	*SwetWing*
Horizontal Tail Wetted Area	The total wetted area of the horizontal tail.	*SwetHt*
Vertical Tail Wetted Area	The total wetted area of the vertical tail.	*SwetVt*
Nacelles Wetted Area	The total wetted area of the nacelles.	*SwetNac*
Pylons Wetted Area	The total wetted area of the pylons.	*SwetPyl*

Stability Analysis Output Parameters

Name	Description	Label
Cruise Static Margin	The static margin at mid cruise conditions.	*SMCr1*
Takeoff Static Margin	The static margin at takeoff conditions.	*SMTo*
Landing Static Margin	The static margin at landing conditions.	*SMLa*
Cruise Tail Deflection	The tail deflection at mid-cruise conditions.	*ihtCr1*
Takeoff Tail Deflection	The tail deflection at takeoff conditions.	*ihtTo*
Landing Tail Deflection	The tail deflection at landing conditions.	*ihtLa*
Cruise Trim Drag	The additional drag due to the tail deflection required to trim the aircraft during cruise.	*CDTrimCr1*
Takeoff Trim Drag	The additional drag due to the tail deflection required to trim the aircraft during takeoff.	*CDTrimTo*
Landing Trim Drag	The additional drag due to the tail deflection required to trim the aircraft during landing.	*CDTrimLa*

Performance Prediction Output Parameters

Name	Description	Label
Fuel Used	The mass of fuel used for the performance profile.	*WfuelPPout*
Final Weight Fraction	The ratio of the weight at the end of the profile to the takeoff weight.	*Wend\0PP*
Flight Time	The flight time for the complete performance profile.	*Tpp*
Flight Range	The total distance travelled during the performance profile.	*Rpp*
Takeoff Distance	The estimated takeoff run length.	*Sto*
Landing Distance	The estimated landing run length.	*Sla*
FAR Takeoff Distance	The estimated FAR takeoff field length,	*FARto*
FAR Landing Distance	The estimated FAR landing field length, including regulation safety factors.	*FARla*
Resultant Takeoff Weight	The takeoff weight for the calculated performance profile.	*W0pp*
Main Cruise Range(No Reserves)	The length of the main cruise section of the calculated performance profile.	*Rcr1PPOut*
Fuel per passenger-kilometre	The amount of fuel consumed during the flight, divided by the product of the number of passengers and the range. This gives a measure of the efficiency of the aircraft.	*Wfuel\NR*

Data Evaluation Window System Parameters

Name	Description	Label
Atmospheric Altitude	Altitude input for atmosphere calculations.	*EVHatm*
Atmospheric DT	Temperature input for atmosphere calculations.	*EVDTatm*
Atmospheric Speed of Sound	Speed of sound output from atmosphere calcs.	*EVasound*
Atmospheric Air Density	Air density output from atmosphere calcs.	*EVRho*
Atmospheric Air Viscosity	Air viscosity output from atmosphere calcs.	*EVnu*
Atmospheric Temperature	Temperature output from atmosphere calcs.	*EVTemp*
Atmospheric Pressure	Pressure output from atmosphere calcs.	*EVPress*
Engine Altitude	Altitude input for engine calculations.	*EVHeng*
Engine Mach No.	Mach number input for engine calculations.	*EVMaeng*
Engine Thrust Setting	Thrust setting input for engine calculations.	*EVTSeng*
Engine Thrust	Thrust value output from engine calculations.	*EVT*
Engine Thrust Ratio	Thrust ratio output from engine calculations.	*EVT\Tnom*
Engine S.F.C.	Engine s.f.c. output from engine calculations.	*EVsfc*
Drag Altitude	Altitude input for drag calculations.	*EVHdrag*
Drag CL	Lift coefficient input for drag calculations.	*EVCLdrag*
Drag Mach No.	Mach number input for drag calculations	*EVMadrag*
Component Drag	The parasite drag, neglecting compressibility and flap effects, output from the drag calcs.	*EVCDcmpn*
Parasite Drag	Total parasite drag output from the drag calcs.	*EVCD0*
Total Drag	Total drag output from the drag calculations.	*EVCD*
Drag Force	The total drag force output from the drag calcs.	*EVdrag*
Compressibility Drag	The compressibility drag increment output from the drag calculations	*EVCDcmpr*
Vortex Drag	The drag due to lift output from the drag calcs.	*EVCDV*
Flap Drag	The drag due to flap deployment from the drag calculations.	*EVCDflap*

Correlation Window System Parameters

Name	Description	Label
Correlation Result -1	The value of the correlation expression evaluated in slot 1.	*CoExp1*
Correlation Result -2	The value of the correlation expression evaluated in slot 2.	*CoExp2*
Correlation Result -3	The value of the correlation expression evaluated in slot 3.	*CoExp3*
"	"	"
Correlation Result -15	The value of the correlation expression evaluated in slot 15.	*CoExp15*

Fuselage Sizing Window System Parameters

Name	Description	Label
Fuselage Sizing Style	Fuselage style as set in the Fuselage Sizing Window.	*FuSiStyle*
Fuselage Sizing Length	Length of the fuselage calculated in the Fuselage Sizing Window.	*FuSiLfuse*
Fuselage Sizing Width	Width of the fuselage calculated in the Fuselage Sizing Window.	*FuSiBfuse*
Fuselage Sizing Height	Height of the fuselage calculated in the Fuselage Sizing Window.	*FuSiHfuse*
Fuselage Sizing Nose Length	Nose length of the fuselage calculated in the Fuselage Sizing Window.	*FuSiLnose*
Fuselage Sizing Tail Length	Tail length of the fuselage calculated in the Fuselage Sizing Window.	*FuSiLtail*

Universal Constants and Conversion Factors

Name	Description	Label
Pi	3.1415927	*Pi*
Gravitational constant	9.80665	*g*
metre-ft conversion	3.280339895	*ft*
metre-nautical mile conversion	0.000539982	*nm*
metre-mile conversion	0.0006214	*mile*
metre-inch conversion	39.37	*in*
kilogram-pound conversion	2.20462218	*lb*
second-minute conversion	1/60	*min*
second-hour conversion	1/3600	*hr*
radian-degree conversion	180/pi	*deg*
m\s - knots conversion	1.943	*knots*
m^2 -ft^2 conversion	10.763910417	*ft2*
Newton-Lbf conversion	4.448225959	*LBF*

BIBL
LONDON